Synthesis and functional studies of transition metal complexes derived from amido and imido P(V) ligands

A thesis

Submitted in partial fulfillment of the requirements

Of the degree of

Doctor of Philosophy

By

Arvind Kumar Gupta

ID: 20113113

Department of Chemistry

Indian Institute of Science Education and Research, Pune

March 2014

Dedicated to

My Mother

For her endless love….

भारतीय विज्ञान शिक्षा एवं अनुसंधान संस्थान, पुणे
INDIAN INSTITUTE OF SCIENCE EDUCATION AND RESEARCH (IISER), PUNE
(An Autonomous Institution, Ministry of Human Resource Development, Govt. of India)
900 NCL Innovation Park, Dr. Homi Bhabha Road, Pune 411008

Dr. R. Boomi Shankar
Assistant Professor
Department of Chemistry,
IISER Pune

CERTIFICATE

Certified that the work incorporated in the thesis entitled "***Synthesis and functional studies of transition metal complexes derived from amido and imido P(V) ligands"*** submitted by **Mr. Arvind Kumar Gupta** was carried out by the candidate, under my supervision. The work presented here or any part of it has not been included in any other thesis submitted previously for the award of any degree or diploma from any other university or institution.

Date: 21st March 2014, Pune

Dr. R. Boomi Shankar
(Research Supervisor)

boomi@iiserpune.ac.in •Ph: +91-20-25908208•Fax: +91-20-25908186

DECLARATION

I declare that, this written submission represents my ideas in my own words and where others' ideas have been included; I have adequately cited and referenced the original sources. I also declare that I have adhered to all principles of academic honesty and integrity and have not misrepresented or fabricated or falsified any idea / data / fact/ source in my submission. I understand that violation of the above will be cause for disciplinary action by the Institute and can also evoke penal action from the sources which have thus not been properly cited or from whom proper permission has not been taken when needed.

Date: 21st March 2014, Pune

Mr. Arvind Kumar Gupta

ID: 20113113

Acknowledgements

I express my reflective gratitude to my research supervisor Dr. R. Boomi Shankar for his precious suggestion, incisive guidance and decisive insights during the entire course of my Ph.D. Research. As a first Ph. D student of his group, it gives me a great pleasure to express my profound sense of gratitude to my research supervisor. I am also thankful to him for giving me freedom to pursue my own ideas and it's my privilege to have worked under his kind guidance. My everlasting gratitude goes towards him.

I thank Prof. K. N. Ganesh, the Director, IISER-Pune, for providing outstanding research facilities and financial support that I have been privileged with, during my stay at IISER-Pune, India. I would like to acknowledge my sincere gratitude to my Research Advisory Committee (RAC) members Dr. V. G. Anand and Dr. Sujit K. Ghosh and former doctoral committee member in Indian Institute of Technology (IIT) Guwahati Prof. P. K. Iyer, Prof. Gopal Das and Dr. C. V. Sastri for their intellectual support, encouragement and valuable suggestions. My honest regards to all the faculty of the Department of Chemistry, IISER-Pune for their motivation and encouragement espe cially to Dr. M. Jayakannan, Dr. M. Jagenmohan and Dr. R. Vaidyanathan.

I acknowledge the help from Archana for the instrumental support for single-crystal X-ray diffraction data, Swati M. Dixit for recording MALDI-TOF and CHN analysis. I am also thankful to Dr. Balamurugan for UV-visible and fluorescence measurements Biplab, Sanjog, somya and Shyamapada for Gas Adsorption measurements, Ananthraj for TGA, Avishek for NMR and Neeraj for PXRD. I am grateful to Mayuresh for the administrative support.

My sincerest thankfulness goes towards my lab mates Anant, Ashok, Mahesh, Vijaykanth, Rajashekar, Arun, Indra and my friends Himashu Jha, Nibidh Chandra, Gunjan, Shiv, Jugal, Anwesha, Sandipdey, Mohan Lal, SandipJadav, Anil, Anu, Biplab Manna, Abhisek, Abhijeet, Aamod, Dinesh, Gopal, Kiran Reddy, Santosh, Arun Tnapare, Pramode, Santosh Panchal, Barun, Chutki, Sohini, Pramod, Bilbi, Abhigyan, Rajkumar, Smita, Kavita, Tanpreet, Kishor, Kiran, Venki. Thesis Room friends Prakash, Dnyaneshwar, Sachin, Maroti for their cooperation during this time span as well as my seniors Dr. Subash, Dr. Himashu Jena, Dr. Mrigendra, Dr. Nihar, Dr. Chipem and Dr. Faizi for their timely help support and also for the wonderful time we shared together.

The thesis remains incomplete without mentioning the motivation blessings and love of my family members for their understanding, encouragement, patience, unending support and blessings in my every endeavor without which my Ph.D. could not be completed. They are the main soul and inspiration for each and every step that I achieve in my life.

Finally I pray to almighty God whose blessings made me able to complete the research work and submit this thesis for Ph.D. degree.

Arvind Kumar Gupta

Table of Contents

Chapter 4: Zn (II) and Cu (II) coordination polymer of an in-situ generated 4-pyridyl (^{4}Py) attached bis(amido)phosphate ligand, showing preferential water uptake over aliphatic alcohols

Chapter 5: Facile formation of stable tris(imido)phosphate trianions as their tri- and hexanuclear Pd(II) complexes in protic solvents

List of Abbreviations Used

A	Appendix
Ac	Acyl
Anal.	Analysis
Ar	Aryl
Bu.	Butyl
Calcd.	Calculated
Cy	Cyclohexyl
DCM	Dichloromethane
DMF	N, N-Dimethyl formamide
DMSO	Dimethyl Sulphoxide
DOSY	Diffusion-Ordered Spectroscopy
ESI	Electron Spray Ionization
Et	Ethyl
EtOH	Ethanol
EPR	Electron Paramagnetic Resonance
mg	milligram
µL	Micro liter
µM	Micro molar
min	minutes
N	Normal
HRMS	High resolution mass spectrometer
hrs	hours
IR	Infrared Spectroscopy
mmol	milli moles
Me	Methyl
MeOH	Methanol
MALDI-TOF	Matrix-Assisted Laser Desorption /Ionization – Time of Flight
MP (mp)	Melting point
MOF	Metal Organic Framework
NMR	Nuclear Magnetic Resonance
ORTEP	Oak Ridge Thermal Ellipsoid Program
PXRD	Powder X-Ray Diffraction
RT	Room Temperature
Ph	Phenyl
Py	Pyridyl
SCXRD	Single Crystal X-Ray Diffraction
TGA	Thermogravimetric Analysis
THF	Tetrahydrofuran
TOF	Time of Flight
DSC	Differential Scanning Calorimetric
TMS	Tetramethylsilane
Pr	Propyl
ppm	parts per million
UV	Ultraviolet

Synopsis

Thesis Title: Synthesis and functional studies of transition metal complexes derived from amido and imido P(V) ligands

Chapter 1: Introduction

In this chapter a survey of the literature pertaining to the chemistry of imido P(V) ligands and their metal complexes has been presented. Traditionally, P(V)-imido moieties are analogous to the various phosphorus oxo anions and have gained immense attention in main group coordination chemistry. Synthetic routes to access these imido-P(V) anions involve the use of highly reactive main-group metal reagents in reaction with a phosphonium salt like $[(PhNH)_4P]Cl$ or phosphoramides such as $[(RNH)_3P{=}E]$ (E = $NSiMe_3$, O, S or Se) or with preformed iminophosphoranes. In these reactions the P(V) ligands can undergo sequential deprotonation leading to the formation of various phosphorus oxo species isoelectronic to H_3PO_4, $H_2PO_4^-$, HPO_4^{2-} and PO_4^{3-}ions. However, due to the highly reactive nature of these metal precursors as well as to the presence of residual metal-alkyl/aryl/halide/silylamide bonds in these complexes, the imido ligand chemistry has largely been limited to main-group metal ions in anhydrous aprotic and non-polar solvents. Hence, the objective of the thesis is to generate amido and imido P(V) complexes of various transition metal ions in a protic and polar medium, understand their diverse structural features and study their functional properties in the areas of catalysis, sorption, self-assembly and host-guest chemistry.

Chapter 2: Amino functionalized P(V) ligands and their supramolecular structures

Chapter 2 describes the synthesis and the H-bond assisted supramolecular organization of the precursor amino phosphonium cations of formula $[P(NHR)_4]^+$ in presence of various acceptor anions. These phosphonium cations offer four H-bonding sites that are arranged in tetrahedral fashion around the central phosphorus atom. This arrangement generates novel supramolecular building blocks that are distinct to the commonly planar NH donor systems such as urea and guanidine. The supramolecular aggregation of these cations in presence of chloride, carboxylate and inorganic anions such as polyoxomatellate ions have been described in detail (Figure 1a, 1b and 1c). The phosphonium chlorides $[P(NHR)_4]Cl$ exhibit N-H…Cl H-bonding interactions and lead to liner, zigzag and helical 1D-chain and 2D-supramolecular structures depending on the steric bulk on amino

substituents. The phosphonium carboxylates were obtained by two routes: anion exchange reaction with phosphonium carboxylates and re-protonation reaction from a neutral phosphine imine [P(NPh)(NhPh)$_3$]. Depending on the steric bulk on the phosphonium cation as well as the topology of the carboxylate moiety (mono, di and tri-carboxylate) interesting 2D- and 3D-supramolecular structures mediated N-H…O interactions were obtained. Finally we have shown for the first time an amino-phosphonium polyoxometalate supramolecular network by employing the phosphonium salts in the polyoxometalate synthesis.

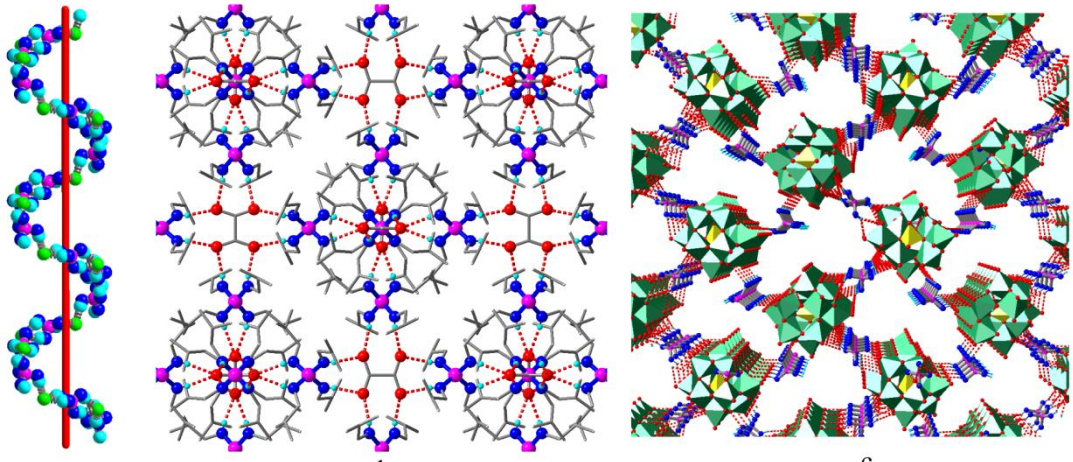

Figure 1

Chapter 3: Amido and imido metal complexes of P(V) ligands featuring 2- and 3-pyridyl substituents

In this chapter, we described the synthesis and the deprotonation chemistry of a series of amino P(V) compounds viz., a phosphonium salt **1**, [P(NH^{2}py)$_4$]Cl, a phosphine imine **2**, [P(N^{2}Py)(NH^{2}Py)$_3$] and a phosphoramide **3**, [PO(NH^{2}Py)$_3$] featuring 2-pyridyl (^{2}Py) substituents. Reaction of **1** or **2** with $AgClO_4$ lead to an unprecedented penta-nuclear Ag (I) cationic complex $[Ag_5(LH_2)_2]^{3+}$ stabilized by two $[P(N^2Py)_2(NH^2Py)_2]^-$ anions $[L]^-$ generated upon deprotonation (Figure 2a). Use of other Ag(I) salts such as AgOTf lead to the formation of the same cationic complex with charge balancing OTf anions. Similar deprotonation reaction of the phosphoramide **3**, in the absence of an external base, has been studied in presence of various silver (I) salts. Interesting examples of octa- and hepta-nuclear Ag(I) complexes coordinated to imido and pyridyl groups were obtained when more reactive Ag(I) salts such as $AgClO_4$ and $AgBF_4$ were used, while the less reactive $AgNO_3$ reacts only with the peripheral pyridyl groups leading to a tri-nuclear cluster. Structural determination of these Ag(I) complexes show that sequential

deprotonation of the ligand amino protons were achieved forming imido P(V) species analogous to the $H_2PO_4^-$ and HPO_4^{2-} ions (Figure 2b). The deprotonation chemistry of the phosphonium salt **1** and the phosphoramide **2** has been studied with other soft metal ions such as Cu(I) and Pd(II) in which the metal complexes were found to be stabilized by the monoanionic ligand $[PO(N^2Py)(NH^2Py)_2]^-$. Similar reactivity studies were performed on the corresponding 3-pyridyl derivatives such as $[P(NH^3Py)_4]Cl$ (**4**), $[P(N^3Py)(NH^3Py)_3]$ (**5**) and $[PO(NH^3Py)_3]$ (**6**). However, no deprotonation of the ligand NH protons were observed. With divalent transition metal ions, the phosphoramide **6** has been shown to form self-assembled M_6L_8 cages or a macrocycle with one free ligand arm. Under hydrothermal conditions in DMF it forms a 2D-coordination polymer for Cu(I) ions.

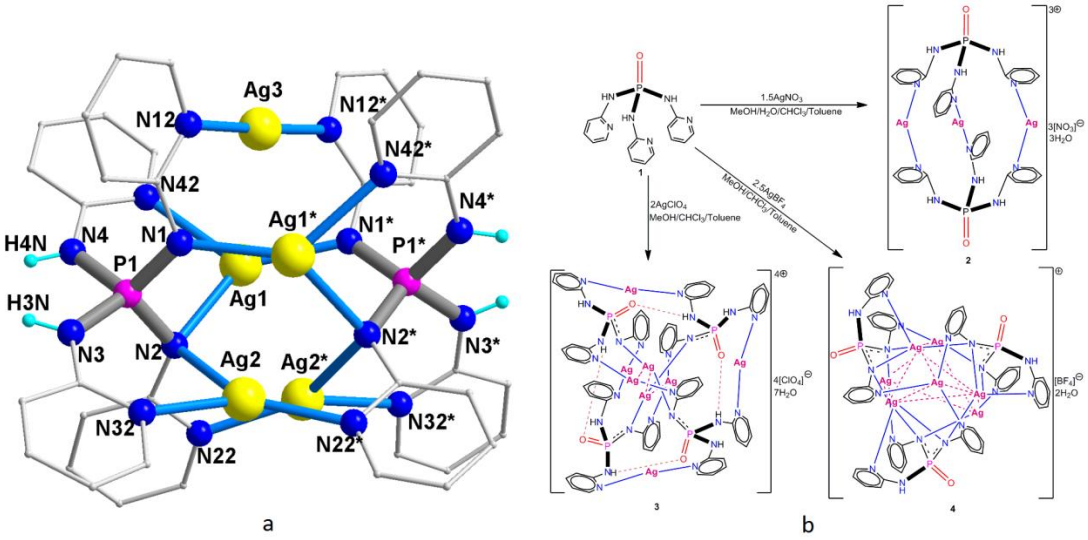

Figure 2

Chapter 4: Zn(II) and Cu(II) coordination polymers of an in-situ generated 4-pyridyl attached bis(amido)phosphate ligand showing preferential water uptake over aliphatic alcohols

In this chapter, we reported the synthesis of the P(V) ligands featuring 4-pyridyl substituents and their reactivity studies leading functional coordination polymers. Thus, the reaction of $[P(NH^4Py)_4]Cl$ (**7**) or $[PO(NH^4Py)_3]$ (**8**) with $Zn(NO_3)_2$ in DMF under hydrothermal conditions at 90 ° has lead to the formation of two polymorphic 2D-coordination polymers of composition $[ZnL(HCO_2)]_\infty$ for the in-situ generated ligand $[PO_2(NH^4Py)_2]^-$, $[L]^-$ (Figure 3a). The activated forms of both of these polymers have shown to exhibit a higher CO_2 uptake over N_2. Interestingly, solvent uptake studies of this

material have revealed a preferentially high uptake capacity for water over aliphatic alcohols such as methanol and ethanol (Figure 3c). This observation has an interesting industrial implication for the purification of bioethanol from water. Similar reactions involving **7** or **8** with $Cu(NO_3)_2$ in DMF under hydrothermal conditions at 90 ° yielded a 1D-coordination polymer of composition $[CuL_2(H_2O)_2]_\infty$ for the same in-situ generated ligand (Figure 3b). Solvent sorption study of this material again shows a preferential adsorption of water over aliphatic alcohol, albeit with a slightly lower uptake capacity. During this reaction we have also isolated a Cu(I) coordination polymer of composition $[Cu(\mathbf{8})L]_\infty$ containing both the neutral (**8**) and the in-situ generated ligand $[L]^-$.

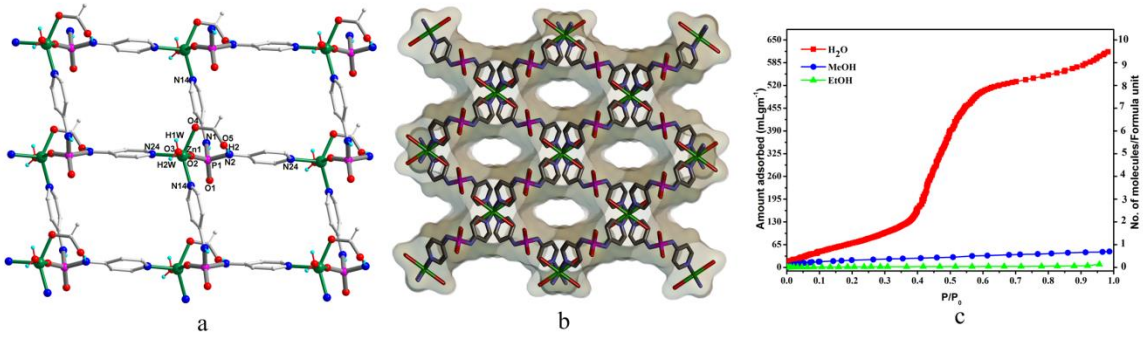

Figure 3

Chapter 5: Facile formation of stable tris(imido)phosphate trianions as their tri-and hexanuclear Pd(II) complexes in protic solvents

In this chapter, employing Pd(II) salts a facile deprotonation route to access the elusive tris(alkylimido)phosphate trianions, $[(RN)_3PO]^{3-}$ (R = ^{t}Bu, ^{c}Hex, ^{i}Pr), analogous to the orthophosphate (PO_4^{3-}) ion in polar and in protic solvents has been described. Using $Pd(OAc)_2$, trinuclear and prismatic Pd(II) clusters of these imido-trianions having the formula $\{Pd_3[(NR)_3PO](OAc)_3\}_n$ (n = 1 or 2)**,** were isolated exclusively in all these reactions in which the trianionic species acts as the tripodal chelating ligand to the trinuclear Pd_3-unit (Figure 4a and 4b). Reactivity studies aiming at the Pd(II) centres in these clusters with nucleophilic reagents such as primary amines ($R'NH_2$) have lead to a new trimeric cluster of formula $\{Pd_3[(NR)_3PO](OAc)_3(R'NH_2)_3\}$ in which the tripodal coordination of the Pd–N_{imido} moieties remained unaffected exemplifying the robustness of the Pd_3-unit in all these clusters (Figure 4c). We have also shown the catalytic activity of these Pd(II) complexes in Mizoroki-Heck type coupling reactions in presence of $Cu(OAc)_2$ as an oxidant (Figure 4d). Use of $PdCl_2$ leads again to the fully deprotonated

species $[(RN)_3PO]^{3-}$ as their corresponding chloro-bridged hexameric clusters in which the six Pd(II) ions were found in an octahedral arrangement (Figure 4e).

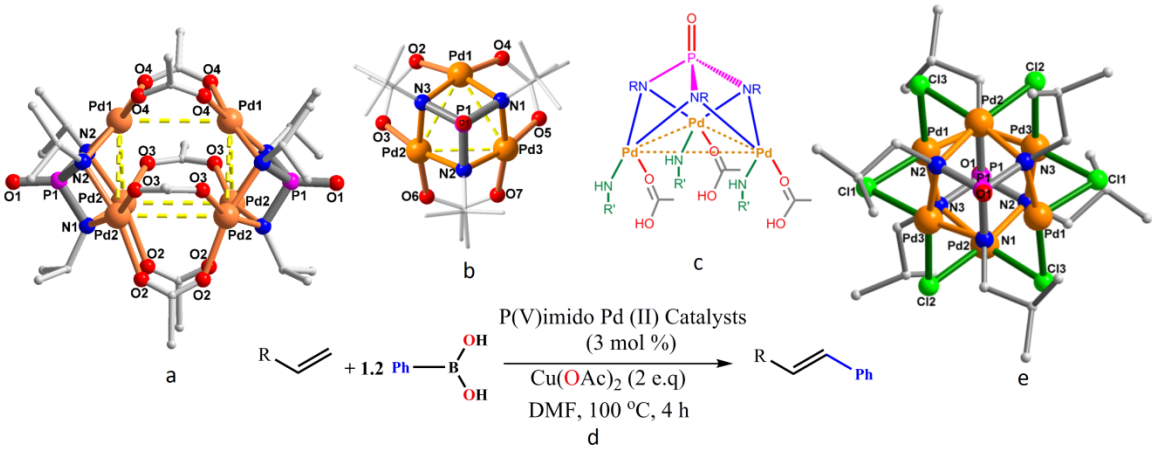

Figure 4

Chapter 6: Tri-nuclear imido-Pd(II) clusters as polyhedral building units for self-assembled neutral cages

In this chapter, starting from the hexameric imido-Pd(II) clusters depicted in figure 4a we described a novel ligand substitution route to access the hitherto unknown neutral polyhedral cages for Pd(II) ions. In an initial observation we found that reaction of benzoic acid with the hexamer $\{Pd_3[(NR)_3PO](OAc)_3\}_2$ results a hexameric complex of composition $\{Pd_3[(NR)_3PO](PhCOO)_3\}_2$. Similarly, reaction of $\{Pd_3[(NR)_3PO](OAc)_2(OH)\}_2$ with 1,1'-ferrocenedicarboxylic acid (FDC-H) replaces the four acetate bridges with FDC bridges $\{Pd_3[(NR)_3PO](FDC)(OH)\}_2$. These reactions showed that the trinuclear $\{Pd_3[(NR)_3PO]\}^{3+}$ motif is stable in solution and can be linked with suitable carboxylate linkers to yield the elusive high-nuclearity neutral cage molecules for Pd(II) ions. In this effort we have synthesized a neutral tetrahedron $[(Pd_3X)_4L_6]$ and a cube $[(Pd_3X)_8L_{12}]$ in the reaction of the hexameric cluster formula $\{Pd_3[(NR)_3PO](OAc)_2(OH)\}_2$ with oxalic acid and 2,5-pyrazine dicarboxylic acid, respectively (Figure 5a and 5b). The vertices of these cages feature a trinuclear polyhedral building unit of formula $[Pd_3X]^{3+}$ in which trianionic tris(iso-propylimido) phosphate X^{3-}, $[PO(N^iPr)_3]^{3-}$, motif acts as a cis-capping ligand for a planar Pd_3-unit. These cis-blocked PBUs act as 60^o acceptors and spontaneously self-assemble in presence of 180^o oxalate linker to give a tetrahedral cage. Use of a 120^o 2, 5-pyrazine dicarboxylate linker leads to the formation of a cubic cage. The void volumes of these tetrahedral and cubic cages were found to be 85.8 and 1000 $Å^3$, respectively. Further, guest encapsulation studies show that

the tetrahedral cage molecule is selective for CCl_4 and benzene over $CHCl_3$, CH_2Cl_2, THF and other substituted benzene derivatives. Guest encapsulation studies for the bigger cubic cage molecule are currently underway.

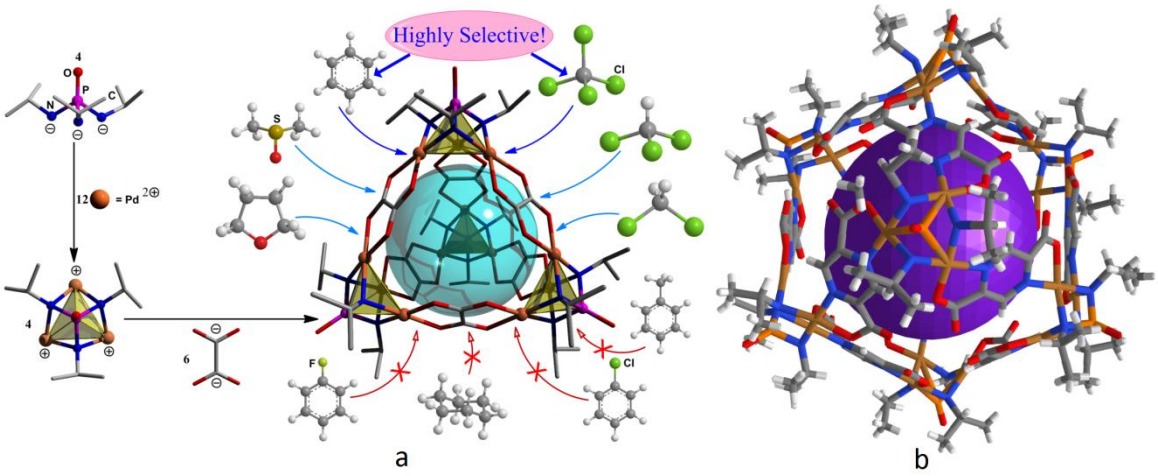

Figure 5

(Compounds numbers in the synopsis are different from those in thesis)

****

List of Publications

1. **Arvind K. Gupta**, Anant K. Srivastava, Indra K. Mahawar and R. Boomishankar "Discrete and Polymeric Cu(II) complexes derived from in-situ generated bis(pyridylamino)phosphate, $[PO_2(NHPy)_2]^-$, ligands" *Cryst. Growth Des.* **2014**, *17*, 1701-1709. ***(Appeared in Spotlight)***

2. **Arvind K. Gupta**, Ashok Yadav and R. Boomishankar "Discrete and polymeric coordination assemblies derived from 3-pyridyl attached flexible phosphoric triamide ligand and copper salts" *PNAS, India, Sect. A Phys. Sci.*, **2014**, *84*, 205-212.

3. **Arvind K. Gupta**, S. Arun Dixith R eddy and R. Boomishankar "Facile formation of stable tris(imido)phosphate trianions as their tri-and hexanuclearPd(II) complexes in protic solvents" *Inorg. Chem.* **2013**, *52*, 7608-7614.

4. **Arvind K. Gupta**, Sanjog S. Nagarkar and R. Boomishankar "Zn(II) coordination polymer of an in-situ generated 4-pyridyl (^{4}Py) attached bis(amido)phosphate ligand, $[PO_2(NH^4Py)_2]^-$ showing preferential water uptake over aliphatic alcohols" *Dalton Trans*. **2013**. *42*, 10964-10974.

5. **Arvind K. Gupta**, Alexander Steiner and R. Boomishankar "Tri-, hepta- and octa-nuclear Ag (I) complexes derived from 2-pyridyl functionalized tris(amido)phosphate ligand" *Dalton Trans*. **2012**, *41*, 9753-9759.

6. **Arvind K. Gupta**, Francis A. S. Chipem and R. Boomishankar "A 2-pyridyl (Py) attached phosphine imine $[P(NPy)(NHPy)_3]$ and an imido phosphinate ion $[P(NPy)_2(NHPy)_2]^-$ in its Ag(I) complex" *Dalton Trans*. **2012**, *41*, 1848-1853.

7. **Arvind K. Gupta**, Aswini Kalita, and R. Boomishankar "Synthesis and supramolecular structures of iso- and heteropolymetallates assisted by organoaminophosphonium cations" *Inorg. Chim. Acta* **2011**, *37*, 152–159.

8.**Arvind K. Gupta**, J. Nicholls, S. Debnath, I. Rosbottom, A. Steiner and R. Boomishankar "Organoaminophosphonium cations as building blocks for hierarchical supramolecular assemblies" *Cryst. Growth Des*. **2011**, *11*, 555-564.

9. **Arvind K. Gupta,** K. R. Ramya, Anant Kumar Srivastava, Shyamapada Nandi, Ashok Yadav and R. Boomishankar "A Neutral Cluster Cage with a Tetrahedral $[Pd^{II}_{12}L_6]$ Framework" *(Under Review).*

10. **Arvind K. Gupta**, Anant K. Srivastava and R. Boomishankar "A tetrakis(amido)phosphonium cation containing 2-pyridyl (^{2}Py) substituents, $[P(N^2Py)_4]^+$, and its reactivity studies with Ag(I) salts" *(Under Review).*

11. R. Boomishankar, P. I. Richards, **Arvind K. Gupta** and A. Steiner "Magnesium and Titanium Complexes of PolyanionicPhosphazenates" *Organometallics* **2010**, *29*, 2515-2520.

12. Ayyakkalai Balamurugan, **Arvind K. Gupta**, R. Boomishankar, Mundalapuddy Laximipathy Reddy and Manickam Jayakannan "Excited State Engineering in One and Three Dimensional Luminescent Frameworks by Heavy Atom Effect" *ChemPlusChem* **2013**, *78*, 737-745.

Chapter 1

Introduction

Abstract

The aim of this chapter is to provide an overall view on the chemistry of imido P(V) ligands and their metal complexes. Traditionally, P(V)-imido moieties are analogous to various phosphorus oxoanions and have gained immense attention in main group coordination chemistry. Synthetic routes to access these imido-P(V) anions involve the use of highly reactive main-group metal reagents in reaction with a phosphonium salt like $[(PhNH)_4P]Cl$ or amidophosphates (phosphoramides) such as $[(RNH)_3P=E]$ (E = $NSiMe_3$, O, S or Se) or with preformed iminophosphoranes. In these reactions the P(V) ligands can undergo sequential deprotonation leading to the formation of various phosphorus oxo species isoelectronic to H_3PO_4, $H_2PO_4^-$, HPO_4^{2-} and PO_4^{3-} ions. However, due to the highly reactive nature of these metal precursors as well as to the presence of residual metal-alkyl/aryl/halide/silylamide bonds in these complexes, the imido ligand chemistry has largely been limited to main-group metal ions in anhydrous aprotic and non-polar solvents. Hence, the objective of the thesis is to generate amido and imido P(V) complexes of various transition metal ions in protic and polar medium, understand their diverse structural features and study their functional properties in the areas of catalysis, sorption, self-assembly and host-guest chemistry.

1.1 P-N ligand platforms: Amido and imido P(V) scaffolds

The first published article based on phosphorus was "De Phosphorisquatuor Observatio" by Johann Elsholz and the first book published dealing with its chemistry was "The Aerial Noctiluca" by Robert Boyle in 1680. In this book, he proposed several possible applications of phosphorus such as preparation of luminous displays etc. which lead to several demonstrations of the incredible light evolved by phosphorus that amplified from the end of the 17th century. One hundred years after the discovery of "cold light" the existence of phosphorus in plants and animals was determined, and its form was established as a compound of phosphoric acid. On that time in 1833 the Duke of Richmond proved that the fertilizing value of bones exist in not in gelatin, nor in the calcium, but also in the phosphoric acid. Three centuries after this discovery, enormous numbers of scientists are working in phosphorus and plenty of applications have been found in all areas of chemistry, from organic chemistry to material chemistry through inorganic chemistry, organometallic chemistry, bio-organic chemistry, bio-inorganic chemistry etc.[1]

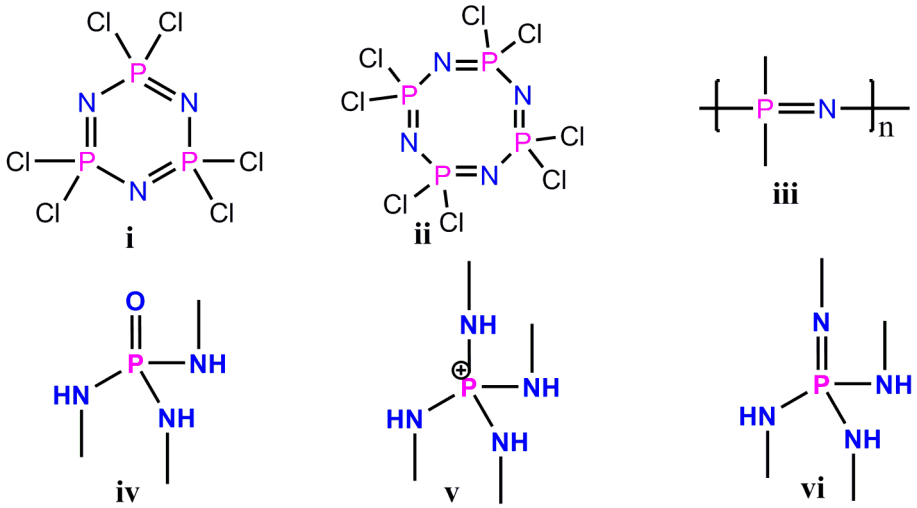

Chart 1.1: Various P-N scaffolds in diverse structural form.

Amido and imido P(V) compounds are very famous class of P-N compounds, which are very popular in main group chemistry and exits in diverse structural forms. They are isoelectronic to Si-O frameworks and play an important role in organic, inorganic, biological and material chemistry. Some representatives of most common P-N scaffolds that are of immense interest in current research are shown in Chart 1.1. Some notable examples include cyclic- (**i** and **ii**) and poly-phosphazenes (**iii**), cyclic-diphosphazanes, phosphoramides (**iv**), phosphonium cations (**v**) and phosphine imine (**vi**). Phosphine

imines are one of the simplest classes of phosphorus nitrogen compounds that are extensively studied in coordination chemistry and catalysis.[2] The imido groups (=NR), conventionally originate from the corresponding amido precursors, are isoelectronic to the oxo group (=O) and are capable to form metal complexes through lone pair of electron available at nitrogen atoms. For example, the trialkyl phosphorane **1**-R_3 acts as a neutral ligand for Lewis-acidic trialkly metal derivatives of Group-13 metal ions (Chart 1.2).[3] In the last two decades, the imino analogues of p-block oxo-anions containing group 14, 15 and 16 elements and their coordination chemistry have been extensively explored. The imino P(V) functionality having different R groups at the P(V) backbone can provide steric bulk to control coordination numbers and facilitates solubility in aprotic solvents and can determine the electronic properties of the ligand to some extent. Over the years, Dehnicke and co-workers,[4] Roesky and coworkers,[5] Chivers and co-workers,[6] Wright and co-workers,[7] Stalke and co-workers,[8] Russell and coworkers,[9] Steiner and coworkers[10] and Stahl and co-workers[11] have elaborated the chemistry of imido analogues of main group oxo anions particularly the chemistry of imido P(V) anions relevant to their structural diversity and reactivities and presented these results in well compiled review articles. Some of the most representative chemistry of these imido-metal complexes of various P(V) scaffolds, that laid the foundation for the subsequent chapters, have been highlighted in the sections below. The chemistry of cyclic-phosphazenes[12] is not covered in this chapter as this thesis deals with the chemistry of acyclic P-N scaffolds.

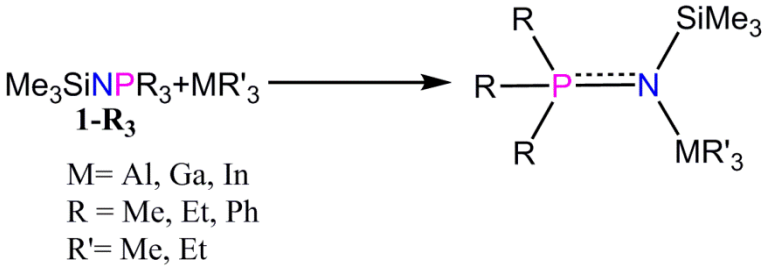

Chart 1.2: Trimethylsilyl trialkyl phosphraneimine as a Neutral donor-ligand

1.1.1 Metal complexes derived from neutral phosphoraneimine ligand

Kurt Dehnicke et al. have synthesized transition metal phosphoraneiminato complexes which contain the $[N{=}PR_3]^-$ ligand moiety. The R groups at the center of the phosphorus atom represent organic substituents. The$[N{=}PR_3]^-$moiety is isoelectronic with various ligand scaffolds, most prominently those found in the silyl imido and silyloxy

complexes. A general method for obtaining these mono functional phosphoraneiminato complexes for divalent transition metal ions is by heating metal halides with silylated phosphoraneimines (**1-R_3**) in presence of sodium fluoride at 160-220 ^oC. Use of NaF in these reactions is to generate the anionic $[N{=}PR_3]^-$ ligand moiety by the expulsion of Me_3Si group as Me_3SiF. These thermally stable donor-acceptor complexes require high temperature reactions for their formation. They exhibit a hetero cubane structure with $[M_4N_4]$ cubic core. The metal center in these cubanes has three N_{imido} contacts and the fourth one from the halide ion (X) (Figure 1.1).

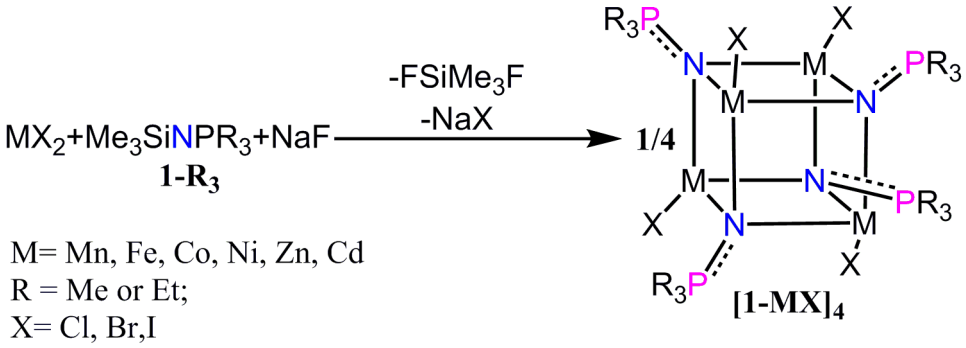

Scheme 1.1: Synthesis of Transition metal complexes of mono functional Phosphoraneimine.

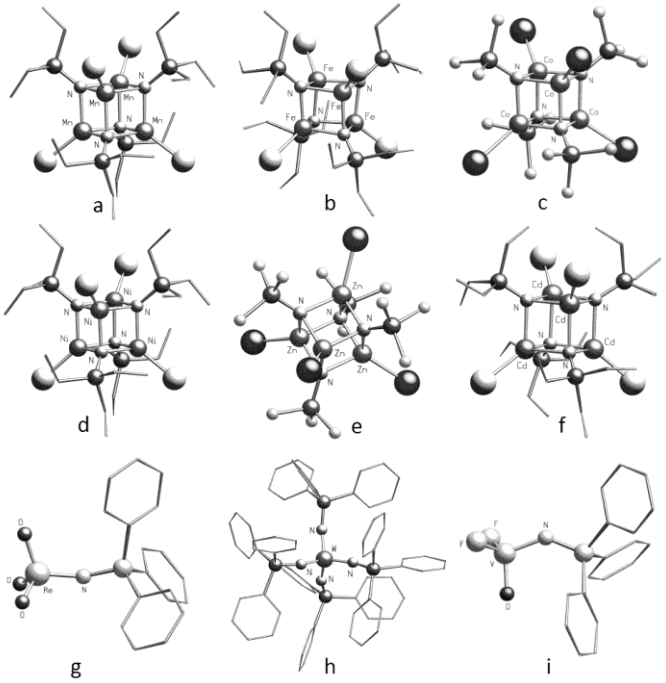

Figure 1.1: Crystal structure of transition metal phosphoraneiminato complexes (a, b, c, d, e and f) having +2 oxidation states with heterocubane (M_4N_4) core, while g, h, i

represents metal complexes in various oxidation states (Adopted from Dehnicke et al. *Coord. Chem. Rev.***1998**, *182*, 19-65).

In comparison, there are only a few examples of phosphoraneiminato complexes of transition metal ions in +1 oxidation state.[13] They can be obtained by the reaction of silylated $Me_3SiNPEt_3$(1-Et_3) with anhydrous Cu(I) trifluromethanesulfonate (triflate) or silver triflate which gave new type of imido complexes with cubane structure for the N_{imido} atoms. Thus, the Cu(I) or Ag(I) ions occupy the edge centres of the cube and N atoms of $[N=PEt_3]^-$ moiety are present at the vertices (Figure 1.2). Apart from these, **1-R_3** has also been subjected to reactions with various 2nd and 3rd row transition metal ions having oxidation states in the range between +1 and +7 to generate the corresponding imido-metal complexes in various structural topologies (Figure 1.1).

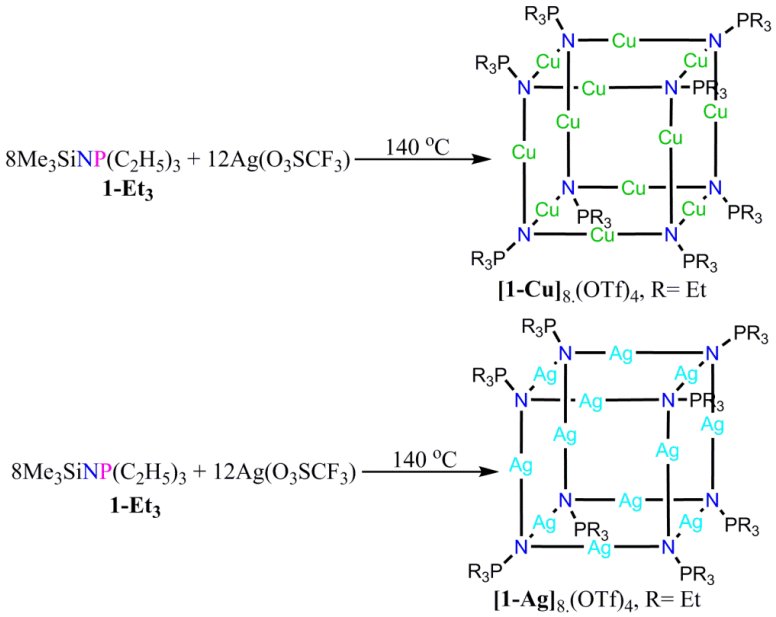

Scheme 1.2: Synthesis of Ag(I)- and Cu(I)-phosphoraneiminato complexes.

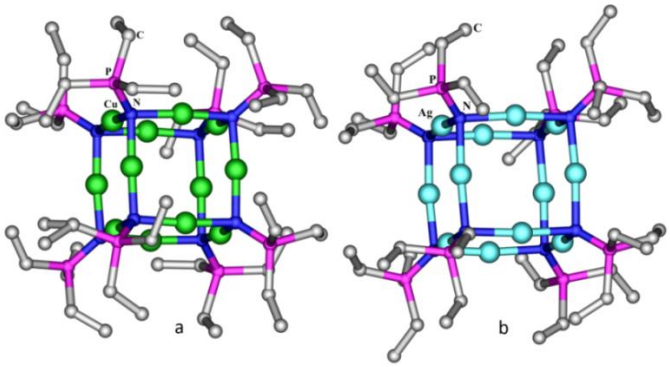

Figure 1.2: Crystal structure of [**1-Cu**]$_8$(OTf)$_4$ and [**1-Ag**]$_8$(OTf).

1.1.2 Metal complexes derived from imido-amido phosphinate scaffolds

In the above mentioned studies by Dehnicke, neutral mono functionalized Phosphoraneamines were used under high-temperature conditions for the generation of the mono-anionic ligand in the corresponding complexes. Hence, in an effort to generate the mono-anionic imido-phosphinate species, analogous to $[H_2PO_2]^-$, Stalke and coworkers have employed the deprotonation reaction of the amino-imino phosphorane precursor. Thus, the reaction of the diphenyl((trimethylsilyl)amino) ((trimethylsilyl)imino) phosphorane, **2-H** was subjected to reactions with alkali-metals or alkali-metal reagents such as MLi and MH.[14] These metal complexes revealed an unexpected coordination of bis(imido)phosphoranate ligand with alkali metals.

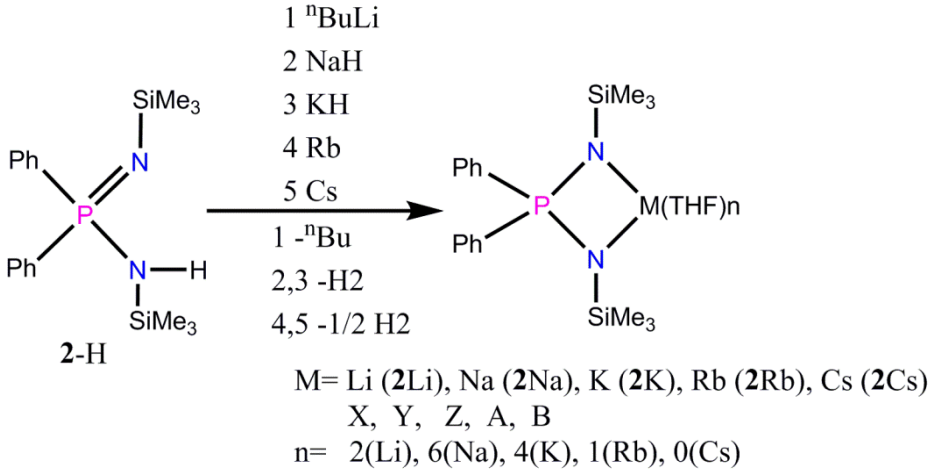

Scheme 1.3: Synthesis of alkali metal complexes of mono anionic imidophosphinate ion.

The Li and K complexes are monomer in the solid state, where the anion is chelating the metal ion, ensuing in four-member kite-shaped PN_2Li (Figure 1.3a) and PN_2K (Figure 1.3c) rings. Lithium atom is coordinated by two THF molecules where as the potassium atom is coordinated by four THF molecules.

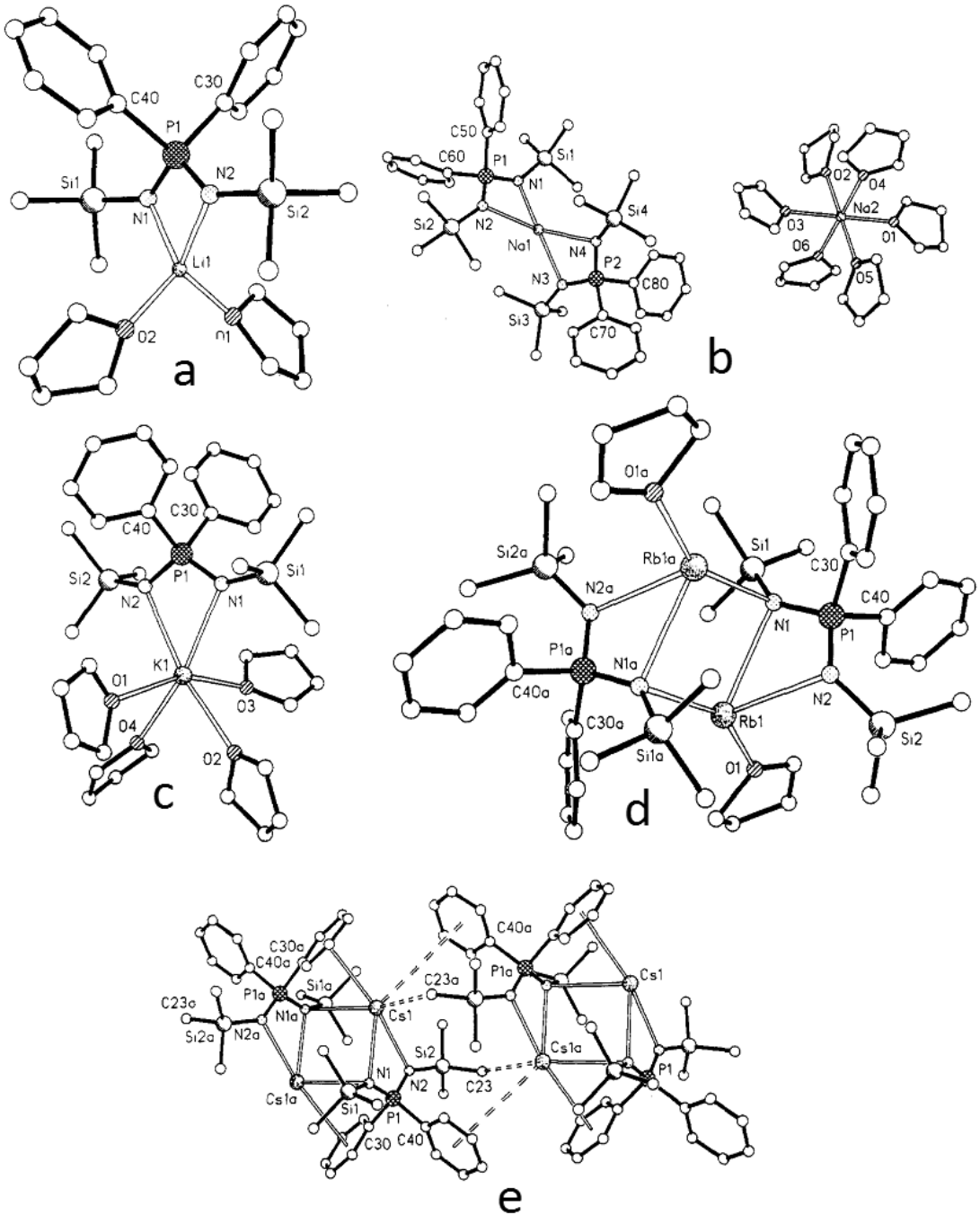

Figure 1.3: Crystal structure of Alkali metal complexes **2Li**, **2Na**, **2K**, **2Rb**, **2Cs** (Adopted from Stalke et al. *Inorg. Chem.* **1993**, *32*, 1977-1981).

In the sodium sodiumate complex, one sodium atom is coordinated by two anions and the charge balancing sodium cation (Figure 1.4b)) is surrounded by six THF molecules. The trimethylsilyl groups of the ligand slot onto each other, leaving the central Na^+ covered with a hydrocarbon surface. The complex is quite soluble, even in non-polar hydrocarbons as the Na^+ cation is surrounded by THF molecules.

The Rb and Cs derivatives form dimer in solid state. The Rb complex has three four-member rings fused to form a stair-shaped structure, where each Rb is coordinated with an additional THF molecule. The Cs metal is not at all coordinated to any THF molecule. The interaction between the π-system of ligand and the Rb metal is very weak, but in case of complex with Cs metal, the phenyl group is surprisingly attractive towards the soft and easy to polarize Cs metal. This remarkable close intramolecular and a weak intermolecular contact of Cs to phenyl ring of ligand leads to formation of an infinite molecular rods.

Stalke et al. have performed the synthesis and detailed structural investigation of alkaline earth metal complexes of aminoiminophosphorane **2-H**.[15] All complexes were monomeric, with metal centre having connections with two monoanionic ligands by two N atoms. The coordination number around the metal centre increases from 4 (Be and Mg complex) via 5 (Ca complex) to 6 (Sr and Ba complex). The extra coordination in case of Ca, Sr and Ba complexes were completed by one and two THF molecules, respectively. As a consequence, the coordination of both the anionic ligands in Sr and Ba complex is different as compared to that in lighter alkaline earth metal complexes. It was found that if the metal remains nearly in plane of one anionic ligand, the plane of second anion undergoes deviation, and the deviation is more pronounced while going from lighter to heavier metal (Be to Ba) containing complexes.

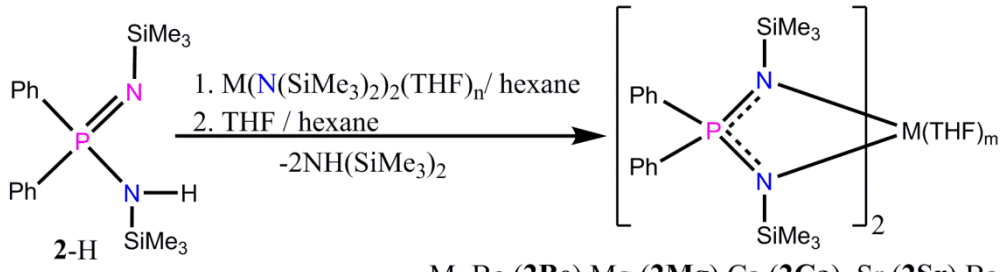

M	Be (**2Be**)	Mg (**2Mg**)	Ca (**2Ca**)	Sr (**2Sr**)	Ba (**2Ba**)
n	0	2	2	2	2
m	0	0	1	2	2

Scheme 1.4: Synthesis of alkaline earth metal complexes of mono anionic imidophosphinate ion.

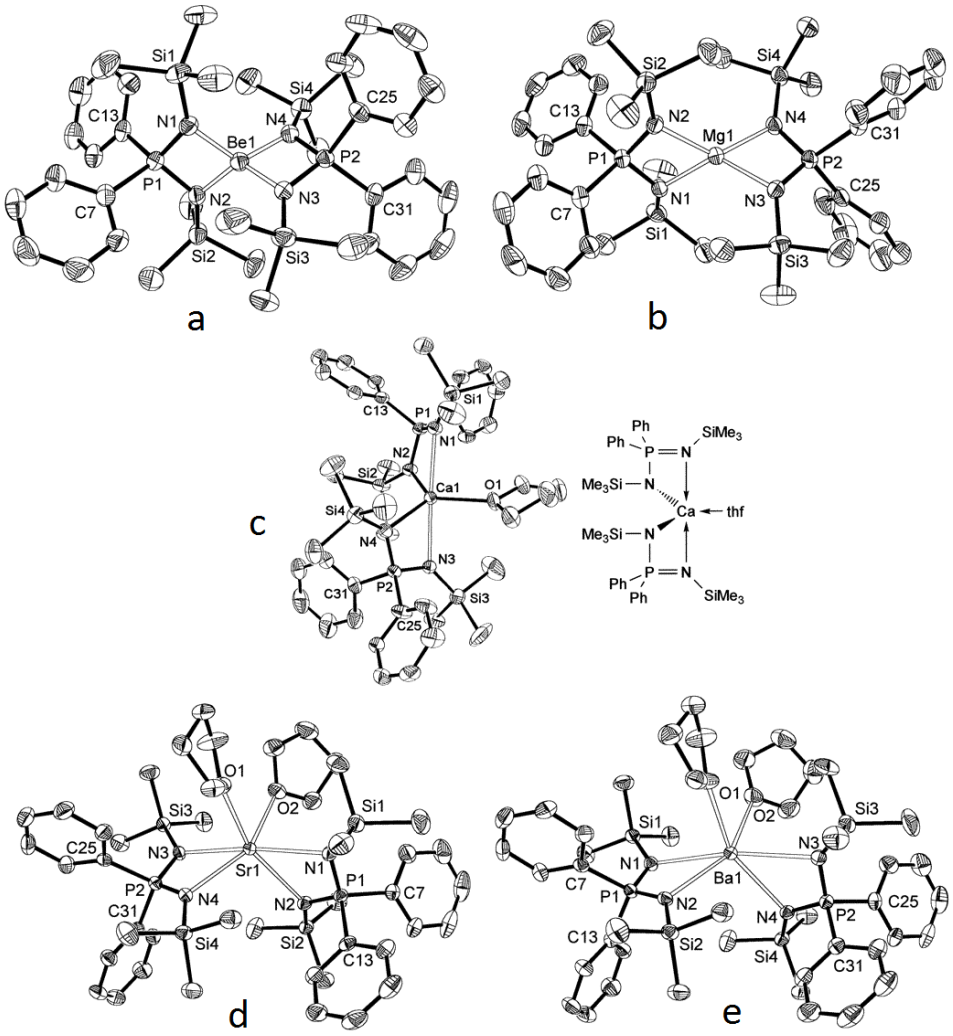

Figure 1.4: Crystal structures of **2Be**, **2Mg**, **2Ca**, **2Sr** and **2Ba** (Adopted from Stalke et al. *Inorg. Chem.***1997**, *36*, 2413-2419).

More recently, in 2006, Collins et al. have shown the reactivity of **2-H** with various Ni(II) sources and obtained interesting examples of mononuclear discrete complexes having PN_2Ni ring(s) (Scheme 1.5). Further, these complexes were investigated as an active catalyst for the polymerization of ethylene.[16] However, All the complexes **2Ni**(allyl), **(2)$_2$Ni** and **2Ni**(Ph)(PPh_3) are all found to yield a dimerizedproduct instead of the polymer. Interestingly, when **2Ni**(Ph)(PPh_3) was employed in these reactions in presence of a selective phosphine scavenger [Rh(acac)(C_2H_4)$_2$], a branched oligoethylene material was obtained.

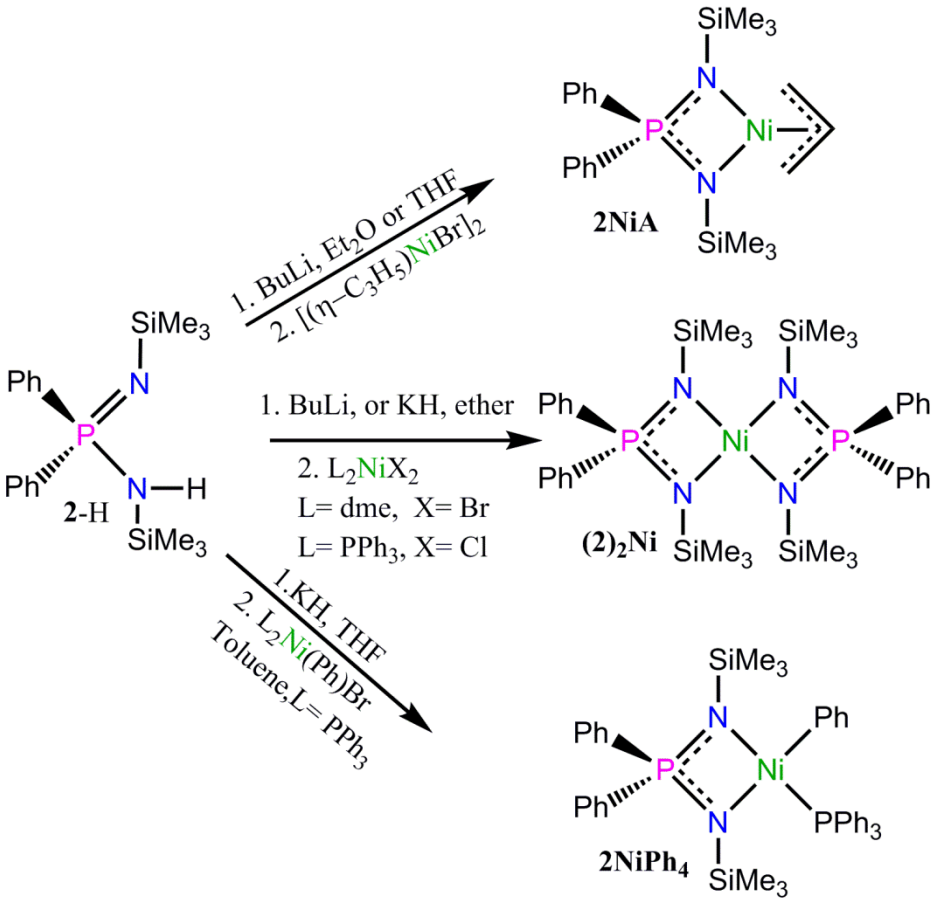

Scheme 1.5: Synthesis of mono-nuclear Ni(II)-imidophosphinate complexes.

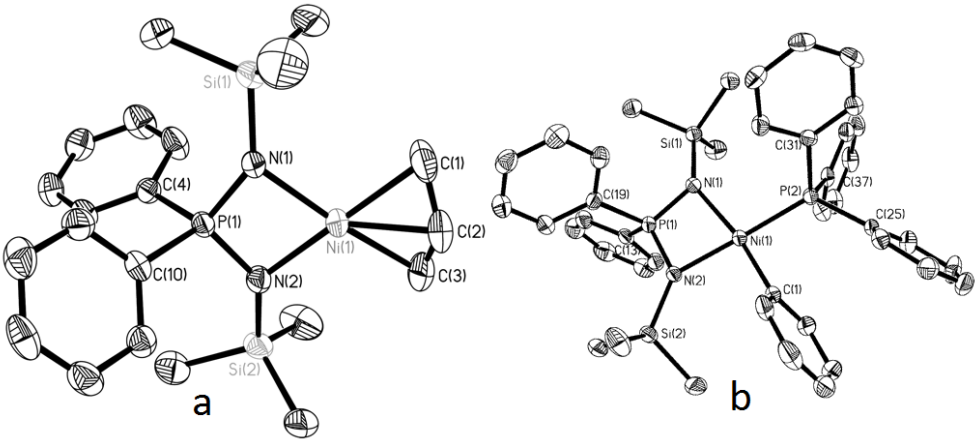

Figure 1.5: Crystal structures of **2Ni**(allyl) and **2Ni**(Ph)(PPh_3) (Adopted from Collins et al. *Organometallics* **2006**, *25*, 2514-2524).

Roesky et al.have synthesized Al(III)-complexes based on iminophosphonamide ligand with chloride, hydride, methyl, amide and diethyl substituents on Al(III) ions. For this they employed monoanionic iminophosphonamide ligand and treated it with various aluminium reagents. As a result interesting structures were obtained having rare four-

membered PN_2Al rings bearing halide, methyl and hydride substituents in addition to the coordination from the two N_{imido} moieties. These organoaluminium compounds were depicted as reagents for various organic syntheses, industrial catalytic processes, as precursor for chemical vapor deposition (CVD) processes and for the preparation of Al-N containing materials.[17]

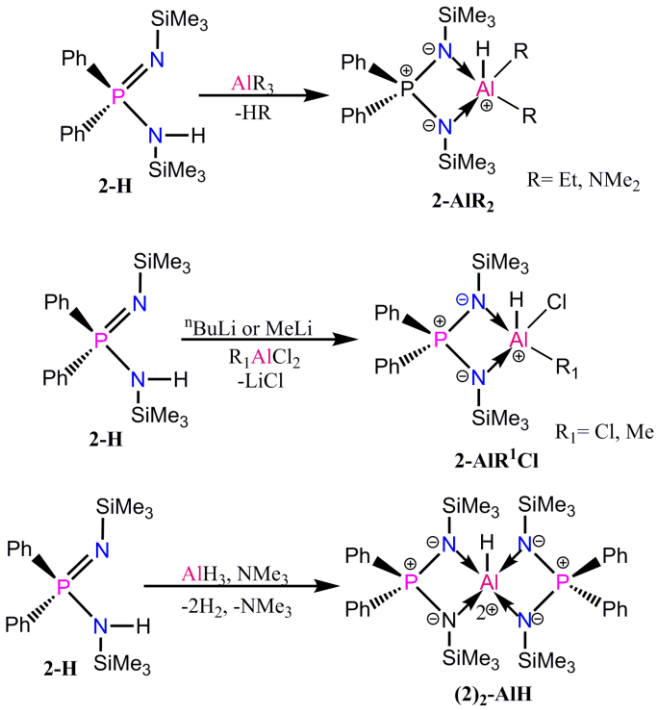

Scheme 1.6: Synthesis of Aluminum imidophosphinate complexes.

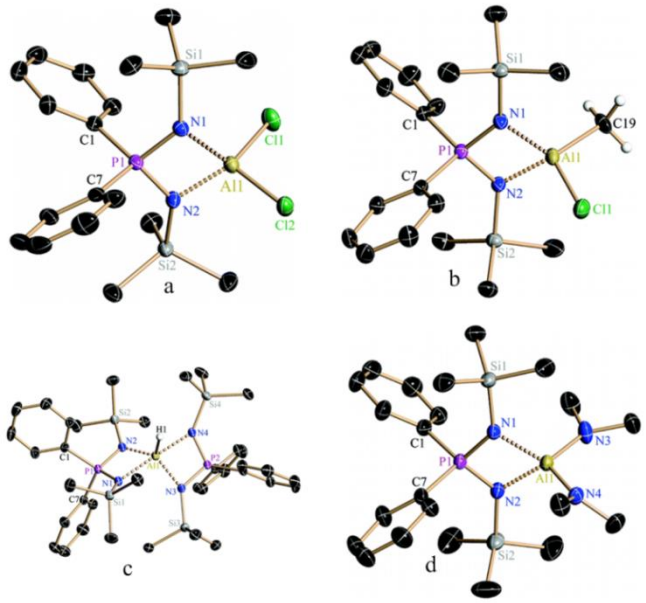

Figure 1.6: Crystal structures of Aluminum imidophosphinate complexes; a: **2-Al**Me_2, b: **2-Al**MeCl, c: **(2)$_2$-AlH**, d: 2-**Al**$(NMe_2)_2$ (Adopted from Roesky et al. *Inorg. Chem.* **2009**, *48*, 9174-9179).

Staschet al. have synthesized a sterically demanding aminoiminophosphorane ligand, $Ph_2P(=NDip)(NHDip)$ [Dip= C_6H_3-2,6-$^iPr_2$], **3-H**. Using this as precursor, examples of a potassium complex as well as a series of heteroleptic Zn(II)-complexes [(**3Zn**Br)$_2$, (**3Zn**Me), (**3Zn**Et), (**3Zn**I)$_2$] and their coordination behavior was compared with related C-N based ligand systems.[18] Interestingly, it had been shown that reduction of (**3Zn**Br)$_2$ and [(**3Zn**I)$_2$ with dimeric Mg(I) reagents such as [{Mg(^{Mes}nacnac)}$_2$] in stoichiometric ratio yielded an unusual dimeric Zn(I) complex, (**3Zn**)$_2$, having a Zn-Zn bond (Scheme 1.7).

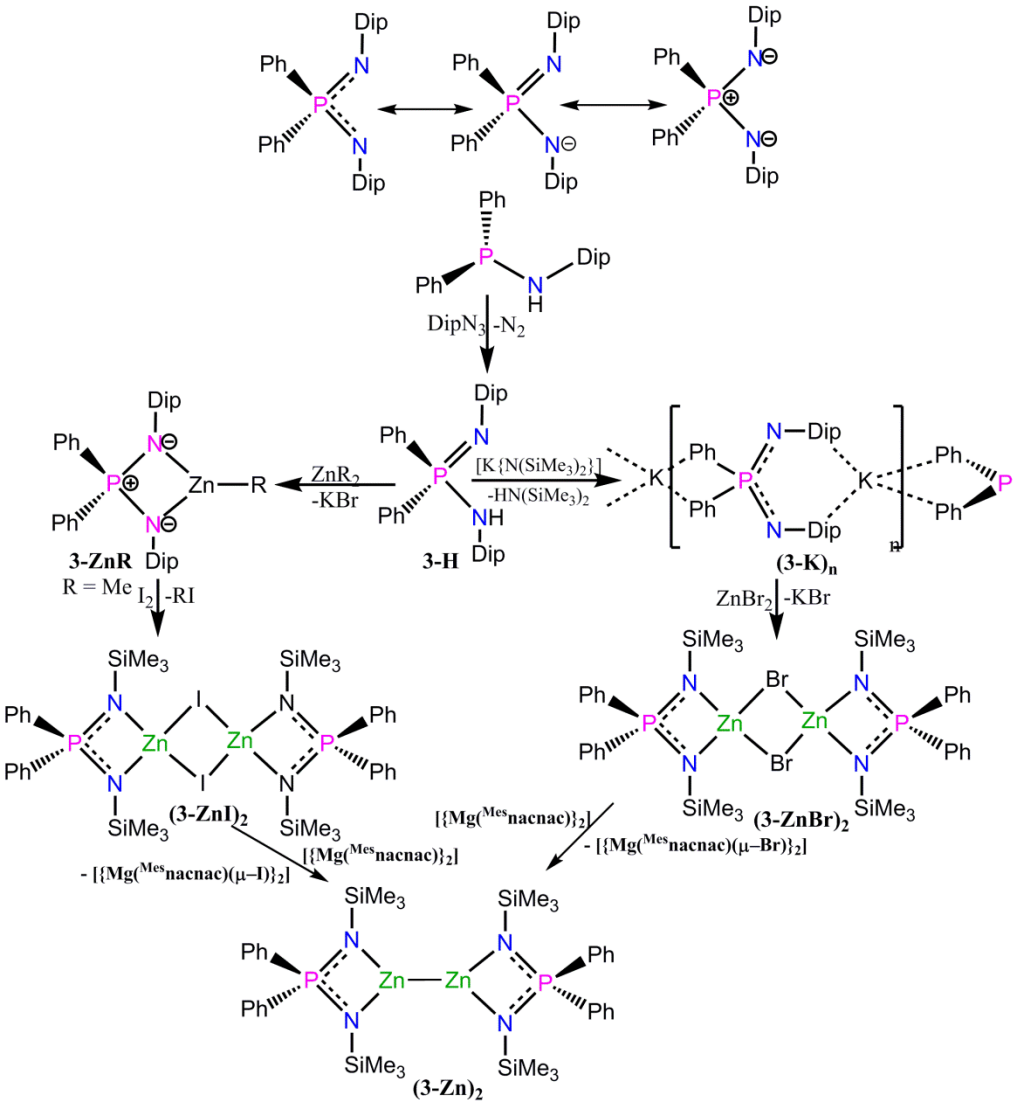

Scheme 1.7: Reaction of the organozinc reagents with **3-H** and their subsequent reactions leading to Zn(I)-imido P(V) complexes.

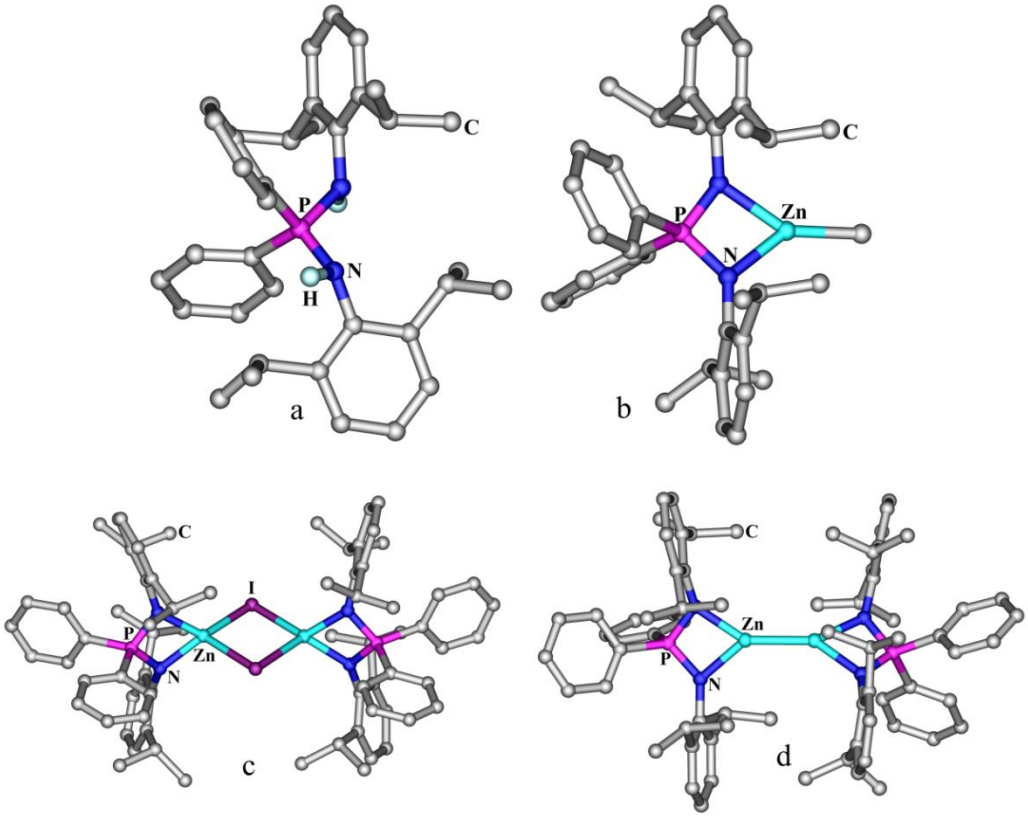

Figure 1.7: Crystal structures of the complexes **3-H** (a), **3-Zn**Me (b), (**3-Zn**I)$_2$ (c) and (**3-Zn**)$_2$ (d).

1.1.3 Metal complexes derived from amido-phosphonate ligands

Chivers et al. have shown the reactivity of chalcogenido bis(amido) phosphonate ligand [PhP(E)(NH^{t}Bu)$_2$] (E= O, S, Se) (**4-EH$_2$**) with ^{n}BuLi to generate dilithium salt of phosphonate dianion [PhP(E)(N^{t}Bu)$_2$]$^{2-}$, analoguous to the phosphite ion [HPO$_3$]$^{2-}$. When the chalcogen is oxygen (E = O), cluster complexes of formula {[(THF)Li$_2$(**4-O**)]$_4$·Li$_2$O} and {(Et$_2$O)$_{0.5}$Li$_2$(**4-O**)]$_4$}were obtained.[19] This former complex is more symmetric consisting of an OLi$_6$ core and four peripheral Li atoms coordinated with THF (Figure 1.9a). Presence of the central O^{2-} ion is attributed to the adventitious water during crystallization. The later complex is less symmetric consisting of a larger [Li(**4-O**)]$_3$ head group and a smaller [Li$_2$(**4-O**)] tail. The two solvated diethyl ether moieties were found to be coordinated to the two Li$^+$ ions that are belonging to two different subgroups (Figure 1.8b). On the other hand, a dimeric structure of formula (**4-S**Li$_2$)$_2$ was obtained for the corresponding thio-phosphonate ligand in which the Li ions and the two N$_{imido}$ sites are found in two kinds of coordination. While one of the Li ions is found in a tricoordinate environment having N$_{imido}$, S$_{thio}$ and O$_{THF}$ and is part of an eight membered P$_2$S$_2$N$_2$Li$_2$ ring, the other Li ion tetra-coordinate featuring two N$_{imido}$ and two O$_{THF}$

contacts (Figure 1.8c). A selenium analogue of this compound, (**4-Se**Li_2)$_2$, has an almost identical structure except that the Se atom on each of the ligand moieties are involved in a bifurcated interaction with the two Li^+ ions (Figure 1.8d).

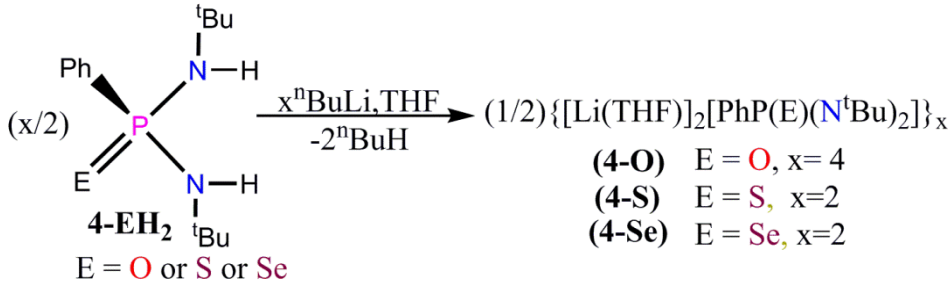

Scheme 1.8: Synthesis of lithium imido/chalcogenido phosphonates.

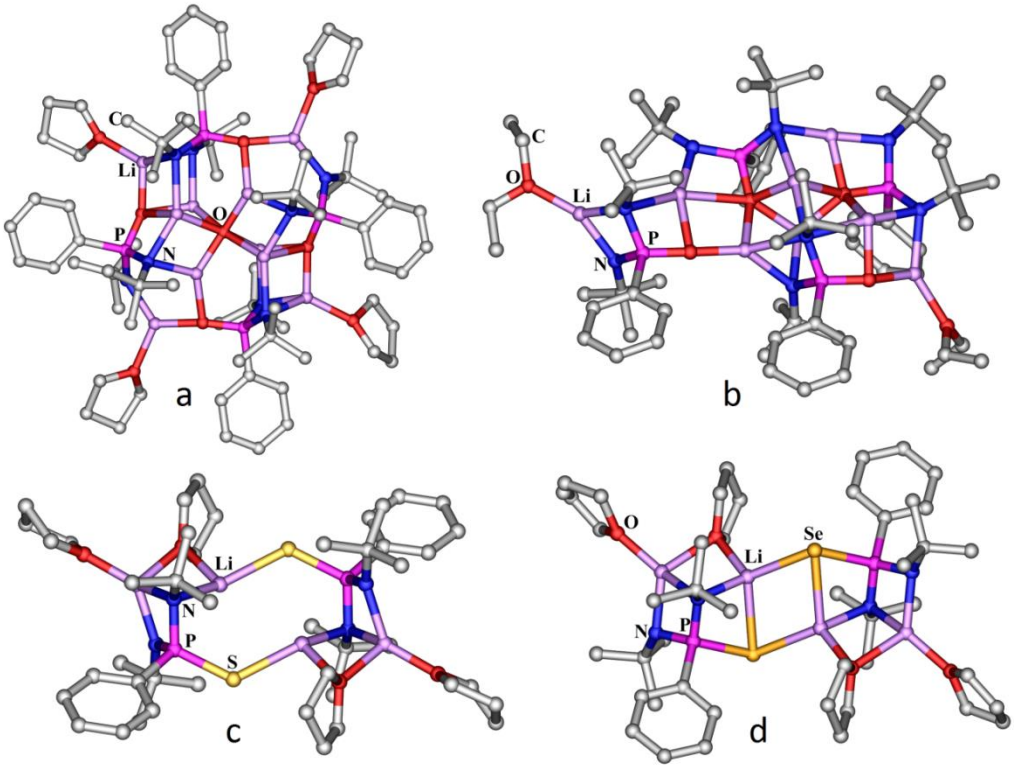

Figure 1.8: Crystal structures of Lithium complexes stabilized by chalcogenido bis(imido)phosphonate ligands.

In an interesting reaction, Russell et al. have shown the reaction of PCl_3 and 3 equivalent of 2-methoxyaniline in THF/NEt_3,followed by the reaction of 2 equivalent of ^{n}BuLi gave the imido P(V) dianion, $[HP(NR)_3]^{2-}$ analoguous to the phosphite anion $[HPO_3]^{3-}$ (Scheme 1.9) The origin of the hydride ion has been tracked to the proton exchange from the amino centre to the phosphorus centre in addition to the metallation of the remaining amido protons.[20] The crystal structure of the complex shows a dimeric centrosymmetric

structure consisting of four Li^+ ions and two ligand moieties. Two distinct ligand environments have been found for the tetra-coordinate Li^+ ions in this structure. In the first environment, the Li^+ ions consists of two N_{imido} contacts from two ligand segments and two from the methoxy side arms. In the second one, it is complexed with two imido nitrogens from one $[HP(NR)_3]^{2-}$ unit and one N_{imido} and one methoxy side arm from the other $[HP(NR)_3]^{2-}$ unit.

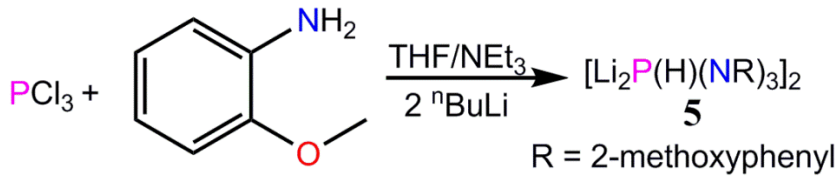

Scheme 1.9: Synthesis of the hexameric imido phosphonate complex **5**.

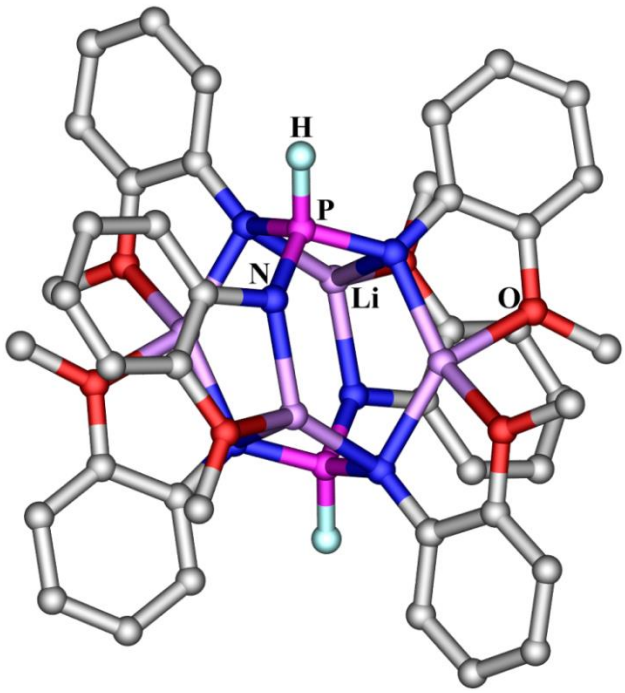

Figure 1.9: Crystal structures **5**.

1.1.4 Metal complexes derived from amido-phosphate ligands

Tris(amido) P(V) ligands are one of the widely studied ligands in deprotonation chemistry resulting in coordination complexes with interesting cage and cluster structures (Scheme 1.9) . Chivers and co-workers have shown that the imido tris(amido) phosphate ligand $P(NSiMe_3)[N(H)^tBu]_3$, **6-H$_3$**, undergoes full deprotonation with ^{n}BuLi and to generate the first example of a heteroleptic tetra-imido phosphate trianion, analogous to $[PO_4]^{3-}$ ion, as a hexameric complex of formula [**6-Li$_3$**]$_2$ (Figure 1.10).[21] This cage assembly consists of a cyclic ladder shaped Li_6N_6 core in which the two

$PNSiMe_3$ groups cap the hexagonal faces of the cage in a μ3 (N,N,N) coordination. Interestingly the two exo-cluster P-N-Si bonds exhibit perfect linearity with a bond angle of 174(2) °. However, the analogous ligand **7-H$_3$** is only doubly deprotonated to result in the formation of the imido anion analogous to $[HPO_3]^{2-}$ ion, owing to the coordination of the phosphoryl oxygen atom (Figure 1.10b). The structure of [**7-Li$_2$**(THF)]$_2$ is a centrosymmetric dimer consisting of four Li^+ cations linked by two dianionic ligand moieties of **7**.

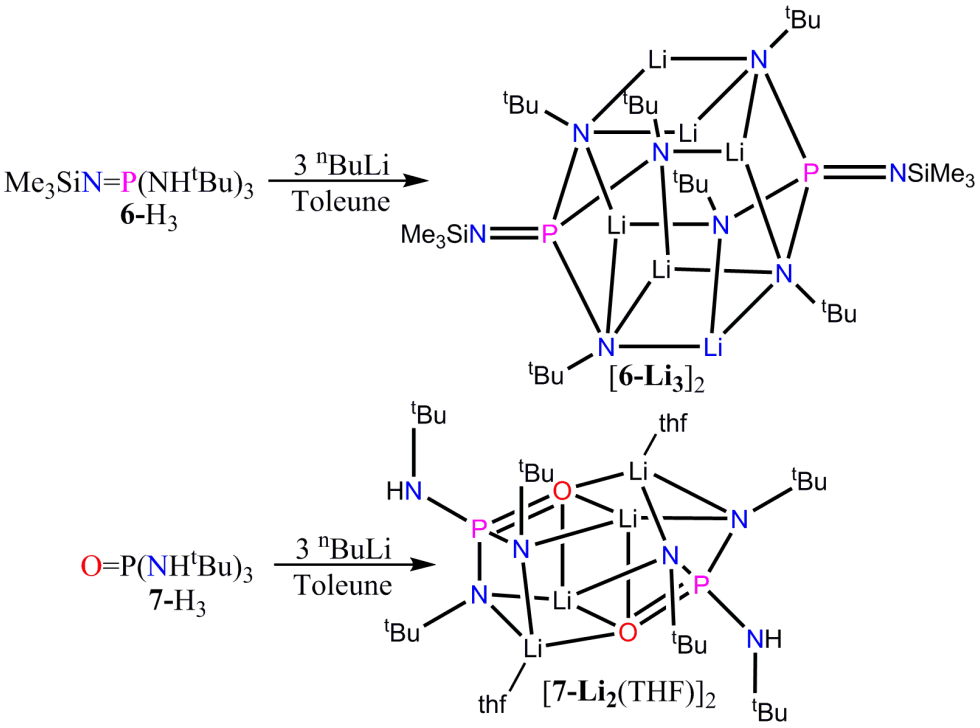

Scheme 1.10: Synthesis of bis- and tris-imido phosphate anions.

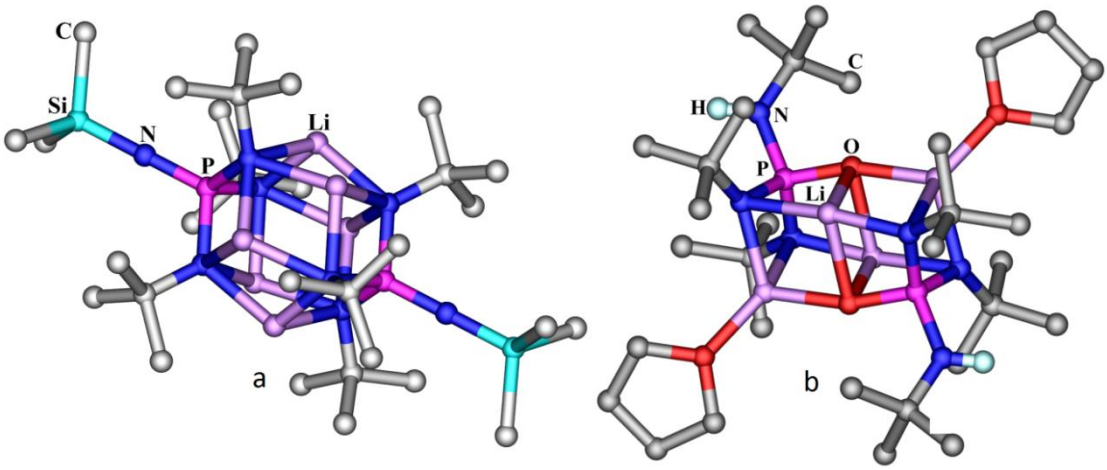

Figure 1.10: Crystal structure of (a) [**6-Li$_3$**]$_2$ and (b) [**7-Li$_2$**(THF)$_2$]$_2$.

The deprotonation chemistry of heteroleptic precursor **6-H$_3$** was further tested with various other organometallic reagents such as $^{n}Bu_2Mg$, Me_2Zn, Et_2Zn and Me_3Al. Surprisingly, these reagents were unable to de-prononate the all the three acidic protons of the ligand. In all these instances only a mono-deprotonation was observed during the initial reactions.[22] However, the Al complex **6-H$_2$Al**Me_2 can be subjected to further deprotonation reactions in presence of ^{n}BuLi or $^{n}Bu_2Mg$ (Scheme 1.10). Thus, deprotonation of the remaining two amino protons of **6-H$_2$Al**Me_2 were successfully performed using 1 or 2 equivalents of ^{n}BuLi, yielding a mono and di-lithiated bimetallic complexes where the coordination sphere of Li was completed by THF. Similarly, reaction of **6-H$_2$Al**Me_2 with $^{n}Bu_2Mg$ resulted in complete deprotonation in which the coordination sphere Mg was completed by THF. However, attempted metallation of **6-H$_2$Al**Me_2 with ^{n}BuLi or $^{n}Bu_2Mg$ resulted in nucleophilic displacement of methylzinc fragment by Li or Mg (Scheme 1.10).

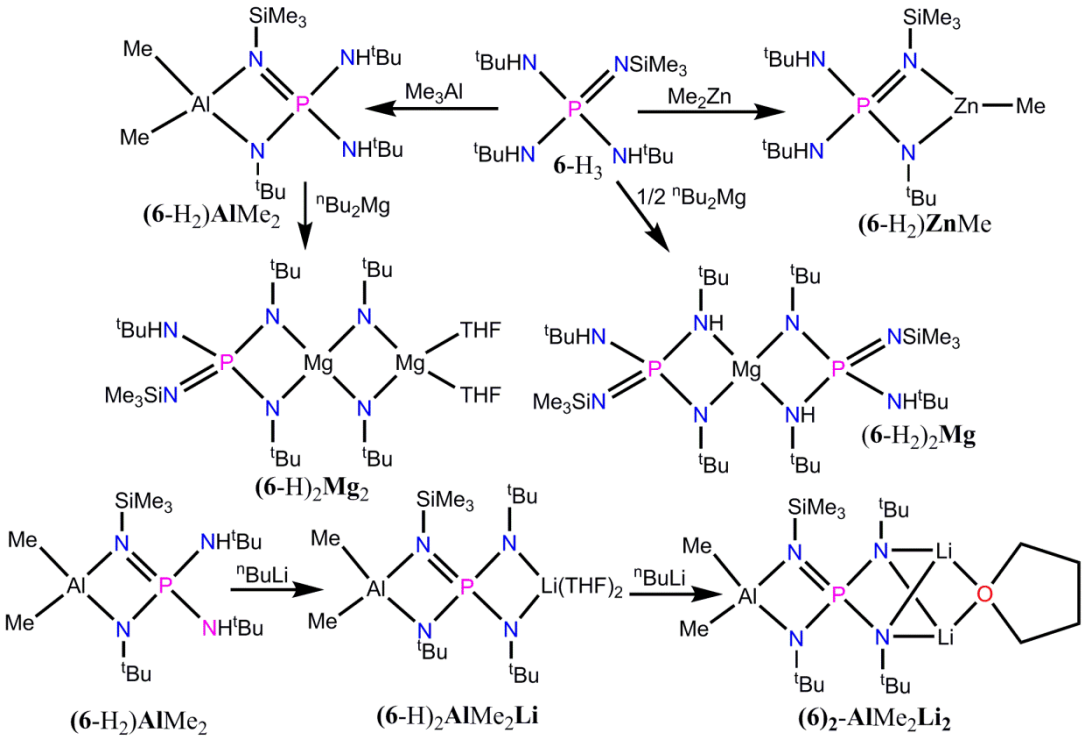

Scheme 1.11: Schematic representation for the synthesis of various imidophosphate complexes.

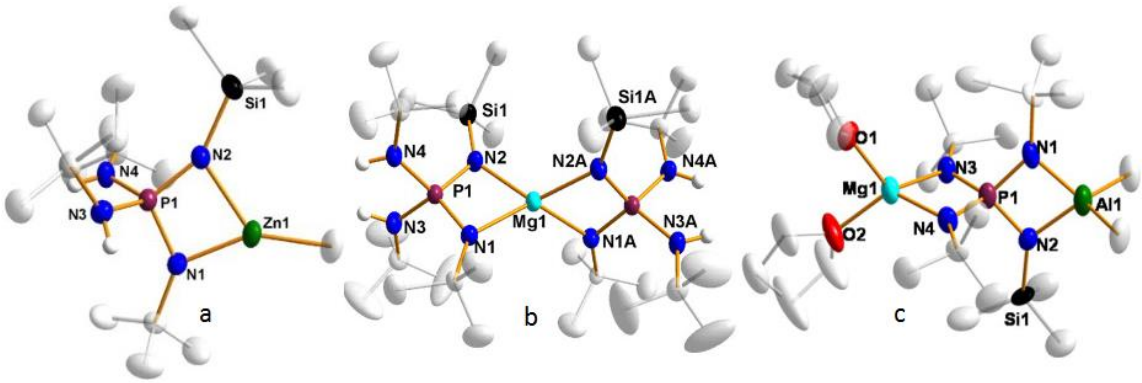

Figure 1.11: Crystal structures of monomeric Zn and Mg complexes derived from **6**-H_3. (Adopted from Chivers et al. *Inorg. Chem.* **2005**, 44, 5778-5788 and *J. Organomet. Chem.* **2007**, *692*, 4327-4336).

In an effort to extend the rich coordination chemistry of imido-P(V) ligand to transition metal ions, Layfield and co-workers studied the coordination chemistry of a related ligand system $[P(NSiMe_3)(NH^tBu)_3]$ (**6-H$_3$**), $[P(NSiMe_3)(NH^cHex)_3]$ (**8-H$_3$**), $[P(NSiMe_3)(NH^nPr)_3]$ (**9-H$_3$**), with manganocene (Cp_2Mn) (Scheme 1.11).[23] Their reactivity studies suggested all the obtained Mn(II) complexes contains of the mono-deprotonated ligand moiety and that the aggregation state in these complexes were determined by the steric effect of the N-substituents on the ligand (Figure 1.11). They have also speculated that multiple deprotonation of **6-H$_3$**, **8-H$_3$** and **9-H$_3$** are seemingly not possible under the employed reaction conditions.

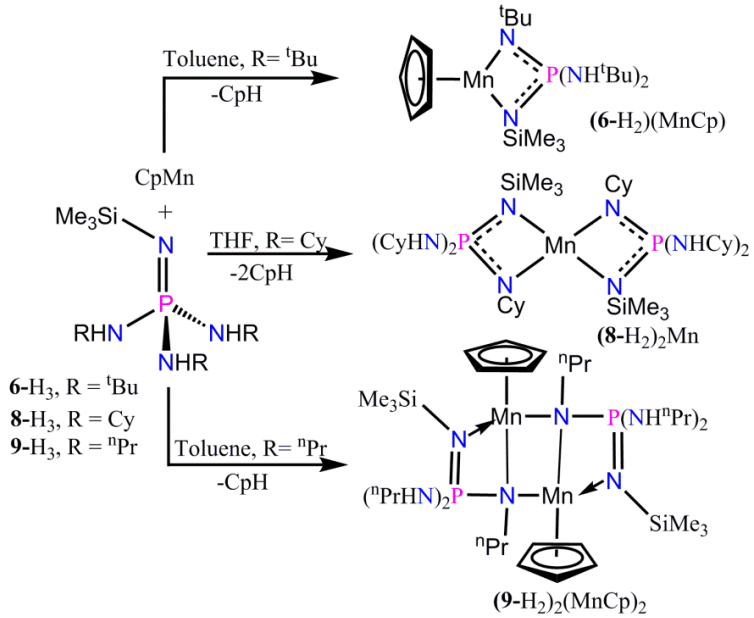

Scheme 1.12: Reactions of the amido(imido)phosphate with manganocene.

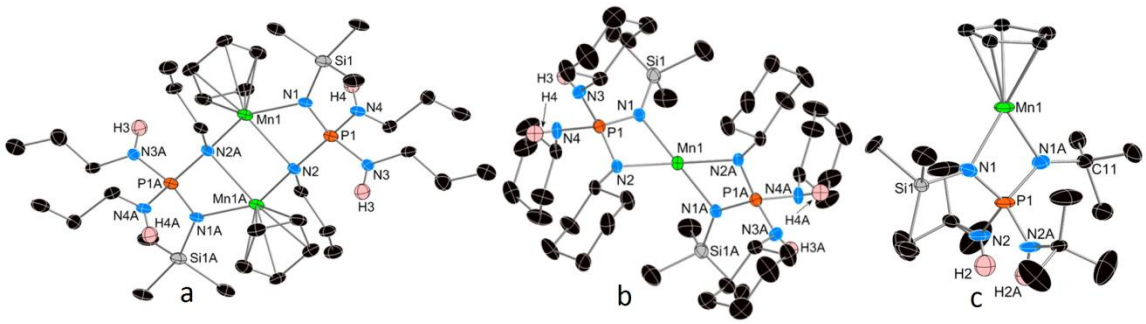

Figure 1.12: Crystal structures of Mn(II)-imidophosphate complex. (Adopted from Layfield et al. *Inorg. Chem.* **2012**, *51*, 9104-9109).

Chivers et al. have also studied the deprotonation in the phosphoramide **7**-H_3 using organoaluminium reagents. Based on the stoichiometry and reaction condition two types of complexes were obtained in these reactions. A 1:1 molar ratio of **7-H$_3$** and Me_3Al at room temperature gave a mixture of products in which the compound (**7**-H_3)(6-H)$AlMe_2$ was obtained as a major product and (**7-H$_2$**)$_2$AlMe as a minor product, as traced by ^{1}H and ^{31}P NMR. However (**7-H$_2$**)$_2$**Al**Me was obtained exclusively when the reaction was performed with 2:1 molar ratio of reagents in refluxing n-hexane.[24] The complex (7-**H$_3$**)(7-**H**)**Al**Me_2 consists of two Al^{3+} centers and two ligand motifs, of which one ligand is doubly deprotonated with one residual amino arm. Whereas, no deprotonation was observed on the other ligand and is found to be coordinated to one of the Al^{3+} centre via its phosphoryl oxygen atom. Both the Al^{3+} ions are tetra-coordinated having two residual methyl groups on each of them. The remaining two contacts on each of these two Al^{3+} ions were respectively provided by two N_{imido} sites from one of the ligand moieties and two phosphoryl oxygens from two different ligands. On the other hand the Al^{3+} ion in the mononuclear complex (**7-H$_2$**)$_2$**Al**Me exhibits a distorted trigonal bipyramidal coordination having two chelating O, N_{imido} ligand contacts and one residual methyl group.

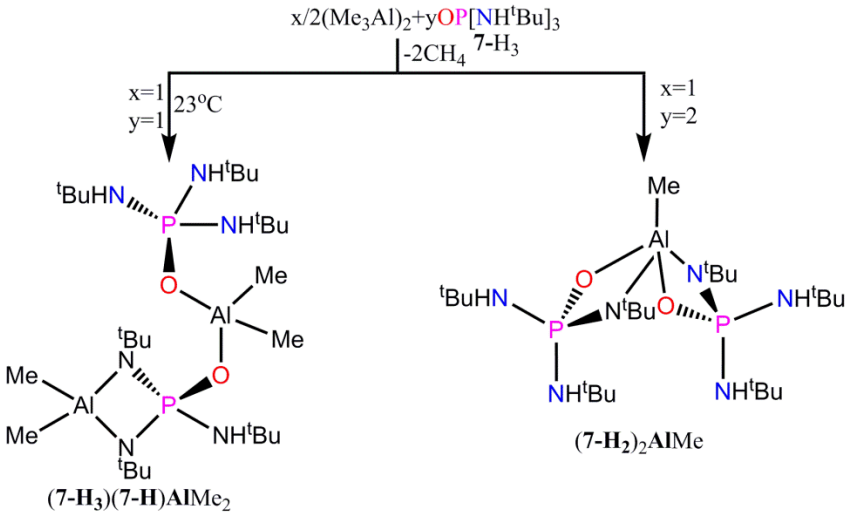

Scheme 1.13: Schematic representation for the synthesis of various Al- imido phosphate complexes derived from **7**-H_3.

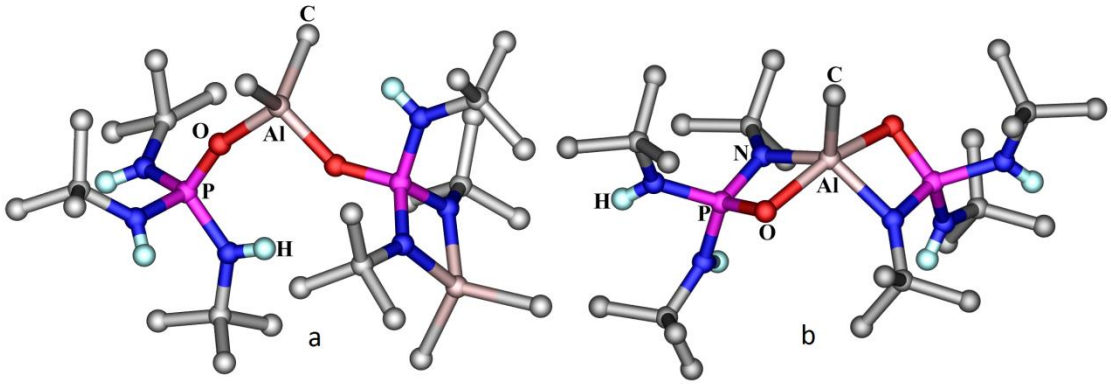

Figure 1.13: Crystal structure of (**7-H$_3$**)(**7-H**)**Al**Me_2 and (**7-H$_2$**)$_2$**Al**Me.

Moving away from the deprotonation chemistry of the phosphoric triamide ligands, reaction of alkyl substituted thiophosphoramides [$SP(NHR)_3$] with organolithium ($LiBu^n$) reagents have also been investigated by Chivers et al. These reactions revealed the effect of steric bulk on both mode of aggregation as well as the further reactivities of the partially lithiated imido-amido thiophosphates.[25] They have shown a route for sequential mono and di-deprotonation, where the multidentate anionic ligand binds to Li^+ ions by a combination of hard (N) and soft (S) donor sites in the complex. They have shown that mono-lithiation of $SP(NHR)_3$ with $LiBu^n$ yields dimer with central Li_2N_2 in case of (**10-H$_2$**)**Li**]$_2$ or Li_2S_2 rings in case of [(**11-H**)(**11-H$_2$**)**Li$_3$**]$_2$. Further lithiation of (**10**--H_2)Li]$_2$ yielded the dianionic species in the corresponding complex (**9-H**)**Li$_2$**(TMEDA). On the other hand further lithiation [(**11-H**)(**11-H$_2$**)**Li$_3$**]$_2$ triggers ligand condensation and sulfurextrusion resulting in the formation of a heterocubane type cluster.

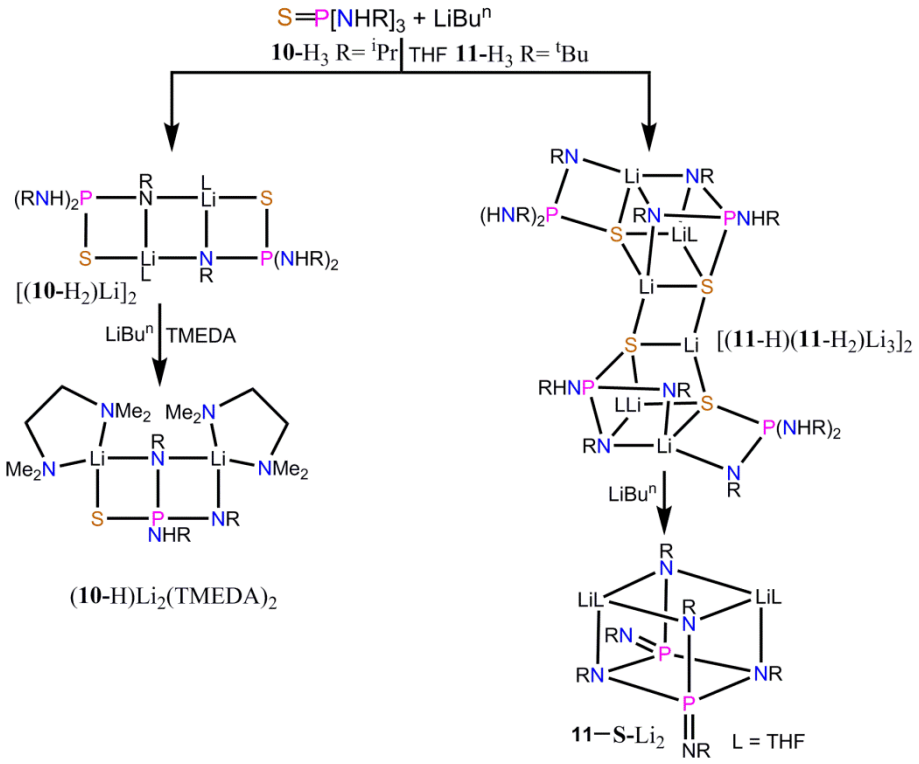

Scheme 1.14: Synthetic routes for the various Li-imido P(V) complexes derived from the thio-amidophosphate **10-H$_3$**.

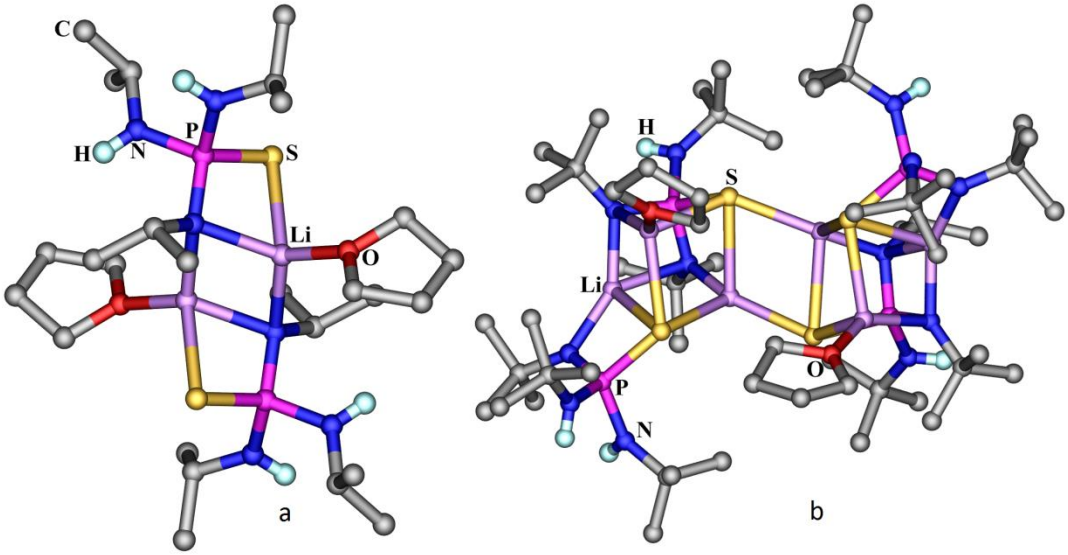

Figure 1.14: Crystal structures of Li-complex derived from **10-H$_3$** stabilized by both hard-soft (N,S) chelation.

Rufanov et al. have synthesized first transition metal complexes of S=P(NHBu^t)$_3$, **11-H$_3$**, by trans-metallation reaction of mono-lithiated species **11-H$_2$**Li with various metal precursors such as [Rh(CO)$_2$Cl]$_2$, [(^{t}BuN)$_2$MoCl$_2$(dme)] and NiBr$_2$(dme).[26] All the obtained complexes **11-H$_2$**Rh(CO)$_2$, (**11-H$_2$**)$_2$Mo(N^{t}Bu)$_2$ and (**11-H$_2$**)$_2$Ni complexes are

monomeric in nature, and supported by mixed N, S coordination. The metal ions in these complexes exhibit diverse coordination geometries; in Rh complex it is square planar, Mo adopts octahedral environment, while in the Ni complex metal is pseudo-tetrahedrally coordinated with the angles varying from 73° to 134°. In Rh and Mo complex the metal has only hard-soft (N,S) chelation mode, but surprisingly the Ni-complex was found to have both hard-soft (N,S) and hard-hard (N,N') chelation mode.

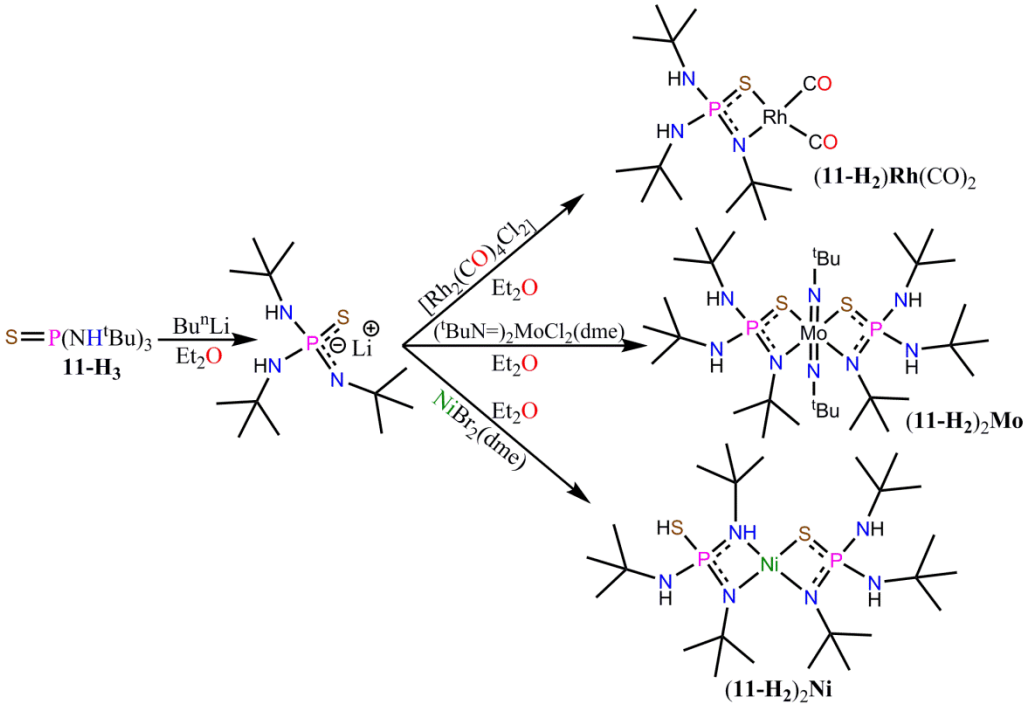

Scheme 1.15: Synthesis of transition metal imido-P(V) complexes derived from **11-H_3** via trans-metalation reactions.

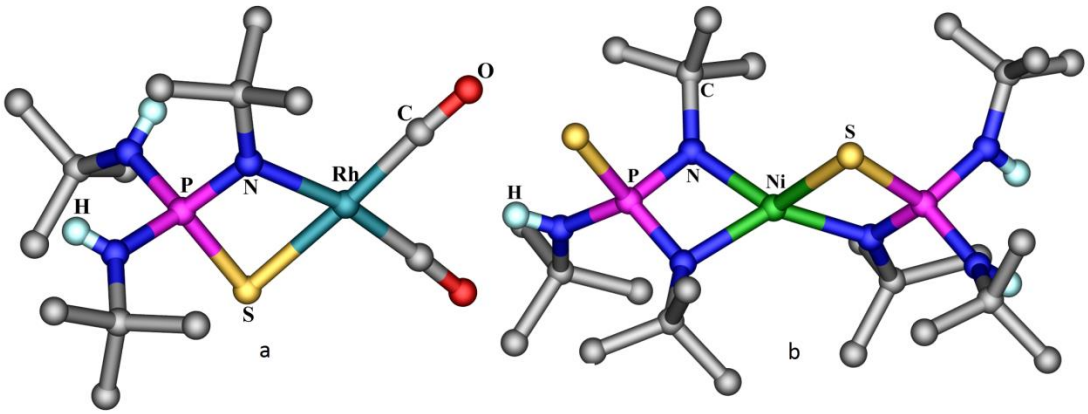

Figure 1.15: Crystal structures of **11-H_2Rh**$(CO)_2$ (a) and $($**11-H_2**$)_2$**N**i featuring the mono anionic thio-imidophosphate ligand.

The first example of the homoleptic tetra-imidophosphate trianion was reported by Wright and co-workers in an unprecedented reaction.[27] The lithium complex was recovered after reaction of diphosphorus tetraiodide with α-naphtylamine and subsequent addition of butyllithium.[15] X-ray structure determination revealed a solvent separated ion pair **12**-Li_3 (Figure1.16)

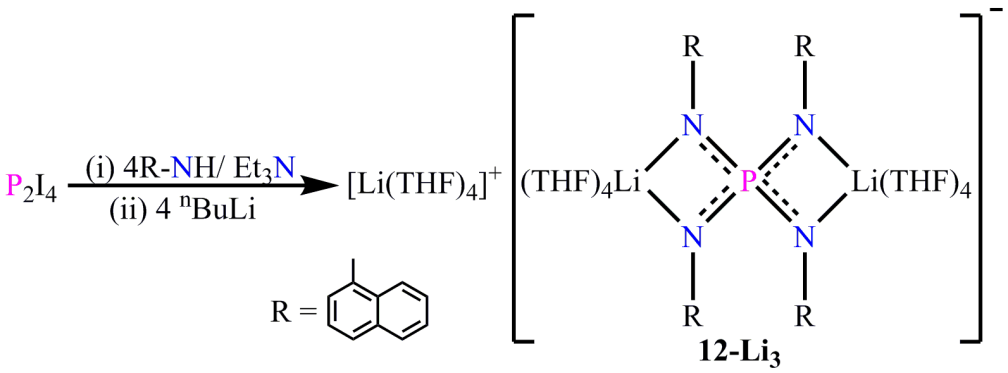

Scheme 1.16: Synthesis of Lithium complex of the tetrakis(imido)phosphate trianion.

The complex anion consists of the trianionic ligand accommodating two lithium ions in two bidentate chelating sites. The cationic complex contains a lithium ion surrounded by four THF molecules.

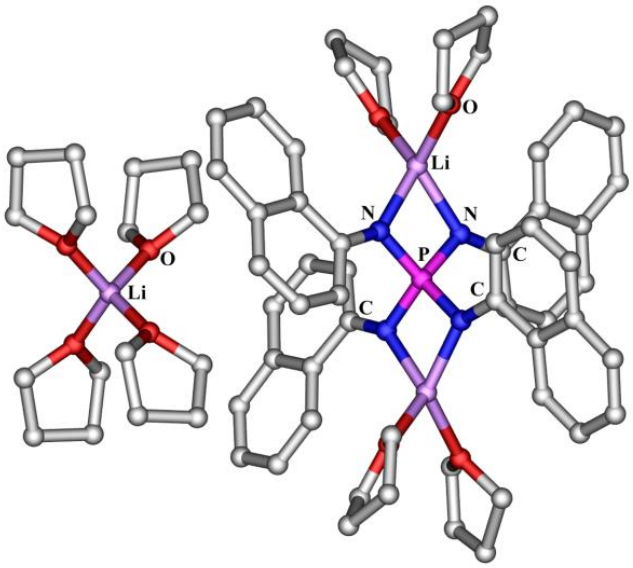

Figure 1.16: Crystal structures of **12-Li_3**.

Subsequently, Steiner and coworkers have shown step-wise deprotonation of tetraanilinophosphonium cation, $[P\{N(H)Ph\}_4]^+$ (**13-H_4**) ,by ^{n}BuLi in THF.[28] Thus, the deprotonation reaction of $[P\{N(H)Ph\}_4]Cl$ generates the neutral phosphine imine $[P\{N(H)Ph\}_3(NPh)]$ (**13-H_3**), monoanionic $[P\{N(H)Ph\}_2(NPh)_2]^-$ (**13-H_2**), dianionic $[P\{N(H)Ph\}(NPh)_3]^{2-}$ (**13-H**) and trianionic $[P(NPh)_4]^{3-}$ (**13**) species upon treatment

with 1, 2, 3 and excess equivalence of ^{n}BuLi. The formations of these imido species were monitored by ^{31}P-NMR and their solid state structures have also been obtained. As the oxo (=O) and imino (=NR) groups as well as hydroxyl (-OH) and amido (-N(H)R) groups are isoelectronic, these neutral, monoanionic, dianionic and trianionic species can be considered as analogues of phosphoric acid (H_3PO_4), dihydrogenphosphate ($H_2PO_4^-$), monohydrogenphosphate (HPO_4^{2-}) and orthophosphate (PO_4^{3-}) ions, respectively. Although the oxo phosphate analogues form highly networked solid state structures, their N anologues have a tendency to form structures with lower dimensionality because of the presence of organic substitution at the N atom. These findings suggests that similar platforms with functionalized ligand periphery can be synthesized which can be utilized as building blocks for materials with unique connectivity patterns.

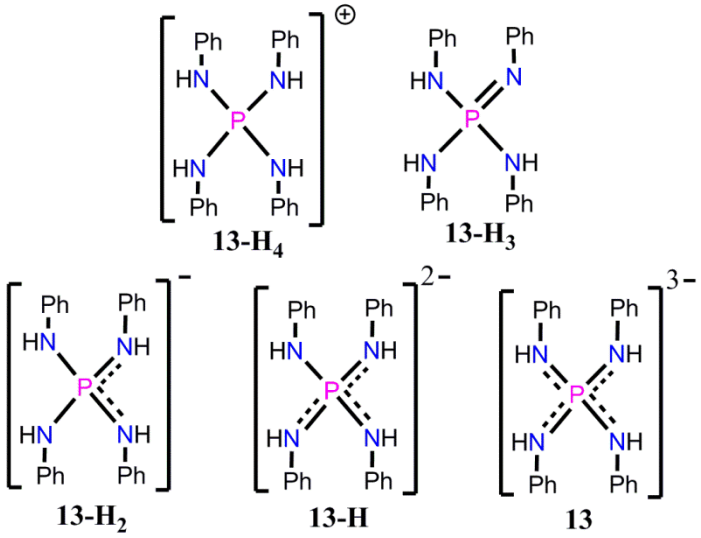

Figure 1.17: Tetraanilino phosphonium cation and its neutral, mono-, di- and tri-anionic forms.

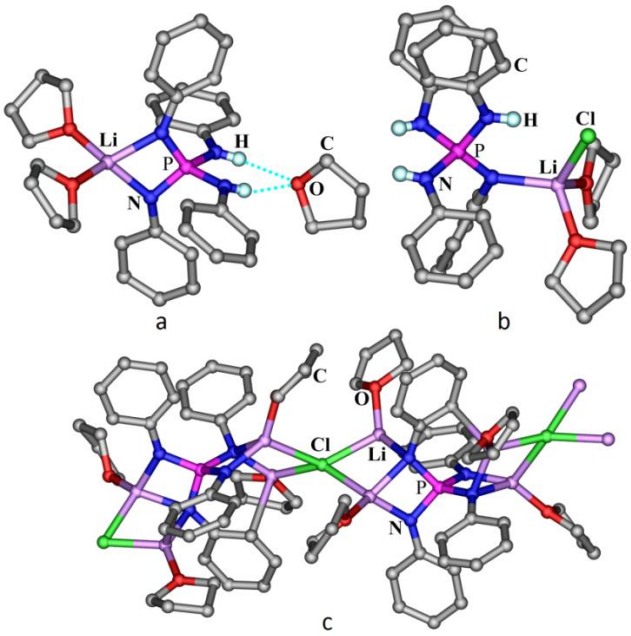

Figure 1.17: Crystal structures of (a) **13Li**$(THF)_{3.5}$, (b) **13LiCl**$(THF)_2$ and (c) $[\{$**13Li**$(THF)_2\}_2Cl]^-$.

1.2 Definition of the problem

By looking at all the above mentioned examples, synthetic routes to access these imido P(V) anions involve the use of highly reactive main-group metal reagents in reaction with a phosphonium salt like $[(PhNH)_4P]Cl$ or phosphates such as $[(RNH)_3P{=}E]$ (E = $NSiMe_3$, O, S or Se) or with preformed iminophosphoranes. However due to the highly reactive nature of the metal precursors as well as to the presence of residual metal-alkyl/aryl/halide/silylamide bonds in these complexes, the imido ligand chemistry has largely been limited to main-group metal ions in anhydrous aprotic and non-polar solvents. Only in very few instances, utilizing trans-metallation reactions, the transition metal derivatives of these imido anions have been realized in aprotic non-polar medium. Chivers and co-workers have also shown that use of transition metal reagents containing Lewis-acidic metal ions such as $CuCl_2$ in reaction with **7**-H_3 under polar environment have lead to P-N bond hydrolysis reaction to generate $(RNH_3)^+$ ion which directs a copper chloride chain assembly of composition $\{[^tBuNH_3]_2[Cu_3(\mu_3\text{-}OH)(\mu_2\text{-}H_2O)Cl_7]\}_n$.[29] Hence, we presumed that use of a less-acidic softer transition metal ion in combination with a stronger conjugate base as a leaving group, as briefly indicated by Dehnicke, it is possible to obtain the transition metal complexes for these imido P(V) anions under ambient conditions. Also by providing further stabilization for these transition metals, via peripheral functional groups on the P(V) backbone, deprotonation at the amido sites could be accelerated. Hence, we were interested in systematically

investigating the ligand chemistry of amido and imido P(V) precursors containing various substituents on the P(V) backbone and subsequently study them for their functional properties.

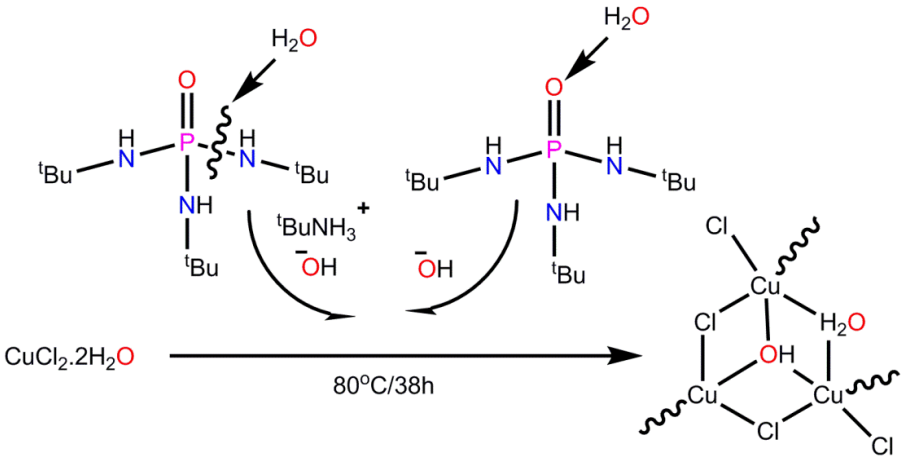

Scheme 1.18: Schematic representation for the solvothrmal reaction of phosphoramide with Cu(II) salt.

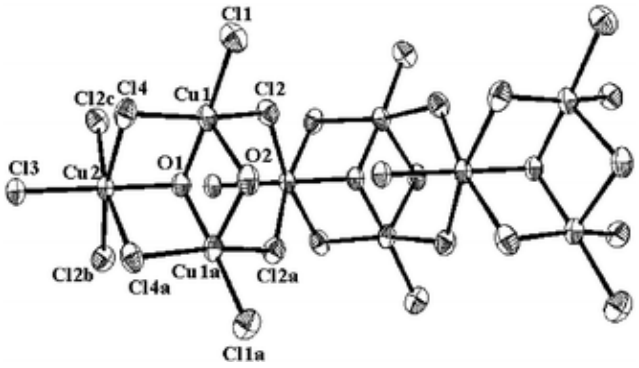

Figure 1.18: Crystal structure of $\{[Cu_3(\mu_3\text{-}OH)(\mu_2\text{-}H_2O)Cl_7]^{2-}\}_n$. (Adopted from Chivers et al. *Chem. Commun.* **2005**, 2339-2341).

Thus the major objectives of this research program are outlined as follows.

- Generating imido P(V) derivatives in a protic and polar medium from reactive transition metal salts to obtain the corresponding polyamido and/or polyimido metal complexes
- Obtain diverse structural architectures by tuning the peripheral functional groups and the ligand geometry attached at the central P(V) atom
- To study the functional properties of these amido/imido P(V) metal complexes in the areas of catalysis, sorption, self-assembling ability and host-guest chemistry

1.3 References

(1) Bertrand, G. *Chem. Rev.* **1994,** *94*, 1161-1162.

(2) (a) Buchard, A.; Auffrant, A.; Klemps, C.; Vu-Do, L.; Boubekeur, L.; Le Goff, X. F.; Le Floch, P. *Chem. Commun*. **2007**, 1502-1504. (b) Alhomaidan, O.; Bai, G.; Stephan, D. W. *Organometallics* **2008**, *27*, 6343-6352. (c) Li, D.; Li, S.; Cui, D.; Zhang, X.; Trifonov, A. A. *Dalton Trans*. **2011**, *40*, 2151-2153. (d) Gamer, M. T.; Rastätter, M.; Roesky, P. W.; Steffens, A.; Glanz, M. *Chem. Eur. J.* **2005**, *11*, 3165-3172. (e) Rastätter, M.; Zulys, A.; Roesky, P. W. *Chem. Eur. J*. **2007**, *13*, 3606-3616. (f) Rastätter, M.; Zulys; A.; Roesky, P. W. *Chem. Commun*. **2006**, 874-876. (g) Boubekeur, L.; Ulmer, S.; Ricard, L.; Mézailles, N.; Le Floch, P. *Organometallics* **2006**, *25*, 315-317.

(3) Schmidbaur, H.; Wolfsberger, W. *Chem. Ber*. **1967**, *100*, 1000.

(4) (a) Dehnicke, K.; Weller, F. *Coord. Chem. Rev.* **1997**, *158*, 103-169. (b) Dehnicke, K.; Krieger, M.; Mass, W. *Coord. Chem. Rev*. **1999**, *182*, 19−65.

(5) Witt, M.; Roesky, H. W., *Chem. Rev.* **1994**, *94*, 1163-1181.

(6) (a) Chivers, T.; Brask, J. K. *Angew. Chem., Int. Ed.* **2001**, *40*, 3960-3976. (b) Chivers, T. *Top. Curr. Chem.* **2003**, *229*,143-159. (c) Chivers, T.; Hilts, R. W. *Coord. Chem. Rev.* **1994**, *137*, 201-232.

(7) Beswick, M. A.; Wright, D. S. *Coor. Chem. Rev.* **1998**, *176*, 373-406.

(8) Fleischer, R.; Stalke, D.*Coord. Chem. Rev.* **1998**, 176, 431-450.

(9) Aspinall, G. M.; Copsey, M. C.; Leedham, A. P.; Russell, C. A. *Coord. Chem. Rev.* **2002**, *227*, 217-232.

(10) Steiner, A.; Zacchini, S.; Richards, P. I. *Coord. Chem. Rev.* **2002**, *227*, 193-216.

(11) Stahl, L. *Coord. Chem. Rev.* **2002**, *210*, 203-250.

(12) (a) Chandrasekhar, V.; Thilagar, P.; Murugesapandian, B. *Coord. Chem. Rev.* **2007**, *251*, 1045-1074. (b) Chandrasekhar, V.; Nagendran, S. *Chem. Soc. Rev.* **2001**, *30*, 193-203. (c) Chandrasekhar, V.; Murugesapandian, B. *Acc. Chem. Res.* **2009**, *42*, 1047-1062. (d) Allen, C. W., Linear, cyclic and polymeric phosphazenes. *Coord. Chem. Rev.* **1994**, *130*, 137-173.

(13) Riese, U.; Faza, N.; Massa, W.; Dehnicke, K. *Angew. Chem., Int. Ed.* **1999**, *38*, 528-531.

(14) Steiner, A.; Stalke, D. *Inor. Chem.***1993**, *32*, 1977-1981.

(15) Fleischer, R.; Stalke, D. *Inor. chem.* **1997**, *36*, 2413-2419.

(16) Stapleton, R. L.; Chai, J.; Taylor, N. J.; Collins, S. *Organometallics* **2006**, *25*, 2514-2524.

(17) Nekoueishahraki, B.; Roesky, H. W.; Schwab, G.; Stern, D.; Stalke, D. *Inorg. chem.* **2009**, *48*, 9174-9179.

(18) Stasch, A. *Chem. Eur. J.* **2012**, *18*, 15105-15112.

(19) Briand, G. G.; Chivers, T.; Krahn, M.; Parvez, M. *Inorg. chem.* **2002**, *41*, 6808-6815.

(20) Burke, L. T.; Hevia-Freire, E.; Holland, R.; Jeffery, J. C.; Leedham, A. P.; Russell, C. A.; Steiner, A.; Zagorski, A. *Chem. Commun.* **2000**, *18* , 1769-1770.

(21) Armstrong, A.; Chivers, T.; Krahn, M.; Parvez, M.; Schatte, G. *Chem. Commun.* **2002**, 2332−2333.

(22) Robertson, S. D.; Chivers, T.; Konu, J. *J. Organomet. Chem*. **2007**, *692*, 4327-4336.

(23) Woodruff, D. N.; McInnes, E. J. L.; Sells, D. O.; Winpenney, R. E. P.; Layfield, R. A. *Inorg. Chem*. **2012**, *51*, 9104-9109.

(24) Blais, P.; Chivers, T.; Schatte, G.; Krahn, M. *J. Organomet. Chem.* **2002**, *646*, 107-112.

(25) Chivers, T.; Krahn, M.; Parvez, M.; Schatte, G. *Chem. Commun*. **2001**, 1922-1923.

(26) Rufanov, K. A.; Zeimer, B.; Meisel, M. *Dalton Trans*. **2004**, 3808-3809.

(27) Raithby, P. R.; Russell, C. A.; Steiner, A.; Wright, D. S. *Angew. Chem., Int. Ed. Engl.* **1997**, *36*, 649-650.

(28) Bickley, J. F.; Copsey, M. C.; Jeffery, J. C.; Leedham, A. P.; Russell, C. A.; Stalke, D.; Steiner, A.; Stey, T.; Zacchini, S. *Dalton Trans.* **2002**, 989-995.

(29) Chivers, T.; Fu, Z.; Thompson, L. K. *Chem. Commun.* **2005**, 2339-2341.

Chapter 2

Amino functionalized P(V) ligands and their supramolecular structures

Abstract

The objective of this Chapter is to synthesize and study the H-bond assisted supramolecular organization of the precursor amino phosphonium cations of formula $[P(NHR)_4]^+$ *in presence of various anions. These phosphonium cations offer four H-bond donor sites that are arranged in tetrahedral fashion around the central phosphorus atom. This arrangement generates novel supramolecular building blocks that are distinct to the commonly planar NH donor systems such as urea and guanidine. The supramolecular aggregation of these cations in presence of chloride, carboxylate and inorganic anions such as polyoxometalate ions have been described in detail. The phosphonium chlorides exhibit H-bonding interactions and lead to liner, zigzag and helical 1D-chain and 2D-supramolecular structures depending on the steric bulk on amino substituents. The phosphonium carboxylates were obtained by two routes: anion exchange reaction with phosphonium carboxylates and re-protonation reaction from a neutral phosphine imine* $[P(NPh)(NhPh)_3]$*. Depending on the steric bulk on the phosphonium cation as well as the topology of the carboxylate moiety (mono, di and tri-carboxylate) interesting 2D- and 3D-supramolecular structures mediated N-H…O interactions were obtained. Finally we have shown for the first an amino-phosphonium polyoxometalate supramolecular network by employing the phosphonium salts in the polyoxometalate synthesis.*

2.1 Introduction

The design and synthesis of functional materials via crystal engineering has been emerged as an active area over the past few decades.[1] Although the main driving force for such approaches is to understand the supramolecular self-assembly process, the ultimate aim is to gain control over the supramolecular assembly processes in order to produce designer crystals.[2] Several strategies have been developed to achieve this. For example, the network topology of metal-organic frameworks can be controlled to a great extent, which has enabled the synthesis of materials with specific properties.[3] As a result, metal-organic frameworks have shown enormous potential for applications ranging from host-guest chemistry, gas storage[4] to catalysis and sensors.[5] Thus the quest for new supramolecular building blocks that are able to generate structures of novel topologies and materials with certain properties, for example metal free organic frameworks, continues to grow at a steady rate.[6]

Phosphonium cations containing alkyl and aryl substituents play an important role in chemical synthesis, for example the Wittig reaction.[7] They have been widely applied as phase transfer catalysts, such as the ring-opening polymerization of epoxides.[8] These compounds also play an important role in many stereoselective syntheses. Chiral tetraamino phosphonium catalysts have been utilized in enantioselective transformations for example the Mannich reaction,[9] the Henry reaction and the hydrophosphonylation of aldehydes.[10] Ooi and co-workers used an enantiopure tetraamino phosphonium phenoxide salt containing a spirocyclic cation as a supramolecular ion-pair catalyst in which the chiral information is transferred to the substrate via hydrogen bonding.[11] Interestingly, it has been shown that organoamino substituted phosphonium cation $[(PhNH)_4P]^+$ can be deprotonated to form anions that are valence isoelectronic to PO_4^{3-}, HPO_4^{2-} and $H_2PO_4^-$ ions.[12] Such ligands can offer binding sites for both Lewis acids and bases. For example, the mono anionic ligand $[(PhNH)_2P(NPh)_2]^-$, which is the N-analogue of the dihydrogen phosphate ion, contains a bidentate N-P-N site for the chelation of metal centres and a bidentate HN-P-NH site that can interact with anions via H-bonding.

Tetra(organoamino)phosphonium cations of general formula $[P(NHR)_4]^+$ exhibit a tetrahedral arrangement of four RNH groups around the central phosphorus atom. As such they offer a unique coordination geometry for hydrogen bonding, which differs from that of the commonly planar NH-donors such as urea and guanidinium (figure 2.1).[13] The crystal structure of $[P(NHPh)_4]Cl$ shows that the $[P(NHPh)_4]^+$ ion binds two

chloride ions via two HN-P-NH chelates, which are located at opposite faces of the cation and are twisted by 90° with respect to each other.[12a]

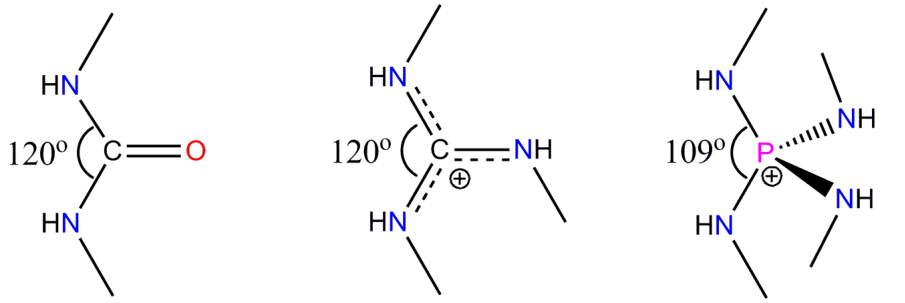

Figure 2.1: Geometrical arrangement of urea, guanidine and phosphonium ions

Encouraged by the unique ligand geometry, we set out to explore the potential of these cations as supramolecular building blocks and the coordination modes of these cations in the presence of a range of anions. In particular, salts of anions containing carboxylate groups promise interesting structures, since these are potential double H-acceptors and thus compatible with the doubly H-donating HN-P-NH moiety of the cation. Carboxylic acids and carboxylic ions, especially those that contain several carboxylic groups, have been widely used as supramolecular synthons.[14] Apart from carboxylates, another interesting class of anions that can engage in multiple H-bonds is those of polyoxometalates. Prompted by this we were also interested in the hydrogen bonded assembly of tetra(organoamino)phosphonium cations with Polyoxometallate cluster anions (POMs). POM anions have widely been used as supramolecular synthons and provide multiple hydrogen bond acceptor sites through terminal and bridging oxo functions.[15-19] In addition, the steric and electronic properties of the $[P(NHR)_4]^+$ ion can be tuned via the modification of the four R-groups. Crystal structures of related organoamino phosphazenes and phosphazenium ions have shown that slight changes of R can have a profound effect on the dimensionality of the H-bonding network.[20] In this chapter, we report on the synthesis of salts of various mono-, di- and tri-carboxylate anions and those of iso- and hetero-polymetalate anions in presence of various $[P(NHR)_4]^+$ ions. The single crystal X-ray analysis of these phosphonium salts reveal the formation of interesting supramolecular structures that are assisted by hydrogen bonding interactions.

2.2 Experimental

2.2.1 General Remarks: All manipulations involving phosphorus halides were performed under dry nitrogen atmosphere in standard Schlenk-glassware. Solvents were dried over potassium (THF, hexane) and sodium (toluene). PCl_5 and primary amines were purchased from Aldrich and used as received. The phosphonium chloride precursors $[P(NHR)_4]Cl$, **2.1** (R = phenyl), **2.2** (R = *n*-propyl), **2.3** (R = *iso*-propyl), **2.4** (R = *iso*-butyl), **2.5** (R = *tert*-butyl) and **2.6** (R = cyclohexyl) were prepared by using the literature reported procedure.[21] The carboxylate and the polyoxometalate precursors were locally procured (SPECTROCHEM and LOBA, India) and used as received. NMR spectra were recorded on a 400 MHz Varian FT spectrometer (^1H NMR: 400.13 MHz, $^{13}C\{^1H\}$ NMR: 100.62 MHz, $^{31}P\{^1H\}$ NMR: 161.97 MHz) at room temperature using $SiMe_4$ (^1H, ^{13}C) and 85% H_3PO_4 (^{31}P) as external standards. FT-IR spectra were taken on a Perkin Elmer spectrophotometer with samples prepared as KBr pellets. Mass spectra for **2.17-2.22** were obtained by Waters Q-Tof Premier & Aquity instrument. TGA and DSC data were obtained on TA instruments model SDT-Q600 and Q-20 machines, respectively. Melting points were obtained using an Electro thermal melting point apparatus and were uncorrected.

2.2.2 Synthesis

2.7: $[P(NHPh)_4]Cl$, **2.1** (100 mg, 0.230 mmol) and sodium acetate (14.28 mg, 0.237 mmol), in 1:1 ratio were taken in methanol (10 mL) and heated to 60-70 °C for 1 hour. The precipitated NaCl was removed by filtration on a celite pad and the solution was left to evaporate slowly at room temperature. Single crystals suitable for X-ray analysis was obtained after 7 days. Yield 70.0 mg (68 %), M.P. 308-310 ^oC,^1H NMR (400 MHz, CD_3OD): δ 2.00 (s, 3H**,** C*H*$_3$), 5.36 (br, 4H**,** N*H*), 7.03 (t, *p*-H, C*H*, $^3J_{H\text{-}H}$ =6.8 Hz), 7.17 (t, *m*-H, C*H*, $^3J_{H\text{-}H}$ =6.8 Hz), 7.23 (d, *o*-H, C*H*, $^3J_{H\text{-}H}$ =6.8 Hz); $^{13}C\{^1H\}$(100 MHz, CD_3OD): δ 21.10 (*C*H$_3$), 121.66 (*o*-*C*), 125.22 (*p*-*C*), 130.67 (*m*-*C*), 138.87 (N-*C*), 175.78 (*C*OO$^-$); ^{31}P NMR (161 MHz, CD_3OD) δ 8.19; FT-IR data in KBr pellet (cm^{-1}) : 3189 [ν (N-H)]; 690, 748, 956, 1031, 1081, 1221, 1280, 1410, 1498 [ν (P-N)]; 1600 [ν (C-O)]. Anal. Calcd. for $C_{50}H_{51}N_8O_2ClP_2$: C, 67.22; H, 5.75; N, 12.54. Found: C, 66.82; H, 5.80; N, 11.39.

2.8: $[P(NHCy)_4]Cl$, **2.6** (100mg, 0.218mmol) and sodium acetate (25mg, 0.218mmol),in 1:1 ratio were taken in methanol (10mL) heated to 60-70 °C for 1 hour. The precipitated NaCl was removed by filtration on a celite pad and the solution was left to evaporate

slowly at room temperature. Colourless crystals suitable of X-ray analysis were formed after 3 days.Yield 77.4 mg (65 %), M.P. 250-252°C ;^{1}H NMR (400 MHz, CD_3OD): δ 1.18-1.92 (m, 40 H**,** CH_2), 2.95 (s, 3H, CH_3), 3.34 (m, 4 H, C*H*), 4.91 (br, 4H, N*H*); ^{13}C{^{1}H}(100 MHz, CD_3OD): δ 24.55 (*C*H_2), 26.52 (*C*H_3), 32.78 (*C*H_2), 36.93 (*C*H_2), 51.94 (*C*H), 180.90 (*C*OO^-); ^{31}P NMR (161 MHz, CD_3OD): δ 21.28; FT-IR data in KBr pellet (cm^{-1}): 3203 [ν (N-H)]; 1591 [ν (C-O)]; 889, 962, 1047, 1238, 1349 [ν (P-N)]. Anal. Calcd. for $C_{28}H_{59}N_4O_4P$: C, 61.51; H, 10.88; N, 10.25. Found: C, 61.37; H, 11.02; N, 9.92.

2.9: To a solution of [P(NH^{i}Bu)$_4$]Cl, **2.4** (100 mg, 0.281 mmol) in 7 mL of methanol, a solution of disodium oxalate (19 mg, 0.141 mmol) in 3 mL of distilled water was slowly added and the resulting solution was heated to 60-70 ^{o}C for half an hour. The precipitated NaCl was removed by filtration on a celite pad and the filtrate was left to evaporate slowly at room temperature. Colourless prismatic crystals suitable of X-ray analysis were formed after one week. Yield 75.9 mg, (74 %) M.P. 145-147 ^{o}C, ^{1}H NMR (400 MHz, CD_3OD): δ 0.95 (d, 24 H, CH_3), 1.72 (m, 4H,C*H*),2.69 (m, 8H, CH_2), 4.87 (br, N*H*);^{13}C{^{1}H}(100 MHz, CD_3OD): δ 20.85 (*C*H_3), 31.43 (*C*H), 50.26 (*C*H_2), 174.84 (*C*OO^-); ^{31}P NMR (161 MHz, CD_3OD):δ 32.22; FT-IR data in KBr pellet (cm^{-1}) : 3189 [ν (N-H)]; 863, 960, 1010, 1082, 1252, 1423, 1470 [ν (P-N)]; 1589 [ν (C-O)]. Anal. Calcd. for $C_{34}H_{80}N_8O_4P_2$: C, 56.17; H, 10.09; N, 15.41. Found: C, 55.71; H, 10.03; N, 14.16.

2.10: [P(NHPh)$_4$]Cl, **2.1** (0.3g, 0.69 mmol) was dissolved in methanol (~10-15ml) and excess KOH pellets (0.250, 4.46 mmol) were added to it under constant stirring. Soon after the addition, a white precipitate of KCl was formed. Stirring was continued until no more KCl formation was observed and distilled H_2O was then added to the solution. Upon the addition of H_2O, the precipitated KCl dissolved and a new white precipitate formed. This precipitate was then filtered under vacuum and washed with H_2O followed by 2mL of ice-cold methanol and diethyl ether yielding a pure sample of **10**, [P(NHPh)$_3$(NPh)]. Yield 240.0 mg (87 %). Single crystals suitable for X-ray analysis was obtained from a solution tetrahydrofuran/Hexane. M.P. 254˚C. NMR data (δ ppm); ^{1}H NMR (MeOD) δ 1.18-1.24 (t, CH_2), δ 3.32-3.34 (q, OCH_2), δ 4.89 (s, N*H*), δ 6.84-6.88 (m, ortho&para C*H*), δ 7.11-7.19 (m, meta C*H*). ^{13}C NMR (MeOD) δ 101.41 (s, C*H*), δ 121.42-121.50 (d, ortho C*H*), δ 122.63 (s, para C*H*), δ 130.34 (s, meta C*H*), δ 143.72 (s, CN).^{31}P{^{1}H} NMR (MeOD) δ -4.28 (s).. IR data (cm^{-1}): 3348 (ν_s N-H), 3020

(ν_s =C-H), 2929 (ν_s C-H), 1595 (ν_s C=C), 1282 (ν_s P=N), 1223 (ν_s P-N), 1074 (ν_s C-N), 914, 748, 690, 607. Anal. Calcd. for $C_{24}H_{23}N_4P_1$: C, 72.35; H, 5.82; N, 14.06. Found: C, 71.13; H, 5.75; N, 13.83.

2.11: To a solution of [$(PhNH)_3P(NPh)$], **2.10** (100 mg, 0.251mmol), in 10 mL of methanol, acetic acid (15.06 mg, 0.251 mmol), was added with constant stirring. The progress of the reaction was monitored with ^{31}P-NMR and the clear solution thus obtained was left for slow evaporation. The compound **2.11** was obtained as a microcrystalline solid after one week. Yield 83.0 mg (72 %). M.P. 308 ^{o}C.^{1}H NMR(400 MHz, CD_3OD): δ 2.00 (s,3H**,** CH_3), 5.36 (br, 4 H**,** N*H*), 7.03 (t, *p*-H, C*H***,** $^{3}J_{H\text{-}H}$ =6.8 Hz), 7.17 (dd, *m*-H, C*H* $^{3}J_{H\text{-}H}$ =6.8 Hz), 7.23(d, *o*-H C*H*, $^{3}J_{H\text{-}H}$ =6.8); ^{13}C{^{1}H}}(100 MHz, CD_3OD): δ 21.10 (*C*H_3), 121.66 (*o*-*C*), 125.22 (*p*-*C*), 130.67 (*m*-*C*), 138.87 (N-*C*) 175.78 (*C*OO^-): ^{31}P NMR (161 MHz, CD_3OD): δ 8.190; FT-IR data in KBr pellet (cm^{-1}): 3189, [ν (N-H)]; 690, 748, 956, 1031, 1081, 1221, 1280, 1410, 1498 [ν (P-N)]; 1600 [ν (C-O)]. Anal. Calcd. for $C_{26}H_{27}N_4O_2P$: C, 68.11; H, 5.94; N, 12.22. Found: C, 67.93; H, 5.78; N, 11.66.

2.12: To a solution of [$(PhNH)_3P(NPh)$], **2.10** (100 mg, 0.251mmol), in 10 mL of methanol, cyclohexane carboxylic acid (32.14 mg, 0.251 mmol), was added with constant stirring. The progress of the reaction was monitored with ^{31}P-NMR and the clear solution thus obtained was left for slow evaporation. Bright yellow crystals suitable for single crystal X-ray diffraction were obtained after one week. Yield 104.0 mg (79 %). Mp: 220˚C. NMR data (δ p.p.m);^{31}P{^{1}H} NMR (MeOD) δ -0.55 (s). ^{1}H NMR (400 MHz, CD_3OD): δ 1.27-1.92 (m, CH_2), δ 2.17 (s, C*H*), δ 4.89 (N*H*), δ 6.88-6.92 (m, o & p-C*H*), δ 7.19-7.28 (m, m-CH); ^{13}C{^{1}H}(100 MHz, CD_3OD): δ 27.60 (*C*H_2), δ 31.74 (*C*H_2), δ 48.78 (s, *C*H). δ 107.22 (s, *C*-N), δ 119.65 (s, o-*C*), δ 122.66 (p-*C*), δ 130.36 (m-*C*), δ 160.59 (*C*OO^-). IR data (cm^{-1}): 3357 (ν_s N-H), 2927, 2852, 1651 (ν C=C), 1552 [ν_s C=O], 1404, 1221(ν_s P-N), 1034, 930, 748. Anal. Calcd. for $C_{31}H_{35}N_4O_2P_1$: C, 70.70; H, 6.70; N, 10.64. Found: C, 67.24; H, 6.88; N, 9.90.

2.13: A 2:1 mixture of [$(PhNH)_3P(NPh)$], **2.10** (100 mg, 0.251mmol) and malonic acid (13 mg, 0.124 mmol), respectively, in a 5 mL solution of methanol was stirred for half an hour. The completion of the reaction was confirmed by ^{31}P-NMR and the clear solution was left for crystallization. Colorless needle-shaped crystals of **2.13** were formed after one week. Yield 92.8 mg (82 %), M.P. 170-171 ^{o}C; ^{1}H NMR(400 MHz, CD_3OD): δ 3.60 (s, 2H**,** CH_2), 4.83 (br, 4 H,N*H*), 6.90 (t, *p*-H, C*H*, $^{3}J_{H\text{-}H}$ =6.8 Hz), 7.03 (dd, *m*-H,

C*H*, $^{3}J_{H-H}$ =6.8), 7.10 (d, *o*-H, C*H*, $^{3}J_{H-H}$ = 6.8); $^{13}C\{^{1}H\}$(100 MHz, CD_3OD): δ 48.27 (CH_2), 121.34 (*o*-*C*), 125.58 (*p*-*C*), 130.94 (*m*-*C*), 138.42 (N-*C*), 174.71 (COO^-); ^{31}P NMR (161 MHz, CD_3OD):δ 8.83; FT-IR data in KBr pellet (cm^{-1}) : 3082 [ν (N-H)]; 690, 748, 978, 1032, 1057, 1081,1222, 1281, 1329, 1407, 1497 [ν (P-N)]; 1600 [ν (C-O)]. Anal. Calcd. for $C_{51}H_{50}N_8O_4P_2$: C, 67.99; H, 5.59; N, 12.44. Found: C, 67.27; H, 5.81; N, 12.11.

2.14: To a solution of [$(PhNH)_3P(NPh)$], **2.10** (100 mg, 0.251mmol) in 10 mL of methanol, a solution of oxalic acid (14.28 mg, 0.130 mmol) in methanol (5 mL) was added and the resulting mixture was refluxed for half an hour. A white precipitate thus obtained was filtered off in sintered glass funnel and dried to get **2.14**. Yield 87.1 mg (78 %), M.P. 263-265 ^{o}C,^{1}H NMR (400 MHz, CD_3OD): δ 4.83 (br, 4 H**,** N*H*), 6.877 (t, *p*-H, C*H*, $^{3}J_{H-H}$ = 6.8 Hz), 7.04 (dd, *m*-H, C*H*, $^{3}J_{H-H}$ = 6.8), 7.12 (d, *o*-H, C*H*,$^{3}J_{H-H}$ = 6.8); $^{13}C\{^{1}H\}$(100 MHz, CD_3OD): δ 119.34 (*o*-*C*), 122.46 (*p*-*C*), 130.14 (*m*-*C*), 142.54 (N-*C)*, 174.84 (COO^-);^{31}P NMR (161 MHz, CD_3OD):δ 8.827; FT-IR data in KBr pellet (cm^{-1}) : 3139,[ν (N-H)]; 690, 748, 976, 1032, 1222, 1281, 1414, 1497 [ν (P-N)]; 1600 [ν (C-O)]. Anal. Calcd. for $C_{50}H_{48}N_8O_4P_2$: C, 67.71; H,5.45; N, 12.63. Found: C, 66.67; H, 5.85; N, 11.91.

2.15: To a solution of [$(PhNH)_3P(NPh)$], **2.10** (100 mg, 0.251mmol) in 5 mL of methanol, a solution citric acid (16.01 mg, 0.083 mmol) dissolved in methanol (5 mL) was added slowly with constant stirring. The progress of the reaction was monitored with ^{31}P-NMR and the clear solution thus obtained was left for slow evaporation. The compound **2.15** was obtained as a microcrystalline solid after one week. Yield 86.9 mg (75 %) M.P. 160-162 ^{o}C,^{1}H NMR(400 MHz, CD_3OD): δ 1.28 (s, 4H, CH_2), 2.85 (1H, O*H*), 4.90 (br, 4 H**,** N*H*), 7.03 (t, *p*-H, C*H*, $^{3}J_{H-H}$ =7.2 Hz), 7.16 (dd, *m*-H, C*H*, $^{3}J_{H-H}$ =7.2 Hz), 7.26 (d, *o*-H, C*H*, $^{3}J_{H-H}$ =7.2 Hz); $^{13}C\{^{1}H\}$(100 MHz, CD_3OD): δ 44.72 (*C*), 74.43 (CH_2), 121.05 (*o*-*C*), 125.27 (*p*-*C*), 130.70 (*m*-*C*), 138.85 (N-*C*), 174.80 (COO^-), 179.00 (COO^-); ^{31}P NMR (161 MHz, CD_3OD):δ 8.24; FT-IR data in KBr pellet (cm^{-1}): 3153, 3083 [ν (N-H)]; 690, 748, 959, 1032, 1058, 1081, 1220, 1280, 1405, 1497 [ν (P-N)]; 1600 [ν (C-O)]. Anal. Calcd. for $C_{78}H_{77}N_{12}O_7P_3$: C, 67.52; H, 5.59; N, 12.11. Found: C, 66.51; H, 5.95; N, 11.82.

2.16: To a solution of [$(PhNH)_3P(NPh)$], **2.10** (100 mg, 0.251mmol) in 10 mL of methanol, a solution of trimesic acid (17.5 mg, 0.083 mmol), in 5 mL solution in methanol was added slowly with constant stirring. The mixture was stirred for half an hour and the precipitated compound was filtered off in a sintered glass funnel and dried.

Single crystals suitable for single crystal X-ray analysis was obtained from a solution of **2.16** In methanol/DMF mixture. Yield 90.5 mg (77 %), M.P. 268-270^{o}C, ^{1}H NMR(400 MHz,$(CD_3)_2SO$)): δ 3.98 (br, 4 H**,** N*H*), 6.879 (t, *p*-H, C*H*, $^{3}J_{H\text{-}H}$ =7.2 Hz), 7.21 (t, *m*-H, C*H*, $^{3}J_{H\text{-}H}$ =7.2), 7.39 (d, *o*-H, C*H*, $^{3}J_{H\text{-}H}$ =7.2), 8.65 (C*H*, trimesic);^{13}C{^{1}H}}(100 MHz, $(CD_3)_2SO$)): δ 118.45 (*C*H, trimesic), 122.14 (*C*), 129.40 (*o*-*C*), 132.87 (*p*-*C*), 134.47 (*m*-*C*), 139.44 (N-*C*), 168.01 (*C*OO^-); ^{31}P NMR (161 MHz, $(CD_3)_2SO$))δ 4.94; FT-IR data in KBr pellet (cm^{-1}): 3082[ν (N-H)]; 690, 748, 978, 1032, 1057, 1081, 1222, 1281, 1329, 1407, 1497 [ν (P-N)]; 1600 [ν (C-O)]. Anal. Calcd. for $C_{81}H_{75}N_{12}O_6P_3$: C, 69.22; H, 5.38; N, 11.96. Found: C, 68.91; H, 5.65; N, 10.76.

(The synthetic procedure used for the preparation of compounds **2.17-2.22** is described here. To a 2:1 mixture of $[P(NHR)_4]Cl$ (**2.3**, **2.4** or **2.6**) and $Na_2MoO_4.2H_2O$/ $Na_2WO_4.2H_2O$ in methanol (10 mL) an approximately 1.6 N HCl was added until the solution pH reaches between 3 and 4. The resulting slurry was heated at 60-70^{o}C with stirring for 45 minutes. The precipitated solid was filtered and washed with ether. The analytical data for the compounds **2.18-2.23** are given below.)

2.17: $[P(NHCy)_4]Cl$, **2.6** (200 mg, 0.46 mmol); $Na_2MoO_4.2H_2O$ (55.65mg, 0.23 mmol). Crystals suitable for X-ray analysis was obtained from a solution of methanol/DMF. Yield 74% (489 mg), M.P. 260-262°C;^{1}H NMR {400 MHz $(CD_3)_2SO$}: δ 1.05-1.82 (m**,** CH_2), 3.34 (m,C*H*), 5.06 (N*H*); ^{13}C{^{1}H} {100 MHz, $(CD_3)_2SO$}: δ 24.92 (*C*H_2), 30.67 (*C*H_2), 34.95 (*C*H_2), 50.00 (*C*H), ^{31}P NMR {161 MHz, $(CD_3)_2SO$}:δ 22.71; FT-IR data in KBr pellet (cm^{-1}): 3345 [ν (N-H)]; 888, 961, 1081, 1349, 1448, 1593 [ν (P-N)]; 951 [ν (Mo=O)]; 843, 710 [ν (Mo-O-Mo)]. ESI(-) spectra: 634.1 $(Mo_4O_{15})^{6-}$, 607.5 $(Mo_4O_{14})^{4-}$.

2.18: $[P(NH^iBu)_4]Cl$, **2.4** (200 mg, 0.56 mmol); $Na_2MoO_4.2H_2O$ (68 mg, 0.28 mmol). Crystals suitable for X-ray analysis was obtained from a solution of methanol/DMF. Yield, 70% (386 mg) M.P. 182-184 ^{o}C; ^{1}H NMR (400 MHz, {$(CD_3)_2SO$}): δ 0.89, 0.90 (2d, CH_3), 1.64, 1.80 (2m, C*H*),2.53,2.60 (2t, CH_2), 4.11 (NH_3^+) 5.07 (t, N*H*);^{13}C{^{1}H}(100 MHz, {$(CD_3)_2SO$}): δ 19.64, 20.00 (*C*H_3), 26.34, 29.30 (*C*H_2), 45.82, 46.88 (*C*H), ^{31}P NMR (161 MHz, {$(CD_3)_2SO$}):δ 32.27; FT-IR data in KBr pellet (cm^{-1}): 3209 [ν (N-H)]; 863, 961, 1009, 1080, 1252, 1421, 1469 [ν (P-N)]; 953 [ν (Mo=O)]; 893, 843, 711 [ν (Mo-O-Mo)]. ESI(-) spectra: 633.1 $(Mo_4O_{15})^{6-}$, 608.5 $(Mo_4O_{14})^{4-}$.

2.19: $[P(NH^iBu)_4]Cl$, **2.4** (200 mg, 0.56 mmol); $Na_2WO_4.2H_2O$ (93 mg, 0.28 mmol). Crystals suitable for X-ray analysis was obtained from a solution of methanol. Yield 68% (690 mg), M.P. 262-264 ^{o}C; ^{1}H NMR {400 MHz, $(CD_3)_2SO$}): δ 0.95 (d, CH_3), 1.71 (m, C*H*), 2.62 (m, CH_2), 5.22 (N*H*); ^{13}C{^{1}H}(100 MHz, {$(CD_3)_2SO$}): δ 20.00

(CH_3), 29.29 (CH_2), 46.88 (*C*H), ^{31}P NMR (161 MHz, {$(CD_3)_2SO$}):δ 32.27; FT-IR data in KBr pellet (cm^{-1}): 3209 [ν (N-H)]; 863, 961, 1009, 1080, 1252, 1421, 1469 [ν (P-N)]; 956 [ν (W=O)]; 888, 801 [ν (W-O-W)]. ESI(-) spectra: 2082.9 (W_9O_{27}), 1726.6 $(W_7O_{27})^{12-}$, 1175.5 $(W_5O_{16})^{2-}$, 703.6 $(W_3O_{10})^{2-}$.

2.20: [P(NH^{i}Pr)4]Cl, **2.3** (200 mg, 0.67 mmol); $Na_2MoO_4.2H_2O$ (81mg, 0.33 mmol). Crystals suitable for X-ray analysis was obtained from a solution of methanol. Yield 65% (568 mg), M.P. 290-295°C;^{1}H NMR (400 MHz), {$(CD_3)_2SO$}: δ 1.30 (d**,** C*H*$_3$), 3.34 (m,C*H*), 4.88 (N*H*); ^{13}C{^{1}H}(100 MHz, {$(CD_3)_2SO$}: δ 24.80 (*C*H_3), 42.98 (*C*H), ^{31}P NMR (161 MHz, {$(CD_3)_2SO$}: δ 0.70, 22.70; FT-IR data in KBr pellet (cm^{-1}): 3220 [ν (N-H)]; 897, 935, 1036, 1123, 1166, 1384, 1430, 1462 [ν (P-N)]; 951 [ν (Mo=O)]; 804, 851, 710 [ν (Mo-O-Mo)]. ESI(-) spectra: 910.2 $^1/_2(PMo_{12}O_{40})^{3-}$, 797.0 $(PMo_5O_{18})^-$, 511.7 $(PMo_3O_{12})^-$.

2.21: [P(NH^{i}Pr)$_4$]Cl, **2.3** (200 mg, 0.67 mmol); $Na_2WO_4.2H_2O$ (110 mg, 0.33 mmol. Yield 58% (616 mg), M.P. 320-325°C;^{1}H NMR (400 MHz, {$(CD_3)_2SO$}: δ 1.12 (d**,** C*H*$_3$), 3.34 (m,C*H*), 4.91 (N*H*); ^{13}C{^{1}H}(100 MHz, {$(CD_3)_2SO$}: δ 24.81 (*C*H_3), 42.97 (*C*H), ^{31}P NMR (161 MHz, {$(CD_3)_2SO$}: δ -14.58, 22.70; FT-IR data in KBr pellet (cm^{-1}): 3203 [ν (N-H)]; 889, 962, 1047, 1238, 1349 [ν (P-N)] 962 [ν (W=O)], 802 [ν (W-O-W)]. ESI(-) spectra: 1647.3 $(W_7O_{23})^{4-}$, 1567.4 $(P_2W_6O_{25})^{4-}$, 1436.0 $^1/_2(PW_{12}O_{40})^{3-}$.

2.22: To a mixture of [P(NHCy)$_4$]Cl, **2.6** (200 mg, 0.46 mmol), $Na_2MoO_4.2H_2O$ (445.28 mg, 1.83 mmol) and sodium arsenate (47.84mg, 0.15 mmol) in methanol (10 mL) an approximately 1.6 N HCl was added until the solution pH reaches between 3 and 4. The resulting slurry was heated at 60-70^{o}C with stirring for 45 minutes. The precipitated solid was filtered and washed with ether. Crystals suitable for X-ray analysis was obtained from a solution of methanol/DMF. Yield 48% (230.88 mg), M.P. 260-262°C;^{1}H NMR (400 MHz, {$(CD_3)_2SO$}: δ 1.05-1.82 (m**,** C*H*$_2$), 2.06 (m,C*H*), 3.36 (br, 4H, N*H*); ^{13}C{^{1}H}(100 MHz, {$(CD_3)_2SO$}: δ 25.00 (*C*H_2), 30.66 (*C*H_2), 34.93 (*C*H_2), 49.90 (*C*H), ^{31}P NMR (161 MHz, {$(CD_3)_2SO$}: δ 22.69; FT-IR data in KBr pellet (cm^{-1}): 3172 [ν (N-H)]; 961, 1017, 1096, 1142, 1448, [ν (P-N)]; 898 [ν (Mo=O)]; 794 [ν (Mo-O-Mo)]. ESI(-) spectra: 951.9 $^1/_2(AsMo_{12}O_{40})^{3-}$, 492.4 $(AsMo_2O_{14})^{11-}$.

2.2.3 Crystallography

Reflections were collected either on a Bruker Smart Apex II CCD diffractometer at 293 K or on a Bruker Smart Apex CCD diffractometer at 100 K using MoK$_\alpha$ radiation (λ = 0.71073 Å). Structures were refined by full-matrix least-squares against F^2 using all

data (SHELX).[22] Non-hydrogen atoms were refined aniostropically. Hydrogen atoms were constraint in geometric positions to their parent atoms, with the exception of N-bound H-atoms which were refined without constraints. Crystallographic data for **2.2**, **2.3**, **2.4**, **2.5**, **2.6**·2H_2O, **2.7**, **2.8, 2.9**, **2.10**·2THF, **2.12**, **2.13**, **2.16**, **2.17**·4DMF, **2.18, 2.19, 2.20**·CH_3OH**,** and **2.22** are listed in Table A1.1, Appendix 1. The crystal structure of **2.4** contains one disordered iso-butyl group and one disordered iso-butylamino group. The solvated molecules of water and THF in the crystal structures of **2.6**.2H_2O and **2.10**.2THF, respectively, are disordered. One phenyl ring in **2.7** and three phenyl rings in **2.13** are disordered, **2.18 c**ontains three disordered c-hexyl groups, the amino groups of the phosphonium groups (P1) and methyl groups of six other i-propyl substitunets in **2.19** are disordered over two positions.Atom positions of the disordered groups in **2.4**, **2.6**.2H_2O, **2.10**.2THF, **2.13**, **2.18** and **2.19** were split over two positions and refined isotropically using similar-distance U-restraints. The disordered phenyl group of **2.7** was split over three positions and isotropically refined. Crystals of **2.4, 2.13, 2.17** and **2.21** diffracted weakly lacking observed reflections at higher angles, thus a cut-off at $2\theta = 45°$ was applied. Although the unit cell parameters of **2.16** show a good fit for Orthorhombic P, both the diffraction pattern and the crystal structure shows monoclinic P symmetry and no sign of twinning. Although a 2θ cut-off was applied for **2.17** and **2.18**, the R-factors of these two compounds could not be improved below 10%.

2.3 Result and discussion

2.3.1 Synthesis

The chlorides [P(NHR)$_4$]Cl, **2.1** (R = phenyl), **2.2** (R = *n*-propyl), **2.3** (R = *iso*-propyl), **2.4** (R = *iso*-butyl), **2.5** (R = *tert*-butyl) and **2.6** (R = cyclohexyl) were prepared according to the literature procedure reported by Huheey and co-workers.[21] The crystal structures of **2.2**, **2.3**, **2.4**, **2.5** and **2.6** were determined by X-ray crystallography and are discussed further below. The structure of **2.1** has been reported earlier by Steiner and co-workers.[12a]

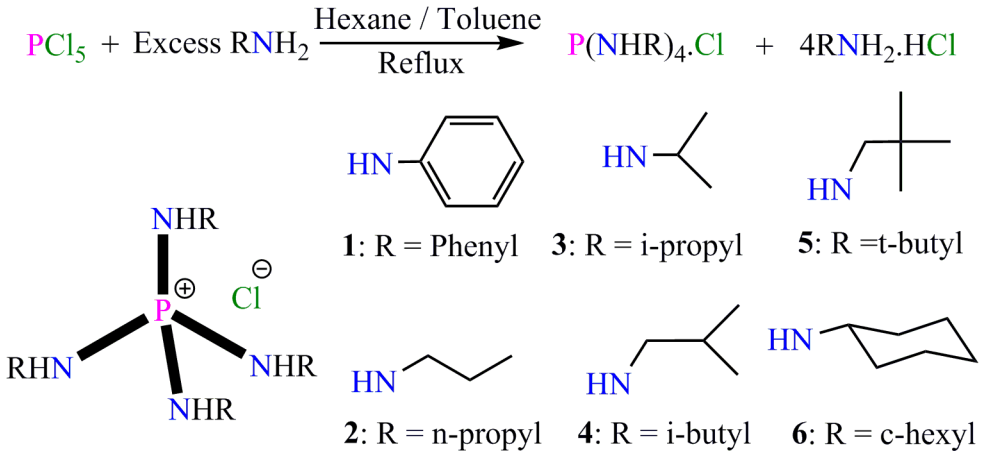

Scheme 2.1: Preparation of various phosphonium salts **2.1** to **2.6**. Reaction conditions: Toluene, 100-120 ^{o}C for **2.1**, **2.4** and **2.6**. Hexane, 70-80 ^{o}C for **2.2** and **2.3**. CCl_4-Toluene mixture, 100-110 ^{o}C for **2.5**.

Two routes have been employed to generate carboxylate salts: The first method constitutes anion exchange of chloride salts with sodium carboxylates, while in the second route, the phosphonium cations were deprotonated with base followed by the reaction of the resulting phosphine imine with a carboxylic acid. Anion exchange reactions were carried out in methanol or in a methanol/water mixture under reflux (Scheme 2.2). The reactions of sodium acetate proceeded with all phosphonium chlorides in methanol with precipitation of sodium chloride. The filtrates of each of these reactions were evaporated to obtain a crystalline solid which showed a strong IR absorption around 1590 cm^{-1} characteristic of the carboxylate group and the absorption bands of N-H (around 3100 cm^{-1}) and P-N bonds (between 550 and 1500 cm^{-1}). Crystals suitable for single crystal X-ray analysis were obtained from the reactions of **2.1** and **2.6**. X-ray crystal structure confirmed that **2.6** underwent complete ion exchange yielding the salt $[P(NHCy)_4][CH_3COO]$, while only partial exchange occurred during the reaction of **2.1**, which gave the mixed anion salt $[P(NHPh)_4]_2[CH_3COO][Cl]$ **2.7**. Unlike sodium acetate, the reactions of disodium oxalate were sluggish for all phosphonium chlorides due to the poor solubility of reactants, except **2.4**, which is partially soluble in water. The X-ray structure of the product of this reaction revealed the formation of $[P(NH^{i}Bu)_4]_2[C_2O_4]$ **2.9**. It should be noted that the ^{31}P-NMR spectra showed no significant change in chemical shifts upon ion exchange reactions in solution.

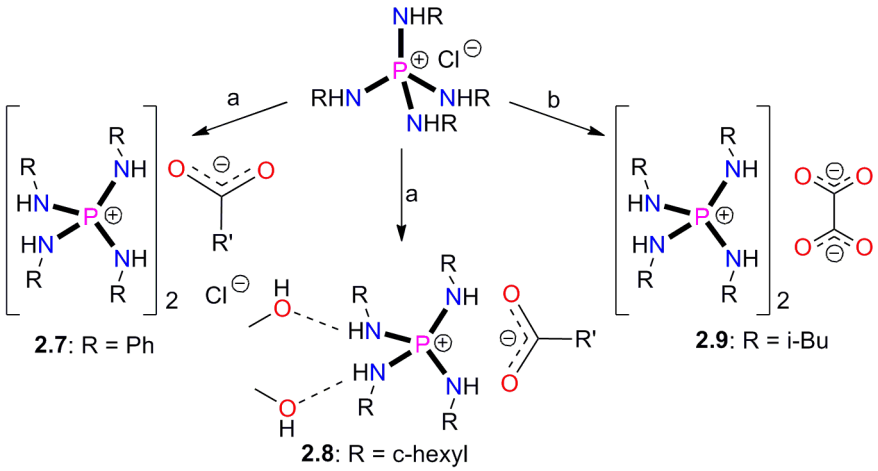

Scheme 2.2: Preparation of various phosphonium carboxylates **2.7** to **2.9**. Reaction conditions: (a) CH_3COONa, MeOH, 65˚-70˚C, -NaCl; (b) $(COONa)_2$, MeOH/H_2O in 1:1 ratio, 65˚-70˚C, -NaCl.

The second route to form carboxylates employs the neutral phosphine imine $[(PhNH)_3P(NPh)]$, which is obtained via deprotonation of **2.1** with a solution of KOH in methanol.[23] The ^{31}P-NMR spectrum of **2.10** shows a considerable upfield shift (δ = -4.3) compared to **2.1**. The infrared spectrum of **2.10** exhibits a very strong band at 1282 cm^{-1} characteristic of the P=N bond. Single crystals suitable of X-ray structure analysis were obtained from THF, which yielded the solvate **2.10**.2THF. In contrast to **2.1**, the chlorides **2.2**, **2.3, 2.4, 2.5** and **2.6** were hydrolyzed in the presence of KOH/MeOH generating the corresponding tris(alkylamino)phosphine oxides.

Reaction of the phosphorane **2.10** with mono carboxylic acids, such as acetic acid and cyclohexane carboxylic acid, in 1:1 molar ratio proceeded spontaneously. The ^{31}P-NMR spectrum of the reaction mixtures shows the presence of the phosphonium ion resonance at around 8.0 ppm and the disappearance of the peak due to **2.10** at δ -4.3 ppm. Extension of this re-protonation strategy to other di- and tri carboxylic acids such as malonic acid, oxalic acid, citric acid and 1, 3, 5-benzenetricarboxylic acid resulted in the formation of the corresponding phosphonium salts. The results of all these reactions are summarized in scheme 2.3. The crystal structures of **2.12**, **2.13** and **2.16** were established by X-ray crystallography.

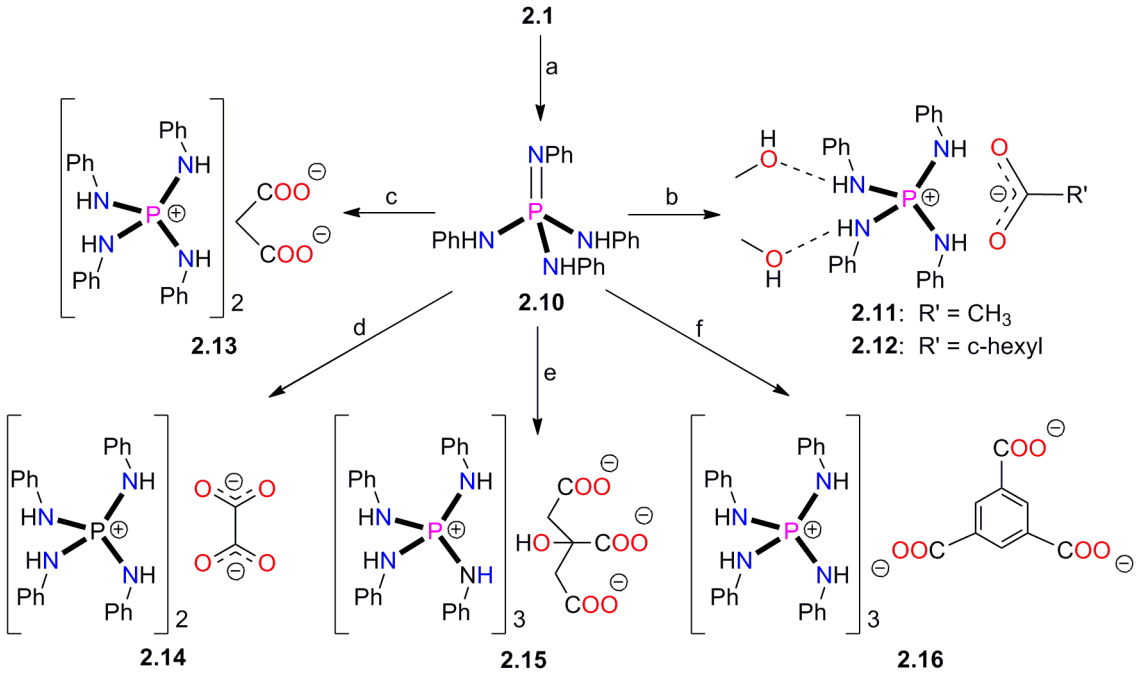

Scheme 2.3: Preparation of various phosphonium carboxylates **2.10** to **2.16**. Reaction conditions: (a) i. KOH/MeOH, -KCl, ii. H_2O; (b) R'COOH, MeOH, 65˚-70˚C; (c) $CH_2(COOH)_2$, MeOH, 65˚-70˚C; (d) $(COOH)_2$, MeOH ratio, 65˚-70˚C; (e) $C(OH)(COOH)(CH_2COOH)_2$, MeOH, 65˚-70˚C; (f) 1,3,5-$C_6H_3(COOH)_3$, MeOH, 65˚-70˚C

The phosphonium polyoxometalate salts **2.17-2.22** were prepared by a slightly modified procedure reported for tetra(alkylammonium) polyoxometalates. Accordingly, the chlorides salts **2.3**, **2.4** and **2.6** were treated with sodium molybdate dihydrate or sodium tungstate dihydrate in refluxing methanol/water mixtures. The pH of the medium was adjusted between 3 and 4 by adding conc. HCl (approx. 1.6 N). The products **2.17-2.22** were obtained as insoluble residues from the reaction mixtures and isolated by filtration (Scheme 2.4).

The single crystal X-ray analysis revealed that the compounds **2.17** and **2.18** contain an octamolybdate $[\beta\text{-}Mo_8O_{26}]^{4-}$ ion and **2.19** contain a decatungstate $[W_{10}O_{32}]^{4-}$ cluster. While the charge balance in **2.17** and **2.19** were provided by four $[P(NHR)_4]^+$ units, **2.18** was obtained as a salt of mixed cations with two $[P(NH^iBu)_4]^+$ and two $(^iBuNH_3)^+$ units. The formation of iso-butyl ammonium cation is due to the high acidity of the reaction medium which triggers cleavage of phosphonium cations in situ. In one of the reactions involving **2.6** and $Na_2WO_4.2H_2O$, the obtained product was totally insoluble in both polar and non-polar solvents including water and hence we were unable to characterize it.

The phosphonium chloride **2.3**, which contains relatively less bulky substituents, upon reaction with $Na_2MoO_4.2H_2O$ under the same conditions has lead to the formation of a keggin cluster instead of a Lindquvist cluster. The crystal structure analysis of **2.20** showed the formation of a phosphamolybdate $[PMo_{12}O_{40}]^{3-}$ cluster stabilized by three $[P(NH^iPr)_4]^+$ ions. Again the high acidity of the reaction medium causes the cleavage of the phosphonium cation producing the phosphate PO_4^{3-} ion in situ. To the best of our knowledge this is the first instance in which a heteropolymolybdate cluster stabilized by organic cations is produced in a two-component reaction. Similarly, reaction of **2.3** with $Na_2WO_4.2H_2O$ also resulted in a keggin type ion for **2.21**. Due to the poor quality X-ray data its crystal structure has not been discussed in this chapter (supporting information). Direct formation of a Keggin type cluster **2.22**, $[P(NHCy)_4]_3[AsMo_{12}O_{40}]$, has been found in a separate reaction involving the phosphonium chloride **2.6**, $Na_2MoO_4.2H_2O$ and sodium arsenate (Na_2HAsO_4).

In addition to crystallography, the phosphonium POM derivatives **2.17-2.22** were characterized by NMR, IR and ESI-Mass spectroscopic techniques. The phosphonium moieties in the compounds **2.17**, **2.18**, **2.19** and **2.22** showed a single peak at $^{31}P\{^1H\}$ NMR. The observed chemical shifts for these compounds are very close to their precursor phosphonium chlorides in d_6-DMSO ($(CD_3)_2SO$). The compounds **2.20** and **2.21** showed two resonances each in the $^{31}P\{^1H\}$ NMR: δ 22.7 & 0.7 ppm for **2.20** and δ 22.7 & -14.6 ppm for **2.21** indicating the presence of phosphonium and phosphate groups. While the phosphonium resonance at 22.7 ppm remains the same for both **2.20** and **2.21**, the phosphate resonance in **2.21** is considerably up field shifted indicating the increased shielding of inner phosphate group by the electron rich W centers.[24] The IR spectra of these compounds show characteristic peaks due to N-H protons (3300 cm^{-1}) and P-N groups (between 550 and 1500 cm^{-1}). In addition, the frequencies due to Mo-O and W-O groups around 750-950 cm^{-1} have been observed. The ESI-mass spectra in the negative ion mode obtained on the samples of **2.17-2.22** indicate the presence of POM clusters by showing peaks at their corresponding ½(*m/z*) values along with other prominent fragment ion peaks.

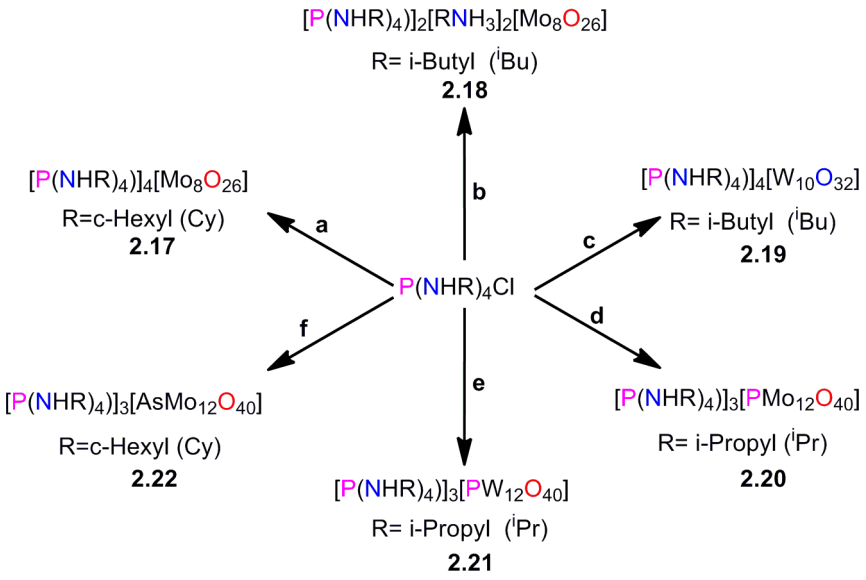

Scheme 2.4: Preparation for various iso- and heteropolymetallates assisted by organoamino-phosphonium cations **2.17** to **2.22**. Reaction conditions: (a) **2.6** , 2 $Na_2MoO_4.2H_2O$, HCl(aq), MeOH, 65-70 ºC; (b) **2.4**, 2 $Na_2MoO_4.2H_2O$, HCl(aq), MeOH, 65-70 ºC; (c) **2.4**, 2 $Na_2WO_4.2H_2O$, HCl(aq), MeOH, 65-70 ºC; (d) **2.3**, 2 $Na_2MoO_4.2H_2O$, HCl(aq), MeOH, 65-70 ºC; (e) **2.3**, $2Na_2WO_4.2H_2O$, HCl(aq), MeOH, 65-70 ºC; (f) 3eq. **2.6**, $12Na_2MoO_4.2H_2O$, Na_2HAsO_4, HCl(aq), MeOH, 65-70 ºC.

2.3.2 Crystal structures

The crystal structure of **2.1** has been reported earlier by Steiner and co-workers.[12a] It showed that the phosphonium cations and the chloride anions engage in hydrogen bonding interactions forming a zigzag one dimensional chain structure. The cations are disk-shaped; its four phenyl groups form a near planar arrangement. As a result there are two pairs of NH groups facing in opposite directions. The two NH bonds of each pair are aligned in parallel, acting as a double H-bond donor toward a chloride ion, which in return binds two phosphonium cations. Compound **2.2**, which contains the least bulky phosphonium cation used this study, crystallizes in space group *C2/c*. It is the only halide structure of this series that does not form chain-type structure, but forms a layered structure with the topology of a (4,4) net. Every phosphonium ion binds to four chloride ions via NH...Cl bonds and in return every chloride ion coordinates to four cations. The 2D-sheet features a series of 12-membered rings, graph set notation[25] $R_4^2(12)$, each containing two phosphonium and two chloride ions.

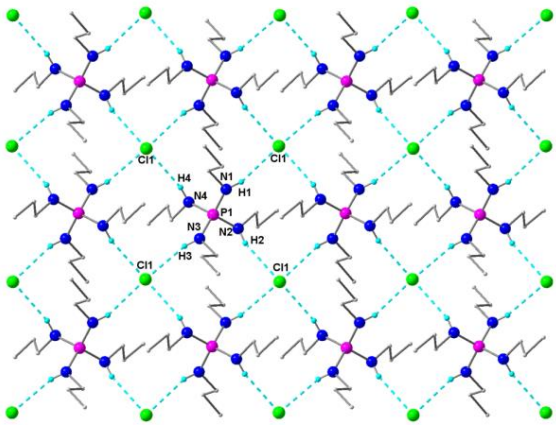

Figure 2.2: (a) Crystal structure of **2.2**.

The crystal structures of **2.3-2.5** exhibits the chain-type topology observed in **2.1** where each link between phosphonium and chloride ions features two H-bonds to give $R_2^1(6)$ ring motifs. The *iso*-propyl derivative **2.3** crystallizes in the tetragonal space group *P-42(1)c*. The cation exhibits point group symmetry S4. The hydrogen bonded assembly of phosphonium and chloride ions forms a linear chain along [001].

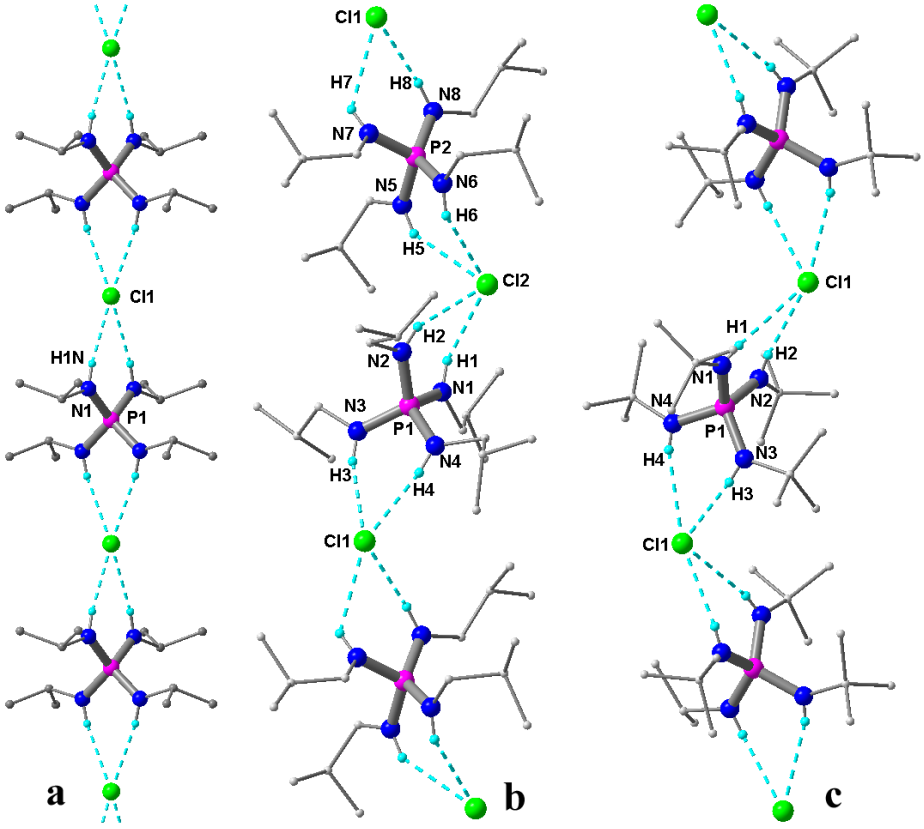

Figure 2.3: 1D-chain structures of **2.3** (a), **2.4** (b) and **2.5** (c).

The supramolecular structures of the *iso*-butyl derivative **2.4** and the *tert*-butyl derivative **2.5**, which crystallise in space groups *P2(1)/c* and *P2(1)2(1)2(1)*, respectively, consist of 1D-*zigzag* chain (Figure 2.3). Crystals of the cyclohexyl derivative **2.6** were obtained in the form of the hydrate **2.6**·$2H_2O$, which crystallizes in space group *C222(1)*. Again, the ionic moieties form a hydrogen bonded chain, which however is curled into a helical structure, containing six units of $[P(NHCy)_4]Cl$ per turn. Every turn contains four of chloride and four phosphonium ions that reside on general positions and two chloride ions and two phosphonium ions occupying two-fold rotation axes. The phosphonium ions that are located on general positions show a coordination behavior equivalent to that observed in **2.1** and **2.3-2.5** involving all NH groups, while the phosphonium ions located on the 2-fold axes engage with only two NH groups in the bridging of chloride ions. The other two NH groups bind to water molecules, which in turn bind to chloride ions and thereby connecting two adjacent helices via H-bonding (Figure 2.4).

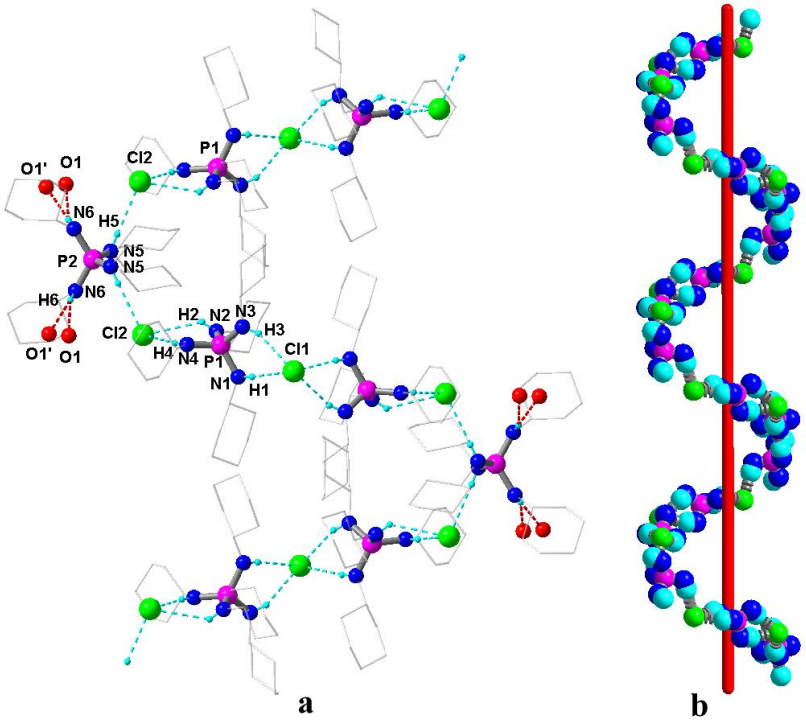

Figure 2.4: (a) 1D-helical chain structure in **6**.$2H_2O$. (b) View along the helical axis.

The hydrogen bond distances and angles found in the phosphonium chlorides range by a close margin which are comparable with those of organoammonium chloride salts.[26] The metric parameters associated with the hydrogen bonding interactions in **2.2-2.6** are given in Table A1.2, Appendix 1. The P-N bond distances found in **2.2-2.6** are similar to **2.1** and $[P(NH_2)_4]Cl$.[27] Comparison of N-P-N bond angles in **2.2-2.6** have lead to some

interesting observations. While the phosphonium bond angles in **2.2** are close to 109°, two varied types of N-P-N bond angles are found for **2.3-2.6** indicating different types of deviations from the ideal tetrahedral angle. More acute angles (avg 100.8(9)°) are observed for N-P-N units involved in chelating hydrogen bonding interactions and wider angles (av.116.46(7)°) are found for the other N-P-N segments present in non-chelating environment (Table A1.3, Appendix 1). Although the exact reason for distortion from the perfect tetrahedral geometry in terms of steric and electronic factors is unclear, it appears to be partially controlled by hydrogen bonding interactions as well.

The crystals of **2.10**.2THF were obtained by slow evaporation of a THF solution of **2.10** at room temperature. The molecule **2.10**.2THF crystallized in the orthorhombic space group *Aba2*. The phosphonium cation occupies a two-fold axis of symmetry featuring two pairs of crystallographically unique N-atoms. The P1-N2 bond distance (1.617(2) Å) is considerably shorter than P1-N1 distance (1.659(2) Å). This distance is somewhat between P-N bond lengths observed in imino- and amino phosphorus compounds. This suggests that the imino group is disordered over the two positions N2 and N2a. Equally the two THF molecules, which are bonded to either side of the phosphonium ion via NH...O contacts, are disordered over two positions. Resolving the disorder gives one THF molecule that is bonded to two amino functions, while the other forms a single contact (Figure 2.5).

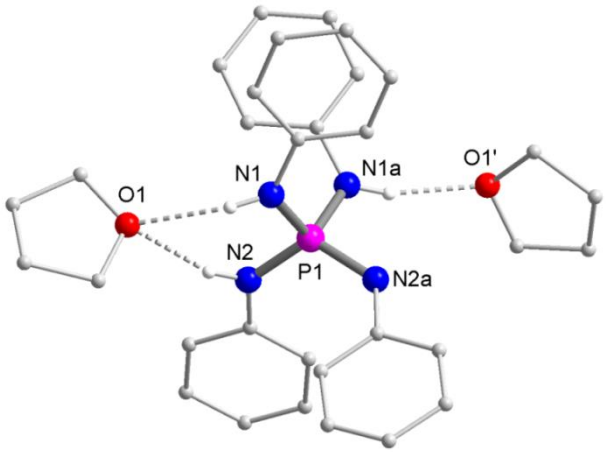

Figure 2.5: Molecular structure of **2.10**. The disordered THF fragments are omitted for clarity. P1-N1: 1.659(2) Å; P1-N2: 1.617(2) Å; N2-P1-N(1): 99.93(12)°; N2-P1-N2a: 118.43(18)°; N2-P1-N1a: 115.00(11)°; N1a-P1-N1: 108.91(17)°. D(N1-H1…O1): 2.20(5) Å; <(N1-H1…O1): 146.9(3)°; D(N1-H1…O1): 2.08(5) Å; <(N1-H1…O1): 162.9(3)°; D(N1-H1…O1): 1.98(5) Å; <(N1-H1…O1): 160.4(3)°.

Structural determination of the phosphonium monocarboxylate salts **2.7**, **2.8** and **2.12** showed interesting supramolecular variations. The structure of **2.7** containing mixed chloride and acetate ions is given in Figure 2.6. It shows the presence of two crystallographically unique phosphonium units (centered on P1 and P2), which are linked together by an alternating array of N-H…O and N-H…Cl hydrogen bonds in a zigzag manner. The chloride ion bonds with the N-H protons in bridging tetradentate coordination equivalent to that found in **2.1**. The acetate ion interacts with its neighbouring phosphonium segments via both bridging pyramidal and chelating bidentate modes giving rise to the 1D-chain propagation.

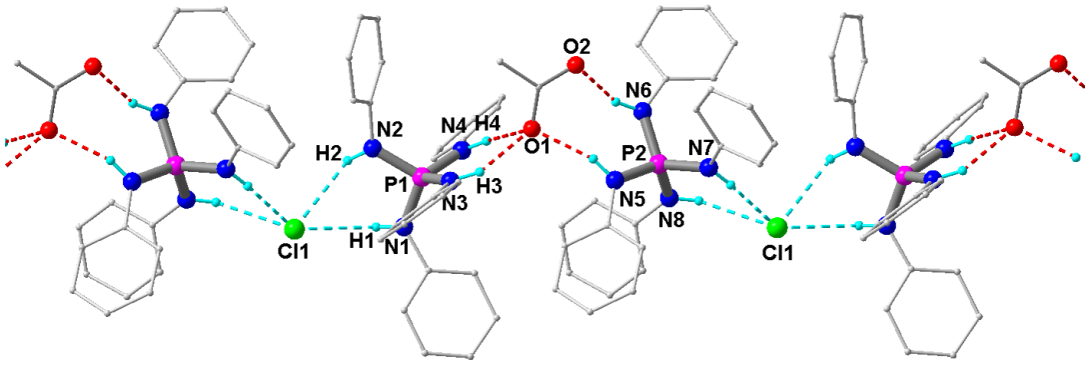

Figure 2.6: Formation of zigzag H-bond assisted chain in **2.7**.

The X-ray structure analysis revealed that **2.8** crystallized in tetragonal space group *P4(3)2(1)2* in which 'P1' and the acetate carbon atoms sit at the 2-fold axes of rotation (Figure 2.7a). Compound **2.12** crystallized in monoclinic space group *P2(1)/c* where the phosphonium and $CyCOO^-$ units take up the general positions (Figure 2.8a). The crystal structures of **2.8** and **2.12** shows that one of their two phosphonium HN-P-NH segments interact with the carboxylate moiety (CH_3COO^-/$CyCOO^-$) through the chelating double hydrogen bond interaction (Figure 2.7a). The other segment engages in H-bonding two methanol molecules which in turn act as a hydrogen bond donor to carboxylate ions of the neighboring phosphonium units. Unlike **2.7**, each carboxylate oxygen is involved in a bifurcated interaction with N-H and O-H protons resulting in the formation of a grid like three dimensional network in **2.8** (Figure 2.7b) and 2D-sheet structure in **2.12** (Figure 2.8b). Although the basic structures of **2.8** and **2.12** are very similar, their supramolecular structures are apparently different. The change in supramolecular structure is presumably attributed to the mode of interaction of solvent molecules with the ionic moieties. A closer look at the grid structure in **2.8** shows the formation of helical chains mediated by solvated methanols which tethers the phosphonium acetate

ion pair segments on either sides of the helix (Figure 2.7c). On the other hand the interaction of methanol, $CyCOO^-$ and two amino protons in **2.12** forms *zigzag* hydrogen bonded chain (Figure 2.8b).

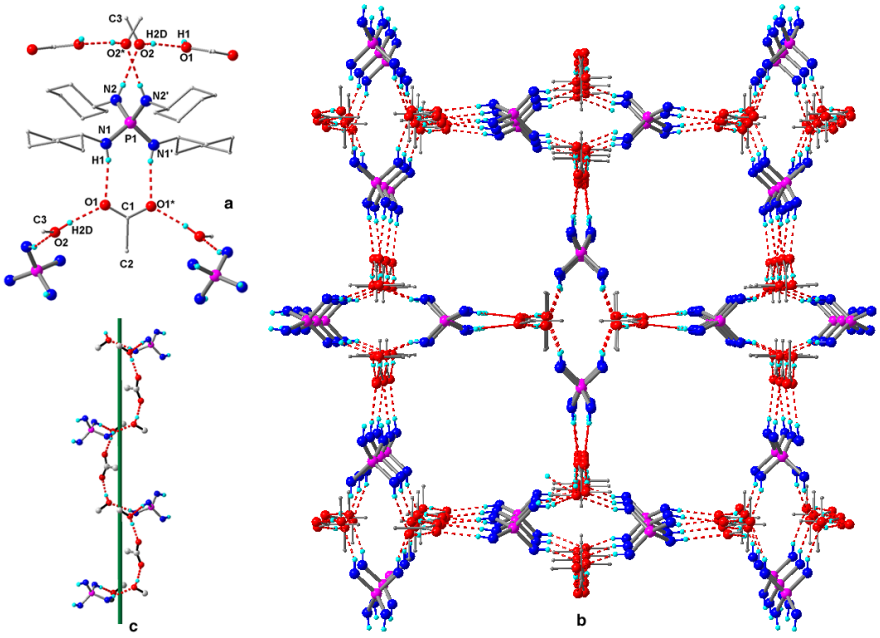

Figure 2.7: (a) Molecular structure of **2.8**, (b) formation of 3D-grid structure via by N-H…O and O-H…O interactions, (c) view of the helical chains within the Grid structure.

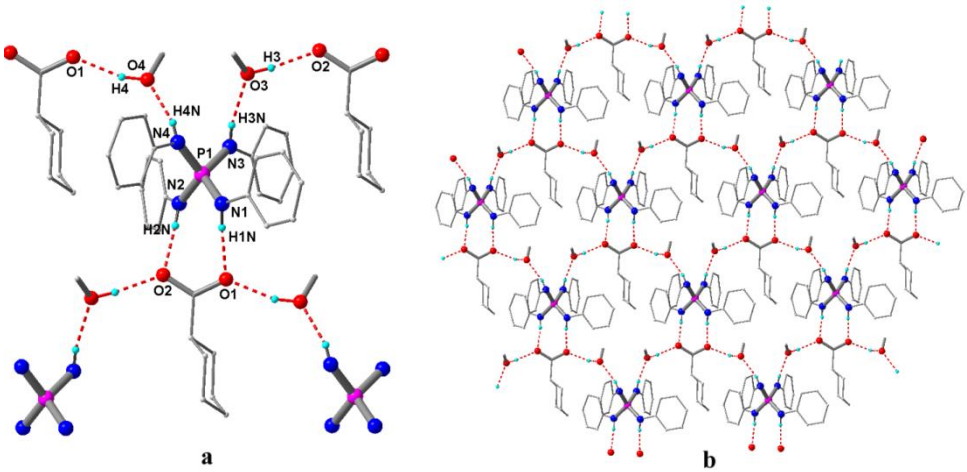

Figure 2.8: (a) Crystal structure of **2.12** and (b) its propagation into 2D-sheet structure.

Thus the helical arrangement in **2.8** leads to 3D-grid structure and the zigzag arrangement in **2.12** leads to 2D-sheet structure. The N-H…O hydrogen bond distances found in **2.8** and **2.12** are stronger measuring around 1.95 (3) Å (avg) and their H-bond angles are close to linearity (avg 170.1(3)º). The corresponding methanol donor R-OH…O^- distances in these salts are found to be shorter (avg 1.83(3) Å) than the acceptor NH…OH (avg 2.06(2) Å) distances. The formation of supramolecular structures in **2.8** and **2.12** also gives rise to large macrocyclic rings. The 44-

membered macrocyclic rings (Figure **2.9a**) in **2.8** contains five phosphonium units, five acetate ions and six methanol molecules (graph set $R_{16}^{12}44$). The 28 membered rings in **2.12** consists of three phosphonium cations, three $CyCOO^-$ ions and four methanol molecules (Figure 2.9b), which adapt to the graph set $R_8^8 28$ topology.

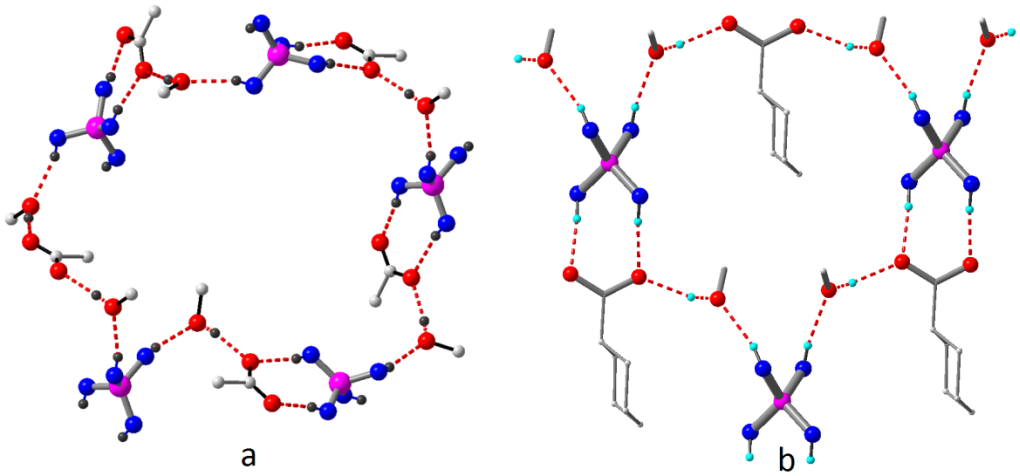

Figure 2.9: (a) Formation of large macrocyclic ring in **2.8** and (b) **2.12**.

The structure of a phosphonium dicarboxylate salt containing the oxalate anion **2.9** is given in Figure 2.10. The compound crystallized in cubic space group *Pn-3n* with its asymmetric unit containing one fourth of the phosphonium moiety and one fourth oxalate ion. The unique oxalate carbon atom is positionally disordered over four sites, pointing to either a vertical or horizontal alignment of the oxalate ions with respect to the phosphonium cation. Analysis of the hydrogen bonding interactions in **2.9** shows the formation of a tightly knitted cubic 3D-network. Each oxalate ion is surrounded by four phosphonium units in a planar fashion which offers four pairs of double H-donors (Figure 2.10a). The oxalate ion in return binds to the four phosphonium units via bifurcated and chelating interactions. On the other hand the phosphonium N-P-N segment on either sides of P-atom is interacting with two oxalate moieties which are aligned orthogonal to each other (Figure 2.10a). Thus the orthogonal arrangement of oxalate ions at alternate positions and their bifurcated H-bonding interactions with phosphonium cations helps the molecule propagate in the 3D-network (Figure 2.10b). The schematic representation of the arrangement of phosphonium (pink spheres) and oxalate ions (black spheres) in the cubic network is shown in (Figure 2.10d) which represents a hitherto unknown type of arrangement of atoms involving amino protons and carboxylate oxygens.[28-29] Each cubic subset of the 3D-network is connected at alternate corners and forms large macrocyclic rings of approximately 14 Å diameters

(Figure 2.10c). These rings are formed by stitching six phosphonium and six oxalate ions as represented by graph set $R_{12}^{6}(28)$ topology in their shortest route.

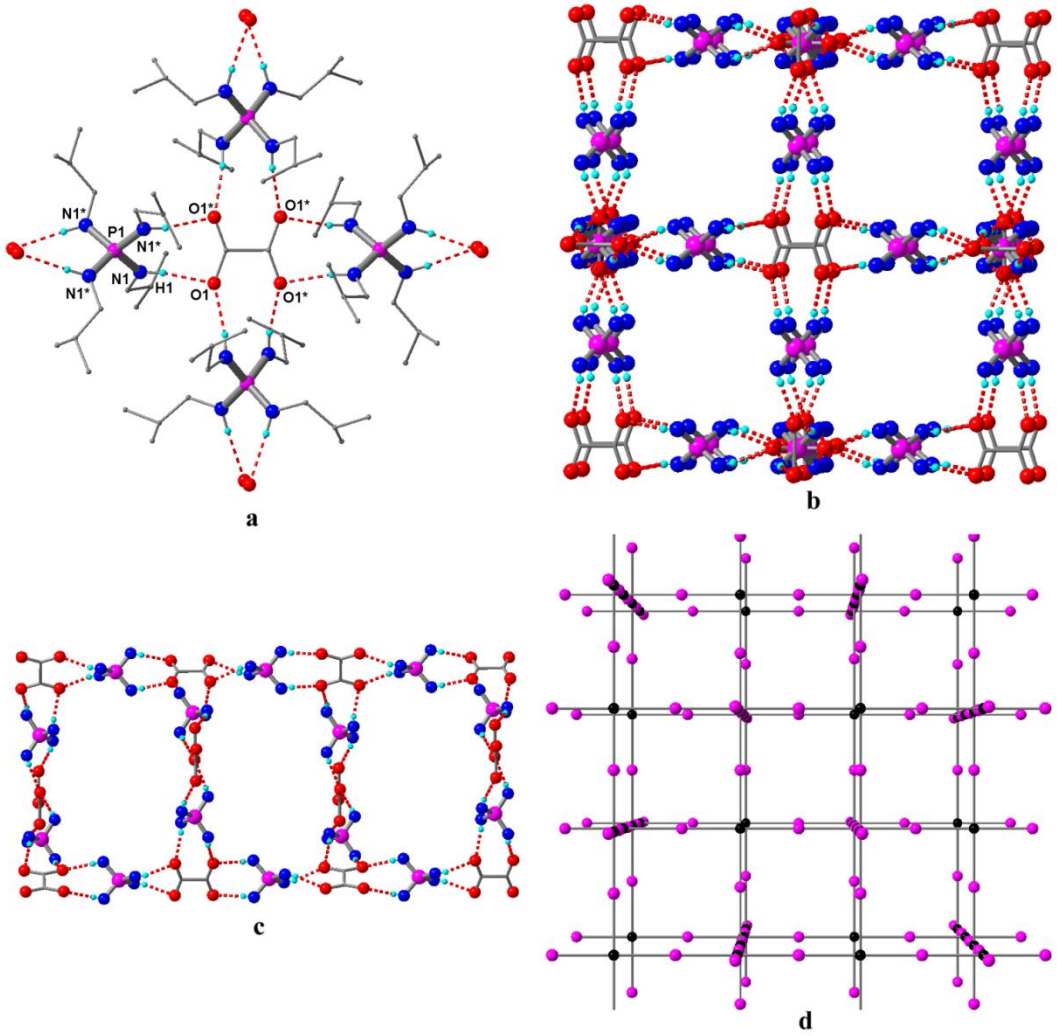

Figure 2.10: (a) Crystal structure of **2.9**. (b) Formation of cubic 3D-network mediated by N-H…O interactions. The *iso*-butyl groups have been omitted for clarity. (c) View of the 28-membered macrocyclic rings, (d) Schematic representation of the arrangement of the cations (pink spheres) and anions (black spheres) in the cubic network.

Moving from rigid oxalate ion to the flexible dicarboxylate ion such as malonate anion gives rise to a completely different supramolecular structure. The malonate salt **2.13** crystallizes in tetragonal space group *I4(1)cd* in which the malonate group and two phosphonium moieties occupy the general positions. The malonate ion interacts with four phosphonium moieties with each of its carboxylate end offers tetradentate interactions to two phosphonium units through chelating and bridging hydrogen bonds analogous to the acetate ion interaction found in **2.7** (figure 2.11a). Unlike the oxalate ion which interacts with four phosphonium units in a planar fashion, the malonate ion in

2.13 hydrogen bonds to four phosphonium units in a concerted manner. The overall result of these hydrogen bonding interactions in **2.13** is the generation of a tubular three dimensional network (Figure 2.11b). The tubular structure can be viewed as the stacking of an array of large macrocyclic rings facilitated by the flexible nature of malonate chains (Figure 2.11c). These rings are nanoscopic in dimensions and are fused by the aid of six phosphonium and six malonate moieties (graph set $R_{12}^{10}(52)$).

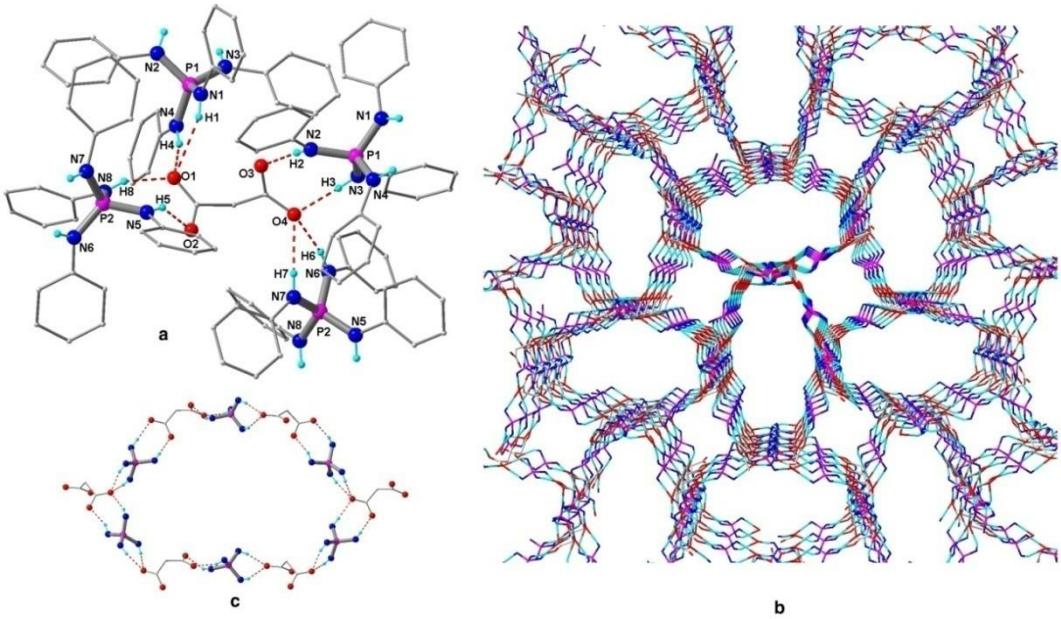

Figure 2.11: (a) Molecular structure of **2.13** and its H-bonded neighbors. (b) View of tubular 3D-structure. The phenyl rings omitted for clarity. (c) 52-membered macrocycle within the tubular assembly.

The phosphonium salt **2.16** containing the 1, 3, 5-benzene tricarboxylate trianion (trimesic anion) crystallized in the monoclinic space group *Pc*. The asymmetric unit of this molecule consists of six phosphonium moieties and two trianions which are labeled for convenience as T1 and T2 (Figure 2.12a). Each trianionic motif is surrounded by six phosphonium cations with every carboxylate end of it is hydrogen bonded to two phosphonium units via tetradentate interactions. The step-wise assembly of the 3D-supramolecular structure can be understood as follows. Out of the six phosphonium moieties, two of them, centered on P1 and P3, are solely involved in hydrogen bonding the trimesic unit labeled T1 into a planar (4, 4) sheet (Figure 2.12b). Likewise, the phosphonium units P2 and P5 tether the trimesic units of T2 in the 2-D manner. The sheets of T1 and T2 are superimposing onto each other which are further linked by the remaining two phosphonium moieties, centered on P4 and P6, leading to a 3-D network.

Formation of the three dimensional structure in **2.16** accompanies two different types of macrocyclic rings (Figure A1.2, Appendix 1). While the individual (4, 4) sheets of T1 and T2 form $R_8^8(44)$ rings, macrocycles situated in-between the sheets of T1 and T2, involving the bridging phosphonium connectors of P4 and P6, form $R_8^7(42)$ rings.

The hydrogen bond details associated with the compounds **2.7**-**2.16** is listed in Table A1.2, Appendix 1. The N-H…O bond distances and angles found in them are comparable to the carboxylate salts of protonated amines.[30] In all these carboxylate salts the phosphonium moieties interact with the carboxylate groups in a chelating double H-interaction. As a result N-P-N bond angles in these salts deviate from ideal tetrahedral angle in which more acute angles of around 100˚ are again found for the N-P-N segments involved in chelating interactions (Table A1.3, Appendix 1).

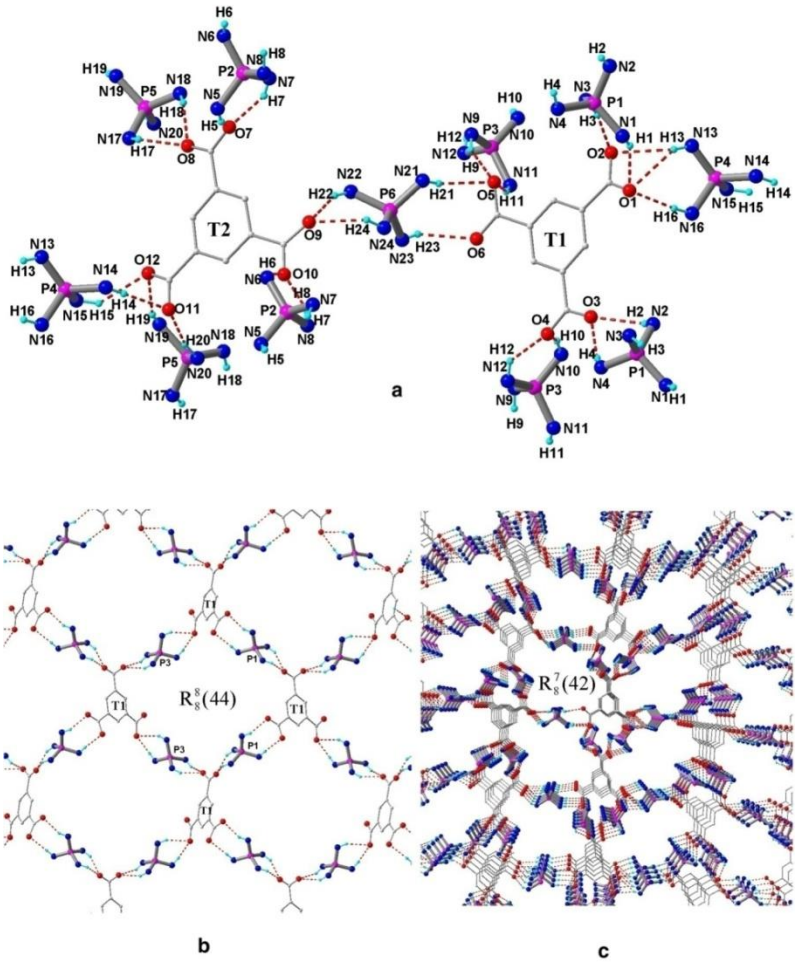

Figure 2.12: (a) Molecular structure of **2.16** with its immediate H-bonded neighbors. The phenyl rings on amino groups have been omitted for clarity. (b) View of the individual planar (4,4)-sheet within the 3D-assembly. (c) Formation of the 3D-supramolecular network mediated by N-H…O interactions.

The compounds **2.17** and **2.18** which contain the octamolybdate $[\beta\text{-}Mo_8O_{26}]^{4-}$ cluster were crystallized from DMF/Methanol. The single crystal X-ray analysis revealed that both of them were crystallized in the monoclinic space group *P2(1)/c*. Compound **2.17** was obtained as solvent adduct containing four DMF molecules. The asymmetric unit of **2.17**.4DMF contains one half of the $[\beta\text{-}Mo_8O_{26}]^{4-}$ unit, two phosphonium cations and two DMF molecules. Similarly, the asymmetric unit of **2.18** includes one half of the $[\beta\text{-}Mo_8O_{26}]^{4-}$ unit, one phosphonium cation and an ammonium cation.

The octamolybdate cluster in **2.17** is surrounded by six phosphonium cations and their c-hexyl substituents provide a tight lipophilic sheath around the cluster core (Figure 2.13a). The $[\beta\text{-}Mo_8O_{26}]^{4-}$ cluster shows an approximate C_{2v} symmetry and interacts with the phosphonium moieties by accepting hydrogen bonds via its terminal and bridging oxo groups. The phosphonium unit centered on P1 hydrogen bonds to the octamolybdate cluster through one of its chelating HN-P-NH segments, while its other HN-P-NH segment bonds with two DMF molecules in a non-chelating fashion. On the other hand, the second phosphonium unit centered on P2 utilizes both of its HN-P-NH chelates in linking the adjacent cluster moieties via hydrogen bonding giving rise to a layered structure with the topology of a (4, 4) net (Figure 2.13b).[31] Viewing the network along the 'c' axis shows that the phosphonium groups of the P1 centers and the DMF molecules hydrogen bonded to them are located above and below the 2D-sheet (Figure 2.13c).

In **2.18** the $[\beta\text{-}Mo_8O_{26}]^{4-}$ cluster is surrounded by four phosphonium and four ammonium cations (Figure 2.14a). The rise in the number of surrounding ligands in **2.18** compared to **2.17** is due to both the decrease in phosphonium steric bulk as well as the smaller size of the $[^{i}BuNH_3]^{+}$ ions. Similar to **2.17**, the phosphonium units in **2.18** are hydrogen bonded to the octamolybdate clusters through its HN-P-NH chelates resulting in a layered arrangement. Interaction of the two $[^{i}BuNH_3]^{+}$ ions with the octamolybdate ions leads to a 1D-chain structure (Figure 2.14c) which runs orthogonal to the sheet structure formed by the phosphonium ions. In total, all these interactions involving phosphonium and ammonium cations give rise to a 3D-grid structure for **2.18** (Figure 2.14b).

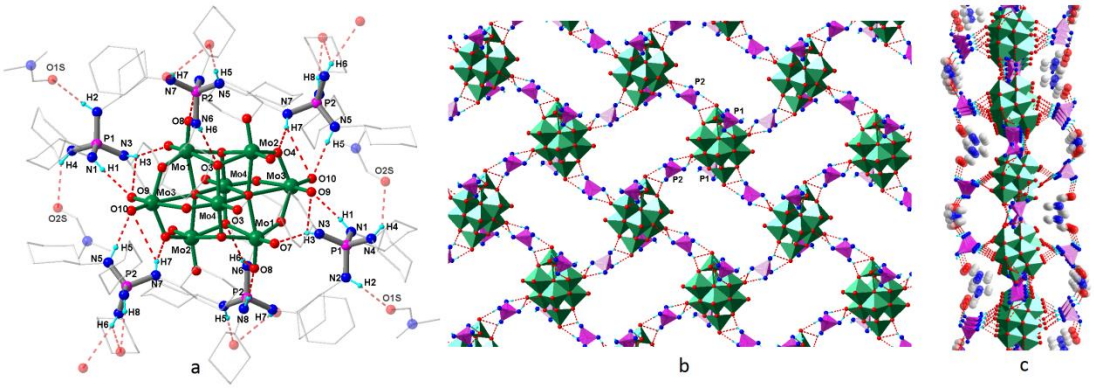

Figure 2.13: (a) Core view of the octamolybdate cluster in **2.17**, (b) view of the 2D-sheet along the [100] plane. The POM units are shown as green octahedron and the phosphonium units as pink tetrahedron. The c-hexyl and DMF molecules are omitted, (c) view along the c axis.

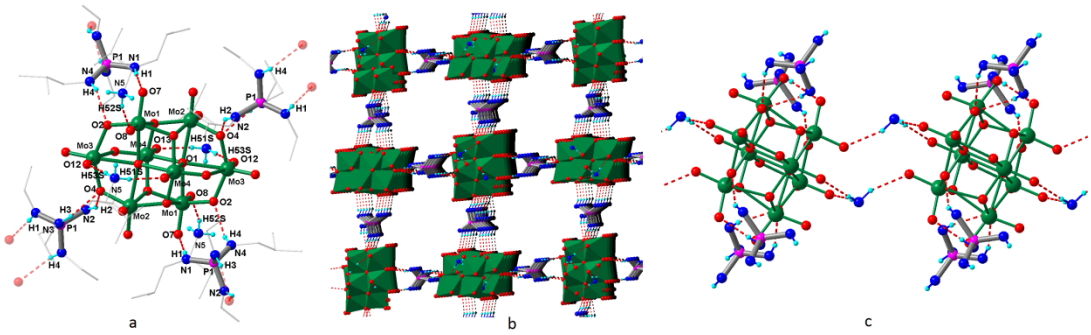

Figure 2.14: (a) Core view of **2.18** showing the arrangement of cations and anions, (b) View of the 3D-framework along the 'a' axis. The POM units are shown as green octahedron; i-butyl groups are omitted.

The compound **2.19** which contains the decatungstate $[W_{10}O_{32}]^{4-}$ cluster, stabilized by four $[P(NH^{i}Bu)_4]^{+}$ ions, is crystallized in the monoclinic spacegroup *P2(1)/n* with its asymmetric unit consisting of two phosphonium cations and one half of the cluster moiety. The point group symmetry exhibited by the anionic cluster is D_{4h}, while a local D_{2d} symmetry is observed at the phosphonium centers. In the crystal structure eight phosphonium units encompass the decatungstate cluster out of which four of them, situated near the corner tungsten atoms (W5), are involved in linking the clusters via HN-P-NH chelates into a 2D-layer. The remaining four phosphonium units that are at the centre act as pillars and connect the adjacent layers into a 3D-network (Figure 2.15).

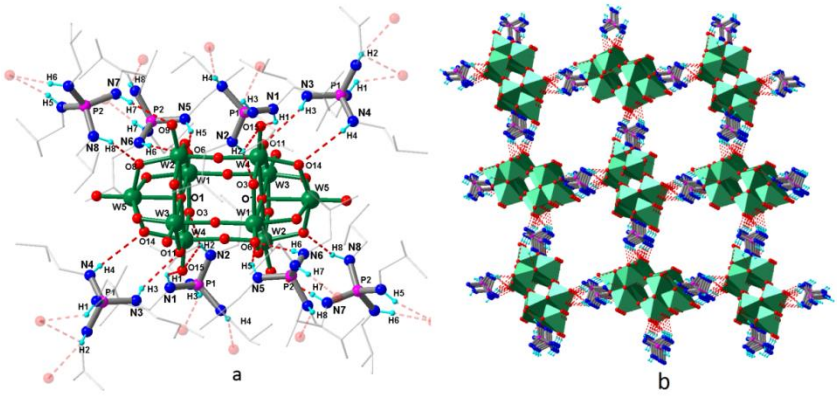

Figure 2.15: (a) Core view of **2.19** showing the arrangement of cations and anions, (b) View of the 3D-framework along the 'a' axis. The POM units are shown as green octahedron; i-butyl groups are omitted.

The Keggin compound **2.20** was crystallized as its methanol adduct in the orthorhombic spacegroup *Pbcn*. The asymmetric unit in **2.20** contains two cluster moieties and a methanol at two-fold axes of symmetry and three $[P(NH^{i}Pr)_4]^+$ ions located at the general positions. The amino groups of one of the phosphonium groups (P1) and i-propyl substituents on the other two phosphonium units are disordered over two positions. Additionally, the oxygen atoms attached to the central phosphate group (P6) in one of the cluster moieties are disordered over two sites. Each phosphamolybdate cluster core is surrounded by eight phosphonium cations and interacts with them via terminal and bridging oxo groups (Figure 2.16a). One of the two HN-P-NH segments in every phosphonium cation makes chelating interactions whereas the other one is engaged in non-chelating contacts.

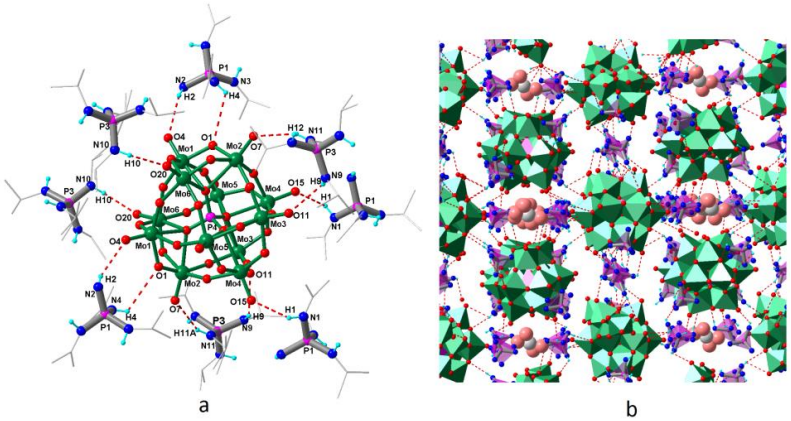

Figure 2.16: (a) View of one of the phosphamolybdate core in **2.20**.CH_3OH and (b) its three dimensional network. Green octahedron represents the Keggin clusters, phosphonium centres as pink tetrahedron and disordered methanol in the space fill model.

Three out of the four amino substituents in each phosphonium unit interacts with two phosphamolybdate clusters and forms a 2D-layer (Figure 2.17) along the [010] plane. The protons of the remaining amino groups (labelled N1, N5 and N10) are projected away from the plane and link the neighbouring layers into a three dimensional network. The construction of supramolecular structure in **2.20** also accompanies the formation of a channel structure. These channels are hydrophilic and are occupied by disordered methanol molecules (Figure 2.16b).

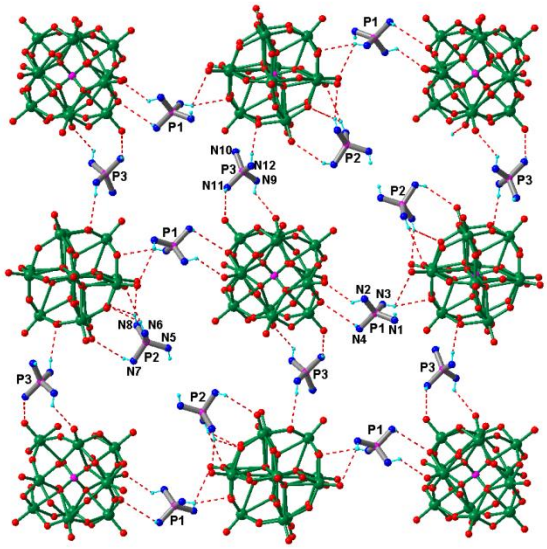

Figure 2.17: Formation of 2D-layers in **2.20**.CH_3OH via the interaction of three amino residues of each phosphonium unit. Note the outward projection of the fourth amino residue from the plane.

The compound **2.22** was crystallized in chiral monoclinic spacegroup *P2(1)* where the $[AsMo_{12}O_{40}]^{3-}$ cluster and three $[P(NHCy)_4]^+$ ions were present in the asymmetric unit. Unlike **7**.CH_3OH, the Keggin cluster in **2.22** is surrounded by only six phosphonium units due to bulkiness of the c-hexyl substituents. Among the three phosphonium units, two of them (P1 and P2 centers) are involved in chelating interactions on either side of their HN-P-NH segments similar to **2.18**. Interestingly the hydrogen bonding interactions in **2.22** have resulted in the formation of a helical 3D-assembly. The stepwise arrangement of the helical assembly can be understood as follows. The interaction of the Keggin cluster with the phosphonium units of P2 first forms a helical chain that runs along the 'a' axis (Figure 2.18b). Each turn of the helical chain contains three cluster moieties and three phosphonium ions. The individual helices are then connected to each other by the bridging interaction of the HN-P-NH chelates centered on P1 forming a 2D-

helical sheet (Figure 2.19). The third phosphonium unit that belong to P3 further connects these 2D-sheets, through a non chelating interaction of its amino groups (N9-H9…O30 and N11-H11…O5), into a 3D-helical assembly (Figure 2.18c). The other two amino groups of P3 (N10-H10 and N12-H12) did not find any suitable hydrogen bond acceptor and remain uncoordinated. It is worthwhile to note here that formation of helical supramolecular assemblies have also been envisaged for $[P(NHCy)_4]^+$ ion in its chloride and acetate salts. Although the exact reason for this is unclear, the bulkiness of the c-hexyl substituents coupled with its structural flexibility have presumably played a vital role.

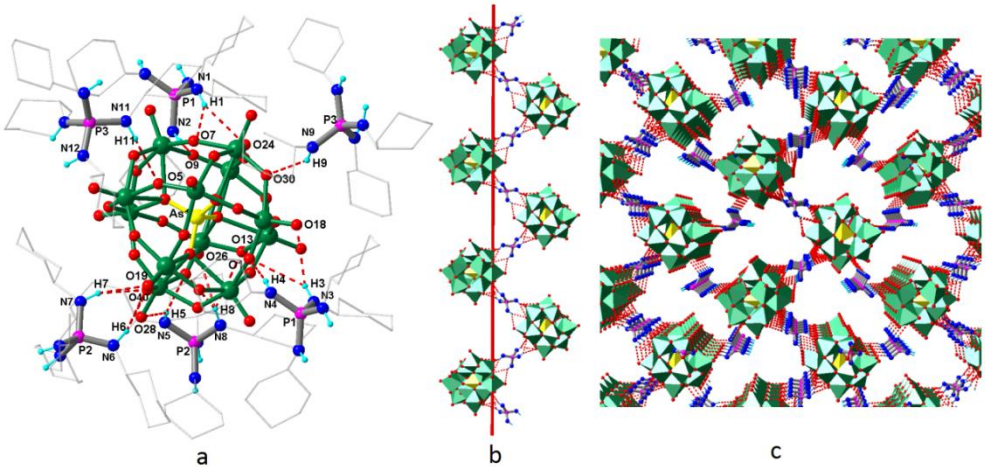

Figure 2.18: (a) View of the phosphamolybdate core in **2.22**, (b) Formation of helical chain mediated by phosphonium centres labelled P2, (c) View of the 3D-helical assembly. Green octahedron represents the Keggin clusters.

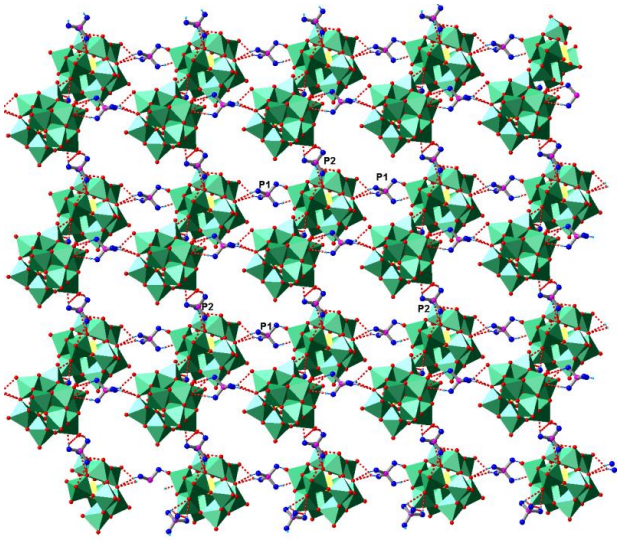

Figure 2.19: 2D-Projecction of the helical sheets along the ab-plane in **2.22**. The Phosphonium unit labeled P1 connects the adjacent helical chains into a 2D-sheet.

The hydrogen bond details related to the compounds **2.17-2.22** are given in Table A1.4, Appendix 1. The N-H…O bond distances observed in all these compounds range from 2.10 to 3.00 Å indicating strong to moderately weak interactions. It has been found that the N-H…O distances associated with terminal M=O groups are stronger compared to those related with M-O-M groups. The P-N bond distances observed in compounds **2.17-2.22** fall in the usual range and found between 1.59 and 1.65 Å (Table A1.4. appendix 1). The phosphonium cations involved only in chelating interactions showed two varied bond angles: the two N-P-N segments which are part of chelating H-bonding showed an acute angle of around 100º (av.), while the other two N-P-N angles were nearly 116º (av.). On the other hand, bond angles of around 109º were found for phosphonium groups in which none of the N-P-N segments have chelating contacts.

2.3.3 Thermal Analysis

Thermogravimetric analysis (TGA) data was obtained on the samples of some of the representative phosphonium carboxylates and polyoxometalates. Thermal behavior of all these samples indicates that their supramolecular structures are stable at sufficiently high temperatures. The TGA curve of **2.8**.2CH_3OH shows an initial weight loss of about 11.5% at 175°C matching with the loss of two solvated methanol molecules. Further weight loss of about 73% is accompanied by decomposition at about 275°C corresponding to the acetate and cyclohexyl groups. The final char-yield at 500 $^{\circ}$C is 15.5 % indicates to the species of formula PN_4. TGA data of **2.9** shows a single weight loss onset at 225 $^{\circ}$C and a complete decomposition at around 380 $^{\circ}$C. The TGA plot of **2.13** reveals a two stage weight loss onset at 150 $^{\circ}$C and upto 275 $^{\circ}$C the observed weight loss is 69% (obtained from DTG analysis) which corresponds to the elimination of all the phenyl groups. A further decrease in weight of about 12% is observed in the temperature region between 275 $^{\circ}$C and 450 $^{\circ}$C indicating the loss of malonate group. The remaining char-yield of 19% at 1000 $^{\circ}$C points to the PN_4 species. The TGA trace of **2.16** shows a sharp decomposition at 250 $^{\circ}$C and a weight reduction of about 60% in the region between 250 $^{\circ}$C and 600 $^{\circ}$C indicating the loss of most of the organic groups. Above 800 $^{\circ}$C (not shown in the figure) a further decline in weight was observed which points to exclusion of the remaining organic species (Figure 2.20).

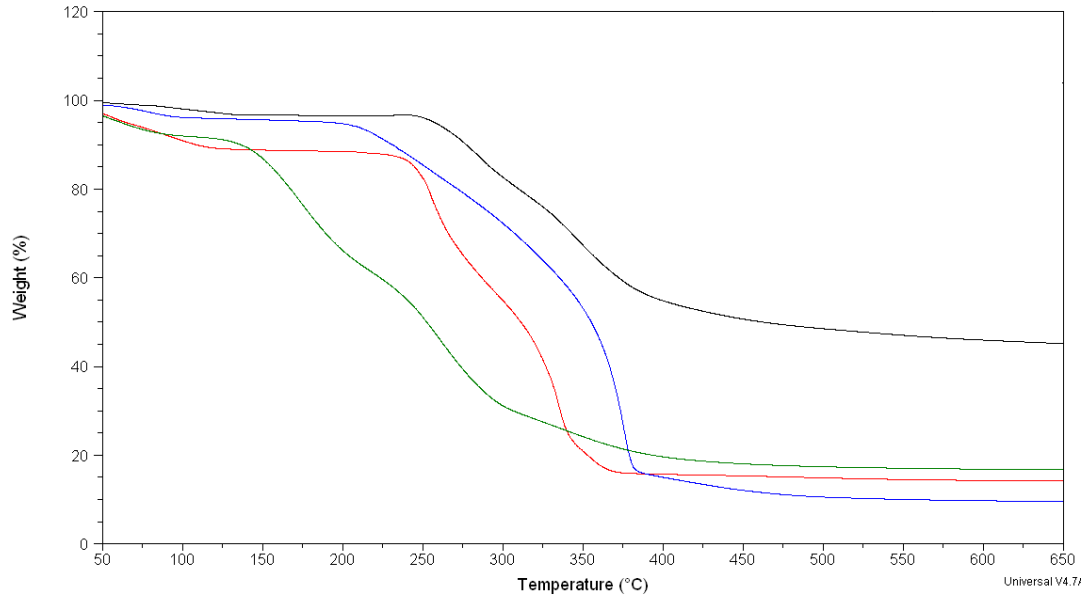

Figure 2.20: TGA trace of the phosphonium carboxylates **2.8**.2CH_3OH (red), **2.9** (blue), **2.13** (green) and **2.16** (black)

Compounds **2.17-2.22** shows that these hybrid solids are stable over a range of temperatures (Figure 2.21). For example crystals of **2.18** decompose around 180 ºC whereas **2.19** and **2.21** begins to decompose around 330 ºC. The TGA trace of **2.17**.4DMF shows an initial weight loss of about 10% onsets at 160 ºC indicating the exclusion of four DMF molecules. A 52% weight loss equivalent to four phosphonium ligands is observed in the temperature region between 290 ºC and 400 ºC at which point the remaining 38% corresponds to $[Mo_8O_{26}]$ cluster. A further 16% loss of weight between 800 ºC and 950 ºC was also observed indicating decomposition of the cluster (not shown). The TGA curve of **2.19** shows a very sharp melting temperature of 103 ºC followed by a weight loss (6.2%) up to 235 ºC indicating the removal of four ^{iso}butyl molecules. A complete decomposition was observed at 310 ºC where all the phosphonium ligands are lost. The final yield of 65% corresponds to the $[W_{10}O_{32}]$ cluster. The TGA traces of all other compounds are quite similar where their corresponding ligands are gradually lost while their cluster cores are relatively stable except for **2.22**. The TGA graph of **2.22** shows a complete decomposition (66%) onset at 290 ºC indicating the loss of cations as well as a huge portion of the cluster. Comparing the TGA curves of **2.20**.CH_3OH and **2.21** reveals that the Keggin cluster in **2.21** is stable upto 1000 ºC while that in **2.20**.CH_3OH decomposes at 450 ºC.

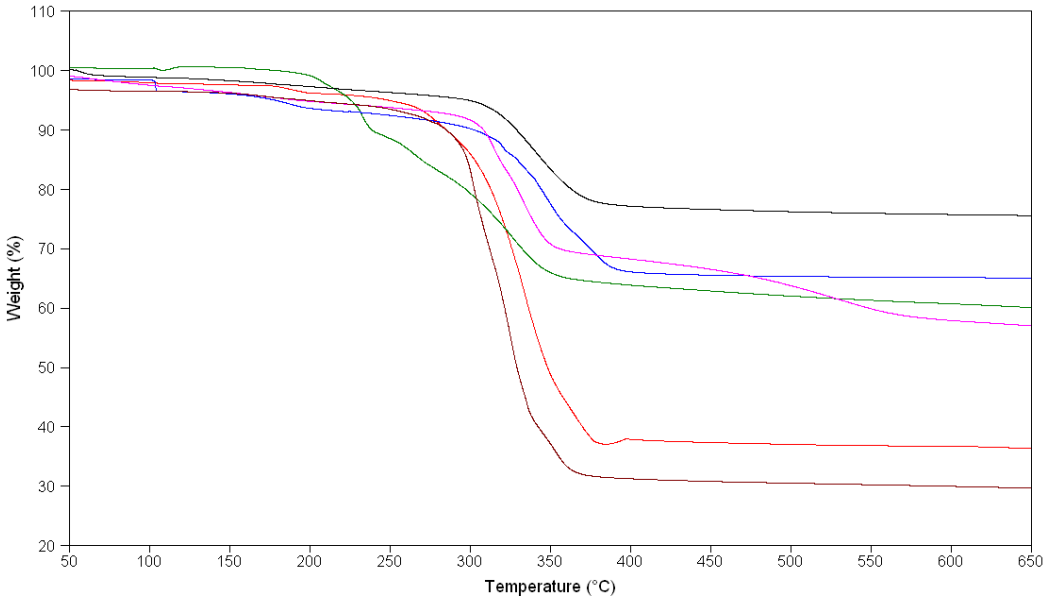

Figure 2.21: TGA curves of the compounds **2.18** (pink), **2.19** (green), **2.20** (blue), **2.21** (red), **2.22** (black) and **2.23** (maroon)

2.4 Conclusion

We have comprehensively studied the supramolecular behavior of organoamino substituted phosphonium cations in presence of halide, carboxylate and polyoxometalate anions respectively. The dimensionality of supramolecular structure exhibited by the phosphonium halides can be varied depending on the steric bulk on the amino substituent. Thus interesting examples of 2D-sheet structures and 1D-structures containing linear, zigzag and helical chains are obtained. The phosphonium cations containing carboxylate anions are prepared by two routes: by anion exchange reactions with phosphonium chlorides and by protonation of neutral phosphine imine, $P(NPh)(NHPh)_3$. While the phosphonium cations containing mono carboxylate anions show solvent assisted supramolecular structures, the corresponding phosphonium di- and tri-carboxylate salts display intricate charge assisted hydrogen bonding interactions forming tightly knit 3D-structures. We have also synthesized six new examples of organic-inorganic hybrid molecules containing phosphonium cations and polyoxometalate anions and studied their supramolecular organization in the solid state. A detailed structural analysis show that the type of supramolecular formed by these compounds depends upon nature of the polyoxometalate ion and steric bulk on the phosphonium ligands. Thus interesting supramolecular structures of 2D-layers, grids, networks and 3D-helical assemblies are obtained. During the course of these studies we have also envisaged the formation of a Keggin type polyoxometalate anion by a facile P-

N bond cleavage reaction. All these compounds are characterized by IR, NMR, and X-ray crystallographic techniques. Thermo-gravimetric studies performed on the phosphonium carboxylates and polyoxometalates show sufficiently high thermal stabilities for their supramolecular assemblies.

2.5 References

(1) (a) Bernstein, J.; Davis, R. E.; Shimoni, L.; Chang, N.-L. *Angew. Chem., Int. Ed. Engl*. **1995**, *34*, 1555. (b) Aakeroy, C. B.; Seddon, K. R. *Chem. Soc. Rev.* **1993**, 397. (c) Desiraju, G. R. *Crystal Engineering. The Design of Organic Solids*; Elsevier: Amsterdam, 1989. (d) David J.; Wolstenholme, D. J.; Weigand, J. J.; Cameron, E. M.; Cameron, T. S. *Cryst. Growth Des*. **2009**, *9*, 282. (e) Aakeröy, C. B.; Nieuwenhuyzen, M. *J. Am. Chem. Soc.* **1994**, *116*, 10983. (f) Katrusiak, A.; Szafrański, M. *J. Am. Chem. Soc.* **2006**, *128*, 15775. (g) Desiraju, G. R. *Acc. Chem. Res.* **2002**, *35*, 565. (h) Desiraju, G. R. *Angew. Chem., Int. Ed.* **2007**, *46*, 565.

(2) (a) Moulton, B.; Zaworotko, M. J. *Chem. Rev.* **2001**, *101*, 1629. (b) Braga, D.; Desiraju, G. R.; Miller, J. S.; Orpen, A. G.; Price, S. L. *CrystEngComm* **2002**, *4*, 500. (c) Hosseini, M. W. *Coord. Chem. Rev.* **2003**, *240*, 157. (d) Braga, D.; Brammer, L.; Champness, N. R. *CrystEngComm* **2005**, *7*, 1. (e) Adams, C. J.; Crawford, P. C.; Orpen, A. G.; Podesta, T. J.; Salt, B. *Chem. Commun.* **2005**, 2457.

(3) (a) Batten, S. R.; Robson, R. *Angew. Chem., Int. Ed.* **1998**, *37*, 1460. (b) Ockwig, N. W.; Delgado-Friedrichs, O.; O' Keeffe, M.; Yaghi, O. M. *Acc. Chem. Res.* **2005**, *38*, 176. (c) Delgado-Friedrichs, O.; O' Keeffe, M.; Yaghi, O. M. *Phys. Chem. Chem. Phys.* **2007**, *9*, 1035. (d) Férey, G. *Chem. Soc. Rev.* **2008**, *37*, 191. (e) Huang, B. L.; Ni, Z.; Millward, A.; McGaughey, A. J. H.; Kaviany, M.; Yaghi, O. M. *Int. J. Heat Mass Transfer* **2007**, *50*, 405.

(4) (a) Collins, D. J.; Zhou, H.-C. *J. Mater. Chem.* **2007**, *17*, 3154. (b) Klontzas, E.; Emmanuel Tylianakis, E.; Froudakis, G. E. *Nano Lett.* **2010**, *10*, 452. (c) Rowsell, J. L. C.; Spencer, E. C.; Eckert, J.; Howard, J. A. K.; Yaghi, O. M. *Science* **2005**, *309*, 1350. (d) Wong-Foy, A. G.; Matzger, A. J.; and Yaghi, O. M. *J. Am. Chem. Soc.* **2006**, *128*, 3494.

(5) (a) Farrusseng, D.; Aguado, S.; Pinel, C. *Angew. Chem., Int. Ed.* **2009**, *48*, 7502. (b) Yang, L.; Kinoshita, S.; Yamada, T.; Kanda, S.; Kitagawa, H.; Tokunaga, M.; Ishimoto,

T.; Ogura, T.; Nagumo, R.; Miyamoto, A.; Koyama, M. *Angew. Chem., Int. Ed.* **2010**, *49*, 5348. (c) Kitagawa, S.; Matsuda, R.; *Coord. Chem. Rev.* **2007**, *251*, 2490. (d) Kitagawa, S.; Kitaura, R.; Noro, S. *Angew. Chem., Int. Ed.* **2004**, *43*, 2334. (e) Bradshaw, D.; Claridge, J. B.; Cussen, E. J.; Rosseinsky, M. J. *Acc. Chem. Res.* **2005**, *38*, 273. (f) Lu, G.; Hupp, J. T. *J. Am. Chem. Soc.* **2010**, *132*, 7832. (f) Lin, W. *Top Catal.* **2010**, *53*, 869.

(6) (a) Desiraju, G. R. *Nature* **2001**, *412*, 397. (b) Sharma, C. V. K. *Cryst. Growth Des.* **2002**, *2*, 465. (d) Desiraju, G. R. *Angew. Chem., Int. Ed.* **2007**, *46*, 8342. (c) Jeffrey, G. A. *An Introduction to Hydrogen Bonding*; Oxford University Press: Oxford, UK, 1997.

(7) (a) *Assymetric Phase Trnasfer catalysis;* Maruoka, K. Ed.; Wiley-VCH: Weinheim, Germany, **2008.** (b) Kosolapoff, G. M. In *Organophosphorus Compounds*, John Wiley and Sons: New York, **1950**. (c) A *Guide to Organophosphorus Chemistry*, Quin, L. D.; Ed.; John Wiley and Sons: New Yark, **2000**. (d) Wittig, G.; Geissler, G. *Liebigs Ann. Chem.* **1953,** *580*, 44. (e) Venkatachalam, T. K.; Samuel P.; Ucken, F. M. *Bioorg. Med. Chem.* **2005,** *13*, 1763. (f) Nam, N. H.; Kim, Y.; You, Y. J.; Hong, D. H.;Kim, H. M.; Ahn, B. Z. *Bioorg. Med. Chem.* **2005,** *11*, 1021.

(8) Rexin, O.; Mülhaupt, R. *J. Polym. Sci. Part A: Poly. Chem.* **2002,** *40*, 864.

(9) Uraguchi, D.; Sakaki, S.; Ooi, T. *J. Am. Chem. Soc.* **2007**, *129*, 12392.

(10) Uraguchi, D.; Ueki. Y.; Ooi, T. *J. Am. Chem. Soc.* **2008**, *130*, 14088.

(11) (a) Uraguchi, D.; Ueki, Y.; Ooi, T. *Science*, **2006**, *326*, 120. (b) Rix, D.; Lacour, J. *Angew. Chem., Int. Ed.* **2010,** *49*, 1918.

(12) (a) Bickley, J. F.; Copsey, M. C.; Jeffery, J. C.; Leedham, A. P.; Russell, C. A.; Stalke, D.;Steiner, A.;Stey, T.; Zacchini, S. *Dalton Trans*. **2004**, 989. (b) Steiner, A.; Zacchini, S.; Richards, P. I. *Coord. Chem. Rev*. **2002**, *227*, 193. Other examples of isoelectronic N-analogues of phosphate derivates can be found at (c) Fleischer, R.; Stalke, D.; *Coord. Chem. Rev.* **1998**, *176*, 431. (d) Raithby, P. R.; Russell, C. A.; Steiner, A.; Wright, D. S. *Angew. Chem. Int. Ed. Engl.* **1997,** *36*, 649. (e) Armstrong, A. F.; Chivers, T.; Krahn, M.; Parvez, M.; G. Schatte, G. *Chem. Commun.* **2002**, 2332. (f) Armstrong, A. F.; Chivers, T.; Krahn, M.; Parvez, M. *Can. J. Chem.* **2005**, *83*, 1768.

(13) (a) Holman, K. T.; Pivovar, A.M.; Swift, J. A.; Ward, M. D. *Acc. Chem. Res.* **2001**, *34*, 107. (b) Schmuck, C.; Wienand, W. *J. Am. Chem. Soc.* **2003**, *125*, 452. (c) Costero, A. M.; Gaviña, P.; Rodríguez-Muñiza, G. M.; Gil, S. *Tetrahedron* **2006**, *62*, 8571. (d) Burke, N. J.; Burrows, A. D.; Mahon, M. F.; Warren, J. E. *Cryst. Growth Des.* **2006**, *6*, 546.

(14) (a) Fitzmaurice, R. J.; Kyne, G. M. Douheret, D.; Kilburn, J. D. *J. Chem. Soc*., *Perkin Trans. 1* **2002**, 841. (b) Bhogala, B. R.; Nangia, A. *Cryst. Growth Des.* **2006**, *6*, 32. (c) Bhogala, B. R.; Vishweshwar, P.; Nangia, A. *Cryst. Growth Des.* **2005**, *5*, 1271. (d) Kolotuchin, S. V.; Fenlon, E. E.; Wilson, S. R.; Loweth, C. J.; Zimmerman, S. C. *Angew. Chem., Int. Ed. Engl.* **1995**, *34*, 2654. (e) Moorthy, J. N.; Natarajan, R.; Mal, P.; Venugopalan, P. *J. Am. Chem. Soc.* **2002**, *124*, 6530.

(15) (a) Bickley, J. F.; Bonar-Law, R.; Lawson, G. T.; Richards, P. I.; Rivals, F.; Steiner, A.; Zacchini, S. *Dalton Trans.* **2003**, 1235-1244. (b) Benson,M. A.; Zacchini, S.; Boomishankar, R.; Chan, Y.; Steiner, A. *Inorg. Chem.* **2007**, *46*, 7097.

(16) (a) Hagrman, P.J.; Hagrman, D.; Zubieta J. *Angew. Chem., Int. Ed.* **1999**, *38*, 2639. (b) Pope, M.Y.; Müller A. *Angew. Chem., Int. Ed. Engl*. **1991**, *30*, 34. (c) Streb C.; Ritchie C.; Long, D.-L.; Kögerler P.; Cronin, L. *Angew. Chem., Int. Ed*. **2007**,*46*, 7579. (e) Zheng, S.-T.; Zhang, J.; Yang, G.-Y. *Angew. Chem., Int. Ed*. **2008**, *47*, 3909.

(17) (a) Ito, T.; Sawada, K.; Yamase, T. *Chem. Lett*. **2003**, *32*, 938. (b) Rheingold, A. L.;White, C. B.; Haggerty, B. S.; Maatta, E. A. *Acta. Crystallogr*. **1993**, *C49*, 756. (c) Alyea, E. C.; Craig, D.; Dance, I.; Fisher, K.; Willett, G.; Scudder, M. *CrystEngComm* **2005**, *7*, 491.

(18) (a) Maguerés, P. Le.; Hubig, S. M.; Lindemann, S. V.; Veya, P.; Kochi, J. K. *J. Am. Chem. Soc.* **2000**, *122*, 10073. (b) Modec, B.; Brenčič, J. V.; Zubieta, J. *J. Chem. Soc. Dalton Trans* **2002**, 1500.

(19) (a) Burkholder, E.; Zubieta, J. *Inorg. Chim.Acta* **2004**, *357*, 279. (b) Wang, X.; Guo, Y.; Li, Y.; Wang, E.; Hu, C.; Hu, N. *Inorg. Chem.* **2003**, *42*, 4135. (c) Zhang, Y.; Zhang, L.; Hao, Z.; Luo, F. *Dalton Trans* 2010, *39*, 7012.

(20) (a) Chatterjee, T.; Sarma, M. ; Das, S. K. *Cryst. Growth Des*. **2010**, *10*, 3149. (b) Upreti, S.; Ramanan, A. *Cryst. Growth Des.* 2006, *6*, 2066. (c) Wang, W.; Xu, L.; Liu, X.; Liu, L. *Inorg. Chem.Commun.* **2009**, *12*, 259. (d) Kobayashi, H.; Ikarashi, K.; Uematsu, K.; Toda, K.; Okawa, H.; Taoyun, Z.; Sato, S. *Inorg. Chim. Acta* 2009, *362*, 238.

(21) Cameron, T. B.; Hanson, H. N.; de la Fuente, G. F.; Huheey, J. E. *Phosphorus, Sulfur Silicon Relat. Elem.* **1993**, *78*, 37.

(22) Sheldrick, G. M. *Acta Crystallogr*. **2008**, *A64*, 112-122.

(23) Some imino derivatives of P(V) compounds as super bases can be seen at (a) Schwesinger, R.; Schlemper, H. *Angew. Chem., Int. Ed. Engl.* **1987**, *26*, 1167. (b) Schwesinger, R.; Link, R.; Wenzl, P.; Kossek, S., Keller, M. *Chem. Eur. J.* **2006**, *12*,

429. (c) Rodima, T.; Mäemets, V.; Koppel, I. *J. Chem. Soc., Perkin Trans. 1* **2000**, 2637. (d) Raab, V.; Gauchenova, E.; Merkoulov, A.; Harms, K.; Sundermeyer, J.; Kovačević, B.; Maksić, Z. B. *J. Am. Chem. Soc.* **2005**, *127*, 15738. (e) Kolomeitsev, A. A.; Koppel, I. A.; Rodima, T.; Barten, J.; Lork, E.; Röschenthaler, G-V.; Kaljurand, I., Kütt, A.; Koppel, I.; Mäemets, V.; Leito, I. *J. Am. Chem. Soc.* **2005**, *127*, 17656.

(24) The ^{31}P-NMR data for some representative POM clusters can be seen at (a) Kozhevnikov, I. V. *Chem. Rev.* **1998**, *98*, 171. (b) Zhang, C-D.; Liu, S-X.; Ma, F-Ji.; Tan, R-K.; Zhang,W.; Su, Z-M. *Dalton Trans*. **2010**, *39*, 8033. (c) Hou,Y.; Xu, L.; Cichon, M. J.; Lense, S.; Hardcastle, K. I.; Hill, C. L. *Inorg. Chem*. **2010**, *49*, 4125.

(25) Etter, M. C. *Acc. Chem. Res.* **1990**, *23*, 120.

(26) Steiner, T.; *Angew. Chem., Int. Ed.* **2002**, *41*, 48 and references therein.

(27) Horstmann, S.; Schnick, W. *Z. Naturforsch.*, **1996**, *B51*, 127.

(28) A survey of the CSD data on the structures of ammonium oxalate shows that the oxalate dianion could take up only three donor hydrogen bonds from the ammonium cation. The fourth one is involved in hydrogen bonding with a solvated molecule. See for example, (a) Taylor, J. C.; Sabine, T. M. *Acta Crystallogr., Sect. B: Struct Crystallogr. Cryst. Chem.* **1972**, *28***,** 3340. (b) Pedersen, B. F. *Acta Crystallogr., Sect. B: Struct. Crystallogr. Cryst. Chem.* **1972**, *28***,** 746. (c) Robertson, J.H. *Acta Crystallogr.* **1965**, *18***,** 410.

(29) Some interesting structures pertaining to alkyl/aryl ammonium carboxylates can be found at (a) Haynes, D. A.; Pietersen, L. K. *CrystEngComm*, **2008**, *10*, 518. (b) Lemmerer, A.; Bourne, S. A.; Fernandes, M. A. *Cryst. Growth Des.* **2008**, *8*, 1106. (c) Yuge, T.; Tohnai, N.; Fukuda, T.; Hisaki, I.; Miyata, M. *Chem. Eur. J.***2007**, *13*, 4163.

(30) (a) Ballabh, A.; Trivedi D. R.; Dastidar, P. *Cryst. Growth Des.* **2005**, *5*, 1545. (b) Trivedi D. R.; Dastidar, P. *Cryst.Growth Des.* **2006**, *6*, 1022. (c) Trivedi D. R.; Dastidar, P. *Cryst. Growth Des.* **2006**, *6*, 2114.

(31) Batten, S. R.; Robson, R. *Angew. Chem., Int. Ed*. **1998**, *37*, 1460.

Chapter 3

Amido and imido metal complexes of P(V) ligands featuring 2- and 3-pyridyl substituents

Abstract

This chapter describes the synthesis and the deprotonation chemistry of a series of pyridylamino (NHPy) functionalized P(V) compounds viz., phosphonium salts, $[P(NHPy)_4]Cl$, phosphine imines $[P(NPy)(NHPy)_3]$ and phosphoramides $[PO(NHPy)_3]$ featuring 2- and 3-pyridyl substituents. Reaction of the phosphonium salt $[P(NH^2Py)_4]Cl$ with 1st row transition metal ions such as Fe^{2+}, Co^{2+} and Ni^{2+} leads to mono-nuclear complexes of formula $\{M[PO(NH^2Py)_3]_2\}$ via the in-situ formation of the phosphoramide ligand $[PO(NH^2Py)_3]$. On the other hand use of Cu^ICl leads to the complex $[CuPO(N^2Py)(NH^2Py)_2Cl]$ where deprotonation of one of the ligand NH protons was observed concomitant with the oxidation of Cu(I) species to the Cu(II) species. In a similar approach, reaction of $[P(NH^2Py)_4]Cl$ with a softer transition metal salt such as $AgClO_4$ lead to an unprecedented penta-nuclear Ag (I) cationic complex $\{Ag_5[P(N^2Py)_2(NH^2Py)_2]_2\}(ClO_4)_3$ where the phosphonium salt has undergone a double-deprotonation without undergoing any cleavage reaction. Use of other Ag(I) salts such as AgOTf again lead to the formation of the same cationic complex with charge balancing OTf anions. Similar deprotonation reaction of the phosphoramide $[PO(NHPy)_3]$ in the absence of an external base has been studied in presence of various Ag(I) salts. Interesting examples of octa- and hepta-nuclear Ag(I) complexes coordinated to imido and pyridyl groups were obtained when more reactive Ag(I) salts such as $AgClO_4$ and $AgBF_4$ were used, while the less reactive $AgNO_3$ reacts only with the peripheral pyridyl groups leading to a tri-nuclear cluster. Structural determination of these Ag(I) complexes show that sequential deprotonation of the ligand amino protons were achieved forming imido P(V) species analogous to the $H_2PO_4^-$ and HPO_4^{2-} ions. The deprotonation chemistry of the phosphonium salt and the phosphoramide has been studied with other soft metal ions such as Pd(II) in which the metal complexes were found to be stabilized by the monoanionic ligand $[PO(N^2Py)(NH^2Py)_2]^-$. Analogous experiments were performed on the corresponding 3-pyridyl derivatives such as $[P(NH^3Py)_4]Cl$, $[P(NPy)(NH^3Py)_3]$ and $[PO(NH^3Py)_3]$. However, no deprotonation of the ligand NH protons were observed. With divalent transition metal ions, the phosphoramide $[PO(NH^3Py)_3]$ has been shown to form self-assembled M_6L_8 cages or a macrocycle with one free ligand arm. Under hydrothermal conditions in DMF it forms a 2D-coordination polymer for Cu(I) ions.

3.1 Introduction

Polyimido derivatives of P(V) compounds have received immense attention in main group chemistry in recent years.[1] This is particularly due to their ability to act as the N-analogues of common phosphorus oxo anions.[2] In this context, phosphorus bound imido anions have received substantial attention.[3] For example, the imido analogues of the respective P(V) oxo species H_3PO_4, $H_2PO_4^-$, HPO_4^{2-} and PO_4^{3-} have been obtained by sequential deprotonation of the phosphonium cation $[(PhNH)_4P]^+$ by n-butyllithium.[4] Chivers and coworkers have shown that tris(organoamino) phosphates of formula $(RNH)_3P{=}E$ (E = NR', O, S or Se) can be deprotonated with a wide variety of organometallic bases such as RLi, R_2Zn, R_2Mg and R_3Al (R is any alkyl or aryl group) generating interesting examples of homoleptic and hetroleptic imido phosphate anions (Figure 3.1). Formation of multi-nuclear metal complexes have been envisaged in many of these reactions, wherein the steric bulk on the imido ligands and nature of the metal ions plays a vital role in controlling their degree of oligomerization.[5,6] Oxidation of some of these metal complexes have shown to form long lived paramagnetic radicals.[7] In addition, complexes of several imino phosphoranes with main group and early transition metal ions were implicated as catalytic systems for olefin oligomerization[8] and polymerization,[9] ring-opening polymerization of lactides,[10] hydroamination[11] and transfer hydrogenation[12] reactions. However, there are no rational routes to obtain the transition metal complexes of these imido P(V) anions in polar and protic solvents. In the previous chapter we have described the synthesis of phosphonium cations of formula $[(RNH)_4P]^+$, in presence of various chloride, carboxylate and polyoxometalate anions, in making designer supramolecular structures aided by hydrogen bonding interactions.[13] In view of the versatile coordination abilities of the imino moiety, we were interested in looking at imido P(V) ligands containing peripheral functional groups and utilize them for obtaining multi-metallic assemblies for various transition metal ions. In this chapter we described the synthesis of various examples amido P(V) derivatives such as phosphonium salts, phosphine imines and phosphoric triamides containing tetra 2- and 3-pyridyl substituents and studied their reactivity studies in presence of various hard and soft transition metal ions. The choice of pyridyl substituents at the P(V) backbone is to facilitate the deprotonation at the phosphorus bound nitrogen center (by withdrawing its electron density) as well as to provide the necessary coordination saturation to the metal ions. Reactivity studies of the phosphonium salt $[P(NH^2Py)_4]Cl$ with divalent transition

metal ions have lead to the mononuclear metal complexes of formula $\{M[PO(NH^2Py)_3]_2\}$ (M = Fe(II), (**3.9**); Co(II), (**3.10**); Ni(II) (**3.11**)) via the in-situ formation of the phosphoramide ligand. A similar reaction with Cu(II) ions gave the discrete complex $\{Cu[PO_2(NH^2Py)_2]_2\}$ (**3.12**) for the in-situ generated bis(amido)phosphate ligand $[PO_2(NH^2Py)_2]^-$. Interestingly, reaction of the phosphoramide $[PO(NH^2Py)_3]$ with CuCl, a reactive soft metal salt, have lead to the mono-deprotonation species $[PO(NPy)(NHPy)_2]^-$ corresponding to the hydrogen phosphate derivative II' (Figure 3.1) as its mono-nuclear complex $[CuPO(N^2Py)(NH^2Py)_2Cl]$ (**3.13**). This suggested that use of a soft metal ion can aid in the generation of various imido P(V) species, depicted in figure 3.1, and can lead to the formation of interesting cluster and cage like molecules. Thus, we employed $[P(NH^2Py)_4]Cl$ and $[PO(NH^2Py)_3]$ with various salts of Ag(I) ions and obtained interesting assemblies for the imido anions of the type II, II' and III' (Figure 3.1).

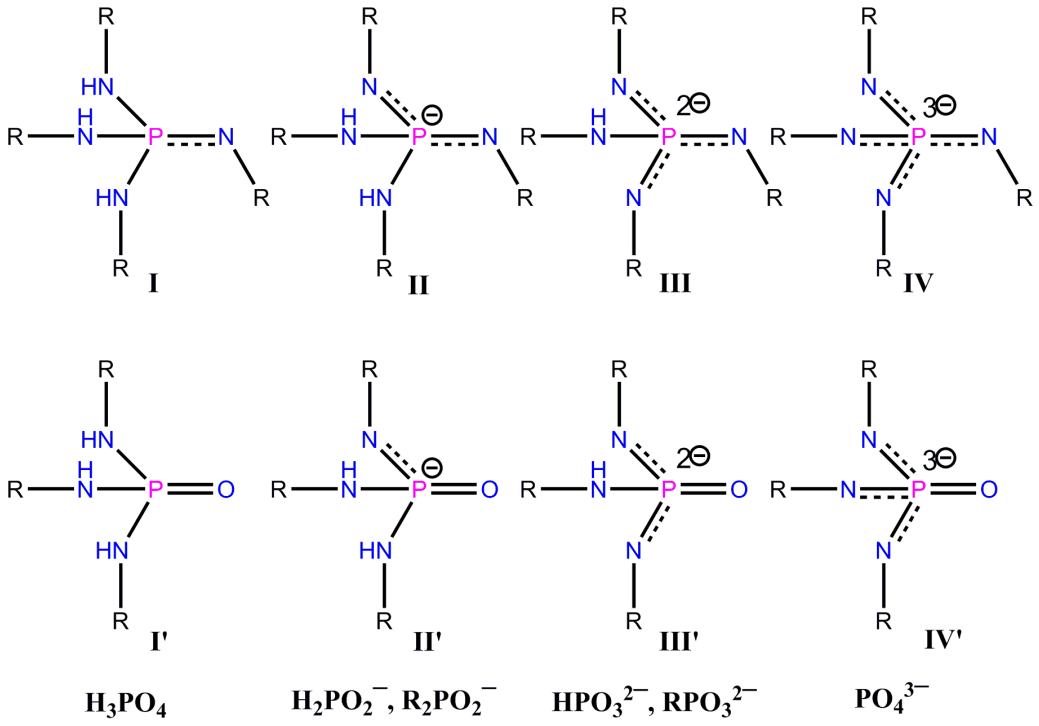

Figure 3.1: N-analogues of various P(V) imido groups (=NR) are iso-electronic to the oxoanions

Use of Pd(II) ions in similar reactions also have shown to give the imido anions of the type II' (Figure 3.1). However, such deprotonation chemistry could not be observed for the corresponding amido P(V) ligands featuring the 3-pyridyl derivatives using Ag(I) ions. Use of transition metal ions in reactions with $[P(NH^3Py)_4]Cl$ or $[PO(NH^3Py)_3]$ gave

cationic cage like assemblies of composition M_6L_8 for the neutral ligand [$PO(NH^3Py)_3$]. However, by controlling the reaction conditions in these reactions in presence of Cu(I) or Cu(II) ions other kinds of assemblies in discrete or polymeric structures could be obtained.

3.2 Experimental section

3.2.1 General Remarks

All manipulations involving phosphorus halides were performed under dry nitrogen atmosphere in standard Schlenk-glassware. Solvents were dried over potassium (THF, hexane) and sodium (toluene). PCl_5, 2- and 3-aminopyridine and metal salts were purchased from Aldrich and Merck and used as received. The $POCl_3$ was purchased locally (SPECTROCHEM, India) and was distilled prior to use. The Cu(I) salt, $[Cu(CH_3CN)_4]PF_6$ was synthesized as reported earlier.[14] NMR spectra were recorded on a 400 MHz Varian FT spectrometer (^{1}H NMR: 400.13 MHz, $^{13}C\{^1H\}$NMR: 100.62 MHz, $^{31}P\{^1H\}$ NMR: 161.97 MHz) at room temperature using $SiMe_4$ (^{1}H, ^{13}C) and 85% H_3PO_4 (^{31}P) as external standards. The solid state (CP-MAS) $^{31}P\{^1H\}$ NMR spectra were obtained on a Bruker 500 MHz spectrometer at a MAS rate of 10.0 KHz. ESI and MALDI-TOF Mass spectra were obtained by Waters Q-Tof Premier & Aquity spectrometer and Applied Biosystem MALDI-TOF/TOF spectrometer, respectively. The solid state UV-visible spectra were obtained from Perkin-Elmer Lambda-950 UV-Visible NIR spectrophotometer with 150 mm integrating sphere. The emission spectra were obtained from Florolog-3 Horiba Jobin Vyon fluorescence spectrophotometer with a 450W Xe lamp as the excitation source. Emission quantum yields were determined by comparison with the emission of a solution of 2-aminopurine (Φ_R = 0.68) in H_2O, employed as a standard.[15] The excitation wavelength used was 327 nm. The quantum yields were then calculated using the expression, $\Phi_S = \Phi_R(A_S/A_R)(n_S^2/n_R^2)$. The subscripts S and R denote sample and reference respectively. Φ is the fluorescence quantum yield; A is the integrated area under the corrected fluorescence spectra, n is the refractive index of the solvent. The solid state emission spectra were obtained from the front face mode. UV-visible spectra were recorded by Perkin-Elmer Lambda-35 spectrophotometer. The emission spectra were obtained from Florolog-3 Horiba Jobin Vyon fluorescence spectrophotometer with a 450W Xe lamp as the excitation source. Elemental analyses were performed on a Vario-EL cube elemental analyzer. FT-IR spectra were taken on a Perkin Elmer spectrophotometer with samples prepared as KBr

pellets. Melting points were obtained using an Electro thermal melting point apparatus and were uncorrected.

3.2.2 Synthesis

3.1: A suspension of PCl_5 (5g, 0.024 mol) in toluene was added drop wise to an excess of 2-aminopyridine (27.10 g, 0.288 mol) in toluene (250 mL) at 0 ^oC. The resulting mixture was refluxed for 4 h by which time a waxy precipitate was obtained. The waxy solid was filtered and washed with cold water to remove the amine hydrochloride by-product. The remaining water insoluble solid was collected, washed with water and dried in vacuum desiccator for 12 hours. Yield 90% (9.46 g), M.P. 205-207 ^oC.^1H NMR (400 MHz, {$(CD_3)_2SO$}): δ 3.14 (br, 4H, N*H*), 6.79 (dd, 4H, C*H*), 7.07 (d, 4H, C*H*), 7.62 (dd, 4H, C*H*) 8.00 (d, 4H, C*H*). ^{13}C {1H}} (100 MHz, {$(CD_3)_2SO$}): δ 113.92, 115.68, 139.27, 147.64, and 154.33. ^{31}P NMR (161 MHz, {$(CD_3)_2SO$}): δ -0.34. FT-IR data in KBr pellet (cm^{-1}): 3339, 3314, and 3113 [ν (N-H)]; 586, 610, 624, 770, 886, 923, 997, 1102, 1152, 1235, 1270, 1296, 1384, 1444, 1485, 1529, 1594 [ν (P-N)]. ESI(+) spectra: 404.17 (M^+). Anal. Calcd. for $C_{20}H_{20}N_8ClP$: C, 54.74; H, 4.59; N, 25.53. Found: C, 54.40; H, 4.54; N, 24.92.

3.2: The compound **3.2** was directly prepared from $POCl_3$ and 2-aminopyridine by a slightly modified literature procedure.[16] $POCl_3$ (5g, 0.0326 mol) was added drop wise to an excess of 2-aminopyridine (36.82g, 0.391 mol) in toluene (250 mL) at 0 ^oC. The resulting mixture was refluxed for 4 h by which time a waxy precipitate was obtained. The waxy solid was filtered and washed with cold water to remove the amine hydrochloride by-product. The remaining water insoluble solid was collected, washed with water and dried in vacuum desiccators for 12 hours. Yield 95% (10.10 g), M.P. 218-220 ^oC.^1H NMR (400 MHz, {$(CD_3)_2SO$}): δ 6.81 (dd, 3H, CH), 7.01 (d, 3H, CH), 7.56 (dd, 3H, CH), 8.10 (d, 3H, CH), 8.60 (br, 3H, NH). $^{13}C\{^1H\}$ (100 MHz, {$(CD_3)_2SO$}): δ 111.27, 116.27, 137.80 , 147.68, 154.45: ^{31}P NMR (161 MHz, {$(CD_3)_2SO$}): δ -4.51; FT-IR data in KBr pellet (cm-1) : 3117 [ν (N-H)]; 611, 637, 724, 803, 774, 803, 877,957, 998, 1061, 1161, 1228, 1267, 1292, 1417, 1449, 1488, 1582, 1598 [ν (P-N)], 1228 [ν (P=O)]. ESI(+) spectra: 327.10 (M+1). Anal. Calcd. for $C_{15}H_{15}N_6OP$: C, 55.21; H, 4.63; N, 25.76. Found: C, 54.54; H, 4.56; N, 25.35.

3.3: A suspension of PCl_5 (5g, 0.024 mol) in toluene was added drop wise to an excess of 3-aminopyridine (27.10 g, 0.288 mol) in toluene (250 mL) at 0 ^oC. The resulting

mixture was refluxed for 4 h by which time a waxy precipitate was obtained. The waxy solid was filtered and washed with cold water to remove the amine hydrochloride by-product. The remaining water insoluble solid was collected, washed with water and dried in vacuum desiccator for 12 hours. Yield 80% (8.40 g) based on P. M.P. 130-132^{o}C.^{1}H NMR (400 MHz, {$(CD_3)_2SO$}): δ 4.55 (br, 4H, N*H*), 7.22 (dd, 4H, C*H*), 7.60 (d, 4H, CH), 8.43 (dd, 4H, C*H*) 8.54 (d, 4H, C*H*). ^{13}C {^{1}H}} (100 MHz, {$(CD_3)_2SO$}): δ 123.74, 124.17, 138.40, 139.43, and 141.58. ^{31}P NMR (161 MHz, {$(CD_3)_2SO$}): δ 0.97. FT-IR data in KBr pellet (cm-1): 3339, 3314, and 3113 [ν (N-H)]; 586, 610, 624, 770, 886, 923, 997, 1102, 1152, 1235, 1270, 1296, 1384, 1444, 1485, 1529, 1594 [ν (P-N)]. ESI(+) spectra: 403.41 (M+). Anal. Calcd. for $C_{20}H_{20}N_8ClP$: C, 54.74; H, 4.59; N, 25.53. Found: C, 54.40; H, 4.54; N, 25.92.

3.5: [$P(NH^2Py)_4$]Cl, **3.1** (0.1g, 0.23 mmol) was dissolved in methanol (~30ml) and excess KOH pellets (0.085g, 1.50 mmol) were added to it under constant stirring. Soon after the addition, a white precipitate of KCl was formed and the stirring was continued until no more KCl formation was observed. The precipitated KCl was then dissolved in distilled water with the evolution of a new white precipitate formed. This precipitate was then filtered under vacuum and washed with H_2O followed by 2 mL of ice-cold methanol and diethyl ether yielding a pure sample of **3.3**, [$P(NHPy)_3(NPy)$]. Single crystals suitable for X-ray analysis was obtained from methanol containing few drops of chloroform. Yield 82% (76 mg) M.P. 240-242 ^{o}C. ^{1}H NMR (400 MHz, {$(CD_3)_2SO$}): δ 3.16 (br, 3H, N*H*), 6.49 (m, 4H**,** C*H*), 6.72 (m, 4H**,** C*H*), 7.27 (m, 4H, C*H*) 7.98 (m, 4H, C*H*). ^{13}C {^{1}H}} (100 MHz, {$(CD_3)_2SO$}): δ 112.60, 113.55, 136.67, 147.26, and 158.93. ^{31}P NMR (161 MHz, {$(CD_3)_2SO$}): δ -11.63; FT-IR data in KBr pellet (cm^{-1}) : 3071 [ν (N-H)]; 586, 637, 736, 776, 921, 945,1004, 1033, 1109, 1155, 1291, 1348, 1405, 1464, 1594 [ν (P-N)]. MALDI-TOF spectra: 403.27 (M+1). Anal. Calcd. for $C_{20}H_{19}N_8P$: C, 59.70; H, 4.76; N, 27.85. Found: C, 59.03; H, 4.38; N, 27.36.

3.6: [$P(NH^3Py)_4$]Cl **3.3** (0.1g, 0.23 mmol) was dissolved in methanol (~30ml) and excess KOH pellets (0.085g, 1.50 mmol) were added to it under constant stirring. Soon after the addition, a white precipitate of KCl was formed and the stirring was continued until no more KCl formation was observed. The precipitated KCl was then dissolved in distilled water with the evolution of a new white precipitate formed. This precipitate was then filtered under vacuum and washed with H_2O followed by 2 mL of ice-cold methanol and diethyl ether yielding a pure sample of **3.8**, [$P(NH^3Py)_3(NPy)$]. Single crystals suitable

for X-ray analysis was obtained from methanol containing few drops of chloroform. Yield 70% (65 mg) based on P. M.P. 155-160 ^{o}C. ^{1}H NMR (400 MHz, {$(CD_3)_2SO$}): δ 4.36 (br, 3H, N*H*), 6.88 (dd, 3H**,** C*H*), 6.96 (dd, 4H**,** C*H*), 7.34(d, 1H, C*H*) 7.53 (dd, 3H, C*H*) 7.68 (dd, 3H, C*H*) 7.90 (d, 1H, C*H*) 8.15 (d, 1H, C*H*). ^{13}C {^{1}H}} (100 MHz, {$(CD_3)_2SO$}): δ 123.71, 124.16, 138.74, 139.53, and 141.64. ^{31}P NMR (161 MHz, {$(CD_3)_2SO$}): δ -8.63; FT-IR data in KBr pellet (cm^{-1}) : 3071 [ν (N-H)]; 586, 637, 736, 776, 921, 945, 1004, 1033, 1109, 1155, 1291, 1348, 1405, 1464, 1594 [ν (P-N)]. ESI (+) spectra: 402.53 (M+1). Anal. Calcd. for $C_{20}H_{19}N_8P$: C, 59.70; H, 4.76; N, 27.85. Found: C, 59.63; H, 4.78; N, 27.83.

3.7: To a solution of $[P(NH^2Py)_4]Cl$, **3.1** (100mg, 0.23 mmol) in methanol (4ml) containing few drops of chloroform, $Mg(NO_3)_2{\cdot}6H_2O$ (30 mg, 0.115 mmol) was added and stirred for few minutes. The solution was then filtered over a thick pad of celite and left for crystallization at room temperature. Colourless crystals of **3.4**, suitable for SCXRD, were obtained after 2 days. Yield 91% (97 mg) M.P. 195-198 °C. ^{1}H NMR (400 MHz, $(CD_3)_2SO$): δ 3.10 (br, 4H, N*H*), 6.81 (dd, 4H, C*H*), 7.05 (d, 4H, C*H*), 7.68 (dd, 4H, C*H*), 8.01 (d, 4H, C*H*). ^{13}C{^{1}H} NMR (100 MHz, $(CD_3)_2SO$): δ 113.89, 115.71, 139.03, 147.57, and 154.38. ^{31}P{^{1}H} NMR (161 MHz, $(CD_3)_2SO$): δ −0.35. FT-IR data in KBr pellet (cm^{-1}): 3450, 3314 and 3113 [ν (N–H)], 586, 610, 624, 644, 771, 874, 927, 972, 997, 1055, 1101, 1151, 1201, 1234, 1269, 1298, 1383, 1460, 1485, 1530, and 1594 [ν (P–N)]. ESI(+) spectra: 403.1546 (M+). Anal. Calcd. for $C_{20}H_{20}N_9O_3P$: C, 51.61; H, 4.33; N, 27.09. Found: C, 52.04; H, 4.28; N, 26.87.

3.8: To a solution of **3.1** (30 mg, 0.068 mmol) in DMF (1 ml) placed in a screw capped glass vessel, 1 M HCl solution in H_2O (1 ml) was added and the final mixture was heated at 90 ^{o}C for 3 days. The reaction mixtures were gradually brought back to room temperature in a period of 24 h to yield a colorless solution. The reaction mixtures were slowly evaporated to dryness on a hot-plate kept at 80 °C to yield a crystalline solid which was found to be a mixture of chloride salt of [(^{C}L)+2H]Cl and the aminopyridine hydrochloride by-product. [(^{C}L)+2H]Cl: Crude yield: 40% (6.8 mg based on P). ^{31}P-NMR (161 MHz, {(D_2O)}: δ -9.31 ppm. MALDI-TOF mass spectrum (m/z): 288.98. FT-IR data in KBr pellet (cm-1): 510, 524, 605, 644, 830, 866, 885, 1024, 1083, 1197, 1233, 1257, 1335, 1406, 1434, 1471, 1530, 1589, 1655, 3024 and 3428.

3.9: To a solution of the ligand $[OP(NH^2Py)_3]$ **3.2** (100 mg, 0.31 mmol) in methanol-Chloroform mixture, $Fe(ClO_4)_2$ (39 mg, 0.15 mmol) in methanol was added. The

mixture was stirred for 1 h, filtered and kept for crystallization. Prismatic light green-colored crystals were obtained after 5 days. Yield: 80% (111 mg, based on P). FT-IR data in KBr pellet (cm-1): 549, 587, 627, 655, 771, 873, 937, 1039, 1149, 1224, 1276, 1330, 1416, 1461, 1505, 1538, 1592, 1608, 1633 and 3461. Anal. Calcd. for $C_{30}H_{30}N_{12}O_{10}P_2Cl_2Fe$: C, 39.71; H, 3.33; N, 18.52. Found: C, 39.51; H, 3.36; N, 18.63.

3.10: To a solution of the ligand $[OP(NH^2Py)_3]$ **3.2** (100 mg, 0.31 mmol) in methanol-Chloroform mixture, $Co(ClO_4)_2 \cdot 6H_2O$ (56 mg, 0.15 mmol) was added. The mixture was stirred for 1 h, filtered and kept for crystallization. Prismatic light red-colored crystals were obtained after 5 days. Yield: 90% (125 mg, based on P). FT-IR data in KBr pellet (cm^{-1}): 525, 548, 588, 627, 656, 746, 772, 873, 927, 1004, 1038, 1165, 1226, 1277, 1320, 1397, 1486, 1507, 1528, 1634, 1665 and 3474. Anal. Calcd. for $C_{30}H_{30}N_{12}O_{10}P_2Cl_2Co$: C, 39.58; H, 3.32; N, 18.46. Found: C, 39.60; H, 3.36; N, 18.74.

3.11: To a solution of the ligand $[OP(NH^2Py)_3]$ **3.2** (100 mg, 0.31 mmol) in methanol-Chloroform mixture, $Ni(ClO_4)_2 \cdot 6H_2O$ (56 mg, 0.15 mmol) in methanol was added. The mixture was stirred for 1 h, filtered and kept for crystallization. Prismatic light green-colored crystals were obtained after 5 days. Yield: 90% (125 mg, based on P). FT-IR data in KBr pellet (cm-1): 503, 587, 636, 773, 872, 926, 1007, 1040, 1090, 1122, 1230, 1332, 1415, 1486, 1538, 1702 and 3442. Anal. Calcd. for $C_{30}H_{30}N_{12}O_{10}P_2Cl_2Ni$: C, 39.59; H, 3.32; N, 18.47. Found: C, 39.21; H, 3.56; N, 18.74.

3.12: *(a)* To a solution of the ligand **3.1** (362 mg, 0.82 mmol) in methanol, $Cu(NO_3)_2$ (100 mg, 0.41 mmol) in methanol was added along with few drops of DMF (N,N-dimethylformamide). The mixture was stirred for 1 h, filtered and kept for crystallization. Prismatic green-colored crystals were obtained after 15 days. Yield: 70% (162 mg, based on Cu). (b) To a solution of the ligand **3.2** (269 mg, 0.82 mmol) in methanol, $Cu(NO_3)_2$ (100 mg, 0.41 mmol) in methanol was added along with few drops of DMF. The mixture was stirred for 1 h, filtered and kept for crystallization. Prismatic green-colored crystals were obtained after 15 days. Yield: 70% (83 mg, based on Cu). M.P. 178-180 ^oC. FT-IR data in KBr pellet (cm^{-1}): 528, 624, 664, 738, 827, 908, 960, 1011, 1071, 1209, 1285, 1330, 1413, 1459, 1504, 1603, 1670, 3175 and 3434. Anal. Calcd. for $C_{20}H_{20}N_8O_4P_2Cu$: C, 42.75; H, 3.59; N, 19.94. Found: C, 42.84; H, 3.56; N, 19.74.

3.12·2DMF: *(a)* To a solution of the ligand **3.1** (237 mg, 0.6 mmol) in methanol, $Cu(ClO_4)_2$ (100 mg, 0.27 mmol) in methanol was added along with few drops of DMF. The mixture was stirred for 1 h, filtered and kept for crystallization. Prismatic green-colored crystals were obtained after 10 days. Yield: 60% (71 mg, based on Cu). *(b)* To a solution of the ligand **3.2** (176 mg, 0.54 mmol) in methanol, $Cu(ClO_4)_2$ (100 mg, 0.27 mmol) in methanol was added along with few drops of DMF. The mixture was stirred for 1 h, filtered and kept for crystallization. Prismatic green-colored crystals were obtained after 10 days. Yield: 70% (83 mg, based on Cu). M.P. 185-187 ^oC. FT-IR data in KBr pellet (cm^{-1}): 524, 578, 769, 825, 933, 1017, 1068, 1118, 1160, 1196, 1384, 1460, 1578, 1617, 1664, 3183 and 3438. Anal. Calcd. for $C_{26}H_{34}N_{10}O_6P_2Cu$: C, 44.10; H, 4.84; N, 19.78. Found: C, 44.34; H, 4.76; N, 19.65.

3.13: To a solution of the ligand $[OP(NHPy)_3]$ **3.2** (100 mg, 0.31 mmol) in methanol-Chloroform mixture, CuCl (58 mg, 0.30 mmol) in methanol was added. The mixture was stirred for 1 h, filtered and kept for crystallization. Prismatic dark green-colored crystals were obtained after 10 days. Yield: 75% (98 mg, based on P) M.P. 185-187 ^oC. FT-IR data in KBr pellet (cm-1): 518, 540, 648, 664, 791, 881, 924, 9947, 1012, 1022, 1108, 1155, 1237, 1277, 1324, 1348, 1384, 1489, 1512, 1574, 1673, 1753 3208 and 3404. Anal. Calcd. for $C_{15}H_{14}N_6OPClCu$: C, 42.46; H, 3.33; N, 19.81. Found: C, 42.35; H, 3.18; N, 19.55.

3.14·$(ClO_4)_3$**:** To a solution of the ligand $[P(NH^2Py)_4]$ (**3.1)** (100 mg, 0.23 mmol) in methanol containing few drops of chloroform (3 mL), kept in a screw capped vial, was carefully layered a solution of $Ag(ClO_4)$ (167 mg, 0.81 mmol) in methanol (3 mL). Toluene (1 mL) was carefully added to this mixture and the slightly cloudy solution was kept in dark for crystallization. Colorless block like crystals were obtained after 12 hours. Yield 57% (130 mg) Crystals of **3.14**·$(ClO_4)_3$ were also obtained in a similar crystallization reaction involving **3.3** (100 mg, 0.25 mmol) and $Ag(ClO_4)$ (129 mg, 0.62 mmol). Yield 65% (160 mg) ^1H NMR(400 MHz, $\{(CD_3)_2SO\}$): δ 4.10 (br, 4H, N*H*), 6.97 (br, 4H, C*H*), 7.24 (br, 2H, C*H*), 7.74 (br, 4H, C*H*), 7.97 (br, 2H, C*H*), 8.24 (br, 2H, C*H*), 8.90 (br, 2H, CH): ^{13}C $\{^1H\}$ (100 MHz, $\{(CD_3)_2SO\}$): δ 116.58, 117.45, 140.27, 150.60, 159.82: ^{31}P NMR (161 MHz, $\{(CD_3)_2SO\}$): δ -2.11; FT-IR data in KBr pellet (cm^{-1}) : 3294 [ν (N-H)]; 508, 739, 850, 913, 1030,1088, 1297,1427, 1445, 1463, 1594 [ν (P-N)]; 625 [ν (Ag-N)]. Anal. Calcd. for $C_{40}H_{36}N_{16}O_{12}P_2Cl_3Ag_5$: C, 29.29; H,

2.21; N, 13.66. Found: C, 28.91; H, 2.28; N, 12.73. MALDI-TOF spectra: 1335.07 ($[Ag_5L_2]^{3+}$) 1228.14 ($[Ag_4L_2]^{2+}$) and 1121.21 ($[Ag_3L_2]^{+}$).

Caution should be used when handling perchlorate salts, since these can be explosive when dry!

3.14·$(OTf)_3$**:** A solution of $[P(NH^2Py)_4]$ **3.1** (100 mg, 0.23 mmol) in methanol (2 mL), DMF (1 mL) and with few drops of chloroform kept in a screw capped vial, was carefully layered with toluene (1 mL) followed by a solution of AgOTf (208.12 mg, 0.81 mmol) in methanol (3 mL). This results in a cloudy solution which was then kept in dark for crystallization. Colorless crystals were obtained after 3 days. Direct mixing of a solution of **3.1** in MeOH/DMF to AgOTf in methanol yielded a white precipitate, which was washed with water and methanol and dried. This precipitate was found to give same mass, NMR and CHN analysis as that of the crystalline sample. Yield 47% (135 mg), M.P. 183-187°C. ^{1}H NMR (400 MHz,$(CD_3)_2SO$): δ 4.13 (br, 4H, N*H*), 6.89 (br,4*H*, C*H*), 7.19 (br, 2H, C*H*), 7.69 (br, 4H, C*H*), 7.91 (br, 2H, CH),8.15 (br, 2H, C*H*), 8.69 (br, 2H, C*H*): $^{13}C\{^1H\}$ NMR (100 MHz, $(CD_3)_2SO$): δ 116.53, 117.58,121.06, 139.97, 150.35, 159.22: $^{31}P\{^1H\}$ NMR (161 MHz, $(CD_3)_2SO$): δ -2.07; FT-IR data in KBr pellet (cm^{-1}): 3310 [ν (N–H)], 506, 596, 742, 819, 925, 1047,1075, 1177, 1234, 1297, 1350, 1426, 1448, 1460, 1594 [ν (P–N)], 1641, 623 [ν (Ag–N)]. Anal. Calcd. for $C_{52}H_{57}F_9N_{19}O_{12}P_2S_3Ag_5$: C, 31.09; H, 2.86; N, 13.25; S, 4.79. Found: C, 30.74; H, 2.40; N, 12.78; S, 4.35. MALDI-TOF spectra: 1340.92 ($[Ag_5L_2]^{3+}$), 1233.04 ($[Ag_4L_2]^{2+}$) and 1127.14 ($[Ag_3L_2]^{+}$).

3.15: To a solution of $[OP(NH^2Py)_3]$ **3.2** (100 mg, 0.306 mmol) in methanol containing few drops of chloroform (3 mL), kept in a screw capped vial, toluene (1mL) was added followed by a careful layering of a solution of $Ag(NO_3)$ (78 mg, 0.460 mmol) in water (3 mL). The resulting slightly cloudy solution was kept in dark for crystallization. Colorless block like crystals were obtained after 10 days. Yield 62% (113 mg, based on P). M.P. 180-182°C, 1H NMR(400 MHz, {$(CD_3)_2SO$}): δ 6.95 (s,3 H, CH_3), 7.18 (br, C*H*), 7.72 (br, C*H*), 8.16 (br, C*H*), 8.96 (s, 4 H, N*H*) : ^{13}C {^1H}} (100 MHz, {$(CD_3)_2SO$}): δ 113.23, 117.12, 139.15, 148.56, 154.24 : ^{31}P NMR (161 MHz, {$(CD_3)_2SO$}): δ -3.68; FT-IR data in KBr pellet (cm-1) : 3443, 3138 [ν (N-H)]; 510, 601, 629, 771, 824, 952, 994, 1053, 1098, 1154, 1207, 1242, 1295, 1384, 1445, 1487, 1574, 1601 [ν (P-N)]; 1207, 1242 [ν (P=O)]; 647, 735 [ν (Ag-N)]. Anal. Calcd. for $C_{30}H_{30}N_{15}O_{11}P_2Ag_3$: C, 31.00; H, 2.60; N, 18.08. Found: C, 31.74; H, 2.58; N, 17.85.

3.16: To a solution of [$OP(NH^2Py)_3$] **3.2** (100 mg, 0.306 mmol) in methanol and chloroform (3 mL), kept in a screw capped vial, toluene (1 mL) was added followed by a careful layering of a solution of $Ag(ClO_4)$ (127 mg, 0.612 mmol) in methanol (3 mL). The resulting slightly cloudy solution was kept in dark for crystallization. Colorless block like crystals were obtained after 3 days. Yield 72%, (149 mg, based on P) ^{1}H NMR (400 MHz, {$(CD_3)_2SO$}): δ 6.93 (br, C*H*), 7.16 (br, C*H*), 7.71 (br, C*H*), 8.16 (br, C*H*), 9.20 (s, 4 H, N*H*): ^{13}C {^{1}H}} (100 MHz, {$(CD_3)_2SO$}): δ 113.51, 117.27, 139.36, 148.78, 154.23: ^{31}P NMR (161 MHz, {$(CD_3)_2SO$}): δ -3.55; FT-IR data in KBr pellet (cm^{-1}) : 3416, 3126 [ν (N-H)]; 636, 724, 775, 958, 1061, 1293, 1418, 1449, 1488, 1598 [ν (P-N)]; 1228 [ν (P=O)]; 1025 [ν (Ag-N)]. Anal. Calcd. for $C_{60}H_{56}N_{24}O_{20}P_4Cl_4Ag_8$: C, 28.13; H, 2.20; N, 13.12. Found: C, 29.00; H, 2.74; N, 13.02.

3.17: To a solution of [$OP(NH^2Py)_3$] **3.2** (100 mg, 0.306 mmol) in methanol and chloroform (3 mL), kept in a screw capped vial, toluene (1 mL) was added followed by a careful layering of a solution of $AgBF_4$ (208 mg, 1.06 mmol) in methanol (3 mL). The resulting slightly cloudy solution was kept in dark for crystallization. Light yellow colored single crystals were obtained in two week. Yield 60% (112 mg, based on P), M.P. 190-192 ^{o}C, ^{1}H NMR(400 MHz, {$(CD_3)_2SO$}): δ 6.88 (br, CH), 7.58 (br, CH), 8.16 (br, CH), 8.72 (br, CH), 8.87 (br, NH): ^{13}C {^{1}H}} (100 MHz, {$(CD_3)_2SO$}): δ 113.57, 115.26, 139.00, 148.69, 154.61: ^{31}P NMR (161 MHz, {$(CD_3)_2SO$}): δ -3.73; FT-IR data in KBr pellet (cm-1) : 3189 [ν (N-H)]; 690, 748, 956, 1031, 1081, 1280, 1410, 1498 [ν (P-N)]; 1221 [ν (P=O)]; 647, 736, 750 [ν (Ag-N)]: Anal. Calcd. For $C_{45}H_{39}BN_{18}O_3F_4P_3Ag_7$: C, 29.78; H, 2.17; N, 13.89. Found: C, 30.11; H, 2.58; N, 13.85.

3.18: To a solution of the ligand [$OP(NH^2Py)_3$] **3.2** (100 mg, 0.31 mmol) in methanol-Chloroform mixture, $Pd(PhCN)_2Cl_2$ (117 mg, 0.31 mmol) in methanol was added. The mixture was stirred for 1 h, filtered and kept for crystallization. Prismatic dark green-colored crystals were obtained after 7 days. Yield: 90% (257 mg, based on P). ^{1}H NMR (400 MHz, {$(CD_3)_2SO$}): δ 6.77 (br, C*H*), 7.36 (br, C*H*), 7.89 (br, C*H*), 8.61 (br, C*H*), 9.22 (s, 4 H, N*H*): ^{13}C {^{1}H}} (100 MHz, {$(CD_3)_2SO$}): δ 112.57, 117.29, 138.43, 148.09, 151.37: ^{31}P NMR (161 MHz, {$(CD_3)_2SO$}): δ -3.88; FT-IR data in KBr pellet (cm^{-1}): 528, 624, 664, 738, 827, 908, 960, 1011, 1071, 1209, 1285, 1330, 1413, 1459, 1504, 1603, 1670, 3175 and 3434. Anal. Calcd. for $C_{30}H_{28}N_{12}O_2P_2Cl_2Pd_2$: C, 38.57; H, 3.02; N, 17.99. Found: C, 38.35; H, 3.18; N, 18.15.

3.18·$4H_2O$**:** To a solution of the ligand $[P(NH^2Py)_4]Cl$ **3.1** (100 mg, 0.23 mmol) in methanol, $Pd(PhCN)_2Cl_2$ (88 mg, 0.23 mmol) in methanol was added. The mixture was stirred for 1 h, filtered and kept for crystallization. Cube like yellow color crystals were obtained after 10 days. Yield: 70% (179 mg, based on P). M.P.178-180 ^oC. The analytical and spectroscopic data of the sample dried at 80 ^oC under vacuum matches with the reported value of **3.18**.

3.19: To a solution of $[P(NH^3Py)_4]Cl$, **3.3**, (117 mg, 0.27 mmol) indry $CHCl_3$ (10 mL), $[Cu(CH_3CN)_4]PF_6$ (100 mg, 0.27 mmol) was added and the reaction mixture was stirred for 1 h. It was then filtered through a celite pad and left for crystallization. After one weak light green crystal of **3.19** were obtained for X-ray analysis. Yield 50 % (124 mg based on Cu) M.P. 215–230. FT-IR data in KBr pellet (cm^{-1}): 2925, 2852, 1734, 1610, 1581, 1501, 1459, 1399, 1256, 1241, 1189, 1101, 1063, 950, 802, 753, 669, and 635.Anal. Calcd for $C_{30}H_{30}Cl_4Cu_2N_{12}O_2P_2$: C, 39.10; H, 3.28; N, 18.24. Found: C, 39.40; H, 3.54; N, 18.92.

3.20: To a solution of the $[OP(NH^3Py)_3]$, **3.4**, (202 mg, 0.62 mmol) in DMF (25 mL) placed in a screw capped glass vessel and a solution of $Cu(NO_3)_2$ (100 mg, 0.41 mmol) was added and the final mixture was heated at 90 °C for three days. The reaction mixture was then slowly brought back to the room temperature in a period of 24 h at which point yellow crystals of **3.20** were obtained. Yield 35% (206 mg, based on Cu). M.P. 200-205. FT-IR data in KBr pellet (cm^{-1}): 3486, 3178, 1585, 1504, 1396, 1332, 1278, 1193, 1062, 944, 804, 698, 655, and 549.Anal. Calcd. for $C_{45}H_{45}Cu_2N_{20}O_9P_3$: C, 43.94; H, 3.69; N, 22.78. Found: C, 53.40; H, 3.54; N, 22.92.

3.2.3 Crystallography

Reflections were collected on a Bruker Smart Apex II diffractometer at 296 K using MoKα radiation (λ = 0.71073 Å) for **3.2**, **3.5**, **3.6**, **3.9**·$2CH_3OH$, **3.10**, **3.11**·$2CH_3OH$, **3.12**·2DMF, **3.14**·$(ClO_4)_3$·$3C_7H_8$·$2CH_3OH$, **3.15**·$3H_2O$, **3.16**·$5CH_3OH$·$3H_2O$, **3.17**·H_2O and **3.18**. The data for **3.2**·C_7H_8, **3.7**·$2H_2O$, **3.12**, **3.13**, **3.14**·$(OTf)_3$·3DMF, **3.18**·$4H_2O$, **3.19** and **3.20** were collected on Bruker Smart Apex Duo diffractometer at 100 K using MoKα radiation (λ = 0.71073 Å).Structures were refined by full-matrix least-squares against F^2 using all data (SHELX).[17] The data for All non-hydrogen atoms were refined aniostropically. Crystallographic data for all the stated above compounds are listed in Table A2.1, Appendix 2. Hydrogen atoms were constraint in geometric positions to their parent atoms. One of the toluene molecules in **3.2**·C_7H_8 was disordered and was refined

isotropically over two sites. Crystals of **3.7**·2H_2O diffracted weakly at higher angles and hence a 2θ = 50 ° cut-off was applied. The nitrate anion in **3.7**·2H_2O was disordered and refined over three positions with SIMU/SAME restraints. The perchlorate and methanol oxygens and one toluene molecule in **3.14**·$(ClO_4)_3$ are disordered. Atom positions of the disordered groups were split over two positions and refined isotropically using similar-distance restraints. Crystals of **3.15** diffracted weakly lacking observed reflections at higher angles and hence a 2θ cut-off of 46° was applied. The solvated DMF molecules and the OTf^- anions in **3.14**·$(OTf)_3$·3DMF were disordered and refined over two positions with SIMU/SAME restraints. Crystals of **3.17**·3H_2O were slightly opaque and diffracted only weakly lacking observed reflections at higher angles and hence a 2θ cut-off at 45° was applied. Although the overall connectivity is not in doubt, care should be taken when evaluating bond lengths and angles. Due to the poor quality of data, atom positions of the nitrate and water moieties were refined isotropically. The nitrate ions were refined with similar-distance restraints and global similar-U restraints were applied to all C, N and O atoms. The structure of **3.17**·3H_2O was refined as a racemic twin. In **3.18**·5CH_3OH·3H_2O the perchlorate anions and solvent molecules are severely disordered along channels that run between the cationic complexes. NMR data suggest that there are about 5 methanol and 3 water molecules per formula unit. The perchlorate ions and solvent molecules were treated as a diffuse contribution to the overall scattering without specific atom positions by SQUEEZE/PLATON. In addition, we also provide a model that attempts to describe the disorder. Isotropic refinement with tight restraints gave tetrahedral ClO_4^- ions, albeit with large thermal parameters; electron difference peaks due to solvents where refined as partially occupied oxygen atoms. In **3.19**·H_2O one pyridyl group is disordered. It was split over two positions and refined isotropically with occupancy factors and similar distance and similar U restraints. Both the BF_4^- anion and the lattice water molecule are disordered over the 3-fold axis. The BF_4^- anion was refined isotropically with similar distance and similar U-restraints. The disordered solvents of DMF and water in the structure of **3.19** have been treated as a diffuse contribution to the overall scattering and removed by the SQUEEZE routine of the PLATON software.

3.2.4 Theoretical Calculations

The molecular geometries of **3.1** and **3.3** were fully optimized at a level of density functional theory employing the hybrid functional B3LYP[18–21] with Pople's basis set 6-

31+G(d,p) where polarization functions were added to all the atoms and diffuse functions to the heavy atoms. For **3.5** and **3.6** the energy minimization and optimization of geometry was done on the molecular structure obtained by X-ray crystallography. The convergence threshold for the energies and residual forces on the atoms during geometry optimization were maintained at 10^{-8} hartree and 4.5×10^{-4} hartree/bohr, respectively. Time-dependent density functional theory (TDDFT) calculations were performed over the optimized geometries to obtain the excitation energies.[22, 23] All the calculations were performed with the development version of Gaussian 03.[24]

3.3Results and Discussions

3.3.1 Synthesis

The phosphonium salts **3.1** and **3.3** were isolated as insoluble residues in the reaction involving PCl_5 and excess of the corresponding amino-pyridine in refluxing toluene (Scheme 3.1). The formation of the salts **3.1** and **3.3** were confirmed by ^{31}P-NMR (δ -0.3 for **3.1** and 0.97 for **3.3**) and ESI-MS spectroscopic (M^+ = 403.2 for **3.1** and 403.4 for **3.3**) techniques (Figure A2.1 and A2.2, Appendix 2). The phosphoramides **3.2** and **3.4** were prepared from $POCl_3$ and 2-aminopyridine by a slightly modified literature procedures (Scheme 3.1).[16]

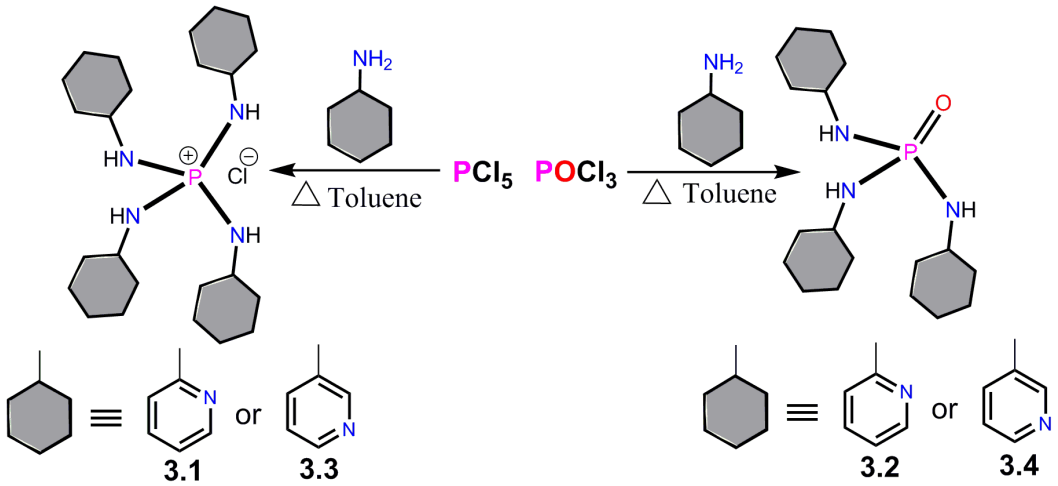

Scheme 3.1: Synthetic schemes for the preparation of **3.1, 3.2, 3.3** and **3.4**.

Although **3.1** and **3.3** are stable in the solid state for a prolonged period of time, their attempted crystallization from their methanolic solutions lead to the formation of the cleaved phosphoramide derivatives **3.2** and **3.4** as indicated by ^{31}P-NMR (δ -4.5 for **3.2** and –3.76 for **3.4**) spectra and X-ray crystallography. The formation of **3.2** and **3.4** is presumably due to the interaction of the pyridyl nitrogens with the acidic protons of the

solvent and thereby increasing the overall positive charge on the cation. Thus, the increased positive charge on the P-atom weakens the P-N bond which undergoes hydrolysis yielding the phosphoramides **3.2** and **3.4**.[25] It has been shown in the previous chapter that $[(PhNH)_4P]Cl$ undergoes mono-deprotonation in alkaline methanol solution to give the neutral imine $(PhNH)_3P{=}NR$.[13a] Hence we treated the salts **3.1** and **3.3** with solid KOH in methanol and isolated the neutral pyridyl substituted phosphine imines **3.5** and **3.6** in quantitative yield (Scheme 3.2). The ^{31}P-NMR spectra of **3.5** and **3.6** shows a strong upfield shift (δ -11.6 for **3.5** and -8.63 for **3.6**) compared to their precursors indicating the presence of the P═N environment.

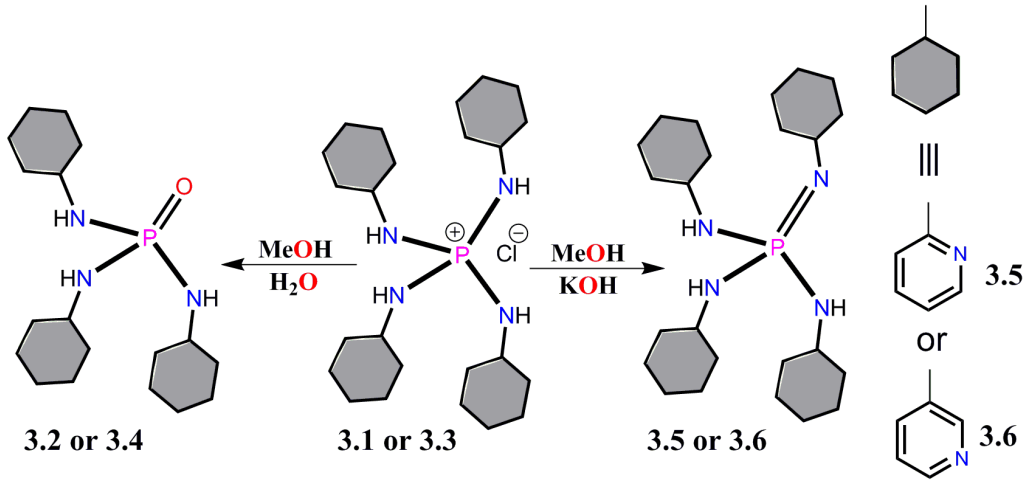

Scheme 3.2: Reaction conditions for the preparation of **3.5** and **3.6** via **3.1** and **3.3**

This prompted us to look for other suitable counter anion which can prevent the P-N bond hydrolysis and provide stability for phosphonium salts to exist in the slightly acidic pH of the methanol medium. We have employed the non-coordinating anions of various electropositive metal ions in the anion exchange reactions and succeeded in one instance where the chloride ion from **3.1** was successfully replaced with the nitrate ion in presence of $Mg(NO_3)_2$ (Scheme 3.3).The ^{31}P-NMR of nitrate salt **3.7** gave a single peak at δ -0.35 which is closely matching with that of **3.1**. The high-resolution mass spectral analysis revealed a characteristic peak in the phosphonium region at *m/z* = 403.15 confirming the absence of the hydrolyzed product (Figure A2.3, Appendix 2). Moreover, the single-crystal X-ray diffraction data collected on the crystal of **3.7** unequivocally supports its existence in the solid state.

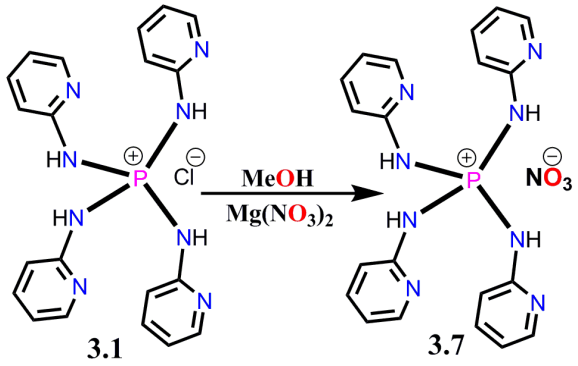

Scheme 3.3: Reaction conditions for the preparation of **3.7**

Further to obtain the transition metal complexes of these amido P(V) ligands we screened all these ligands in presence of divalent transition metal ions. The reaction of **3.1** with the perchlorate salts of Fe^{2+}, Co^{2+} and Ni^{2+} proceeded smoothly at room temperature as observed by a visible color change in solution. Single crystal X-ray analysis of the crystals obtained from these reaction mixtures have shown the formation of the mono-nuclear complex of formula $\{M[PO(NH^2Py)_3]_2\}$ (M = Fe(II) **3.9**; Co(II) **3.10**; Ni(II) **3.11**) in which **3.1** has undergone a P−N bond cleavage reaction instead of the N-H bond deprotonation. Formation of these complexes have been observed in a direct reaction of $[PO(NH^2Py)_3]$ (**3.2**) with these metal salts (Scheme 3.4).

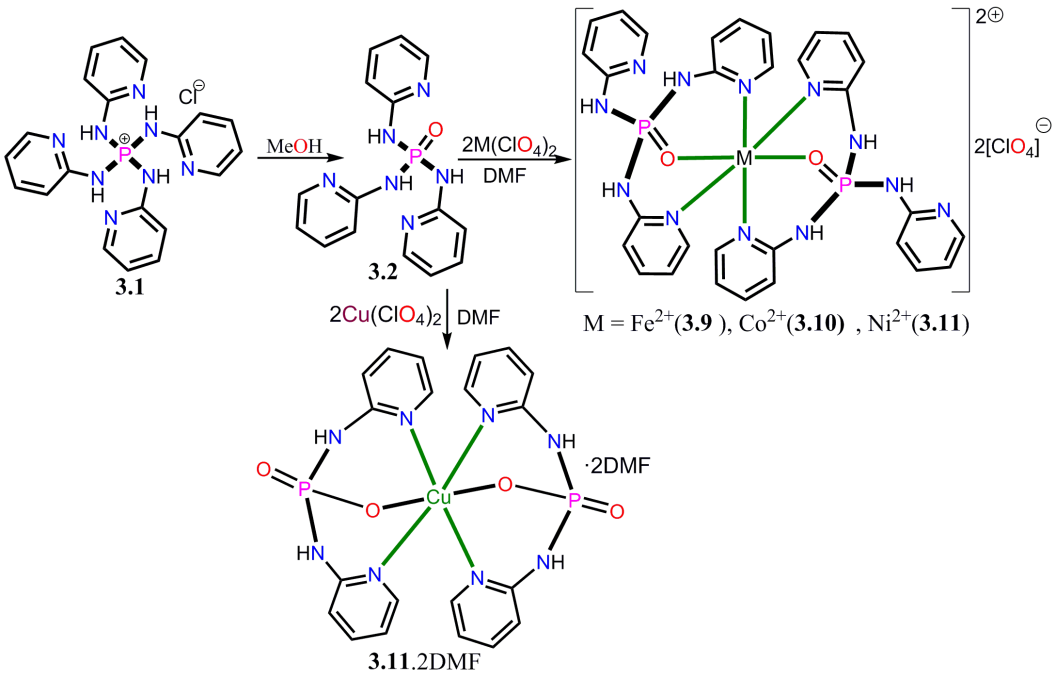

Scheme 3.4: Reaction conditions for the preparation of **3.9**, **3.10, 3.11** and **3.11**·2DMF

Interestingly, reaction of **3.1** with $Cu(NO_3)_2$ at room-temperature gave rise to a further cleaved in-situ generated ligand $[PO_2(NH^2Py)_2]^-$ $(^CL)^-$, in the corresponding complex

3.12. Performing the reaction at hydrothermal conditions at 90 °C with the view of obtaining the dianionic phosphonate ligand $[PO_3(NH^2Py)]^{2-}$ $(^CL)^{2-}$ results in the same complex **3.12** as no further cleavage was observed. This might be attributed to the stable arrangement of the octahedral Cu(II) ions in the N,N,O-coordination of the monoanionic ligand $(^CL)^-$. The same complex as a solvated molecule of **3.12**·2DMF was obtained when the reaction was performed with $Cu(ClO_4)_2$ at room temperature. The stability of **3.12**·2DMF in solution was confirmed by its MALDI-TOF mass spectrum which gave a peak at m/z = 674.9 corresponding to the species [**3.12**·DMF+K]$^+$ (Figure A2.6, Appendix 2). Formation of **3.12** and **3.12**·2DMF were observed when the reactions were performed with **3.2** instead of **3.1**.

In an effort to deliberately synthesize the in-situ ligand $(^CL)^-$ we treated the DMF solutions of **3.1** with 1M solution of HCl in water at 90 °C for 72 hrs and the solution was evaporated to dryness on a hot-plate to yield a solid sample (Scheme 3.5). MALDI-TOF mass spectrum of this sample gave a prominent peak at *m/z* = 288.98 pertaining to the species $[(^CL)+K]^+$, in addition to the peaks due to the corresponding pyridyl amine hydrochloride by-products. The ^{31}P-NMR of the solid shows peak at δ -9.34 ppm, for $[(^CL)+2H]^+$ which is considerably up-field shifted from the corresponding phosphonium precursors (Figure A2.7 and A2.8, Appendix 2). However, efforts to prepare the neutral derivative $[(^CL)+H]$ by subjecting these hydrochloride salts with bases such as Na_2CO_3, $NaHCO_3$, $(NH_4)_2CO_3$ and Et_3N did not result in a clean reaction. These observations clearly indicate that the in-situ formation of $(^CL)^-$ offer a facile reaction pathway to obtain the complex **3.12**. A similar reaction of **3.2** with a 1M solution of HCl in water at room temperature did not yield the in-situ ligand $(^CL)^-$ as observed from the mass-spectra, although **3.12** can be obtained from **3.1** and Cu(II) salts at room temperature. This observation suggests that in addition to the acidity of the reaction medium, the Lewis acidity of the Cu(II) ions play a crucial role for the in-situ ligand synthesis via a metal-assisted P-N bond cleavage pathway.

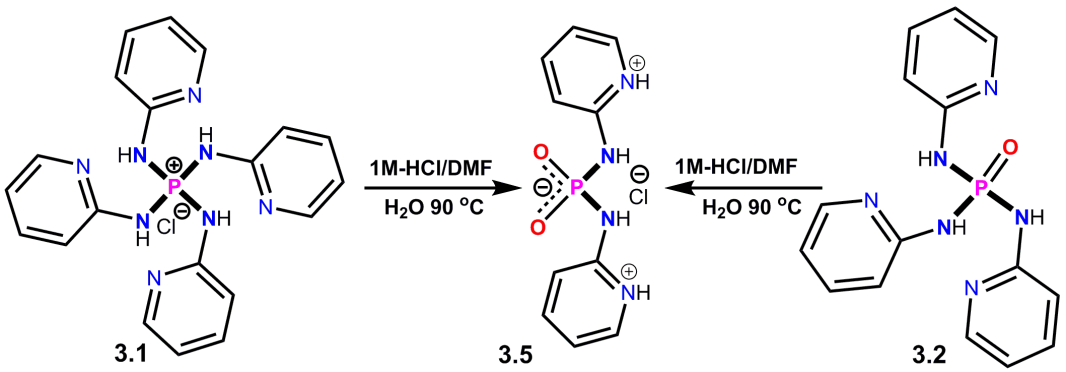

Scheme 3.5: High temperature reaction of **3.1** and **3.2** with a 1M HCl solution

In an effort to arrest the P-N bond cleavage, we set out to employ salts of certain soft transition metal ions, of 1st and 2nd row, which offers reduced Lewis acidities in comparison with the divalent 1st row transition metal ion. Thus, the reaction of **3.2** with $Cu^{I}Cl$ MeOH/$CHCl_3$ gave dark green colour crystals of **3.13** after 10 days. The crystallographic analysis showed that the phosphoramide ligand **3.2** has undergone a mono deprotonation with the formation of a mononuclear Cu(II) complex {Cu[PO(N^2Py)(NH^2Py)$_2$]Cl} in which Cu(I) has been oxidised to Cu(II) (Scheme 3.6). The in situ oxidation of Cu(I) to Cu(II) is attributed to the dissolved oxygen in the reaction solvents.

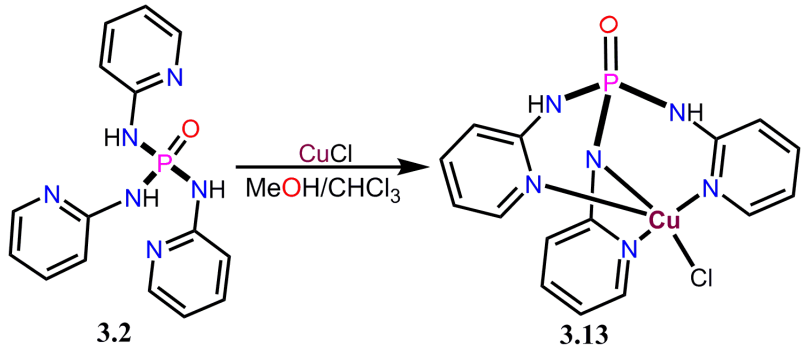

Scheme 3.6: Reaction conditions for the preparation of the **3.13**

Encouraged by the facile formation of **3.13**, we expected that the phosphonium salt **3.1** or neutral phosphoramide **3.2** will undergo deprotonation in presence of soft reactive metal salts. Accordingly, the phosphonium salt **3.1** was allowed to react, in slow diffusion, with excess silver perchlorate in methanol/toluene mixture. Colorless crystals of **3.14**·$(ClO_4)_3$ as a solvent adduct (of $2CH_3OH$ and $3C_7H_8$) was obtained after 12 hours. The crystallographic analysis showed that the phosphonium salt **3.1** has undergone a double deprotonation with the formation of a penta-nuclear silver complex. To the best

of our knowledge this is the first instance where the N-analogue of a phosphinate ion (of the type $H_2PO_4^-$) is obtained under such mild reaction condition. Formation of **3.14**·$(ClO_4)_3$ was also confirmed in a similar reaction involving **3.3** and excess silver perchlorate (Scheme 3.7). The ^{1}H-NMR spectrum of **3.14**·$(ClO_4)_3$ shows the formation of three new signals in the aromatic region indicating the presence of two different types of pyridyl rings. The ^{31}P-NMR spectrum of **3.14**·$(ClO_4)_3$ is again downfield shifted compared to **3.3** and shows a single peak at δ -2.1 pointing to coordination of imino nitrogens to the Ag^+ ions. The MALDI-TOF mass spectroscopy of **3.14**·$(ClO_4)_3$ in DMSO shows the presence of various cationic species in solution corresponding to $[Ag_5L_2]^{3+}$, $[Ag_4L_2]^{2+}$ and $[Ag_3L_2]^+$ at m/z centered at 1335, 1228 and 1121 respectively, confirming the parent cluster in solution.

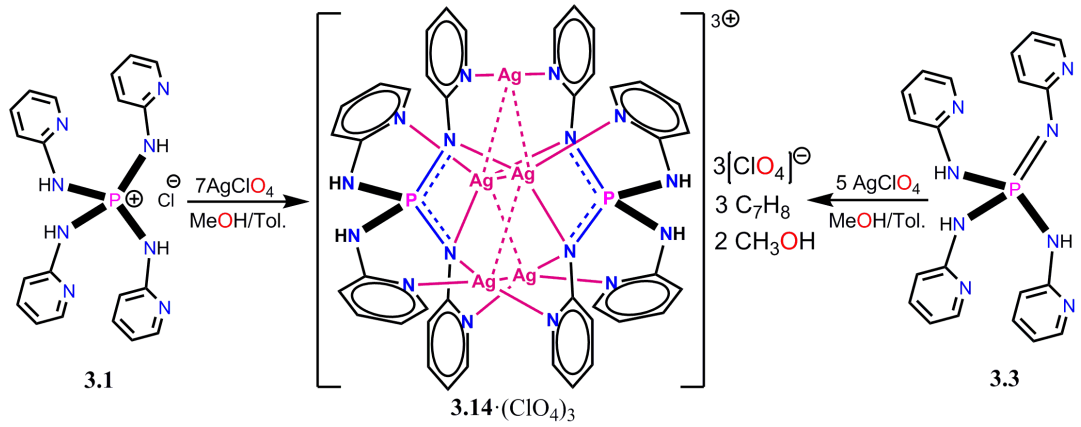

Scheme 3.7: Preparation of the complex **3.14**·$(ClO_4)_3$ from **3.1** and **3.5**

In an attempt to obtain the imido anions $[P(NH^2Py)(N^2Py)_3]^{2-}$ or $[P(N^2Py)_4]^{3-}$ of the type III or IV (Figure 3.1) stabilized by Ag(I) ions, we chose to react the phosphonium salt **3.1** in presence of the more reactive silver triflate salt (AgOTf). Although the reaction proceeded spontaneously forming the crystalline material in less than 72 h, the structural determination of this compound revealed the formation of a similar penta-nuclear Ag(I) complex **3.14**·$(OTf)_3$ stabilized by two $[P(N^2Py)_2(NH^2Py)_2]^-$ $(LH_2)^-$ mono-anions (Scheme A2.1, Appendix 2).

Subsequently to understand the Ag(I) mediated deprotonation chemistry of **3.2**, it was treated separately with excess of AgOAc, $AgNO_3$, $AgClO_4$, $AgBF_4$, $AgPF_6$, AgOTf and $AgSbF_6$ under similar reaction conditions. Crystalline products were obtained in three instances where formation of **3.15** $[Ag_3(^OLH_3)_2]^{3+}$, **3.16** $[Ag_8(^OLH_2)_4]^{4+}$ and **3.17** $[Ag_8(^OLH)_3]^+$, ($[PO(NH^2Py)_3]$ = $^OLH_3$; $[PO(N^2Py)(NH^2Py)_2]^-$ = $(^OLH_2^-)$; $[PO(N^2Py)_2(NH^2Py)]^{2-}$ = $(^OLH)^{2-}$), as colorless crystals in two weeks (Scheme 3.8). The

single crystal X-ray analysis showed the mono- and di-anions of the type II' and III' (Figure3.1) were formed in the reactions involving $AgClO_4$ and $AgBF_4$ salts, respectively. On the other hand, deprotonation of the ligand protons was not observed in the structure of **3.15** obtained in the reaction of **3.2** with $AgNO_3$. These initial observations suggested that the degree of deprotonation depends on the increasing reactivity of the Ag (I) salts. Although, we expected that the highly reactive AgOTf and $AgSbF_6$ might lead to the tri-anion of the type IV (Figure3.1), we have not been able to isolate a crystalline product in these reactions so far. The ^{31}P-NMR (in d_6-DMSO) spectra of the metal complexes **3.15** (δ -5.2), **3.16** (δ +1.5) and **3.17** (δ +9.3) are progressively downfield shifted and closely matches with the literature reported values for the similar amido and imido P(V) species. Unlike the solution NMR, The ^{31}P CP-MAS NMR of the crystalline samples of **3.15**, **3.16** and **3.17** show less pronounced shifts and gives single peaks centered at δ -2.08, -1.78 and -0.95, respectively (Figure A2.10, Appendix 2). In order to understand the preferential formation of mono and di-anions ($(^{O}LH_2)^{-}$) and ($^{O}LH)^{2-}$) in reactions of Ag(I) salts, we separately treated **3.2** with excess (8 eq.) of $AgClO_4$ and $AgBF_4$ in DMSO under stirring conditions. The ^{31}P-NMR (d_6-DMSO) of the reaction mixture in each of these reactions after two days showed two peaks at δ +9.3 and +1.5 (in addition to the free ligand peak at δ -4.9) indicating the presence of both $(^{O}LH_2)^{-}$ and $(^{O}LH)^{2-}$ ions, although in different ratios (Figure A2.11, Appendix 2). While the ratio of mono- and di-anions in the former reaction is 2:1, the obtained ratio in the latter reaction is found to be 1:1. These observations can lead to the inference that the reactivity of $AgBF_4$ with **3.2** is slightly higher than that of $AgClO_4$ forming the mono and di-anion in almost equal proportion. The ESI-MS studies of the crystalline samples of **3.15**, **3.16** and **3.17** in methanol provided confirmation for the presence of the parent clusters in solution (Figure A2.12, A2.13 and A2.14, Appendix 2). Thus for **3.15** and **3.17**, we observed peaks at *m/z* 972.9 and 1726.5 corresponding to the species $[Ag_3(LH_3)_2]^{3+}$ and $[Ag_7(LH)_3]^{+}$, respectively. Similarly for **3.16**, a series of peaks at *m/z* 540.9, 759.1, 1186.7 were observed corresponding to $\{[Ag_8(LH_2)_4](ClO_4)_{4-n}\}^{n+}$ ions (n = 4, 3, 2). In all these cases a major peak at *m/z* 433.0 was observed matching with the smallest fragment $[Ag(LH_3)]^{+}$. In addition, signals corresponding to several prominent fragment ions, with different Ag to ligand ratio, were found in all these spectra.

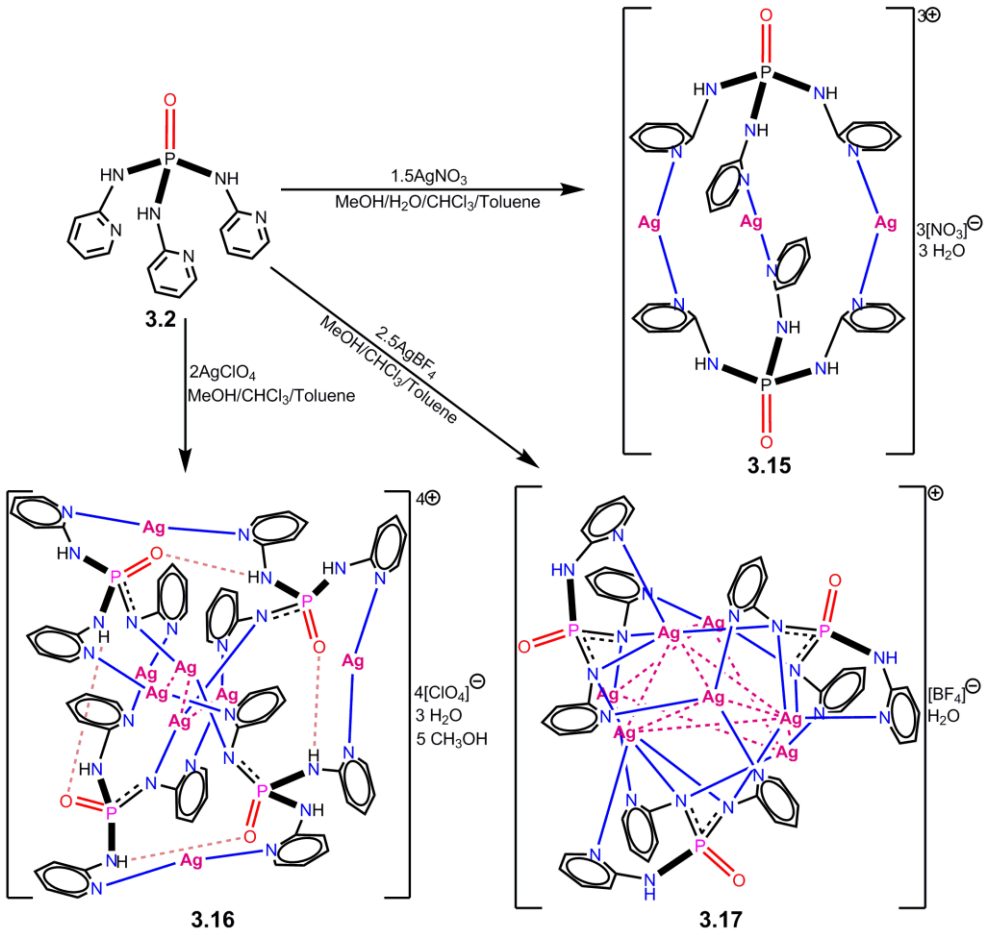

Scheme 3.8: Reaction conditions for the preparation of the Ag (I) clusters.

As it is evident that use of reactive and soft metal salts assists in the generation of imido P(V) anions, we choose to explore this chemistry with other such metal ions. In these studies we found that, the reaction of **3.1** with $Pd(CH_3CN)_2Cl_2$ in $MeOH/CHCl_3$ gave $\{Pd[PO(N^2Py)(NH^2Py)_2Cl\}_2 \cdot 4H_2O$, **3.18**·$4H_2O$ via the in-situ formation of **3.2**. The crystallographic analysis shows that **3.2** has undergone a mono-deprotonation stabilizing the dinuclear Pd(II) complex. Direct reaction of **3.2** with $Pd(CH_3CN)_2Cl_2$ gave the same complex **3.18** as a de-solvated polymorph (Scheme 3.9).

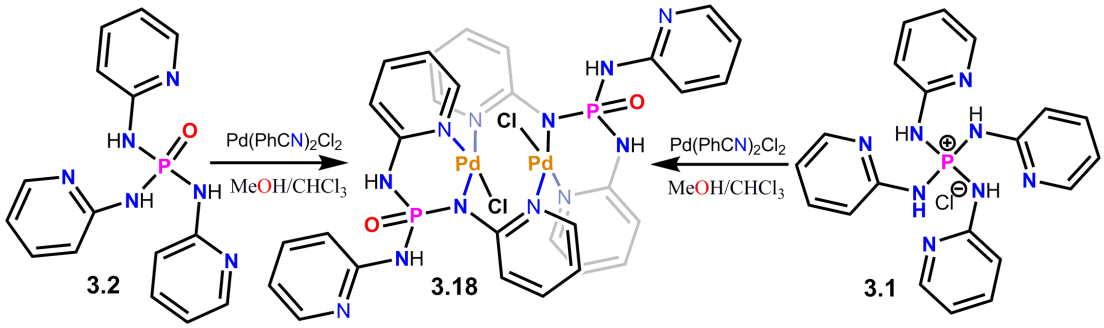

Scheme 3.9: Reaction conditions for the preparation of **3.18** via **3.1** and **3.2**

Reactions of the phosphonium cation **3.3** with di-cationic transition metal ions in methanol have found to give $[M_6L_8]^{12+}$ type self-assembled cage structures as reported before featuring the in-situ generated phosphoramide ligand **3.7**.[26] Unlike **3.2**, reaction of **3.4** with $PdCl_2$ gave the $[M_6L_8]^{12+}$ cage as no N-H bond deprotonation was observed for **3.4**. Hence in an attempt to obtain other kinds of self-assemblies based on these ligands, we chose to treat them with various kinds of copper salts as copper can adopt to various coordination geometries and oxidation states by subtle changes in the reaction conditions. Thus we first treated **3.3** with a Cu(I) salt such as $Cu(MeCN)_4PF_6$ in dry $CHCl_3$ at room temperature. Crystals obtained from this reaction have shown the formation of a new complex of formula $[(PO(NH^3Py)_3)CuCl_2]_2$, **3.19**, in which **3.3** has undergone a P-N bond cleavage reaction and Cu(I) has been oxidised to Cu(II).[27] The in-situ oxidation of Cu(I) to Cu(II) is attributed to the dissolved oxygen in the reaction solvent. The origin of the chloride ions that are bound to the copper atoms can be tracked to the anionic chloride present in **3.6**. It is interesting to note that the direct reaction of the phosphoramide **3.4** with Cu(II) ions leads to the formation of nanoscopic $[M_6L_8]^{12+}$ cage, whereas in the present instance a macrocyclic Cu(II) complex **3.19** has been obtained via the in situ formation of **3.6**. In another reaction, treatment of **3.4** with $Cu(NO_3)_2$ in DMF under hydrothermal conditions have lead to a cationic coordination polymer $\{[Cu_2(PO(NH^3Py)_3)_3](NO_3)_2\}_\infty$, **3.20**, wherein the precursor Cu(II) was reduced to a Cu(I) species. A similar observation was also made when **3.3** was treated with $Cu(NO_3)_2$ in DMF (Scheme 3.10). Although we anticipated a Cu(II) complex in these reactions, formation of a Cu(I) coordination polymer is believed to be formed by the reducing nature of DMF at high temperatures. Several reactions have been reported for the reduction of coinage metal ions such as Cu^{2+} and Ag^+ effected by DMF. It has been proposed that during these reactions DMF is converted into to Me_2NH and CO_2 via the intermediate carbamic acid Me_2NCOOH.[28]

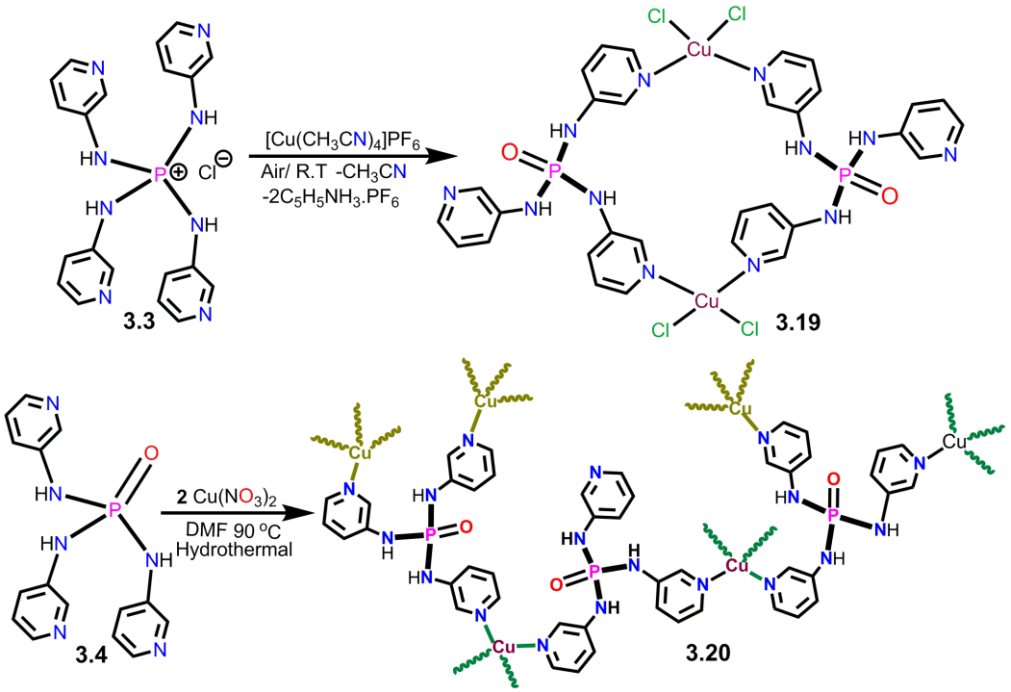

Scheme 3.10: Synthesis of the compounds **3.19** and **3.20**

3.3.2 Crystal Structures

The phosphonium salt **3.1** could not be crystallized owing to its unstable nature in polar protic solvents. Hence a DFT (B3LYP 6-31+G (d,p)) level energy minimized structure was obtained for **3.1** to understand the basic interactions in the molecule. The calculations show that in the ground state two of its four amino protons are involved in hydrogen bonding interactions with the chloride ion in a chelating manner (Figure 3.2a). The other two amino protons are intra-molecularly hydrogen bonded with the two adjacent pyridyl nitrogens. The remaining pyridyl groups are thus available for solvent interactions. The neutral phosphine imine **3.5** crystallized in the monoclinic *P2(1)/c* space group at room temperature. As anticipated, the P−N_{imino} distance (P1−N4: 1.574(2) Å) is considerably shorter than the other P−N distances (av. 1.636(2) Å). The nitrogens of the imino moiety (N4 and N42) accept hydrogen bonds from the neighboring amino groups (H3 and H2 respectively) whereas, the amino group (N1−H1) situated along the same side of it acts as a hydrogen bond donor to N32 (Figure 3.2b). Theoretical calculation based on the structure further confirm this observation as the HOMO of **3.3** is primarily located on the imino group and partly to the pyridyl ring attached to N3. The pyridyl amino moiety that belongs to N1 contributes to the LUMO of the molecule (Figure A2.16, Appendix 2).

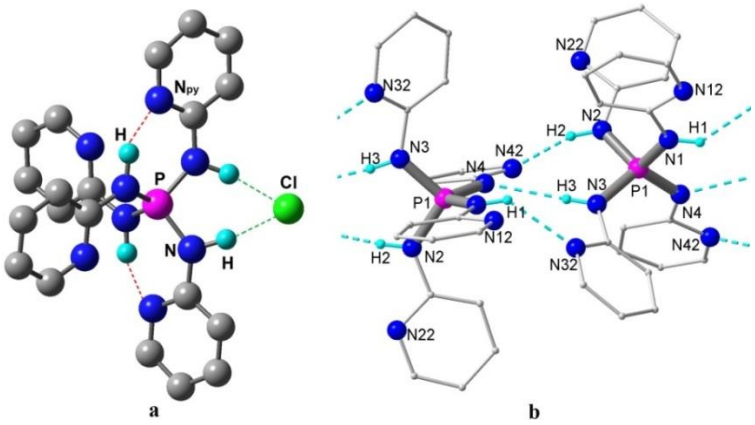

Figure 3.2: (a) Energy minimized structure of **3.1** obtained by DFT calculation (B3LYP 6-31+G (d,p)) (b) Crystal structure of **3.5** showing the formation of a 1D-chain mediated by N−H...N hydrogen bonding interactions

Although there was one previous report pertaining to the crystal structure of **3.2**, we have observed a new polymorph of this compound in our present study. While the previously reported structure was obtained in monoclinic, *P2(1)/n* space group,[16] the present one, crystallized during the slow cleavage of **3.1** in methanol, was solved in hexagonal space group *R-3*. The asymmetric unit of **3.2** contains one third of the molecule as the structure assumes an overall C3 symmetry along the axis of the P═O bond (Figure 3.3a). Each pyridyl amino moiety acts a donor (via N-H group) as well as an acceptor (via pyridyl nitrogen) of inter-molecular hydrogen bonding. The cumulative effect of these interactions leads to the formation of a 2D-hexagonal network mediated by N-H…N interactions (Figure 3.3a). Each unit of **3.2** interacts with three immediate neighboring molecules and involved in fusing the adjacent hexagonal unit. While the donor-acceptor interaction of each pyridyl amino group forms an eight membered ring represented by graph set $R_2^2 8$ notation,[29] formation of a 36-membered ($R_6^6 36$) ring was observed within each hexagonal network. It is also worthwhile to note that in the previous instance (in *P2(1)/n* symmetry), the structure propagates as a one dimensional chain mediated by both N-H…N and N-H…O interactions. However, in **3.2** the phosphoryl oxygens are rendered above and below the hexagonal 2D-plane and remains non-interacting with the amino protons. In one of the crystallization reactions involving **3.2** and AgOAc we observed the formation of a toluene adduct of **3.2** (**3.2**·C_7H_8), instead of the expected Ag(I) complex. This is attributed to the solvent incompatibilities of **3.2** and AgOAc under the given reaction conditions resulting in the crystallization of **3.2**·C_7H_8. The structural description of **3.2**·C_7H_8 has been provided in the Figure A2.19 and A2.20,

Appendix 2. The structure of **3.2**·C_7H_8 was obtained in monoclinic *P2(1)/c* space group. The asymmetric unit consists of four molecules of $PO(NH^2Py)_3$ and four toluene molecules. The metric parameters associated with P–N and P=O bonds are comparable with the reported structures of **3.2**. In the crystal structure of **3.2**.C_7H_8, two of the three amino protons in each ligand are inter-molecularly interacting with two pyridyl nitrogens forming an H-bonded dimer. These dimers are further connected through the third amino protons and phosphoryl oxygens resulting in a 1D-chain structure (Figure 3.3b). Interestingly, the packing diagram of **3.2**·C_7H_8 shows a 1D-channel structure in which solvated toluene molecules are occupied in the void space.

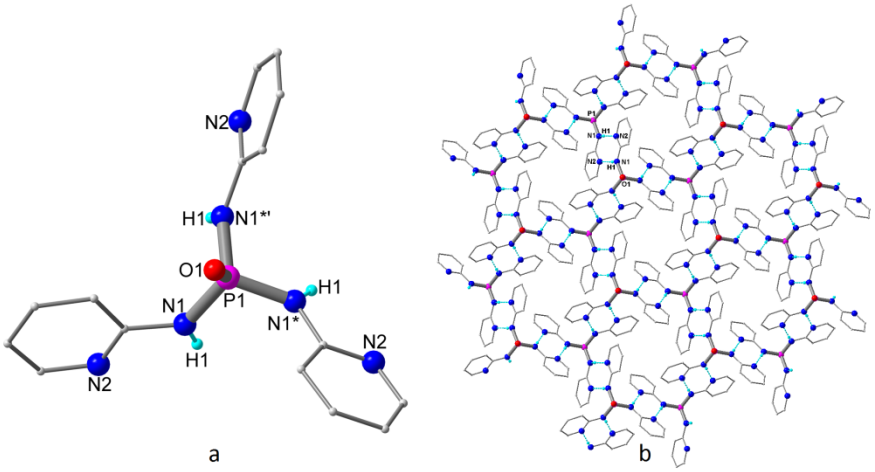

Figure 3.3: (a) Molecular structure of **3.2** obtained during the crystallization of **3.1** (b) Formation of the hexagonal network in **3.2** mediated by N-H…N interactions

Crystals of **3.7** suitable for Single crystal X-ray diffraction (SC-XRD) were obtained from the slow evaporation of its solution in methanol. The molecular structure was solved in the triclinic space group *P-1* comprising of the phosphonium cation, one nitrate ion in three disordered positions and two solvated molecules of water in its asymmetric unit (Figure 3.4a). The observed P-N bond distances were found to be in the range between 1.598 and 1.646 Å as observed for related aryl- or alkyl amino phosphonium compounds. Two of the four N-H bonds were involved in inter-molecular hydrogen bonding interactions with pyridyl N-sites originating from same segments (from two other molecules) in a complementary fashion. These N-H…N interactions thus propagate in a head to tail fashion and result in the formation of a 1D-double chain structure (Figure 3.4b).

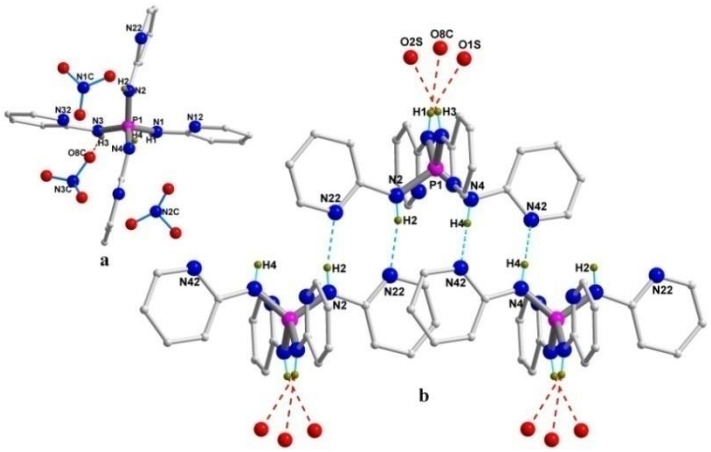

Figure 3.4: (a) Molecular structure of **3.7**·$2H_2O$ (b) Formation of 1D-chain structure in **3.7**·$2H_2O$ mediated N-H…N interactions

The remaining N-H sites are projected away from the double-chain (above and below) and involved in hydrogen bonding interactions with the solvated water molecules and one of the disordered nitrate motifs. These hydrogen bonded water molecules further interact with the nitrate ions and connect the adjacent chains to form a 2D-layered structure (Figure A2.21, Appendix 2). The metric parameters associated with these H-bonds point to very strong interactions. As a result of these H-bonding interactions two varied types of N-P-N bonds were found in the structure deviating from the tetrahedral angle (109.4°). The shortest angle of 100.24(2)° is found in the N2-P1-N4 segment involved in the complementary N-H…N interaction and is part of an eight-membered $R_2^2 8$ ring (graph set notation).[29] Similarly the shorter angle of 104.39(2)° is found for the N1-P1-N3 segment located on the other side of the double chain. Whereas, the remaining four distances were longer and range between 110.54(2)° and 116.73(2)° and were associated with the mixed N-H…N and N-H…O interactions located inside and above the double-chain, respectively.

Like **3.1**, the phosphonium salt **3.3** could not be crystallized due to its instability in polar solvents. Thus, we obtained an optimized structure by DFT (B3LYP 6-31+G (d,p)) calculation using Gaussian 03 software to understand the interactions in this molecule. From the optimized structure it is apparent that the chloride ion is involved in a chelating H-bonding interaction with two of the four N-H groups, while the remaining two N-H groups that are attached to the phosphorus atom might participate in H-bonding with the pyridyl nitrogens (Figure 3.5a).

Crystals of **3.6**·1/2H_2O suitable for single crystal X-ray analysis was obtained from its methanolic solution. The phosphine imine derivative was crystallized as **3.6**·1/2H_2O and solved in the monoclinic space group *P2(1)/c*. The asymmetric unit consists of four unique molecules of **3.8** and two solvated water molecules (Figure 3.5b). The P-N_{imino} (av. 1.591(17) Å) distances are considerably shorter than the P-N_{amino} (av. 1.635 (18) Å) distances as observed for the 2-pyridyl attached phosphine imine described earlier.

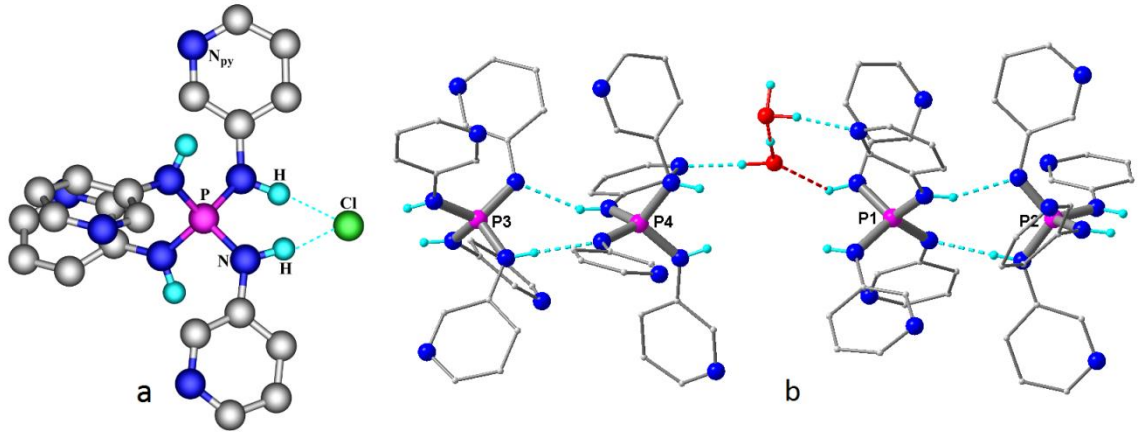

Figure 3.5: (a) Energy minimized structure of **3.3** obtained by DFT calculation (B3LYP 6-31+G (d,p)) (b) Crystal structure of **3.6** showing the formation of a 1D-chain mediated by N−H...N hydrogen bonding interactions

Formation of an intricate H-bonded three-dimensional (3-D) network was observed in **3.6**·1/2H_2O, due to the interaction of the N-H and O-H groups with Lewis basic imino and pyridyl nitrogens and water oxygens. Formation of the 3D-network in this molecule can be understood as follows. First, the imino nitrogens in each of the four **3.6**·1/2H_2O segments is involved in H-bonded interaction with the neighbouring N-H protons in a head to tail fashion and forms a dimeric structure. Thus, the asymmetric unit consists of two such dimers consisting of the graph set[29] $R_2^2 8$ type rings which are connected to each other via the H-bonding interactions from the solvated molecules of water. These individual dimers are further connected to each other through N-H...N interactions and results in the form of a zigzag 2D-sheet like structure (Figure 3.5b). The solvated water molecules are located between these 2D-sheets and connect them to form a 3D-network (Figure A2.22, Appendix 2).

The crystal structure of {Fe[$PO(NH^2Py)_3]_2$} **3.9**·2H_2O and **3.11**·2CH_3OH, {Ni[$PO(NH^2Py)_3]_2$} were solved in space group *P-1* with its asymmetric unit featuring

two unique one half segments of the complex, two perchlorate anions and two molecules of methanol respectively. Similarly **3.10**, {Co[PO(NH^{2}Py)$_3$]$_2$} was solved in *P2(1)/c* with one-half of the molecule in the assymetric unit (Figure 3.6). In all these three structures, the metal ions take up a distorted octahedral geometry consisting of four equatorial $N_{pyridyl}$ contacts and two axial contacts from the phosphoryl oxygens. Each ligand moiety offers two $N_{pyridyl}$ bonds to the metal centre while the third ones projected away from the metal centre and involved in H-bonding interaction with the amino protons (Figure 3.6a). Additionally, the other amino protons are also found to be interacting with the perchlorate anions through hydrogen bonding.

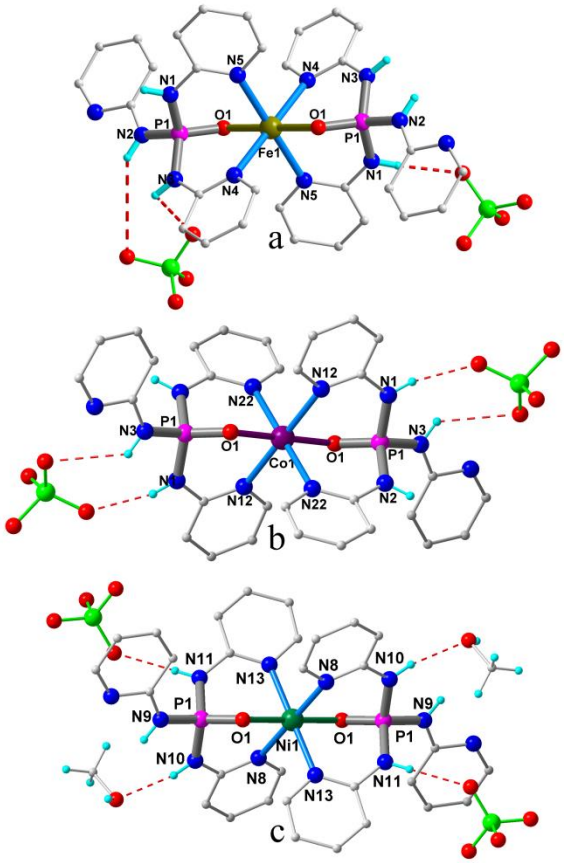

Figure 3.6: Molecular structure of **3.9** (a), **3.10** (b), **3.11** (c).

The copper (II) imido complex **3.13**·DMF was crystallized in the monoclinic space group *P2(1)/n* featuring the whole molecule in the asymmetric unit. The molecular core consist of one Cu(II) atom which is held by the tetra-dentate coordination from the anionic ligand moiety ($^{O}LH_2)^-$ through its three $N_{pyridyl}$ and one N_{imido} sites and one coordinated chloride ion. Thus, the coordination environment around the metal centre is distorted trigonal bipyramidal with three equatorial $N_{pyridyl}$ contacts. The charge balance is restored with one chloride anion attached with Cu(II) atom (Figure 3.7). Interestingly,

formation of the complex **3.13** is facilitated by the redox non-innocent behavior of the phosphoramide in which the ligand reduction (deprotonation) is concomitantly balanced by the oxidation of the metal ion.

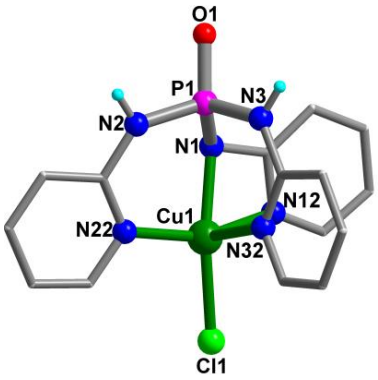

Figure 3.7: The Molecular structure of the mononuclear complex in **3.13**

The molecular structure of **3.11** was solved in the tetragonal space group *I41/acd*. The asymmetric unit of it consists of a Cu(II) ion in one half occupancy and one $(L^1)^-$ ligand moiety. The molecular core consists of a dicationic Cu-center and the charge balance is restored by two $(^CL)^-$ ligands. The coordination geometry around the Cu(II) atom is distorted octahedral featuring four $N_{pyridyl}$ contacts and two O^- coordination derived from the chelating tridentate N, N, O coordination of the two $(^CL)^-$ ligands (Figure 3.8a). The uncoordinated phosphoryl oxygens were involved in a bifurcated H-bonding interaction with protons of the pyridyl amino moieties in which every phosphoryl oxygen atom is part of two eight-membered $R_2^2 8$ rings. The net effect of these H-bonding interactions gave rise to a three dimensional supramolecular network for the structure of **3.12**. The packing diagram of this H-bonded 3D-network shows a tightly packed structure along the tetragonal lattice and shows a very narrow pore along the c-axis with a diameter of 3.870 Å (Figure 3.8b). The calculated void space is around is 284.5 $Å^3$ which amounts to only 3% of the unit-cell volume.

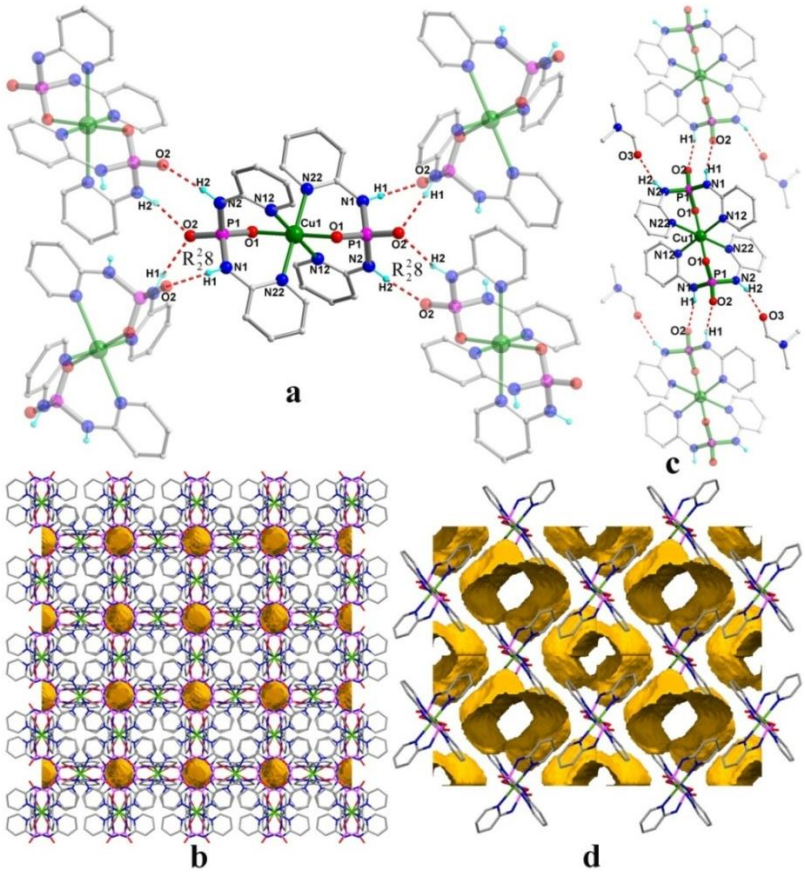

Figure 3.8: The molecular structure and H-bonding interactions in (a) **3.12** and (c) **3.12**·2DMF. Connolly contact surface view of a 2x2x2 packing structure in 3 (b) and **3.12**·2DMF (d) using a probe radius of 1.2 Å and a grid spacing of 0.2 Å

In contrast, the molecular structure of **3.12**·2DMF was solved in the monoclinic space group *P2(1)/n*. As observed before the core structure as well as the octahedral coordination around the Cu(II) center remains same. However, the H-bond assisted supramolecular network in **3.12**·2DMF leads only to a 1D-chain structure (Figure 3.8c). This is due to one of the ligand amino protons in **3.12**·2DMF is engaged in H-bonding with the solvated DMF. This interaction not only prevents the proximity of the adjacent complex but also destroys the bifurcated interaction at the P=O group that was present in **3.12**. As a result, packing diagram of the molecule shows a larger pore with distances ranging from 6.777 Å to 13.835 Å. The channel volume inside is calculated to be 534.5 $Å^3$ (34.3% of the unit cell volume) which are occupied by the solvate molecules of DMF (Figure 3.8d). The metric parameters associated with the P-N, P-O, Cu-N and Cu-O in both **3.12** and **3.12**·2DMF are consistent with the literature reported values.

The compound **3.14**·$(ClO_4)_3$ crystallized in the centro-symmetric orthorhombic space group *Pccn*. The molecular core consists of a tri-cationic cluster of five Ag(I) ions which

are held together by two anionic $[L]^-$ ligands. The charge balance in the molecule is restored by the presence of three perchlorate anions (Figure 3.9a). Each anionic ligand binds to the five Ag(I) ions through its four pyridyl and two imino nitrogens in a hexadentate mode. Among the five Ag(I) ions, four of them are involved in coordination with either one or two imido sites. While one of the imino nitrogens (N1) makes a shorter contact (2.219(4) Å) and bonds with Ag1, the other one (N2) hosts two Ag centers, Ag1−N2: 2.391(4) and Ag2−N2: 2.490(5), at slightly longer distances. The fifth unique silver ion (Ag3) is located at the two fold axis of symmetry and is coordinating only with two pyridyl nitrogens. The P−N bond distances due to the imido nitrogens (av. 1.60(5)) in **3.15** are slightly longer than the imino distance found in **3.3**. This indicates the anionic charge of the ligand in **3.14**·$(ClO_4)_3$ is delocalized between the two imido groups. The complex **3.14**·$(OTf)_3$ crystallizes as **3.14**·$(OTf)_3$·3DMF from its reaction mixture in methanol, toluene and DMF. SC-XRD analysis shows that it crystallizes in the triclinic space group *P-1*. The asymmetric unit consists of the complete $[Ag_5L_2]^{3+}$ core, three disordered triflate (OTf^-) anions and three DMF molecules. The core structure of **3.14**·$(OTf)_3$ resembles very closely to that of **3.14**·$(ClO_4)_3$ featuring two doubly deprotonated hexadentate ligands $(LH_2)^-$ bonded to a tricationic cluster of five Ag(I) ions (Figure 3.9b). The P-N_{imido} distances (P1-N3, P1-N4, P2-N5 and P2-N6: average, 1.604(5) Å) are slightly shorter than the P-N_{amido} distances (P1-N1, P1-N2, P2-N7 and P2-N8: average, 1.668(5) Å) suggesting the delocalized nature of the anionic charge between the two imido moieties house on each P-atom. Four of the five Ag(I) ions in **3.14**·$(OTf)_3$ are found in a tricoordinate environment of which two of them (Ag1 & Ag3) contains two N_{imido} and one $N_{pyridyl}$ contacts. The remaining three Ag(I) ions have two $N_{pyridyl}$ bonds each, as Ag5 does not make any N_{imido} contacts. While, two of the three disordered triflates were engaged in H-bonding interactions with the Lewis acidic bidentate amido protons (HN-P-NH) in a chelating fashion, the third triflate is bonded to one of the Ag(I) ion at a slightly longer distance (Ag5-O1S: 2.595(16) Å).

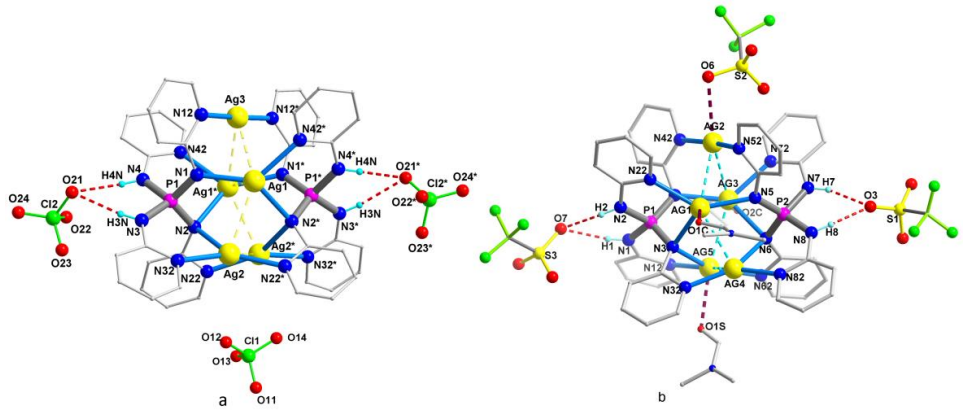

Figure 3.9: (a) Molecular structure of **3.14**·$(ClO_4)_3$ showing the cationic cluster and the perchlorate anions. (b) Molecular structure of **3.14**·$(OTf)_3$ showing the cationic cluster and the triflate anions.

Apart from the Lewis basic imido sites that are bonded to Ag(I) ions, each ligand in **3.14**·$(ClO_4)_3$ also offers a bidentate HN-P-NH site which binds to a perchlorate anion via H-bonding. Interestingly, the solid state packing of the molecule reveals the formation of a grid like structure with open channels (Figure 3.10a). These channels are occupied by solvated toluene and methanol molecules in an alternate fashion. While the hydrophobic toluenes are situated closer to the aromatic rings of the cluster, the anionic perchlorates encapsulate the methanol molecules (Figure A2.23, Appendix 2).

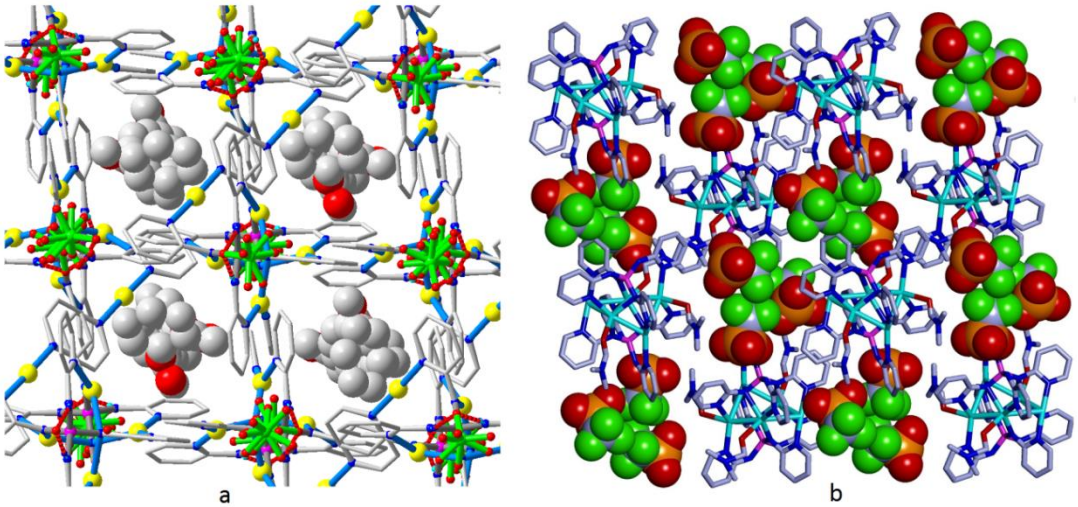

Figure 3.10: (a) Packing structure of **3.14**·$(ClO_4)_3$ showing the solvated channels containing toluene and methanol (b) Packing Diagram of **3.14**·$(OTf)_3$ indicating the presence of triflates anions and DMF molecules in the packing structure (as CPK model).

Unlike **3.14**·$(ClO_4)_3$ where the solvated methanol and toluene were located in the porous channels arising from the grid-like packing of the cluster and anions, the three DMFs in

3.14·$(OTf)_3$·3DMF are coordinated to three Ag(I) ions (Ag1, Ag3 and Ag5) resulting in the formation of a densely packed structure in which two distinct cavities were observed for DMF and triflates (Figure A2.24, Appendix 2). The average Ag-Ag distances were measured to be 2.984(10) Å which is slightly longer than those found in metallic silver (2.880 Å).[22]

Formation of the high-nuclearity Ag(I) complexes in **3.14**·$(ClO_4)_3$ and **3.14**·$(OTf)_3$ are unprecedented and attributed to the tetrahedral nature of the phosphorus center. Further, the pyridyl rings of the ligands in **3.14**·$(ClO_4)_3$ and **3.14**·$(OTf)_3$ are rendered in a cisoidal fashion and encapsulate the metal centers from both sides. Although, there are a few examples for penta-nuclear Ag(I) clusters,[30] compounds **3.14**·$(ClO_4)_3$ and **3.14**·$(OTf)_3$ are the second examples of such a discrete cluster with all nitrogen coordination. The only other example where a $[Ag_5L_4]^{5+}$ cluster was stabilized by the ligand 3,6-di (2-pyridyl)-pyridazine containing bulky trimethylsilyl group at the 4-position.[31] The Ag−Ag distances found in **3.14**·$(ClO_4)_3$ and **3.14**·$(OTf)_3$ are in the range between 2.9647(7) Å (Ag1−Ag2) and 3.1772(12) Å (Ag2−Ag2*) and are closely comparable to those found in metallic silver (2.880 Å).[32]

The compound **3.15**·$3H_2O$ crystallized in the chiral monoclinic space group *P2(1)*. The asymmetric unit consists of two crystallographically independent tri-cationic cluster cores, six nitrate anions and six molecules of water. The Ag(I) cations in **3.15** are found in two-coordinate environment and are bonded to pyridyl nitrogens from two different ligands (Figure 3.11a). The Ag−N distances in **3.15** range from 2.129(16) to 2.206(18) Å, and the N–Ag–N angles are in between 167.8(6)° and 177.6(8)°. The cationic motif can be viewed as a trigonal bipyramidal cage structure in which the three Ag(I) centers forming the equatorial plane and the two P-atoms taking up the axial sites. The average Ag–Ag separation within the cluster is 6.052(7) Å matching closely with other $[Ag_3L_2]^{3+}$ cages containing relatively bulky tripodal ligands. Each $[Ag_3(^{O}LH_3)_2]^{3+}$ unit in **3.15** offers suitable binding pockets for three nitrate anions which are held closer to the cationic cluster via H-bonding interactions with the amino protons. Further, two of the three Ag(I) ions in each tri-cationic cluster make long-contacts with the nitrate oxygens (avg. Ag–O distance: 2.716(6) Å) that are housed at the adjacent cluster unit leading to an 1D-chain structure. While the $[Ag_3L_2]^{3+}$ type cages are well documented for many tripodal N-donor ligands, formation of such a molecule in the present instance is driven by the relative reactivities of the Ag(I) salts. The ligand moieties in **3.15** are C_3-

symmetric and resemble the "TrieCassyn" symbol of the "Isle of Man" flag. While one of the ligands in a given $[Ag_3(^{O}LH_3)_2]^{3+}$ unit shows a clockwise rotation (Δ) of its pyridyl arms, those of the other one shows an anti-clockwise rotation (Λ) (Figure3.11b and 3.17c). Hence each of the tri-cationic motifs in the crystal structure of **3.15** is a racemate.

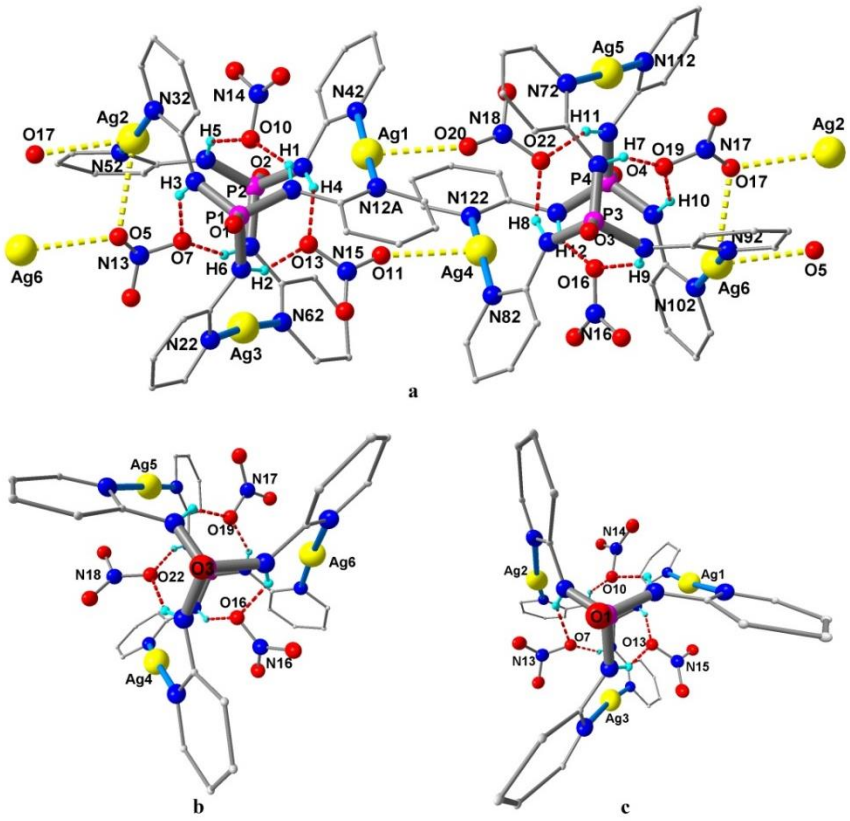

Figure 3.11: (a) Molecular structure of **3.15** showing the interaction between the two tri-cationic motifs. Solvated water molecules have been omitted for clarity. The central projection of the anti-clockwise (b) and clockwise (c) rotation of the ligand arms in **3.15**.

The molecule **3.16**·$5CH_3OH·3H_2O$ crystallized in the monoclinic space group *C2/c*. The molecular core comprises of the tetra-cationic cluster of eight Ag(I) ions which are held together by four anionic ($^{O}LH_2^-$) ligands. The charge balance is restored by the presence of four perchlorate anions that are disordered over five positions. Each of the four anionic ligands of type II' (Figure3.12a) binds to four Ag(I) ions through one imido and three pyridyl nitrogens. All the eight Ag(I) centers in **3.16**·$5CH_3OH·3H_2O$ are involved in a linear coordination in which two of them, Ag1 and Ag2, are located inside the cluster core and bonded solely with the imido groups. Thus, Ag1 is bonded to N3 and N9 and Ag2 is bonded to N6 and N12, respectively. The remaining six Ag(I) ions are situated along the either ends of the cluster, as two triangular units, and interact with the pyridyl nitrogens (Figure3.12a). While the average Ag–N_{imino} distance in

3.16·5CH_3OH·3$H_2O$is 2.122 (7) Å, the Ag−$N_{pyridyl}$ contacts are found between 2.141(9) and 2.230(9) Å. The P−N_{imino} distances (av. 1.610 (8) Å) are marginally shorter than the other P−N_{amino} distances (av. 1.666 (8) Å) indicating the delocalized nature of the anionic charge inside the cluster. There are three short Ag−Ag contacts viz., Ag1−Ag5: 2.753(1), Ag1−Ag2: 2.9084(1) and Ag2−Ag3: 2.7658(11), connecting the two inner (Ag1 and Ag2) and two outer (Ag3 and Ag5) cations.

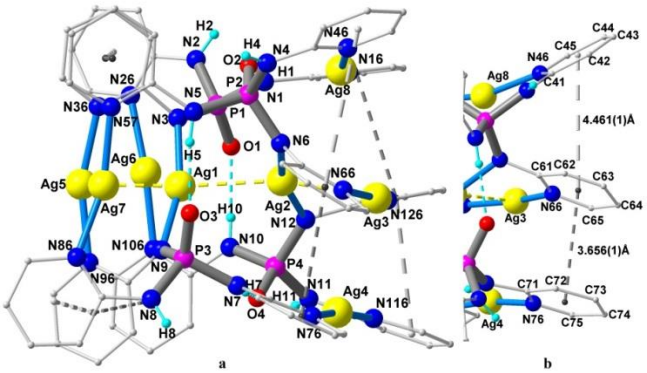

Figure 3.12: (a) View of the octa-nuclear cluster in **3.16**·5CH_3OH·3H_2O (b) closer view of one of the four π-π stacked triads.

The phosphoryl oxygens are intra-molecularly hydrogen bonded, in a concerted manner, to one of the amino protons of the adjacent imido phosphate ligands. The remaining amino groups are hydrogen bonded to either perchlorate anions or the solvated water molecules (Figure A2.25, Appendix 2). Further, the twelve pyridyl rings of the four ($^{O}LH_2^-$) ligands, situated along the cluster rims, form a set of four π-π stacked triads. Within a given triad the inter-ligand π-π interaction is stronger (av. 3.71(2) Å) than that of the intra-ligand (av. 4.12(4) Å) interaction (Figure 3.12b). Formation of the 3D-supramolecular assembly was also observed as the outer Ag(I) centres form weak contacts with perchlorate and water oxygens (Figure 3.12b).

The molecular structure of **3.17**·H_2O was solved in the chiral hexagonal space group *R3*. The asymmetric unit consists of one third of the molecule where the ligand ($^{O}LH^{2-}$) and two Ag(I) ions (Ag1 and Ag2) take up the general positions. The third unique Ag(I) centre, labeled Ag3, the tetraflouroborate anion and the water molecules sit at the three fold axis of symmetry and have one third occupancies each (Figure 3.13a). Each of the three ligands in **3.17**·H_2O is bonded to five Ag(I) ions through its two imido (N1 and N2) and three pyridyl (N12, N22 and N32) nitrogens. Three varied types of coordination is found for the Ag(I) ion in **3.17**·H_2O: an almost linear coordination for Ag1 (N1 and

N12*), a tetra-coordination for Ag2 (N1, N2, N2** and N32) and a nearly planar tri-coordination for Ag3 (N22, N22* and N22**). While N1 forms the shorter (Ag1−N1: 2.139(7) Å) and the longer (Ag2−N1: 2.698(8) Å) contacts to Ag(I) ions, N2 interacts with two Ag2 ions at moderate distances (Ag2−N2: 2.392(6) Å and Ag2*−N2: 2.286(6) Å). The Ag−$N_{pyridyl}$ distances are similar to **3.15**·$3H_2O$ and **3.16**·$5CH_3OH.3H_2O$ and ranges from 2.14(1) Å (Ag1−N12) to 2.331(5) Å (Ag2−N32). It is worthwhile to note the arrangement of seven Ag (I) ions in **3.17**·H_2O where the three crystallographically unique Ag centers are located in different layers. While the first and second layers contain the respective triangular arrays of Ag1 and Ag2 ions, Ag3 forms the third layer and serves as the capping unit (Figure 3.13b). Thus, the structure of the cationic Ag7 core can be viewed as a mono-capped distorted prismane in which the two triangular units of Ag1 and Ag2 deviate by an angle of 11.9°. The Ag−Ag distances in **3.17**·H_2O are found between 2.899(1) (Ag2–Ag3) and 3.218(1) (Ag1–Ag1*) Å and compares closely to those found in metallic silver (2.88 Å).[32] In the solid state the molecule arranges in the form of a 2D-hexagonal sheet through hydrogen bonding interactions (Figure 3.13c). The cationic core consists of three Lewis-acidic NH sites that are bonded to three anionic BF_4 units through N-H...F H-bonding interactions. In addition, the two water molecules, disordered over three sites, interact with the phosphoryl oxygens from the neighboring clusters.

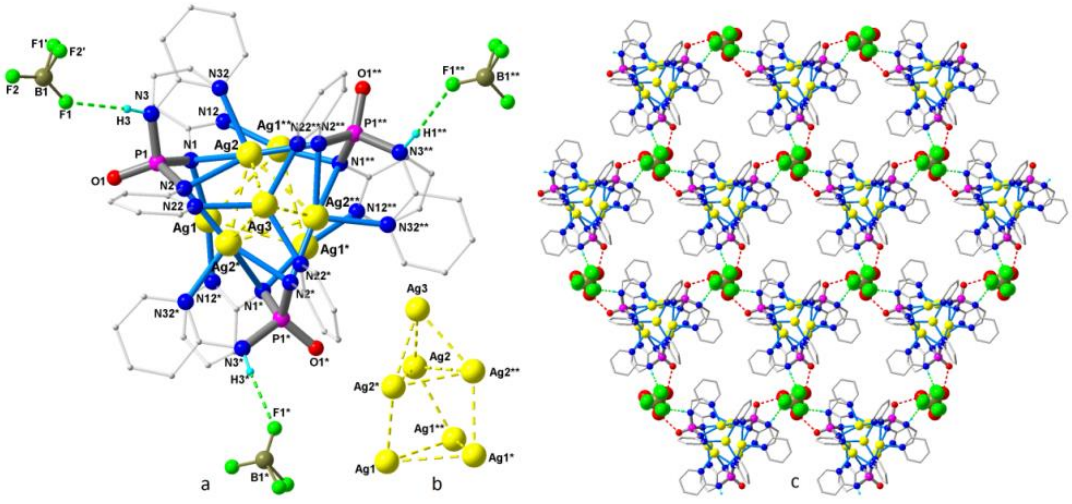

Figure 3.13: (a) The Molecular structure of the hepta-nuclear cluster in **3.17**·H_2O (b) inner view of the Ag_7 core (c) formation of a 2D-hexagonal sheet structure aided by H-bonding interactions.

Although there are a number of reports pertaining to the structures of hepta- and octa-nuclear Ag(I) clusters,[33,34] most of them have been obtained in presence of soft chalcogen

(S or Se) or π-donor ligands. To the best of our knowledge, this is the first report on such hepta- and octa-nuclear complexes containing all nitrogen coordination. Further, the pyridyl rings of the ligands in **3.15**, **3.16** and **3.17** are arranged in a mutually cis-fashion and involved in encapsulating the cluster moieties. The P=O groups in all these cases are pointing away from cluster center and remain non-coordinating. Furthermore, the observed mono- and di-deprotonation of the ligand protons in **3.14**, **3.16** and **3.17** is driven by the relative reactivities of the Ag(I) salts as well as the acidic nature of the amino protons in the precursor ligands indicated by their pKa[36] values (4.35 in case of **3.5** and 4.01 in case of **3.2**) in MeOH (Figure A2.26, Appendix 2).

The crystal structure of **3.18**.4H_2O was solved in cubic space group *Fd-3c* with one-half of the molecule in the asymmetric unit (Figure 3.14). The unit-cell packing suggests a Z value 96 for an overall volume of 121253 Å whereas the crystal structure of **3.18** was solved in monoclinic space group *C2/c* with one-half of the molecule in asymmetric unit. The unit-cell volume in **3.18** is found to be 3470 $Å^3$ with Z = 4. In both cases, the molecular core consist of a dinuclear Pd(II) assembly supported by two mono-deprotonated phosphate ligands ($^{O}LH_2^-$). The coordination geometry around each Pd(II) centre is square planar with two $N_{pyridyl}$ trans-contacts from two different ligand moieties, one imido nitrogen and one chloride ion.

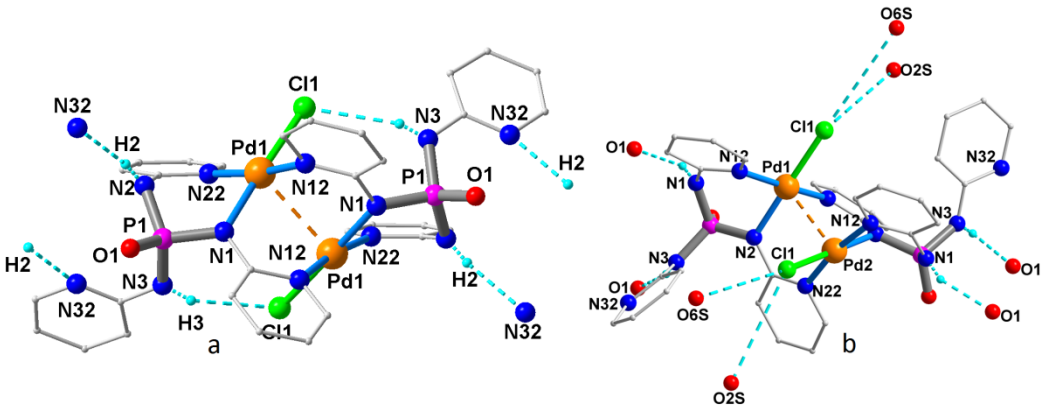

Figure 3.14: The Molecular structure of the di-nuclear Pd(II) complex in **3.18** (a) and **3.18**.4H_2O (b)

While the core structures in **3.18** and **3.18**.4H_2O are similar, their supramolecular structures were drastically different. Of the two amino protons in each ligand moiety in **3.18**, one of them is intra-molecularly H-bonded to the chloride ion (N3-H3…Cl1) and other one is inter-molecularly H-bonded to the free pyridyl nitrogen of the neighboring assembly (N2-H2…N32). As a result of this inter-molecular interaction, a 1D-chain like

structure mediated by the H-bonding interactions is obtained in **3.18**. However, such N-H…N and N-H…Cl interactions are absent in **3.18**.4H_2O as the amino protons and the chloride ions are H-bonded to the solvate molecules of water. The packing diagram of **3.18**.4H_2O reveals that the solvated molecules are located in two distinct channels: one of them consisting of the metal bound chloride ion and the other one consisting of the amino groups. However such a channel structure is absent in case of **3.18** (Figure 3.15).

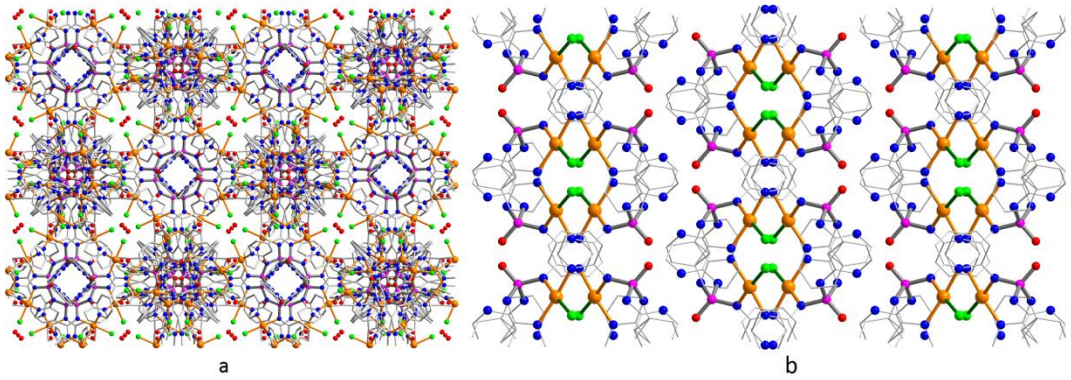

Figure 3.15: (a) Packing structure of 3.23 along c-axis in **3.18**·4H_2O (b) in **3.18**

The 20-membered Cu(II)-macrocycle **3.19** was crystallized in the monoclinic space group *P2(1)/n* with its asymmetric unit featuring one Cu(II) ion, two metal bound chloride ions and one phosphoramide ligand moiety. The phosphoramide ligand is bidentate and is coordinated with two metal centres forming a macrocycle with one of its pyridyl donors remain uncoordinated (Figure 3.16a). It is interesting to compare the orientation of the phosphoramide ligand in the $[M_6L_8]^{12+}$ cages reported earlier and in the macrocyclic compound **3.19**. In these cages for octahedral metal ions (such as Co^{2+}, Ni^{2+}, Cu^{2+}, Zn^{2+} and Cd^{2+}) the three pyridyl arms are oriented *syn* to the phosphoryl oxygen (P=O), while in the square planar Pd^{2+} containing cage they are oriented *anti* with respect to the P=O motif.[35] However, in **3.19** the two coordinated pyridyl arms are oriented *syn* and the uncoordinated arm is aligned *anti* with respect the P=O moiety. As a result of this disparate arrangement, the phosphoramide ligand could not form the $[M_6L_8]^{12+}$ type cage in the present instance. One of the three amino protons in **3.19** is engaged in H-bonding interactions with the metal-bound chloride and form a 1D-chain like structure. Due to these N-H...Cl interactions (N1-H1...Cl2) a new eighteen membered macrocycle, represented by graph set $R_2^2 18$ notation[29], is formed between the two 20-membered parent macrocycles (Figure 3.16b). These chains are further connected by N-H...N_{py} (N2-

H2...N33) and N-H...$O_{phosphoryl}$ interactions (N3-H3...O1) resulting in a herringbone type 2D-network packing (Figure 3.16c).

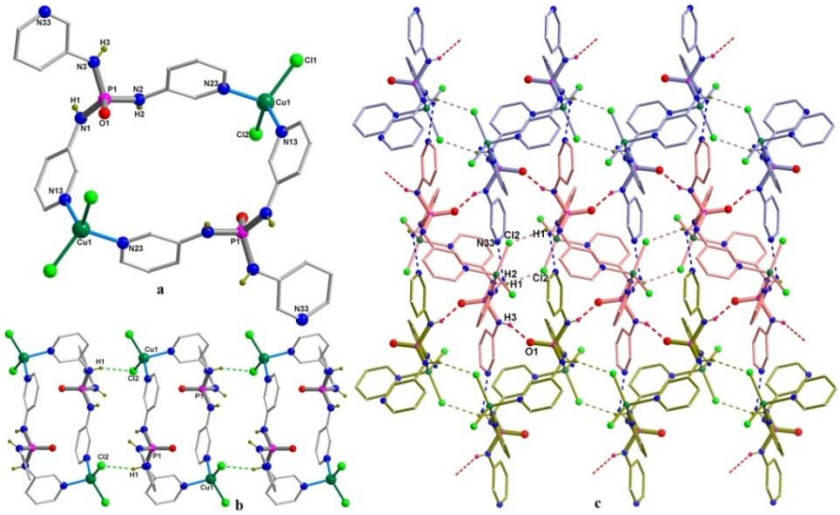

Figure 3.16: (a) View of the 20-membered macrocycle in **3.19** (b) view of the N-H...Cl assisted 1D- chain structure in (c) view of the herringbone type 2D-sheet structure in **3.19** mediated by N-H...O and N-H...O interactions

The coordination polymer **3.20** was crystallized as **3.20**.xS (S = disordered DMF and water molecules which are not resolved) and solved in the triclinic space group *P-1*. The asymmetric unit consists of two Cu(I) ions, there neutral ligand motifs of **3.2**, and two nitrate ions which restores the charge balance in the molecule. Of the three ligand motifs two of them (those of P2 and P3) are located in tridentate C_3-symmetric coordination with three Cu(I) centres, while one of them (belong to P1) is bidentate and connect the Cu(I) centres from two different layers. Thus, the pyridyl arms of these ligand motifs have different orientations with respect to the P=O moieties: all the three pyridyl arms in the tridentate ligands have *anti* orientation and one of the three arms in the bidentate ligand have *syn* orientation. Each Cu(I) atom is having a tetrahedral geometry in which the three in-plane coordination comes from the pyridyl N-sites of the tridentate ligand units. The fourth coordination is provided by one of the pyridyl N-site from the bidentate ligand. The cumulative effect of all these interactions is a double-layer hexagonal network in which the bidentate ligand set acts as a bridge between the two layers. A closer look at the network reveal a bi-nodal double layer **hcb** topology[37] for **3.20** in which tridentate P-centres acts as three-connected nodes and each Cu(I) ion acts as a four-connected node, whereas the bidentate ligand acts as a linker strut between the layers (Figure 3.17). The metric parameters associated with the Cu-N and P-N bonds are consistent with the literature reported values. The nitrate anions are located in between

the layers and involved in H-bonding interaction with the amino protons. The packing diagram of the molecule shows the presence of a channel structure between the two layers which are occupied by the solvated molecules. The solvent free volume excluding the nitrate anions is found to be 865.18 $Å^3$ which amounts to 25.5% of the unit cell volume (Figure A2.26, Appendix 2).

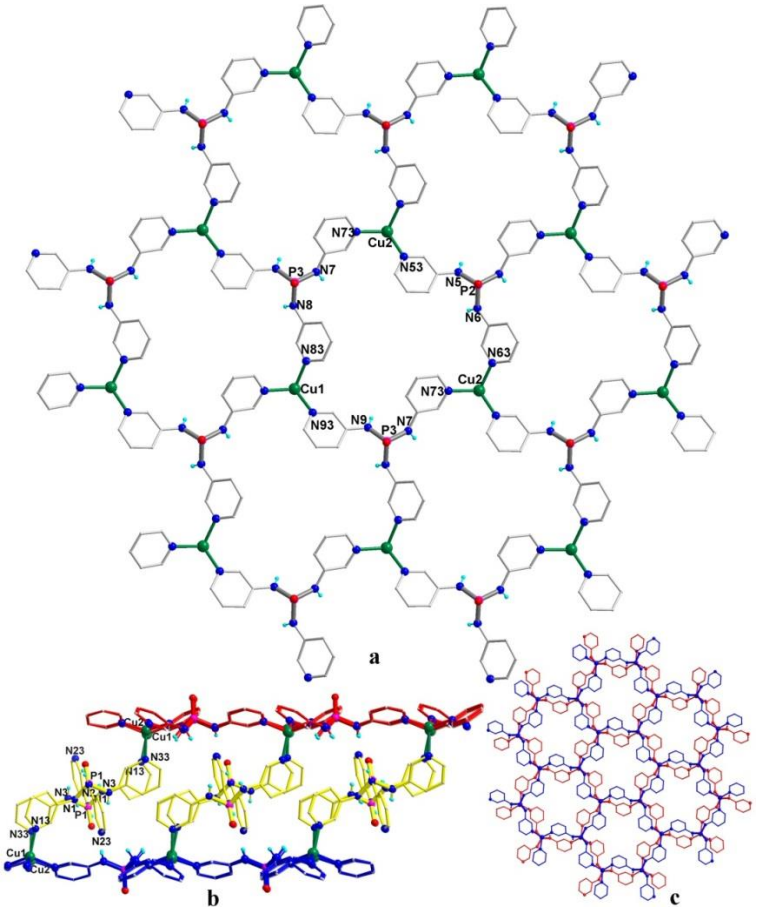

Figure 3.17: View of an individual cationic hexagonal sheet structure in **3.20** (b) bridging coordination of the bidentate phosphoramide ligand (shown in yellow) connecting the two hexagonal sheets (red and blue); (c) overlay of the two hexagonal sheets in **3.20**.

3.3.3 UV-Visible and Fluorescence spectra of the Ag(I) complexes

The UV-visible spectrum of **3.5** in DMSO shows a single absorption at ~284nm (Figure 3.18a) and is largely different from that obtained in methanol which gave four different peaks at 230nm, 255 nm, 290 nm and 320 nm (please refer to the figure 3.26a (Figure A2.27, Appendix 2). The transitions in methanol are due to the pyridyl chromophore's ($n \rightarrow \pi^*$ and $\pi \rightarrow \pi^*$) transitions as well as due to their interactions with the solvent methanol. On the other hand, such solvent interactions are absent in DMSO (aprotic polar) giving rise to only a single absorption. The UV-visible spectrum of the complex

3.14·$(ClO_4)_3$ is blue-shifted compared to **3.5** and absorbs at ~270nm. It is also worthwhile to note a low energy band at ~315nm indicating different kinds of transitions involving amino and metal bound imido groups in **3.14**·$(ClO_4)_3$. The emission signatures of **3.5** and **3.14**·$(ClO_4)_3$ have vibronic structures and show values at 354 (λex = 365 nm) and 350 nm (λex = 307 nm), respectively. Further, the fluorescence intensity of **3.14**·$(ClO_4)_3$ is fairly quenched and somewhat blue shifted from **3.5**. The florescence quenching is presumably due to depletion of electron densities at the imino sites caused by its coordination to Ag (I) ions. Interestingly, the solid state fluorescence spectra of **3.5** and **3.14**·$(ClO_4)_3$ shows emission bands at 480 (λex = 364 nm) and 380 nm (λex = 342 nm) indicating significant quenching as well as blue shift for **3.14**·$(ClO_4)_3$ in comparison with its solution spectra (Figure 3.18b).

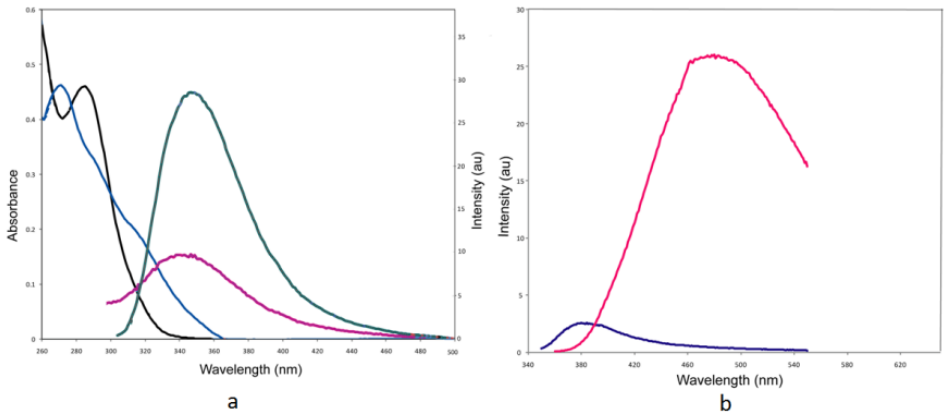

Figure 3.18: (a) UV-Visible **3.5** (black) and **3.14**·$(ClO_4)_3$ (blue) and Emission spectra of **3.5** (green) and **3.14**·$(ClO_4)_3$ (red) in DMSO. (b) Solid State emission spectra taken on the front face mode, **3.5** (pink) and **3.14**·$(ClO_4)_3$ (blue)

The UV-visible spectra of the compounds **3.2**, **3.15**, **3.16** and **3.17** in DMSO show a single absorption due to the pyridyl amino chromophores and ranges between 282 nm (for **3.17**) and 285 nm (for **3.2**) (Figure 3.19a). These values are found to be red shifted in the solid state by about 50 nm (Figure 3.19b) and ranges from 332 nm (for **3.2**) to 337 nm (for **3.17**) indicating that these transitions are predominantly n→π* in nature. The solution emission spectra of the ligand **3.2** and the complex **3.15** in DMSO show an almost equal maxima and intensities at 325 nm. Similarly the emission maxima of **3.16** and **3.17** are nearly same at 328 and 330 nm, respectively, but show a quenching of florescence intensities by a factor of 50%. The observed florescence quenching can presumably due to the depletion of electron densities caused by the coordination of Ag(I) ions to the imido sites. The solid state florescence spectra of these compounds are again

red shifted by about 50 nm confirming the n→π* transitions and ranges from 389 nm (for **3.2**) to 397 nm (for **3.17**) (Figure 3.19d). Interestingly, as we move from the free ligand **3.2** to the Ag(I) complexes coordinated to neutral (**3.15**), mono-anionic (**3.16**) and di-anionic (**3.17**) ligands, the florescence intensities in the solid state decreases progressively. Although, such an effect can be expected in the solution emission spectra as well, the presumable dynamic nature of the Ag–N bonds in dilute solutions precludes such an observation. The calculated quantum yields of 0.065 (for **3.2**), 0.045 (for **3.15**), 0.020 (for **3.16**) and 0.018 (for **3.17**) in DMSO solutions, were very low compared to the reference 2-aminopurine.

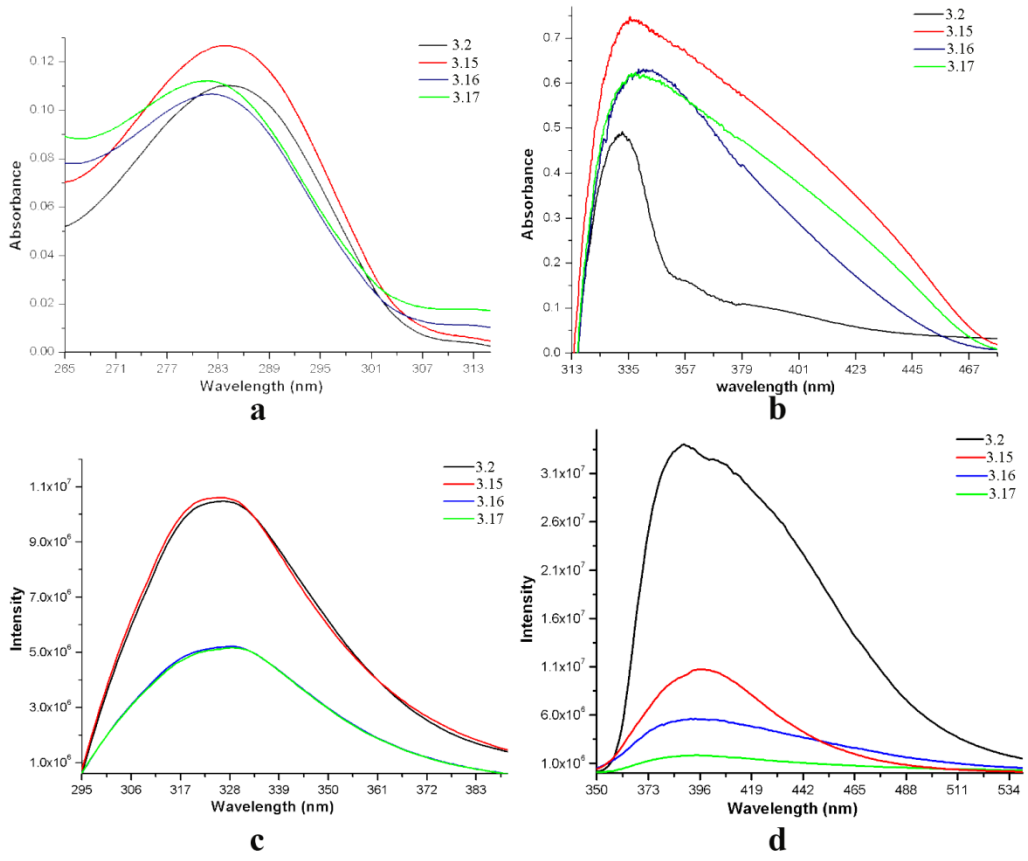

Figure 3.19: UV-visible spectra of the compounds **3.2**, **3.15**, **3.16** and **3.17**(a) in DMSO solution and (b) in the solid state. Florescence spectra of the compounds **3.2**, **3.15**, **3.16** and **3.17** (c) in DMSO solution (λex = 327 nm) and (d) in the solid state florescence (λex = 390 nm).

3.4 Conclusions

In summary, we have synthesized the new phosphonium cations and phosphoramide ligands containing 2 and 3-pyridyl substituents. Reactivity studies of **3.1** and **3.3** with KOH in methanol have resulted in the formation of the corresponding neutral phosphine imines. Treatment of **3.1** and **3.2** ligand with 1st row transition metal salts have resulted in a P–N bond cleavage in which the in situ generated phosphoramide ligand tris(amido)phosphate [$PO(NH^2Py)_3$] and bis(amido)phosphate [$PO_2(NH^2Py)_2]^-$ yields interesting kinds of mononuclear complexes. To prevent the P–N bond cleavage we have established a facile anion exchange route that stabilize the highly labile tetrakis(2-pyridylamino)phosphonium cation in the solution as well as in solid state. An interesting Cu(II) complex of the mono-anionic phosphoramide ligand [$OP(N^2Py)(NH^2Py)_2]^-$ has been obtained in the reaction of **3.2** with Cu^ICl. The reaction of **3.1** with Ag(I) salts gave a pentanuclear Ag(I) imido-phosphate complex [$Ag_5(LH_2^-)]^{3+}$ in which the homoleptic imido phosphate anion [$P(N^2Py)_2(NH^2Py)_2]^-$ acts as a hexadentate cisoidal ligand. Utilizing the slight variations in the reactivities of the Ag(I) salts, sequential deprotonation of the ligand amino protons in **3.2** was achieved forming imido P(V) species analogous to the di hydrogen phosphate and mono hydrogen phosphate ions in the form of tri-, hepta- and octa-nuclear Ag(I) complexes starting from the 2-pyridylamino functionalized phosphonium salt and 2-pyridyl-functionalized tris(amido) phosphate. The acidic nature of the amino protons of **3.2** and **3.5** has been validated by a preliminary pka measurement. Similarly the reaction of **3.1** and **3.2** with Pd(II) ions gave the dinuclear Pd(II) assembly stabilized by two [$OP(N^2Py)(NH^2Py)_2]^-$ ligands. Solid and solution state fluorescence spectra of the 2-pyridyl ligands and Ag(I) complexes show a sequential quenching of fluorescence intensities from the free ligand to the Ag(I) complex containing the mono and di-anionic imido P(V) ligands. Such an observation has been made for the first time in imido-P(V) chemistry. Treatment of the 3-pyridyl attached phosphonium salt **3.3** with various metal salts of copper have again resulted in a P-N bond cleavage in which the in-situ generated phosphoramide ligand [$PO(NH^3Py)_3$], yields interesting kinds of self-assemblies in discrete and polymeric frameworks.

3.5 References

(1) (a) Chivers, T.; Brask, J. K. *Angew. Chem., Int. Ed.* **2001**, *40*, 3960-3997. (b) Aspinall, G. M.; Copsey, M. C.; Leedham, A. P.; Russell, C. A. *Coord. Chem. Rev*. **2002**, *227*, 217-232. (c) Steiner, A.; Zacchini, S.; Richards, P. I. *Coord. Chem. Rev*. **2002**, *227*, 193-216.

(2) (a) Edelmann, F.T. *Coord. Chem. Rev.* **1994**, *137*, 403-481. (b) Bailey, P.J.; Pace, S. *Coord. Chem. Rev.* **2001**, *214*, 91-141. (c) Aspinall, G. M.; Copsey, M. C.; Leedham, A. P.; Russell, C. A. *Coord. Chem. Rev*. **2002**, *227*, 217-232. (d) Stahl, L. *Coord. Chem. Rev.*, 2002, **210**, 203-250.

(3) (a) Steiner, A.; Zacchini, S.; Richards, P. I. *Coord. Chem. Rev*. **2002**, *227*, 193-216. (b) P Raithby, P. R.; Russell, C. A.; Steiner, A.; Wright, D. S. *Angew. Chem. Int. Ed. Engl.* **1997**, *36*, 649-650. (c) Burke, L. T.; Freire, E. H.; Holland, R.; Jeffery, J. C.; Leedham, A. P.; Russell, C. A.; Steiner, A.; Zagorski, A. *Chem. Commun*. **2000**, 1769-1771.

(4) Bickley, J. F.; Copsey, M. C.; Jeffery, J. C.; Leedham, A. P.; Russell, C. A.; Stalke, D.; Steiner, A.; Stey, T.; Zacchini, S. *Dalton Trans*. **2004**, 989-995.

(5) (a) Armstrong, A.; Chivers, T.; Krahn, M.; Parvez, M.; Schatte, G. *Chem. Commun.*, **2002**, 2332-2333. (b) Robertson, S. D.; Chivers, T. ; Konu, J. *J. Organomet. Chem.* **2007**, *692*, 4327-4336. (c)Armstrong, A.; Chivers, T.; Krahn M.; Parvez, M. *Can. J. Chem.* **2005**, *83*, 1768-1778.

(6) (a) Chivers, T.; Krahn, M.; Parvez, M.; Schatte, G. *Chem. Commun.* **2001**, 1922-1923. (b) Chivers, T.; Krahn, M.; Schatte, G.; Parvez, M. *Inorg. Chem.* **2003**, 43, 3994-4005. (c) Armstrong, A.; Chivers, T.; Parvez, M.; Schatte, G.; Boeré, R. T. *Inorg. Chem.* **2004**, *44*, 3453-3460.

(7) Armstrong, A.; Chivers, T.; Parvez, M.; Boeré, R. T. *Angew. Chem., Int. Ed.* **2004**, 43, 502-505.

(8) (a) Buchard, A.; Auffrant, A.; Klemps, C.; Vu-Do, L.; Boubekeur, L.; Le Goff, X. F.; Le Floch, P. *Chem. Commun*. **2007**, 1502-1504. (b) Sauthier, M.;Fornié -Cámer, J.; Toupet, L.; Réau, R. *Organometallics* **2000**, *19*, 553-562.

(9) (a) Zhang, C.; Sun, W-H.; Wang, Z-X. *Eur. J. Inorg. Chem.* **2006**, 4895-4902. (b) Masuda, J. D.; Wei, P.; Stephan, D. W. *Dalton Trans.* **2003**, 3500-3505. (c) Alhomaidan, O.; Beddie, C.; Bai, G.; Stephan, D. W. *Dalton Trans*. **2009**, 1991- (d) Yadav, K.; Mc Cahill, J. S. J.; Bai, G.; Stephan, D. W. *Dalton Trans*. **2009**, 1636. (e) Le Pichon, L.;

Stephan, D. W.; Gao, X.; Wang, Q. *Organometallics* **2002**, *21*, 1362. (f) Alhomaidan, O.; Bai, G.; Stephan, D. W. *Organometallics* **2008**, *27*, 6343-6352. (g) Li, D.; Li, S.; Cui, D.; Zhang, X.; Trifonov, A. A. *Dalton Trans*. **2010**, *40*, 2151.

(10) (a) Buchard, A.; Platel, R. H.; Auffrant, A.; Le Goff, X. F.; Le Floch, P.; Williams, C. K. *Organometallics* **2010**, *29*, 2892-2900. (b) Sun, H.; Ritch, J. S.; Hayes, P. G. *Inorg. Chem.* **2011**, *50*, 8063. (c) Gamer, M. T.; Rastätter, M.; Roesky, P. W.; Steffens A.; Glanz, M. *Chem. Eur. J.* **2005**, *11*, 3165. (d) Rastätter, M.; Zulys, A.; Roesky, P. W. *Chem. Commun.* **2006**, 874-876. (e) Gamer, M. T.; Roesky, P. W.; Palard, I.; Le Hellaye, M.; Guillaume, S. M. *Organometallics* **2007**, *26*, 651-657. (f) Ireland, B. J.; Wheaton, C. A.; Hayes, P. G. *Organometallics* **2010**, *29*, 1079-1084.

(11) (a) Rastätter, M.; Zulys, A.; Roesky, P. W. *Chem. Eur. J.* **2007**, *13*, 3606-3616. (b) Rastätter, M.; Zulys, A.; Roesky, P. W. *Chem. Commun*. **2006**, 874-876. (c) Panda, T. K.; Zulys, A.; Gamer, M. T.; Roesky, P. W. *Organometallics* **2005**, *24*, 2197-2202.

(12) (a) Buchard, A.; Heuclin, H.; Auffrant, A.; Le Goff, X. F.; Le Floch, P. *Dalton Trans.* **2009**, 1659-1667. (b) Cadierno, V.; Díez, J.; García-Álvarez; J.; Gimeno, J. *Organometallics* **2005**, *24*, 2801-2810. (c) Boubekeur, L.; Ulmer, S.; Ricard, L.; Mézailles, N.; Le Floch, P. *Organometallics* **2006**, *25*, 315.

(13) (a) Gupta, A. K.; Nicholls, J.; Debnath, S.; Rosbottom, I.; Steiner, A.; Boomishankar, R. *Cryst. Growth Des.* **2011**, *11*, 555-564. (b) Gupta, A. K.; Kalita, A.; Boomishankar, R. *Inorg. Chim. Acta* **2011**, *372*, 152-159.

(14) Monzyk, B.; Crumbliss, A. L.; Kubas, G. J. *Inorg. Synth.* **1990**, *28*, 68-69.

(15) Berlman, I. B. Handbook of Fluorescence Spectra of Aromatic Molecules, Academic Press, New York, **1965**.

(16) Gholivand, K.; Alavi, M. D.; Pourayoubi, M. *Z. Kristallogr.* **2004**, *219*, 124-126.

(17) Sheldrick, G. M. *Acta Crystallogr*. **2008**, *A64*, 112-122.

(18) Hohenberg, P.; Kohn,W. *Phys. Rev*. **1964**, *136*, B864.

(19) Kohn, W.; Sham, L. *Phys. Rev*. **1965**, *140*, A1133.

(20) Becke, A. D. *J. Chem. Phys*. **1993**, *98*, 5648.

21: Lee, C.; Yang, W.; Parr, R. G. *Phys. Rev. B* **1988**, *37*, 785-789.

(22) Casida, M. E. *Recent Advances in Density Functional Methods, Part I, Chapter 5; Chong, D. P., Ed.; World Scientific: Singapore* **1995**, p 155.

(23) Gross, E.; Dobson, J.; Petersilka, M. T. *Top. Curr. Chem*. **1996**, *181*, 81.

(24) Frisch, M. J.; Trucks, G. W.; Schlegel, H. B.; Scuseria, G. E.; Robb, M. A.; J. R.; Montgomery, J. A.; Vreven Jr., T.; Kudin, K. N.; Burant, J. C.; Millam, J. M.; Iyengar, S.

S.; Tomasi, J.; Barone, V.; Mennucci, B.; Cossi, M.; Scalmani, G.; Rega, N.; Petersson, G. A.; Nakatsuji, H.; Hada, M.; Ehara, M.; Toyota, K.; Fukuda, R.; Hasegawa, J.; Ishida, M.; Nakajima, T.; Honda, Y.; Kitao, O.; Nakai, H.; Klene, M.; Li, X.; Knox, J. E.; Hratchian, H. P.; Cross, J. B.; Bakken, V.; Adamo, C.; Jaramillo, J.; Gomperts, R.; Stratmann, R. E.; Yazyev, O.; Austin, A. J.; Cammi, R.; Pomelli, C.; Ochterski, J. W.; Ayala, P.; Morokuma,Y. K.; Voth, G. A.; Salvador, P.; Dannenberg, J. J.; Zakrzewski, V. G.; Dapprich, S.; Daniels, A. D.; Strain, M. C.; Farkas, O.; Malick, D. K.; Rabuck, A. D.; Raghavachari, K.; Foresman, J. B.; Ortiz, J. V.; Cui, Q.; Baboul, A. G.; Clifford, S.; Cioslowski, J.; Stefanov, B. B.; Liu, G.; Liashenko, A.; Piskorz, P.; Komaromi, I.;Martin, R. L.; Fox, D. J.; Keith, T.; Al-Laham, M. A.; Peng, C. Y.; Nanayakkara, A.; Challacombe, M.; Gill, P. M. W.; Johnson, B.; Chen, W.; Wong, M. W.; Gonzalez, C.; Pople, J. A. *Gaussian 03, Revision E.01*, Gaussian, Inc., Wallingford CT, **2004**.

(25) Various base assisted cleavage pathways of organoamino phosphonium cations can be seen at Marchenko, A. P.; Koidan, G. N.; Pinchuk, A. M. *Zh. Obshch. Khim*. **1984**, *54*, 2691, (*J. Gen. Chem*. **1984**, *54*, 2405).

(26) Li, X.-J.; Jiang, F.-L.; Wu, M.-Y.; Zhang, S.-Q.; Zhou, Y.-F.; Hong, M.-C. *Inorg. Chem.* **2012**, *51*, 4116-4122.

(27) Tsuji, J.; Kezuka, H.; Takayanagi, H.; Yamamoto, K. *Bull. Chem. Soc. Jpn.* **1981**, *54*, 2369-2373.

(28) Pastoriza-Santos, I.; Liz-Marzán, L. M. *Langmuir* **1999**, *15*, 948-951. (b) Mukherjee, A.; Chakrabarty, R.; Patra, G. K. *Inorg. Chem. Comm.* **2009**, *12*, 1227-1230.

(29) Etter, M. C. *Acc. Chem. Res.* **1990**, *23*, 120.

(30) (a) Richards, P. I.; Bickley, J. F.; Boomishankar, R.; Steiner, A. *Chem. Commun.* **2008**, 1656-1658. (b) Liu, C. W.; Chang, H.-W.; Fang, C.-S.; Sarkar, B.; Wang, J.-C. *Chem. Commun.* **2010**, *46*, 4571-4573. (c) Konno, T.; Okamoto, K. *Inorg. Chem.* **1997**, *36*, 1403-1406. (d) Wang, J.;Luo, Q.-H.; Shen, M-C.; Huang, X.; Wu, Q.-J. *J. Chem. Soc. Chem. Commun.* **1995**, 2373-2374. (e) Gonzalez-Duarte, P.;Sola, J.;Vives, J.; Solans, X. *J. Chem. Soc. Chem. Commun.* **1987**, 1641-1642. (f) C. W. Liu and B.-J. Liaw *Inorg. Chem.* 2000, **39**, 1329-1332.

(31) Constable, E. C.; Housecroft, C. E.; Neuburger, M.; Reymann, S.; Schaffner, S. *Chem. Commun.* **2004**, 1056-1057.

(32) Greenwood, N. N.; Earnshaw, A. *Chemistry of the Elements*, Pergamon Press: New York, **1989**, p 1368.

(33) (a) Liu, C. W.; Shang, I-J.; Wang, J-C.; Keng, T-C. *Chem. Commun.*, **1999**, 995-996. (b) Tang, K.; Jin, X.; Yan, H.; Xie, X.; Liu, C.; Gong, Q. *J.Chem. Soc. Dalton Trans.* 2001, 1374-1377. (c) Liu, C. W.; Hung, C-M.; Haia, H-C.; Liaw, B-J.; Liou, L-S.; Tsai Y-F.; Wang, J-C. *Chem. Commun.* **2003**, 976-977. (d) Liu, C. W.; Chang, H-W.; Fang, C-S.; Sarkar, B.; Wang, J-C. *Chem. Commun.* **2010**, *46*, 4571-4573. (e) Block, E.; Gernon, M.; Kang, H.; Ofori-Okai, G.; Zubieta, J. *Inorg. Chem.* **1989**, *28*, 1263-1271. (f) Dance, I. G**.;** Fitzpatrick, L. J.; Craig, D. C.; Scudder, M. L. *Inorg. Chem.* **1989**, *28*, 1853-1861. (g) Vicente, J.; Gonza´lez-Herrero, P.; García-Sánchez, Y.; Jones, P. G. *Inorg. Chem.* **2009**, *48*, 2060-2071. (h) Liu, C. W.; Chang, H-W.; Sarkar, B.; Saillard, J-Y.; Kahlal, S.; Wu, Y-Y. *Inorg. Chem.* **2010**, *49*, 468-475.

(34) (a) Wang, Q-M.; Mak, T. C. W. *Angew. Chem., Int. Ed.* **2001**, *40*, 1130-1133. (b) Wu, H-B.; Huang, Z-J.; Wang, Q-M. *Chem. Eur. J.* **2010**, *16*, 12321-12323. (c) Zhao, X-L., Wang, Q-M.; Mak, T. C. W. *Inorg. Chem.* **2003**, *42*, 7872-7876. (d) Wei, Q-H.; Zhang, L-Y.; Yin, G-Q.; Shi, L-X.; Chen, Z-N. *J. Am. Chem. Soc.* **2004**, *126*, 9940-9941. (e) Matsumoto, K.; Tanaka, R.; Shimomura, R.; Nakao, Y. *Inorg. Chim. Acta.* **2000**, *304*, 293-296. (f) Zhao, X-L.; Mak, T. C.W. *Polyhedron* **2006**, *25*, 975-982.

(35) Li, X.-J.; Jiang, F.-L.; Wu, M.-Y.; Zhang, S.-Q.; Zhou, Y.-F.; Hong, M.-C. *Inorg. chem.* **2012**, *51*, 4116-4122.

(36) Sooväli, L.; Rodima, T.; Kaljurand, I.; Kütt, A.; Koppel I. A.; Leito, I. *Org. Biomol. Chem.*, **2006**, *4*, 2100-2105.

(37) O'Keeffe, M.; Yaghi, O. M. *Chem. Rev.* **2012**, *112*, 675-702.

Chapter 4

Zn (II) and Cu (II) coordination polymer of an in-situ generated 4-pyridyl (^{4}Py) attached bis(amido)phosphate ligand, showing preferential water uptake over aliphatic alcohols

Abstract

In this chapter, starting from the P(V) ligands featuring 4-pyridyl substituents interesting kinds of functional coordination polymers supported by the in-situ generated bis(amido)phosphate ligand $[PO_2(NH^4Py)_2]^-$ (abbreviated as $[L]^-$) were obtained. Thus, the reaction of $[P(NH^4Py)_4]Cl$ or $[PO(NH^4Py)_3]$ with $Zn(NO_3)_2$ in DMF under hydrothermal conditions at 90 °C has lead to the formation of two polymorphic 2D-coordination polymers of composition $[ZnL(HCO_2)]_\infty$. A similar reaction with $Cu(NO_3)_2$ gave a 1D- coordination polymer of composition $[CuL_2(H_2O)_2]_\infty$. The activated forms of the 2D-polymer $[ZnL(HCO_2)]_\infty$ has shown to exhibit a higher CO_2 uptake over N_2. Whereas no appreciable gas uptake characteristic could be observed for the Cu(II) coordination polymer, $[CuL_2(H_2O)_2]_\infty$. Interestingly, solvent uptake studies of both of these materials have revealed a preferentially high uptake capacity for water over aliphatic alcohols such as methanol and ethanol. Although the Cu(II) coordination polymer, $[CuL_2(H_2O)_2]_\infty$ shows a lower water uptake capacity compared to that of the Zn(II) coordination polymer, $[ZnL(HCO_2)]_\infty$, it shows a better stability as indicated by their adsorption profiles. During the formation of $[CuL_2(H_2O)_2]_\infty$ we have also isolated a Cu(I) coordination polymer of composition $[Cu(PO(NH^4Py)_3L]_\infty$ containing both the neutral $[PO(NH^4Py)_3]$ and the in-situ generated ligand $[L]^-$.

4.1 Introduction

Rational design of functional framework materials such as metal-organic frameworks (MOFs) or porous coordination polymers (PCPs) has been the focus area of interest for several research groups.[1,2] This is attributed to both the novel structural topologies exhibited by these materials and their utility in the areas of separation, storage, enantio-selective catalysis, sensors, drug delivery etc.[3,4] These materials are traditionally synthesized by the use of various 'organic linkers' in combination with 'metal cluster nodes' in the form of their oxide or hydroxide building units. Typical 'organic linkers' include neutral and/or anionic ligands such as 4,4-bipyridine and/or 1,4-benzene dicarboxylate and their other analogues which are shown to form families of porous framework materials with tunable pore dimensions.[5] Over the years, several ligand systems have been tried as 'organic linkers' in order to establish the relationship between various framework compositions and the observed functionality.[6] In this effort, phosphorus centred ligand motifs viz., phosphonate monoesters, carboxylated phosphines, phosphine oxides and phosphonium salts have received recent attention, as they can provide a flexible peripheral ligand platform around the central phosphorus.[7,8] Further, the framework based on the ligand $[PO(C_6H_4\text{-}pCO_2H)_3]$ and Zn^{2+} ion has shown to selectively uptake light weight gases in its pore in a reversible manner.[7a] In another report, the MOF based on Ba^{2+} ion and the phosphonate monoester ligand tetraethyl 1, 3, 6, 8-pyrenetetraphosphonate have shown to exhibit very high hydrophobicity and stability towards water.[8b] In the previous chapter we have described the chemistry of amino-functionalized P(V) derivatives[9] and have shown the reactivity of certain flexible multi-site ligands such as the pyridylamino functionalized phosphonium cation, $[P(NH^2Py)_4]^+$ and the phosphoric triamide, $[PO(NH^2Py)_3]$ (^{2}Py = 2-pyridyl) leading to novel examples of Ag(I) clusters.[10] Further, Hong and co-workers have shown that the analogous 3-pyridyl ligand $[PO(NH^3Py)_3]$ is also flexible along the N-P-N bond and can exist in syn or anti-conformation in self-assembled $[M_6L_8]^{12+}$ complex cages depending on the metal ions.[11] In view of the current interest in specifically synthesizing rigid or flexible/dynamic coordination polymers we set out to employ the amino-P(V) ligands containing 4-pyridyl substituents, as we presumed that presence of multiple 4-pyridyl substituents on the tetrahedral P(V) backbone would facilitate the formation of infinite polymeric structures.

This chapter describes the synthesis of two new polymorphic two-dimensional coordination polymers, {[ZnL(HCO_2)].DMF.H_2O}$_\infty$ (**4.3**), ({[ZnL(HCO_2)(H_2O)].DMF}$_\infty$ (**4.4**) and one-dimensional coordination polymer {[$CuL_2(H_2O)_2$].2DMF.$2H_2O$}$_\infty$ (**4.5**) derived from the in-situ generated bis(amido)phosphate ligand L^- (L^- = $[PO_2(NH^4Py)_2]^-$: ^{4}Py = 4-pyridyl). The ligand L^- was generated by a facile metal-assisted P-N bond hydrolysis reaction from the corresponding phosphonium salt **4.1**, $[P(NH^4Py)_4]Cl$ or from the neutral phosphoric triamide **4.2**, $[PO(NH^4Py)_3]$. Interestingly, L^- exhibits variable modes of coordination giving rise to a 2D-sheet structure for Zn(II) ions and a 1D-chain structure for the Cu(II) ions. During these studies we have also isolated and characterized in low yields a new tetrahedral Cu(I) based 2D-coordination polymer, {[Cu(**4.2**)L].DMF.$2H_2O$}$_\infty$ (**4.7**). The formation of this 2D-network is mediated by the tridentate N, N, N-coordinating mode of **4.2** while L^- acts as a support ligand to provide the coordination saturation to the Cu(I) center. Although, there is a lot of literature precedence for the MOFs and PCPs based on the in-situ generated ligand in carbon chemistry, it is extremely rare in literature where functional MOFs and PCPs were stabilized by in-situ generated ligands obtained via the P-N bond cleavage pathway. In addition, vapor sorption studies on the activated sample of **4.3, 4.4** and **4.5** reveals the selective adsorption of water vapor over aliphatic alcohols. Use of MOFs and PCPs for the selective separation of water and alcohols has gained a lot of recent attention[12] with aspirations in the purification of Bioethanol industrially.[13] Removal of the last 4% azeotropic mixture of water from Bioethanol is very difficult by usual distillation procedures and thus microporous MOF materials offer an attractive platform to effect this separation.

4.2 Experimental

4.2.1 General Remarks

All manipulations involving phosphorus halides were performed under dry nitrogen atmosphere in standard Schlenk-glassware. Solvents were dried over potassium (thf, hexane) and sodium (toluene). PCl_5 and 4-aminopyridine were purchased from Aldrich and used as received. The $POCl_3$ was purchased locally (SPECTROCHEM, India) and was distilled prior to use. The metal salts were purchased locally and used as received. NMR spectra were recorded on a 400 MHz Jeol FT spectrometer (^{1}H NMR: 400.13 MHz, $^{13}C\{^1H\}$NMR: 100.62 MHz, $^{31}P\{^1H\}$ NMR: 161.97 MHz) at room temperature using $SiMe_4$ (^{1}H, ^{13}C) and 85% H_3PO_4 (^{31}P) as external standards. ESI and MALDI-TOF

Mass spectra were obtained by Waters Q-Tof Premier & Aquity spectrometer and Applied Biosystem MALDI-TOF/TOF spectrometer, respectively. The powder X-ray diffraction data were obtained from a Bruker D8 Advance diffractometer. Thermal analysis data has been obtained from a Perkin-Elmer STA-6000 thermogravimetric analyzer. Elemental analyses were performed on a Vario-EL cube elemental analyzer. FT-IR spectra were taken on a Thermo-scientific Nicolet 6700 spectrophotometer with samples prepared as KBr pellets. Melting points were obtained using an Electro thermal melting point apparatus and were uncorrected. Electron paramagnetic resonance (EPR) spectrum was obtained on a Bruker EMX EPR spectrometer.

4.2.2 Synthesis

4.1: A suspension of PCl_5 (5g, 0.024 mol) in chloroform was added drop wise to an excess of 4-aminopyridine (27.10 g, 0.288 mol) in chloroform (250 mL) at 0^o C. The resulting mixture was refluxed for 12 h by which time a waxy precipitate was obtained. The waxy solid was filtered and washed with cold water to remove the amine hydrochloride by-product. The remaining water insoluble solid was collected, washed with water and dried in vacuum desiccator for 12 hours. Yield 80% (8.40 g) based on P. M.P. 192-195^{o}C. ^{1}H NMR (400 MHz, {$(CD_3)_2SO$}): δ 8.28 (br, 4H, N*H*), 8.03 (dd, 4H**,** C*H*), 6.94 (d, 4H**,** C*H*), 7.62 (dd, 4H, C*H*). ^{13}C {^{1}H}} (100 MHz, {$(CD_3)_2SO$}): δ 150.45, 148.72, and 114.70. ^{31}P NMR (161 MHz, {$(CD_3)_2SO$}):δ -3.74. FT-IR data in KBr pellet (cm^{-1}): 3459, [ν (N-H)]; 598, 666, 828, 995, 1211, 1327, 1491, and 1603 [ν (P-N)]. ESI (+) spectra: 403.1550 (M^+). Anal. Calcd. for $C_{20}H_{20}N_8ClP$: C, 54.74; H, 4.59; N, 25.53. Found: C, 55.12; H, 4.97; N, 25.88.

4.2: $POCl_3$ (5g, 0.0326 mol) was added drop wise to an excess of 4-aminopyridine (36.82g, 0.391 mol) in chloroform (250 mL) at 0 ^{o}C. The resulting mixture was refluxed for 12 h by which time a waxy precipitate was obtained. The waxy solid was filtered and washed with cold water to remove the amine hydrochloride by-product. The remaining water insoluble solid was collected, washed with water and dried in vacuum desiccator for 12 hours. Yield 90% (10.827 g) based on P. M.P. 187-190^o C. ^{1}H NMR (400 MHz, {$(CD_3)_2SO$}): δ 7.06 (dd, 3H, C*H*), 8.23 (dd, 3H, C*H*), 8.89 (br, 3H**,** N*H*). ^{13}C{^{1}H}} (100 MHz, {$(CD_3)_2SO$}): δ 150.45, 149.12, 112.88: ^{31}P NMR (161 MHz, {$(CD_3)_2SO$}):δ -5.64; FT-IR data in KBr pellet (cm^{-1}) : 3452 [ν (N-H)]; 604, 662, 774, 826, 953, 1002, 1066,1214, 1330, 1410, 1505, 1596 [ν (P-N)], 1283[ν (P=O)]. ESI (+) spectrum:

327.1114 (M+1). Anal. Calcd. for $C_{15}H_{15}N_6OP$: C, 55.21; H, 4.63; N, 25.76. Found: C, 54.54; H, 4.56; N, 25.35.

4.3: To a solution of the ligand **4.1** (219mg, 0.1mmol) in DMF (10mL) placed in a screw capped glass vessel, a solution of $Zn(NO_3)_3$ (145 mg, 0.1mmol) in H_2O (10mL) was added and the final mixture was heated at 90 ^oC for three days. The reaction mixture was then slowly brought back to the room temperature in a period of 24 h at which point colorless crystals of **4.3** was obtained. Yield 35% (116 mg) based on Zn. M.P. 315-318 ^oC FT-IR data in KBr pellet (cm^{-1}): 3540 [ν (N-H)]; 562, 662, 769, 835, 926, 1026, 1092, 1216, 1342, 1381, 1435, 1473, 1519, 1567, 1615, and 1673. Anal. Calcd. for $C_{11}H_{11}N_4O_4PZn$: C, 36.74; H, 3.08; N, 15.58. Found: C, 54.54; H, 4.56; N, 25.35.

4.4: To a solution of the ligand **4.2** (164 mg, 0.1mmol) in DMF (10 mL) placed in a 10 screw capped glass vessel, a solution of $Zn(NO_3)_2$ (145 mg, 0.1mmol) in H_2O (10mL) was added and the final mixture was heated at 90 °C for three days. The reaction mixture was then slowly brought back to the room temperature in a period of 24 h at which point colorless crystals of **4.4** was obtained. Yield 60% (200 mg) based on Zn. M.P. 318-320°C. FT-IR data in KBr pellet (cm^{-1}): 661, 771, 833, 919, 1025, 1064, 1340, 1425, 1463, 1551, 1616, 2859, 2944, 2989, 3031, 3116, 3200, and 3513. Anal. Calcd. for $C_{11}H_{11}N_4O_4PZn$: C, 36.74; H, 3.08; N, 15.58. Found: C, 36.55; H, 3.56; N, 15.70.

4.5: *(a)* To a solution of the ligand **4.1** (438mg, 0.2 mmol) in DMF (10mL) placed in a screw capped glass vessel, a solution of $Cu(NO_3)_3$ (120 mg, 0.1mmol) in H_2O (10mL) was added and the final mixture was heated at 90 ^oC for three days. The reaction mixture was then slowly brought back to the room temperature in a period of 24 h at which point dark blue colored crystals of **4.5** was obtained. Yield 45% (174 mg) based on Cu. *(b)* To a solution of the ligand **4.2** (327mg, 0.2 mmol) in DMF (10mL) placed in a screw capped glass vessel, a solution of $Cu(NO_3)_3$ (120 mg, 0.1mmol) in H_2O (10mL) was added and the final mixture was heated at 90 ^oC for three days. The reaction mixture was then slowly brought back to the room temperature in a period of 24 h at which point dark blue colored crystals of **4.5**.2DMF.$2H_2O$ was obtained. Yield 40% (155 mg) based on Cu. M.P. 282-284^o C. FT-IR data in KBr pellet (cm^{-1}): 3419 [ν (N-H)]; 520, 670, 839, 912, 1022, 1079, 1215, 1319, 1341, 1387, 1413, 1460, 1508, and 1617[ν (P-N)]. Anal. Calcd. for $C_{20}H_{24}N_8O_6P_2Cu$: C, 40.17; H, 4.05; N, 18.74. Found: C, 40.20; H, 4.08; N, 18.35. A small number of pale yellow colored crystals of **4.6** were also

present in the vessel as a minor product in both of these reactions in less than <1% yields based on Cu.

4.6: To a solution of **4.1** (30 mg, 0.068 mmol) in DMF (1 ml) placed in a screw capped glass vessel, 1 M HCl solution in H_2O (1 ml) was added and the final mixture was heated at 90 ^oC for 3 days. The reaction mixtures were gradually brought back to room temperature in a period of 24 h to yield a colorless solution. The reaction mixtures were slowly evaporated to dryness on a hot-plate kept at 80 °C to yield a crystalline solid which was found to be a mixture of chloride salt of **4.6** and the amino-pyridine hydrochloride by-product. Single crystals of **4.6** suitable for X-ray diffraction was obtained from slow evaporation of its mixture in methanol and water (v/v). Crude yield: 50% (8.5 mg based on P). ^{31}P-NMR (161 MHz, {(D_2O}): δ -12.62 ppm. MALDI-TOF mass spectrum (m/z): 288.97. FT-IR data in KBr pellet (cm^{-1}): 515, 563, 624, 766, 777, 876, 949, 982, 1080, 1167, 1244, 1332, 1430, 1438, 1632, 1665 and 3376.

4.7: *(a)* To a mixture of ligand **4.1** (438mg, 1 mmol) and the $Cu(NO_3)_3$ (120 mg, 0.5 mmol) kept in a screw capped vessel was added 20 mL DMF and the final mixture was heated at 90 ^oC for three days. The reaction mixture was then slowly brought back to the room temperature in a period of 24 h at which point pale yellow colored crystals of **4.6** was obtained. Yield 5% (19 mg) based on Cu.*(b)* To a mixture of $Cu(NO_3)_3$ (120 mg, 0.5 mmol) and the ligand **4.2** (327 mg, 1 mmol) kept in a screw capped vessel was added 20 mL DMF and the final mixture was heated at 90 ^oC for three days. The reaction mixture was then slowly brought back to the room temperature in a period of 24 h at which point pale yellow colored crystals of **4.5** was obtained. Yield: 5% (19 mg based on Cu). mp: 240-242 ^oC. FT-IR data in KBr pellet (cm^{-1}): 528, 664, 827, 908, 960, 1011, 1071, 1209, 1285, 1330, 1413, 1459, 1504, 1603 1670 and 3434. Anal. Calcd. for $C_{53}H_{65}N_{21}O_{11}P_4Cu_2$: C, 44.73; H, 4.60; N, 20.67. Found: C, 44.38; H, 4.70; N, 20.34.

4.2.3 Crystallography

Reflections were collected on a Bruker Smart Apex Duo diffractometer at 100 K using MoK_α radiation (λ = 0.71073 Å) for **4.1**, **4.2**, **4.3**, **4.4, 4.5, 4.6** and **4.7**. The data for **4.2**.$CH_3OH.H_2O$ was collected on Bruker Smart Apex II diffractometer at 296 K using MoK_α radiation (λ = 0.71073 Å). Structures were refined by full-matrix least-squares against F^2 using all data (SHELX).[14] Crystallographic data for **4.1**, **4.2**·CH_3OH·H_2O, **4.3**, **4.3a**, **4.4, 4.5, 4.5a, 4.6** and **4.7** are listed in (Table A3.1, Appendix 3). All non-hydrogen

atoms were refined aniostropically if not stated otherwise. Hydrogen atoms were constrained in geometric positions to their parent atoms. The solvated DMF in **4.5** was disordered and hence was split over two positions and refined isotropically with occupancy factors and similar-distance and similar U restraints. The solvated methanol, water and DMF molecules in **4.3a, 4.5** and **4.5a** could not be precicely located as they were disordered along the channel and have been treated as a diffuse contribution to the overall scattering without specific atom positions by SQUEEZE/PLATON. In addition, we also provide a disorder model in which the electron difference peaks due to solvents were refined as partially occupied O-atoms. Presence of methanol and water molecules in **4.5a** is further quantified by TGA analysis. In **4.6**, two pyridyl rings and the methyl groups of the DMF were disordered. All the disordered groups were split over two positions and refined isotropically with occupancy factors and similar-distance and similar U restraints.

4.2.4 Low pressure sorption measurements

Low pressure gas solvent sorption measurements were carried out by using Belsorpmax (Bel Japan) equipment. All the gases and solvents used were of 99.999% purity. To obtain a guest free sample of **4.3a**, **4.3b** and **4.5b** was heated under vacuum for 7 h at 120 °C. Prior to each adsorption measurement the sample was pre-treated at 120 °C under vacuum for 3 h with the help of BelPrepvacII equipment and purged with nitrogen on cooling. The adsorption and desorption isotherms were monitored at 298K for solvents, 77K for nitrogen and 195K for carbon dioxide.

4.3 Results and Discussions

4.3.1 Synthesis

The ligands **4.1** and **4.2** were synthesized from a slightly modified procedure from the analogous 2-pyridyl attached derivatives reported in chapter 3.[10] This involves the addition of eight equivalence of 4-amino pyridine to PCl_5 (in case of **4.1**) and six equivalence of 4-amino pyridine to $POCl_3$ (in case of **4.2**) in chloroform, respectively and refluxing the mixture for 12 hours. Subsequent work up with acidified water in the respective reactions gave the ligands **4.1** and **4.2** in good yields (Scheme 4.1). The formation of the ligands **4.1** and **4.2** were confirmed by the ^{31}P-NMR spectra (**4.1**: δ -3.74 and **4.2**: δ -5.64) in d_6-DMSO and by the ESI (+) mass spectra (**4.1**: m/z 403.1 and **4.2**: m/z 327.1) in methanol showing the presence of these ligands in dilute solutions

(Figure A3.1 and A3.2, Appendix 3). Further, the molecular structures of both these compounds were confirmed by X-ray crystallography. Interestingly, it is to be noted that the tetra 2-pyridyl attached phosphonium chloride salt could not be crystallized owing to its unstable nature in polar protic solvents. This is due to the interaction of the acidic protons of the solvent with the pyridyl groups cleaving one of the P−N bonds and forms the triamide $[PO(NH^2Py)_3]$.[10a] On the other hand, **4.1** is sufficiently stable in methanol, due to the increased separation between the P-N bonds and the nitrogens of the ^{4}Py groups, and could be crystallized from a solvent mixture of methanol/chloroform.

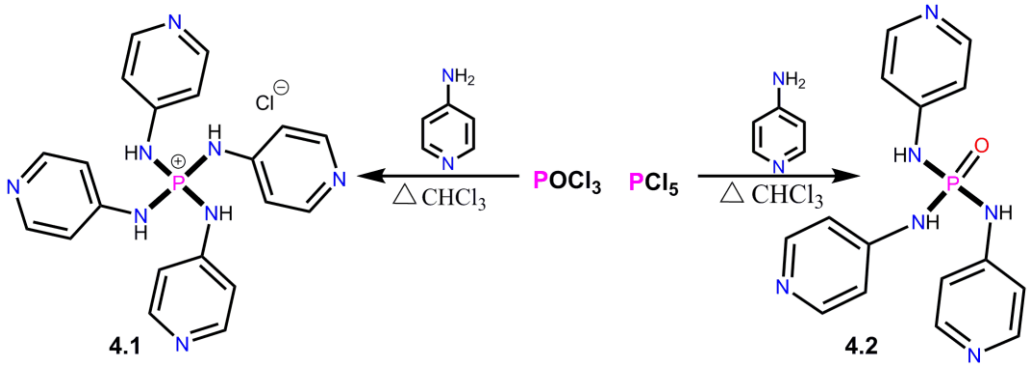

Scheme 4.1: Synthetic schemes for the preparation of **4.1** and **4.2**.

After synthesizing the ligands **4.1** and **4.2**, we subjected them to metallation studies under various conditions with the view of generating porous coordination polymers. Crystallization reactions of **4.1** and **4.2** at room temperature with metal salts of Cu(II), Zn(II), Ag(I) etc., have lead to rapid complexation and precipitation. Hence, we attempted these reactions under hydrothermal conditions at a moderate temperature of around 90 °C. Thus, the reaction of **4.1** in DMF with a solution of $Zn(NO_3)_2$ in water at 90 °C under hydrothermal conditions for 3 days gave the crystals of the 2D-coordination polymer **4.3** ($\{[ZnL(HCO_2)].DMF.\ H_2O\}_\infty$). The origin of the formate anion $(HCO_2)^-$ can be tracked to the hydrolytic cleavage of the solvent DMF at higher temperatures producing the formate anion $(HCO_2)^-$ and dimethyl ammonium cation $(Me_2NH_2^+)$. Literature precedence for the presence of both these species as anions (in case of $HCO_2)^-$ or charge balancing cations (in case of $Me_2NH_2^+$) in PCPs has been observed in several instances.[15] A similar reaction of **4.2** in DMF with a solution of $Zn(NO_3)_2$ in water at 90 °C under hydrothermal conditions for 3 days gave the polymorphic crystal **4.4**, ($\{[ZnL(HCO_2)(H_2O)].DMF\}_\infty$), in which the metal centre of the complex features an extra coordinated water on the Zn(II) ion instead of the solvated water. The in-situ formation of the bis(amido)phosphate ligand $(L)^-$ is attributed to the Lewis-acidic nature

of the Zn(II) salt triggering a metal-assisted P-N bond hydrolysis at some point in the reaction (Scheme 4.2).

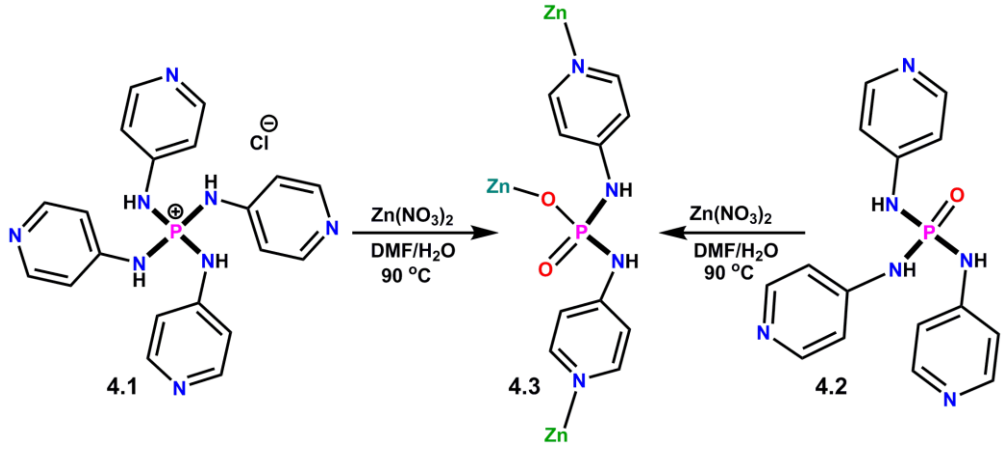

Scheme 4.2: Reaction of **4.1** and **4.2** with $Zn(NO_3)_2$

The reaction of the ligands **4.1** or **4.2** in DMF with a solution of $Cu(NO_3)_2$ in water at 90 °C under hydrothermal conditions for 3 days gave **4.5**.2DMF.2H_2O as a blue color block-like crystalline material in good yield. Single crystal X-ray analysis of the material revealed the presence of the anionic ligand L^-, rather than **4.3** or **4.4**, forming a 1D-macrocyclic chain polymer consisting of the core composition for **4.5** as $[CuL_2(H_2O)_2]$. The in-situ formation of the bis(amido)phosphate ligand $(L)^-$ is again attributed to the Lewis-acidic nature of the Cu(II) salt triggering a metal-assisted P-N bond hydrolysis at the high reaction temperatures and pressure (Scheme 4.3). The EPR spectrum of the crystals of **4.5** at room temperature showed a single line spectrum typical of a Cu(II) ion with a *g* value of 1.973 (Figure A3.3, Appendix 3). Magnetic measurements on the microcrystalline solid of **4.5** show a paramagnetic behavior consistent with the isolated metal ion with S = ½ spin (Figure A3.4 and A3.5, Appendix 3).

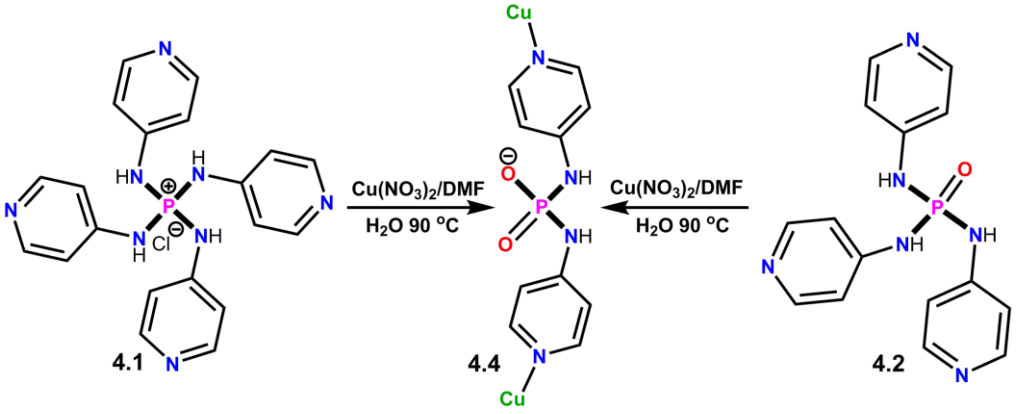

Scheme 4.3: Reaction of **4.1** and **4.2** with $Cu(NO_3)_2$.

In support of this observation control experiments with only the ligands **4.1** and **4.2** under similar reaction conditions were performed, respectively, to see the presence of any hydrolytically cleaved product. The ^{31}P-NMR spectra of the reaction mixtures before and after the experiment showed no change in the chemical shift values (**4.1**: δ -3.74 and **4.2**: δ -5.64) indicating the stable nature of these ligands in the absence of metal ions. Literature survey indicates that such metal-assisted P-N bond hydrolysis were already observed in some instances where the P(V) centers were bound to N-containing heterocycles.[16] Recently, Sokolov and co-workers have reported Cd^{2+} containing coordination polymers based on the P(V) ligands $[(HOCH_2)_3PO]$ and $[(HOCH_2)_2PO_2]^-$.[17] Noticeably, the phosphinate $[(HOCH_2)_2PO_2]^-$ which is structurally analogous to L^- was formed in-situ in the reaction of the corresponding phosphine $[P(CH_2OH)_3]$ with Cd^{2+} ions in MeOH solution via the initial formation of the phosphine oxide $[(HOCH_2)_3PO]$ followed by a P-C bond hydrolysis reaction.

In order to check the formation of the in-situ ligand L^- under metal free conditions, we treated the precursors **4.1** and **4.2** in DMF with a 1M solution of HCl in water at 90 °C under hydrothermal conditions for 72 hrs. Slow evaporation of these reaction mixtures at 80 °C on a hot plate resulted in the mono-chlorinated salt $[PO_2(NH^4PyH)_2]Cl$, **4.6**, as a micro-crystalline solid (Scheme 4.4). MALDI-TOF mass spectra of this sample gave prominent peaks at m/z = 288.98 pertaining to the species $[\mathbf{4.6}+K]^+$. The ^{31}P-NMR of **4.6** in D_2O show peaks at -12.62 ppm which is considerably up-field shifted from the corresponding precursors **4.1** and **4.2** (Figure A3.6 and A3.7, Appendix 3). Further the formation of **4.6** was confirmed by single-crystal X-ray diffraction which shows that one of the two pyridyl N-sites were protonated.

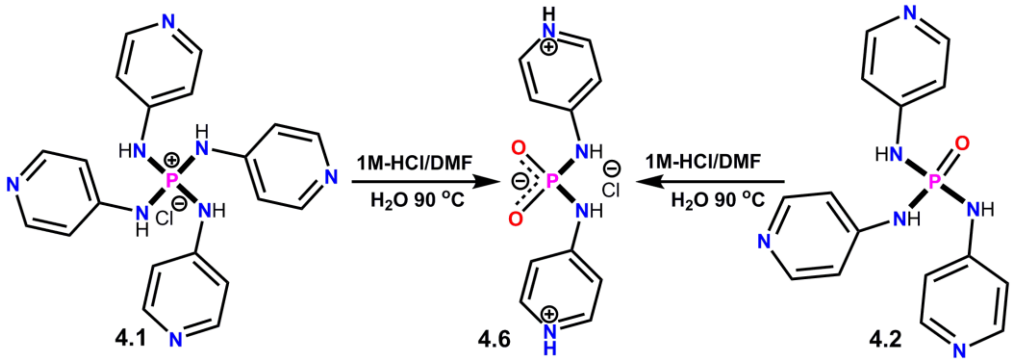

Scheme 4.4: High temperature reaction of **4.1** and **4.2** with a 1M HCl solution.

However, treatment of **4.2** with a 1M solution of HCl in water at room temperature did not yield the in-situ ligand as observed by presence of the parent species in the mass-spectra (Figure A3.8, Appendix 3) This observation suggests that in addition to the acidity of the reaction medium, the Lewis acidity of the metal ions plays a crucial role for the in-situ ligand synthesis via a metal-assisted P-N bond cleavage pathway.

During these reactions ($Cu(NO_3)_2$ with **4.1** or **4.2**) it has been observed that a few small pale yellow crystals in addition to the major quantities of the crystals of **4.5**.2DMF.2H_2O were also formed. Single crystal analysis of these pale yellow crystals show the formation a Cu(I) 2D-coordination network **4.7**.DMF.2H_2O with the core composition of **4.7** as [Cu(**4.2**)(L)] (Scheme 4.5). Formation of the complex **4.7**.DMF.2H_2O is due to the mildly reducing nature of the reaction solvent DMF causing the in-situ reduction of some of the Cu(II) ions to Cu(I) ions. Repeating the reaction with **4.1** or **4.2** in the absence of added water (a DMF solution of $Cu(NO_3)_2$ instead of its aqueous solution) produced the material **4.7**.DMF.2H_2O in pure, although in low yields. Attempts to synthesize **4.7**.DMF.2H_2O from Cu(I) sources (such as $[Cu(MeCN)_4]PF_6$) or from Cu(II) salts in presence of NH_3 as external base were unsuccessful. This is probably due to the acidity of medium being lowered in both these instances preventing the in-situ formation of the L^- ligand.

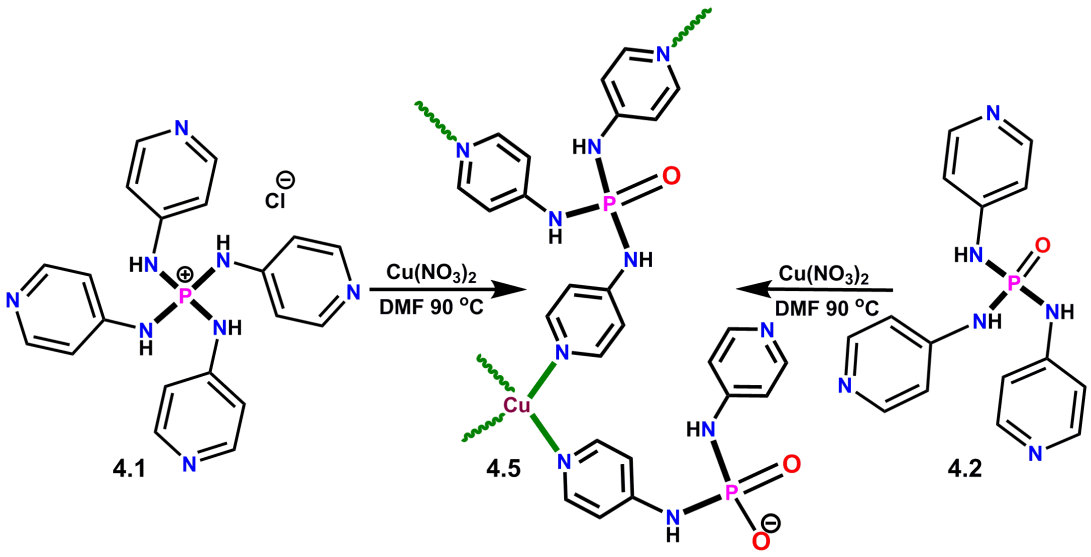

Scheme 4.5: Formation of Cu(I) coordination polymer **4.5** from the reaction of **4.1** and **4.2**.

4.3.2 Crystal structures

The molecular structure of the phosphonium salt **4.1** was shown in the Figure **4.1**a. It crystallized in the cubic space group *I-43d* with its asymmetric unit consisting of one fourth of the phosphorus center attached to a crystallographically unique amino-pyridyl moiety and one-fourth equivalence of the chloride ion. All the four P−N bonds are same due to the presence of a four-fold axis of symmetry and measures at 1.631(2)Å. Two varied types of N−P−N bond-angles are found in the crystal structure of **4.1** and are marginally deviated from the tetrahedral angle of 109.4 (Table A3.2, Appendix 3). While the previously reported aryl- or alkylamino phosphonium chlorides were shown to form interesting kinds of 1D- or 2D-supramolecular structures mediated by N-H…Cl interactions, such extended interactions are not found in the crystal structure of **4.1**. All the four N-H protons are equivalent and involved in hydrogen bonding with the chloride ions, which are located adjacent to these N-H sites, at one fourth occupancies each. In addition, these chloride ions are hydrogen bonded to one of the aryl proton (H22) of the pyridyl ring in a non-classical manner (C-H…Cl).

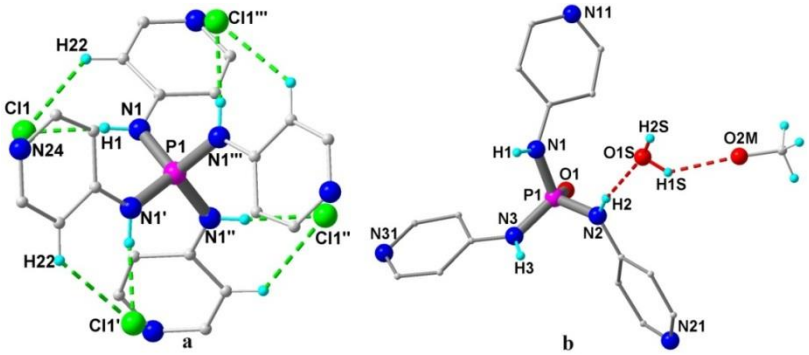

Figure 4.1: Molecular Structures of **4.1** (a) and **4.2** (b)

The phosphoric triamide **4.2** was crystallized in the monoclinic non-centric space group *Pc* as **4.2**.$CH_3OH.H_2O$, with its asymmetric unit consisting of the complete ligand and the solvated molecules of methanol and water (Figure **4.1**b). Unlike **4.1**, the amino protons in **4.2**.$CH_3OH.H_2O$ are involved in intricate hydrogen bonding interactions with the pyridyl nitrogens and the solvated H_2O leading to a 3D-supramolecular network. Interaction of one of the amino protons (N1−H1) with the nearby P═O group (O1) initially forms a 1D-chain structure along the c-axis. Interaction of the second amino-proton (N3−H3) with the pyridyl groups (N21) that belongs to N2 connects the adjacent chains resulting in a 2D-sheet structure running along the bc-plane (Figure 4.2a). Finally,

the solvated water molecules act as a linker between the individual 2D-sheets and connects the remaining amino protons (N2-H2…O1S) and one of the pyridyl nitrogens (O1S-H2S…N31) forming the 3D-network. The solvated molecules of methanol are located along the 1D-channel inside the network and involved in H-bonding with water (O1S-H1S…O2M) and the remaining pyridyl moiety (O2M-H2M…N11) (Figure 4.2b).

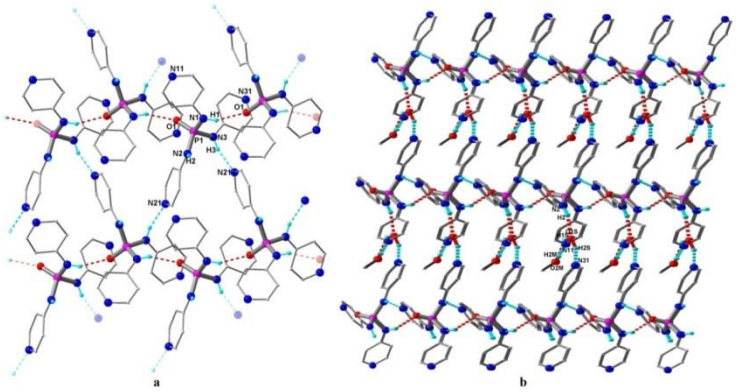

Figure 4.2: (a) View of the H-bonded 2D-sheet in **4.2** formed by the interaction of amino protons with P=O and pyridyl groups; (b) formation the 3D-network mediated by the solvated water molecules. The layers are slightly offset to show the 3D-nature of the network.

The Zn(II) coordination polymer **4.3** crystallized in the orthorhombic space group *Pbca*. It consists of a distorted tetrahedral Zn(II) centre surrounded by three L^- ligands and a formate anion. Among the three L^- ligands, two of them coordinate via pyridyl nitrogens while the third one is attached through its phosphate (O3) oxygen. Thus, L^- acts as a tridentate N,N,O-ligand and each Zn(II) centre acts as a 3-connected node for the formation of a 2D-network with the topology of a (3,3) sheet (Figure 4.3). The 2D-sheet has the shape of a zigzag chain along the c-axis and contains a series of 28-membered macrocycles. The formate ion provides the necessary coordination saturation to the Zn(II) centre and is intra-molecularly hydrogen bonded to one of the amino protons via its free C=O groups (N2-H2…O4). Further, hydrogen bonding between the remaining amino groups and the phosphoryl oxygens connects the individual 2D-sheets to form a 3D-network. A series of eight-membered $R_2^2 8$ rings are involved in linking the 2D-sheets facilitating the formation of the 3D-network (Figure 4.3).

The packing diagram of the molecule shows the presence of 1D-pores (8.6Å x 7.5Å) including van der Walls distances) along the a-axis which are occupied by the solvated molecules of DMF and water. Exchange studies with methanol on the crystals of

4.3indicate that the DMF molecules are completely exchanged with methanol (**3a**) (Figure 4.5) (Color code for solvent atoms: oxygen: orange; hydrogen: dusty green; nitrogen: light blue; carbon: light pink) in 10 days in a single crystal to single crystal manner. The solvent accessible space calculated by the Mercury software[18] on **4.3** and **4.3a** is found to be 33.6% (1365.5 Å) and 32.8% (1322.6 Å) of the unit cell volume, respectively (Figure 4.6a).

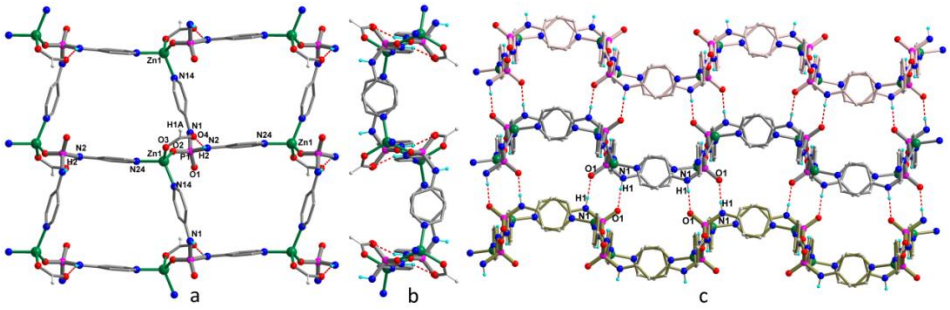

Figure 4.3: (a) View of the 2D-sheet in **4.5**.DMF.H_2O along the ab-plane; (b) zigzag view of the 2D-sheet along the c-axis; (c) formation of the 3D-network mediated H-bonding interactions.

The crystal structure of the polymorph **4.4** was solved in the monoclinic space group *P2(1)/n*. It contains the Zn(II) ion in distorted trigonal bipyramidal (TBP) geometry featuring three L^- ligands (two equatorial N-sites and one axial O-site), one equatorial O-site from the formate and the fifth axial O-site from water. The net effect is the formation of a 2D-coordination polymer similar to that found in **4.3** except that the topology of the zigzag sheet is slightly different from that of **3** attributed to the TBP geometry at the metal centre in **4.4**. Unlike **4.3**, the 3D-assembly in **4.4** is facilitated by the interaction of the coordinated water with the phosphoryl and formate oxygen atoms (Figure 4.4).

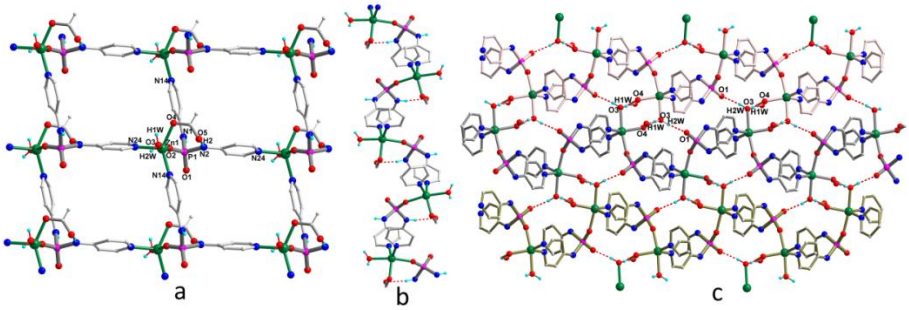

Figure 4.4: View of the 2D-sheet in **4.5**.DMF.H2O along the ab-plane; (b) zigzag view of the 2D-sheet along the c-axis; (c) formation of the 3D-network mediated H-bonding interactions.

The solvent accessible void in **4.4** is lower than that of **4.3** and is calculated to be 22% (401.8 Å) of the unit cell volume (Figure 4.6b) indicating the flexible nature of the $[ZnL(HCO_2)]_\infty$ framework with respect to the solvated groups (**4.3** contain solvated DMF and water, **4.3a** contain disordered methanol and water and **4.4** contain disordered DMF). The solvent disorder in **4.3a** could not be resolved and hence they are refined as partially occupied oxygen atoms. In **4.4** the whole DMF molecule was disordered over two positions of which only one of them is shown in the packing (Figure 4.5).

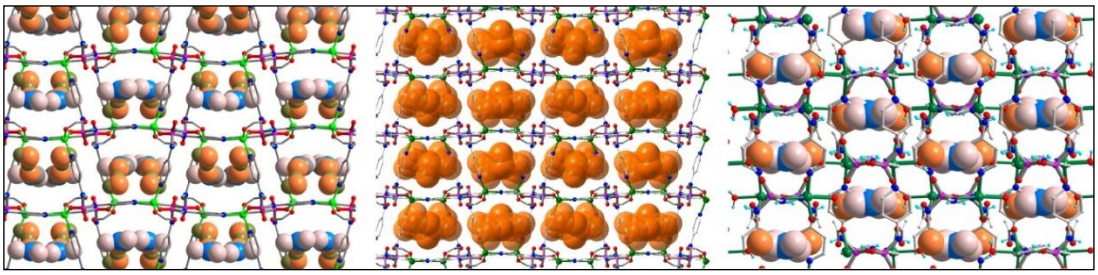

Figure 4.5: Packing diagram of **4.3** (left), **4.3a** (middle) and **4.4** (right) with solvated molecules shown in space fill representation.

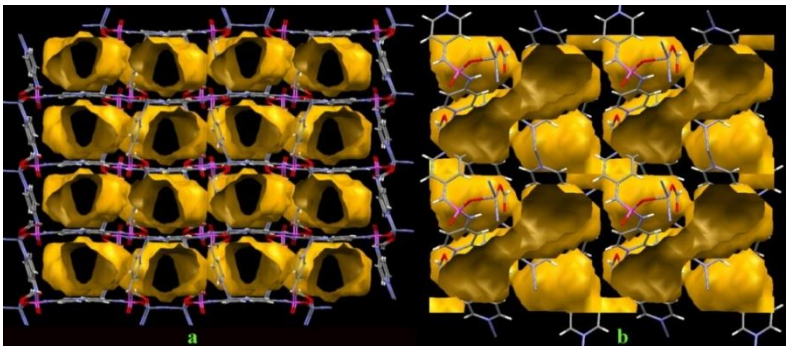

Figure 4.6: Connolly surface view of the packing structure of **4.3a** along the a-axis (a) and **4.4** along c-axis (b) indicating the solvent accessible voids

The one-dimensional Cu(II)-coordination polymer **4.5** was crystallized in the orthorhombic space group *Cccm*. The asymmetric unit of **4.5** consists of an unique Cu(II) center having one fourth of an occupancy, half of the phosphate ligand $(L)^-$ and a half occupied coordinated water molecule. Thus the overall formula of the 1D-chain can be represented as $[Cu(L)_2(H_2O)_2]_\infty$ and the dicationic charge of the complex is balanced by the presence of two $(L)^-$ ligands. The solvated DMF and water molecules were found with positional disorder with one half occupancies for each of them in the asymmetric unit. The molecular core consists of a distorted octahedral Cu(II) center consisting of four equatorial pyridyl ligands from four $(L)^-$ ligands in a planar fashion and two coordinated water molecules at the axial sites. Each anionic ligand coordinates through

only its pyridyl nitrogens and bridges the two adjacent Cu(II) centers in a 'V'-shaped manner with the formation of a contiguous $Cu_2(L)_2$ square-grids. Although such kinds of Cu(II) based coordination polymers were known in the literature, they were all formed in presence of neutral N-donor ligands and the obtained chains were cationic in nature.[19] It is interesting to compare the coordination of $(L)^-$ in **4.5** to that found in its 1:1 zinc complex of formula $[Zn(L)(HCO_2)]_\infty$.[13] In this 2D-network due to the higher oxophilicity of Zn(II) ions, the ligand was found in a tridentate coordination involving two $N_{pyridyl}$ and one anionic O^- coordination. Where as in **4.5**, the ligand is found in only a bidentate coordination to two Cu(II) atoms resulting in a 1D-chain structure.

Further, the two coordinated water molecules are both equivalent and engage in hydrogen bonding interaction with the uncoordinated P-O groups of the adjacent orthogonally oriented 1D-chains to form a tightly knit 3D-network. While the 24-membered $Cu_2(L)_2$ macrocycles form the core of the 1D-chain, a series of H-bonded $R_4^4 12$ rings were involved in the construction of the 3D-network (Figure 4.7). TOPOS analysis[20] on **4.5** shows the presence of a $(4\text{-c})_2$, 8-c bi-nodal **scu** net as represented by the Schläfli symbol of $(4^4.6^2)_2(4^{16}.6^{12})$ (first symbol for the $(L^2)^-$ ligand and the second one for the Cu atoms).[21] Each ligand moiety acts as a 4-connected node (pink spheres, with two short and two long contacts) and each Cu atom (green spheres, with four short and four long contacts) serves as an 8-connected node leading to a 3D H-bonded network (Figure 4.5b). The metric parameters associated with these H-bonds are very strong which measures at 2.705(3) Å for the donor-acceptor distance (O1…O2) and the pertaining O2–H2…O1 angle measuring at 160.8(3)°. The packing diagram of the hydrogen bonded 3D-network in **4.5** shows the presence of a solvated channel which are occupied by the disordered molecules of DMF and water (Figure 4.5c). The channel volume calculated by using the Mercury software,[18] after excluding the solvate molecules, gave 32.6% of the unit cell volume which measures about 1068 $Å^3$. The two diameters of the pores inside **4.5** are measured to be 13.158 Å and 14.942 Å. In order to obtain a guest free material, the solvated DMFs in **4.5** were exchanged with methanol in a single crystal to single crystal manner. The X-ray analysis of the crystals soaked in methanol for a period of 10 days indicated a complete guest exchange leading to the formation of a new methanol adduct **4.5a** ($\{[Cu(L)_2(H_2O)_2]\cdot 2CH_3OH\cdot 2H_2O\}_\infty$). The unit cell parameters of **4.5a** are similar to that of **4.5** and solved in the orthorhombic space

group *Cccm*. Comparison of the channel structures along the c-axis in both these crystals indicate that the void space observed in **4.5** is retained in **4.5a** as well.

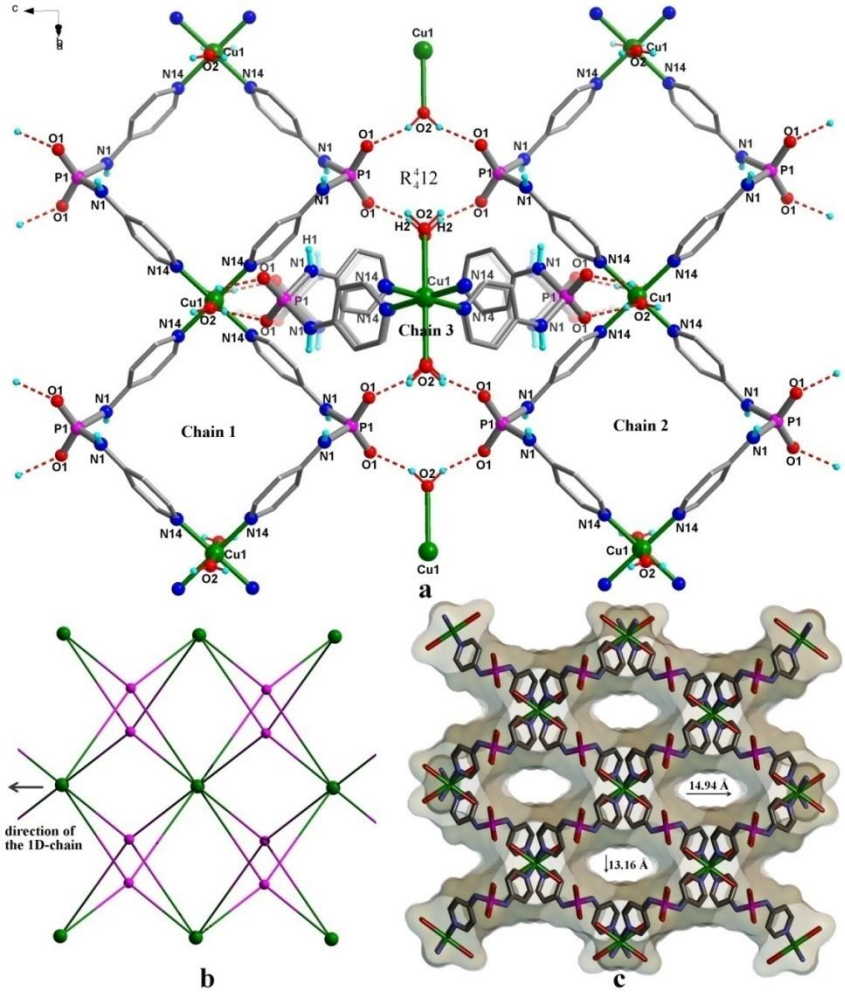

Figure 4.7: (a) View of the 1D-chain polymer in **4.3**.2DMF.2H_2O; (b) hydrogen bonding interaction of orthogonally oriented neighboring chains leading to the 3D-network.

The molecular structure of the in-situ ligand derivative **4.6** was solved in the orthorhombic space group *Pca2(1)* (Figure 4.8a). The asymmetric unit consists of the Zwitterionic segment of $[L+2H]^+$ featuring the monoanionic (non-protonated) P-O terminals and the dicationic protonated pyridyl segments, an environment very similar to that of L^- in **4.3**. The charge balance is restored in the form of a chloride ion originating from the HCl source. Due to the presence of the four protic hydrogen atoms and the electronegative anionic segments it exhibits rich hydrogen bonding interactions in the crystal lattice. The chloride ion is involved in a bifurcated H-bonding interaction with two Zwitterionic units via the amino proton (H2) of one unit and one protonated pyridyl moiety (H24) of the other unit. These two Zwitterionic units are further bridged by the other amino proton (H1) and one of the phosphoryl oxygen atoms (O1) from a third

Zwitterionic moiety leading to the formation of a one-dimensional chain structure consisting of contiguous 18 membered rings (Figure 4.8b). Further these 1D-double chains were connected through the N-H···O interactions of the other protonated pyridyl ring (H14) and the second phosphoryl oxygen atom (O2) to yield the 2D-hydrogen bonded network (Figure 4.8c). The metric parameters associated with these H-bonding indicate very strong interactions between the donor and acceptor atoms (Table A3.3, Appendix 3).

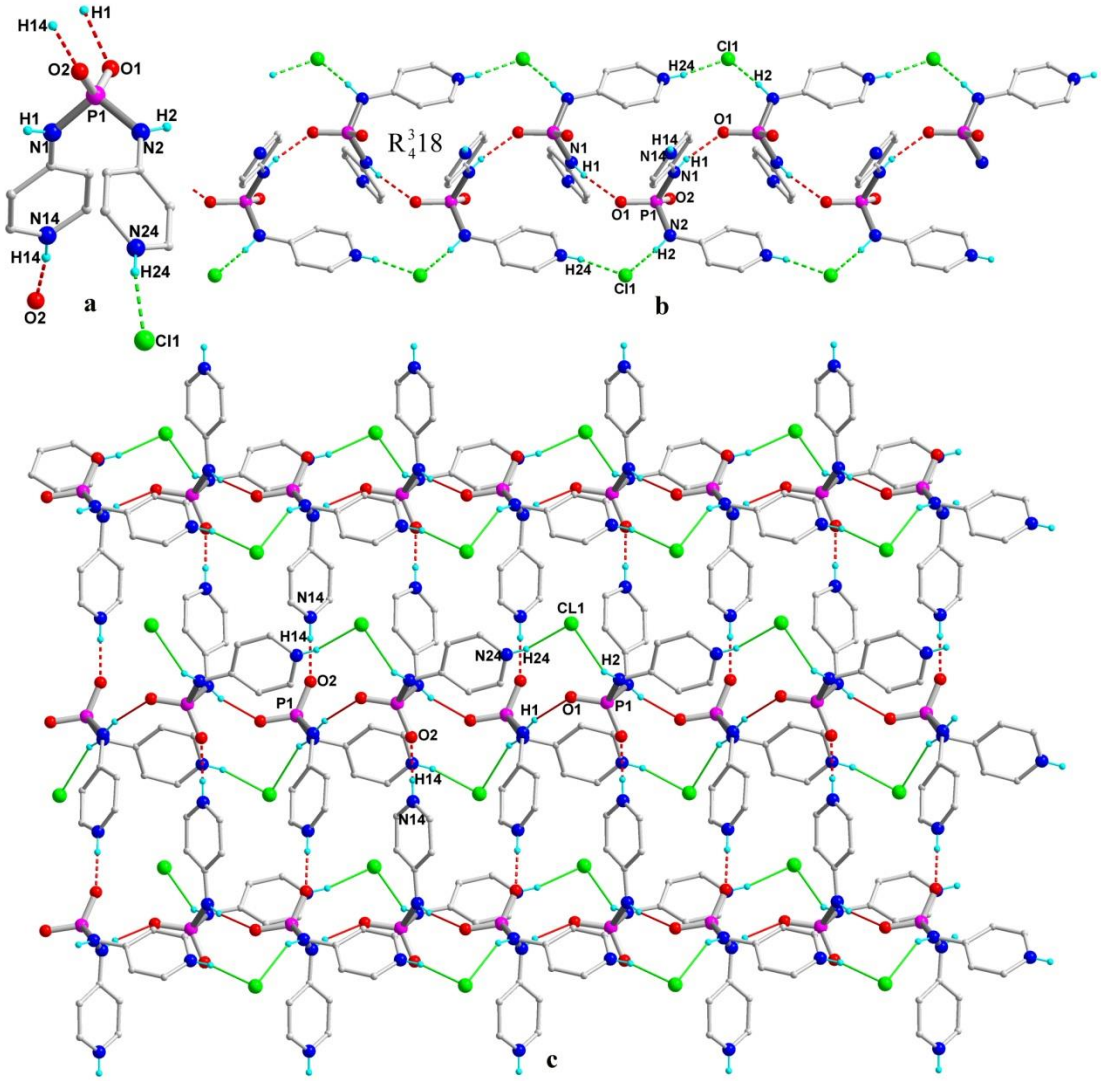

Figure 4.8: (a) Molecular structure of **4.6** with immediate H-bonded segments; (b) Formation of the 1D-chain structure comprising of the continuous 18 membered macrocycles mediated by $N_{pyridyl}$-H…Cl, N_{amino}-H…Cl and N_{amino}-H…O=P interactions; (c) Formation of the 2D sheet-like assembly due to $N_{pyridyl}$-H…O=P interactions

The Cu(I) coordination polymer **4.7** with the mixed ligand configuration was solved in the monoclinic space group *P2(1)/c*. At the core of the molecule resides the tetrahedral

Cu(I) ion coordinated to four pyridyl donor ligands, three from the ligand **4.2** and one from the anionic ligand L^-. Each neutral ligand (**4.2**) in turn is bonded to three tetrahedral Cu(I) center and aids in the 2D-network propagation (Figure 4.9a). The cumulative effect of these interactions is the formation of a zigzag 2D-layer in which both the Cu(I) center and the neutral ligand **4.2** acts as 3-connected node (Figures 4.9a and 4.9b). The TOPOS software analysis for **4.7** gave a Schläfli symbol of 6^3 for a uninodal net with a distorted **hcb** network topology (Figure 4.9c).[21] The role of L^- is merely to provide the coordination saturation for the metal centre through one of its pyridyl groups and to restore the charge balance in the network. The other pyridyl group of L^- is uncoordinated and remains alternately above and below the 2D-sheet.

The packing diagram of the molecule shows the formation a 3D-assembly in which the 2D-layers are inter-digitated onto each other and involved in H-bonding interactions. The zigzag nature (Figure 4.9b) of the network allows each 2D-sheet to participate in H-bonding interactions with six other sheets (three above and three below). The amino protons of the ligand 4.**7** in a given sheet are involved in H-bonding with the P=O groups of the L^- ligands from the adjacent sheets (N3-H3…O2). Further the anionic ligands L^- from the neighboring sheets occupy the space inside the channel and involve in H-bonding interactions among themselves forming $R_2^2 8$ rings (N4-H4…O2) providing additional support for the 3D-assembly (Figure 4.9d). The remaining amino protons are hydrogen bonded to solvated (DMF and water) molecules located in the channels. The packing diagram of the molecule shows a narrow pore along the b-axis with a void volume of 274.09 $Å^3$ which amounts to only 8% of the unit cell volume. Due to the smaller void volume and the oxygen sensitive nature this material we were unable to perform the guest exchange and sorption studies for **4.7**.

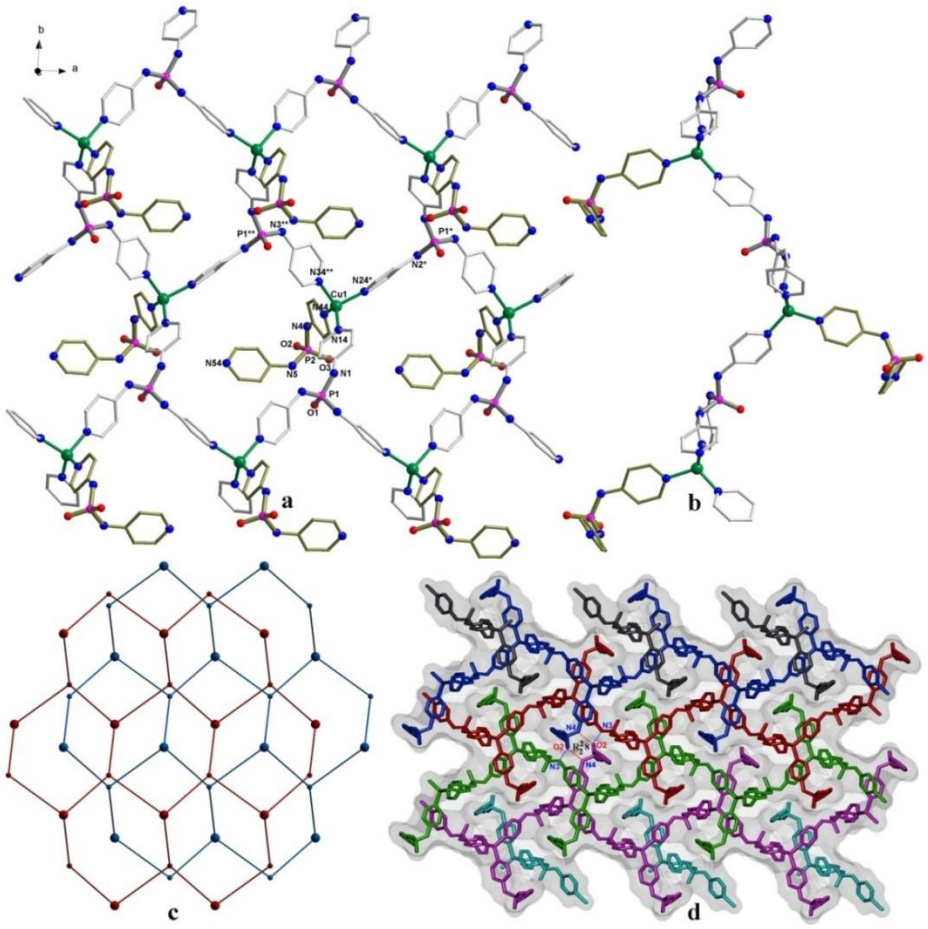

Figure 4.9: (a) View of the 2D-sheet in **4.7**.DMF.2H_2O along the ab-plane. The neutral ligand **4.2** is shown with light-grey colored bonds and the anionic ligand L^- is shown with dull-green bonds (b) zigzag view of the 2D-sheet along the a-axis. (c) Offset view of the hexagonal network in **4.7**.DMF.2H_2O smaller and bigger spheres represent P and Cu nodes, respectively. (d) Formation of H-bonded 3D structure in **4.7**.DMF.2H_2O. The individual sheets are colored differently for better viewing and representative H-bonding points are indicated as dotted lines.

4.3.3 Thermal and guest exchange studies of the coordination polymers

The thermogravimetric analysis (TGA) graph of **4.3** shows no staged weight loss and decomposes at temperature above 130 °C. But, that of **4.3a** shows an initial weight loss of 8% at 75 °C corresponding to the loss of the solvated molecules (1·CH_3OH and 1·H_2O). Beyond this temperature the material remains stable until it reaches 180 °C at which point decomposition of the framework was observed. The TGA graph of the de-solvated sample of **4.3b**, obtained by evacuating **4.3a** at 120 °C for 5 hours, shows almost no weight loss until 180 °C and decomposes straight away above this temperature (Figure 4.10).

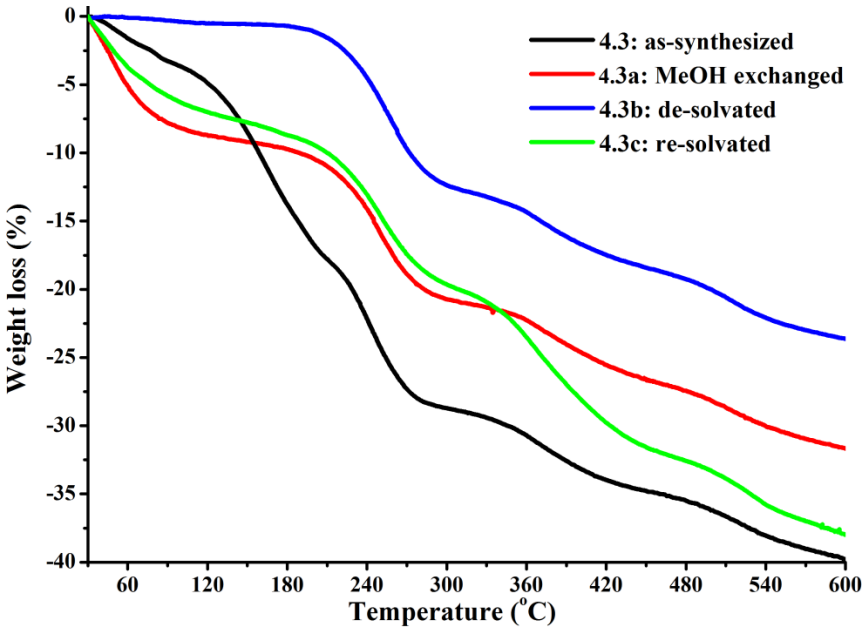

Figure 4.10: TGA graphs for various samples of **4.3**

The powder diffraction (PXRD) of the as-synthesized **4.3** and methanol exchanged **4.3a** are nearly the same whereas that of **4.3b** (de-solvated) shows changes in the diffraction patterns due to the loss of solvents. Soaking **4.3b** in methanol for few days (3 days) generates **4.3c** (re-solvated) which has a matching PXRD pattern as that of **4.3a** (Figure 4.11).

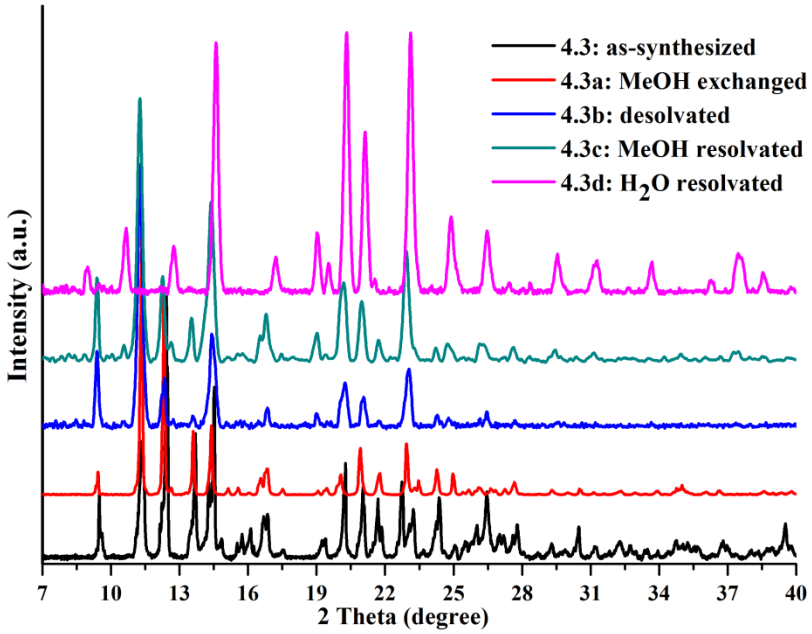

Figure 4.11: The PXRD patterns for various samples of **4.3**

The TGA graph of **4.4** shows a three staged weight loss: first one due to the loss of coordinated H_2O, second one due to the loss of DMF and the third one attributed to

framework decomposition (Figure 4.12). The TGA of **4.4a** (MeOH exchanged) exhibits an analogous trend except that the first weight loss is due to MeOH and the second one due to coordinated H_2O. Notably, the TGA of **4.4b** (de-solvated) and **4.4c** (MeOH re-solvated) matches closely with that of **4.3b** and **4.3c**, respectively (Figure 4.14). A similar trend has also been observed in their PXRD patterns indicating the de- and re-solvated phases of both **4.3** and **4.4** are the same (Figure 4.13 and 4.15).

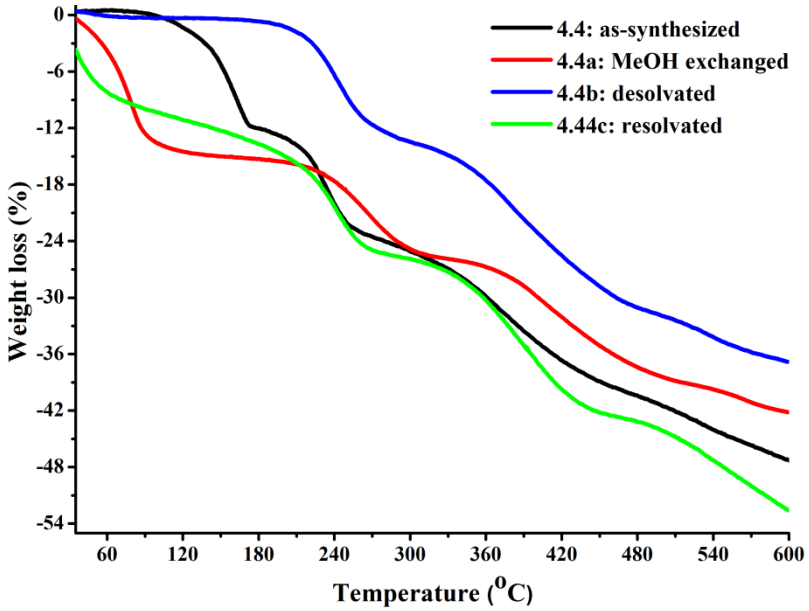

Figure 4.12: TGA graphs for various samples of **4.4**

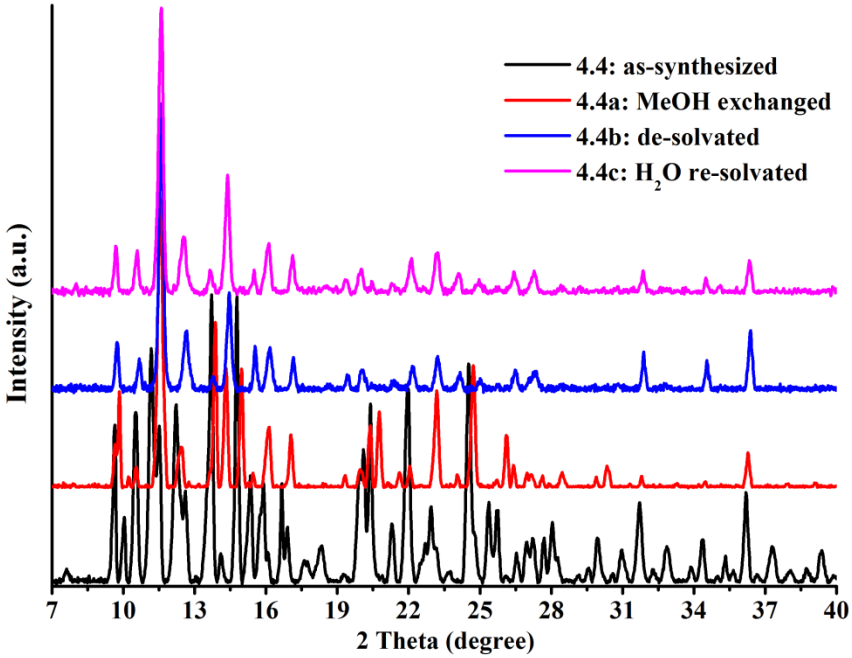

Figure 4.13: The PXRD patterns for various samples of **4.4**

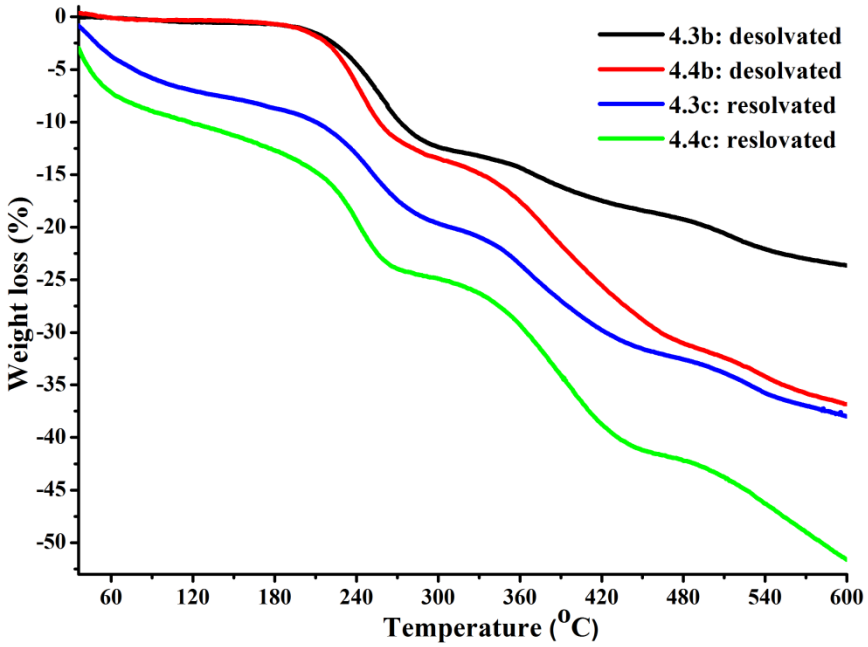

Figure 4.14: TGA comparison plots for de-solvated and re-solvated samples of **4.3** and **4.4**

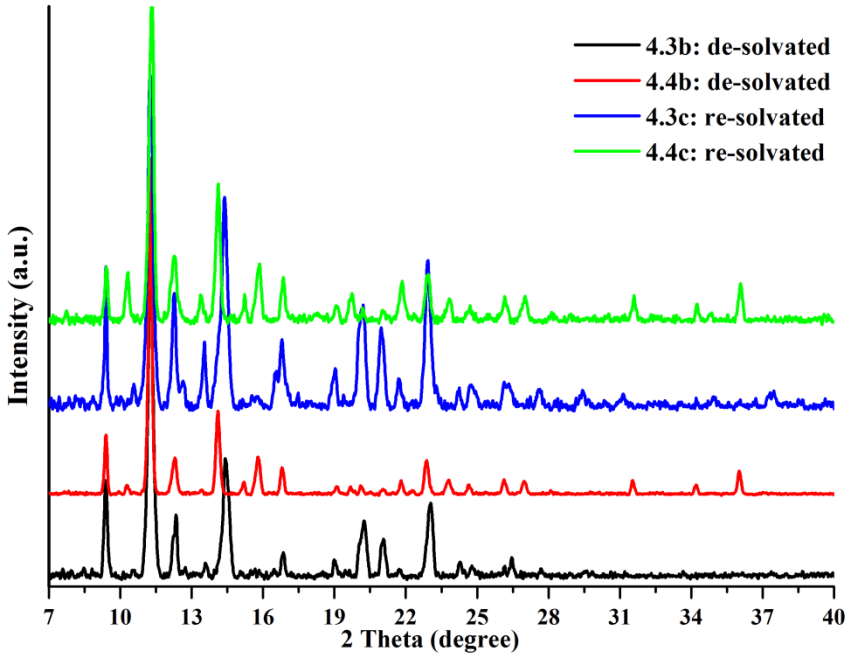

Figure 4.15: Comparative PXRD patterns for de-solvated and re-solvated samples of **4.3** and **4.4**

The TGA of the crystalline sample of **4.5** shows a gradual weight loss of about 20% up to a temperature of 230 °C corresponding to the loss of all the solvent molecules present in the structure. Above this temperature the percentage weight loss is high and abrupt which is attributed to the framework decomposition (Figure 4.16). The TGA graph of the methanol exchanged sample **4.5a**, shows an initial weight loss of about 14% below 100

°C matching with the removal of solvated molecules of methanol and water. A second weight loss of about 5% occurs in the temperature region between 170 °C and 230 °C suggesting the loss of two coordinated water molecules. Above this temperature an abrupt weight loss occurs as before indicative of the framework decomposition. TGA analysis on the desolvated sample of **4.5b**, obtained by evacuating **4.5a** at 90 °C overnight, shows no significant weight loss up to 190 °C and completely decomposes above 220 °C indicating that the framework remained intact up to this temperature.

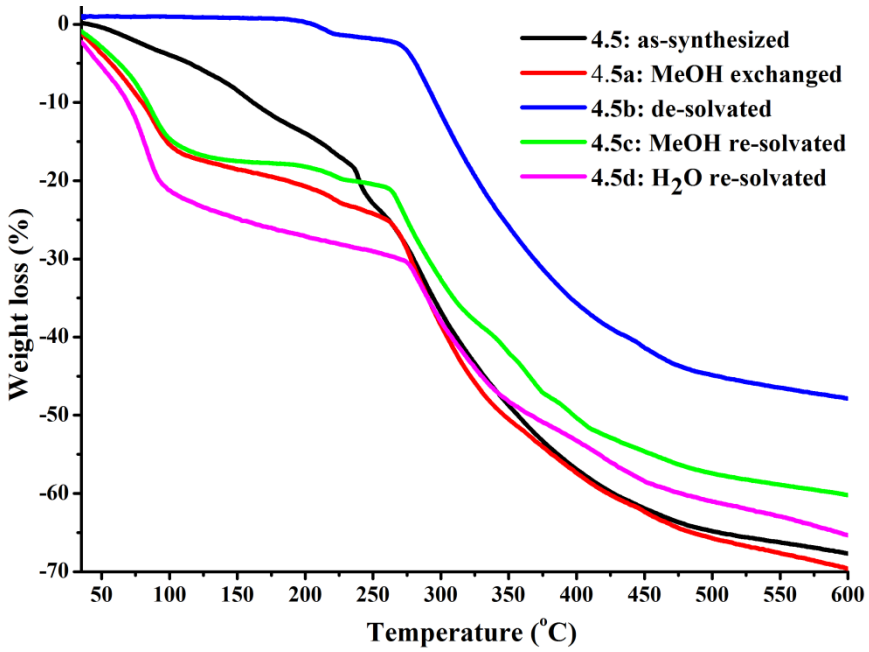

Figure 4.16: (a) TGA graphs for various samples of **4.5**

The powder X-ray diffraction (PXRD) patterns of the samples of **4.5** and **4.5a** were closely matching, albeit a slight variation in the intensities for some of the observed peaks (Figure 4.17). On the other hand, the PXRD pattern of the desolvated sample **4.5b** shows deviations to that of the pristine sample indicating some changes in the crystal packing. This might be owing to the partial or complete loss of the coordinated water upon desolvation although the shape of the crystals remained intact and opaque after evacuation. Soaking **4.5b** in methanol for three days resolvates it and revokes the crystallinity in the sample (**4.5c**). This is evidenced by a visible color change of the sample from dark green to bright blue and reappearance of the PXRD patterns due to **4.5a**. The TGA analysis of **4.5c** also matches with that of **4.5a** consistent with the complete resolvation. Interestingly, resolvation of **4.5b** in water takes place within 30 minutes confirming the absence of the coordinated water molecules (one or both) in **4.5b**

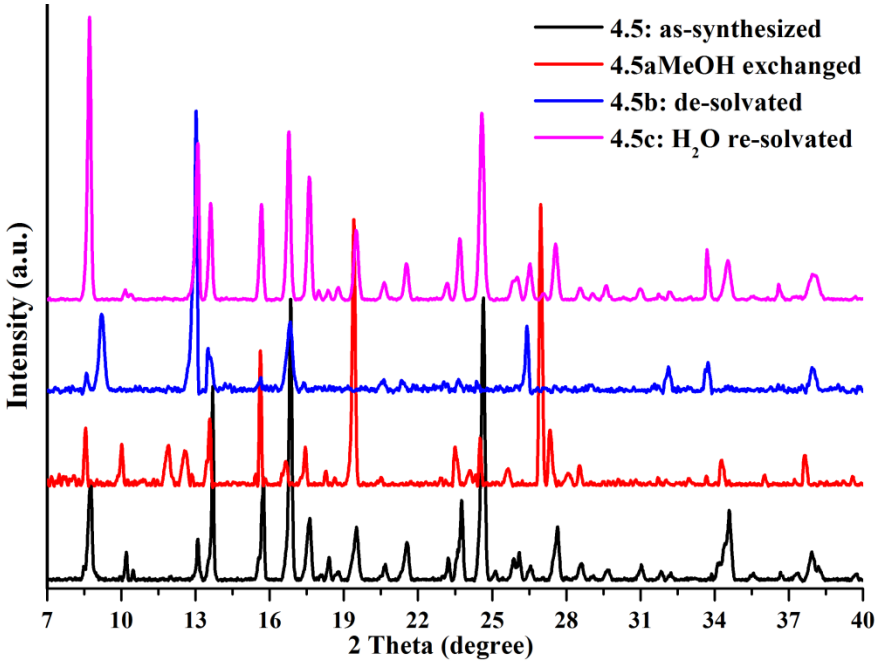

Figure 4.17: The PXRD patterns for various samples of **4.5**

4.3.4 Gas and Solvent adsorption studies of the coordination polymers

Gas adsorption measurements showed that **4.3b** uptakes $N_2$and CO_2 at 77 K and 195 K, respectively (Figure 4.18). The CO_2 sorption shows an uptake with a type I behavior whereas that of N_2 shows type II behavior. The seemingly better uptake of CO_2 over N_2 can be attributed to the larger quadrupole moment of CO_2 (compared to N_2), which favors a better interaction with the polar P=O and C=O groups that are located inside the molecular pores. However, the adsorption data measured for these gases at room temperature did not show appreciable uptake characteristics (Figure A3.9, Appendix 3).

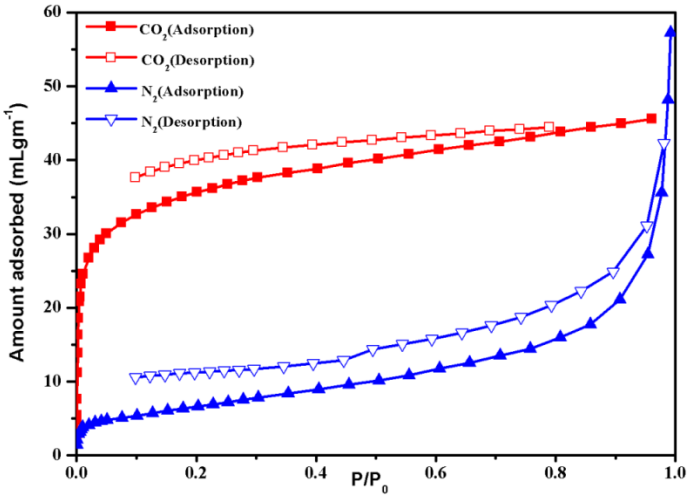

Figure 4.18: CO_2 and N_2adsorption (filled symbols) and desorption (open symbols) isotherms for **4.3**b at 195 K and 77K

In view of the polar nature of the pores present in **4.3b**, vapor sorption measurements for polar solvents such as water, methanol and ethanol were performed (Figure 4.18). The adsorption of water shows a clear uptake step at P/Po = 0.35 and the final value at P/Po = 1.0 corresponds to ten water molecules per formula unit. The observed isotherm indicates that there is a possible adsorption-dependent structural rearrangement, which is attributed to the flexible nature of the framework. In contrast, methanol was adsorbed to a very small value corresponding to one molecule per formula unit. Ethanol in fact did not show any adsorption at all. PXRD profiles of the various resolvated (H_2O, MeOH and EtOH) samples show that there is a significant change in patterns for the H_2O re-solvated sample. On the other hand, the PXRD profiles of MeOH and EtOH resolvated samples resemble closely that of **4.3a** (Figure 4.19 and Figure A3.10 Appendix 3). This could be due to the smaller size of the water molecules, as they can undergo a better diffusion inside the pores than the alcohols and can cause a minor structural deformation. Also, the amino protons in **4.3** can more effectively participate in H-bonding with water than with alcohols favoring the adsorption of water vapor over alcohols. Further, from the crystal structures of **4.3** and **4.4**, a possible change in geometry for the Zn^{2+} ions could be speculated, from tetrahedral (in **4.3b**) to five-coordinate (TBP) environment upon water re- solvation.

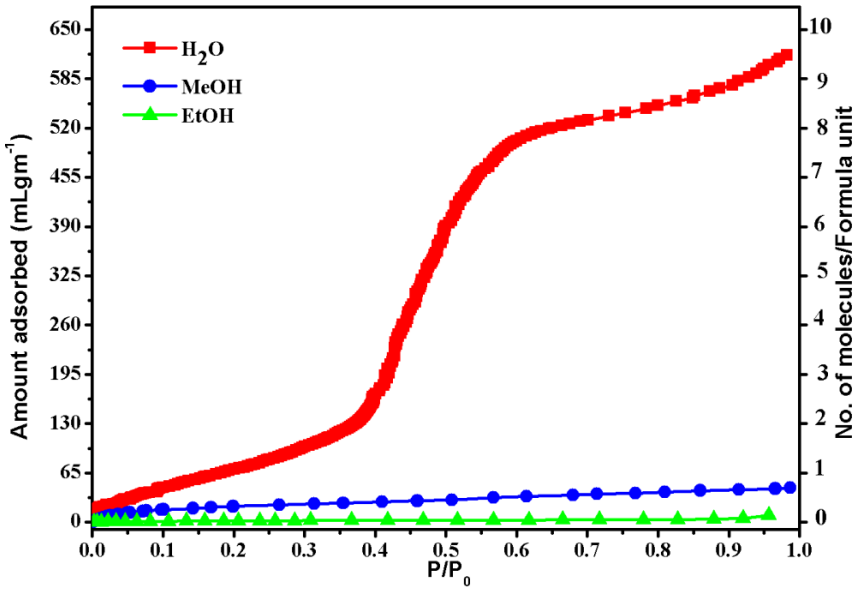

Figure 4.19: Solvent adsorption isotherms for **4.3b** at 298K

Although the volume of the packing cavity in **4.5a** is quite suitable for gas uptake studies, due to the narrow dimensions of the pore windows (2.6 Å x 6.7 Å), excluding the van der Waals radii, no appreciable gas uptake characteristics could be observed for

this material. The CO_2 and N_2 adsorption isotherms for the activated sample of **4.5b** measured at 150 K and 77K, respectively, indicates that the observed values are characteristic of a surface adsorption (Figure 4.20).

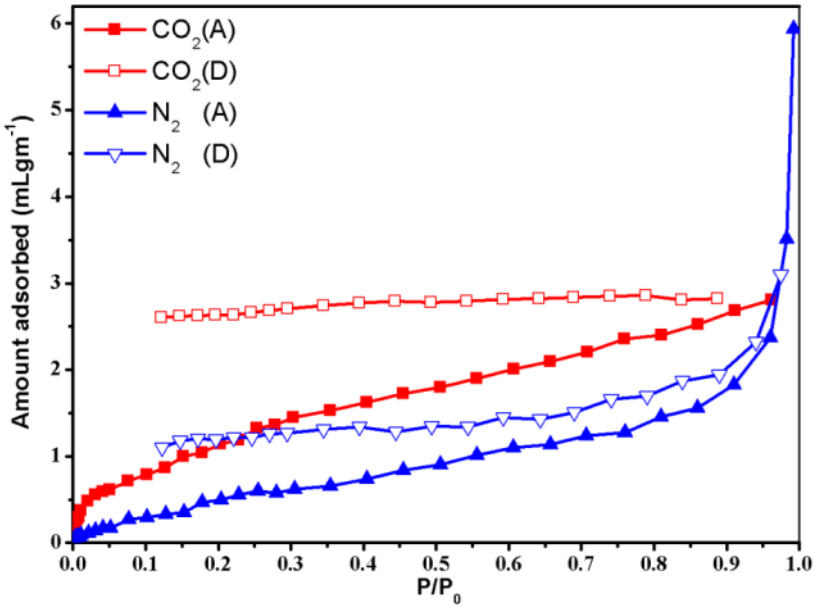

Figure 4.20: CO_2 and N_2 adsorption (filled symbols) and desorption (open symbols) isotherms for **4.5**b at 195 K and 77K

In contrast, solvent sorption studies for water, methanol and ethanol vapors measured on **4.5b** shows an interesting trend among these solvents. The adsorption isotherm of water indicates a gradual uptake and the final value at P/P_o = 1.0 corresponds to five and a half water molecules per formula unit (Figure 4.21). The adsorption isotherm for methanol reveals that the uptake was sluggish and the final value corresponds only to one methanol per formula unit of the network. The bulkier ethanol did not adsorb at all suggesting that **4.5b** uptakes water vapors preferential over aliphatic alcohols. This could be attributed both to its smaller pore diameter and to the presence of donor-acceptor type H-bonding interactions between the coordinated and solvated molecules of water. Although the Zn(II) polymer **4.3b** is better in terms of the water uptake capacity (10 molecules per formula unit), its water adsorption isotherm indicated a minor structural rearrangement. However, **4.5b** exhibits a better stability as indicated by its gradual uptake isotherm and sharp PXRD profiles (for both **4.5b** and **4.5d**). Further from the nearly identical solid state UV-visible spectral profiles and FT-IR peaks the structural stability of the de-solvated and water re-solvated samples were confirmed (Figure 4.22 and 4.23).

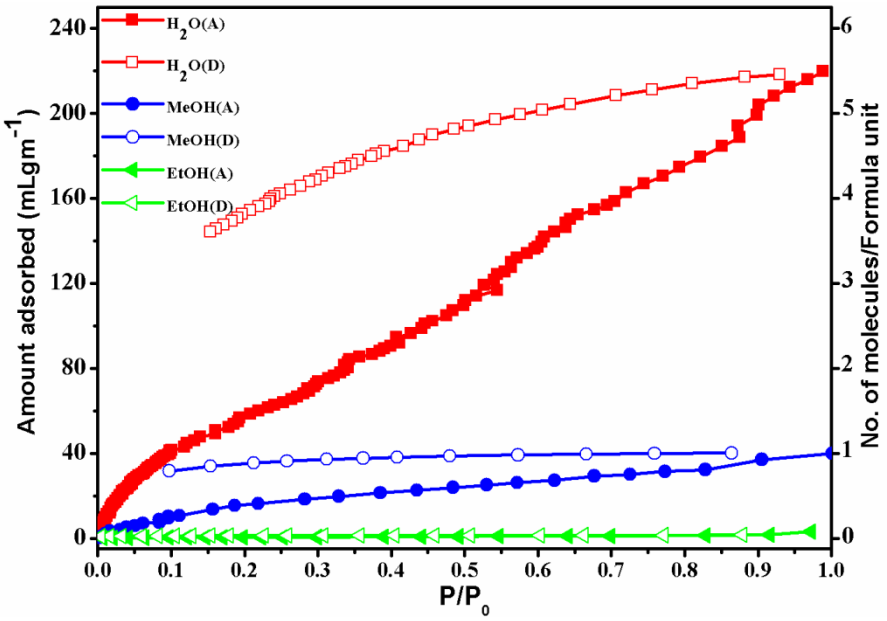

Figure 4.21: The solvent adsorption isotherms for **4.5b** at 298 K (filled symbols: adsorption and open symbols: desorption).

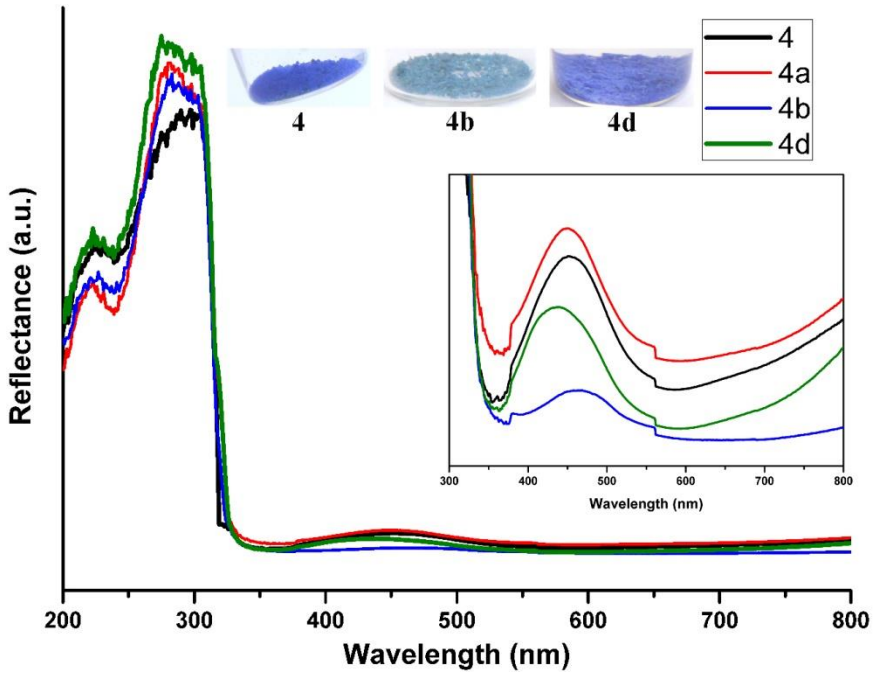

Figure 4.22: Solid state diffuse reflectance UV-Visible spectra for **4.5**. Inset showing the close view of the d-d bands in the region between 300 and 800 nm. Crystal colours of the as-synthesized, de-solvated and water re-solvated samples of **4** are provided in the inset as well.

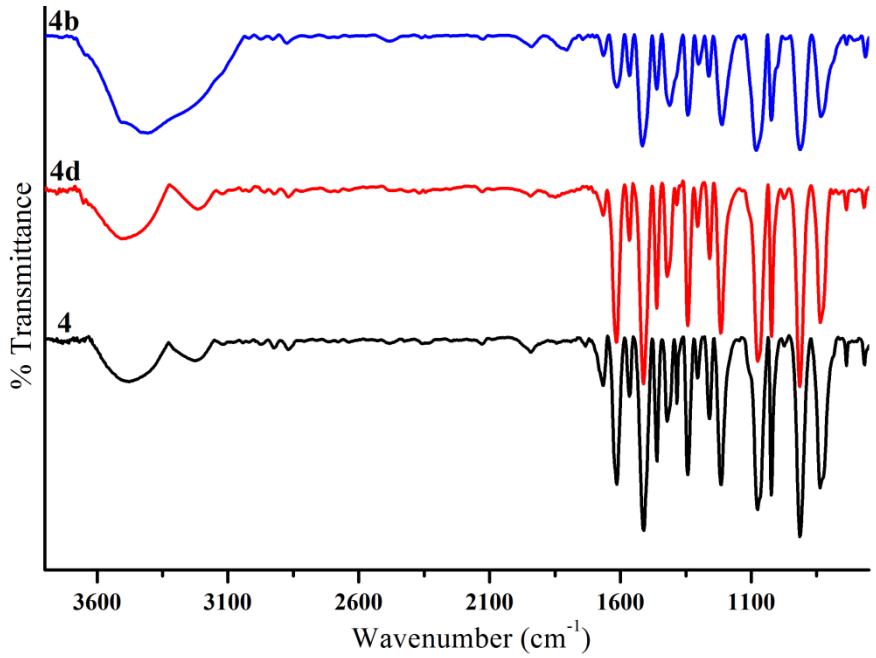

Figure 4.23: FTIR Spectrum for various samples of **4.5**

4.4 Conclusions

In summary, we have synthesized examples of Zn(II) and Cu(II) coordination polymer from an in-situ generated ligand $[PO_2(NH_4Py)_2]^-$. The in-situ formation of this ligand was achieved in P-N bond cleavage reaction from the corresponding phosphonium salt $[P(NH_4Py)_4]Cl$ or from neutral phosphoric triamide $[OP(NH_4Py)_3]$. The structural analysis of $[CuL_2(H_2O)_2]_\infty$ shows that the ligand is bonded to the Cu(II) ions via its pyridyl nitrogen atoms while the phosphorus bound oxygen atoms are involved in a intermolecular H-bonding interactions yielding a 3D-network in **scu** topology. Both coordination polymer exhibit a narrow porous network and shows selectivity for polar guest molecules. The porosity of $[ZnL(HCO_2)]_\infty$ assembly was determined by gas adsorption studies showing a higher uptake capacity for CO_2 over N_2. No appreciable gas uptake characteristic could be observed for the Cu(II) coordination polymer,$[CuL_2(H_2O)_2]_\infty$. Remarkably, the de-solvated for of the Zn(II) coordination polymer, $[ZnL(HCO_2)]_\infty$, shows a very high uptake of water adsorption over aliphatic alcohols. Although the Cu(II) coordination polymer,$[CuL_2(H_2O)_2]_\infty$, shows a slightly lower uptake capacity for water adsorption, it exhibits a better stability than the Zn(II) polymer. An interesting 2D Cu(I)-coordination polymer in **hcb** topology contains both neutral (**4.2**) and anionic $(L^2)^-$ ligands was obtained as a minor product along with **4.5**.

4.5 References

(1) (a) Hoskins, B. F.; Robson, R. *J. Am. Chem. Soc.* **1989**, *111*, 5962–5964. (b) Chui, S. S.-Y.; Lo, S. M.-F.; Charmant, J. P. H.; Orpen, A. G.; Williams, I. D. *Science* **1999**, *283*, 1148–1150. (c) Li, H.; Eddaoudi, M.; O'Keeffe, M.; Yaghi, O. M. *Nature* **1999**, *402*, 276–279. (d) Dinca, M.; Long, J. R. *Angew. Chem., Int. Ed.* **2008**, *47*, 6766–6779. (e) Vittal, J. J. *Coord. Chem. Rev.* **2007**, *251*, 1781-1795. (f) Ferrey, G.; Serre, C. *Chem. Soc. Rev.* **2009**, *251*, 1380-1399. (g) Eddaoudi, M.; Kim, J.; Rosi, N. L.; Vodak, D. T.; Wachter, J. O,; Keeffe, M.; Yaghi, O. M. *Science* **2002**, *295*, 469-472. (h) Lee, Y. E.; Jang, S. Y.; Suh, P. M. *J. Am. Chem. Soc.* **2005**, *127*, 6374-6381. (i) An, J.; Shade, C. M.; C-Czegan, D. A.; Petoud, S.; Rosi, N. L. *J. Am. Chem. Soc.* **2011**, *133*, 1220-1223. (j) Ma, S.; Zapata, F.; Lobkovsky, E. B.; Yang, J.; Chen, B. *Inorg. Chem.* **2006**, *45*, 5718-5720. (k) Aijaz, A.; Lama, P.; Bharadwaj, P. K. *Inorg. Chem.* **2010**, *49*, 5883-5889. (m) Kitagawa, S.; Uemura, K. *Chem. Soc. Rev.* **2005**, *34*, 109-119.

(2) (a) Ghosh, S. K.; Zhang, J.-P.; Kitagawa, S. *Angew. Chem., Int. Ed.* **2007**, *46*, 7965-7968. (b) Hanson, K.; Calin, N.; Bugaris, D.; Scancella, M.; Sevov, S. C. *J. Am. Chem. Soc.* **2004**, *126*, 10502-10503. (c) Serre, C.; Mellot-Draznieks, C.; Surble, S.; Audebrand, N.; Filinchuk, Y.; Ferey, G. *Science* **2007**, *315*, 1828-1831. (d) Kubota, Y.; Takata, M.; Matsuda, R.; Kitaura, R.; Kitagawa, S.; Kobayashi, T. C. *Angew. Chem., Int. Ed.* **2006**, *45*, 4932-4936. (e) Maji, T. K.; Mastuda, R.; Kitagawa, S. *Nat. Mater.* **2007**, *6*, 142-148. (f) Matsuda, R.; Kitaura, R.; Kitagawa, S.; Kubota, Y.; Belosludov, R. V.; Kobayashi, T. C.; Sakamoto, H.; Chiba, T.; Takata, M.; Kawazoe, Y.; Mita, Y. *Nature* **2005**, *436*, 238-241. (g) Frey, G.; Mellot-Draznieks, C.; Serre, C.; Millange, F.; Dutour, J.; Surble, S.; Margiolaki, I. *Science* **2005**, *309*, 2040-2042. (h) James, S. L. *Chem. Soc. Rev.* 2003, 32, 276-288.

(3) (a) Yaghi, O. M.; Li, G.; Li, H. *Nature* **1995**, *378*, 703-706. (b) Batten, S. R.; Robson, R. *Angew. Chem. Int. Ed.* **1998**, *37*, 1460-1494. (c) Ockwig, N. W.; Delgado-Friedrichs, O.; O'Keeffe, M.; Yaghi, O. M. *Acc. Chem. Res.* **2005**, *38*, 176-182. (d) Delgado-Friedrichs, O.; O'Keeffe, M.; Yaghi, O. M. *Phys. Chem. Chem. Phys.* **2007**, *9*, 1035-1043. (e) Férey, G. *Chem. Soc. Rev.* **2008**, *37*, 191-214. (f) Huang, B.L.; Ni, Z.; Millward, A.; McGaughey, A. J. H.; Kaviany, M.; Yaghi, O. M. *Int. J. Heat Mass Transfer* **2007**, *50*, 405-411. (g) Rosi, N. L.; Eckert, J.; Eddaoudi, M.; Vodak, D. T.; Kim, J.; O'Keeffe, M.; Yaghi, O. M. *Science* **2003**, *300*, 1127-1129.

(4) (a) Collins, D. J.; Zhou, H.-C. *J. Mater. Chem.* **2007**, *17*, 3154-3160. (b) Klontzas, E.; Emmanuel Tylianakis, E.; Froudakis, G. E. *Nano Lett.* **2010**, *10*, 452-454. (c) Rowsell, J. L. C.; Spencer, E. C.; Eckert, J.; Howard, J. A. K.; Yaghi, O. M. *Science* **2005**, *309*, 1350-1354. (d) Wong-Foy, A. G.; Matzger, A. J.; Yaghi, O. M. *J. Am. Chem. Soc.* **2006**, *128*, 3494-3495. (e) Ma, J.-P.; Yu, Y.; Dong, Y.-B. *Chem. Commun.* **2012**, *48*, 2946-2948. (f) Lee, J.; Farha, O. K.; Roberts, J.; Scheidt, K. A.; Nguyen, S. T.; Hupp, J. T. *Chem. Soc. Rev.* **2009**, *38*, 1450-1459. (g) Seo, J. S.; Whang, D.; Lee, H.; Im Jun, S.; Oh, J.; Jeon, Y. J.; Kim, K. *Nature* **2000**, *404*, 982-986.

(5) (a) Eddaoudi, M.; Moler, D. B.; Li, H.; Chen, B.; Reineke, T. M.; O'keeffe, M.; Yaghi, O. M., *Acc. Chem. Res.* **2001**, *34*, 319-330. (b) Ockwig, N. W.; Delgado-Friedrichs, O.; O'Keeffe, M.; Yaghi, O. M., *Acc. Chem. Res.* **2005**, *38*, 176-182. (c) Chen, B.; Xiang, S.; Qian, G., *Acc. Chem. Res.* **2010**, *43*, 1115-1124.

(6) (a) Serre, C.; Mellot-Draznieks, C.; Surble, S.; Audebrand, N.; Filinchuk, Y.; Ferey, G. *Science* **2007**, *315*, 1828–1831. (b) Kitagawa, S.; Kitaura, R.; Noro, S. I. *Angew. Chem. Int. Ed.* **2004**, *43*, 2334-2375.(c) Horike, S.; Shimomura, S.; Kitagawa, S. *Nat. Chem.***2009**, *1*,695–704. (d) Férey, G., *Chem. Soc. Rev.* **2008**, *37*, 191-214 (e) Deng, H.; Doonan, C. J.; Furukawa, H.; Ferreira, R. B.; Towne, J.; Knobler, C. B.; Wang, B.; Yaghi, O. M. *Science* **2010**, *327*, 846-850.

(7)(a) Humphrey, S. M.; Oungoulian, S. E.; Yoon, J. W.; Hwang, Y. K.; Wise E. R.;Chang, J.-S. *Chem. Commun.* **2008**, 2891-2893. (b) Humphrey, S. M.; Allan, P. K.; Oungoulian, S. E.; Ironside M. S.; Wise, E. R. *Dalton Trans.* **2009**, 2298-2305.

(8) (a) Iremonger, S. S.; Liang, J.; Vaidhyanathan, R.; Martens, I.; Shimizu, G. K. H.; Daff, T. D.; Aghaji, M. Z.; Yeganegi S.; Woo, T. K. *J. Am. Chem. Soc.* **2011**, *133*, 20048-20051. (b) Taylor, J. M.; Vaidhyanathan, R.; Iremonger, S. S.; Shimizu, G. K. H. *J. Am. Chem. Soc.* **2012**, *134*, 14338-14341.

(9) (a) Gupta, A. K.; Nicholls, J., Debnath, S.; Rosbottom, I.; Steiner A.; Boomishankar, R. *Cryst. Growth Des*. **2011**, *11*, 555-564. (b) Gupta, A. K.; Kalita A.; Boomishankar, R. *Inorg. Chim. Acta* **2011**, *372*, 152-159.

(10) (a) Gupta, A. K.; Chipem, F. A. S.; Boomishankar, R. *Dalton Trans*. **2012**, *41*, 1848-1853. (b) Gupta, A. K.; Steiner A.; Boomishankar, R. *Dalton Trans*. **2012**, *41*, 9753-9759.

(11) (a) Li, N.; Jiang, F.-L.; Chen, L.; Li, X.-J.; Chen, Q.-H.; Hong, M.-C. *Chem. Commun.*, **2011**, *47*, 2327-2329. (b) Li, X.-J.;Jiang, F.-L.;Wu, M.-Y.; Zhang, S.-Q.; Zhou U.-F.; Hong, M.-C. *Inorg. Chem*. **2012**, *51*, 4116-4122.

(12) (a) Shigematsu, A.; Yamada, T.; Kitagawa, H. *J. Am. Chem. Soc.* **2012**, *134*, 13145-13147. (b) Gu, J.-Z.; Lu, W.-G.; Jiang, L.; Zhou, H.-C.; Lu, T.-B. *Inorg. Chem.* **2007**, *46*, 5835-5837. (c) Chen, B.; Ji, Y.; Xue, M.; Fronczek, F. R.; Hurtado, E. J.; Mondal, J. U.; Liang, C.; Dai, S. *Inorg. Chem.* **2008**, *47*, 5543-5545. (d) Gupta, A. K.; Nagarkar, S. S.; Boomishankar, R. *Dalton Trans.* **2013**, *42*, 10964-10974.

(13) (a) Kim, S.; Dale, B. E. Biomass Bioenergy 2004, 26, 361-375. (b) Lipnizki, F.; Field R. W.; Ten, P. K. *J. Membr. Sci.* **1999**, 153, 183-210. (c) Uchida, S.; Kawamoto R.; and Mizuno, N. *Inorg. Chem.* **2006**, *45*, 5136-5144.

(14) Sheldrick, G. M. *Acta Crystallogr.* **2008**, *A64*, 112-122.

(15) Lin, X. M.; Fang, H. C.; Zhou, Z. Y.; Chen, L.; Zhao, J. W.; Zhu, S. Z.; Cai, Y. P. *CrystEngComm* **2009**, *11*, 847–854.

(16) (a) Kingsley, S.; Chandrasekhar, V. *Inorg. Chem*. **2001**, *40*, 6057-6060. (b) Chandrasekhar, V.; Kingsley, S.; Lam, K. C.; Rheingold, A. L., *Inorg. Chem*. **2000**, *39*, 3238-3242.

(17) Anyushin, A. V.; Mainichev, D. A.; Moroz, N. K.; Abramov, P. A.; Naumov, D. Y.; Sokolov, M. N.; Fedin, V. P. *Inorg. Chem.* **2012**, *51*, 9995-10003.

(18) Macrae, C. F.; Edgington, P. R.; McCabe, P.; Pidcock, E.; Shields, G. P.; Taylor, R.; Towler M.; van de Streek, J. *J. Appl. Cryst.* **2006**, *39*, 453-457.

(19) (a) Díaz, P.; Benet-Buchholz, J.; Vilar, R.; White, A. J. *Inorg. Chem.***2006**, *45*, 1617-1626. (b) Lazarou, K. N.; Psycharis, V.; Terzis, A.; Raptopoulou, C. P. *Polyhedron* **2011**, *30*, 963-970. (c) Noro, S.-I.; Kitaura, R.; Kondo, M.; Kitagawa, S.; Ishii, T.; Matsuzaka, H.; Yamashita, M. *J. Am. Chem. Soc.* **2002**, *124*, 2568-2583. (d) Withersby, M. A.; Blake, A. J.; Champness, N. R.; Cooke, P. A.; Hubberstey, P.; Realf, A. L.; Teat, S. J.; Schröder, M. *J. Chem. Soc., Dalton Trans.* **2000**, 3261-3268.

(20) Blatov, V.; Shevchenko, A.; Serezhkin, V. *J. Appl. Crystallogr.* **2000**, *33*, 1193-1193.

(21) O'Keeffe, M.; Yaghi, O. M. *Chem. Rev.* **2012**, *112*, 675-702.

Chapter 5

Facile formation of stable tris(imido)phosphate trianions as their tri-and hexanuclearPd(II) complexes in protic solvents

Abstract

In this chapter, employing Pd(II) salts a facile deprotonation route to access the elusive tris(alkylimido)phosphate trianions, $[(RN)_3PO]^{3-}$ (R = ^{t}Bu ,^{i}Bu, ^{c}Hex, ^{i}Pr), analogous to the orthophosphate (PO_4^{3-}) ion in polar and in protic solvents has been described. Using $Pd(OAc)_2$, trinuclear and prismatic Pd(II) clusters of these imido-trianions having the formula $\{Pd_3[(NR)_3PO](OAc)_3\}_n$ (R = ^{t}Bu, ^{c}Hex, ^{i}Pr), (n = 1 or 2), were isolated exclusively in all these reactions in which the trianionic species acts as the tripodal chelating ligand to the trinuclear Pd_3-unit. Use of $PdCl_2$ leads again to the fully deprotonated species $[(RN)_3PO]^{3-}$(R =^{t}Bu, ^{i}Bu, ^{c}Hex, ^{i}Pr),as their corresponding chloro-bridged hexameric clusters in which the six Pd(II) ions were found in an octahedral arrangement except for the most bulky ^{t}Bu substituents on the imido-phosphate ligands. Further, for the chloro-bridged hexameric clusters two types of arrangement have been found for the two trinuclear Pd_3-subunits. An eclipsed arrangement of the two Pd_3-subunits was found for the imido-phosphate ligand featuring ^{t}Bu substituents and for the rest of them (R = ^{i}Bu or ^{c}Hex or ^{i}Pr) a staggered (octahedral) was observed. Reactivity studies aiming at the Pd(II) centers in the acetate-bridged clusters with nucleophilic reagents such as primary amines ($R'NH_2$) have lead to a new trimeric cluster of formula $\{Pd_3[(NR)_3PO](OAc)_3(R'NH_2)_3\}$ in which the tripodal coordination of the Pd-N_{imido} moieties remained unaffected exemplifying the robustness of the Pd_3-unit in all these cluster. We have also shown the catalytic activity of some of these Pd(II) complexes in Mizoroki-Heck type coupling reactions in presence of $Cu(OAc)_2$ as an oxidant.

5.1 Introduction

Imido analogues of common phosphorus oxo-anions have been the topic of extensive research interest in main group chemistry and are employed as ligands in coordination chemistry.[1] Metal complexes of several P(V) imido anions were developed as catalytic systems for olefin oligomerization and polymerization, ring-opening polymerization of lactides, hydroamination and transfer hydrogenation etc.[2] Current synthetic procedures to access these imido P(V) anions involve the use of highly basic organometallic-reagents in reaction with a phosphonium salt[3] like $[(NHPh)_4P]Cl$ or phosphoramides[4] such as $[(RNH)_3P{=}E]$ (E = $NSiMe_3$, O, S or Se), or performed iminophosphorane.[5] However due to the highly reactive nature of the metal precursors employed in the reactions as well as the presence of residual metal-alkyl/aryl/silylamide bonds in these complexes, their stability have largely been limited to anhydrous aprotic and non-polar solvents. It has also been noticed that use of Lewis acidic transition metal ions such as cu^{2+} ions in these deprotonation reactions has lead to the cleavage of P-N bonds instead of the N-*H* deprotonation.[6] Hence we started looking at using salts of soft transition metal ions as a source of base to generate the P(V) bound polyimido species in polar medium, which would allow us to discover the potential of these species for wider synthetic applications. Encouraged by the remarkable utility of Palladium and its compounds in various organic bond-activation reactions,[7] we employed the salts of Pd(II) ions in deprotonation reactions with tris(alkylamido)phosphate ligands, $[(NHR)_3PO]$. In this chapter, we report on the facile syntheses of the fully deprotonated tris(imido)phosphate trianions of the type $[(RN)_3PO]^{3-}$ starting from $[(NHR)_3PO]$ and $Pd(OAc)_2$ in polar solvents such as $CH_3OH/CH_3CN/(CH_3)_2SO$ etc. These highly basic anions were isolated as their corresponding tri- and hexa-nuclear Pd(II) clusters of the type $\{Pd_3[(NR)_3PO](OAc)_3\}_n$ (**5.6**, R = ^{t}Bu, n = 1; **5.7** ,R = ^{C}Hex, n = 2; **5.8**, R = ^{i}Pr, n= 2) or as mixed-bridged clusters of the type $\{Pd_3[(N^{i}Pr)_3PO](OAc)_2(OR')\}_2$ (**5.9** R' = Me; **5.10**, R' = H) depending upon the R and R' groups and the reaction solvents (Scheme 5.1). Use of $PdCl_2$ in place of $Pd(OAc)_2$ leads again to the fully deprotonated species $[(RN)_3PO]^{3-}$ as their corresponding chloro-bridged hexameric clusters $\{Pd_3[(NR)_3PO](Cl)_3\}_2$ (**5.11**, R = ^{t}Bu; **5.12,** R = ^{C}Hex; **5.13**, R = ^{i}Pr; **5.14**, R = ^{i}Bu). All these complexes contain one or two triangular Pd_3-motifs in which the Pd(II) atoms are bound to three chelating N_{imido} moieties.

Further reactions at the Pd(II) centers in the hexameric acetate-bridged Pd_6-clusters with nucleophilic reagents such as primary amines (R"NH_2) leads to a trimeric species of

formula $\{Pd_3[(NR)_3PO](OAc)_3(R''NH_2)_3\}$, obtained via the symmetrical cleavage of the hexamer. This suggests that the three Pd-N_{imido} moieties attached to the Pd_3-subunit exhibits a remarkable stability and remains unaffected during the cleavage reaction. To the best of our knowledge, the Pd(II) complexes reported here are the first isolated examples of metal complexes obtained in protic solvents that feature the highly basic imido-phosphate trianions $[(RN)_3PO]^{3-}$ as ligands. Although it has been described in the chapter 3 that the imido anions analogous to $H_2PO_4^-$ and HPO_4^{2-} ions can be generated by using certain reactive Ag(I) salts from the P(V) moieties having sufficiently acidic N-*H* groups, the imido trianion corresponding to the orthophosphate (PO_4^{3-}) ion remains elusive in all these Ag(I) mediated reaction so far.[8] In addition, we have explored the preliminary catalytic activity of these Pd(II) complexes in Mizoroki-Heck (M-H) type coupling reaction of phenyl boronic acid with alkenes.

5.2 Experimental section

5.2.1 General Remarks

All manipulations involving phosphorus halides were performed under dry nitrogen atmosphere in standard Schlenk-glassware. Solvents were dried over potassium (hexane) and sodium (toluene). The primary amines were purchased from Merck or from Aldrich and used as received. The halide precursor $POCl_3$ was purchased locally (SPECTROCHEM, India) and was distilled prior to use. The ligands **5.1**H_3 and **5.2**H_3 were synthesized using literature methods.[9] NMR spectra were recorded on a Jeol 400 MHz spectrometer (^{1}H NMR: 400.13 MHz, $^{13}C\{^1H\}$NMR: 100.62 MHz, $^{31}P\{^1H\}$ NMR: 161.97 MHz) or on a Bruker 500 MHz (^{1}H NMR: 500.00 MHz, $^{13}C\{^1H\}$NMR: 125.725 MHz, $^{31}P\{^1H\}$ NMR: 202.404 MHz) spectrometer at room temperature using $SiMe_4$ (^{1}H, ^{13}C) and 85% H_3PO_4 (^{31}P). The 2D-DOSY experiments were performed on a Bruker 500 MHz NMR with standard pulse program ledbpgp2S using bipolar gradient pulse pair and two spoiling gradients.[10a] The gradient strength was changed from 2 to 95% with linear type of ramp and other parameters such as the diffusion time (Δ = 40-50 ms), sine-shaped pulse length (δ = 1.1 - 2.1 ms) and relaxation delay (D1 = 4-8 s) were also employed.[10b] The electron spray ionization (ESI) mass spectra in the positive ion mode were recorded in a Waters-SYNAPT-G2 high resolution spectrometer. The matrix-assisted laser desorption ionization time-of-flight (MALDI-TOF) spectra were obtained on an Applied Biosystem MALDI-TOF/TOF spectrometer. Fourier transform infrared (FT-IR) spectra were taken on a Perkin-Elmer spectrophotometer with samples prepared

as KBr pellets. Melting points were obtained using an Electro thermal melting point apparatus and were uncorrected.

5.2.2 Synthesis

5.3-H_3**:** $POCl_3$ (5 ml, 8.23 g 0.0536 mol) was added drop wise to an excess of isopropyl amine (23.12 ml, 16.69 g, 0.282 mol) in toluene (250 mL) at 0 ^oC. The resulting mixture was slowly brought to room-temperature and stirred for 4 h. The precipitated iso-propylammonium chloride was removed by filtration. The filtrate was reduced to 80 mL and hexane (50 mL) was added to it and left at -15 ^oC for 2 days to yield a white impure solid. The impure solid was purified by sublimation at 120 ^oC / $1x10^{-3}$Torr. Yield 75 % (8.90g, based on P). M.P. 122-125 ^oC; 1H-NMR (400 MHz, $CDCl_3$: δ 1.14 (s, 18H, CH_3), 2.15 (br, 3H, NH) 3.35 (septet, 3H, C*H*); 13C-NMR (100 MHz, $CDCl_3$: δ 26.00, 43.25; ^{31}P-NMR (161 MHz, $CDCl_3$): δ 12.84. FT-IR data in KBr pellet (cm^{-1}): 3498, 3197, 1638, 1464, 1427, 1384, 1168, 1121, 933, 897, 794, 542; ESI(+): 222.17 $[M+H]^+$, 199.08 $(M–(C_3H_7NH))^+$. Anal. Calcd. for $C_9H_{24}N_3OP$: C, 48.85; H, 10.93; N, 18.99. Found: C, 49.14; H, 10.76; N, 18.74.

5.4-H_3**:** $POCl_3$ (5 ml, 8.23 g 0.0536 mol) was added drop wise to an excess of isobutyl amine (28.61 ml, 21.1 g, 0.288mol) in toluene (250 mL) at 0 ^oC. The resulting mixture was refluxed for 4 h at room temperature a white precipitate formed. The iso-butylammonium chloride was removed by filtration and washed with toluene. The volume of the filtrate was reduced to 80 mL and hexane (50 mL) was added, and after 2 days at -15 ^oC a colorless crystals were formed. Yield 80% (11 g, based on P). M.P. 118-120^oC, ^{1}H NMR(400 MHz, $CDCl_3$: δ 0.92 (s,18H**,** CH_3), 1.84 (septet, 3H,C*H*), 2.62 (br, 3H**,** N*H*), 2.67 (d, 6H, CH_2): ^{13}C {^{1}H}} (100 MHz, , CD_3Cl_3: δ 22.20, 32.11, 47.33: ^{31}P NMR (161 MHz, $CDCl_3$: δ 18.88; FT-IR data in KBr pellet (cm^{-1}) : 3438, 3183, 1664, 1617, 1460, 1384, 1196, 1118, 1068, 1017, 933, 825, 769, 578. ESI(+): 264.36 $[M+H]^+$, Anal. Calcd. for $C_{12}H_{30}N_3OP$: C, 54.73; H, 11.48; N, 15.96. Found: C, 54.55; H, 11.88; N, 15.76.

5.6: To a solution of [$OP(NH^tBu)_3$], **5.1**H_3, (20 mg, 0.08 mmol) in methanol and palladium acetate $Pd(OAc)_2$ (51 mg, 0.24 mmol) in acetonitrile was added. The resulting mixture was stirred for 1 h and kept for crystallization. Orange block like crystals were obtained after 5 days. Yield 90 % (52 mg, based on P). M.P. 205-208 ^oC; ^{1}H-NMR (400 MHz, {$(CD_3)_2SO$}): δ 1.20 (s, 27H, CH_3), 2.04 (s, 9H, CH_3COO); ^{13}C-NMR (100 MHz,

{$(CD_3)_2SO$}): δ 27.63, 32.20, 52.88 179.19; ^{31}P-NMR (161 MHz, {$(CD_3)_2SO$}): δ 69.04; FT-IR data in KBr pellet (cm^{-1}): 3454, 1728, 1561, 1413, 1275, 1175, 1041, 976, 752, 634; ESI(+): 778 $(M+Na)^+$, 698 $(M–C_4H_9)^+$. Anal. Calcd. for $C_{18}H_{36}N_3O_7PPd_3$: C, 28.57; H, 4.80; N, 5.55. Found: C, 28.60; H, 4.60; N, 5.38.

5.7: To a solution of [$OP(NH^cHex)_3$], **5.2**H_3, (20mg, 0.06 mmol) in methanol and palladium acetate $Pd(OAc)_2$ (40 mg, 0.18 mmol) in methanol was added . The resulting mixture was stirred for 1 h and kept for crystallization. Dark orange prismatic crystals were obtained after 10 days. Yield 70 % (69 mg, based on P). M.P. 180-182^{o}C; ^{1}H-NMR (400 MHz, {$(CD_3)_2SO$}): δ 1.08 (m, 24H, CH_2), 1.60 (m, 12H, C*H*), 1.75 (m, 12H, CH_2), 2.25 (s, 18H, CH_3COO), 2.74 (m, 24H, CH_2); ^{13}C-NMR (100 MHz, {$(CD_3)_2SO$}): δ 25.12, 25.48, 27.44, 38.65, 55.38, 178.66; ^{31}P-NMR (161 MHz, {$(CD_3)_2SO$}): δ 73.03; FT-IR data in KBr pellet (cm^{-1}): 3332, 1649, 1451, 1414, 1113, 1018, 647; ESI(+): 1694 $(M+Na)^+$, 836 $(M/2)^+$. Anal. Calcd. for $C_{48}H_{84}N_6O_{14}P_2Pd_6$: C, 34.53; H, 5.07; N, 5.03. Found: C, 33.87; H, 5.04; N, 4.88.

5.8: A mixture of [$OP(NH^iPr)_3$], **5.3**H_3, (20 mg, 0.09 mmol) and palladium acetate $Pd(OAc)_2$ (60 mg, 0.27 mmol) in THF was stirred for 1 h and kept for crystallization. Plate like orange coloured crystals were obtained after 10 days. Yield 75% (98 mg, based on P). M.P. 198-200 ^{o}C; ^{1}H-NMR (400 MHz, {$(CD_2)_4O$}): δ 1.19 (d, 36H, CH_3), 2.68 (septet, 6H, C*H*), 2.47 (s, 18H, CH_3COO); ^{13}C-NMR (100 MHz, {$(CD_2)_4O$}): δ 22.53, 28.84,52.20, 183.33; ^{31}P-NMR (161 MHz, {$(CD_2)_4O$}): δ 78.87; FT-IR data in KBr pellet (cm^{-1}): 3338, 1611, 1552, 1425, 1261, 1140, 1019, 692; MALDI-TOF/TOF: 1423 $(M)^+$, 1365 $(M–C_3H_7NH)^+$. Anal. Calcd. for $C_{30}H_{60}N_6O_{14}P_2Pd_6$: C, 25.21; H, 4.23; N, 5.88. Found: C, 25.35; H, 4.24; N, 5.77.

5.9: A mixture of [$OP(NH^iPr)_3$], **5.3**H_3, (20 mg, 0.09 mmol) and palladium acetate $Pd(OAc)_2$ (60 mg, 0.27 mmol) in methanol were stirred for 1 h and kept for crystallization. Orange block like crystals were obtained in 12 hours. Yield 85% (105 mg, based on P). M.P. 180-182^{o}C; ^{1}H-NMR (400 MHz, CD_3OD: δ 1.12 (d, 36H, CH_3), 2.49 (s, 12H, CH_3COO), 2.69 (septet, 6H, C*H*), 3.12 (s, 6H, OCH_3); ^{13}C-NMR (100 MHz, CD_3OD): δ 24.59, 25.29, 42.87, 53.74, 173.88; ^{31}P-NMR (161 MHz, CD_3OD): δ 73.60; FT-IR data in KBr pellet (cm^{-1}); 3335, 1603, 1550, 1420, 1257, 1140, 1019, 722, 690; MALDI-TOF/TOF: 1369 $(M)^+$. Anal. Calcd. for $C_{28}H_{60}N_6O_{12}P_2Pd_6$: C, 24.49; H, 4.40; N, 6.12. Found: C, 24.08; H, 4.15; N, 5.94.

5.10: A mixture of [OP(NH^{i}Pr)$_3$], **5.3**H$_3$, (20 mg, 0.09 mmol) and palladium acetate Pd(OAc)$_2$ (60 mg, 0.27 mmol) in dimethyl sulfoxide (DMSO) were stirred for 1 h and kept for crystallization. Orange block like crystals were obtained after 5 days. Yield 75% (101 mg, based on P). M.P. 220-222 ^{o}C; ^{1}H-NMR (400 MHz, {(CD$_3$)$_2$SO}): δ 1.10 (d, 36H, C*H*$_3$), 2.68 (s, 12H, C*H*$_3$COO), 2.74 (septet, 6H, C*H*), 2.84 (s, 2H, O*H*); ^{13}C-NMR (100 MHz, {(CD$_3$)$_2$SO}): δ 25.67, 25.85, 50.03, 177.14; ^{31}P-NMR (161 MHz, {(CD$_3$)$_2$SO}): δ 73.67; FT-IR data in KBr pellet (cm^{-1}): 3677, 1646, 1532, 1426, 1255, 1143, 1025, 696; MALDI-TOF/TOF: 1423 (M+DMSO)$^{+}$, 671 (M/2)$^{+}$. Anal. Calcd. for $C_{30}H_{68}N_6O_{14}P_2S_2Pd_6$: C, 24.00; H, 4.57; N, 5.60. Found: C, 24.83; H, 4.11; N, 5.88.

5.11: A mixture of [OP(NH^{t}Bu)$_3$], **5.1**H$_3$ (20mg, 0.076 mmol) and bis(benzonitrile)palladium(II) chloride Pd(PhCN)$_2$Cl$_2$ (87 mg, 0.23 mmol) in methanol was stirred for one an hour and kept for crystallization . Dark orange prisms like crystals were obtained after 10 days. Yield 80% (83 mg, based on P). M.P. 180-182^{o}C, ^{1}H NMR(400 MHz, {(CD$_3$)$_2$SO}): δ 1.08 (m,12H, C*H*$_2$), 1.60 (m, 6H, C*H*), 1.75 (m, 12H, C*H*$_2$), 2.25 (s, 18H, C*H*$_3$), 2.74 (m, 3H, C*H*) : ^{13}C {^{1}H}} (100 MHz, {(CD$_3$)$_2$SO}): δ 113.23, 117.12, 139.15, 148.56, 154.24 : ^{31}P NMR (161 MHz, {(CD$_3$)$_2$SO}): δ 77.30; FT-IR data in KBr pellet (cm^{-1}) : 3430, 1635, 1384, 1310, 1220, 1092, 1024, 827, 773; MALDI-TOF/TOF: 1404 (M+K)$^{+}$. Anal. Calcd. for $C_{24}H_{54}N_6O_2P_2Cl_6Pd_6$: C, 21.01; H, 3.97; N, 6.13. Found: C, 21.21; H, 4.01; N, 5.97.

5.12: A mixture of **[**OP(NH^{c}Hex)$_3$], **5.2**H$_3$ (20 mg, 0.060 mmol) and bis(benzonitrile)palladium(II) chloride Pd(PhCN)$_2$Cl$_2$ (68 mg, 0.117 mmol) in THF, was stirred for one an hour and kept for crystallization. Orange plates like crystals were obtained after 10 days. Yield 85% (77 mg, based on P). M.P. 196-200 ^{o}C, ^{1}H-NMR (400 MHz, {(CD$_3$)$_2$SO}): δ 1.11 (m, 24H, C*H*$_2$), 1.56 (m, 12H, C*H*), 1.74 (m, 12H, C*H*$_2$), 2.70 (m, 24H, C*H*$_2$); ^{13}C-NMR (100 MHz, {(CD$_3$)$_2$SO}): δ 25.10, 27.54, 38.60, 55.40; ^{31}P-NMR (161 MHz, {(CD$_3$)$_2$SO}): δ 73.59; FT-IR data in KBr pellet (cm-1) : 3489, 1624, 1422, 1346, 1296, 1235, 1155, 1102, 1058, 997, 941, 888, 765, 737; MALDI-TOF/TOF: 1520 (M)$^{+}$. Anal. Calcd for $C_{36}H_{66}N_6O_2P_2Cl_6Pd_6$: C, 28.30; H, 4.35; N, 5.50 Found: C, 28.44.; H, 4.39; N, 5.18.

5.13: A mixture of **[**OP(NH^{i}Pr)$_3$], **5.3**H$_3$ (20 mg, 0.090 mmol) and bis(benzonitrile)palladium(II) chloride Pd(PhCN)$_2$Cl$_2$ (104 mg, 0.271 mmol) in methanol stirred for half an hour. Orange block like crystals were obtained within one day. Yield 80%(93 mg, based on P). M.P. 180-182^{o}C, ^{1}H NMR(400 MHz, {(CD$_3$)$_2$SO}): δ 1.12

(d,18 H**,** CH_3), 2.49 (s, 12 H, CH_3), 2.69 (septet, 3H, C*H*), 3.12 (s, 6H**,** CH_3): **^{13}C** {^{1}H}} (100 MHz, {$(CD_3)_2SO$}): δ 24.59, 25.29, 42.87, 53.74, 173.88 : ^{31}P NMR (161 MHz, {$(CD_3)_2SO$}): δ 77.60; FT-IR data in KBr pellet (cm^{-1}) : 3403, 1635, 1466, 1416, 1383, 1361, 1310, 1167, 1138, 1049, 1015, 973, 911, 841, 791, 578; MALDI-TOF/TOF: 1326 $(M+K)^+$. Anal.Calcd. for $C_{28}H_{60}N_6O_{12}P_2Pd_6$: C, 24.49; H, 4.40; N, 6.12. Found: C, 31.74; H, 2.58; N, 17.85.

5.14: To a solution of [$OP(NH^iBu)_3$], **5.4**H_3 (20 mg, 0.076 mmol) in methanol, bis(benzonitrile)palladium(II) chloride $Pd(PhCN)_2Cl_2$ (87 mg, 0.23 mmol) in methanol and acetonitrile was added and stirred for an hour and kept for crystallization. Orange block like crystals were obtained after 5 days. Yield 80% (83 mg, based on P). M.P. 205-208^{o}C, ^{1}H NMR(400 MHz, {$(CD_3)_2SO$}: δ 0.98 (s,18H**,** CH_3), 2.04 (septet, 3H,C*H*), 2.72 (br, 3H**,** N*H*), 2.97 (d, 6H, CH_2): ^{13}C {^{1}H}} (100 MHz, {$(CD_3)_2SO$}: δ 24.22, 31.34, 48.98:^{31}P NMR (161 MHz, {$(CD_3)_2SO$}): δ 76.44; FT-IR data in KBr pellet (cm^{-1}) : 3461, 1667, 1578, 1521, 1469, 1400, 1369, 1261, 1159, 1105, 1029, 975, 818, 765, 522; MALDI-TOF/TOF: 1371 $(M)^+$. Anal. Calcd. for $C_{18}H_{36}N_3O_7PPd_3$: C, 28.61; H, 4.67; N, 5.56. Found: C, 29.01; H, 4.88; N, 5.13.

5.15: To a solution of **5.6**H_3 (30 mg, 0.04 mmol) in methanol, cyclohexylamine (12.0 mg, 14μL, 0.12 mmol) was added. The resulting mixture was stirred for 30 minutes and kept for crystallization. Pale yellow colored solid was obtained upon slow evaporation. Yield 80% (72 mg, based on P). M.P. 143-145 ^{o}C; ^{1}H-NMR (400 MHz, CD3OD: δ 1.28 (m, 12H, CH_2), 1.33 (s, 27H, CH_3), 1.65 (m, 3H, C*H*), 1.88 (m, 6H, CH_2), 2.08 (br, 6H, NH_2), 2.63 (s, 9H, CH_3*COO*), 2.74 (m, 12H, CH_2); ^{13}C-NMR (100 MHz, CD_3OD): δ 25.08, 25.79, 27.66, 32.50, 38.02, 40.86, 52.86, 179.35; ^{31}P-NMR (161 MHz, CD_3OD): δ 72.01; FT-IR data in KBr pellet (cm^{-1}): 3477, 1718, 1619, 1568, 1408, 1283, 1145, 1032, 968,748, 625; MALDI-TOF/TOF: 1077 $(M+Na)^+$. Anal. Calcd. for $C_{36}H_{75}N_6O_7PPd_3$: C, 41.01; H, 7.17; N, 7.97. Found: C, 41.03; H, 7.83; N, 7.22.

5.16: *Method A:* To a solution of **5.7**.H_2O (30 mg, 0.017 mmol) in methanol, cyclohexylamine (11 mg, 13μL, 0.10 mmol) was added. The resulting mixture was stirred for 30 minutes and kept for crystallization. Platelike pale yellow colored crystals were obtained after 7 days. Yield 80% (32 mg, based on P). *Method B:* To a mixture of [$PO(NH^cHex)_3$], **5.2**H_3, (20mg, 0.06 mmol) and palladium acetate $Pd(OAc)_2$(40 mg, 0.18 mmol) in methanol, cyclohexylamine (17 mg, 20 μL, 0.18 mmol) was added. The resulting mixture was stirred for half an hour. Platelike pale yellow colored crystals were

obtained after 10 days. Yield 80% (56 mg, based on P). M.P. 198-200 ^{o}C; ^{1}H-NMR (400 MHz, {$(CD_3)_2SO$}): δ 1.08 (m, 24H, C*H*), 1.53 (m, 6H, C*H*), 1.73 (m, 24H, CH_2), 2.49 (s, 9H, CH_3COO), 2.19 (m, 6H, NH_2), 2.74 (m, 18H, CH_2); ^{13}C-NMR (100 MHz, {$(CD_3)_2SO$}): δ 25.19, 25.66, 31.21, 34.49, 36.15, 40.94, 50.02, 177.18; ^{31}P-NMR (161 MHz, {$(CD_3)_2SO$}): δ 74.07; FT-IR data in KBr pellet (cm^{-1}): 3463, 1629, 1448, 1281, 1103, 894, 845, 712; ESI(+): 1132 $(M)^+$, 955 $(M–3(OAc))^+$. Anal. Calcd. for $C_{42}H_{81}N_6O_7PPd_3$: C, 44.55; H, 7.21; N, 7.42. Found: C, 44.18; H, 7.97; N, 6.97.

5.17: *Method A:* To a solution of **5.8** (30 mg, 0.02 mmol) in methanol, cyclohexylamine (12 mg, 14μL, 0.12 mmol) was added. The resulting mixture was stirred for 30 minutes and kept for crystallization. Platelike pale yellow colored crystals were obtained after 5 days. Yield 70% (28 mg, based on P). Note: **5.17** can also be obtained from a similar reaction of **5.9** with cyclohexylamine. *Method B:* To a mixture of [$OP(NH^iPr)_3$], **5.3**H_3, (20 mg, 0.09 mmol) and palladium acetate $Pd(OAc)_2$ (60 mg, 0.27 mmol) in methanol, cyclohexylamine (27 mg, 30 μL, 0.27 mmol) was added and stirred for 30 minutes and kept for crystallization. Platelike pale yellow colored crystals were obtained after 5 days. Yield 80% (73 mg, based on P). M.P. 215-217 ^{o}C; ^{1}H-NMR (400 MHz, CD_3OD: δ 1.13 (d, 18H, CH_3), 1.29 (septet, 3H, C*H*), 1.51 (m, 3H, C*H*), 1.71 (m, 12H, CH_2), 2.41 (m, 18H, CH_2) 2.63 (s, 9H, CH_3COO), 3.12 (br, 6H, NH_2): ^{13}C-NMR (100 MHz, CD_3OD): δ 22.39, 25.81, 29.32, 33.84, 34.67, 35.16, 52.91, 179.15; ^{31}P-NMR (161 MHz, CD_3OD): δ 73.67; FT-IR data in KBr pellet (cm^{-1}): 3465, 1640, 1574, 1496, 1395, 1196, 1037, 849; ESI(+): 1035 $(M+Na)^+$, 856 $(M–3(OAc)+Na)^+$. Anal. Calcd. for $C_{33}H_{69}N_6O_7PPd_3$: C, 39.16; H, 6.87; N, 8.30. Found: C, 40.34; H, 7.00; N, 8.08.

5.2.3 Crystallography

Reflections were collected on a Bruker Smart Apex Duo diffractometer at 100 K using MoKα radiation (λ = 0.71073 Å) for **5.4**-H_3, **5.6**, **5.7**·H_2O, **5.8**·2H_2O, **5.9**, **5.10**·2DMSO, **5.11**·2H_2O, **5.12**·DMF, **5.13**, **5.16**·2H_2O and **5.17** and on a Bruker Smart Apex II diffractometer at 273 K for **5.3**-H_3 and **5.14** (Table A4.1, Appendix 4). Structures were refined by full-matrix least-squares against F^2 using all data (SHELX97).[11] All non-hydrogen atoms were refined aniostropically if not stated otherwise. Hydrogen atoms were constrained in geometric positions to their parent atoms. Crystals of **5.8**.2H_2O and **5.9** were weakly diffracting at higher angles and hence a 2θ = 50 ° cut-off was applied. Two of the three cyclohexyl groups in the asymmetric unit of **5.7**.H_2O were disordered. The cyclohexyl moiety of the primary amino group in the asymmetric unit of **5.16** was

similarly disordered. Atom positions of the disordered C-atoms were isotropically refined over two positions using similar distances and similar U-restraints. Five C-atoms and one O-atom in **5.8**.2H_2O had slightly bad ellipsoids and hence were refined with partial isotropic parameters. The solvated DMSO molecule in the asymmetric unit of **7.10** was disordered and is freely refined over two positions using similar distances and similar U-restraints. The water molecules in **5.7**.H_2O and **5.8**.2H_2O were disordered as well and isotropically refined. The solvated methanol, water molecules in **5.11** could not be precicely located as they were disordered and have been treated as a diffuse contribution to the overall scattering without specific atom positions by SQUEEZE/PLATON.

5.3 Result and Discussions

5.3.1 Synthesis

The phosphoric triamide ligands, [$(NHR)_3PO$] (**5.1**-H_3, R = ^{t}Bu; **5.2**-H_3, R = ^{c}Hex; **5.3**-H_3, R = ^{i}Pr and **5.4**-H_3, R = ^{i}Bu), were prepared by a slightly modified literature procedure.[4d,8] The reactivity of these ligands were further tested with $Pd(OAc)_2$ in an appropriate polar solvent at room temperature with the view of obtaining various imido-P(V) derivatives (Scheme 5.1). Crystals of {$Pd_3[(N^tBu)_3PO](OAc)_3$} (**5.6**) and {$Pd_3[(N^cHex)_3PO](OAc)_3\}_2$ (**5.7**) were obtained from the respective reaction of **5.1**-H_3 and **5.2**-H_3 with $Pd(OAc)_2$ in MeOH within 10 days. On the other hand, it has been observed that reaction of **5.3**-H_3 under similar conditions in MeOH gave {$Pd_3[(N^iPr)_3PO](OAc)_2(OMe)\}_2$ (**5.9**) as a major compound. When the solvent system is changed to $(CH_3)_2SO$, crystals of {$Pd_3[(N^iPr)_3PO](OAc)_2(OH)\}_2$.2$(CH_3)_2SO$ (**5.10**.2DMSO) were formed, exclusively.

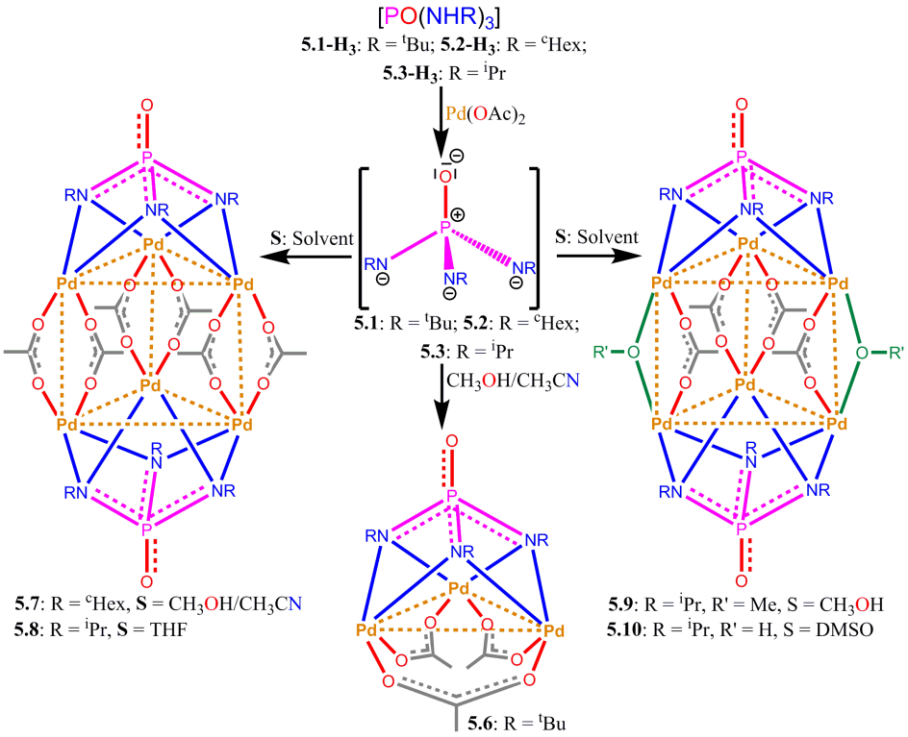

Scheme 5.1: Synthetic routes to access the tri- and hexanuclear Pd(II) clusters of the tris(alkylimido) phosphate trianions.

Formation of these mixed-bridged clusters **5.9** and **5.10** was attributed to the dynamic nature of bridging OAc groups in $[Pd_3(OAc)_6]$ (**5.5**) where it exists as a mixture of **5.5** and $[Pd_3(OMe)_2(OAc)_4]$ (**5.5**a) in MeOH as observed by the diffusion-ordered ^{1}H-NMR spectroscopy (^{1}H-DOSY).[12] Similarly, in a solvent containing a large excess of water (such as DMSO) it exists as a mixture of **5.5** and $[Pd_3(OH)_2(OAc)_4]$ (**5.5**b). Hence, it is evident that formation of **5.9** and **5.10** is mostly due to the reaction of **5.3** with **5.5**a and **5.5**b, respectively. Finally crystals of the all-acetate bridged species $\{Pd_3[(N^iPr)_3PO](OAc)_3\}_2$ (**5.8**) were exclusively obtained from the corresponding reaction in tetrahydrofuran. The ^{31}P-NMR spectra of the reaction mixture of **5.3** and $Pd(OAc)_2$ after 12 h gave three signals at δ 77.7 (minor), 72.5 (major), 65.8 (minor) in the cluster region indicating that there are three species in solution having the anionic ligand species **5.3**. The peaks at δ 77.7 and 72.5 indicate the presence of two hexameric clusters, while the minor peak at 65.8 is due to a trimeric species, suggesting that the formation of the hexameric cluster proceeds via a trimeric species similar to **5.6** (Figure A4.1, Appendix 4). The ^{1}H-DOSY measurement of the reaction mixture of **5.3**H_3 and **5.5** in CD_3OD after 15 hours at the acetate region shows the presence of at least two major species in solution (Figure A4.2, Appendix 4). The first one at a diffusion rate of log D = -8.98 shows the presence of an all acetate species (major **5.8**) and the second one at log

D = -9.33 corresponds to **5.9** (similar to **5.5**a which gives more than one OAc peak in ^{1}H-DOSY).[12] On the other hand, the reaction mixture of **5.1**-H_3 and **5.5** and that of **5.2**-H_3 and **5.5** in methanol after 12 hours shows a single peak in the ^{31}P-NMR spectra in the cluster region indicating the formation of **5.6** and **5.7** in their respective reactions. Absence of the mixed-bridged species in these reactions might be due to (a) the faster reactivity of **5.5** with the ligands **5.1**H_3 and **5.2**-H_3 and (b) the stronger steric-hindrance exhibited by the bulky ^{c}Hex and ^{t}Bu substituents for smaller bridging (methoxy or hydroxy) groups. The ^{31}P-NMR spectra of all the isolated compounds gave a single peak in the range between δ 78.9 and 69.0 (Figure A4.3, Appendix 4). Further, the structure of all these clusters as well as ligands in solution has been confirmed by ESI(+) or MALDI-TOF mass spectra showing the isotopic distribution of peaks centered at the values corresponding to their $[M^{+}]$ or $[M+Na]^{+}$ ions along with other prominent fragment ion peaks (Figure A4.4-A4.17, Appendix 4).

The reactivity of these ligands also tested with $Pd(PhCN)_2Cl_2$ in polar solvents at room temperature leading to the formation of imido-P(V) trianions as hexanuclear chloro-bridged clusters (Scheme 5.2). Crystals of $\{Pd_3[(NR)_3PO](Cl)_3\}_2$ (**5.11**: R = ^{t}Bu, **5.12**: R = ^{c}Hex, **5.13**: R = ^{i}Pr, **5.14**: R = ^{i}Bu) were obtained from the respective reaction of **5.1**, **5.2**, **5.3** and **5.4** with $Pd(PhCN)_2Cl_2$ in MeOH within 10 days. The ^{31}P-NMR of these compounds gave a single peak around the region between δ 77.0-77.5 ppm consistent with the signal for the imido-trianions. Further, the ESI(+) or MALDI-TOF mass spectra these compounds gave an isotopic distribution of peaks centered at the values corresponding to their $[M^{+}]$ or $[M+Na]^{+}$ ions along with other prominent fragment ion peaks (Figure A4.4-A4.17, Appendix 4).

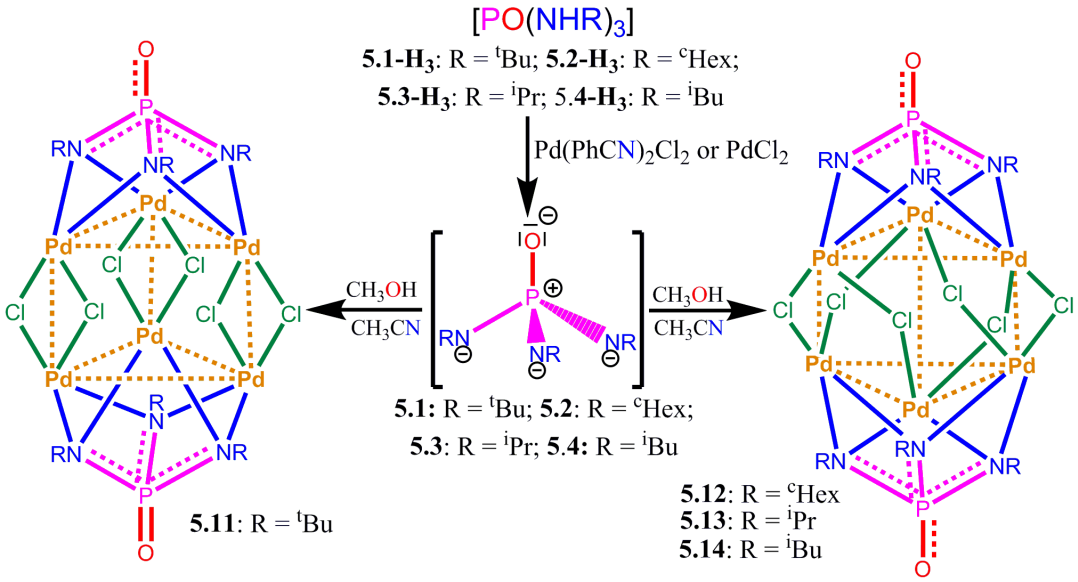

Scheme 5.2: Synthetic routes to access the tri- and hexanuclearPd(II) clusters of the tris(alkylimido) phosphate trianions

5.3.2 Crystal Structures

The crystal structure of ligand **5.3-H$_3$** was obtained in the orthorhombic space group *Pnma* with its asymmetric unit consisting of one half of the ligand moiety. The ligand **5.4-H$_3$** was crystallized in monoclinic space group *P2(1)/c* with its asymmetric unit consisting of four unique ligand moieties (Figure 5.1). Similar to the crystal structures of the previously characterized phosphoramides (5.1 and 5.2), **5.3-H$_3$** and **5.4-H$_3$** exhibit interesting kinds of H-bonding mediated by inter-molecular N-H…O interactions between the amino protons and phosphorus bound oxo functionalities (Figure A4.18, Appendix 4).

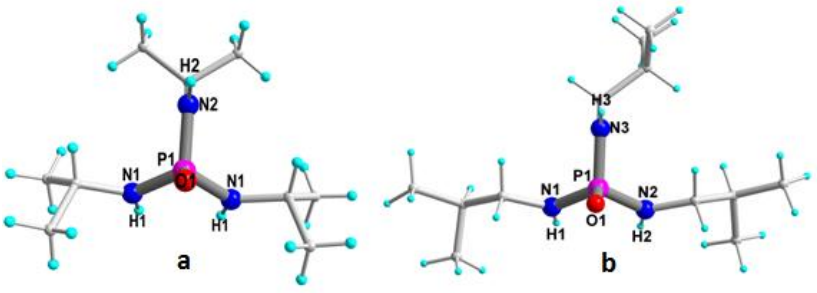

Figure 5.1: Crystal Structure of **5-H$_3$** and **5.4-H$_3$**.

The trinuclear species **5.6** crystallized in the orthorhombic space group *Cmc2(1)*. The molecular core consists of one fully deprotonated ligand **5.1**, three Pd(II) atoms and three charge balancing acetate ions (Figure 5.2a). The imido-ligand is hexadentate and is

involved in bridging the three equilaterally arranged Pd(II) atoms in a chelating fashion. Each Pd(II) atoms is located at a square planar coordination of two N-sites from **5.1** and two O-sites from the three bridging acetate units. It is interesting to compare the structure of **5.6** with the solid state structure of the precursor $Pd(OAc)_2$.[13] In the solid state $Pd(OAc)_2$ exists in the form of a trimer as $Pd_3(OAc)_6$ (**5.5**) with a central triangular Pd_3 unit sandwiched between three bridging carboxylate units on either side of it remained intact and help to restore the charge balance in the molecule. Each imido-nitrogen is bonded to two Pd(II) centers at almost equal distances ranging from 2.052(3) to 2.061(3) Å indicating the trianionic charge is equally delocalized on the three N-sites. Similarly the Pd-O distances found in **5.6** are almost equal pointing to the delocalized nature of the carboxylate charges.

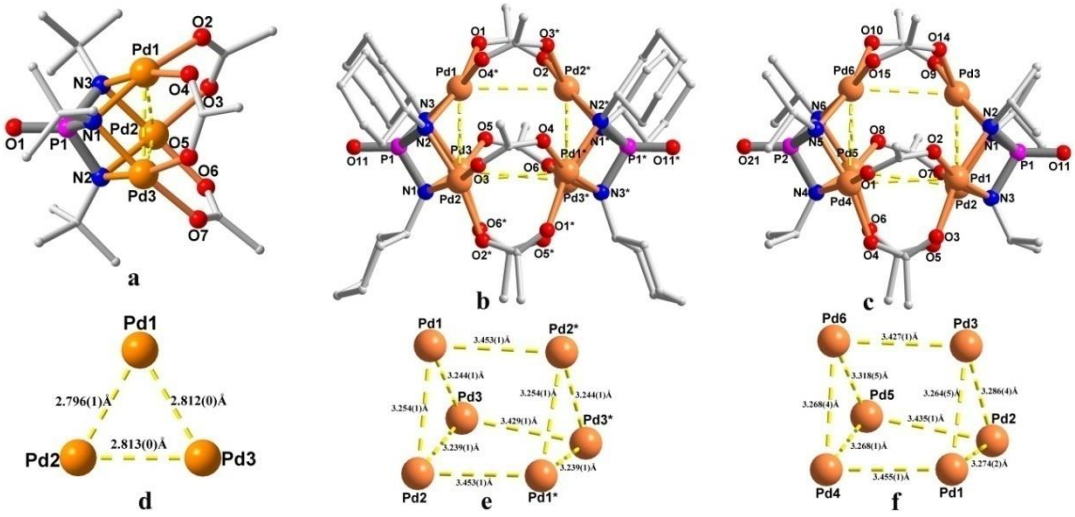

Figure 5.2: Molecular structures of **5.6** (a) **5.7** (b) and **5.8** (c). The Pd_3 subunits of **5.6** (d); the Pd_3-subunits stacked upon each other in an eclipsed manner in **5.7** (e) and **5.8** (f).

The molecules **5.7** and **5.8** are iso-structural and crystallized as **5.7**.H_2O and **5.8**.$2H_2O$, respectively. The molecular structure of **5.7**.H_2O was solved in the orthorhombic space group *C222(1)* with one-half of the molecule in the asymmetric unit (Figure 5.2b). The crystal structure of **5.8**.$2H_2O$ was obtained in the monoclinic space group *C2/c* featuring the complete molecule in its asymmetric unit (Figure 5.2c). The molecular cores in **5.7**.H_2O and **5.8**.$2H_2O$ consists of a hexameric Pd_6 cluster in a prismatic geometry sandwiched between two tris(imido)phosphate ligands (**5.2** or **5.3**). The prismatic Pd_6 cluster can be viewed as a pair of planar Pd_3-subunits (of the type found in **5.6** as well as in **5.5**) that are stacked upon each other in a nearly eclipsed manner. Each imido-phosphate ligand acts as a hexadentate cisoidal ligand and is bonded in a chelating

fashion to the triangular Pd_3 unit. These individual Pd_3 units are further connected by six carboxylate ligands (Harris Notation: 2.1.1 coordination)[14] completing the hexameric structure. A closer look at these structures reveal that these six carboxylate ligands are interacting in a set of two and connect a pair of Pd(II) centers from the adjacent triangular units. Thus, these prismatic Pd_6 cluster assemblies contain three such Pd_2-pairs and each of them is held together by two bridging carboxylate ligands.

The mixed bridged cluster **5.9** crystallized in the monoclinic space group *P2(1)/c* featuring the whole molecule in the asymmetric unit. The molecule **5.10**.2DMSO crystallized in the monoclinic space group *C2/c* and contains one half of the molecule and one solvated DMSO molecule in the asymmetric unit.

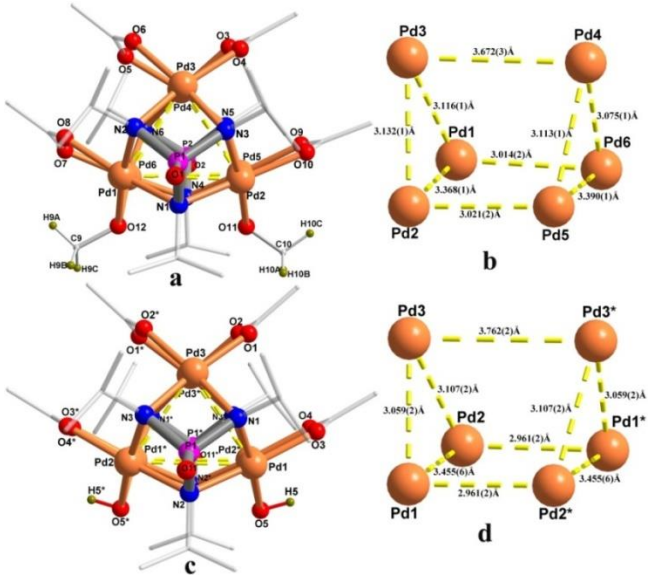

Figure 5.3: Molecular structures of **5.9** (a) and **5.10** (c) showing their two Pd_3 subunits stacked upon each other in an eclipsed manner. Prismatic view of the six Pd(II) centers in **5.9** (b) and **5.10** (d)

The core structures of **5.9** and **5.10** resemble closely to that of **5.8** and contain two μ^2-bridging methoxy and hydroxy groups, respectively, in place of two of the six acetate groups (Figure 5.3a and 5.3c). Two of the three Pd_2 pairs present in the prismatic cluster of **5.9** and **5.10** possess the mixed bridged environment with one acetate moiety and one methoxy/hydroxy unit each, while the third pair contains only acetate bridges. The two hydroxyl groups present in **5.9** are hydrogen bonded to two solvated disordered molecules of DMSO (Figure 5.4). The Pd-N and Pd-O distances found in **5.7**.H_2O and **5.8**.2H_2O, **5.9** and **5.10**.2DMSO are similar and comparable to that found in **5.6**.

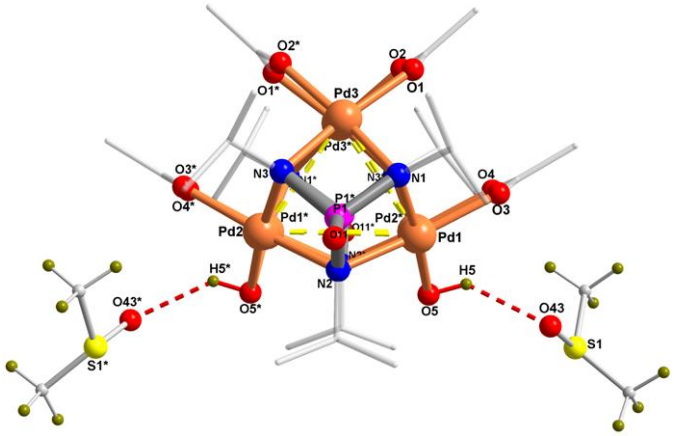

Figure 5.4: Eclipsed view of the structure of **5.10**.2DMSO containing two H-bonded DMSO molecules

The molecular structure of **5.11** was solved in the hexagonal space group *P6(3)/m* with one-sixth of cluster assembly in the asymmetric unit. The molecular core in **5.11** is closely similar to those of **5.7** or **5.8** consisting of the Pd_6 cluster in the prismatic geometry sandwiched between two tris(imido)phosphate ligand. Like before the Pd_3 subunits that are stacked upon each other in a nearly eclipsed manner. These individual Pd_3 units are further connected by six chloride ions completing the hexameric structure (Figure 5.5). The molecular structure of **5.12**.DMF and **5.14** were solved in the monoclinic space group *P2(1)/c* with one-half of the molecule in the asymmetric unit whereas **5.13** was solved in the monoclinic space group *P2(1)/n* with one-half of the molecule in the asymmetric unit (Figure 5.6). Interestingly unlike **5.11**, the molecular structures of **5.12**, **5.13**.DMF and **5.14** consist of the octahedral arrangement of the six Pd(II) atoms in which the two Pd_3 subunits in each of them are still capped by the tris(imido)phosphate ligands (**5.2**, **5.3** and **5.4**) in a cisoidal manner. Construction of these octahedral Pd_6 clusters can be regarded as the stacking of two triangular Pd_3 subunits onto each other in a nearly staggered manner. While each of the three Pd_2-pairs in **5.11** is bridged by an isolated pair of chloride ions similar to the prismatic acetate bridged clusters, the chloride ions in **5.12**, **5.13**.DMF and **5.14** are alternating bridging between the adjacent Pd(II) atoms resulting in a more-effective bonding environment in the octahedral assembly (Figure 5.6).

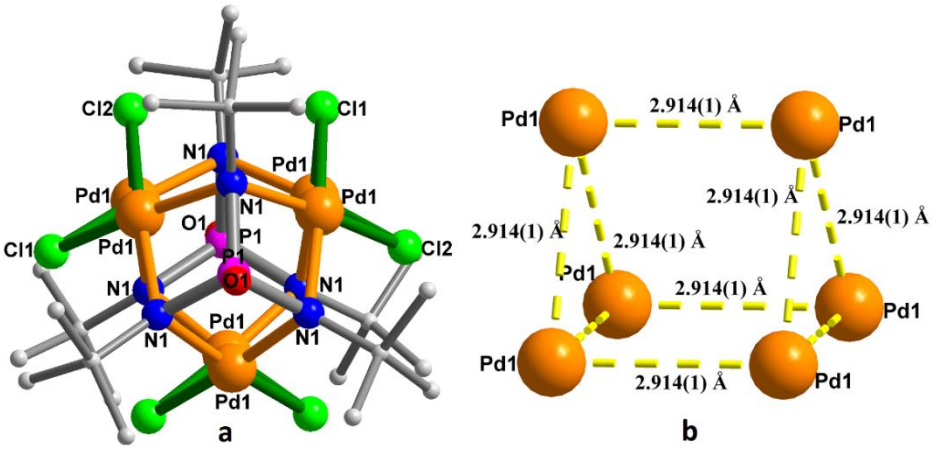

Figure 5.5: (a) Molecular structure of **5.11** showing the eclipsed arrangement of the two Pd_3 subunits; (c) view of the prismatic cluster core in **5.11**.

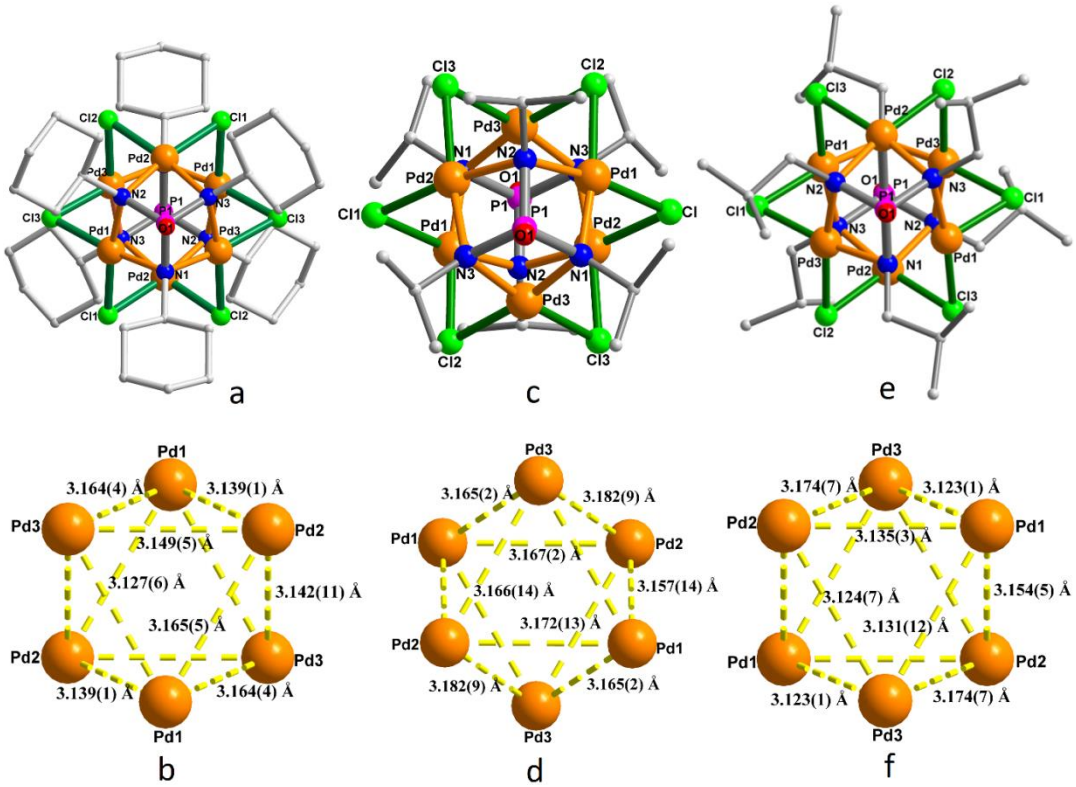

Figure 5.6: Molecular structures of **5.12** (a) **5.13** (c) and **5.14** (e) showing the staggered arrangement of the two Pd_3 subunits; view of the octahedral cluster cores in **5.12** (b) **5.13** (d) and **5.14** (f).

It is interesting to compare the Pd-Pd distances found in these trimeric and hexameric assemblies. The two unique Pd-Pd distances of 2.796(0) and 2.813(1) Å, found in the trimeric assembly of **5.6** (Figure 5.2d), are considerably shorter than those found in the crystal structures of $Pd_3(OAc)_6$ (**5.5**, av. 3.151(13) Å).[13] But in the hexameric assemblies

of **5.7**, **5.8**, **5.9** and **5.10**, the Pd-Pd distances found within the triangular segment are slightly longer than those found in **5.5** owing to the open bridging coordination of the acetate groups between the two Pd_3 subunits. A further look at the interplanar Pd-Pd distances found along the three rims of the prismatic assemblies reveal large deviations for the mixed-bridged clusters **5.9** and **5.10** in comparison with the all acetate bridged clusters **5.7** and **5.8**. Thus, in **5.9** and **5.10** two of the three rim distances are relatively much shorter (**5.9**: 3.018(2) Å (average); **5.10**: 2.961(2) Å) than the third (**5.9**: 3.672(3) Å; **5.10**: 3.762(2) Å) as the shorter ones are found at the Pd_2-pairs containing mixed (OAc and OR') bridging groups (Figure 5.3b and 5.3d). All three interplanar Pd-Pd distances found in **5.7** (av. 3.445(1) Å) and **5.8** (av. 3.439(1) Å) are very much similar to each other (Figure 5.2e and 5.2f). As a consequence, the mean-plane deviation between the two triangular Pd_3-subunits in **5.9** and **5.10** are larger at 14 and 15°, respectively, while those found in **5.7** and **5.8** are deviated minimally by an angle of 1°. However, in the chloro-bridged clusters all the Pd-Pd distances are nearly same and are relatively shorter compared to the all-acetate-bridged clusters **5.7** and **5.8**. Particularly, the prismatic assembly of **5.11** features the shortest Pd-Pd distances of av. 2.914(1) Å observed for the hexameric clusters and is comparable to some of the rim distances of **5.9** and **5.10**. The Pd-Pd found distances in the octahedral clusters are in the range from 3.12 (5) to 3.17 (6) which on average are intermediate between the chloro- and acetate-bridged prismatic assemblies.

A Cambridge structural database (CSD) search on the structures of palladium containing hexameric complexes indicate that the prismatic clusters observed in our reactions are rather unprecedented. Although a handful number of octahedral structures are reported,[15] there are very few examples known for the prismatic arrangement of the six Pd(II) ions.[16] Hence, we presume that the key requirements for obtaining such prismatic arrangement of the Pd(II) clusters are the intact Pd_3-unit in its local structure and ligand sets which minimizes the steric crowding in between the two Pd_3 subunits in the eclipsed form. In case of **5.7** and **5.8** vís-a-vís **5.9** and **5.10** the acetate bridges largely relieve the steric congestions in the molecule to facilitate a prismatic arrangement of the six Pd(II) atoms. However, as discussed above the chloro-bridged hexamers exhibit a considerably shorter Pd-Pd distances which forces the two Pd_3-subunits to take-up a staggered conformation giving rise to an octahedral cluster. Even though crystalline $Pd(OAc)_2$ exists in the form of a discrete trimeric Pd_3-unit, most ligand displacement reactions tend to destroy this

arrangement. In this regard the tripodal nature of the ligand moieties in **5.2, 5.3** and **5.4** proves to be compatible, sterically and electronically, to provide a structurally rigid triangular motif by tethering the Pd_3 unit together from one side of it.

5.3.3 Reactivity Studies of tri- and hexanuclear Pd(II) complexes

In order to test the robustness of tripodally chelated $(Pd{-}N_{imido})_3$ moieties in **5.6**, **5.7**, and **5.8**, we studied the reactivity of these complexes in the presence of a primary amine which acts as a nucleophilic reagent to the Pd(II) ions. Thus, the reaction of **5.6**, **5.7**, and **5.8** with stoichiometric equivalents of cyclohexylamine in MeOH proceeds spontaneously as observed by a visual color change in solution (from orange to yellow) from which yellow-colored crystalline solids of **5.15**, **5.16**, and **5.17**, respectively, were obtained (Scheme 5.3). Single-crystal X-ray analysis of the crystals of **5.16** and **5.17** indicates the presence of a new trinuclear species of the formula $\{Pd_3[(NR)_3PO](OAc)_3(^cHexNH_2)_3\}$ (**5.16**, R= ^{c}Hex; 5.**17**, R= ^{i}Pr), while a similar structure for **5.15** (R = ^{t}Bu) was confirmed by a combined ^{31}P NMR and mass spectral analysis. These new trinuclear assemblies were obtained via a nucleophilic attack on the Pd(II) ions by the amino groups, and in fact, **5.16** and **5.17** were obtained from a symmetrical cleavage of the hexanuclear assemblies in **5.7** and **5.8**, respectively. While such an amine-triggered cleavage of a dinuclear Pd(II) species to a mononuclear complex has been observed previously,[17] formation of **5.15**, **5.16**, and **5.17** in the present instance is attributed to the rigid tripodal chelation of the imido-phosphate which provides the necessary stability to the Pd_3 units.

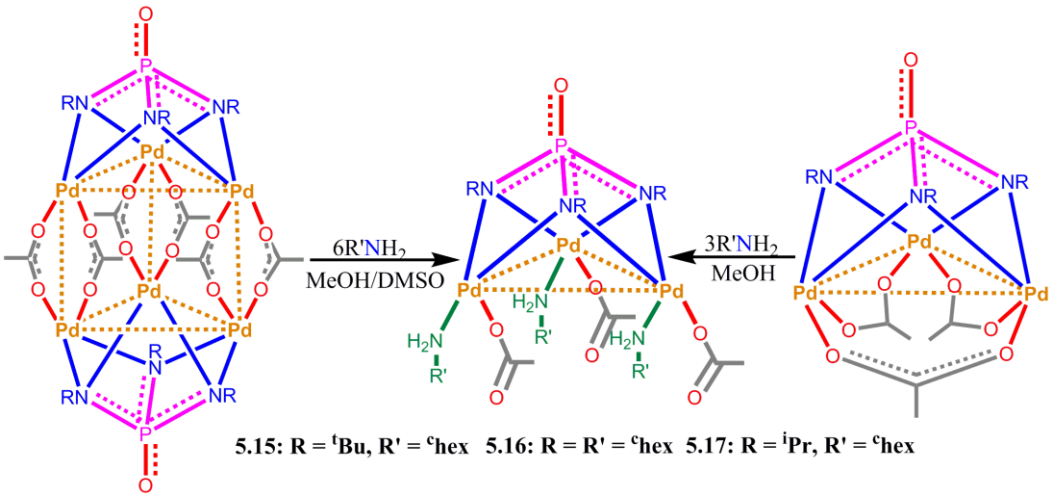

Scheme 5.3: Synthetic routes to access the tri- and hexanuclear Pd(II) clusters of the tris(alkylimido) phosphate trianions

In addition, formation of **5.16**/**5.17** has been observed in a direct reaction involving the phosphoramide precursor **5.2**H_3/**5.3**H_3, $Pd(OAc)_2$, and cyclohexylamine. The preferential deprotonation of **5.2**H_3/**5.3**H_3 over cyclohexyl-amine confirms that the trianionic species **5.2**/**5.3** provides a vital stability to keep triangular Pd_3 motifs intact. The ^{31}P-NMR spectra of the compounds **5.14** (δ 72.05), **5.15** (δ 73.50), and **5.16** (δ 73.67) in CD_3OD gave a single peak in the cluster region. Furthermore, from the mass spectral data, their existence in solution has been confirmed.

The single crystal X-ray analysis of **5.16** and **5.17** reveal that these clusters are iso-structural in the solid state. The asymmetric unit of **5.16**.2H_2O contains one third of the molecule as it was crystallized in the trigonal space group *P3-c1* (Figure 5.7a). The molecular structure of **5.17** was solved in the monoclinic space group *P2(1)/n*, in which the asymmetric unit contains the whole molecule (Figure 5.7). As observed before one side of the Pd_3-plane in **5.16** and **5.17** were found with the tripodally chelating imido-ligand, while the other side of it contains three hanging cyclohexyl amines and three acetate moieties. The Pd-N, Pd-O and Pd-Pd distances found in **5.16** and **5.17** are comparable to those found in the hexameric complexes. Further the H-bonding interactions between the acetate anions and amino protons result in the formation of a two-dimensional hexagonal network for **5.16** (Figure 5.7b) and 1D-zigzag chain for **5.17** (Figure 5.9).

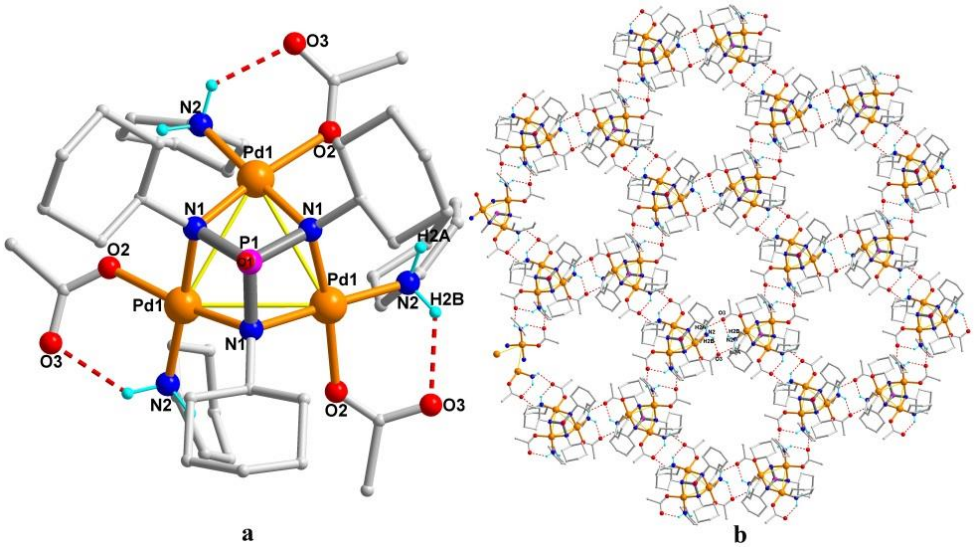

Figure 5.7: Crystal structure (a) and formation of a hexagonal 2D-structure (b) in **5.16**.2H_2O.

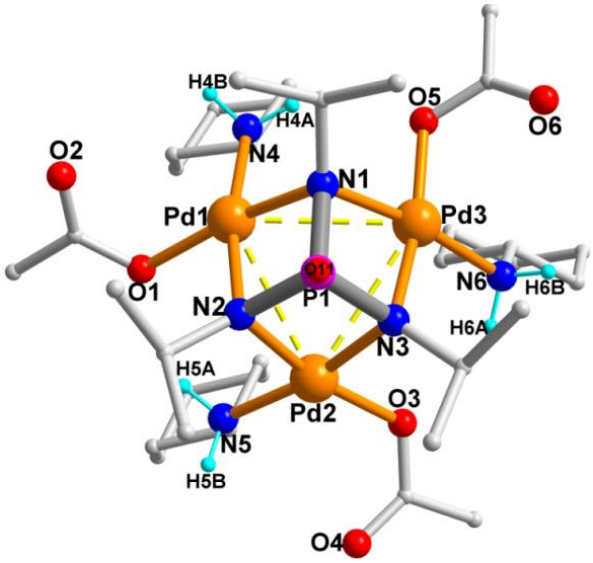

Figure 5.8: Crystal structure of the trinuclear cluster **5.17**

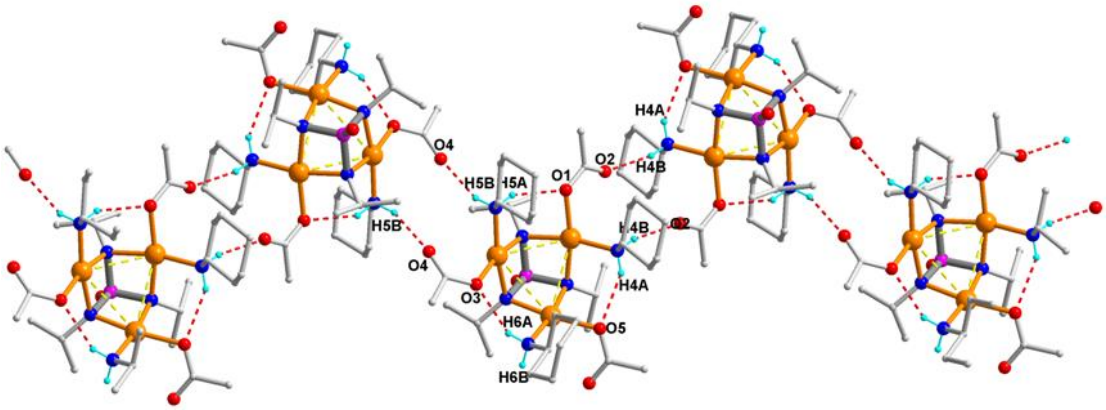

Figure 5.9: formation of a 1D-chain structure in **5.17**

5.4 Application in Catalytic Reactions

Inspired by their rigid Pd-N_{imido} tripodal motifs, we were curious to see whether the Pd(II) atoms in these clusters are still active for catalytic reactions. As these imido-motifs are strongly bound to the Pd(II) atoms, we thought a catalytic reaction that utilizes the Pd(II) ions as an active catalyst would be more suitable to examine. Hence we employed these complexes in the Mizoroki-Heck type reactions in which the Pd(II) species catalyzes the coupling reaction of phenyl boronic acid with alkenes.[18,19] Thus, the treatment of phenyl boronic acid (1.2 equiv) with n-butyl acrylate (**5.18**a) in presence of the trinuclear complex **5.6** (3 mol %) and $Cu(OAc)_2$ (2 equiv) in DMF at 100 °C for 4 h leads to the corresponding phenylated trans-alkene derivative (**5.19**a) in 90 % isolated yield (Scheme 5.4).

The reaction was also tested with the hexameric complexes **5.7** and **5.8** under same conditions which gave the alkene product **5.19**a in 90% and 95% yields, respectively. Similarly, we have tried the coupling reaction with few more alkenes such as methyl acrylate (**5.18**b), c-hexyl acrylate (**5.18**c) and styrene (**5.18**d) in presence of all these three cluster motifs. Noticeably, **5.9** acts as a better catalyst for all these substrates yielding the coupled products **5.19**b-d in 90 %, 95 % and 98 % yields, respectively (Table 5.1). As observed before,[18c] the catalytic reaction presumably proceeds via the trans-metallation of the phenyl boronic acid with Pd(II) complexes followed by insertion of the alkene substrate that subsequently undergoes β-hydride elimination in presence of $Cu(OAc)_2$, which acts both as an acetate source as well as an oxidant in the catalytic cycle. Similar studies aiming at the reactivity and the catalytic studies for the chloro-bridged hexameric clusters are currently under study.

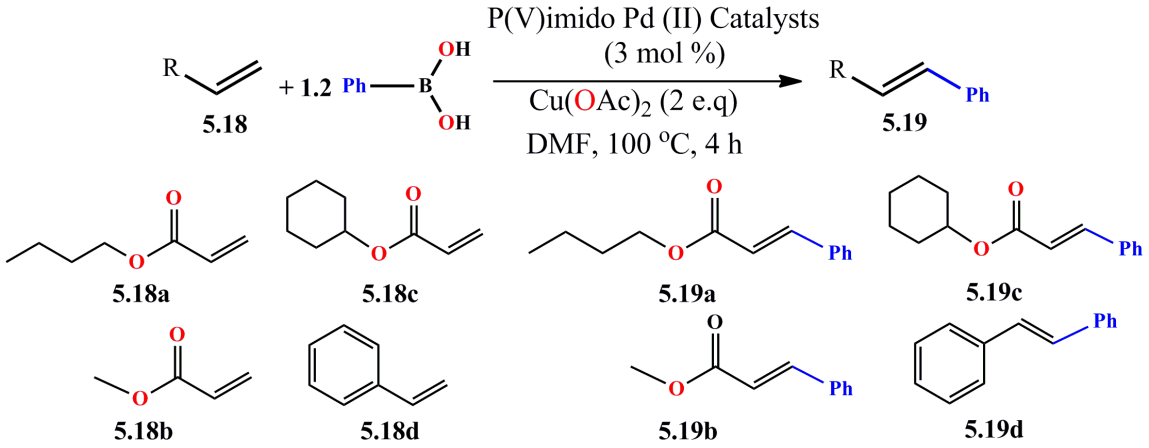

Scheme 5.4: M-H type reaction of $PhB(OH)_2$ with various alkenes.

Table 5.1 M−H Type Reaction of $PhB(OH)_2$with Alkenes

Starting Material	Coupled Product	% Yield of the Product		
		Catalyst **5.6**	Catalyst **5.7**	Catalyst **5.9**
5.18a	5.19a	90	90	95
5.18b	5.19b	90	92	90
5.18c	5.19c	92	90	95
5.18d	5.19d	95	95	98

5.5 Conclusions

In conclusion we have shown that $Pd(OAc)_2$ provides a facile deprotonation route to access the highly basic tris(alkylimido) phosphate trianions, $[(RN)_3PO]^{3-}$, in polar and in protic solvents. Tri or hexa-nuclear Pd(II) clusters of these trianions were isolated exclusively in all these reactions in which the trianionic species acts as a tripodal

chelating ligand to the trinuclear Pd_3-unit. Employing of $PdCl_2$ leads again to the fully deprotonated species $[(RN)_3PO]^{3-}$ as their corresponding chloro-bridged hexameric clusters. We observed two types of arrangement for the chloro-bridged hexameric clusters from the crystal structures. A prismatic arrangement of the Pd_6-assembly was observed for the trianionic imido-phosphate ligand featuring the most bulky ^{t}Bu substituents, while for other substituents such as ^{c}Hex, ^{i}Pr and ^{i}Bu on the imido-P(V) backbone an octahedral cluster assembly was obtained. Reactivity studies on the hexameric clusters featuring the acetate groups with primary amines have lead to a symmetric cleavage of the prismatic assemblies in which the tripodally chelated $(Pd\text{-}N_{imido})_3$ moieties remained unaffected. The robustness of the Pd_3-unit in all these clusters is expected to offer a stable platform for catalytic reactions in which the trianionic ligand would act as a perfect spectator ligand and the substrate will approach the Pd(II) ions from the side that is trans to the $Pd\text{-}N_{imido}$ sites. Also, the crystalline nature of these imido-Pd_3 motifs is an added advantage as it can assist in isolating various organic-intermediate species and thus would provide useful inputs on understanding reaction mechanisms. We have also demonstrated the catalytic activity of these complexes in M-H type coupling reactions which proves that these clusters are worthy candidates for catalytic applications.

5.6 References

(1) (a) Chivers, T.; Brask, J. K. *Angew. Chem., Int. Ed.* **2001**, *40*, 3960-3976. (b) Steiner, A.; Zacchini, S.; Richards, P. I. *Coord. Chem. Rev*. **2002**, *227*, 193-216. (c) Raithby, P. R.; Russell, C. A.; Steiner, A.; Wright, D. S. *Angew. Chem., Int. Ed. Engl.* **1997**, *36*, 649-650. (d) Armstrong, A.; Chivers, T.; Parvez, M.; Boeré, R. T. *Angew. Chem., Int. Ed.* **2004**, *43*, 502-505. (e) Aspinall, G. M.; Copsey, M. C.; Leedham, A. P.; Russell, C. A. *Coord. Chem. Rev*. **2002**, *227*, 217-232. (f) Stahl, L. *Coord. Chem. Rev*. **2002**, *210*, 203-250. (g) Scherer, O.; Kerth, J.; Sheldrick, W. S. *Angew. Chem., Int. Ed.* **1984**, *23*, 156-157.

(2) (a) Buchard, A.; Auffrant, A.; Klemps, C.; Vu-Do, L.; Boubekeur, L.; Le Goff, X. F.; Le Floch, P. *Chem. Commun*. **2007**, 1502-1504. (b) Alhomaidan, O.; Bai, G.; Stephan, D. W. *Organometallics* 2008, *27*, 6343-6352. (c) Li, D.; Li, S.; Cui, D.; Zhang, X.; Trifonov, A. A. *Dalton Trans*. **2011**, *40*, 2151-2153. (d) Gamer, M. T.; Rastätter, M.; Roesky, P. W.; Steffens, A.; Glanz, M. *Chem. Eur. J.* **2005**, *11*, 3165-3172. (e) Rastätter, M.; Zulys, A.; Roesky, P. W. *Chem. Eur. J*. **2007**, *13*, 3606-3616. (f) Rastätter, M.; Zulys; A.; Roesky, P.

W. *Chem. Commun*. **2006**, 874-876. (g) Boubekeur, L.; Ulmer, S.; Ricard, L.; Mézailles, N.; Le Floch, P. *Organometallics* **2006**, *25*, 315-317.

(3) (a) Bickley, J. F.; Copsey, M. C.; Jeffery, J. C.; Leedham, A. P.; Russell, C. A.; Stalke, D.; Steiner, A.; Stey, T.; Zacchini, S. *Dalton Trans.* **2002**, 989-995. (b) Gupta, A. K.; Nicholls, J.; Debnath, S.; Rosbottom, I.; Steiner, A.; Boomishankar, R. *Cryst. Growth Des.* **2011**, *11*, 555-564.

(4) (a) Armstrong, A. Chivers, T.; Krahn, M.; Parvez, M.; Schatte, G. *Chem. Commun.* **2002**, 2332-2333. (b) Chivers, T.; Krahn, M.; Parvez, M.; Schatte, G. *Chem. Commun.* **2001**, 1922-1923. (c) Armstrong, A.; Chivers, T.; Parvez, M.; Schatte, G.; Boeré, R. T. *Inorg. Chem.* **2004**, *43*, 3453-3460. (d) Chivers, T.; Krahn, M.; Schatte, G.; M. Parvez, *Inorg. Chem.* **2003**, *42*, 3994-4005. (e) Woodruff, D. N.; McInnes, E. J. L.; Sells, D. O.; Winpenney, R. E. P.; Layfield, R. A. *Inorg. Chem.* **2012**, *51*, 9104-9109. (f) Robertson, S. D.; Chivers, T.; Konu, J. *J. Organomet. Chem.* **2007**, *692*, 4327-4336. (g) Armstrong, A.; Chivers, T.; Krahn, M.; Parvez, M. *Can. J. Chem.* **2005**, *83*, 1768-1778. (h) Rufanov, K. A.; Zeimer, B.; Meisel, M. *Dalton Trans.* **2004**, 3808-3809.

(5) (a) Dehnicke, K.; Weller, F.*Coord. Chem. Rev.* **1997**, *158*, 103-169.(b) Dehnicke, K.; Krieger, M.; Mass, W. *Coord. Chem. Rev.* **1999**, *182*, 19-65.

(6) Chivers, T.; Fu, Z.; Thompson, L. K. *Chem. Commun.* **2005**, 2339-2341.

(7) (a) Lyons, T. W.; Sanford, M. S. *Chem. Rev.* **2010**, *110*, 1147-1169. (b) Chen, X.; Engle, K. M.; Wang, D.-H.; Yu, J.-Q. *Angew. Chem., Int. Ed.* **2009**, *48*, 5094-5115.

(8) (a) Gupta, A. K.; Chipem, F. A. S.; Boomishankar, R. *Dalton Trans*. **2012**, *41*, 1848-1853. (b) Gupta, A. K.; Steiner, A.; Boomishankar, R. *Dalton Trans*. **2012**, *41*, 9753-9759.

(9) Audrieth, L. F.; Toy, A. D. F. *J. Am. Chem. Soc*. **1942**, *64*, 1553-1555.

(10) (a) Wu, D.; Chen, A.; Johnson, C. S., Jr. *J. Mag. Reson., Ser. A* **1995**, *115*, 260-264. (b) Kerssebaum, R. DOSY and Diffusion by NMR. In *Users guide for XWinNMR 3.5, Version 1.0*; Bruker Bio Spin GmbH: Rheinstetten, Germany, 2002.

(11) Sheldrick, G. M. *Acta Crystallogr.* **2008**, *A64*, 112.

(12) Nosova, V. M.; Ustynyuk, Y. A.; Bruk, L. G.; Temkin, O. N.; Kisin, A. V.; Storozhenko, P. A. *Inorg. Chem*. **2011**, *50*, 9300-9310.

(13) (a) Cotton, F. A.; Han, S. *Rev. Chim. Miner.* **1983**, *20***,** 496-503. (b) Cotton, F. A.; Han, S. *Rev. Chim. Miner.* **1985**, *22***,** 277-284. (c) Bakhmutov, V. I.; Berry, J. F.; Cotton, F. A.; Ibragimov, S.; Murillo, C. A. *Dalton Trans.* **2005**, 1989-1992. (d) Kozitsyna, N. Y.; Nefedov, S. E.; Dolgushin, F. M.; Cherkashina, N. V.; Vargaftik, M. N.; Moiseev, I. I.

Inorg. Chim. Acta **2006**, *359*, 2072-2086. (e) Skapski, A. C.; Smart, M. L. *Chem. Commun.* **1970**, 658-659.

(14) Coxall, R. A.; Harris, S. G.; Henderson, D. K.; Parsons, S.; Tasker, P. A.; Winpenny, R. E. P. *J. Chem. Soc. Dalton Trans.* **2000**, 2349-2356.

(15) (a) Klein, H.-F.; Mager, M.; Flörke, U.; Haupt, H.-J. *Organometallics* **1992**, *11*, 3915-3917. (b) Halvagar, M. R.; Fard, Z. H.; Dehnen, S. *Inorg. Chem.* **2009**, *48*, 7373-7377. (c) Mednikov, E. G.; Dahl, L. F. *Dalton Trans.* **2003**, 3117-3125.

(16) Holah, D. G.; Hughes, A. N.; Krysa, E.; Markewich, R. T.; Havighurst, M. D.; Magnuson, V. R. *Polyhedron*, **1997**, *16*, 2789-2796.

(17) Pratap, R.; Parrish, D.; Gunda, P.; Venkataraman, D.; Lakshman, M. K. *J. Am. Chem. Soc.* **2009**, *131*, 12240-12249.

(18) (a) Du, X.; Suguro, M.; Hirabayashi, K.; Mori, A.; Nishikata, T.; Hagiwara, N.; Kawata, K.; Okeda, T.; Wang, H. F.; Fugami, K.; Kosugi, M. *Org. Lett.* **2001**, *3*, 3313−3316. (b) Zhang, Y.-H.; Shi, B.-F.; Yu, J.-Q.*J. Am. Chem. Soc.* **2009**, *131*, 5072−5074. (c) Zhang, S.; Shi, L.; Ding, Y. *J. Am. Chem. Soc.* **2011**, *133*, 20218−20229.

(19) For the conventional Pd(0)-catalyzed M-H type coupling reactions, see: (a) Mizoroki, T.; Mori, K.; Ozaki, A. *Bull. Chem. Soc. Jpn.* **1971**, *44*, 581−584. (b) Heck, R. F.; Nolley, J. P., Jr. *J. Org. Chem.* **1972**, *37*, 2320-2322.

Chapter 6

Trinuclear imido-Pd(II) clusters as polyhedral building units for self-assembled neutral cages

Abstract

In this chapter, starting from the hexameric imido-Pd(II) clusters we described a novel ligand substitution route to access the hitherto unknown neutral polyhedral cages for Pd(II) ions. In an initial observation we found that reaction of benzoic acid with the hexamer $\{Pd_3[(N^iPr)_3PO](OAc)_3\}_2$ *results a hexameric complex of composition* $\{Pd_3[(N^iPr)_3PO](PhCOO)_3\}_2$*. Similarly, reaction of* $\{Pd_3[(N^iPr)_3PO](OAc)_2(OH)\}_2$ *with 1,1'-ferrocenedicarboxylic acid (FDC-H) replaces the four acetate bridges with two FDC bridges* $\{Pd_3[(N^iPr)_3PO](FDC)(OH)\}_2$*. These reactions showed that the trinuclear* $\{Pd_3[(N^iPr)_3PO]\}^{3+}$ *motif is stable in solution and can be linked with suitable carboxylate linkers to yield the elusive high-nuclearity neutral cage molecules for Pd(II) ions. In this effort we have synthesized a neutral tetrahedron* $[(Pd_3X)_4L_6]$ *and a cube* $[(Pd_3X)_8L_{12}]$ *in the reaction of the hexameric cluster formula* $\{Pd_3[(N^iPr)_3PO](OAc)_2(OH)\}_2$ *with oxalic acid and 2,5-pyrazine dicarboxylic acid, respectively. The vertices of these cages feature a trinuclear polyhedral building unit of formula* $[Pd_3X]^{3+}$ *in which trianionic tris(iso-propylimido) phosphate* X^{3-}, $[PO(N^iPr)_3]^{3-}$, *motif acts as a cis-capping ligand for a planar* Pd_3*-unit. These cis-blocked PBUs act as* 60^o *acceptors and spontaneously self-assemble in presence of* 180^o *oxalate linker to give a tetrahedral cage. Use of a* 120^o *2,5-pyrazine dicarboxylate linker leads to the formation of a cubic cage. The void volumes of these tetrahedral and cubic cages were found to be 85.8 and 1000* $Å^3$*, respectively. However, such cage assemblies were not obtained when non-chelating carboxylate linkers were employed in these reactions. Furthermore, guest encapsulation studies show the tetrahedral cage molecule is selective for* CCl_4 *and benzene over* $CHCl_3$, CH_2Cl_2*, THF and other substituted benzene derivatives. Guest encapsulation studies for the bigger cubic cage molecule are currently underway.*

6.1 Introduction

Over the years, self-assembled molecular architectures derived from abiological systems have evolved in to an intense field of research in supramolecular chemistry.[1] These processes take inspiration from the nature itself, wherein the highly complex functional structures of cells, viruses, nucleo-bases and peptide-based assemblies were obtained by spontaneous self-assembly pathways.[2] Synthetic approaches to artificial assemblies involve the use of small and simple molecular building blocks, which react in a cooperative manner to yield highly organized structures.[3] Besides their structural novelty, these assemblies reveal promising applications in host-guest chemistry viz., guest recognition, chemical sensing, protection and entrapment of reactive molecules and catalysis in their confined space.[4] Polyhedral cages derived from metal-ligand coordination bonds belong to one such notable class of self-assembled systems amongst several known supramolecular entities.[5] Most often these polyhedral structures were assembled from isolated metal ions in combination with neutral N-donor bridging ligands leading to the formation of cationic assemblies.[6] Use of multi-anionic bridging ligands yield anionic assemblies in general except in few cases where neutral cages were obtained.[7] Conversely, it has been shown that bimetallic paddlewheel motifs of formula $[M_2(COO)_4]$ can be used as cluster vertices for building charge neutral polyhedral assemblies which are termed as metal-organic polyhedra (MOPs).[8] However, rational routes to access these kinds of MOPs have largely been limited to the dinuclear clusters of certain metal ions. This could be attributed to the lack of precise control over the reactivity of such cluster motifs favoring the formation of extended two- or three-dimensional structures.[9] Moreover it is difficult to find suitable auxiliary groups[10] for such cluster assemblies that can protect some of its metal-coordination sites to specifically obtain discrete MOPs.

This chapter describes a novel ligand substitution route to access elusive examples of neutral Pd(II)-containing MOPs, starting from the imido-Pd(II) clusters reported earlier in chapter 5. In this chapter, we have shown the utility of the trinuclear imido-Pd(II) cluster motif $[Pd_3(N^iPr)_3PO]$, denoted as $[Pd_3X]^{3+}$, as a new polyhedral building unit (PBU) for obtaining large charge-neutral cluster cages. These PBUs, which are cis-protected with the trianionic imido-phosphate $[PO(N^iPr)_3]^{3-}$ (X^{3-}) ligands, self-assemble in presence of suitable anionic linker ligands to yield interesting platonic solids in tetrahedral and cubic topologies. A dodecanuclear neutral tetrahedral cage $[(Pd_3X)_4L_6]$

(L^{2-} = C_2O_4), **6.3**, was obtained when the PBU precursor $\{Pd_3[(NR)_3PO](OAc)_2(OH)\}_2$ (**5.10**·2DMSO) was subjected to the ligand substitution reaction with oxalic acid, a chelating dicarboxylic acid. Use of pyrazine dicarboxylic acid having slightly different chelating angles, have resulted in a cubic cage assembly $[(Pd_3X)_6L_{12}]$ (L^{2-} = $[C_4H_2N_2(COO)_2]^{2-}$), **6.7**. Use of this unique $[Pd_3X]^{3+}$ unit as a polyhedral vertex is aided by the chelating cis-coordination of the imido-phosphate ligand that keeps the Pd_3-motif intact from one side of its plane leaving the other side of it to indulge towards cage formation in presence of chelating linker carboxylates. Although there are a few examples known for Pd(II) and Pt(II) containing discrete assemblies, to the best of our knowledge,[11] this is the first instance where multi-nuclear Pd(II)-clusters form the vertex of neutral polyhedrons. However, such cage assemblies were not obtained when non-chelating carboxylate linkers were employed in these reactions. The tetrahedral cage **6.3** exhibits remarkable ability to encapsulate a wide range of neutral guest solvents (from polar to non-polar). Further, we have also described the stability, gas adsorption and the solvent encapsulation studies of the tetrahedral cage assembly **6.3** in detail.

6.2 Experimental section

6.2.1 General Remarks

All manipulations involving phosphorus halides were performed under dry nitrogen atmosphere in standard Schlenk-glassware. Solvents were dried over potassium (THF, hexane) and sodium (toluene). The primary amines were purchased from Merck or from Aldrich and used as received. $POCl_3$ was purchased locally and was distilled prior to use. Benzoic acid, isonicotinic acid (INA-H), 1,1'-ferrocenedicarboxylic (FDC-H) acid, oxalic acid, 2,5-pyridinedicarboxylic acid (PDC-H), 2, 5-pyarzinedicraboxylic (PZDC-H) acid dihydrate and ferric oxalate hexahydrate were purchased from Aldrich and used as received. The buffer solutions were prepared from either NaOAc-AcOH mixture or Na_2HPO_4/NaH_2PO_4-NaOH mixture or K_2HPO_4 in water. NMR spectra were recorded on a Jeol 400 MHz spectrometer (^{1}H NMR: 400.13 MHz, $^{13}C\{^1H\}$NMR: 100.62 MHz, $^{31}P\{^1H\}$ NMR: 161.97 MHz) or on a Bruker 500 MHz (^{1}H NMR: 500.00 MHz, $^{13}C\{^1H\}$NMR: 125.725 MHz, $^{31}P\{^1H\}$ NMR: 202.404 MHz) spectrometer at room temperature using $SiMe_4$ (^{1}H, ^{13}C) and 85% H_3PO_4 (^{31}P). The 2D-DOSY experiments were performed on a Bruker 500 MHz NMR with standard pulse program ledbpgp2S using bipolar gradient pulse pair and two spoiling gradients.[12a] The gradient strength was changed from 2 to 95% with linear type of ramp and other parameters such as the

diffusion time (Δ = 40 -50 ms), sine shaped pulse length (δ = 1.1 - 2.1 ms) and relaxation delay (D1 = 4 - 8 s) were also employed.[12b] The MALDI-TOF spectra were obtained on an Applied Biosystem MALDI-TOF/TOF spectrometer. The powder X-ray diffraction data were obtained from a Bruker D8 Advance diffractometer. Thermal analysis data has been obtained from a Perkin-Elmer STA-6000 thermogravimetric analyzer. Fourier transform infrared (FT-IR) spectra were taken on a Thermo-scientific Nicolet 6700 spectrophotometer with samples prepared as KBr pellets. Melting points were obtained using an Electro thermal melting point apparatus and were uncorrected.

6.2.2 Synthesis

6.1: To a solution of **5.10**·2DMSO (20 mg, 0.013 mmol) in methanol, benzoic acid C_6H_5COOH (10 mg, 0.08 mmol) in methanol was stirred for 1 hour and kept for crystallization. Platelike orange-colored crystals were obtained after 7 days. Yield: 95% (22 mg) mp: 215-217 ^oC. ^1H NMR (400 MHz, {$(CD_3)_2SO$}): δ 1.73 (d, 72H, C*H*$_3$), 2.02 (m, 12H, C*H*), 7.73 (dd, 2H, C*H*), 7.81 (dd, 3H, C*H*), 8.05 (dd, 3H, C*H*): $^{13}C\{^1H\}$ (100 MHz, {$(CD_3)_2SO$}): δ 25.78, 54.10, 127.32, 128.01, 136.53, 138.89: $^{31}P\{^1H\}$ NMR (161 MHz, {$(CD_3)_2SO$}): δ 72.82; FT-IR data in KBr pellet (cm^{-1}): 674, 694, 731, 753, 786, 864, 954, 1025, 1136, 1176, 1265, 1353, 1409, 1452, 1572, 1612, 2977 and 3423. Anal. Calcd. $C_{60}H_{72}N_6O_{14}P_2Pd_6$: C, 40.00; H, 4.03; N, 4.66. Found: C, 40.21; H, 4.13; N, 4.22.

6.2: To a solution of **5.10**·2DMSO (20 mg, 0.013 mmol) in methanol, 1, 1 Ferrocenedicarboxylic acid (FDC-H) $(Cp)_2Fe(COOH)_2$ (7.21 mg, 0.026 mmol) in methanol was added. The mixture was stirred for 1 h, filtered and kept for crystallization. Dark orange-colored crystals were obtained in 10 days. Yield: 60% (13 mg) mp: 225-227 ^oC. FT-IR data in KBr pellet (cm^{-1}): 539, 669, 745, 953, 1021, 1141, 1198, 1257, 1317, 1364, 1401, 1437, 1490, 1588, 1652 and 3386. Anal. Calcd. $C_{42}H_{58}N_6O_{12}P_2Fe_2Pd_6$: C, 30.55; H, 3.54; N, 5.09. Found: C, 30.21; H, 3.73; N, 5.22.

Preparation of Tetrahedral Cage (DMSO⊂6.3): To a stirred solution of **5.10**·2DMSO (20 mg, 0.013 mmol) in methanol (2 mL) oxalic acid (3 mg, 0.027 mmol) was added and the solution was heated at 80 ^oC for 30 min to give an orange coloured precipitate. The resulting mixture was filtered and the residue was washed with 10 mL portions of methanol and dried under vacuum overnight. Yield 95% (34 mg, based on P). M.P. 232-234 ^oC, ^1H NMR (400 MHz, {$(CD_3)_2SO$}): δ 2.10 (br, 72H**,** C*H*$_3$), 2.56 (br, 12H, C*H*): $^{13}C\{^1H\}$ (100 MHz, {$(CD_3)_2SO$}): δ 31.20, 42.20, 51.38 : $^{31}P\{^1H\}$ NMR (161 MHz, {$(CD_3)_2SO$}): δ 73.57 ; FT-IR data in KBr pellet (cm^{-1}) : 3451, 2966, 2926, 1638, 1497,

1409, 1384, 1353, 1309, 1268, 1138, 1020, 802, 722, 659. Anal. Calcd for $C_{50}H_{90}N_{12}O_{29}P_4SPd_{12}$: C, 21.79; H, 3.29; N, 6.10. Found: C, 21.98; H, 3.58; N, 6.20. Single crystals suitable for X-ray diffraction analysis were obtained from slow evaporation of its solution in DMSO.

Preparation of the Guest free Tetrahedral Cage (6.3b): To a stirred solution of [$OP(NH^iPr)_3$], (20 mg, 0.09 mmol) in methanol (5 mL) palladium acetate $Pd(OAc)_2$ (60 mg, 0.27 mmol) and oxalic acid (12 mg, 0.14 mmol) was added and the solution was heated at 60 ^oC for 30 min to give an orange coloured precipitate **6.3a**. The resulting mixture was filtered and the residue was washed with 10 mL portions of methanol and dried under vacuum overnight to yield the guest free cage **6.3b**. Yield 90% (231 mg, based on P). M.P. 228-230 ^oC, ^1H NMR (400 MHz, {$(CH_3)_2CO$}): δ 1.73 (d, 72H, C*H*$_3$), 2.02 (m, 12H, C*H*): $^{13}C\{1H\}$ (100 MHz, {$(CH_3)_2CO$}): δ 25.78, 54.10, 174: $^{31}P\{1H\}$ NMR (161 MHz, {$(CH_3)_2CO$}): δ 72.82; FT-IR data in KBr pellet (cm^{-1}) : 3457,2962, 2933, 1618, 1507, 1429, 1394, 1363, 1313, 1262, 1151, 1080, 819, 733 and 657. Anal. Calcd. for $C_{48}H_{84}N_{12}O_{28}P_4Pd_{12}$: C, 21.53; H, 3.16; N, 6.28. Found: C, 21.71; H, 3.19; N, 6.18.

General procedure for preparation of Guest⊂6.3 (Guests: Benzene, CCl_4, $CHCl_3$, CH_2Cl_2 and THF) and Guest⊄6.3 (toluene, chlorobenzene, fluorobenzene and cyclohexane): DMSO⊂**6.3** (10 mg, 0.004 mmol) was dissolved in 2 mL of the guest solvent and stirred at a warm temperature of about 35-40 °C until the solvents were evaporated to dryness. Crystalline orange colored solid was recovered from the reaction vessel. Single crystals suitable for X-ray diffraction were obtained in a direct reaction involving **5.10**·2DMSO (10 mg, 0.07 mmol) and oxalic acid (1.2 mg, 0.013 mmol) in the corresponding solvents by slow-evaporation. In case of CCl_4 few drops of methanol was added for getting a homogeneous solution and the obtained crystals were again re-crystallized from CCl_4/benzene mixture for a better X-ray data.

C_6H_6⊂6.3: Yield 90% (9.5 mg, based on P). M.P. 224-226 ^oC, ^1H NMR (400 MHz, {$(CH_3)_2CO$}): δ 1.73 (d, 72H**,** C*H*$_3$), 2.02 (m, 12H, C*H*) 7.32 (s, 6H, C*H*) : **^{13}C** {^1H}} (100 MHz, {$(CH_3)_2CO$}): δ 26.90, 54.53, 133.74, 174.44: ^{31}P NMR (161 MHz, {$(CH_3)_2CO$}): δ 72.80; FT-IR data in KBr pellet (cm^{-1}) : 3423, 2964, 2924, 1791, 1635, 1353, 1278, 1135, 1016, 947, 858, 804, 727, 651. Anal. Calcd. for $C_{54}H_{90}N_{12}O_{28}P_4Pd_{12}$: C, 23.53; H, 3.29; N, 6.10. Found: C, 23.91; H, 3.68; N, 6.13.

CCl_4⊂6.3: Yield 75% (7.5 mg, based on P). M.P. 225-227 ^oC, ^1H NMR (400 MHz, {$(CH_3)_2CO$}): δ 1.74 (d, 72H**,** C***H***$_3$), 2.02 (m, 12H, C*H*) : **^{13}C** {^1H}} (100 MHz, {$(CH_3)_2CO$}): δ 31.21, 54.58, 99.96, 174.86: ^{31}P NMR (161 MHz, {$(CH_3)_2CO$}): δ 72.83; FT-IR data in KBr pellet (cm^{-1}) : 3430, 2967, 2924, 2866, 1635, 1461, 1437, 1384, 1266, 1168, 1136, 1018, 951, 807, 723, 682. Anal. Calcd. for $C_{49}H_{84}N_{12}O_{28}P_4Cl_4Pd_{12}$: C, 20.78; H, 2.99; N, 5.94. Found: C, 20.61; H, 2.88; N, 6.01.

$CHCl_3$⊂6.3: Yield 80% (8 mg, based on P). M.P. 220-222 ^oC, ^1H NMR(400 MHz, {$(CH_3)_2CO$}): δ 1.75 (d, 27H**,** C*H*$_3$), 2.02 (m, 9H, C*H*) 7.30 (s, 1H, C*H*): **^{13}C** {^1H}} (100 MHz, {$(CH_3)_2CO$}): δ 27.63, 32.20, 79.67, 174.47: ^{31}P NMR (161 MHz, {$(CH_3)_2CO$}): δ 72.82; FT-IR data in KBr pellet (cm^{-1}) : 3428, 2965, 1701, 1405, 1353, 1260, 1134, 1016, 946, 783, 720, 649, 570. Anal. Calcd. for $C_{49}H_{85}N_{12}O_{28}P_4Cl_3Pd_{12}$: C, 21.04; H, 3.06; N, 6.01. Found: C, 21.23; H, 3.08; N, 6.13.

CH_2Cl_2⊂6.3: Yield 80% (8.5 mg, based on P). M.P. 228-230 ^oC, ^1H NMR(400 MHz, {$(CH_3)_2CO$}): δ 1.73 (d, 72H**,** C*H*$_3$), 2.02 (m, 12H, C*H*$_3$) 5.59 (s, 2H, C*H*$_2$) : **^{13}C** {^1H}} (100 MHz, {$(CH_3)_2CO$}): δ 31.15, 49.05, 53.34, 174.73: ^{31}P NMR (161 MHz, {$(CH_3)_2CO$}): δ 72.81; FT-IR data in KBr pellet (cm^{-1}) : 3424, 2965, 1717, 1617, 1401, 1352, 1320, 1135, 1016, 948, 858, 802, 727, 650, 520 . Anal. Calcd. for $C_{49}H_{86}N_{12}O_{28}P_4Cl_2Pd_{12}$: C, 21.30; H, 3.14; N, 6.08. Found: C, 21.73; H, 3.48; N, 5.70.

THF⊂6.3: Yield 90% (8 mg, based on P). M.P. 203-205 ^oC, ^1H NMR(400 MHz, {$(CH_3)_2CO$}): δ 1.38 (br, 4H, C*H*$_2$), 1.74 (d, 4H, C*H*$_2$), 2.02 (m, 72H**,** C*H*$_3$), 3.80 (m, 4H, C*H*) : **^{13}C** {^1H}} (100 MHz, {$(CH_3)_2CO$}): δ 25.14, 29.68, 55.29, 67.19, 174.00: ^{31}P NMR (161 MHz, {$(CH_3)_2CO$}): δ 72.80; FT-IR data in KBr pellet (cm^{-1}) : 3438, 2926, 1726, 1637, 1460, 1384, 1355, 1280, 1136, 1072, 996, 806, 725, 679. Anal. Calcd. for $C_{52}H_{92}N_{12}O_{29}P_4Pd_{12}$: C, 22.71; H, 3.37; N, 6.11. Found: C, 22.35; H, 3.78; N, 6.43.

6.4: To a solution of **5.10**·2DMSO (20 mg, 0.013 mmol) in methanol, isonicotinic acid (INA-H) (C_6H_4NCOOH) (3.2 mg, 0.026 mmol) in methanol was added. The mixture was stirred for 1 h, filtered and kept for crystallization. Thin rod-shape yellow-colored crystals were obtained after 10 days. Yield: 40% (13 mg) mp: 206-208^oC. FT-IR data in KBr pellet (cm^{-1}): 675, 711, 729, 776, 862, 993, 1058, 1144, 1260, 1376, 1416, 1452, 1549, 1624, 2936 and 3448.

6.5: To a solution of **5.10**·2DMSO (20 mg, 0.013 mmol) in methanol, 2, 5 pyridinedicarboxylic acid (PDC-H) {$C_6H_3N(COOH)_2$} (13 mg, 0.0. mmol) in methanol

was added. The mixture was stirred for 1 h, filtered and kept for crystallization. Plate like yellow-colored crystals were obtained in 7 days. Yield: 90% (6.3 mg). mp: 212-215 ^{o}C. ^{1}H NMR (400 MHz, {(CD_3OD}): δ 1.73 (d, 18H**,** C*H*$_3$), 2.74 (m, 3H, C*H*), 7.89 (d, 3H, C*H*), 8.56 (d, 3H, C*H*), 9.02 (d, 3H, C*H*), 12.06 (s, 3H, COO*H*) : **^{13}C** {^{1}H}} (100 MHz, {($CH_3)_2CO$}): δ 26.40, 51.16, 80.24,140.18, 142.66, 143.88, 155.29, 174.24: ^{31}P NMR (161 MHz, {($CH_3)_2CO$}): δ 74.84. FT-IR data in KBr pellet (cm^{-1}): 501, 559, 641, 694, 751, 782, 883, 952, 1020, 1160, 1251, 1290, 1308, 1401, 1430, 1471, 1577, 1600, 1694 and 3470. Anal. Calcd. for $C_{30}H_{36}N_6O_{13}PPd_3$: C, 34.68; H, 3.49; N, 8.09. Found: C, 34.32; H, 3.68; N, 8.19.

6.6: *Method A:* To a solution of **5.10**·2DMSO (100 mg, 0.23 mmol) in methanol, 2, 5 pyrazinedicarboxylic acid dihydrate (PZDC-H) {$C_6H_2N_2(COOH)_2.2H_2O$} (88 mg, 0.23 mmol) in methanol was added. The mixture was stirred for 1 h, filtered and kept for crystallization. Cube like orange-color crystals were obtained after 10 days. *Method B*: To a solution of **6.6** (10 mg, 10 μmol) in methanol, **5.10**·2DMSO (21.1 mg, 15 μmol) in DMSO was added the mixture was stirred for 1 h, filtered and kept for crystallization. Cube like orange-color crystals were obtained. Yield: 70% (44 mg) mp: 222-225 ^{o}C.^{1}H NMR (400 MHz, {($CD_3)_2SO$}): δ 0.93 (d, 144H, C*H*$_3$), 2.81 (m, 24H, C*H*), 9.12 (2.81 (m, 24H, C*H*); **^{13}C** {^{1}H}} (100 MHz, {($CD_3)_2SO$}): δ 26.22, 53.35, 80.32, 139.89, 142.71, 142.85, 156.03, 174.34: ^{31}P NMR (161 MHz, {($CD_3)_2SO$}): δ 73.32; FT-IR data in KBr pellet (cm^{-1}): 530, 542, 672, 717, 878, 992, 1032, 1168, 1272, 1336, 1484, 1489, 1523, 1652, 1726 and 3461.

6.7: To a solution of **5.10**·2DMSO (20 mg, 0.013 mmol) in methanol, 2,5 pyrazinedicarboxylic acid dihydrate (PZDC-H) {$C_6H_2N_2(COOH)_2.2H_2O$} (163 mg, 0.23 mmol) in methanol was added. The mixture was stirred for 1 h, filtered and kept for crystallization. Cube like yellow color crystals were obtained after 10 days. Yield: 85% (12 mg). mp: 216-218 ^{o}C. ^{1}H NMR (400 MHz, {($CD_3)_2SO$}): δ 1.26 (d, 18H**,** C*H*$_3$), 2.12 (m, 3H, C*H*), 9.12 (s, 3H, C*H*), 9.32 (s, 3H, C*H*), 11.84 (s, 3H, COO*H*) : **^{13}C** {^{1}H}} (100 MHz, {($CD_3)_2SO$}): δ 26.90, 53.54, 80.44, 140.09, 142.91, 143.12, 157.24, 174.44: ^{31}P NMR (161 MHz, {($CD_3)_2SO$}): δ 72.27. FT-IR data in KBr pellet (cm^{-1}): 527, 555, 633, 707, 893, 902, 950, 1035, 1163, 1288, 1316, 1407, 1437, 1588, 1652 and 3461. Anal. Calcd. for $C_{30}H_{33}N_9O_{13}PPd_3$: C, 31.13; H, 3.19; N, 12.10. Found: C, 34.52; H, 3.15; N, 12.29.

6.2.3 Crystallography

Reflections were collected on a Bruker Smart Apex Duo diffractometer at 100 K using MoKα radiation (λ = 0.71073 Å) for **6.1**·CH_3OH·H_2O, **6.2**, DMSO⊂**6.3**, C_6H_6⊂**6.3**, $CHCl_3$⊂**6.3**, CH_2Cl_2⊂**6.3**, C_7H_8⊄**6.3**, C_6H_5Cl⊄**6.3** and C_6H_5F⊄**6.3, 6.4**, **6.5**·4DMSO, **6.6**·8H_2O and **6.7**. For CCl_4⊂**6.3**, the data was collected on a Bruker D8 Venture fitted with a micro focus detector at 100 K using CuKα radiation ((λ = 1.54178 Å). Structures were refined by full-matrix least-squares against F^2 using all data (SHELX).[13] Crystallographic data for all these compounds are listed in (Table A5.1, Appendix 5). All non-hydrogen atoms were refined aniostropically if not stated otherwise. Hydrogen atoms were constrained in geometric positions to their parent atoms. Crystals of **6.2**, C_6H_6⊂**6.3** and C_7H_8⊄**6.3** were weakly diffracting at higher angles and hence a 2θ = 50 ° cut-off was applied. Both the encapsulated and solvated DMSO molecules in the asymmetric unit of {DMSO⊂**6.3**·10DMSO·5H_2O} were disordered and freely refined isotropically over two positions using similar distances and similar U-restraints. The remaining solvated atoms in it were not precisely identified and hence were refined as partially occupied water oxygen atoms. We have also provided a better refined structure of this molecule (DMSO⊂**6.3**) with the solvated atoms in its packing cavity is treated as a diffuse contribution to the overall scattering without specific atom positions by SQUEEZE/PLATON. Similarly for C_6H_6⊂**6.3**, CH_2Cl_2⊂**6.3**, $CHCl_3$⊂**6.3,** C_7H_8⊄**6.3**, C_6H_5Cl⊄**6.3** and C_6H_5F⊄**6.3**, the encapsulated solvents were disordered and refined over two positions with SAME/SADI commands in the SHELX. For all the solvent encapsulated structures, except that of {DMSO⊂**6.3**·10DMSO·5H_2O}, the solvated atoms in the packing cavities were treated as a diffuse contribution to the overall scattering without specific atom positions by SQUEEZE/PLATON. However, for C_7H_8⊄**6.3**, and C_6H_5Cl⊄**6.3** one molecule of each of these solvents was kept in the packing cavity. A few C, N and O atoms in some of the structures exhibited slightly bad ellipsoids and were refined with partial isotropic parameters. In case of **6.7** the solvated atoms in the molecule were treated as diffuse contribution to the overall scattering without specific atom positions by SQUEEZE/PLATON.

6.2.4 Low Pressure Gas Sorption Measurements

Low pressure gas sorption measurements were performed using Micromeritics 3-Flex surface area and porosimetry analyzer. All the gasses used were of high purity

(99.9999%). To get all isotherms, about 50 mg of the sample **6.3b** was activated by heating the sample at 80°C under vacuum for 6 hours and was directly loaded to the analysis port. Prior to the start of analyses, the sample was again evacuated for 2 hours under turbo vacuum pump. N_2 (77K), H_2 (77K) and CO_2 (195K, 263K, 273K & 298K) sorption isotherms were obtained for this material. Heat of adsorption for CO_2 was calculated from CO_2 adsorption isotherms (263K, 273K & 298K) using DFT model; pore size distribution was calculated from 195K CO_2 isotherm using DFT model.

6.3 Result and Discussions

6.3.1 Synthesis

To demonstrate the general utility of ligand substitution strategy, we chose to employ the less bulky acetate-bridged hexanuclear Pd(II) cluster **5.8** or its derivative **5.10**.2DMSO in reactions with various mono- and di- carboxylic acids. The reaction of benzoic acid with the hexanuclear Pd-imido complex $\{Pd_3[(NR)_3PO](OAc)_3\}_2$ (**5.8**) in methanol resulted a complete replacement of the acetate groups with benzoate groups resulting in a hexameric complex of composition $\{Pd_3[(NR)_3PO](PhCOO)_3\}_2$ (**6.1**) (Scheme 6.1). Similar reaction of **5.8** with 1,1'-ferrocenedicarboxylic acid in DMSO gave the complex $\{Pd_3[(NR)_3PO](FDC)(OH)\}_2$, **6.2** (via **5.5b**), in which four acetate bridges were replaced with two ferrocene dicarboxylate (FDC) bridges and the remaining two positions were occupied by hydroxyl groups as observed in case of **5.10** (Scheme 6.2). The MALDI-TOF mass spectra of these compounds gave isotopic distribution of signals cantered at *m/z*=1891 and 1688, respectively, showing their existence in solution. The SC-XRD analysis of **6.1** and **6.2** confirmed the formation of the same prismatic structures indicating the retention of the parent structures of **5.8** or **5.10** when a mono-carboxylic acid or a cis directed dicarboxylic acid with suitable spacer groups is employed in ligand substitution reactions.

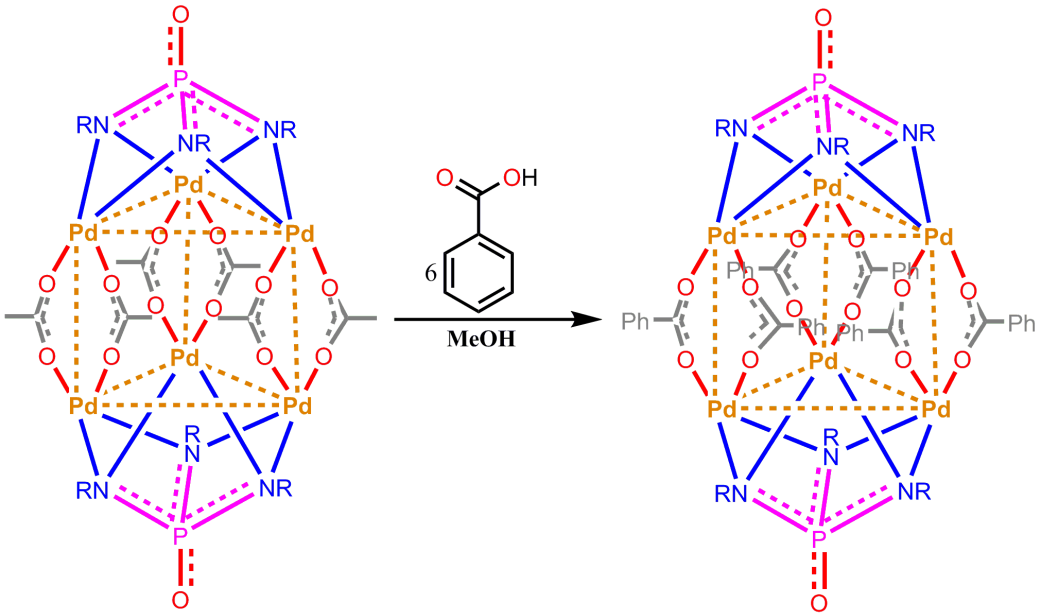

Scheme 6.1: Synthesis of hexanuclear Pd(II) clusters of the tris(alkylimido) phosphate trianions.

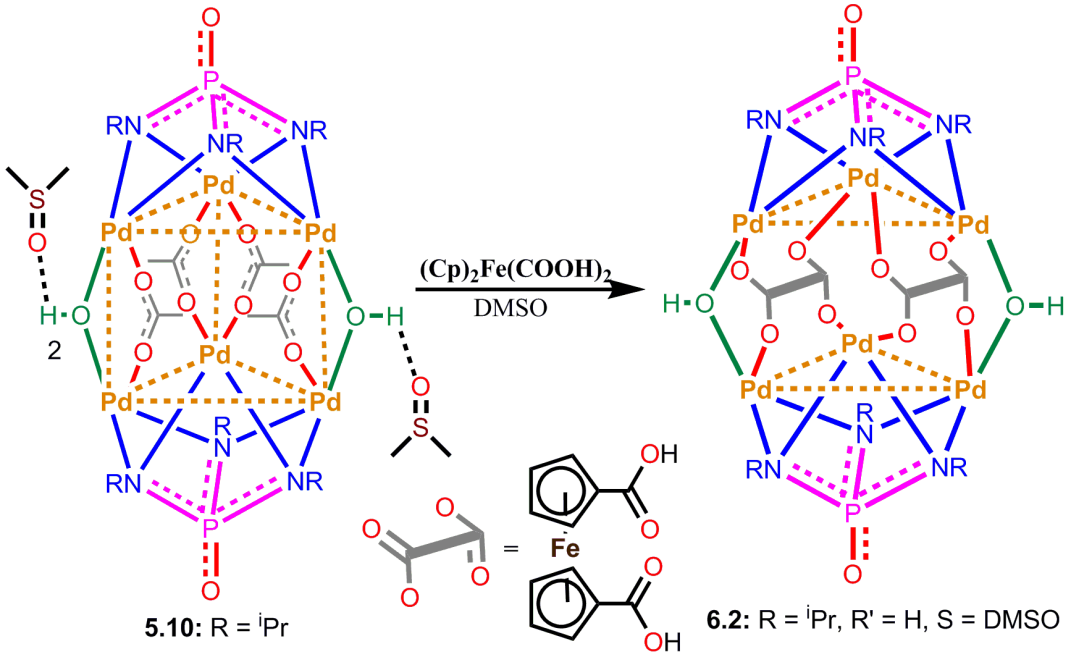

Scheme 6.2: Synthesis of the hetero-bimetallic hexanuclear Pd(II) cluster **6.2**.

Thus, from the structures of **5.6**-**5.10** and from **6.1** and **6.2** it is evident that the two oxygen atoms of a carboxylate group cannot act as a geminal-coordinating ligand to a single Pd(II) ion and hence a wide-angle chelating ligand is required for obtaining larger assemblies based on these imido-Pd(II) PBUs. Since the three Pd(II) atoms in these PBUs are separated by an angle of 60° with two vacant coordinating sites at 90° angle on

each of them, we envisioned that a wide-angle chelating linker dicarboxylate such as oxalate would lead to the formation of a larger assembly. Thus the reaction of the PBU precursor **5.10** in reaction with oxalic acid which acts a 180° bridging ligand gave the dodecanuclear neutral tetrahedral cage {$[Pd_3(N^iPr)_3PO]_4(C_2O_4)_6$}, **6.3**. Formation of the tetrahedral cage assembly can be understood to take place in a three component reaction involving the trianionic imido-phosphate $[(N^iPr)_3PO]^{3-}$, X^{3-}, ligands, Pd^{2+} ions and the oxalate linker ligands (L^{2-}) to generate the neutral cage, $[(Pd_3X)_4L_6]$ via the formation of a $[Pd_3X]^{3+}$ PBU (Figure 6.1).

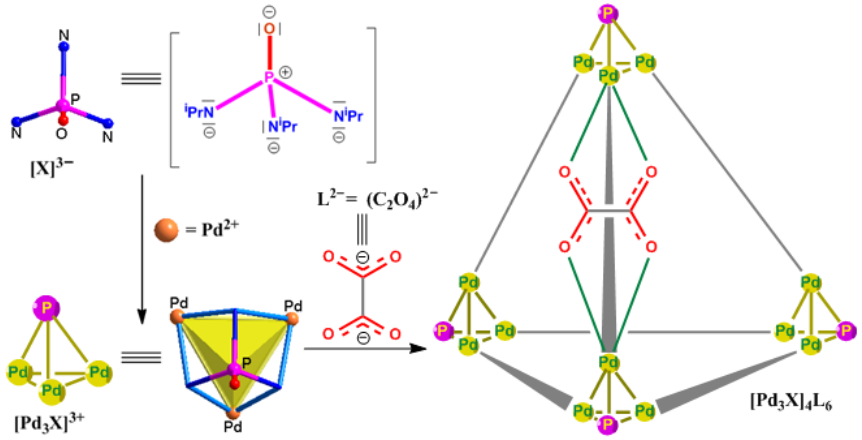

Figure 6.1: Schematic diagram showing the formation of the tetrahedral assembly **6.3**

The tetrahedral cage assembly of DMSO⊂**6.3** (⊂ denotes encapsulation) was synthesized in a facile ligand substitution reaction involving the cis-blocked hexanuclear Pd-imido complex **5.10**·2DMSO and oxalic acid in methanol (Scheme 6.3). The ^{31}P-NMR of DMSO⊂**6.3** in d_6-DMSO gave a sharp peak at δ = 73.6 ppm confirming the formation of a unique product. The MALDI-TOF mass spectrum of DMSO⊂**6.3** in methanol gave two isotopic distribution of signals centered at *m/z* = 2717 and 2795 corresponding to [**6.3**+K]$^+$ and [DMSO⊂**6.3**+K]$^+$ ions, respectively. The ^{1}H-NMR diffusion ordered spectroscopy (^{1}H-DOSY) of the bulk sample of DMSO⊂**6.3** in d_6-DMSO shows the presence of a single species in solution with a diffusion rate of log *D* = -9.74. The guest free cage of **6.3** can be obtained in a one pot reaction involving $[(NH^iPr)_3PO]$, $Pd(OAc)_2$ and oxalic acid in methanol. The obtained solid (**6.3a**) was filtered and dried in the vacuum for overnight to yield the guest free cage **6.3b** (Figures 6.2-6.5).

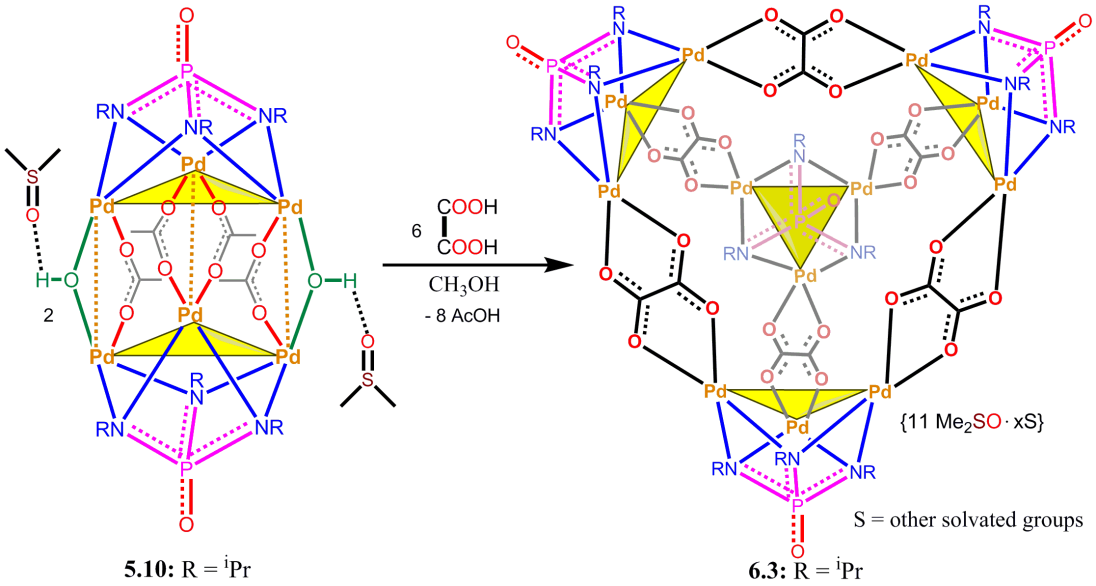

5.10: R = ^{i}Pr **6.3:** R = ^{i}Pr

Scheme 6.3: Synthesis of Tetrahedral cage molecule DMSO⊂**6.3**

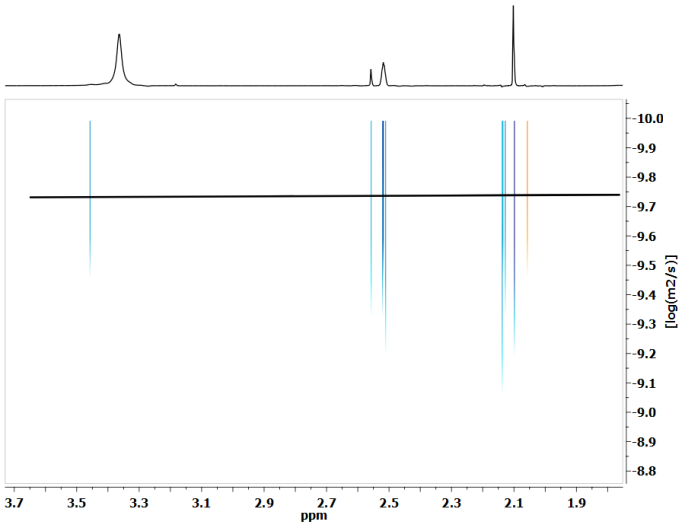

Figure 6.2: ^{1}H-2D- DOSY NMR spectrum of DMSO⊂**6.3** in d_6-Me_2SO

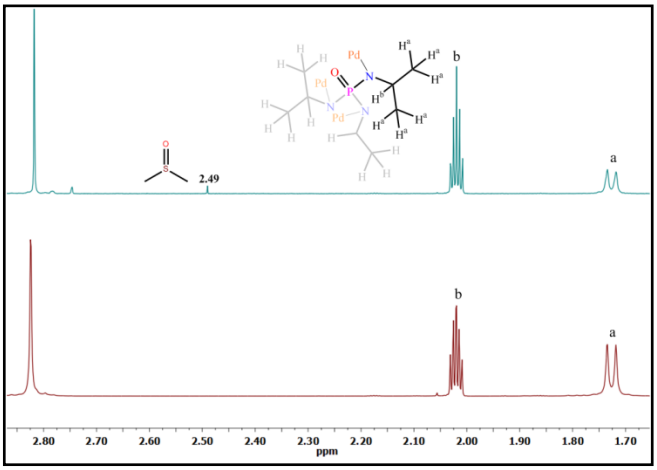

Figure 6.3: ^{1}H NMR spectra of DMSO⊂**6.3** and **6.3b**d_6-Me_2CO

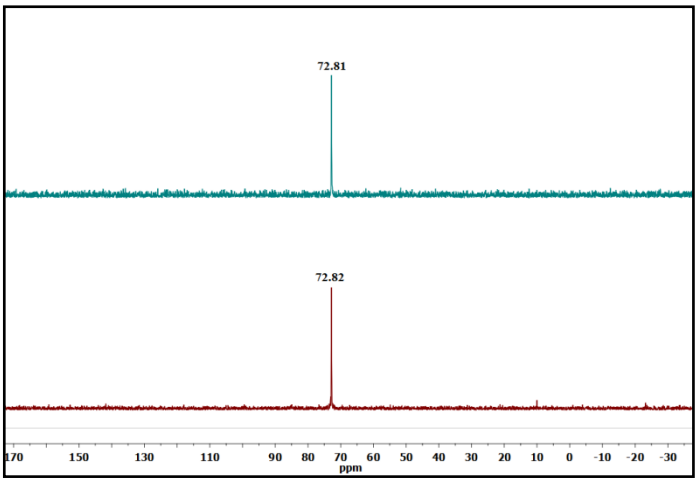

Figure 6.4: ^{31}P NMR spectra of DMSO⊂**6.3** and **6.3b** in d_6-Me_2CO

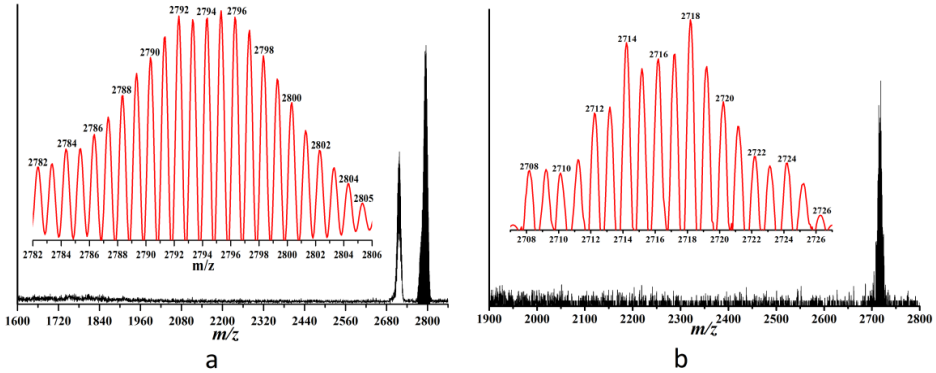

Figure 6.5: MALDI-TOF Mass spectrum of DMSO⊂**6.3** in MeOH (a) and **6.3b** in toluene showing only the guest free cage

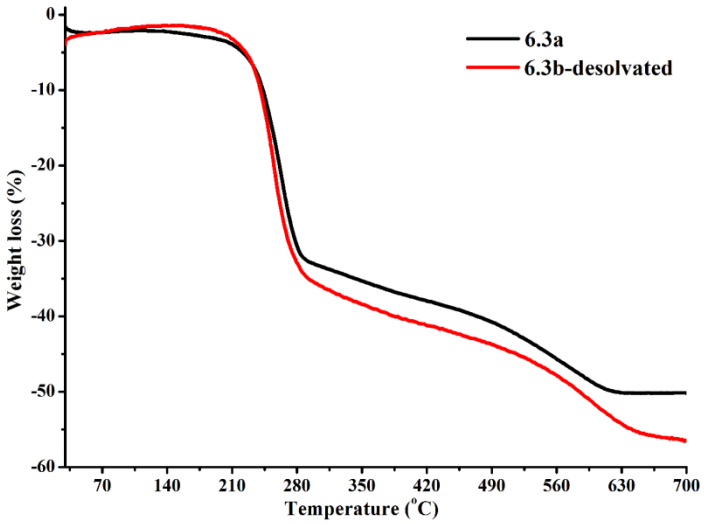

Figure 6.6: Thermogravimetric (TGA) curves of **6.3a** (black-line) and **6.3b** (red-line) showing the stability of the sample after desolvation.

An interesting barrel shaped assembly consisting of ten Pd(II) ions and four trianionic imido ligands was obtained when the PBU precursor **5.10**·2DMSO was treated with a non-chelating isonicotinic acid (INA-H) having linear linker functionalities. Formation of the decameric barrel shaped assembly $\{Pd_5[(N^iPr)_3PO]_2(INA)_2(OH)_2\}_2$, **6.4**, was obtained in a dimerization reaction via the initial displacement of the four acetate bridges in **5.10** with two INA ($C_6H_4NCOO^-$) linkers. A new $[Pd_5(OH)_2X_2]^{2+}$ PBU was then obtained by the elimination of a molecule of $Pd(OAc)_2$ in each of the two hexameric units to form the barrel shaped assembly. Formation of the decameric barrel shaped assembly again demonstrates the need of the chelating linker ligands in obtaining the polyhedral assemblies based on these Pd(II) containing PBUs.

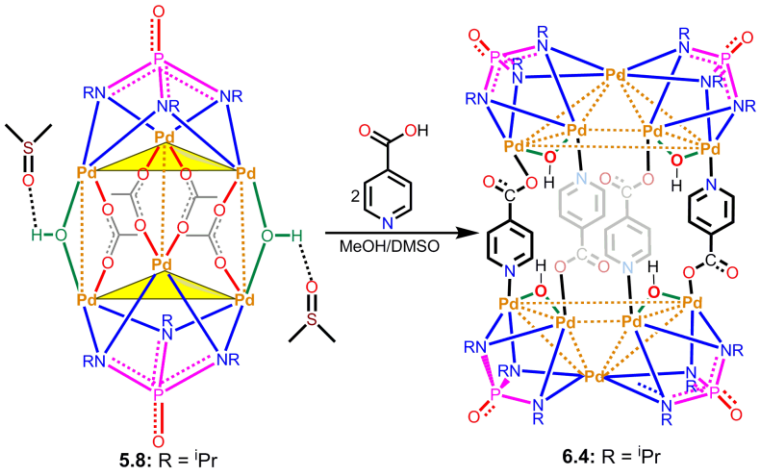

Scheme 6.4: Synthesis of decanuclear Pd(II) clusters of the tris(alkylimido) phosphate trianions.

Use of 2,5-pyridine dicarboxylic acid (PDC-H) in reaction with **5.10**·2DMSO gave only a trinuclear cluster assembly $\{[Pd_3(N^iPr)_3PO]_8(PDC)_{12}\}$, **6.5**, where the chelating 2-pyridyl carboxylate ends are attached to each of the three Pd(II) centres while the other carboxylic acid (at the 5-position) is un-reacted (Scheme 6.5). In order to obtain a larger assembly based on the 90° pyridine carboxylate chelating segment, we chose to employ the symmetric pyrazine-2,5-dicarboxylic acid (PZDC-H) in reaction with the PBU precursor **5.10**·2DMSO. Thus, the 1:3 reaction of **5.10**.2DMSO with PZDC-H in MeOH/DMSO gave a cubic cage assembly of composition $\{[Pd_3(N^iPr)_3PO]_8(PZDC)_{12}\}$, **6.6**. Formation of the cubic cage **6.6** can be understood as follows. Each of the $[Pd_3X]^{3+}$ PBU offer a three 60° acceptor sites which are connected by the chelating 120° linker PZDC units to yield a neutral cubic cage assembly of composition $\{[Pd_3X]_8L_{12}\}$. Interestingly, the cubic cage **6.6** can be obtained in a step-wise manner via the trinuclear

cluster fragment {[$Pd_3(N^iPr)_3PO](PZDC)_3$}, **6.7**. Thus the initial 1:6 reaction of **5.10**.2DMSO with PZDC-H gave **6.7** which upon further reaction with 1.5 eq. of **5.10**·2DMSO gave the cubic cage **6.6**.

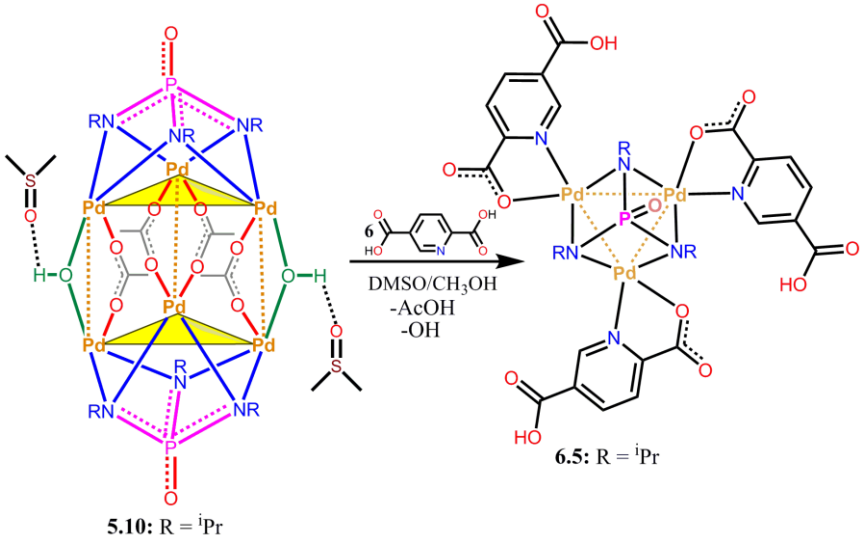

Scheme 6.5: Synthesis of trinuclear Pd(II) complex of the tris(alkylimido) phosphate trianions.

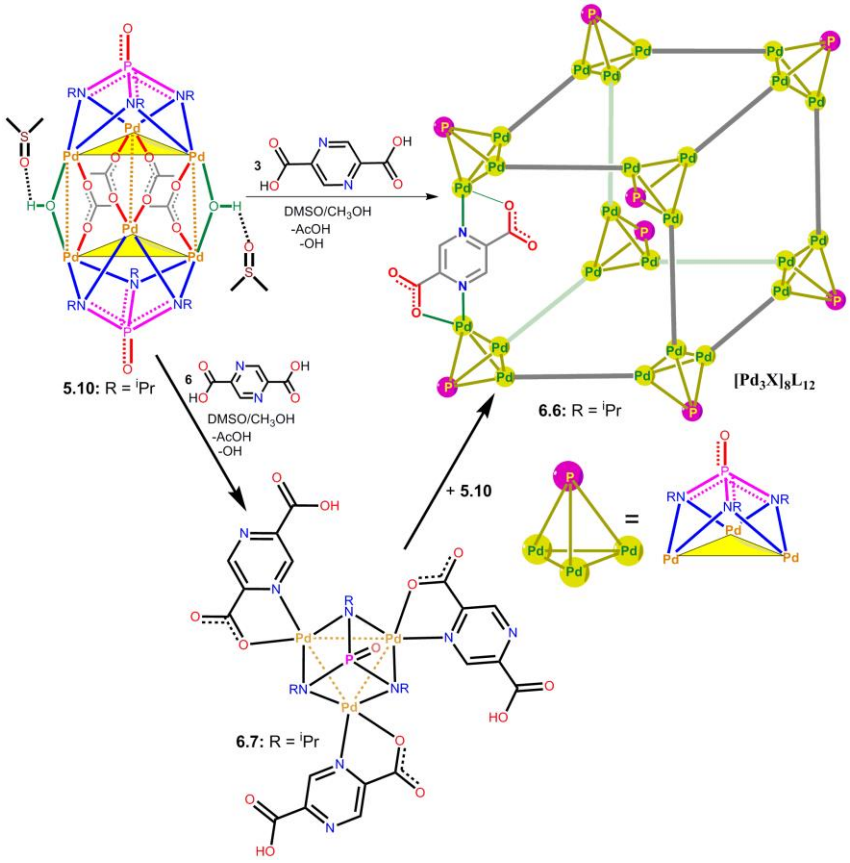

Scheme 6.6: Synthesis of tetradeceicos Pd(II) cage of the tris(alkylimido) phosphate trianions.

6.3.2 Crystal Structures

The crystal structure of **6.1**was solved in monoclinic space group *P2(1)/c* containing the whole molecule in the asymmetric unit (Figure 6.7). The molecular core in **6.1** consists of a hexameric Pd_6 cluster (similar to **5.8**) in a prismatic geometry sandwiched between two tris(imido)phosphate ligands **5.3**. The prismatic Pd_6 cluster can be viewed as a pair of planar Pd_3 subunits that are stacked upon each other in a closely eclipsed manner. Each imido-phosphate ligand acts as a hexadentate cisoidal ligand and holds the triangular Pd_3 unit in chelating fashion from one side of its plane. These individual Pd_3 units are further connected by six benzoate ligands completing the hexameric structure. Similar to the structure of **5.8**, these six benzoate ligands are grouped in a set of two and connect a pair of Pd(II) atoms from the adjacent triangular units. Thus these prismatic Pd_6 cluster assemblies contain three such Pd_2 pairs, and each of them is held together by two bridging benzoate ligands.

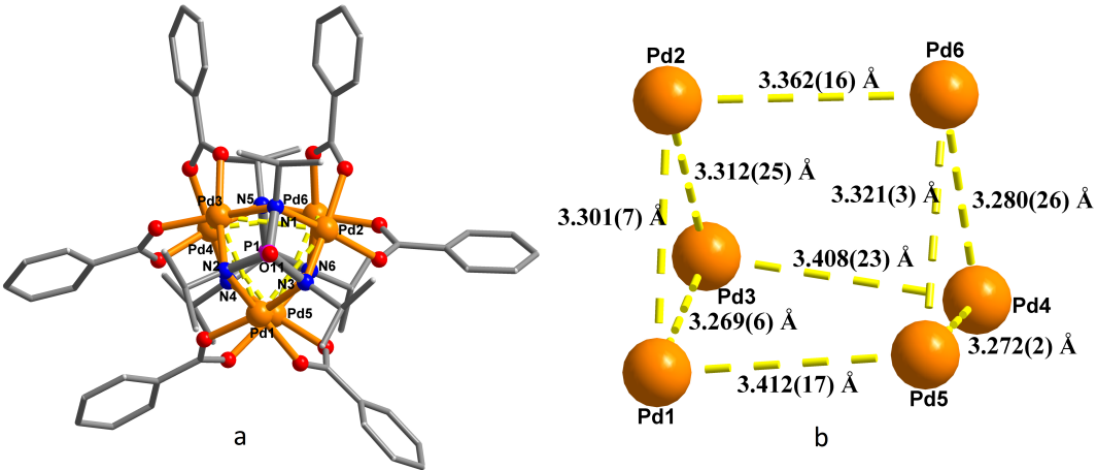

Figure 6.7: (a) Molecular structure of **6.1** showing the eclipsed arrangement of the two Pd_3 subunits; (b) view of the prismatic cluster core in **6.1**.

The hetero-bimetallic cluster **6.2** was crystallized as **6.2**.DMSO in the monoclinic space group *Ia* featuring whole molecule in the asymmetric unit. The core structures of **6.2** resemble closely that of the **5.10** containing two μ^2-bridging hydroxy groups except that in place of the four acetate bridges, two ferrocene dicarboxylate (FDC) bridged are present (Figure 6.8a). Two of the three Pd_2 pairs present in the prismatic cluster of **6.2** possess mixed-bridged environment with one FDC moiety and one hydroxyl unit each, while the second pair contains only FDC bridges. Further the two ferrocenyl moieties serve as linkers to the three Pd_2 pairs and provide additional support to the prismatic structure.

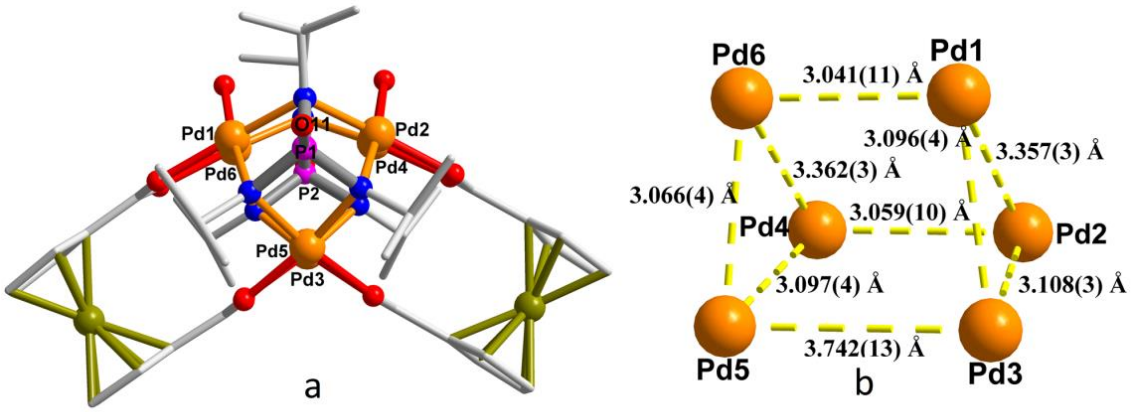

Figure 6.8: (a) Molecular structure of **6.2** showing the eclipsed arrangement of the two Pd_3 subunits; (b) view of the prismatic cluster core in **6.2**.

The molecular structure of the tetrahedral assembly DMSO⊂**6.3**·10DMSO·5H_2O was solved in orthorhombic space group *Cmcm*. Each vertex of the tetrahedral cage consists of a planar-cluster of three Pd(II) cations which are capped by three chelating N_{imido} sites from $[PO(N^iPr)_3]^{3-}$ (X^{3-}), trianions yielding a tetrahedral $[Pd_3X]^{3+}$ PBU. These PBUs are further connected by bridging interaction of the six oxalate (L^{2-}) ions and complete the tetrahedral cage assembly of composition $[(Pd_3X)_4L_6]$ (Figure 6.8 and 6.9). The building up of the tetrahedral cage assembly in **6.3** can be visualized as follows. The Pd(II) sites in these PBUs are located at an angle of nearly 60° (average 61.130(1)°) to each other and offers two cis-oriented coordinating sites at about 90° angle (average 82.427(1)°) each. Thus, each Pd_3-polygon acts as a 60° acceptor that is linked by the 180° chelating oxalate connector to form the tetrahedral MOP assembly. The wide-angle chelation of the oxalate bridges are perfectly compatible with the cisoidal sites at the Pd(II) atoms to give a neatly assembled tetrahedral cage. The metric parameters associated with Pd-Pd, Pd-O and Pd-N bonds in the $[Pd_3X]^{3+}$ PBU are closely matching with those found in **5.10**.2DMSO (average Pd-Pd = 3.123(1) Å, Pd-N = 2.024(5) Å, Pd-O = 2.058(4) Å and P-N = 1.688(5) Å). The average Pd-Pd distances within the triangular Pd_3-unit is 3.123(1) Å and is matching closely with those observed in **5.10**.2DMSO.

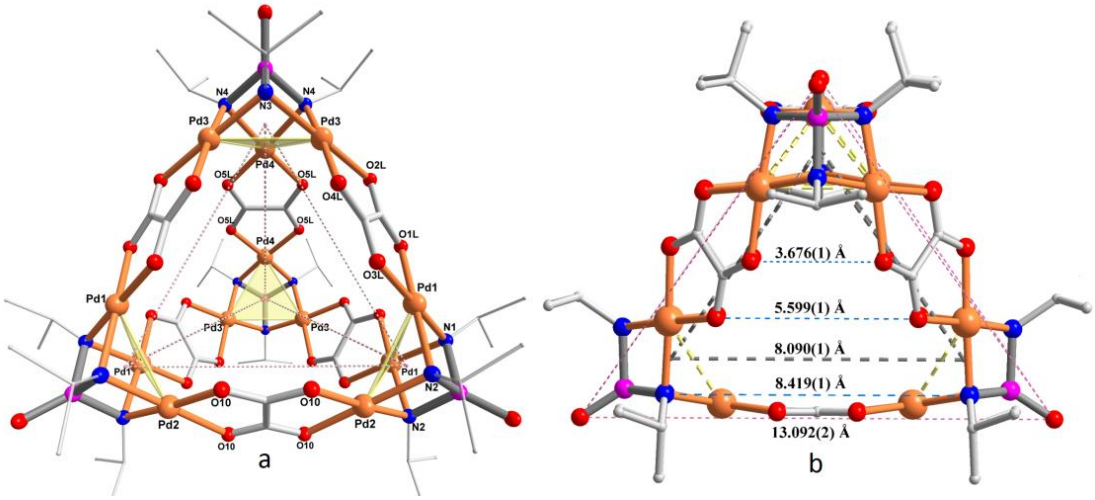

Figure 6.9: (a) Molecular structure of the cage assembly of **6.3** from SC-XRD. The encapsulated DMSO has been omitted for clarity. (b) View of the various portal, edge and central distances measured in the crystal structure of **6.3**.

The barrel shaped assembly of **6.4** was crystallized as **6.4**·6DMSO in the triclinic space group *P-1* having the one-half of the molecule and three solvated DMSO molecules in the asymmetric unit. The molecular core in **6.4** consists of a decameric assembly of ten Pd(II) ions consisting of two square pyramidal $[Pd_5(OH)_2X_2]^{2+}$ subunits that are connected by four anionic INA pillars resulting in a charge-neutral assembly. Each of the $[Pd_5(OH)_2X_2]^{4+}$ subunits consists of two corner-shared triangular segments, Pd1-Pd2-Pd5 and Pd3-Pd4-Pd5, that are cis-capped with the trianionic imido(phosphate), X^{3-}, moieties. As a result of the square-pyramidal arrangement, two varied types of coordination environments are found for the Pd(II) atoms in these pentameric subunits. The four Pd(II) atoms that constitute the square-plane (Pd1 to Pd4) consists of two N_{imido} sites, one coordination from μ^2-hydroxo group and one $N_{pyridyl}$ or carboxylate coordination from the INA ligand (these coordinations are reversed in the symmetry related counter parts in other Pd_5 subunit). On the other hand, the corner-shared Pd(II) ion (Pd5) located at the apical position is solely connected to four N_{imido} sites from two different imido-P(V) ligands. As a result of these unsymmetrical coordination environments, the Pd-Pd distances in **6.4** are spread over a broad range between 3.004(43) and 3.389(51) Å. The shorter ones are found at the pairs (Pd1-Pd5 and Pd3-Pd5) involving the corner sharing atom and the longer pairs are located away from it.

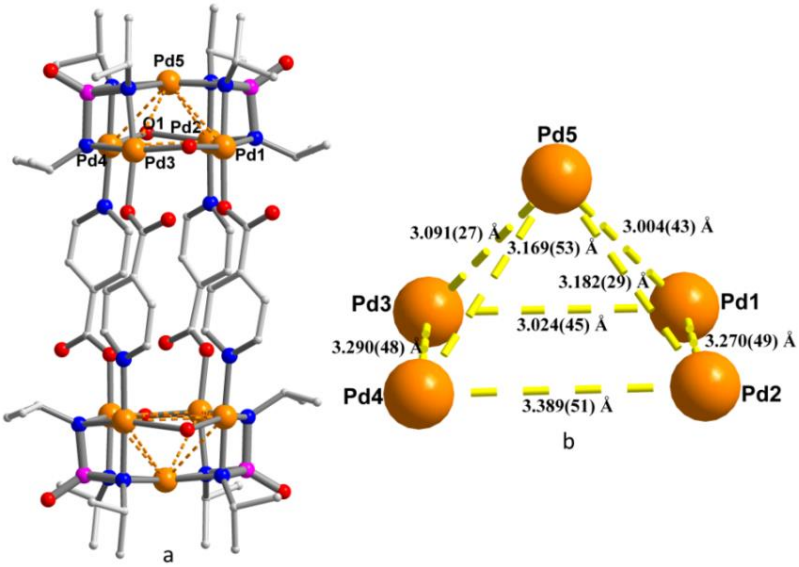

Figure 6.10: (a) Molecular structure of **6.4** showing the eclipsed arrangement of the two Pd_5 subunits; (c) view of the square-pyramidal cluster core in **6.4**.

The molecular structures of the trinuclear assemblies **6.5** and **6.7** are solved in the monoclinic space groups *P2(1)/c* and *P2(1)*, respectively. The core structures of **6.5** and **6.7** are both same consisting of a planar array of three Pd(II) ions cis-caped with the trianionic imido-phosphate ligand, X^{3-}, and the chelating pyridyl carboxylate subunits. The O-atom adjacent to N,O-chelating site as well as the coordinating groups (COOH in case of 6.5 and $N_{pyridyl}$ and COOH in case of **6.7**) that are located trans to N,O-chelates are un-coordinated. In **6.5** one of the three protons that are attached to the un-coordinated carboxylic acid is in an H-bonding interaction while the other two are H-bonded to the solvate molecules (water or methanol) located inside the packing pores. On the other hand, the packing structure of **6.7** shows the presence of a hexagonal pore structure which is symmetrically decorated with the free carboxylic acid groups (all the three) that interacts with the channel solvates. The void volume calculated by using Mercury software in **6.5** is 1182 $Å^3$ (25%) and in **6.7** is 861 $Å^3$ (44.5%). In addition to their packing structural variations, these trinuclear assemblies are potential synthons as metallo-ligands for the construction of hetrometallic porous assemblies.

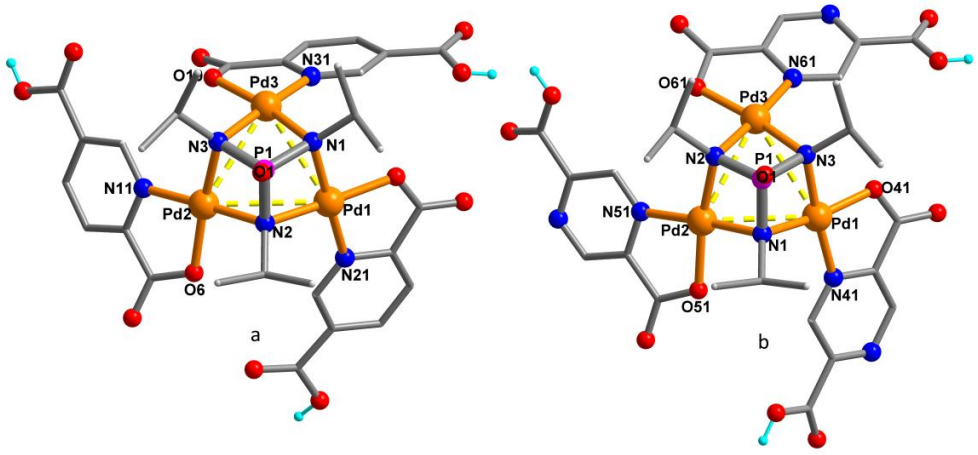

Figure 6.11: Molecular structure of (a) **6.5** and (b) **6.7**.

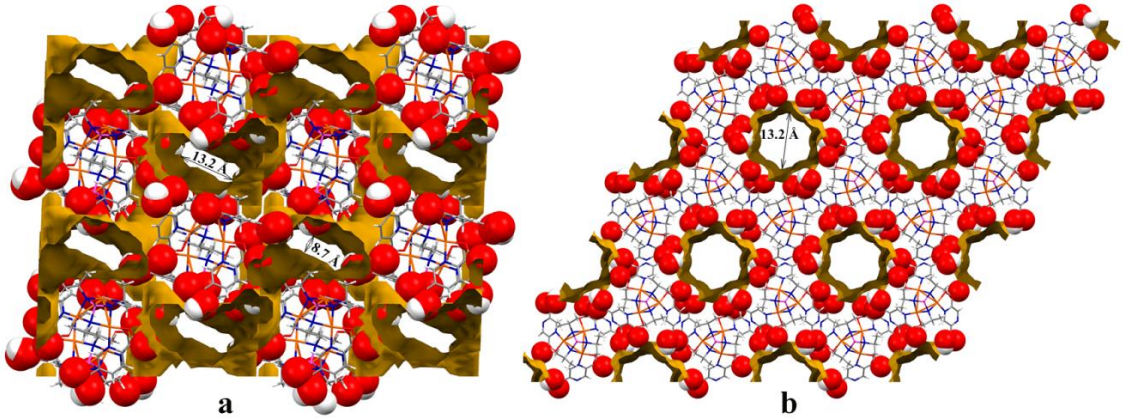

Figure 6.12: Packing diagram of (a) **6.5** and (b) **6.7** along the 'b' axis showing the packing channels decorated with the free carboxylic acid groups.

The cubic MOP of **6.6** was solved in orthorhombic space group *Fddd* with its asymmetric unit consisting of one fourth of the cage assembly. As in the tetrahedral assembly of **6.3**, each of the cubic vertex consists of the tetrahedral $[Pd_3X]^{3+}$ PBU having a planar array of three Pd(II) ions cis-capped by three chelating N_{imido} sites from $[PO(N^iPr)_3]^{3-}$ (X^{3-}), trianions. These PBUs are further connected by bridging interaction of the 12 PZDC linker ligands (L^{2-}) ions to complete the cube cage assembly of composition $[(Pd_3X)_8L_{12}]$ (Figure 6.16). The building up of the cubic cage in **6.6** can be envisaged as follows. The three Pd(II) sites in these PBUs are considered as 60° acceptors (average 61.130(1)°) with two vacant cis-directed coordination sites on each of them at about angle of 90° (average 82.427(1)°). These PBUs are then linked by the 120° chelating PZDC connectors giving rise to the cubic MOP assembly **6.6**. The two ends of the PZDC ligands having a mixed $N_{pyridyl}$ and $O_{carboxylate}$ sites provides a perfect chelation for the cisoidal coordination sites at the Pd(II) ions in the cubic cage. The metric

parameters associated with Pd-Pd, Pd-O and Pd-N bonds in the $[Pd_3X]^{3+}$ PBU are closely matching with those found in **5.10**.2DMSO (average Pd-Pd = 3.194(1) Å, Pd-N = 2.061(1) Å, Pd-O = 2.076(1) Å and P-N = 1.648(0) Å). The average Pd-Pd distances within the triangular Pd_3-unit is 3.123(1) Å and is matching closely with those observed in **5.10**·2DMSO.

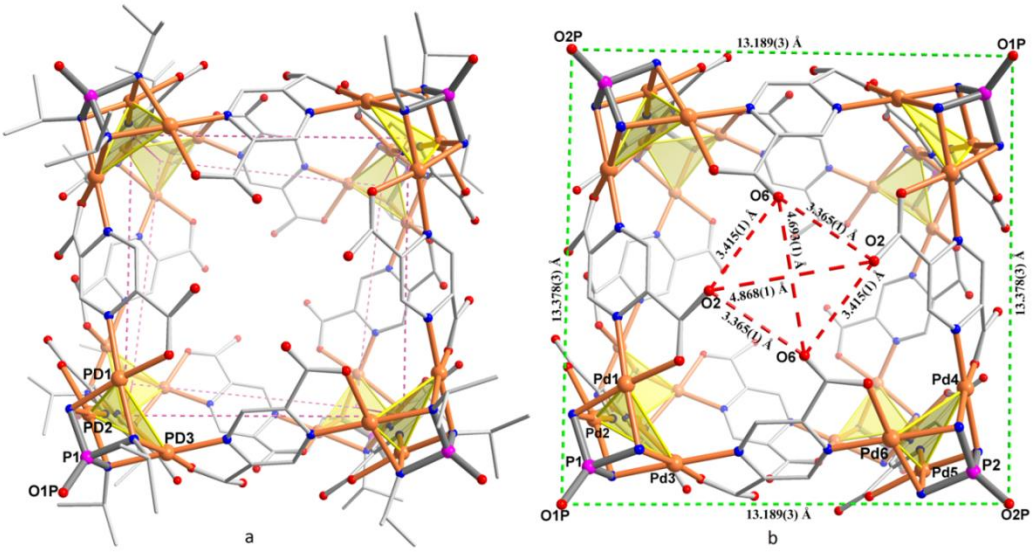

Figure 6.13: (a) Molecular structure of the cage assembly of **6.6** from SC-XRD. (b) View of the portal distances measured in the crystal structure of **6.6**.

6.3.3 Cavity volume calculations for 6.3 and 6.6

Owing to the presence of distinct molecular cavities in the tetrahedral (6.3) and cubic (6.6) assemblies, detailed pore volume calculations were preformed on their crystal structures. The crystal packing of DMSO⊂**6.3**·10DMSO·$5H_2O$ shows the presence of densely filled solvated groups which occupy ~ 49 % of the unit cell volume (6618 $Å^3$). The void space calculated in 6.7 is 33380 $Å^3$ which again amounts to about 49% of the unit-cell volume. A closer look at the packing structure of **6.3** reveals two distinct types of voids: first one is a smaller intrinsic cavity containing an encapsulated DMSO and the second one is the larger extrinsic pore located along the b-axis featuring at least 10 DMSO molecules per formula unit (Figure 6.15). Though, the packing structure of the cubic cage **6.6** also shows the presence of the intrinsic as well as extrinsic cavities, the solvate molecules present in them could not be located due to its huge solvent accessible volume in the crystal lattice. The intrinsic cavities in **6.3** and **6.6** were determined by MSROLL software calculations[14] with a fixed probe radius of 1.3 Å (Table 6.1)[15] which gave cavity volumes of 85.8 and 1009.3 $Å^3$, respectively. The corresponding cavity

surfaces in **6.3** and **6.6** are found to be 100.8 and 534.3 $Å^2$, respectively (Table 6.1 and 6.2). The portals of the cage are housed along the four faces of the tetrahedron with aperture distances ranging from 3.676(1) to 8.419(1) Å and the average outer edge-lengths calculated between the peripheral P=O groups measure at 13.093(1) Å (Figure 6.9b). The cubic cage shows symmetrical portal diameters along the six faces of the cube which measures at 4.781(1) Å (average). The narrow portal diameters in **6.6** can be attributed to the uncoordinated carboxylate oxygen atoms of the PZDC moieties that are projected towards the cubic face centers. Considering that some non-porous tetrahedral palladium clusters are known, the host structure of **6.3** represents a smallest cavity cage molecule with a definite volume of 85.84 $Å^3$.[16] Although the oxalate bridges have widely been employed for making extended solids in 1-, 2- and 3-dimensional structures,[17] only in few instances discrete molecular entities are reported based on this ligand.[18] Though, there are a few scattered reports in literature for the use of PZDC linkers,[19] construction of MOFs/MOPs based on this ligand is rather unexplored. In fact, the cubic cage of **6.6** could be the largest charge neutral cage known for the Pd/Pt self-assembled structures.

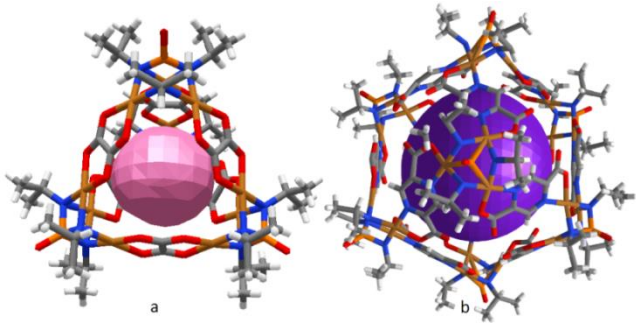

Figure 6.14: View of the intrinsic cavities inside (a) **6.3** and (b) **6.6** by a surface.

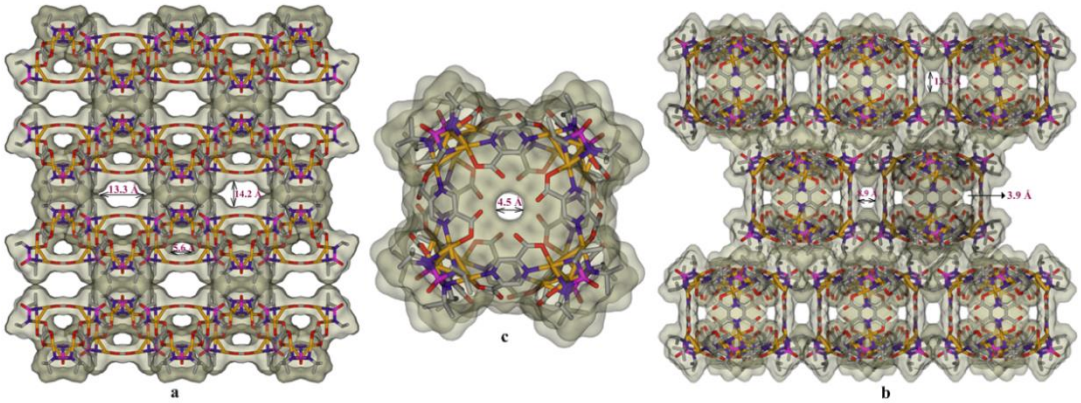

Figure 6.15: Surface overlay view of the packing structures of (a) **6.3** along the c-axis and (b) **6.6** along the b-axis showing the presence of two distinct types of voids. (c) View of intrinsic cavity in **6.6** along the c- axis.

Table 6.1: Volume and area calculated for intrinsic cavity of **6.3** from MSROLL calculations

Probe Radius (Å)	Surface Area ($Å^2$)	Volume ($Å^3$)
1.27	102.094	86.963
1.28	101.666	86.580
1.29	101.248	86.205
1.3	100.841	85.835
1.4	97.225	82.420
1.5	94.142	79.337

[a]The probe escapes from the cavity upon lowering the radius below 1.27 Å.

Table 6.2: Volume and area calculated for intrinsic cavity of **6.7** from MSROLL calculations

Probe Radius (Å)	Surface Area ($Å^2$)	Volume ($Å^3$)
1.3	534.328	1009.338
1.4	525.225	998.233
1.5	523.048	996.407

[a]The probe escapes from the cavity upon lowering the radius below 1.3Å.

6.3.4 Gas Sorption Analysis for 6.3

Furthermore, intrinsic porosity of **6.3** has been determined by gas adsorption studies for CO_2, N_2 and H_2 for the activated solvent free sample **6.3b**. From the adsorption profile it is evident that CO_2 exhibits a higher uptake capacity of 3.4 mmol/g at 195K compared to N_2 (2.4 mmol/g at 77K) and H_2 (1.9 mmol/g at 77K) (Figure 6.17). The better CO_2 uptake can be attributed to its effective interactions with the polar oxalate bridges in **6.3**. The pore size distribution calculated from the 195K CO_2 uptake profile indicates that the majority of the pores are centered on 5 Å diameters which are closely matching with the central portal distances of **6.3**. The BET and Langmuir surface areas in **6.3b** based on its 195K CO_2 uptake profile are calculated to be 293.24 (correlation coefficient = 0.9998) and 459.58 (correlation coefficient=0.9999) m^2/g, respectively. Further, based on the 263, 273 and 298 K adsorption data, the isosteric heat of adsorption (Q_{st}) for CO_2 in **6.3b** was calculated to be 37 kJ/mol (Figure 6.18). The gas adsorption studies for cubic cage assembly **6.6** are currently underway.

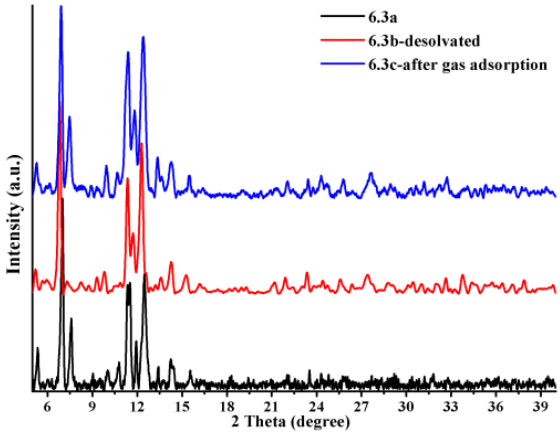

Figure 6.16: The PXRD patterns for the various samples of **6.3** showing the crystallinity and structural stability after gas adsorption.

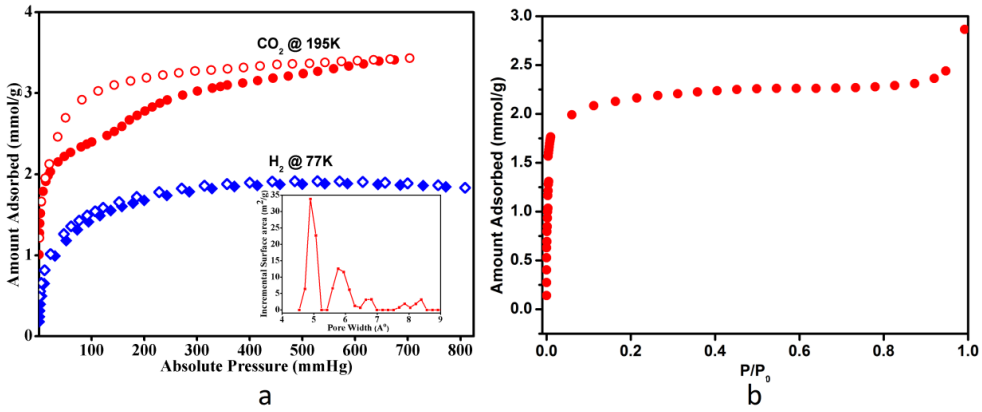

Figure 6.17: (a) Red: CO_2 adsorption at 195K and Blue: H_2 adsorption at 77K. Open symbols represent desorption. Inset: pore size distribution in **6.3** calculated from 195K CO_2 data. (b) N_2 adsorption at 77K, desorption branch has not been shown as it was too slow.

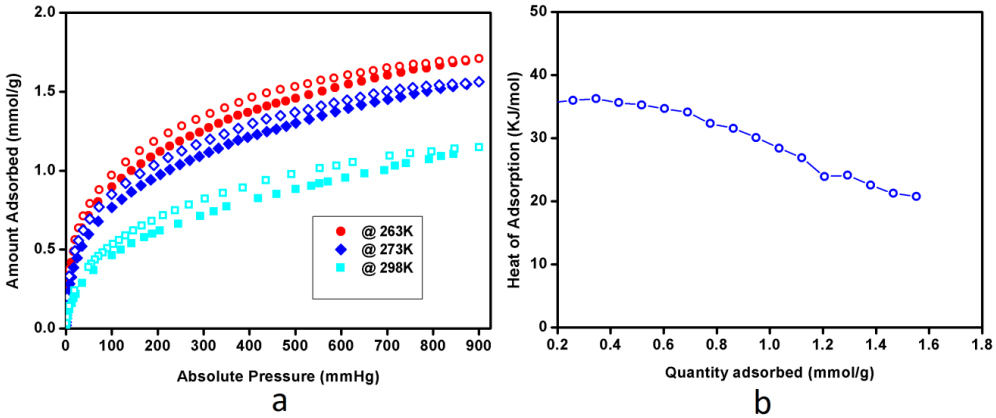

Figure 6.18: (a) CO_2 isotherms at three different temperatures. The open symbols in all cases represent desorption. (b) Heat of adsorption (Q_{st}) vs loading graph for CO_2 at **6.3**. Q_{st} for CO_2 adsorption on the cluster calculated from 263, 273, and 298 K isotherms using DFT modelling.

6.3.5 Guest Encapsulation Studies for 6.3

In view of the prominent intrinsic cavity present in **6.3**, inclusion studies for several neutral guest solvents were performed. Thus, DMSO⊂**6.3** readily dissolves in non-polar solvents such as benzene, toluene, halobenzenes, $CHCl_3$, CH_2Cl_2, CCl_4 and tetrahydrofuran (THF) forming the corresponding solvent encapsulated cage assemblies such as C_6H_6⊂**6.3**, CH_2Cl_2⊂**6.3**, $CHCl_3$⊂**6.3**, CCl_4⊂**6.3** and THF⊂**6.3** as orange colored powders (Table 6.3). The ^{1}H-NMR spectra of these samples show distinct peaks due to the guest solvents: δ = 7.32 (C_6H_6), 5.59 (CH_2Cl_2), 7.30 ($CHCl_3$) and 1.38 and 3.80 (THF) ppm (Figure 6.21). The MALDI-TOF mass spectra of all these guest included samples show prominent isotropic distribution of peaks corresponding to [Guest⊂**2**+K]$^+$ ions: *m/z* 2795 (C_6H_6), 2793 (CH_2Cl_2),[20] 2836 ($CHCl_3$), 2870 (CCl_4) and 2789 (THF) (Figure A5.1 to 5.10, Appendix 5).

Table 6.3: List of guest molecules screened for encapsulation within the host structure of **6.3** and the corresponding observations

Guest	**Surface Area [Å^2]**	**Molecular Volume [Å^3]**	**Encapsulation observed for cage 6.3**	**Crystal structure**
CH_2Cl_2	83.62	60.83	Yes	Yes
$CHCl_3$	99.58	74.68	Yes	Yes
DMSO	96.3	76.40	Yes	Yes
THF	105.33	85.92	Yes	No
CCl_4	115.38	88.69	Yes	Yes
C_6H_6	114.95	99.16	yes	Yes
C_6H_6F	120.77	103.83	No	Yes
C_6H_{12}	129.29	111.48	No	No
C_6H_5Cl	143.58	129.00	No	Yes
$C_6H_5(CH_3)$	149.16	134.77	No	Yes

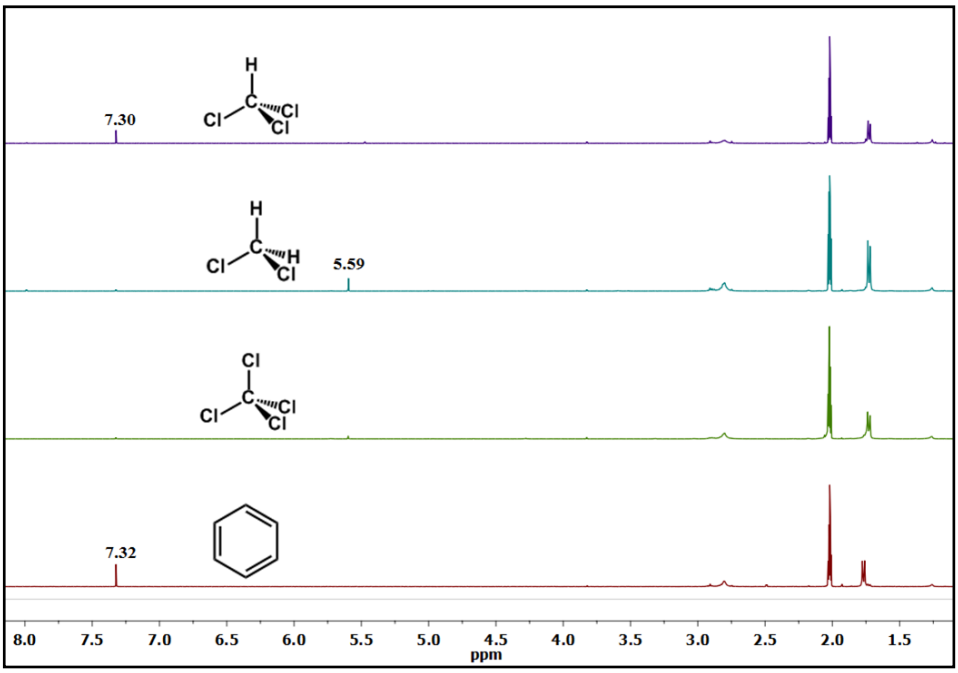

Figure 6.19: ^{1}H NMR spectra of $CHCl_3$⊂**6.3**, CH_2Cl_2⊂**6.3**, CCl_4⊂**6.3,** THF⊂**6.3** and C_6H_6⊂**6.3** in d_6-acetone

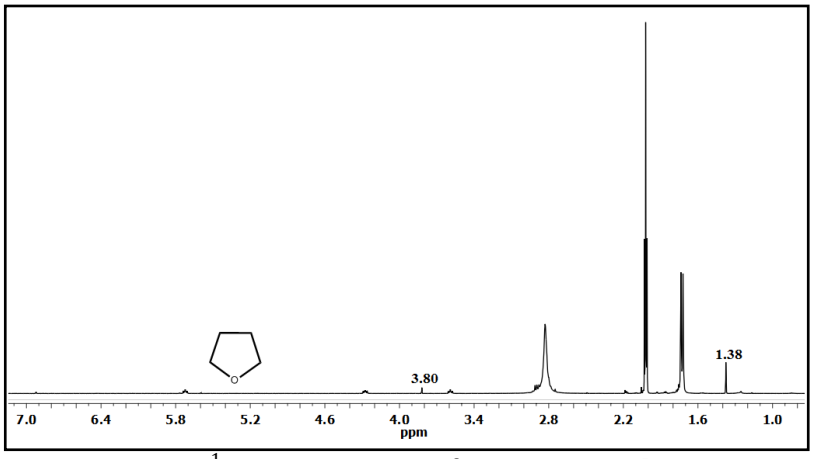

Figure 6.20: ^{1}H NMR spectra of THF⊂**6.3** in d_6-acetone

Further, SC-XRD analyses were performed on the crystals of **6.3** grown directly from the reaction mixture of **5.10**·2DMSO and oxalic acid in the respective solvents. The molecular structure of CCl_4⊂**2** shows that all the four chloride atoms are symmetrically housed at the center of the tetrahedral faces which facilitates a tight packing of CCl_4 inside **6.3**. Unlike CCl_4⊂**6.3**, $CHCl_3$⊂**6.3** and CH_2Cl_2⊂**6.3** reveal positional disorders for the guest molecules at the intrinsic cavity of **6.3** (Figure 6.21a). This suggests that the sizes of these two solvents are relatively smaller compared to the size of the cavity. This observation is consistent with the respective volumes of 60.83, 74.68 and 88.69 Å^3 for CH_2Cl_2, $CHCl_3$ and CCl_4 as the latter one is closer to the free volume of the empty cage. Similarly for the formation of C_6H_6⊂**6.3**, the symmetry and planarity of the phenyl ring

allows its lateral encapsulation through the cage portals although the volume of benzene is slightly larger (99.16 $Å^3$) than the measured cavity volume (Figure 6.25). However, crystals grown from toluene (V = 135 $Å^3$), C_6H_5F (V = 104 $Å^3$) and C_6H_5Cl (V = 129 $Å^3$) have shown that these solvents entered only at the extrinsic cavity and the DMSO present at the intrinsic cavity of **6.3** remains un-disturbed in all these instances. (Figure 6.24). Thus, it is apparent that guest molecules having volumes above 100 $Å^3$ are unable to enter the smaller intrinsic cavity and **6.3** acts as a molecular flask that can separate benzene from other substituted benzene derivatives and cyclohexane (V = 111.5 $Å^3$).

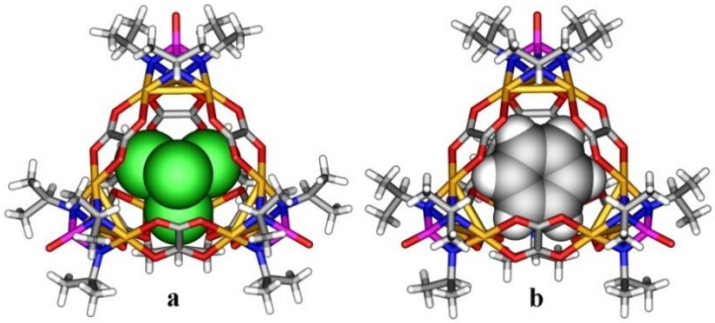

Figure 6.21: Molecular structures of (a) CCl_4⊂**6.3** (b) C_6H_6⊂**6.3**. The disordered solvated molecules are omitted for clarity.

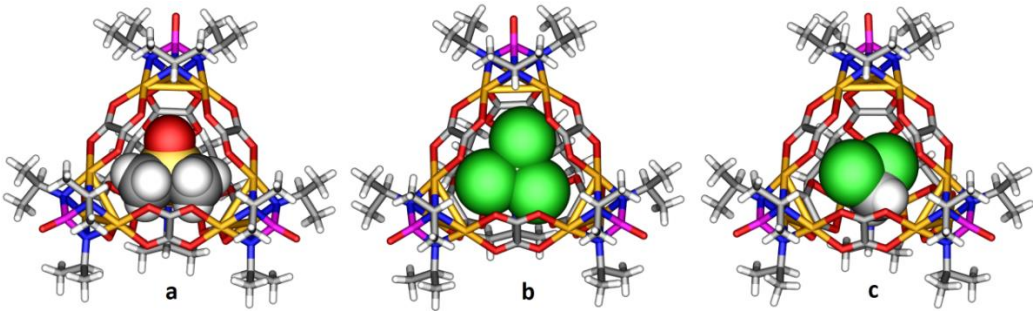

Figure 6.22: Molecular structures of (a) DMSO⊂**6.3** (b) $CHCl_3$⊂**6.3** (c) CH_2Cl_2⊂**6.3**. The disordered solvated molecules are omitted for clarity.

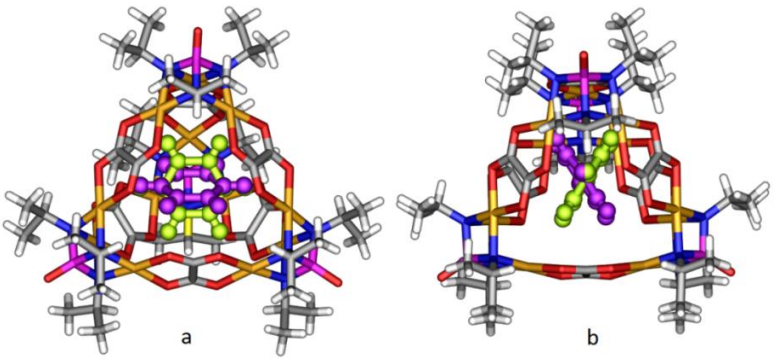

Figure 6.23: Molecular structure of C_6H_6⊂**6.3** along the (a) C_3-axis and (b) C_2-axis showing the disordered benzene guest molecule refined over two positions.

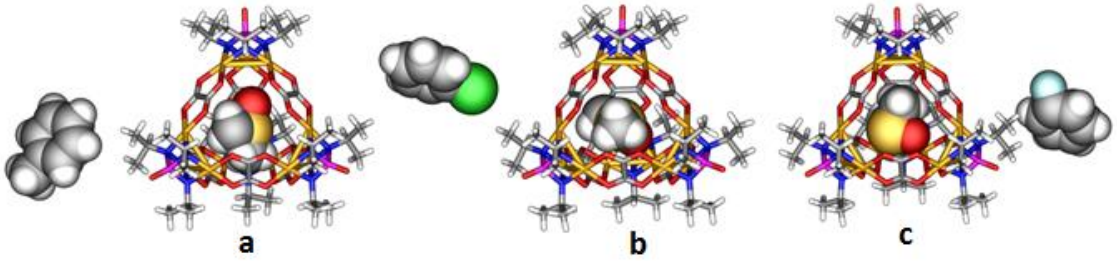

Figure 6.24: Molecular structures of (a) C_7H_8⊄**6.3** (b) C_6H_5Cl⊄**6.3** (c) C_6H_5F⊄**6.3** with the encapsulated DMSO

The selectivity of **6.3** for benzene and CCl_4 encapsulation over other competitive solvents such as CH_2Cl_2, $CHCl_3$ and THF has been derived from mass spectral, NMR and crystallographic analysis. Thus, treatment of DMSO⊂**6.3** with a mixture of equal amounts (0.5 mL) of all these five solvents gave C_6H_6⊂**6.3** as indicated by its characteristic peak centered at *m/z* = 2795 in the MALDI-TOF mass spectrum. Crystallographic experiments on the crystals (four different crystals were screened) grown from this solvent mixture confirm the exclusive formation of C_6H_6⊂**6.3**. Also, the ^{1}H-NMR of the obtained crystals in d_6-Me_2CO showed a signal at δ = 7.32 ppm due to C_6H_6⊂**6.3**. Analogous experiments with only chlorinated solvents showed the preferential encapsulation of CCl_4 over CH_2Cl_2 and $CHCl_3$ (Figure 6.25). Exchange experiments performed separately on CH_2Cl_2⊂**6.3** and $CHCl_3$⊂**6.3** with benzene and CCl_4 show a similar trend which again demonstrates the stronger binding affinities of the cage for both benzene and CCl_4. The poorly resolved mass-spectral profile of **6.6** precludes such solvent encapsulation studies for the cubic assembly. However, we are currently exploring the utility of the cage assembly as molecular containers for performing reactions inside its intrinsic cavity.

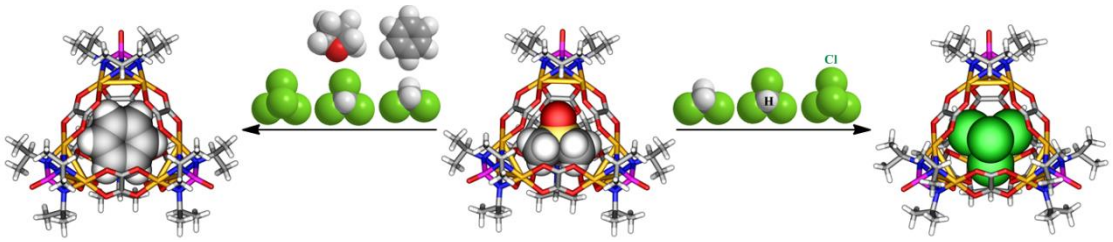

Figure 6.25: Selective Guest Encapsulation Studies

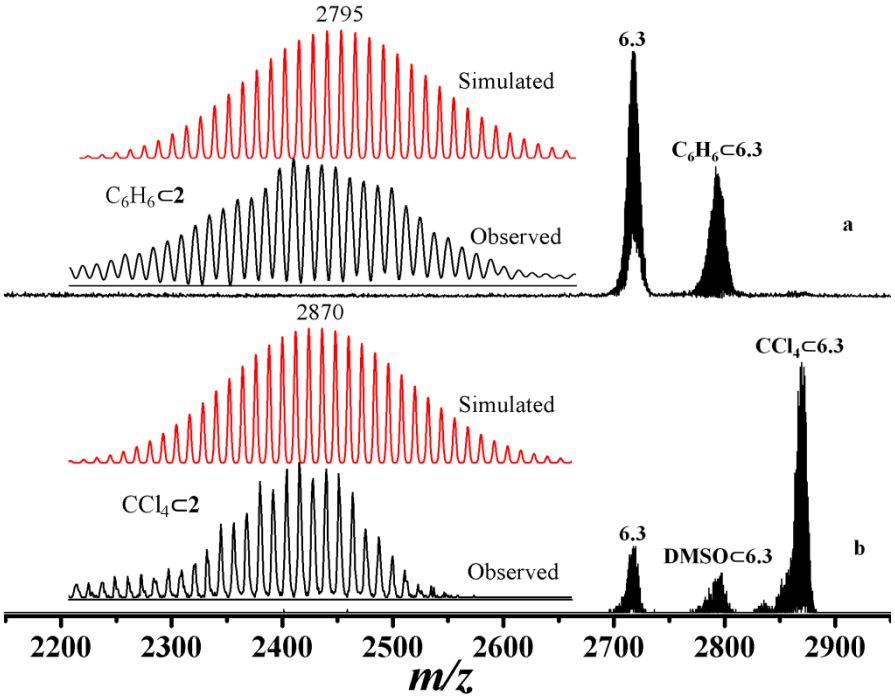

Figure 6.26: MALDI-TOF mass spectrum of the samples of DMSO⊂**6.3** treated with a mixture of (a) benzene, CCl_4, CH_2Cl_2, $CHCl_3$ and THF and (b) only chlorinated solvents. Insets show the corresponding Guest⊂**6.3** isotopic patterns.

6.4 Stability Studies of 6.3

In order to check the robustness the tetrahedral cage **6.3** for various applications we set out to check their stabilities viz., thermal stabilities, pH dependant stabilities and stability under competitive reaction conditions. Such studies for the cubic assembly are currently underway in our laboratory.

6.4.1Thermogravimetric analysis

The TGA graphs of all these solvent encapsulated assemblies show that an initial weight loss of about 10 % was observed for most solvents below 200 °C and in all these cases the onset of cage decomposition is observed around 240 °C.

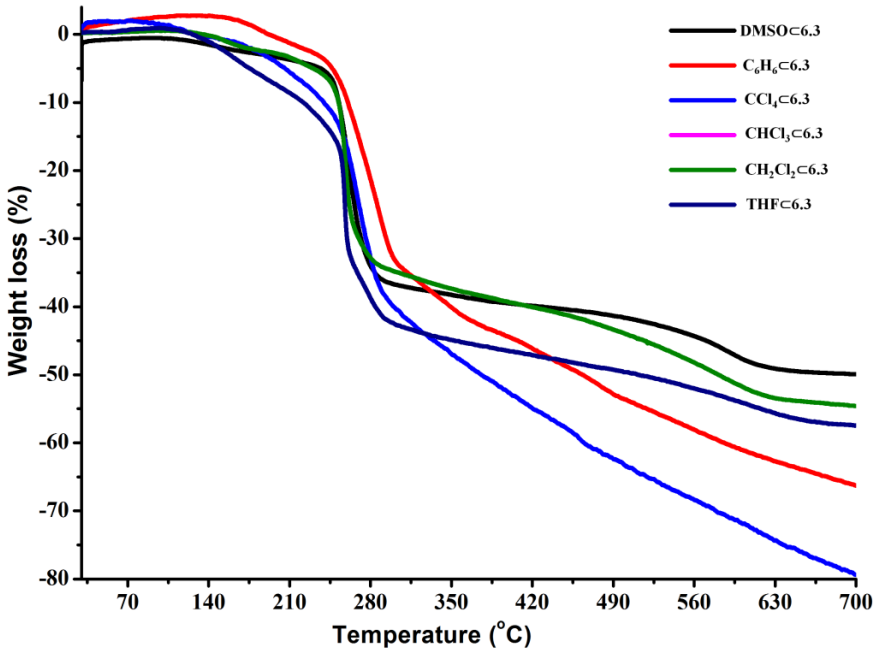

Figure 6.27: Thermogravimetric (TGA) curves of $CHCl_3$⊂**6.3**, CH_2Cl_2⊂**6.3**, CCl_4⊂**6.3** C_6H_6⊂**6.3** and THF⊂**6.3**

6.4.2 pH dependant stability studies

In a typical pH stability experiment 1 mg (0.0004 mmol) of DMSO⊂**6.3** was stirred with 0.5 mL of a buffer solution and 0.5 mL of acetone for 10-12 hours at 50°C. The resultant solution was subjected to mass spectral analysis. The MALDI-TOF mass spectra of DMSO⊂**6.3** treated with various pH buffer solutions is given in the figure 6.30. From the mass spectral analysis it is evident that the tetrahedral cage assembly of **6.3** was intact in the pH range between 3.5 and 9. However at pH 3.5 the concentration of the cage was very low as observed from very weak mass spectral signatures in the cage region. In fact no cage peak was observed for buffer solutions below pH 3.5. To further validate these observations we took ^{31}P-NMR spectra of these samples at slightly higher concentrations. For this purpose 3 mg (0.0012 mmol) of DMSO⊂**6.3** was stirred with 0.35 mL of a buffer solution and 0.4 mL of acetone for 10-12 hours at 50°C. The ^{31}P-NMR reveal that the peak due to the $[Pd_3X]^{3+}$ PBU was retained in the pH range between 4.5 and 9. However, this peak was absent for the sample treated with the pH = 3.5 solution (Figure 6.31). These experiments suggest that the cage structure is retained for a wide pH range and could be useful for encapsulation and controlled release of guest molecules. Spectral studies on samples treated with pH > 9 buffer solutions could not be performed due to poor solubility at the cage assembly in these solutions. The buffer solutions were prepared in 10 mL quantities in 200 mM concentrations as below.

The buffer solution of pH = 3.5 and 4.5 were prepared by mixing the appropriate quantities of NaOAc-AcOH solutions monitored by the pH meter. For the buffer solutions between pH = 6.0 and 8.0, Na_2HPO_4/NaH_2PO_4-NaOH mixtures were used in appropriate ratio monitored by the pH meter. The buffer solution of pH = 9 was prepared from K_2HPO_4 and NaOH in water.

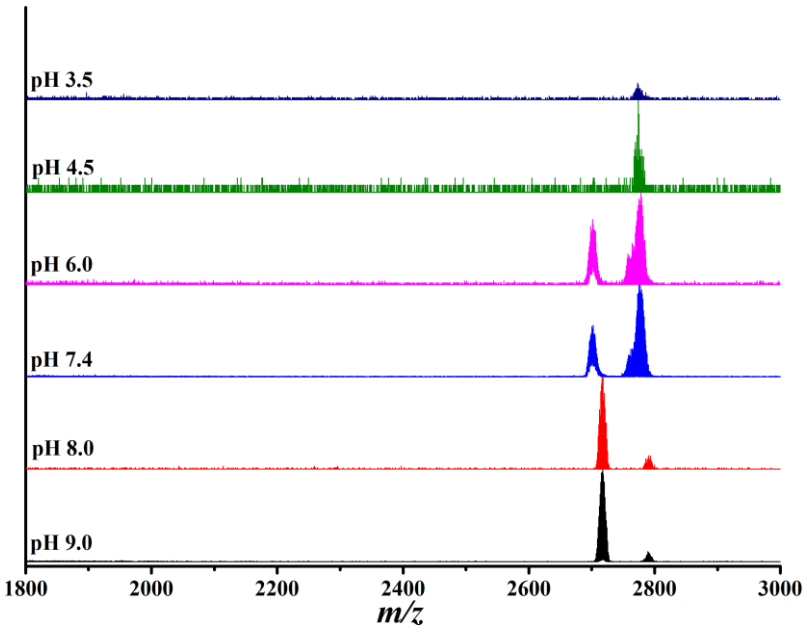

Figure 6.28: MALDI-TOF Mass spectra for DMSO⊂**6.3**in various pH buffer solutions showing the isotopic distribution of peaks due to **6.3** and/or DMSO⊂**6.3**.

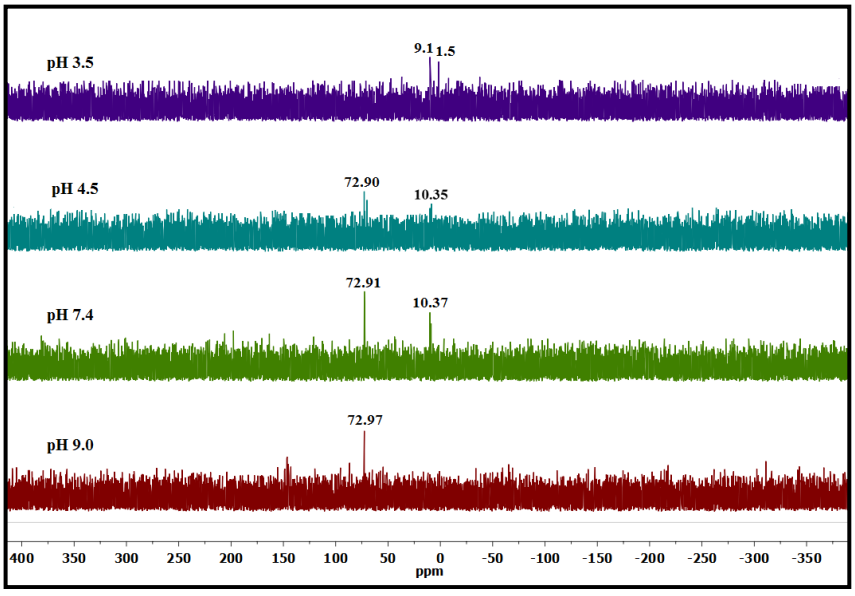

Figure 6.29: ^{31}P-NMR spectra for DMSO⊂**6.3** in various pH buffer solutions showing the signal due to the trianionic imido-phosphate trianion in the PBU segments around δ = 72.9 ppm. The noisy baseline is due to the lower concentrations of **6.3** in the buffer solutions.

6.4.3 Preferential formation of 6.3 under competitive conditions

In order to see the formation of the cage assembly of **6.3** in presence of an indirect oxalate source, we treated 1.2DMSO with $Fe_2(C_2O_4)_3 \cdot 6H_2O$. Thus to a stirred solution of **5.10**·2DMSO (10 mg, 0.007 mmol) in methanol (2 mL) and iron (III) oxalate hexa-hydrate (4 mg, 0.013 mmol) in methanol (2 mL) was added and the resulting mixture was heated for 30 min at 80 ^{o}C. Then the solvents were evaporated to dryness to yield a crude sample. The MALDI-TOF mass spectrum of this sample showed the formation of DMSO⊂**6.3** along with ferric acetate $\{Fe_3O(OAc)_6(H_2O)_3]OAc\}$[21]. Further confirmation was obtained from SC-XRD when this crude sample was crystallized from methanol/DMSO mixtures which gave the same structural parameter as that of DMSO⊂**6.3**·10DMSO·$5H_2O$.

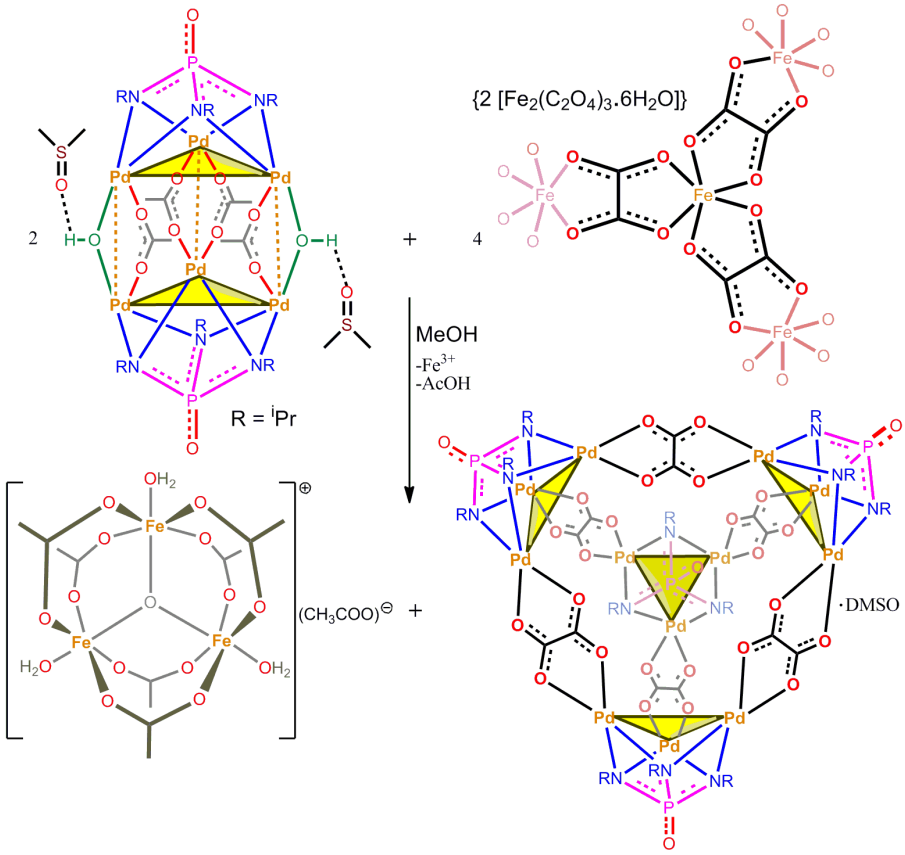

Scheme 6.7: Synthesis of the tetrahedral cage assembly of DMSO⊂**6.3** from an indirect oxalate source

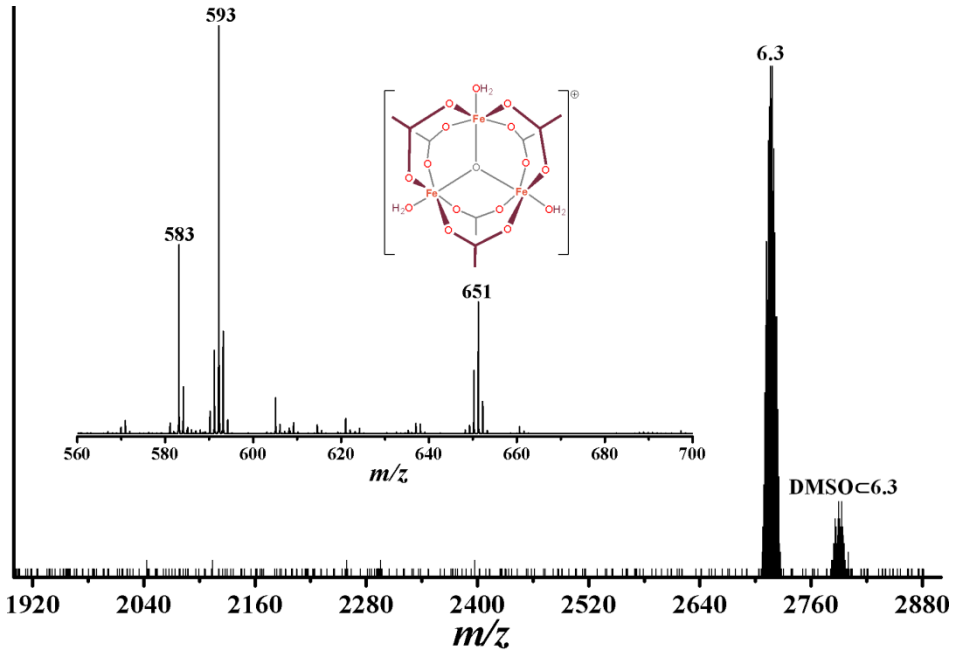

Figure 6.30: MALDI-TOF Mass spectrum of the reaction mixture of **5.10**.2DMSO, oxalic acid and $Fe_2(C_2O_4)_3 \cdot 6H_2O$ in methanol. Inset shows the partial mass spectrum of the sample in the *m/z* region between 500 and 700 showing the formation of ferric oxalate minor product $\{Fe_3O(OAc)_6(H_2O)_3]OAc\}$. The *m/z* centered at 651 corresponds to the cation $\{Fe_3O(OAc)_6(H_2O)_3]\}^+$ and *m/z* centered at 593 corresponds to the species $[Fe_3O(OAc)_6]^+$.

6.4.4 Theoretical Calculations

Further information pertaining to solvent binding energies and cage deformation energies for **6.3** was derived from theoretical calculations by taking coordinates from the corresponding crystal structures. Density Functional Theory (DFT) with dispersion corrected B97-D[22] functional has been employed for these calculations using Gaussian 09 software[23]. Single point energy calculations were performed on the crystal structures using LALN2DZ basis set for palladium atom in conjunction with the cc-pVTZ basis set (for all other atoms).

The binding energies for the host-guest systems as internal energies are calculated as follows:

$$\text{Binding energy} = E_{\text{host-guest}} - E_{\text{host}\ldots\ldots\text{guest}}$$

Where, $E_{\text{host-guest}}$ is the total energy of the system which comprised of guest located at the centre of the cage and $E_{\text{host}\ldots\ldots\text{guest}}$ is the total energy of the system where guest is at 30 Å away from the center of the cage.

To determine the structural changes with the encapsulation of guest in the host cage, we calculated the deformation energy[24] and it is written as

$$\text{Deformation energy} = E_{host} - E_{host}^{enc}$$

Where, E_{host} is the total energy of the optimized empty cage, E_{host}^{enc} is obtained by removal of the guest molecule from the host cage followed by a single point energy calculation on the corresponding structure.

Among the host-guest complexes that are screened, $C_6H_6\subset$**6.3** (-36.81 kcal/mol) shows more binding energy compared to other solvents as observed from the Table 6.4. Of the three chlorinated solvents tested, CCl_4 is more preferred over other solvents. This is attributed due to (a) the symmetric shape of CCl_4 compared to others and (b) the volume compatibility of CCl_4 with the host cage for efficient encapsulation. Further, to check the structural integrity of **6.3** upon guest encapsulation, cage deformation energies were calculated.[24] The obtained deformation energies are below 1 kcal/mol for all the host-guest systems studied, which are too low to cause any significant distortion to the parent assembly.

Table 6.4 Binding and deformation energies (kcal/mol) calculated using DFT/B97-D level of theory

Complex	Guest volume[25] (Å^3)	Binding energy	Deformation energy
DMSO⊂**6.3**	76.36	-36.11	0.47
$C_6H_6\subset$**6.3**	99.16	-36.81	0.32
$CCl_4\subset$**6.3**	88.69	-25.66	0.92
$CHCl_3\subset$**6.3**	74.68	-24.98	0.64
$CH_2Cl_2\subset$**6.3**	60.83	-22.50	0.78

6.5 Conclusions

In conclusion, we have demonstrated a novel ligand substitution strategy to build polyhedral clusters and cages utilizing the $[Pd_3X]^{3+}$ cationic PBUs and various linker carboxylate anions in which the $[(N^iPr)_3PO]^{3-}$ (X^{3-}) moiety acts as a novel trianionic cis-blocking agent for a planar Pd_3-motif. Although the imido P(V) moieties are well documented for their coordination chemistry and catalysis, use of these ligands as anionic cis-blocking agents in metallo-supramolecular cage chemistry has so far been unprecedented. Thus for the first time we have shown the formation of charge neutral Pd(II) polyhedral assemblies in tetrahedral and cubic topologies. The inherent stability of

these cage assemblies stems from the cooperative effects of chelating tripodal N_{imido} interactions and the chelating linker ligands at the Pd(II) centers. The intrinsic porosity of tetrahedral cage assembly was determined by gas adsorption studies showing a higher uptake capacity for CO_2 over N_2 and H_2. Guest encapsulation inside this cage assembly was examined with a large selection of solvents ranging from non-polar to polar and separate competitive binding experiments have shown the preferential encapsulation of benzene and CCl_4 over other related aromatic or chlorinated solvents. DFT calculations gave a highest binding-affinity for benzene and shows guest encapsulation keeps the cage structure intact. An unusual barrel shaped decameric assembly consisting of fused square-pyramidal polyhedral motifs and linear non chelating isonicotinate bridges were obtained, during these studies. Trinuclear imido-Pd(II) assemblies containing uncoordinated, N-donor and carboxylic acid functionalities were synthesized which are useful synthons for further self-assembly reactions. Syntheses of other kinds of Platonic or Archimedean polyhedra utilizing these new found $[Pd_3X]^{3+}$ PBUs and various suitable linker ligands is the current focus of research in our group.

6.6 References

(1) (a) Lehn, J.-M. *Science* **2002**, *295*, 2400-2403. (b) Stoddart, J. F. *Nat. Chem.* **2009**, *1*, 14-15. (c) McKinlay, R. M.; Cave, G. W.; Atwood, J. L. *Proc. Natl. Acad. Sci. USA* **2005**, *102*, 5944-5948.

(2) (a) Douglas, T.; Young, M. *Science* **2006**, *312*, 873-875. (b) Douglas, T.; Young, M. *Nature* **1998**, *393*, 152-155. (c) Uchida, M.; Klem, M. T.; Allen, M.; Suci, P.; Flenniken, M.; Gillitzer, E.; Varpness, Z.; Liepold, L. O.; Young, M.; Douglas, T. *Adv. Mater.* **2007**, *19*, 1025-1042. (d) Bhatia, D.; Surana, S.; Chakraborty, S.; Koushika, S. P.; Krishnan, Y. *Nat. Commun.* **2011**, *2*, 339. (e) MacGillivray, L. R.; Atwood, J. L. *Nature* **1997**, *389*, 469-472.

(3) (a) Hof, F.; Craig, S. L.; Nuckolls, C.; Rebek Jr., J. *Angew. Chem. Int. Ed.* **2002**, *41*, 1488-1508. (b) Wieser, C.; Dieleman, C. B.; Matt, D. *Coord. Chem. Rev.* **1997**, *165*, 93-161. (c) Baldini, L.; Casnati, A.; Sansone, F.; Ungaro, R. *Chem. Soc. rev.* **2007**, *36*, 254-266. (d) Szejtli, J. *Chem. Rev.* **1998**, *98*, 1743-1754. (e) Mecozzi, S.; Rebek Jr., J. *Chem. Eur. J.* **1998**, *4*, 1016-1022. (f) Liu, Y.; Hu, C.; Comotti, A.; Ward, M. D. *Science* **2011**, *333*, 436-440.

(4) (a) Pluth, M. D.; Bergman, R. G.; Raymond, K. N. *Science* **2007**, *316*, 85-88. (b) Swiegers, G. F.; Malefetse, T. J. *Chem. Rev.* **2000**, *100*, 3483-3538. (c) Wang, Z. J.;

Clary, K. N.; Bergman, R. G.; Raymond, K. N.; Toste, F. D. *Nat. Chem.* **2013**, *5*, 100-103. (d) Ajami, D.; Rebek Jr., J. *Proc. Natl. Acad. Sci. USA* **2007**, *104*, 16000-16003. (e) Schwarzmaier, C.; Schindler, A.; Heindl, C.; Scheuermayer, S.; Peresypkina, E. V.; Virovets, A. V.; Neumeier, M.; Gschwind, R.; Scheer, M. *Angew. Chem. Int. Ed.* **2013**, *52*, 10896-10899. (f) Mal, P.; Breiner, B.; Rissanen, K.; Nitschke, J. R. *Science* **2009**, *324*, 1697-1699. (g) Yoshizawa, M.; Klosterman, J. K.; Fujita, M. *Angew. Chem. Int. Ed.* **2009**, *48*, 3418-3438. (h) Clever, G. H.; Tashiro, S.; Shionoya, M. *Angew. Chem. Int. Ed.* **2009**, *48*, 7010-7012. (i) Cram, D. J.; Tanner, M. E.; Thomas, R. *Angew. Chem. Int. Ed.* **1991**, *30*, 1024-1027.

(5) (a) Cook, T. R.; Zheng, Y.-R.; Stang, P. J. *Chem. Rev.* **2012**, *113*, 734-777. (b) Pluth, M. D.; Bergman, R. G.; Raymond, K. N. *Acc. Chem. Res.* **2009**, *42*, 1650-1659. (c) Saalfrank, R. W.; Burak, R.; Breit, A.; Stalke, D.; Herbst-Irmer, R.; Daub, J.; Porsch, M.; Bill, E.; Müther, M.; Trautwein, A. X. *Angew. Chem. Int. Ed.* **1994,** *33*, 1621-1623. (b) Chakrabarty, R.; Mukherjee, P. S.; Stang, P. J. *Chem. Rev.* **2011**, *111*, 6810-6918. (c) Leininger, S.; Olenyuk, B.; Stang, P. J. *Chem. Rev.* **2000**, *100*, 853-908. (d) Fujita, M.; Tominaga, M.; Hori, A.; Therrien, B. *Acc. Chem. Res.* **2005**, *38*, 369-378. (f) Ronson, T. K.; Zarra, S.; Black, S. P.; Nitschke, J. R. *Chem. Commun.* **2013**, *49*, 2476-2490.

(6) (a) Stang, P. J.; Olenyuk, B. *Angew. Chem. Int. Ed.* **1996**, *35*, 732-736. (b) Fujita, M.; Oguro, D.; Miyazawa, M.; Oka, H.; Yamaguchi, K.; Ogura, K. *Nature* **1995**, *378*, 469-471. (c) Bar, A. K.; Raghothama, S.; Moon, D.; Mukherjee, P. S. *Chem. Eur. J.* **2012**, *18*, 3199-3209. (d) Lu, Z.; Knobler, C. B.; Furukawa, H.; Wang, B.; Liu, G.; Yaghi, O. M. *J. Am. Chem. Soc.* **2009**, *131*, 12532-12533.

(7) (a) Caulder, D. L.; Powers, R. E.; Parac, T. N.; Raymond, K. N. *Angew. Chem. Int. Ed.* **1998**, *37*, 1840-1843. (b) Caulder, D. L.; Raymond, K. N. *Acc. Chem. Res*. **1999**, *32*, 975-982. (c) Saalfrank, R. W.; Burak, R.; Breit, A.; Stalke, D.; Herbst-Irmer, R.; Daub, J.; Porsch, M.; Bill, E.; Müther, M.; Trautwein, A. X. *Angew. Chem. Int. Ed.* **1994,** *33*, 1621-1623. (d) Liu, G.; Ju, Z.; Yuan, D.; Hong, M. *Inorg. Chem.* **2013**, 52, 13815-13817. (d) Clegg, J. K.; Li, F.; Jolliffe, K. A.; Meehan, G. V.; Lindoy, L. F. *Chem. Commun*. **2011**, 47, 6042-6044.

(8) (a) Li, J. R.; Zhou, H. C. *Angew. Chem. Int. Ed.* **2009**, *48*, 8465-8468. (b) Li, J.-R.; Zhou, H.-C. *Nat. Chem.* **2010**, *2*, 893-898. (c) Ni, Z.; Yassar, A.; Antoun, T.; Yaghi, O. M. *J. Am. Chem. Soc.* **2005**, *127*, 12752-12753. (d) Chun, H. *J. Am. Chem. Soc.* **2008**, *130*, 800-801.

(9) (a) Murray, C. A.; Cardin, C. J.; Greenland, B. W.; Swift, A.; Colquhoun, H. M. *Inorg. Chem.* **2013,** *52*, 10424-10430. (b) Li, J.-R.; Yu, J.; Lu, W.; Sun, L.-B.; Sculley, J.; Balbuena, P. B.; Zhou, H.-C. *Nat. Commun.* **2013**, *4*, 1538.

(10) (a) Leininger, S.; Olenyuk, B.; Stang, P. J. *Chem. Rev.* **2000**, *100*, 853-908. (b) Seidel, S. R.; Stang, P. J. *Acc. Chem. Res.* **2002**, *35*, 972-983. (c) Fujita, M.; Tominaga, M.; Hori, A.; Therrien, B. *Acc. Chem. Res.* **2005**, *38*, 369-378. (d) Fujita, M.; Umemoto, K.; Yoshizawa, M.; Fujita, N.; Kusukawa, T.; Biradha, K. *Chem. Commun.* **2001**, 509-518.

(11) (a) Mukherjee, P. S.; Das, N.; Kryschenko, Y. K.; Arif, A. M.; Stang, P. J. *J. Am. Chem. Soc.* **2004**, *126*, 2464-2473. (b) Bar, A. K.; Gole, B.; Ghosh, S.; Mukherjee, P. S. *Dalton Trans.* **2009**, 6701-6704. (c) Bar, A. K.; Shanmugaraju, S.; Chi, K.-W.; Mukherjee, P. S. *Dalton Trans.* **2011**, *40*, 2257-2267.

(12) (a) Wu, D; Chen, A; Johnson, Jr., C. S; *Mag. Reson., J; Ser. A* **1995**, *115*, 260-264.

(b) Kerssebaum, R. DOSY and Diffusion by NMR. In *Users guide for XWinNMR 3.5, Version 1.0*; BrukerBioSpin GmbH: Rheinstetten, Germany, **2002**.

(13) Sheldrick, G. M. *ActaCrystallogr.***2008**, *A64*, 112-122.

(14) Connolly, M. L. *J. Mol. Graph*. **1993**, *11*, 139-141.

(15) Barbour, L. J. *Chem. Commun.* **2006**, 1163-1168.

(16) (a) Lawrence, S.; Williams, D., *Chem. Commun.* **1997**, 285-286. (b) Mingos, D. M. P.; Vilar, R., *J. Organomet. chem.* **1998,** *557* (1), 131-142. (c) Vilar, R.; Michael, D.; Mingos, P., *J. Cluster Sci.* **1996**, 7, 663-675.

(17) (a) Kawato, T.; Uechi, T.; Koyama, H.; Kanatomi, H.; Kawanami, Y. *Inorg. Chem.* **1984**, *23*, 764-769. (b) Rao, C. N. R.; Natarajan, S.; Vaidhyanathan, R. *Angew. Chem. Int. Ed.* **2004**, *43*, 1466-1496.

(18) Ling, J.; Wallace, C. M.; Szymanowski, J. E.; Burns, P. C. *Angew. Chem. Int. Ed.* **2010**, *49*, 7271-7273.

(19) (a) Cai, B.; Yang, P.; Dai, J.-W.; Wu, J.-Z. *CrystEngComm* **2011**, *13*, 985-991. (b) Pan, Y.; Ma, D.; Liu, H.; Wu, H.; He, D.; Li, Y., *J. Mater. Chem*. **2012**, *22*, 10834-10839. (c) Beobide, G.; Castillo, O.; Luque, A.; García-Couceiro, U.; García-Terán, J. P.; Román, P. *Inorg. chem.* **2006**, *45*, 5367-5382.

(20) A small amount of NaI is added to obtain a well resolved $[CH_2Cl_2 \subset \mathbf{2}+Na]^+$ ion signals.

(21) (a) Cotton F. A., Advanced Inorganic Chemistry, *Wiley, New York,* **1980**, 154-155. (b) Catterick, J.; Thornton, P. *Adv. Inorg. Chem. Radiochem.* **1977**, *20*, 291-362. (c) Cannon R. D.; White R. P., *Prog. Inorg. Chem.***1988**, *36*, 195-298.

(22) Grimme, S. *J. Comput. Chem.* **2006**, *27*,1787-1799.

(23) Frisch, M. J. *et al.* Gaussian 09, Revision C.01 Gaussian, Inc.: Wallingford, CT, **2010**.

(24) Ramya, K. R.; Venkatnathan, A. *Comp. Theo. Chem.* **2013**, *1023*, 1-4.

(25) Ronson, T. K.; Giri, C.; Beyeh, N. K.; Minkkinen, A.; Topić, F.; Holstein, J. J.; Rissanen, K.; Nitschke, J. R. *Chem. Eur. J.* **2013**, *19*, 3374-3382.

Summary and Conclusions

In summary the present thesis has dealt with the coordination and supramolecular chemistry of functionalized phosphorus nitrogen (P-N) scaffolds and their applications in storage, sensing and in catalysis. We have synthesized various alkylamino phosphonium salts of formula $[P(NHR)_4]^+$ and studied their supramolecular chemistry in presence of various counter anions such as halides, carboxylates and polyoxometallates. The dimensionality of supramolecular structure exhibited by the phosphonium halides can be varied depending on the steric bulk on the amino substituents. Therefore interesting examples of 2D-sheet structures and 1D-structures containing linear, zigzag and helical chains are obtained. The phosphonium cations containing carboxylate anions are prepared by two routes: by anion exchange reactions with phosphonium chlorides and by protonation of neutral phosphine imine, $[P(NPh)(NHPh)_3]$.

We have also synthesized six new examples of organic-inorganic hybrid molecules containing phosphonium cations and polyoxometalate anions and studied their supramolecular organization in the solid state. A detailed structural analysis show that the type of supramolecular formed by these compounds depends upon nature of the polyoxometalate ion and steric bulk on the phosphonium ligands. Therefore interesting supramolecular structures of 2D-layers, grids, networks and 3D-helical assemblies are obtained. During the course of these studies we have also envisaged the formation of a Keggin type polyoxometalate anion by a facile P–N bond cleavage reaction.

Subsequently, we have synthesized several pyridyl functionalized P(V) scaffolds such as phosphonium salts, phosphine imines and phosphoric triamides and studied their coordination chemistry in presence various metal salts. Treatment of 2-pyridyl substituted phosphonium salts and phosphine oxides with 1st row transition metal salts have resulted in a P–N bond cleavage in which the in situ generated phosphoramide ligand tris(amido)phosphate $[PO(NH^2Py)_3]$ and bis(amido)phosphate $[PO_2(NH^2Py)_2]^-$ yields interesting kinds of mononuclear complexes. To prevent the P–N bond cleavage we have established a facile anion exchange route that stabilize the highly labile tetrakis(2-pyridylamino)phosphonium cation in the solution as well as in solid state. We developed a mild synthetic route for obtaining imido P(V) species which are isoelectronic analogues to common phosphorus oxo-anions such as H_3PO_4, $H_2PO_4^-$, HPO_4^{2-} and PO_4^{3-} ions. For example the reaction of phosphoramide ligand with Cu^ICl gave Cu(II) complex of mono-anionic phosphoramide ligand $[OP(N^2Py)(NH^2Py)_2]^-$. The reaction of phosphonium salt $[P(NH^2Py)_4]Cl$ with Ag(I) salts gave a pentanuclear Ag(I)

imido-phosphate complex $[Ag_5(LH_2^-)]^{3+}$ in which the homoleptic imido phosphate anion $[P(N^2Py)_2(NH^2Py)_2]^-$ acts as a hexadentate cisoidal ligand. Employing the slight variations in the reactivities of the Ag(I) salts, sequential deprotonation of the phosphoramide ligand amino protons was achieved forming imido P(V) species analogous to the di hydrogen phosphate and mono hydrogen phosphate in the form of hepta- and octa-nuclear Ag(I) complexes starting from 2-pyridylamino functionalized phosphonium salt and 2-pyridyl-functionlized tris(amido)phosphate. Similarly the reaction of phosphonium salt and phosphoramide ligand with Pd(II) ions gave the dinuclear Pd(II) assembly stabilized by two $[OP(N^2Py)(NH^2Py)_2]^-$ ligands.

Treatment of the 3-pyridyl attached phosphonium salt with various metal salts of copper have again resulted in a P–N bond cleavage in which the in-situ generated phosphoramide ligand $[PO(NH^2Py)_3]$, yields interesting kinds of self-assemblies in macrocyclic, cage and 2D-coordination polymers. Further, we have synthesized Zn(II) and Cu(II) coordination polymer from an in-situ generated ligand $[PO_2(NH^4Py)_2]^-$. The in-situ generated ligand was achieved in P–N bond cleavage reaction from the corresponding phosphonium salt $[P(NH^4Py)_4]Cl$ or from phosphoramide $[PO(NH^4Py)_3]$. Both coordination polymer exhibit a narrow porous network and shows selectivity for polar guest molecules. The porosity of $[ZnL(HCO_2)]_\infty$ assembly was determined by gas adsorption studies showing a higher uptake capacity for CO_2 over N_2. No appreciable gas uptake characteristic could be observed for the Cu(II) coordination polymer, $[CuL_2(H_2O)_2]_\infty$. Remarkably, the de-solvated form of the Zn(II) coordination polymer, $[ZnL(HCO_2)]_\infty$, shows a very high uptake of water adsorption over aliphatic alcohols. Although the Cu(II) coordination polymer,$[CuL_2(H_2O)_2]_\infty$, shows a lower uptake capacity for water adsorption, it exhibits a better stability than the Zn(II) polymer.

Interestingly, treatment of Pd(II) salts in reaction with alkyl derivatives of the phosphoramide ligands such as $[PO(NHR)_3]$, gave the most basic imido(phosphate) trianions $[(RN)_3PO]^{3-}$ as its tri- and hexanuclear metal complexes in protic and polar solvents. Tri or hexa-nuclear Pd(II) clusters of these trianions were isolated exclusively in all these reactions in which the trianionic species acts as a tripodal chelating ligand to the trinuclear Pd_3-unit. A similar reaction with $PdCl_2$ leads again to the fully deprotonated species $[(RN)_3PO]^{3-}$ as their corresponding chloro-bridged hexameric Pd(II) clusters. We observed two types of arrangement for the chloro-bridged hexameric clusters from the crystal structures. A prismatic arrangement of the Pd_6-assembly was

observed for the trianionic imido-phosphate ligand featuring the most bulky ^{t}Bu substituents, while for other substituents such as ^{c}Hex, ^{i}Pr and ^{i}Bu on the imido-P(V) backbone gave an octahedral cluster assembly. Reactivity studies on the hexameric clusters featuring the acetate groups with primary amines have lead to a symmetric cleavage of the prismatic assemblies in which the tripodally chelated $(Pd\text{-}N_{imido})_3$ moieties remained unaffected. We have also demonstrated the catalytic activity of these complexes in M-H type coupling reactions which proves that these clusters are worthy candidates for catalytic applications.

We have established a novel ligand substitution approach to build polyhedral clusters and cages utilizing the $[Pd_3X]^{3+}$ cationic PBUs and various linker carboxylate anions in which the $[(N^{i}Pr)_3PO]^{3-}$ (X^{3-}) moiety acts as a novel trianionic cis-blocking agent for a planar Pd_3-motif. Thus for the first time we have shown the formation of charge neutral Pd(II) polyhedral cage assemblies in tetrahedral and cubic topologies. The intrinsic porosity of the tetrahedral cage was determined by gas adsorption studies showing a higher uptake capacity for CO_2 over N_2 and H_2. Guest encapsulation inside this cage assembly was examined with a large selection of solvents ranging from non-polar to polar and separate competitive binding experiments have shown the preferential encapsulation of benzene and CCl_4 over other related aromatic or chlorinated solvents. DFT calculations gave a highest binding-affinity for benzene and shows guest encapsulation keeps the cage structure intact. An unusual barrel shaped decameric assembly consisting of fused square-pyramidal polyhedral motifs and linear non chelating isonicotinate bridges were obtained, during these studies. Trinuclear imido-Pd(II) assemblies containing uncoordinated, N-donor and carboxylic acid functionalities were synthesized which are useful synthons for further self-assembly reactions.

In short, this thesis work involved the design of main group P-N based ligands in transition metal chemistry in constructing novel self-assembled structures in clusters, cages and framework architectures. The chemistry and observations reported in this thesis will lay foundation for the development of new functional materials having great potential in the areas of catalysis, sorption, self-assembly and host-guest chemistry.

Appendix

Chapters 2-6

Appendix 1

Table A1.1: Crystallographic Data

Compound	**2.2**	**2.3**	**2.4**
Chemical formula	$C_{12}H_{32}ClN_4P$	$C_{12}H_{32}ClN_4P$	$C_{16}H_{32}ClN_4P$
Formula weight	298.84	298.84	354.94
Temperature (K)	100(2)	100(2)	100(2)
Crystal system	Monoclinic	Tetragonal	Monoclinic
Space group	C2/c	P42(1)c	P2(1)/c
a (Å); α (°)	12.586(3); 90	10.1654(18); 90	14.251(3); 90
b (Å); β(°)	12.583(3); 106.12(4)	10.1654(18); 90	13.333(7); 108.98(5)
c (Å); γ (°)	22.569(12); 90	8.2342(13); 90	10.3373(3); 90
V ($Å^3$); Z	3433.7(12); 8	850.9(3); 2	4364.8(18); 8
ρ (calc.) mg m^{-3}	1.156	1.166	1.080
μ(Mo K_α) mm^{-1}	0.309	0.311	0.252
$2\theta_{max}$ (°)	56	56	45
R(int)	0.0172	0.0186	0.0673
Completeness to θ	93.9 %	97.2 %	99.7 %
Data / param.	3913 / 183	987 / 47	5685 / 387
GOF	1.018	1.098	1.033
R1 [F>4σ(F)]	0.0328	0.0241	0.0782
wR2 (all data)	0.0914	0.0646	0.2144
max. peak/hole (e.$Å^{-3}$)	0.425 / -0.272	0.246/-0.142	0.893 / -0.423

Compound	**2.5**	**2.6.2H_2O**	**2.7**
Chemical formula	$C_{16}H_{40}ClN_4P$	$C_{72}H_{146}Cl_3N_{12}P_3$	$C_{50}H_{51}ClN_8P2$
Formula weight	354.94	298.84	893.38
Temperature (K)	100(2)	100(2)	100(2)
Crystal system	Monoclinic	Orthorhombic	Triclinic
Space group	P2(1)2(1)2(1)	C222(1)	P-1
a (Å); α (°)	9.262(3); 90	18.0375(7); 90	10.290(3); 75.659(7)
b (Å); β(°)	14.898(4); 90	24.8828(7); 90	13.821(7); 78.223(5)
c (Å); γ (°)	15.923(10); 90	19.1713(6); 90	17.274(5); 78.223(6)
V ($Å^3$); Z	2197.3(10); 4	8604.5(5); 4	2330.2(12); 2
ρ (calc.) mg m^{-3}	1.073	1.089	1.273
μ(Mo K_α) mm^{-1}	0.250	0.208	0.200
$2\theta_{max}$ (°)	50	48	50
R(int)	0.0195	0.0961	0.0230
Completeness to θ	98.9 %	99.8 %	91.3 %
Data / param.	3813 / 227	6994 / 434	7531 / 551
GOF	1.058	0.996	1.004
R1 [F>4σ(F)]	0.0330	0.0495	0.0746
wR2 (all data)	0.0803	0.1471	0.1707
max. peak/hole (e.$Å^{-3}$)	0.299 / -0.147	0.440 / -0.212	0.421 / -0.451

Compound	**2.8**	**2.9**	**2.10.THF**
Chemical formula	$C_{28}H_{59}N_4O_4P$	$C_{17}H_{40}N_4O_2P$	$C_{32}H_{39}N_4O_2P$
Formula weight	546.76	363.50	542.64
Temperature (K)	296(2)	296(2)	100(2)
Crystal system	Tetragonal	Cubic	Orthorhombic
Space group	P4(3)2(1)2	Pn-3n	Aba2
a (Å); α (°)	14.6698(5); 90	19.8212(18); 90	19.654(8); 90
b (Å); β(°)	14.6698(5); 90	19.8212(18); 90	8.211(3); 90
c (Å); γ (°)	15.4509(7); 90	19.8212(18); 90	18.478(8); 90
V ($Å^3$); Z	3325.1(2); 4	7787.4(12); 12	2982(2); 4
ρ (calc.) mg m^{-3}	1.092	0.930	1.209
μ(Mo K_α) mm^{-1}	0.309	0.119	0.127
$2\theta_{max}$ (°)	56	50	50
R(int)	0.0172	0.1170	0.0485
Completeness to θ	100 %	99.4 %	99.6 %
Data / param.	4173 / 178	1156 / 59	2506 / 182
GOF	0.892	1.017	1.025
R1 [F>4σ(F)]	0.0424	0.0764	0.1064
wR2 (all data)	0.1087	0.2913	0.1095
max. peak/hole (e.$Å^{-3}$)	0.136 / -0.197	0.230 / -0.495	0.235 / -0.191

Compound	**2.12**	**2.13**	**2.16**
Chemical formula	$C_{33}H_{43}N_4O_4P$	$C_{51}H_{50}N_8O_4P_2$	$C_{81}H_{75}O_6N_{12}P_3$
Formula weight	590.68	900.93	1405.44
Temperature (K)	100(2)	296(2)	296(2)
Crystal system	Monoclinic	Tetragonal	Monoclinic
Space group	P2(1)/c	I4(1)cd	Pc
a (Å); α (°)	9.543(2); 90	33.3989(10); 90	24.3854(17); 90
b (Å); β(°)	37.633(8); 110.51(3)	33.3989(10); 90	16.3995(7); 90.737(2)
c (Å); γ (°)	9.453(2); 90	18.2549(12); 90	18.7063(13); 90
V ($Å^3$); Z	3179.8(12); 4	20363.1(16); 16	7480.8(9); 4
ρ (calc.) mg m^{-3}	1.156	1.175	1.248
μ(Mo K_α) mm^{-1}	0.309	0.136	0.141
$2\theta_{max}$ (°)	50	45	50
R(int)	0.0302	0.1390	0.0844
Completeness to θ	98.5 %	99.2 %	99.5 %
Data / param.	5548 / 405	6611 / 572	23994 / 1837
GOF	1.029	0.849	0.9
R1 [F>4σ(F)]	0.0420	0.0570	0.0690
wR2 (all data)	0.1051	0.1573	0.2138
Flack parameter	-	-0.15(13)	
max. peak/hole (e.$Å^{-3}$)	0.304 / -0.366	0.317 / -0.153	0.912 / -0.755

Compound	**2.17.**4DMF	**2.18**	**2.19**
Chemical formula	$C_{108}H_{192}Mo8N_{10}O30P$	$C_{40}H_{100}Mo_8N_4O_{26}P_2$	$C_{64}H_{154}N_{116}O_{32}P_4W_{10}$
Formula weight	3142.22	1966.76	3622.41
Temperature (K)	100(2)	100(2)	100(2)
Crystal system	Monoclinic	Monoclinic	Monoclinic
Space group	P2(1)/c	P2(1)/c	P2(1)/n
a (Å); α (°)	19.259(8); 90	11.018(7); 90	17.184(12); 90
b (Å); β(°)	20.372(8); 90	17.647(12); 90	16.871(11); 96.95(4)
c (Å); γ (°)	19.070(8); 90	19.398(14); 90	19.348(12); 90
V ($Å^3$); Z	7111.9(5); 2	3771.7(4); 2	5568.2(6); 8
ρ (calc.) mg m^{-3}	1.467	1.732	2.161
μ(Mo K_α) mm^{-1}	0.798	1.399	10.410
$2\theta_{max}$ (°)	50	56	48
R(int)	0.0784	0.0614	0.0863
Completeness to θ	99.2 %	99.6 %	98.4 %
Data / param.	12477 / 754	9321 / 408	8398 / 581
GOF	1.124	1.023	1.023
R1 [F>4σ(F)]	0.1064	0.0497	0.0497
wR2 (all data)	0.3173	0.1008	0.1008
max. peak/hole (e.$Å^{-3}$)	2.922 / -1.079	1.735 / -1.707	- 1.735 / -1.707

Compound	**2.20**·CH_3OH	**2.22**
Chemical formula	$C_{37}H_{96}Mo_{12}N_{12}O_{41}P_4$	$C72H_{144}AsMo_{12}N_4O_{40}P_3$
Formula weight	2640.42	3137.10
Temperature (K)	100(2)	100(2)
Crystal system	Orthorhombic	Monoclinic
Space group	Pbcn	P2(1)
a (Å); α (°)	19.904(9); 90	14.5412(6); 90
b (Å); β(°)	21.237(9); 90	17.5150(7); 90.49(2)
c (Å); γ (°)	39.930(16); 90	22.4630(9); 90
V ($Å^3$); Z	16880.8(12); 8	5684.4(4); 2
ρ (calc.) mg m^{-3}	2.078	1.833
μ(Mo K_α) mm^{-1}	1.881	1.685
$2\theta_{max}$ (°)	43	50
R(int)	0.0726	0.0847
Completeness to θ	98.3 %	99.4 %
Data / param.	9269 / 923	19305 / 1262
GOF	1.255	1.029
R1 [F>4σ(F)]	0.1139	0.0468
wR2 (all data)	0.2648	0.1186
Flack parameter	-	0.828(15)
max. peak/hole (e.$Å^{-3}$)	1.139 / -1.274	1.369 / -0.884

Table A1.2: Hydrogen bonding distances (Å) and angles (○) for the compounds **2.2–2.6**

Compound	D-H...A	d(H...A)Å	d(D...A)Å	<(DHA)˚
2.2	N(1)-H(1)...Cl(1)	2.474(19)	3.2683(13)	160.6(16)
	N(2)-H(2)...Cl(1)#1	2.468(19)	3.2394(13)	160.8(16)
	N(3)-H(3)...Cl(1)#2	2.460(19)	3.2593(13)	164.8(16)
	N(4)-H(4)...Cl(1)#3	2.477(19)	3.2943(13)	166.7(16)
	Symmetry transformations used to generate equivalent atoms:			
	#1 -x+1/2,-y+3/2,-z+1 #2 x+1/2,y+1/2,z #3 -x+1,-y+1,-z+1			
2.3	N(1)-H(1N)...Cl(1)	2.50(9)	3.343(11)	168.8(21)
2.4	N(1)-H(1)...Cl(1)#1	2.779(25)	3.485(2)	161.77(24)
	N(2)-H(2)...Cl(1)#1	2.474(27)	3.217(2)	172.02(27)
	N(3)-H(3)...Cl(1)#2	2.442(22)	3.237(2)	167.58(21)
	N(4)-H(4)...Cl(1)#2	2.632(24)	3.351(2)	165.65(23)
	Symmetry transformations used to generate equivalent atoms:			
	#1 -x+1,y+1/2,-z+1/2 #2 x+1/2,y,z			
2.5	N(1)-H(1)...Cl(2)	2.492(3)	3.234(5)	142.31(29)
	N(2)-H(2)...Cl(2)	2.399(3)	3.221(6)	155.64(28)
	N(3)-H(3)...Cl(1)	2.357(3)	3.208(6)	162.63(30)
	N(4)-H(4)...Cl(1)	2.400(2)	3.223(6)	155.65(37)
	N(5)-H(5)...Cl(2)#1	2.466(2)	3.243(6)	147.47(37)
	N(6)-H(6)...Cl(2)#1	2.619(9)	3.338(14)	139.48(78)
	N(6')-H(6')...Cl(2)#1	2.373(5)	3.221(10)	162.13(61)
	N(7)-H(7)...Cl(1)	2.595(2)	3.200(7)	126.74(40)
	N(8)-H(8)...Cl(1)	2.362(7)	3.209(10)	161.66(41)
	Symmetry transformations used to generate equivalent atoms:			
	#1 x-1,y,z			
2.6.2H_2O	N(1)-H(1)...Cl(1)#2	2.50(2)	3.277(3)	172(4)
	N(2)-H(2)...Cl(2)	2.76(4)	3.329(3)	133(4)
	N(3)-H(3)...Cl(1)#2	2.52(3)	3.230(3)	151(4)
	N(4)-H(4)...Cl(2)	2.51(2)	3.279(3)	169(4)
	N(5)-H(5)...Cl(2)#3	2.57(2)	3.382(3)	176(4)
	N(6)-H(6)...O(1)	2.31(3)	3.091(9)	162(4)
	N(6)-H(6)...O(1')	2.24(3)	3.026(17)	165(4)
	Symmetry transformations used to generate equivalent atoms:			
	#1 x-1,y,z #2 -x+1,-y+1,z-1/2			

Table A1.3: Selected P-N bond lengths and N-P-N bond angles for compounds **2.2-2.6**

Compound	Bond lengths	Bond Angles
2.2	P(1)-N(2): 1.6173(12) P(1)-N(3): 1.6206(12) P(1)-N(1): 1.6207(11) P(1)-N(4): 1.6229(12)	N(2)-P(1)-N(3): 109.54(6) N(2)-P(1)-N(1): 109.26(6) N(3)-P(1)-N(1): 109.39(6) N(2)-P(1)-N(4): 109.43(6) N(3)-P(1)-N(4): 109.66(6) N(1)-P(1)-N(4): 109.55(6)
2.3	P(1)-N(1): 1.6114(12)	N(1)#1-P(1)-N(1): 114.72(4) N(1)#2-P(1)-N(1): 99.41(8) N(1)#3-P(1)-N(1): 114.72(4)
2.4	P(1)-N(3): 1.605(5) P(1)-N(1): 1.611(5) P(1)-N(2): 1.612(5) P(1)-N(4): 1.613(5) P(2)-N(7): 1.602(7) P(2)-N(8): 1.607(6) P(2)-N(5): 1.608(5) P(2)-N(6'): 1.633(9) P(2)-N(6): 1.656(11)	N(3)-P(1)-N(1): 113.3(2) N(3)-P(1)-N(2): 111.8(2) N(1)-P(1)-N(2): 101.4(2) N(3)-P(1)-N(4): 102.7(2) N(1)-P(1)-N(4): 113.3(3) N(2)-P(1)-N(4): 114.8(3) N(7)-P(2)-N(8): 101.5(3) N(7)-P(2)-N(5): 112.9(3) N(8)-P(2)-N(5): 111.8(3) N(7)-P(2)-N(6'): 124.2(4) N(8)-P(2)-N(6'): 102.6(4) N(5)-P(2)-N(6'): 103.4(4) N(7)-P(2)-N(6): 98.9(5) N(8)-P(2)-N(6): 131.1(5) N(5)-P(2)-N(6): 99.9(4)
2.5	P(1)-N(2): 1.6234(18) P(1)-N(4): 1.6240(18) P(1)-N(3): 1.6280(18) P(1)-N(1): 1.6317(18)	N(2)-P(1)-N(4): 114.23(10) N(2)-P(1)-N(3): 116.12(9) N(4)-P(1)-N(3): 99.26(9) N(2)-P(1)-N(1): 99.54(10) N(4)-P(1)-N(1): 114.46(9) N(3)-P(1)-N(1): 114.10(10)
2.6.2H_2O	P(1)-N(3): 1.603(3) P(1)-N(4): 1.604(3) P(1)-N(2): 1.613(3) P(1)-N(1): 1.618(3) P(2)-N(5)#1:1.618(3) P(2)-N(5): 1.618(3) P(2)-N(6): 1.622(3) P(2)-N(6)#1: 1.622(3)	N(3)-P(1)-N(4): 110.89(15) N(3)-P(1)-N(2): 116.00(15) N(4)-P(1)-N(2): 100.63(14) N(3)-P(1)-N(1): 100.04(13) N(4)-P(1)-N(1): 118.18(17) N(2)-P(1)-N(1): 111.92(15) N(5)#1-P(2)-N(5): 121.7(2) N(5)#1-P(2)-N(6): 107.79(15) N(5)-P(2)-N(6): 100.62(14) N(5)#1-P(2)-N(6)#1: 100.62(14) N(5)-P(2)-N(6)#1: 107.79(15) N(6)-P(2)-N(6)#1: 119.6(2)

Table A1.4: Hydrogen bonding parameters for the compounds **2.17-2.22**

Compound	D-H...A	d(H...A)	d(D...A)	<(DHA)
2.17	N(1)-H(1)...O(9)#2	2.10	2.954(17)	171.6
	N(2)-H(2)...O(1S)	2.32	2.96(3)	131.2
	N(3)-H(3)...O(7)#2	2.12	2.941(17)	160.4
	N(4)-H(4)...O(2S)#3	2.32	3.02(2)	139.6
	N(5)-H(5)...O(10)	2.09	2.945(17)	174.5
	N(6)-H(6)...O(8)#4	2.60	3.308(18)	140.0
	N(6)-H(6)...O(3)#4	2.64	3.426(16)	152.8
	N(7)-H(7)...O(4)	2.41	3.222(16)	157.6
	N(8)-H(8)...O(8)#4	2.07	2.921(17)	169.7
	Symmetry transformations used to generate equivalent atoms:			
	#1 -x+2,-y,-z+1 #2 -x+1,-y,-z+1 #3 x,y-1,z #4 -x+2,y+1/2,-z+1/2			
2.18	N(1)-H(1)...O(7)#2	2.30	3.159(4)	176.8
	N(2)-H(2)...O(4)#3	2.27	3.013(4)	144.4
	N(3)-H(3)...O(4)#3	2.13	2.947(4)	158.1
	N(4)-H(4)...O(2)#2	2.24	3.010(4)	149.7
	N(5)-H(51S)...O(13)#1	2.11(3)	2.957(4)	173(5)
	N(5)-H(52S)...O(8)#4	2.16(3)	2.965(4)	158(5)
	N(5)-H(53S)...O(12)	2.03(3)	2.875(4)	171(5)
	Symmetry transformations used to generate equivalent atoms:			
	#1 -x+2,-y,-z+1 #2 x,y+1,z #3 -x+2,y+1/2,-z+1/2 #4 -x+1,-y,-z+1			
2.19	N(1)-H(1)...O(15)#2	2.21	2.871(17)	133.0
	N(2)-H(2)...O(3)#2	2.60	3.397(17)	155.7
	N(3)-H(3)...O(11)#3	2.48	3.099(17)	129.9
	N(4)-H(4)...O(14)#3	2.90	3.73(2)	162.6
	N(5)-H(5)...O(6)#4	2.28	3.066(19)	151.3
	N(6)-H(6)...O(6)#4	2.24	3.058(18)	158.7
	N(7)-H(7)...O(9)#3	2.30	3.149(18)	171.0
	N(8)-H(8)...O(8)#3	2.16	2.918(16)	147.2
	Symmetry transformations used to generate equivalent atoms:			
	#1 -x,-y+2,-z+2 #2 x+1,y-1,z #3 -x+1/2,y-1/2,-z+3/2 #4 x,y-1,z			
2.20	N(1)-H(1)...O(15)#3	2.98	3.38(5)	110.4
	N(2)-H(2)...O(4)#4	2.42	3.01(4)	126.3
	N(3)-H(3)...O(39)#5	2.65	3.48(5)	160.5
	N(4)-H(4)...O(1)#4	3.00	3.51(4)	119.7
	N(1')-H(1')...O(39)#5	2.92	3.33(5)	110.9
	N(2')-H(2')...O(32)#6	2.57	3.11(5)	121.8

	N(3')-H(3')...O(1)#4	2.42	3.26(5)	165.8
	N(4')-H(4')...O(15)#3	2.58	3.01(5)	111.9
	N(5)-H(5)...O(24)#7	2.69	3.35(3)	134.6
	N(6)-H(6)...O(26)	2.65	3.31(4)	135.1
	N(7)-H(7)...O(40)	2.81	3.37(4)	124.1
	N(8)-H(8)...O(26)	2.42	3.04(3)	130.2
	N(8)-H(8)...O(30)	2.44	3.27(4)	159.9
	N(9)-H(9)...O(11)	2.50	3.07(3)	124.4
	N(10)-H(10)...O(20)#8	2.42	3.13(3)	139.8
	N(11)-H(11A)...O(7)	2.76	3.50(3)	144.4
	N(12)-H(12)...O(34)#9	2.57	3.42(3)	173.9
	Symmetry transformations used to generate equivalent atoms:			
	#1 -x+1,y,-z+3/2 #2 -x,-y,-z+1 #3 -x+3/2,y-1/2,z #4 -x+1,y-1,-z+3/2 #5 x+1,y,z			
	#6 -x+1,-y,-z+1 #7 x+1/2,-y+1/2,-z+1 #8 -x+1/2,y-1/2,z #9 x,y+1,z			
2.21	N(1)-H(1)...O(24)	2.48	3.223(13)	144.6
	N(1)-H(1)...O(9)	2.61	3.364(13)	146.5
	N(2)-H(2)...O(9)	2.53	3.364(12)	164.0
	N(3)-H(3)...O(18)#1	2.72	3.455(14)	144.7
	N(4)-H(4)...O(1)#1	2.29	3.138(11)	169.0
	N(5)-H(5)...O(14)#2	2.44	3.240(13)	156.0
	N(6)-H(6)...O(19)#1	2.40	3.120(13)	141.4
	N(7)-H(7)...O(40)#1	2.53	3.245(13)	140.6
	N(7)-H(7)...O(19)#1	2.62	3.357(13)	144.7
	N(8)-H(8)...O(14)#2	2.45	3.275(12)	160.1
	N(9)-H(9)...O(30)#1	2.86	3.622(14)	148.2
	N(10)-H(10)...O(22)#3	3.05	3.37(2)	104.0
	N(11)-H(11)...O(5)#3	2.76	3.503(13)	145.5
	N(12)-H(12)...O(22)#3	3.06	3.275(14)	97.1
	Symmetry transformations used to generate equivalent atoms:			
	#1 x-1,y,z #2 -x+1,y-1/2,-z #3 -x+1,y+1/2,-z+1			

Table A1.5: Selected P-N bond lengths and N-P-N bond angles for compounds **17-22**

Compound	Bond lengths	Bond Angles
2.17	P(1)-N(3): 1.587(15) P(1)-N(2): 1.635(14) P(1)-N(1): 1.635(15) P(1)-N(4): 1.638(13) P(2)-N(5): 1.610(13) P(2)-N(7): 1.622(14) P(2)-N(8): 1.625(14) P(2)-N(6): 1.628(13)	N(3)-P(1)-N(2): 111.0(8) N(3)-P(1)-N(1): 105.2(8) N(2)-P(1)-N(1): 114.8(7) N(3)-P(1)-N(4): 114.1(8) N(2)-P(1)-N(4): 102.4(7) N(1)-P(1)-N(4): 109.6(8) N(5)-P(2)-N(7): 101.8(7) N(5)-P(2)-N(8): 115.3(8) N(7)-P(2)-N(8): 112.0(8) N(5)-P(2)-N(6): 110.8(8) N(7)-P(2)-N(6): 114.7(8) N(8)-P(2)-N(6): 102.8(7)
2.18	P(1)-N(3): 1.605(3) P(1)-N(2): 1.611(4) P(1)-N(1): 1.619(4) P(1)-N(4): 1.620(4)	N(3)-P(1)-N(2): 103.02(16) N(3)-P(1)-N(1): 110.8(2) N(2)-P(1)-N(1): 114.7(2) N(3)-P(1)-N(4): 113.2(2) N(2)-P(1)-N(4): 110.6(2) N(1)-P(1)-N(4): 104.7(2)
2.19	P(1)-N(1): 1.607(14) P(1)-N(3): 1.608(15) P(1)-N(4): 1.62(2) P(1)-N(2): 1.624(15) P(2)-N(8): 1.607(16) P(2)-N(6): 1.609(13) P(2)-N(7): 1.613(15) P(2)-N(5): 1.627(15)	N(1)-P(1)-N(3): 111.5(8) N(1)-P(1)-N(4): 116.4(10) N(3)-P(1)-N(4): 102.8(10) N(1)-P(1)-N(2): 99.6(8) N(3)-P(1)-N(2): 115.3(9) N(4)-P(1)-N(2): 112.0(10) N(8)-P(2)-N(6): 112.7(8) N(8)-P(2)-N(7): 101.2(8) N(6)-P(2)-N(7): 114.5(8) N(8)-P(2)-N(5): 114.4(9) N(6)-P(2)-N(5): 100.7(8) N(7)-P(2)-N(5): 114.0(9)
2.21	P(1)-N(4'): 1.61(2) P(1)-N(1'): 1.61(2) P(1)-N(3): 1.61(2) P(1)-N(1): 1.61(2) P(1)-N(4): 1.61(2)	N(4')-P(1)-N(1')119(2) N(3)-P(1)-N(1)106(2) N(3)-P(1)-N(4)103(2) N(1)-P(1)-N(4)117(2) N(4')-P(1)-N(3')107(2)

	P(1)-N(3'): 1.62(2) P(1)-N(2): 1.62(2) P(1)-N(2'): 1.62(2) P(2)-N(5): 1.60(3) P(2)-N(6): 1.60(3) P(2)-N(8): 1.62(3) P(2)-N(7): 1.65(3) P(3)-N(10): 1.60(3) P(3)-N(11): 1.60(2) P(3)-N(9):1.61(3) P(3)-N(12): 1.62(2)	N(1')-P(1)-N(3')110(2) N(3)-P(1)-N(2)121(2) N(1)-P(1)-N(2)105(2) N(4)-P(1)-N(2)105(2) N(4')-P(1)-N(2')106(2) N(1')-P(1)-N(2')102(2) N(3')-P(1)-N(2')113(2) N(5)-P(2)-N(6): 107.7(17) N(5)-P(2)-N(8): 119.7(15) N(6)-P(2)-N(8): 104.0(15) N(5)-P(2)-N(7): 104.6(17) N(6)-P(2)-N(7): 118.4(17) N(8)-P(2)-N(7): 103.2(18) N(10)-P(3)-N(11): 117.5(14) N(10)-P(3)-N(9): 104.8(13) N(11)-P(3)-N(9): 104.6(13) N(10)-P(3)-N(12): 106.0(12) N(11)-P(3)-N(12): 104.2(13) N(9)-P(3)-N(12): 120.6(15)
2.22	P(1)-N(4): 1.606(10) P(1)-N(2): 1.610(10) P(1)-N(1): 1.624(9) P(1)-N(3): 1.640(9) P(2)-N(6): 1.582(11) P(2)-N(7): 1.603(9) P(2)-N(8): 1.607(11) P(2)-N(5): 1.608(10) P(3)-N(12): 1.566(12) P(3)-N(9): 1.606(10) P(3)-N(11): 1.611(10) P(3)-N(10): 1.632(13)	N(4)-P(1)-N(2): 121.0(6) N(4)-P(1)-N(1): 108.6(5) N(2)-P(1)-N(1): 101.5(5) N(4)-P(1)-N(3): 101.7(4) N(2)-P(1)-N(3): 107.5(5) N(1)-P(1)-N(3): 117.4(5) N(6)-P(2)-N(7): 102.3(5) N(6)-P(2)-N(8): 118.2(7) N(7)-P(2)-N(8): 109.0(6) N(6)-P(2)-N(5): 109.0(6) N(7)-P(2)-N(5): 118.6(6) N(8)-P(2)-N(5): 100.7(5) N(12)-P(3)-N(9): 121.3(6) N(12)-P(3)-N(11): 106.6(6) N(9)-P(3)-N(11): 104.1(5) N(12)-P(3)-N(10): 98.0(8) N(9)-P(3)-N(10): 107.9(8) N(11)-P(3)-N(10): 120.0(7)

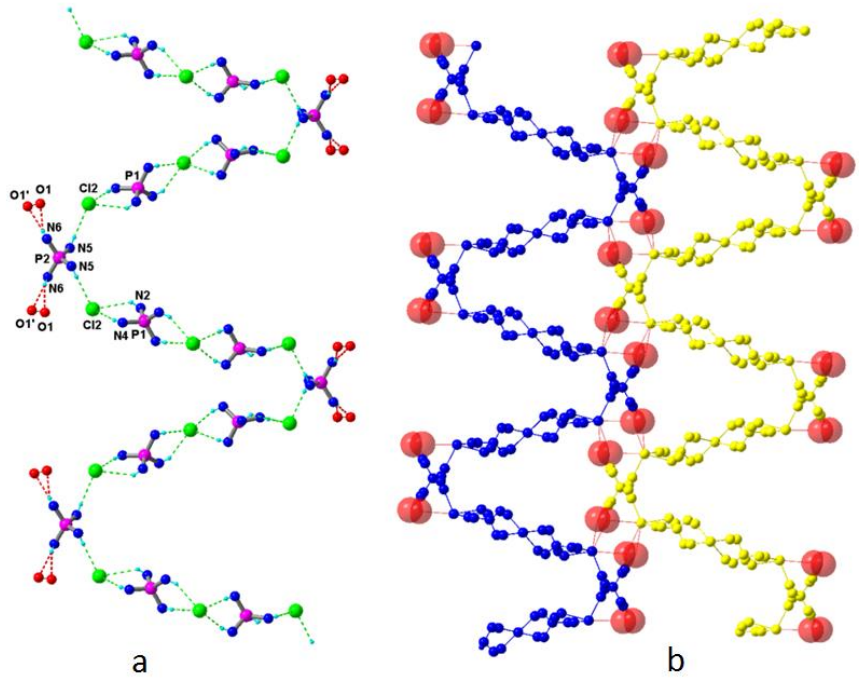

Figure A1.1: Formation of 1D-helical chains (a) and 2D-helical sheets (b) in **6**.2H_2O. Two adjacent helical chains are connected by water molecules via O(H)…Cl interactions. The hydrogen atoms on the disordered oxygen positions (O1 and O1) could not be precisely located

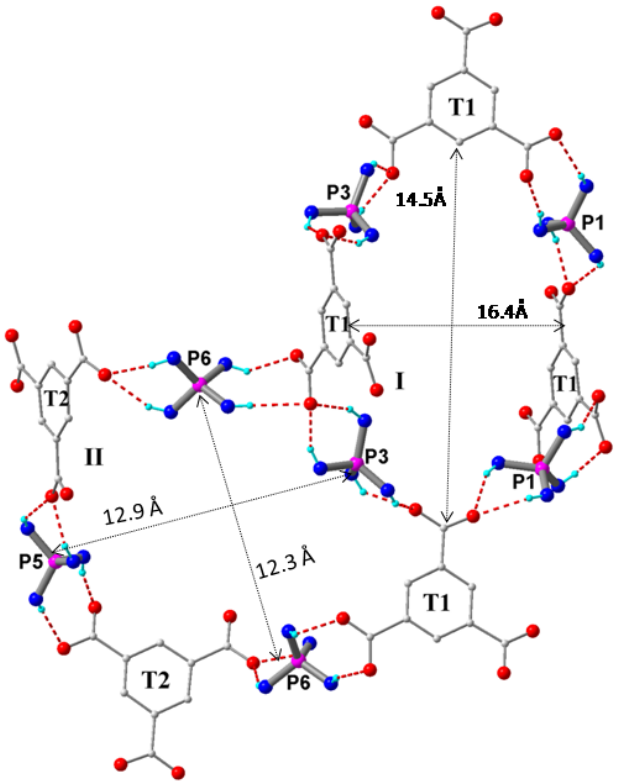

Figure A1.2: Formation of the two orthogonal rings I and II in **16**.

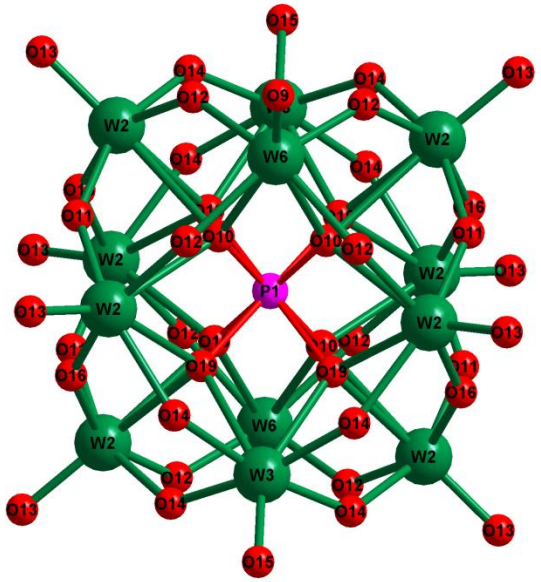

Figure A1.3: Core view of one of the $[PW_{12}O_{40}]^{3-}$ cluster moieties in **8**. Phosphonium*i-pr* amino substituents could not be modeled properly due to the strongly absorbing nature of the 'W' atoms and hence the structure was not solved completely.

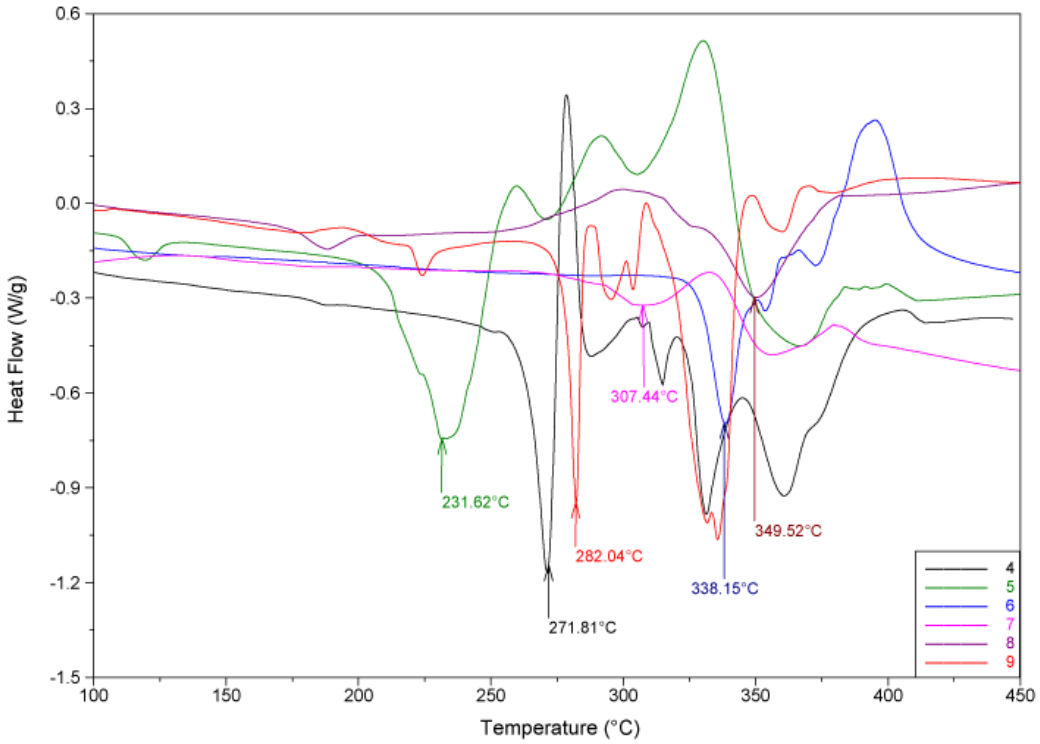

Figure A1.4: DSC traces of the phosphoniumpolyoxometallates**2.17-2.22**

Appendix 2

Table A2.1:Crystallographic Data

Compound	**3.2**	**3.2**·C_7H_8	**3.5**
Chemical formula	$C_{15}H_{15}N_6OP$	$C_{15}H_{15}N_6OP$	$C_{20}H_{19}N_8P$
Formula weight	326.30	418.43	402.40
Temperature (K)	100(2)	200(2)K	100(2)
Crystal system	Hexagonal (Trigonal)	Monoclinic	Monoclinic
Space group	R-3	$P2_1/c$	P2(1)/c
a (Å); α (°)	10.1012(10); 90	21.975(3); 90	9.596(16); 90
b (Å); β(°)	10.1012(10); 90	17.625(2); 130.373(6)	19.40(3); 105.19(4)
c (Å); γ (°)	28.4343(6); 120	29.216(3); 90	11.0279(17); 90
V ($Å^3$); Z	2512.57(7); 6	8620.7(18); 16	1980.7(6); 4
ρ (calc.) mg m^{-3}	1.294	1.290	1.349
μ(Mo K_α) mm^{-1}	0.177	0.154	0.163
$2\theta_{max}$ (°)	56	50	56
R(int)	0.0172	0.1152	0.0810
Completeness to θ	99.8 %	99.5 %	95.1 %
Data / param.	1390 / 74	15154 / 1039	4720 / 262
GOF	1.153	1.007	0.911
R1 [F>4σ(F)]	0.0421	0.0537	0.0416
wR2 (all data)	0.1367	0.1414	0.1080
max. peak/hole (e.$Å^{-3}$)	0.560 / -0.241	0.698 / -0.437	0.248 / -0.306

Compound	**3.6**	**3.7**·$2H_2O$	**3.9**·$2CH_3OH$
Chemical formula	$C_{40}H_{40}N_{16}OP_2$	$C_{20}H_{24}N_9O_5P$	$C_{32}H_{38}N_{12}O_{12}Cl_2P_2Fe$
Formula weight	822.82	501.45	907.34
Temperature (K)	296(2) K	100(2)K	296(2)
Crystal system	Monoclinic	Triclinic	Triclinic
Space group	P2(1)/c	P-1	P-1
a (Å); α (°)	20.160(6) ; 90°	9.037(3); 72.948(7)	8.422(2); 74.417(10)
b (Å); β(°)	10.068(3) ; 92.66(2)°	9.746(4); 80.443(7)	13.821(4); 87.394(10)
c (Å); γ (°)	39.744(10) ; 90°	14.391(5); 86.902(7)	18.7755(5); 79.619(10)
V ($Å^3$); Z	8058.5(4) ; 8	1194.9(8); 2	7349.2(4); 2
ρ (calc.) mg m^{-3}	1.356	1.394	1.553
μ(Mo K_α) mm^{-1}	0.164	0.166	0.974
$2\theta_{max}$ (°)	56	50	50
R(int)	0.0896	0.0770	0.0355
Completeness to θ	98.6	92.4 %	90 %
Data / param.	19730 / 1075	3894 / 339	6504 / 535
GOF	0.818	1.055	1.312
R1 [F>4σ(F)]	0.0498	0.0864	0.0402
wR2 (all data)	0.1329	0.2601	0.1183
max. peak/hole (e.$Å^{-3}$)	0.384 / -0.423	0.970/ -0.668	0.847 / -0.482

Compound	**3.10**	**3.11**·2CH_3OH	**3.12**
Chemical formula	$C_{30}H_{30}N_{12}O_{10}Cl_2P_2Co$	$C_{32}H_{38}N_{12}O_{12}Cl_2P_2Ni$	$C_{20}H_{20}N_8O_4P_2Cu$
Formula weight	909.04	974.29	561.92
Temperature (K)	296(2)	296(2)	100(2)
Crystal system	Monoclinic	Triclinic	Tetragonal
Space group	P2(1)/c	P-1	I4(1)/acd
a (Å); α (°)	13.5524(13); 90	8.483(5); 73.716(3)	19.418(3); 90
b (Å); β(°)	15.7132(17); 95.27(7)	13.8856(7); 87.237(3)	19.418(3); 90
c (Å); γ (°)	8.5749(8); 90	18.861(11); 79.323(2)	25.392(4); 90
V ($Å^3$); Z	1818.3(3); 2	2095.7(11); 2	9574(3); 16
ρ (calc.) mg m^{-3}	1.521	1.544	1.559
μ(Mo K_α) mm^{-1}	1.671	0.741	1.091
$2\theta_{max}$ (°)	50	56	50
R(int)	0.1335	0.1235	0.0453
Completeness to θ	99.4 %	98.2 %	100 %
Data / param.	3190 / 259	10263 / 557	2995 / 160
GOF	1.071	1.018	1.045
R1 [F>4σ(F)]	0.0993	0.0416	0.0283
wR2 (all data)	0.2979	0.1946	0.0856
max. peak/hole (e.$Å^{-3}$)	0.902 / -0.678	0.248 / -0.306	0.383/ -0.325

Compound	**3.12**·2DMF	**3.13**	**3.14**·$(ClO_4)_3$·3C_7H_8·2CH_3OH
Chemical formula	$C_{26}H_{34}N_{10}O_6P_2Cu$	$C_{18}H_{21}N_7O_2PClCu$	$C_{63}H_{62}Ag_5Cl_3N_{16}O_{14}P_2$
Formula weight	708.11	497.38	1974.93
Temperature (K)	100(2)	100(2)	100(2)
Crystal system	Monoclinic	Monoclinic	Orthorhombic
Space group	P2(1)/n	P2(1)/n	Pccn
a (Å); α (°)	11.080(3); 90	14.297(4); 90	27.1792(9); 90
b (Å); β(°)	10.009(3); 90.584(2)	9.412(3); 112.9(6)	10.8631(4); 90
c (Å); γ (°)	14.0334(4); 90	16.752(5); 90	24.8914(8); 90
V ($Å^3$); Z	1556.19(8); 2	2075.2(10); 4	7349.2(4); 4
ρ (calc.) mg m^{-3}	1.511	1.592	1.785
μ(Mo K_α) mm^{-1}	0.863	1.290	1.534
$2\theta_{max}$ (°)	50	50	46
R(int)	0.0347	0.0383	0.0875
Completeness to θ	100 %	100 %	99.8 %
Data / param.	3860 / 207	3649 / 273	5276 / 466
GOF	1.060	1.103	1.076
R1 [F>4σ(F)]	0.0358	0.0669	0.0402
wR2 (all data)	0.1027	0.1929	0.1183
max. peak/hole (e.$Å^{-3}$)	0.310/ -0.334	2.963 / -1.412	0.847 / -0.482

Compound	**3.14**·$(OTf)_3$·3DMF	**3.15**·$3H_2O$	**3.16**·$5CH_3OH·3H_2O$
Chemical formula	$C_{52}H_{57}Ag_5F_9N_{19}O_{12}P_2S_3$	$C_{30}H_{36}Ag_3N_{15}O_{14}P_2$	$C_{45}H_{41}Ag_7BF_4N_{18}O_4P_3$
Formula weight	2008.64	1216.29	1832.77
Temperature (K)	100(2)K	296(2)K	296(2)K
Crystal system	Triclinic	Monoclinic	Hexagonal
Space group	P-1	$P2_1$	$R3$
a (Å); α (°)	11.624(4); 80.501(6)	14.0273(12); 90	14.1261(3) ; 90
b (Å); β(°)	16.726(5); 74.225(7)	22.194(2); 98.846(5)	14.1261(3) ; 90
c (Å); γ (°)	19.060(6); 78.162(6)	14.8103(13); 90	24.5724(14); 120
V ($Å^3$); Z	3466.6(19); 2	4556.0(7); 4	4246.4(3); 3
ρ (calc.) mg m^{-3}	1.940	1.773	2.150
μ(Mo K_α) mm^{-1}	1.622	1.422	2.528
$2\theta_{max}$ (°)	50.06	45	56
R(int)	0.0522	0.1091	0.0527
Completeness to θ	99.5 %	98.7 %	99.6 %
Data / param.	12199 / 890	11649 / 1004	4402 / 254
GOF	1.018	1.002	1.038
R1 [F>4σ(F)]	0.0516	0.0929	0.0395
wR2 (all data)	0.1442	0.2545	0.1226
Flack parameter	-	0.58(6)	-
max. peak/hole (e.$Å^{-3}$)	2.548/ -1.182	1.911/ -0.962	1.181 / -0.791

Compound	**3.17·H_2O**	**3.18**	**3.18**·$4H_2O$
Chemical formula	$C_{45}H_{41}Ag_7BF_4N_{18}O_4P_3$	$C_{30}H_{28}N_{12}O_2P_2Cl_2Pd_2$	$C_{30}H_{36}N_{12}O_6P_2Cl_2Pd_2$
Formula weight	1832.77	934.32	1006.38
Temperature (K)	296(2)K	296(2)	100(2)
Crystal system	Hexagonal	Monoclinic	Cubic
Space group	$R3$	C2/c	Fd-3c
a (Å); α (°)	14.1261(3) ; 90	26.55(3); 90	49.495(6); 90
b (Å); β(°)	14.1261(3) ; 90	9.075(3); 119.74(7)	49.495 (6); 90
c (Å); γ (°)	24.5724(14); 120	16.592(17); 90	49.495 (6); 90
V ($Å^3$); Z	4246.4(3); 3	3470.6(6); 4	121253(27); 96
ρ (calc.) mg m^{-3}	2.150	1.720	0.923
μ(Mo K_α) mm^{-1}	2.528	1.820	0.908
$2\theta_{max}$ (°)	56	50	56
R(int)	0.0527	0.1778	0.3922
Completeness to θ	99.6 %	99.2 %	99.9%
Data / param.	4402 / 254	3401 / 226	6318 / 249
GOF	1.038	1.073	1.388
R1 [F>4σ(F)]	0.0395	0.0722	0.0786
wR2 (all data)	0.1226	0.2306	0.2757
max. peak/hole (e.$Å^{-3}$)	1.181 / -0.791	1.352 / -1.350	1.270 / -0.936

Compound	**3.19**	**3.20**
Chemical formula	$C_{30}H_{30}Cl_4Cu_2N_{12}O_2P_2$	$C_{45}H_{45}Cu_2N_{20}O_9P_3$
Formula weight	921.48	1230.00
Temperature (K)	100(2) K	100(2) K
Crystal system	Monoclinic	Triclinic
Space group	P2(1)/n	P -1
a (Å); α (°)	13.339(2) ; 90°	11.750(18); 112.16(3)°
b (Å); β(°)	8.562(11) ; 110.15(4)°	15.464(2) ; 90.66(3)°
c (Å); γ (°)	17.512(2) ; 90°	20.275(3) ; 95.21(3)°
V ($Å^3$); Z	1877.6(5) ; 2	3393.5(9) ; 2
ρ (calc.) mg m^{-3}	1.630	1.204
μ(Mo K_α) mm^{-1}	1.551	0.756
$2\theta_{max}$ (°)	50	56
R(int)	0.0369	0.0462
Completeness to θ	97.9	97.8
Data / param.	3242 / 235	16777/ 712
GOF	1.033	1.098
R1 [F>4σ(F)]	0.0337	0.0483
wR2 (all data)	0.0870	0.1256
max. peak/hole (e.$Å^{-3}$)	0.745 / -0.489	0.549/ -0.581

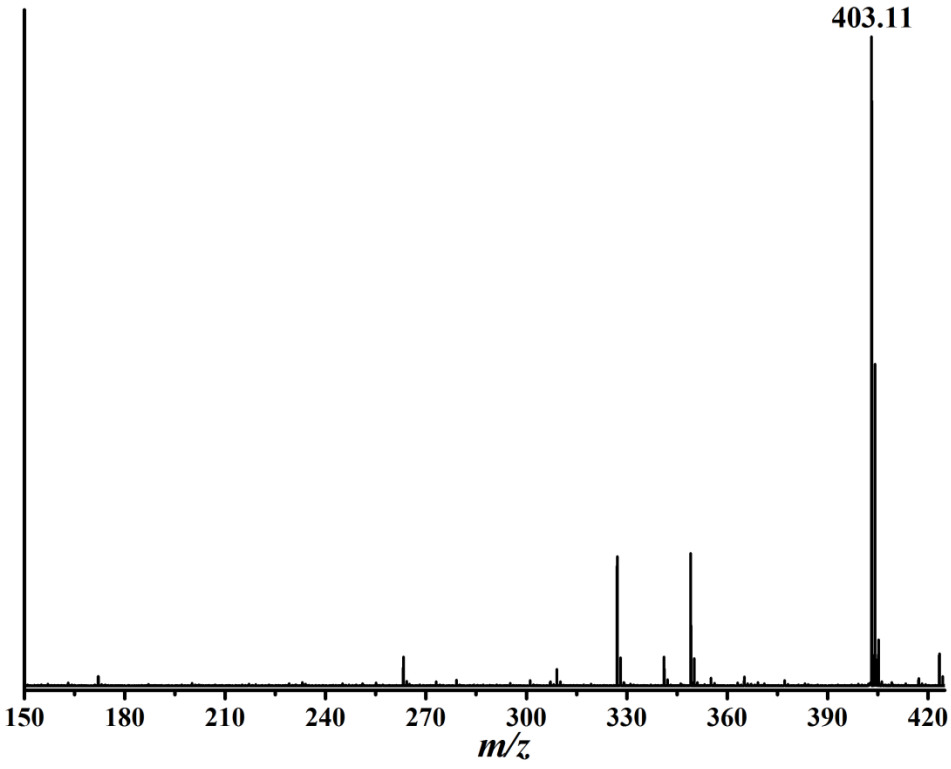

Figure A2.1: High-Resolution ESI(+) mass spectrum of **3.1**

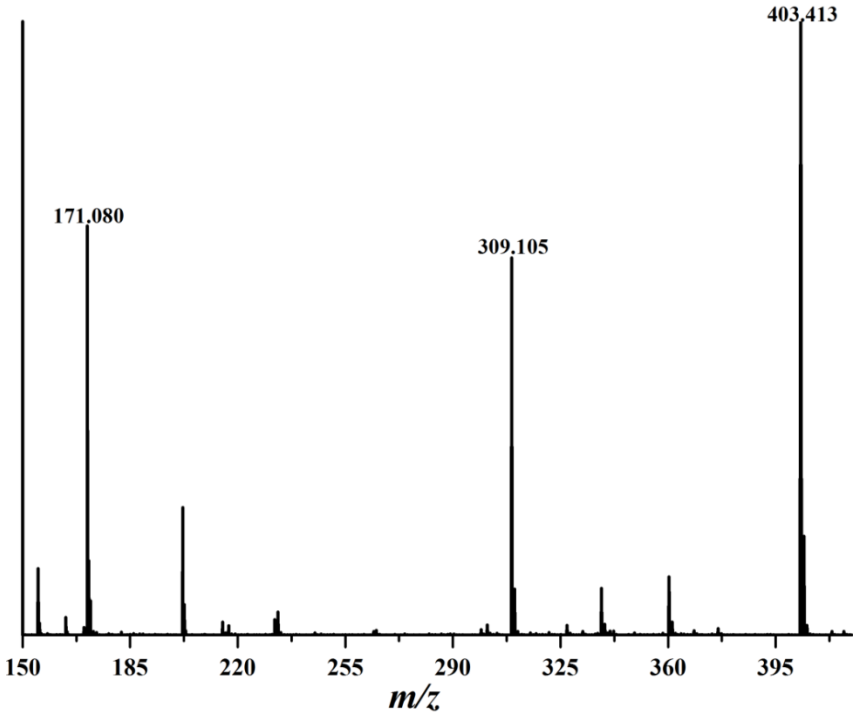

Figure A2.2: High-Resolution ESI (+) mass spectrum of **3.3**

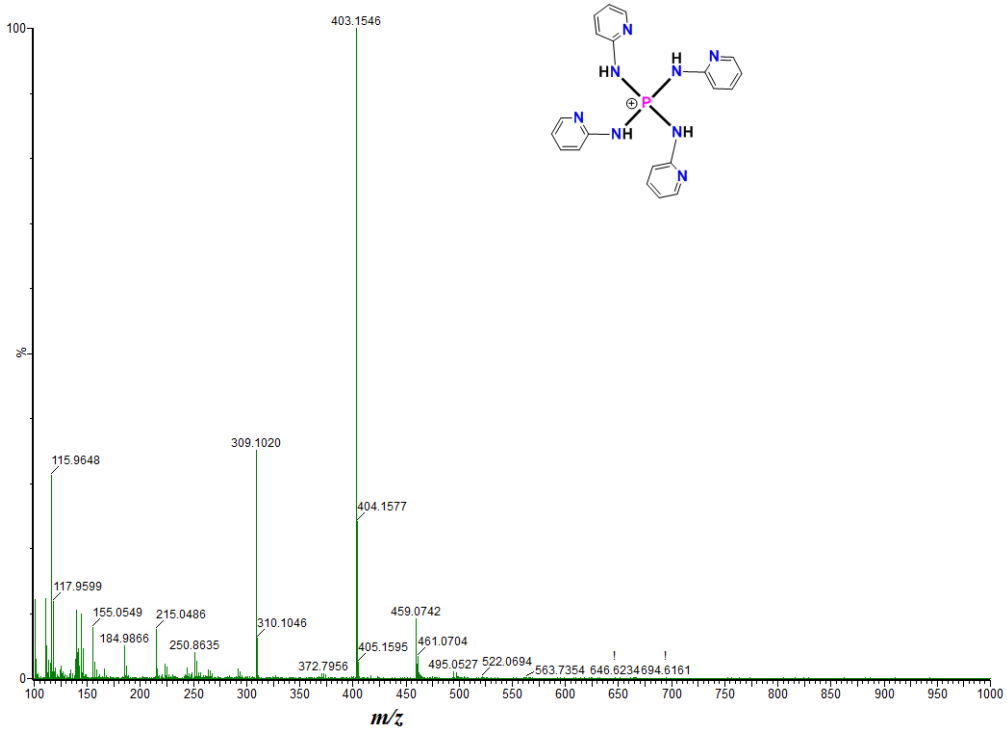

Figure A2.3: High-Resolution ESI (+) mass spectrum of **3.7**

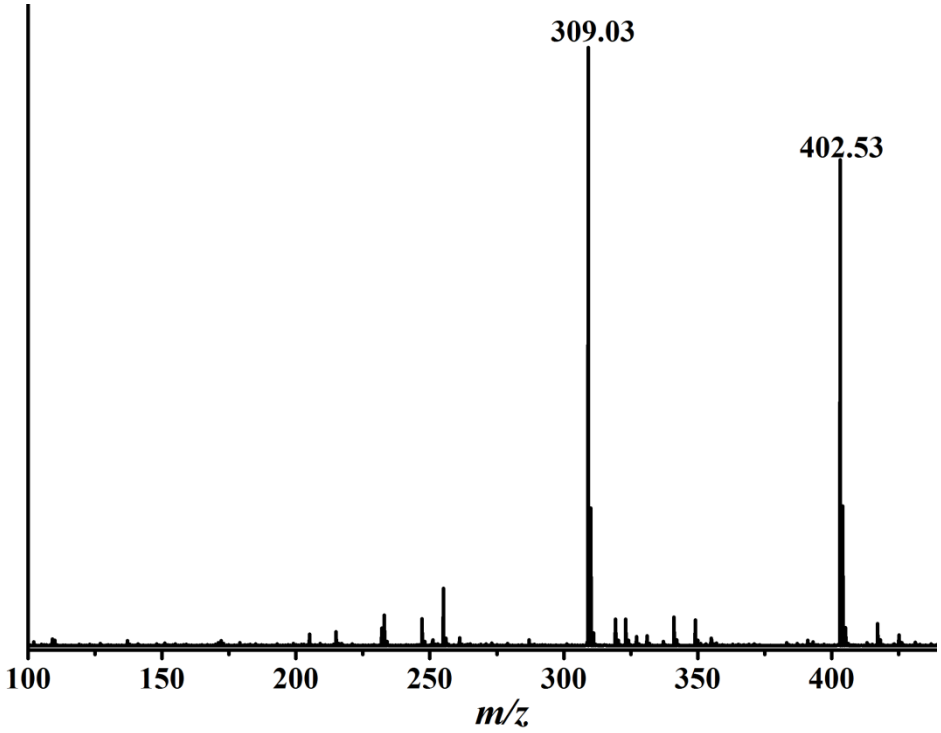

Figure A2.4: High-Resolution ESI (+) mass spectrum of **3.5**

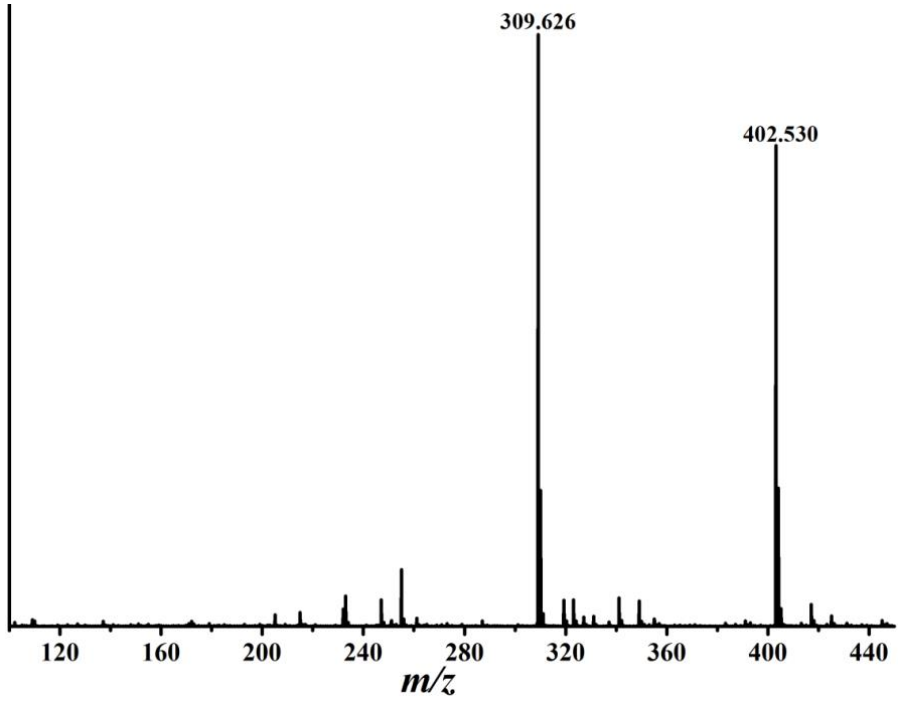

Figure A2.5: High-Resolution ESI (+) mass spectrum of**3.6**

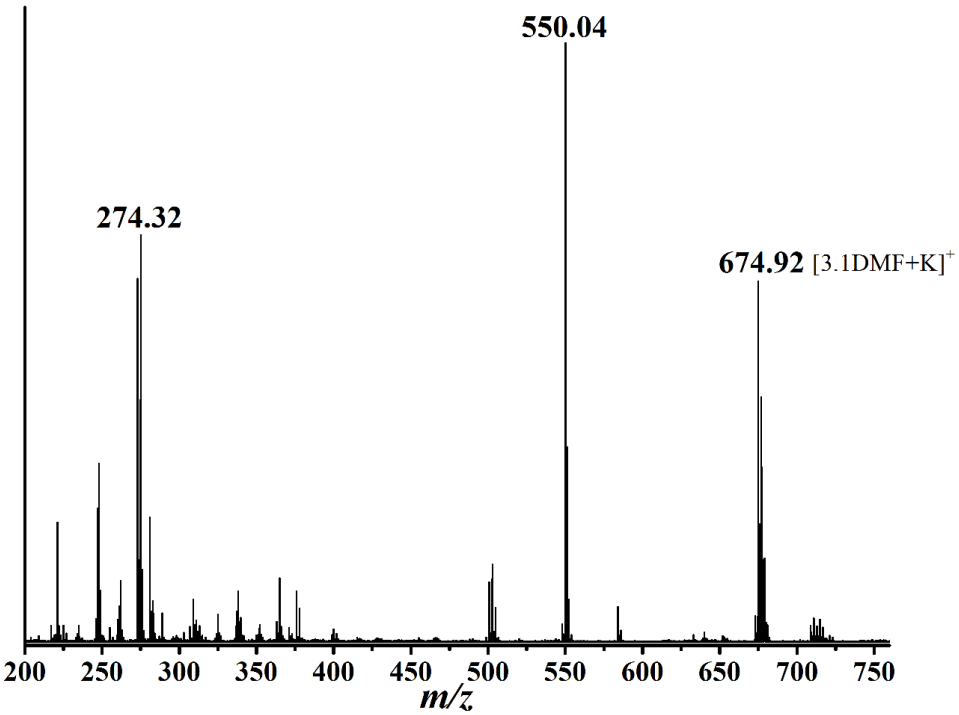

Figure A2.6: MALDI-TOF Spectrum of [**3**.1DMF+K]$^{+}$.

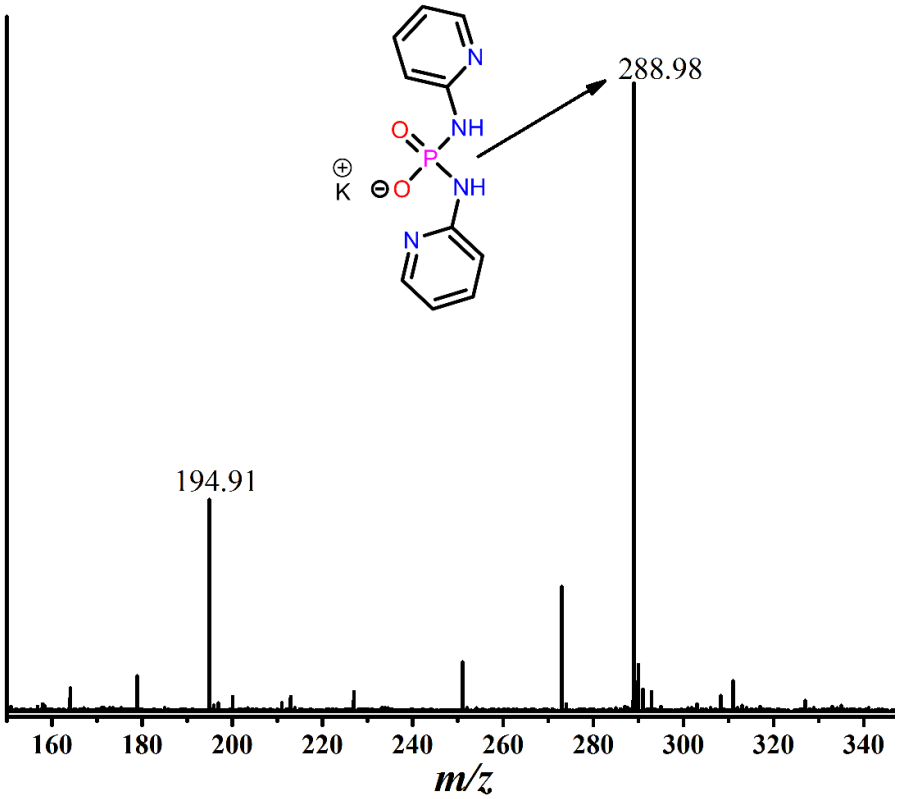

Figure A2.7: MALDI-TOF Mass spectrum of (^{c}**L**)$^{-}$.

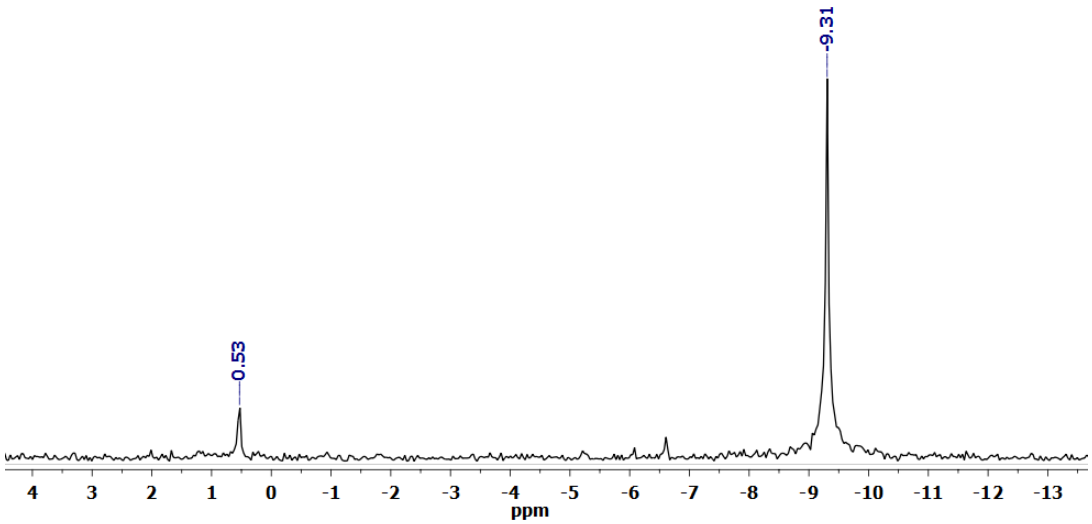

Figure A2.8: ^{31}P-NMR spectra of (^{c}**L**)$^{-}$.

Treatment of 1 with 1M HCl Experiment at 25 °C: To a solution of **6** (30 mg, 0.1 mmol) in MeOH (1 ml) placed in a screw capped glass vessel, 1 M HCl solution in H_2O (1 ml) was added and the final mixture was stirred at room temperature for 15 h. The MALDI-TOF mass spectrum of this reaction mixture gave a prominent peak at m/z 365.0 corresponding to the phosphoramide precursor 6 as its potassium adduct. A minor peak at m/z = 274.98 corresponding to [L^1+Na] was also observed indicating the sluggishness of this reaction at room temperature.

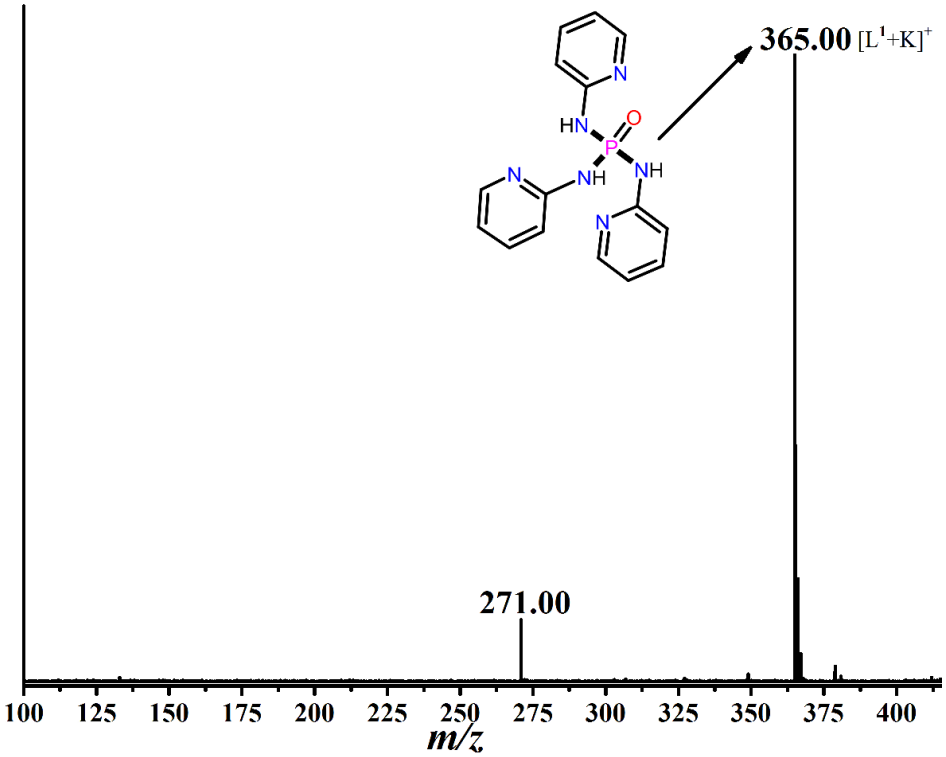

Figure A2.9:MALDI-TOF Mass spectrum of **6** treated with1M HCl at room temperature.

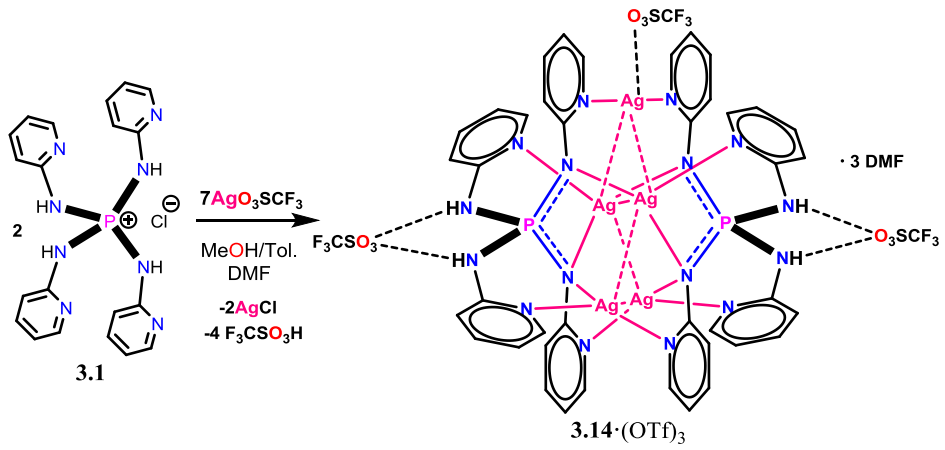

Scheme A2.1: Preparation of the complex **3.14**· $(OTf)_3$ from **3.1**

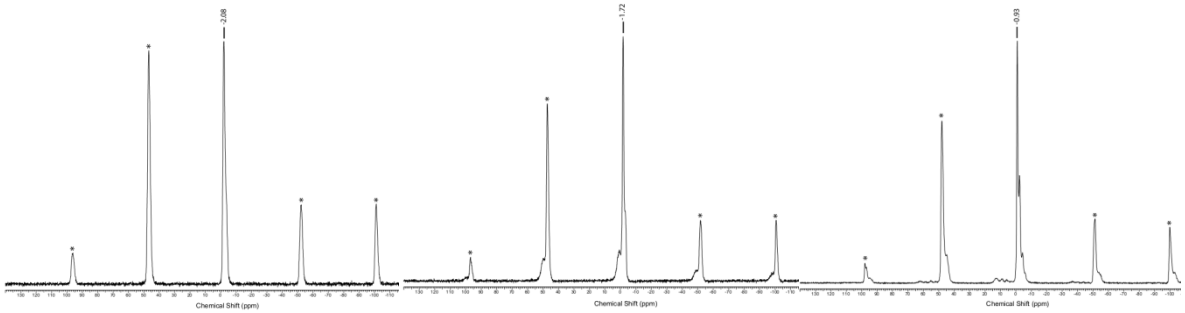

a b c

Figure A2.10: Solid state ^{31}P-CP-MAS NMR spectra of **3.15** (a), **3.16** (b) and **3.17** (c) recorded at a spinning rate of 10 KHz. The peaks denoted with asterisks are spinning side bands

The solid-state NMR spectra were measured on a Bruker Avance DSX 500 spectrometer operating at 202.40 MHz for ^{31}P. All spectra were collected using a 4 mm triple resonance probe and zirconia rotors. The ^{31}P{^{1}H} MAS NMR spectra were measured at a MAS rate of 10 kHz with ^{1}H TPPM decoupling during acquisition at an *rf* field of *ca.* 83 kHz. A ^{31}P $\pi/3$ pulse length of 2.1 μs with a recycle delay of 120.0 s was used.

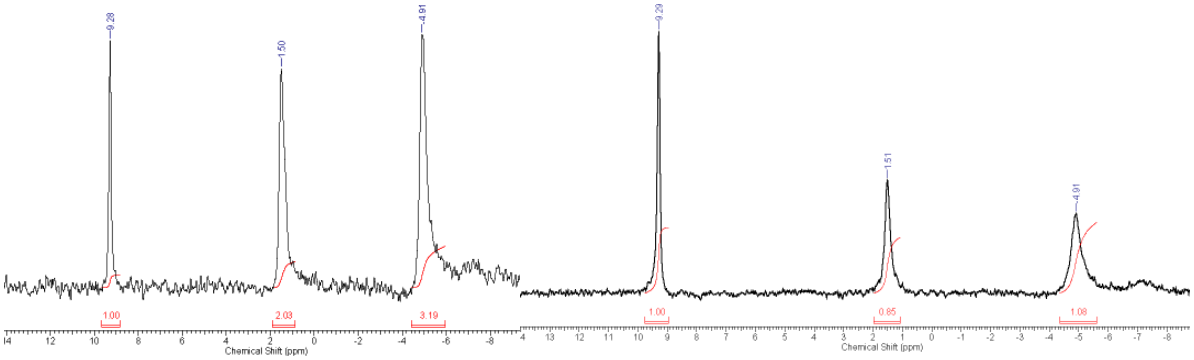

Figure A2.11: Solution ^{31}P- NMR spectra (in d_6-DMSO) of reaction mixtures of **3.2** with (a) excess of $AgClO_4$ and (b) excess of $AgBF_4$ indicating the formation of **3.16** and **3.17** at different ratios after three days.

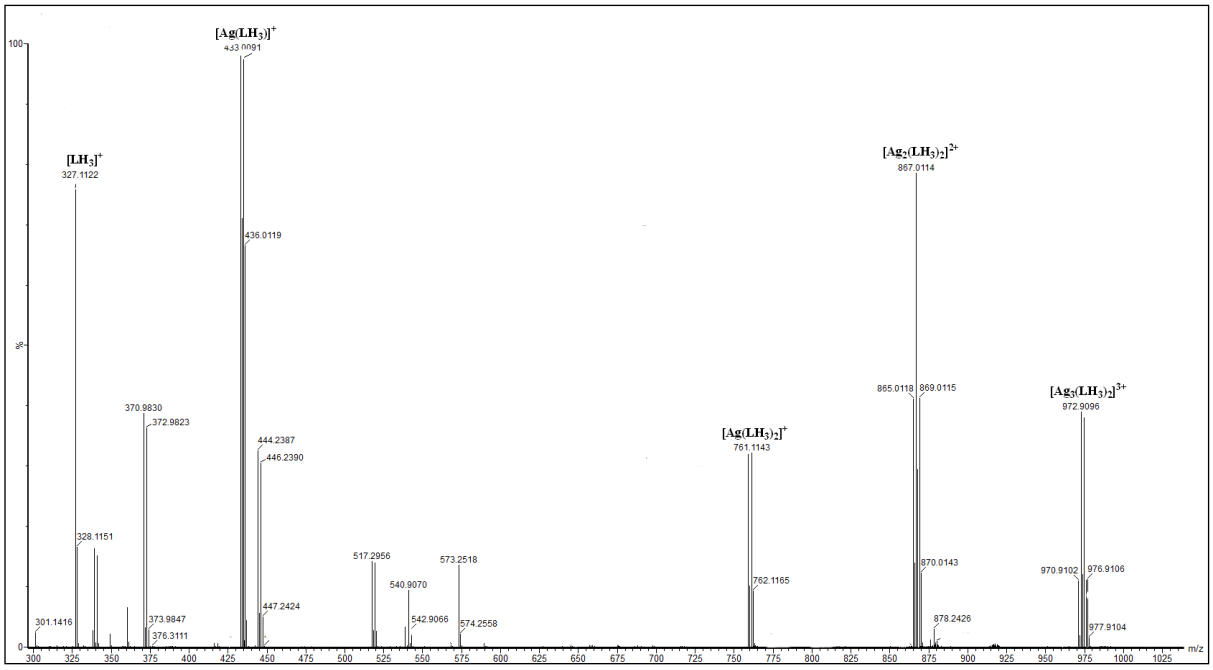

Figure A2.12: ESI (+) Mass spectra of **3.15**.

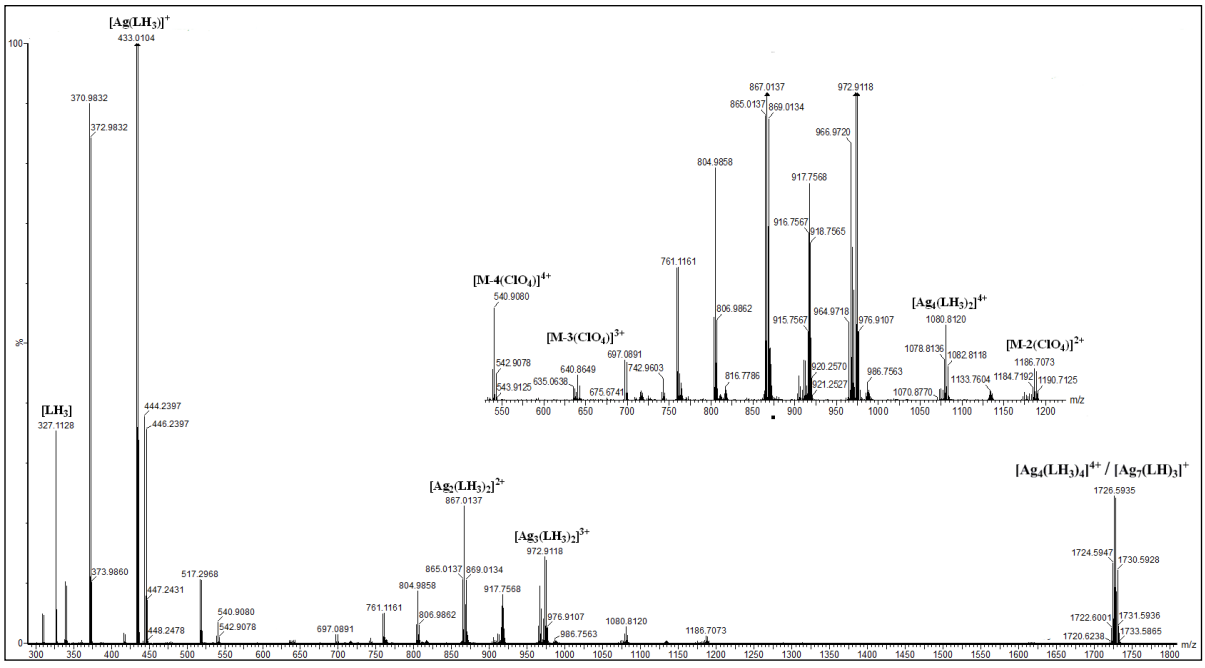

Figure A2.13: ESI (+) mass spectra of **3.16**

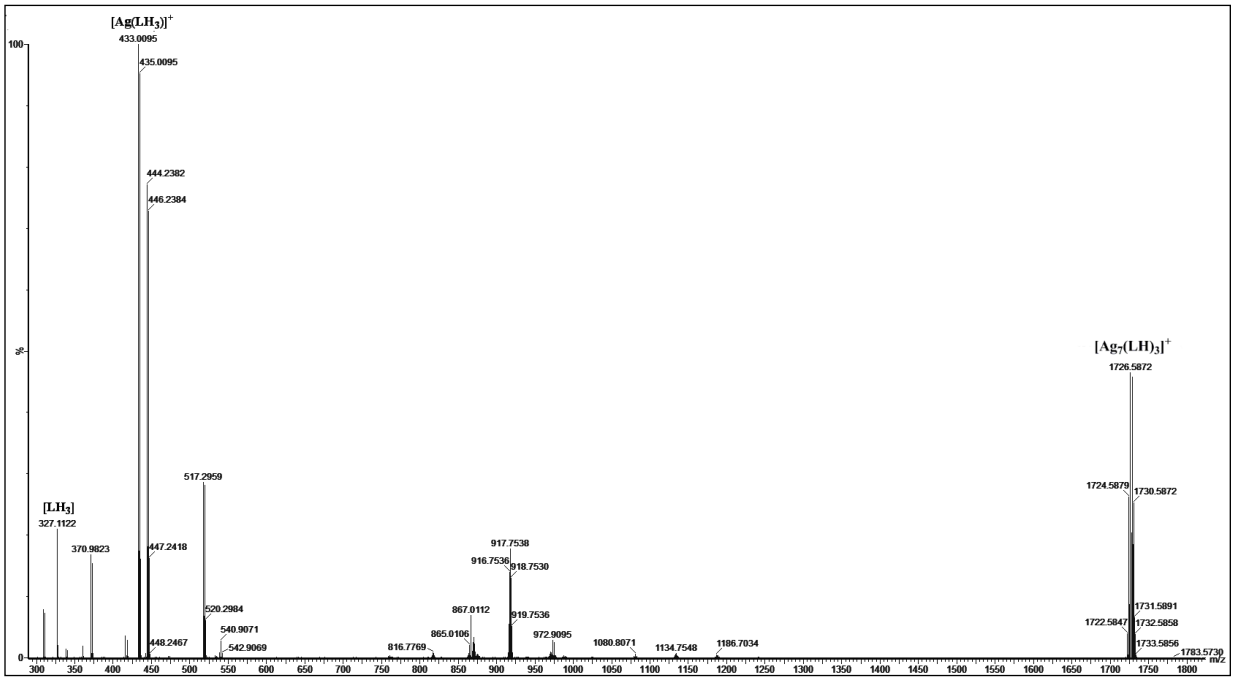

Figure A2.14:ESI (+) mass Spectra of **3.17**.

As the set of ligands and metal ions used are same, many of the peaks were found to be common in all of them. The peak at *m/z* 433.0 corresponds to smallest fragment $[Ag(LH_3)]^+$ and was observed in all the spectra. While the peak at *m/z* 1726.5 corresponds to the cationic core of **3.17**, a similar peak was found in the spectra of **3.16** as well. Although the exact reason for this is unclear, we attribute this to the presence of both mono- and di-anionic imido P(V) species in dilute solutions. Concurrently, the peak at *m/z* 540.9, corresponding to the tetra-cationic core in **3.16** was also found in the spectra of **3.17**.

Theoretical Calculation for 3.1 and 3.5:

DFT Calculations

The molecular geometries were fully optimized at a level of density functional theory employing the hybrid functional B3LYP[1-4] with Pople's basis set 6-31+G(d,p) where polarization functions were added to all the atoms and diffuse functions to the heavy atoms. The convergence threshold for the energies and residual forces on the atoms during geometry optimization were maintained at 10^{-8} hartree and 4.5×10^{-4} hartree/bohr, respectively. The calculation was performed with the development version of Gaussian 03.[5]

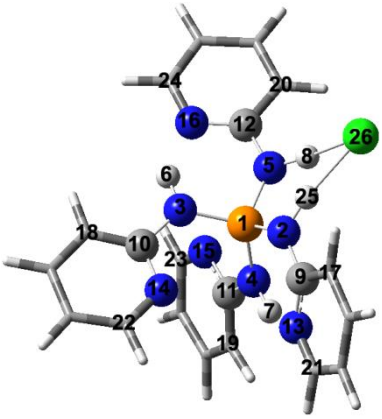

Figure A2.15: Optimized structure of**3.5**

Table A2.2: Optimized parameters for **3.1**

Parameter	**Values**
P1-N2	1.65268Å
P1-N3	1.66442Å
P1-N4	1.66444Å
P1-N5	1.65261Å
N2-H25	1.05658Å
N5-H8	1.05663Å
H25-*Cl*26	2.03875Å
H8-*Cl*26	2.03843Å
N5-H25-*Cl*26	158.10407°
N2-H8-*Cl*26	158.10403°
N13-H7	1.85984Å
N16-H6	1.85977Å
N4-H7…N13	143.69295°
N3-H6…N16	143.63515°
H8-Cl26-H25	59.57691°
C9-N2-P1-N3	100.02229°
C9-N2-P1-N4	-24.45477°
C9-N2-P1-N5	-147.10213°
P1-N2-C9-N13	9.27696°
P1-N5-C12-N16	9.29545°
N2-C9-N13-H7	8.39337°
N5-C12-N16-H6	8.38103°

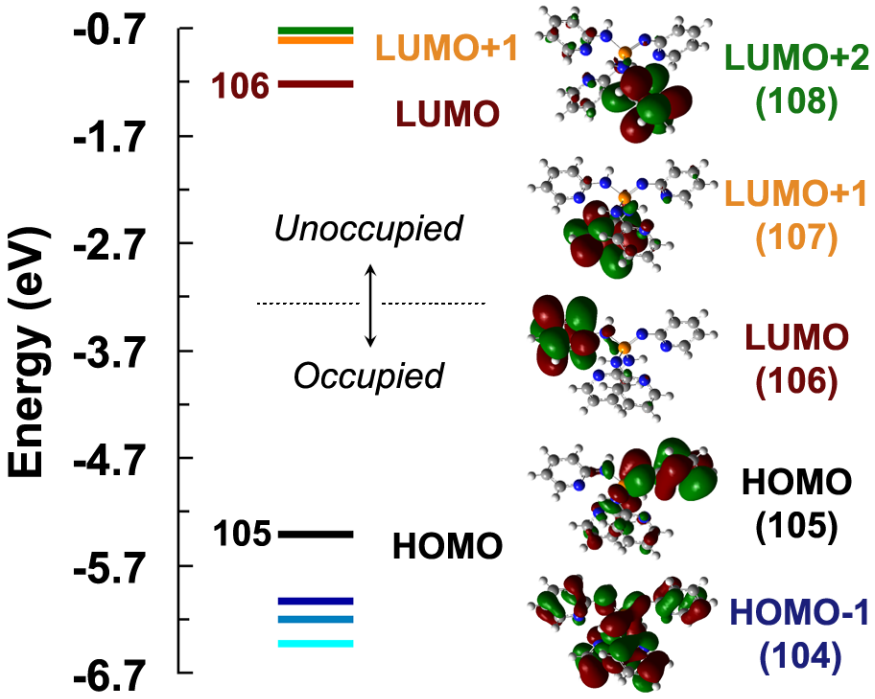

Figure A2.16: Density Functional Theory (DFT) derived molecular orbital energy levels of **3.5**

Table A2.3: Optimized Geometries in Cartesian Coordinates for **3.1**

P	-0.00003395	0.44186378	-0.00005894
N	0.43603269	-0.48844790	-1.30952925
N	-0.43595854	-0.48855766	1.30936090
N	1.26891757	1.48327082	0.19120134
N	-1.26897933	1.48319328	-0.19120878
H	1.45055568	-0.42317163	-1.50590852
H	-1.45045354	-0.42318233	1.50590608
H	0.94619930	2.47493490	0.36095471
H	-0.94631330	2.47491866	-0.36098657
C	-0.32247869	-1.52374371	-1.85551469
N	-1.59671379	-1.60067463	-1.45804215
C	-2.36060592	-2.56927423	-1.98280338
C	-1.90058437	-3.49119640	-2.91991961
C	-0.56405584	-3.39837898	-3.32717744
C	0.24720019	-2.40600970	-2.79216816
C	0.32264867	-1.52370940	1.85545661
N	1.59686086	-1.60065406	1.45789699
C	2.36083498	-2.56912140	1.98276779
C	1.90093431	-3.49090799	2.92008273
C	0.56443581	-3.39808216	3.32742749
C	-0.24690925	-2.40584240	2.79230790
C	2.62066013	1.39465667	-0.17844160
N	3.03155110	0.39564921	-0.96833738
C	4.33131747	0.34254046	-1.30672086
C	5.26782366	1.28279739	-0.89752911
C	4.82338669	2.34142584	-0.09323273
C	3.48952390	2.40377531	0.27996436
C	-2.62073560	1.39443935	0.17840716
N	-3.03148191	0.39550094	0.96846960
C	-4.33124268	0.34225064	1.30684449
C	-5.26787958	1.28231082	0.89748664
C	-4.82359354	2.34086653	0.09301956

C	-3.48973153	2.40334570	-0.28018142
H	-3.39032770	-2.59737798	-1.63343209
H	-2.56314926	-4.25209161	-3.31778125
H	-0.15888316	-4.09536151	-4.05502735
H	1.28742986	-2.30471662	-3.08388762
H	3.39053148	-2.59724412	1.63332047
H	2.56357333	-4.25169675	3.31802389
H	0.15934521	-4.09495060	4.05543227
H	-1.28712016	-2.30454908	3.08409610
H	4.61875105	-0.49052348	-1.94388158
H	6.30454302	1.19774628	-1.20429024
H	5.51455664	3.10931720	0.24123662
H	3.10264845	3.20857301	0.89511488
H	-4.61856823	-0.49075012	1.94413581
H	-6.30458869	1.19715703	1.20425480
H	-5.51487314	3.10860094	-0.24158308
H	-3.10295677	3.20809122	-0.89546098
Cl	-0.00045201	4.24414740	0.00008908

Table A2.4: Optimized Geometries in Cartesian Coordinates for **3.5**

P	0.00000000	0.00000000	0.00000000
N	0.00000000	0.00000000	1.57259501
N	1.46738400	0.00000000	-0.81249952
N	-1.00654510	1.21729937	-0.58672040
N	-0.58664326	-1.53389802	-0.44689420
H	1.57079592	-0.75750606	-1.50143700
H	-1.24778494	1.86375555	0.18282114
H	-1.31795040	-1.82133395	0.19237213
C	-0.35171273	0.98321939	2.46214147
N	-1.03979299	2.08534804	2.07118686
C	-1.37635681	3.00330611	2.99133090
C	-1.07104204	2.89866022	4.34286422
C	-0.36559244	1.75804407	4.75870318
C	-0.00494297	0.80083925	3.82622173
C	2.37379821	1.05353857	-0.80844639
N	2.07981707	2.10552314	-0.03460299
C	2.95056767	3.12350984	0.00017366
C	4.13922303	3.15190876	-0.72538019
C	4.43365839	2.04798223	-1.53597917
C	3.54850002	0.98005761	-1.58508645
C	-1.28230234	1.56604842	-1.90055615
N	-0.92011173	0.69984790	-2.85726805
C	-1.19589470	1.01880419	-4.13018936
C	-1.84255939	2.18954109	-4.51649171
C	-2.22006897	3.08677184	-3.50803871
C	-1.93930296	2.78318639	-2.18403464
C	-0.39367318	-2.38658382	-1.53299500
N	0.71070633	-2.24977787	-2.27879157
C	0.89871702	-3.09127834	-3.30678637
C	0.02254099	-4.11965146	-3.63322722
C	-1.12367070	-4.27070660	-2.84129927
C	-1.34394121	-3.39927436	-1.78587193
H	-1.92370010	3.86677607	2.61602219
H	-1.37112332	3.67296901	5.04074510
H	-0.09993745	1.62564337	5.80440897
H	0.54497782	-0.09185153	4.10259631
H	2.67388399	3.95516467	0.64487893

H	4.80807896	4.00325679	-0.65933856
H	5.34777485	2.02134939	-2.12249045
H	3.74819800	0.10655179	-2.19763071
H	-0.88139911	0.28961825	-4.87450635
H	-2.04274474	2.39267305	-5.56302262
H	-2.72487674	4.01632775	-3.75596845
H	-2.20984211	3.45787810	-1.37809995
H	1.80579841	-2.93032253	-3.88502064
H	0.22777664	-4.77711508	-4.47068921
H	-1.84272994	-5.05667092	-3.05342595
H	-2.23294200	-3.48058332	-1.16788389

DFT calculations for **3.3**:

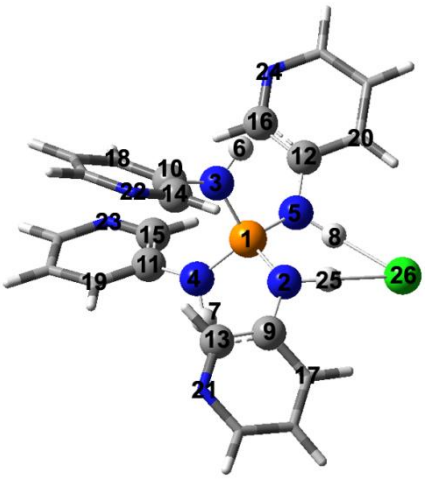

Figure A2.17: Optimized structure of **3.5**

Table **A2.5**: Optimized parameters for **3.3**

Parameter	**Values**
P1-N2	1.64680
P1-N3	1.66067
P1-N4	1.65914
P1-N5	1.64807
N2-H25	1.05577
N5-H8	1.05743
H25-Cl26	2.04058
H8-Cl26	2.02493
X13-H7	2.70103
X16-H6	2.74984
H8-Cl26-H25	58.60037
C9-X13-H7	71.89536
C12-X16-H6	68.64894
C9-N2-P1-N3	105.29630
C9-N2-P1-N4	-13.33901
C9-N2-P1-N5	-140.44071
P1-N2-C9-X13	-41.91922
P1-N5-C12-X16	-40.98234
N2-C9-X13-H7	60.33047
N5-C12-X16-H6	63.00766

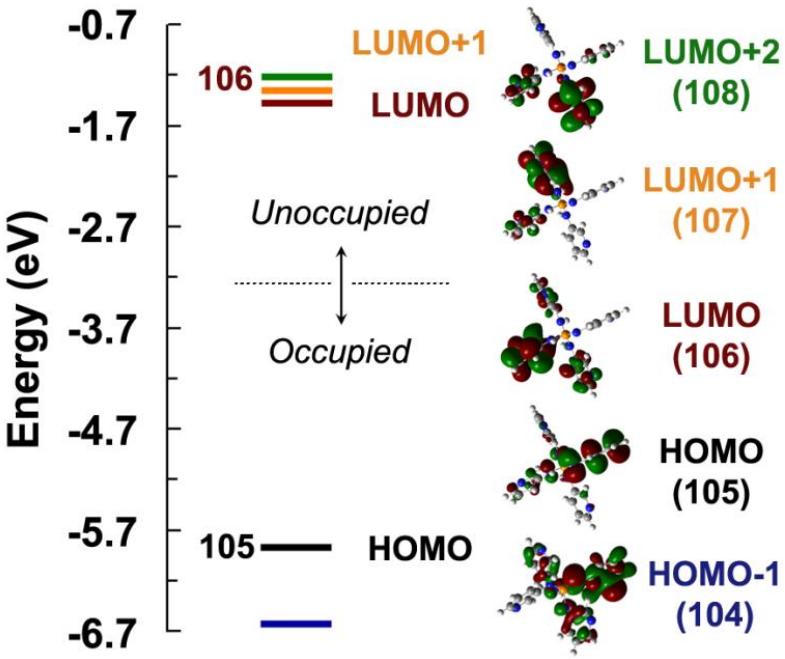

Figure A2.18: Density Functional Theory (DFT) derived molecular orbital energy levels of **3.6**

Table **A2.6**: Optimized Geometries in Cartesian Coordinates for **3.6**

P	0.00000000	0.00000000	0.00000000
N	0.00000000	0.00000000	1.66062951
N	1.59580236	0.00000000	-0.45399776
N	-0.99685363	-1.25437320	-0.38603008
N	-0.66034869	1.25206329	-0.84153870
H	-0.75643447	-0.53892278	2.07148706
H	1.76770582	0.43665903	-1.35585127
H	-1.71553819	-0.97887025	-1.11113731
H	-1.61840707	1.00592021	-1.21051438
C	0.77712472	0.76036354	2.59013123
C	0.81865767	2.15917959	2.53836097
N	1.52347413	2.90387564	3.39775031
C	2.18632441	2.27231080	4.37458538
C	2.17713734	0.88325010	4.53438668
C	1.46798544	0.11044313	3.61746579
C	2.66200248	-0.83800565	0.02623631
C	2.75017612	-2.18058129	-0.36436118
N	3.74493967	-2.99091740	0.01295899
C	4.70357786	-2.47585292	0.79394781
C	4.71605868	-1.14582929	1.22326400
C	3.67266640	-0.30828405	0.83195956
C	-1.37735392	-2.39471402	0.37103078
C	-0.48386143	-3.12292306	1.17123377
N	-0.83868006	-4.20062616	1.88052614
C	-2.10665630	-4.62010199	1.79417248
C	-3.06583214	-3.98069886	1.00293487
C	-2.70393675	-2.84498210	0.28479747
C	-0.05507493	2.31904495	-1.56358640
C	1.06491312	3.03305787	-1.11042231
N	1.61952226	4.04367070	-1.79096352
C	1.05780660	4.40599314	-2.94971234
C	-0.07368387	3.77420134	-3.47470681

C	-0.63841885	2.70999743	-2.77938476
H	0.25100486	2.69491828	1.78176622
H	2.74018156	2.90492308	5.06403848
H	2.72084676	0.41951035	5.35121305
H	1.44649848	-0.97305196	3.68892330
H	1.98846383	-2.60832717	-1.01304430
H	5.50093591	-3.15653498	1.08273874
H	5.52496740	-0.77651390	1.84557998
H	3.63858558	0.73340040	1.13355811
H	0.56043037	-2.82925053	1.24064469
H	-2.36182888	-5.50340719	2.37446636
H	-4.08150707	-4.36087070	0.95619914
H	-3.41528670	-2.30747466	-0.33632764
H	1.53617236	2.78528931	-0.16414049
H	1.52687306	5.23518310	-3.47349315
H	-0.50137505	4.10516074	-4.41593207
H	-1.51289449	2.18195727	-3.15016242
Cl	-3.15504028	0.02203788	-2.12424747

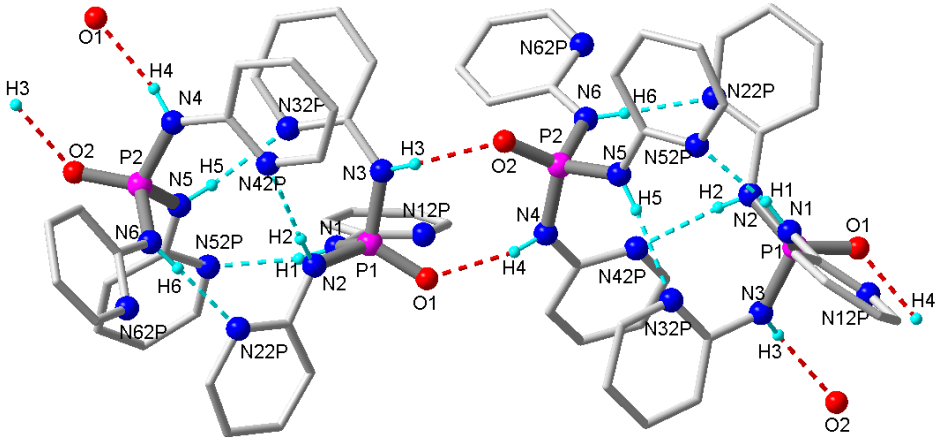

Figure A2.19: Crystal Structure of **3.2**·C_7H_8

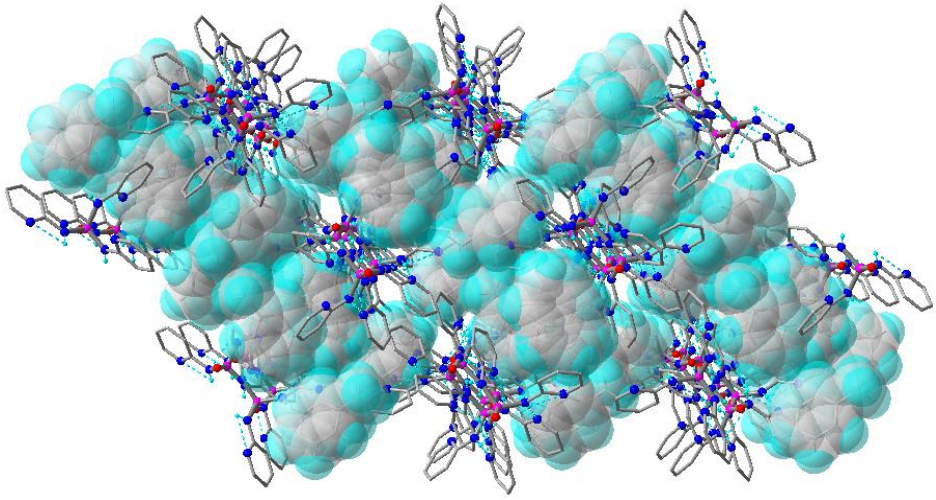

Figure A2.20: Packing diagram of **3.2**.C_7H_8

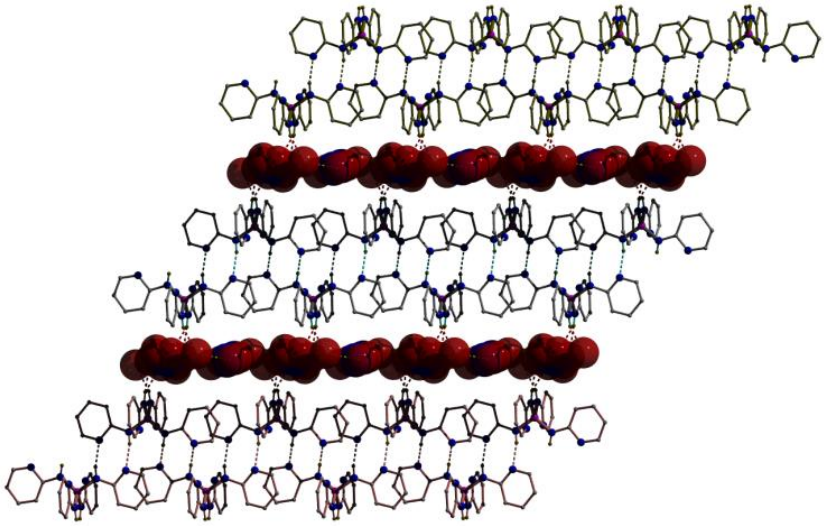

Figure A2.21: Formation of 2D-layred structure of **3.7** mediated by hydrogen bonded solvated water and disordered nitrate motifs

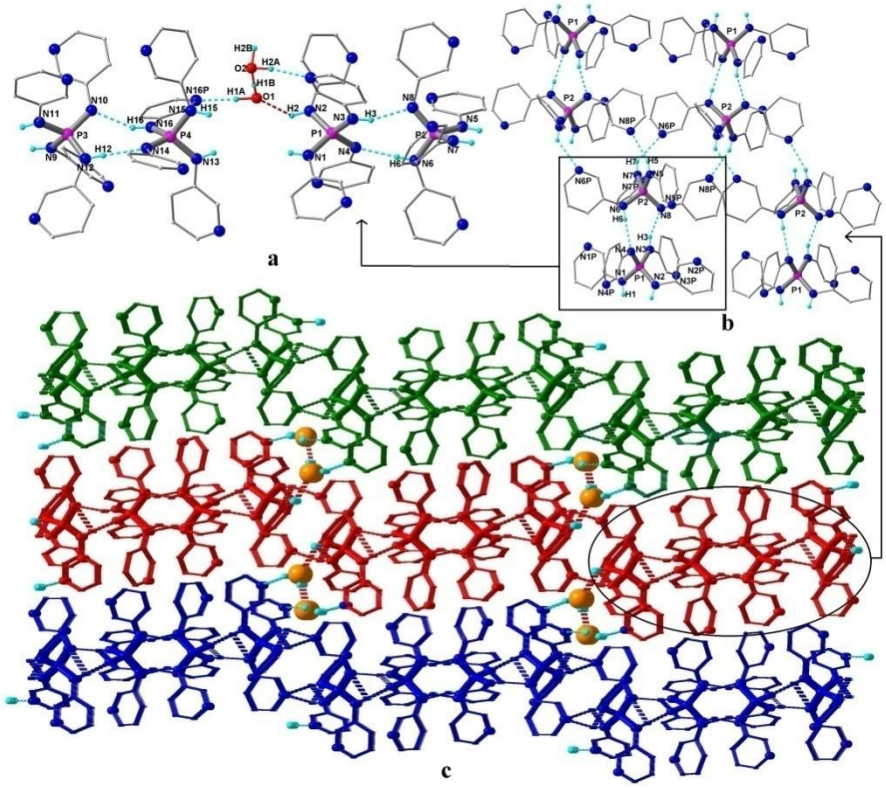

Figure A2.22: (a) Molecular structure of **3.8** in its asymmetric unit; (b) formation of 2D-sheet structure in **3.7**·1/2H_2O mediated by N-H...N interactions; (c) view of the 3D-network in **3.7**·1/2H_2O in which the individual 2D-sheets are connected by the solvated

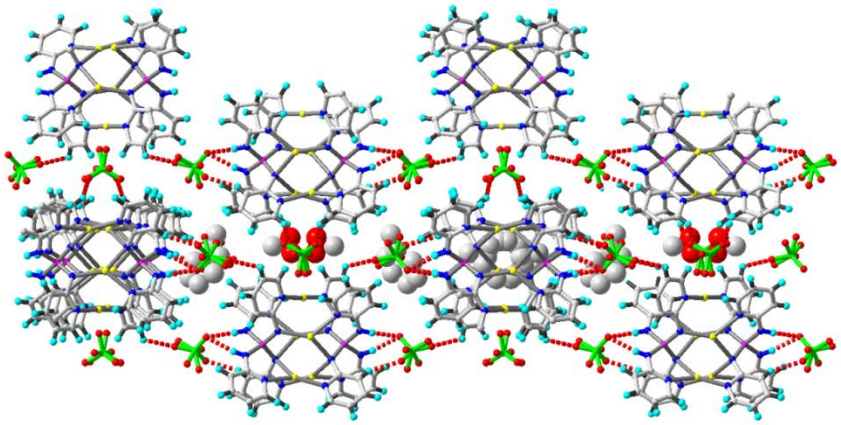

Figure A2.23: View down the channel structure of **4** showing the inner arrangement of solvated toluene and methanol molecules

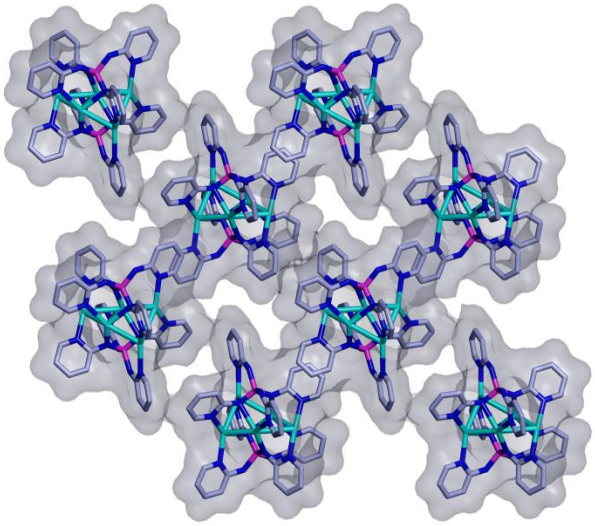

Figure A2.24: Surface overlay view of **3.16**·3DMF, the cationic core showing two distinct cavities available for DMF (smaller) and triflates (larger). Colour Code: nitrogen, blue; carbon, light grey; phosphorus, purple; fluorine, green; oxygen, red; sulphur, yellow; silver, cyan

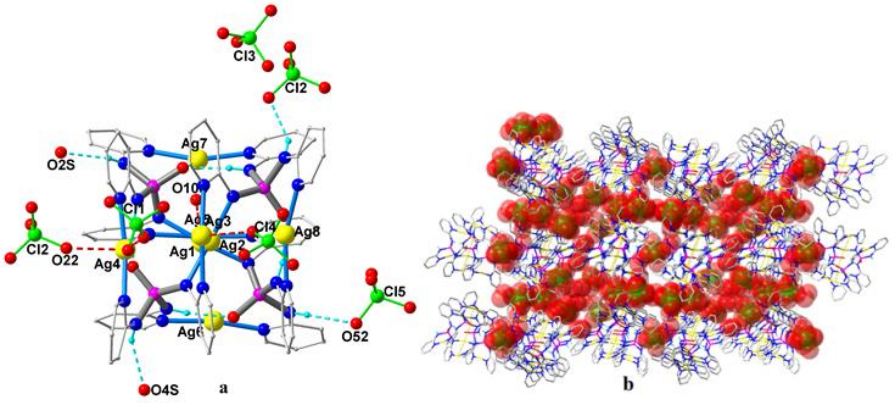

Figure A2.25: (a) View of the octa-nuclear cluster in **3.16**·5CH_3OH.3H_2O along with coordinated and H-bonded perchlorates. The disordered perchlorate groups are omitted; (c) packing diagram of **3.16**·5CH_3OH.3H_2O showing 1D-solvent channel

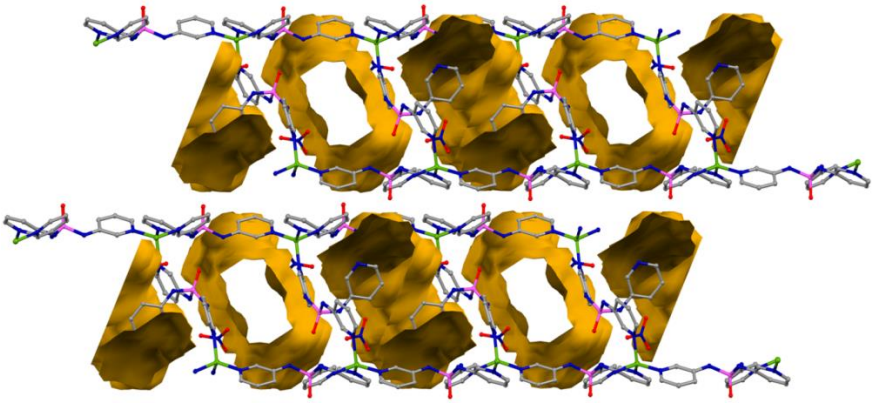

Figure A2.26: Connolly surface view of the 2x2x2 packing diagram of **3.20** showing the solvent accessible voids.

pka calculations for 3.2 and 3.3

In order to probe the base strength of **3.3**, a preliminary pk_a measurement in methanol was carried out by using UV-visible spectroscopy. A dilute solution of **3.3** in methanol was titrated against dilute sulphuric acid (0.025 molar in methanol) and the absorption bands were recorded after every addition (Figure 3.26a). The observed spectral changes (depletion of the intensity at ~220 and increase in intensity at ~240 and ~315 nm) indicate that upon addition of H_2SO_4, protonation at the imino site occurs initially. Further addition of the acid lead to the cleavage of the protonated species (**3.3**H^+) yielding the phosphate derivative **3.2** in its protonated form. This was evidenced by a parallel titration of **3.2** with 0.025 M H_2SO_4 in methanol and monitoring the spectral band at ~315 nm (Figure 3.26b). The pk_a of **3.2** was obtained from the Henderson-Hammette plot of log [**3.2**]/[**3.2**H^+] vs log [H^+].[37] The obtained pk_a of 4.35 shows the acidic nature of the amino protons, despite the molecule having several basic N-sites. Although this value is an approximation, as the measurements were carried out in non-aqeuous medium, it explains the propensity of **3.2** or **3.3** for deprotonation under mild conditions.

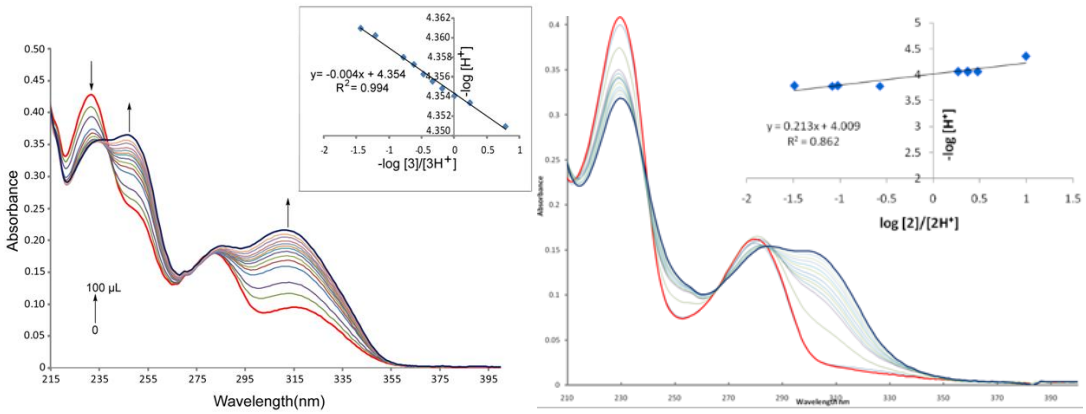

Figure A2.27: (a) Titration of **3.5** with 0.025 molar H_2SO_4 in methanol. The inset shows the Henderson-Hammette plot of log [**3.5**]/[**3.5**H^+] vs pH (b) Parallel Titration of **3.2** with 0.025 M H_2SO_4 in MeOH. The inset shows the Henderson-Hammette plot of log [**3.2**]/[**3.2**H^+] vs pH

The pka of a base (or a conjugate acid) can be obtained by the Hammettes equation, which is used for the dissociation reaction of an acid in aqueous medium and given by following equation

3.3$H^+ + H_2O \rightleftharpoons$ **3** $+ H_3O^+$

$$H_0 = pKa + \log\frac{[3.3]}{[3.3H^+]}$$

Where $[3.3H^+]$ and [3.3] are molar concentration of conjugate acid and base respectively. H_0 is called Hammette's acidity function, which is given by the following reaction

$$H_0 = -log\frac{a_{H^+} f_{3.3}}{f_{3.3H^+}}$$

The factors f_3 and f_{3H^+} are the acidity co-efficients of the base and the conjugate acid. The parameter a_{H^+} is the activity of the proton: for dilute solution H_0 is replaced by pH. A plot of pH versus $\log\frac{[3.3]}{[3.3H^+]}$ is a straight line with unit slope and *pH= pKa when [3.3] = [3.3H$^+$]*. The factor $\log\frac{[3.3]}{[3.3H^+]}$ can be determined from following relation.

$$\frac{[3]}{[3H^+]} = \frac{[A_3 - A]}{[A - A_{3H^+}]}$$

Where A_{3H^+} and A_3 are the absorbance (at the analytical wavelength) of the pure $3.3H^+$ and 3.3 respectively. And *A* is the absorbance (at same wavelength) of any solution in which $3.3H^+$ is partially ionized.

$$\frac{[3.3]}{[3.3H^+]} = \frac{[3.3]}{\{[C] - [3.3]\}}$$

Where [C] = Molar concentration of compound in experimental solution.

$$[3.3] = \frac{A(\lambda_1)\varepsilon_{3.3H^+}(\lambda_2) - A(\lambda_2)\varepsilon_{3.3H^+}(\lambda_1)}{\varepsilon_{3.3}(\lambda_1)\,\varepsilon_{3.3H^+}(\lambda_2) - \varepsilon_{3.3}(\lambda_2)\,\varepsilon_{3H^+3}(\lambda_1)}$$

εis molar extinction coefficient. Generally two wavelengths (λ_1 andλ_2) were chosen on both side of isobestic point.

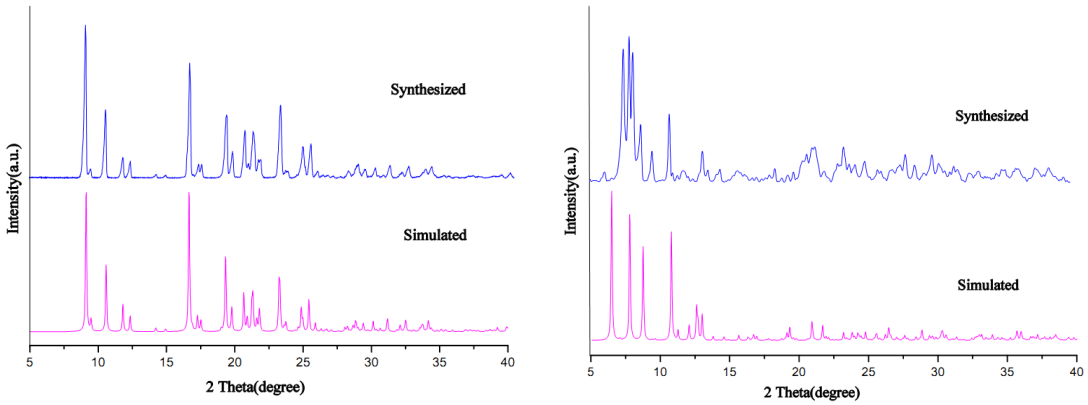

Figure A2.28: PXRD pattern for **3.5**(left) and **3.14**·$(ClO_4)_3$(right). The slight mismatch of the experimental and simulated pattern for 4 is presumably due to the presence of solvated molecules in the single crystal X-ray data.

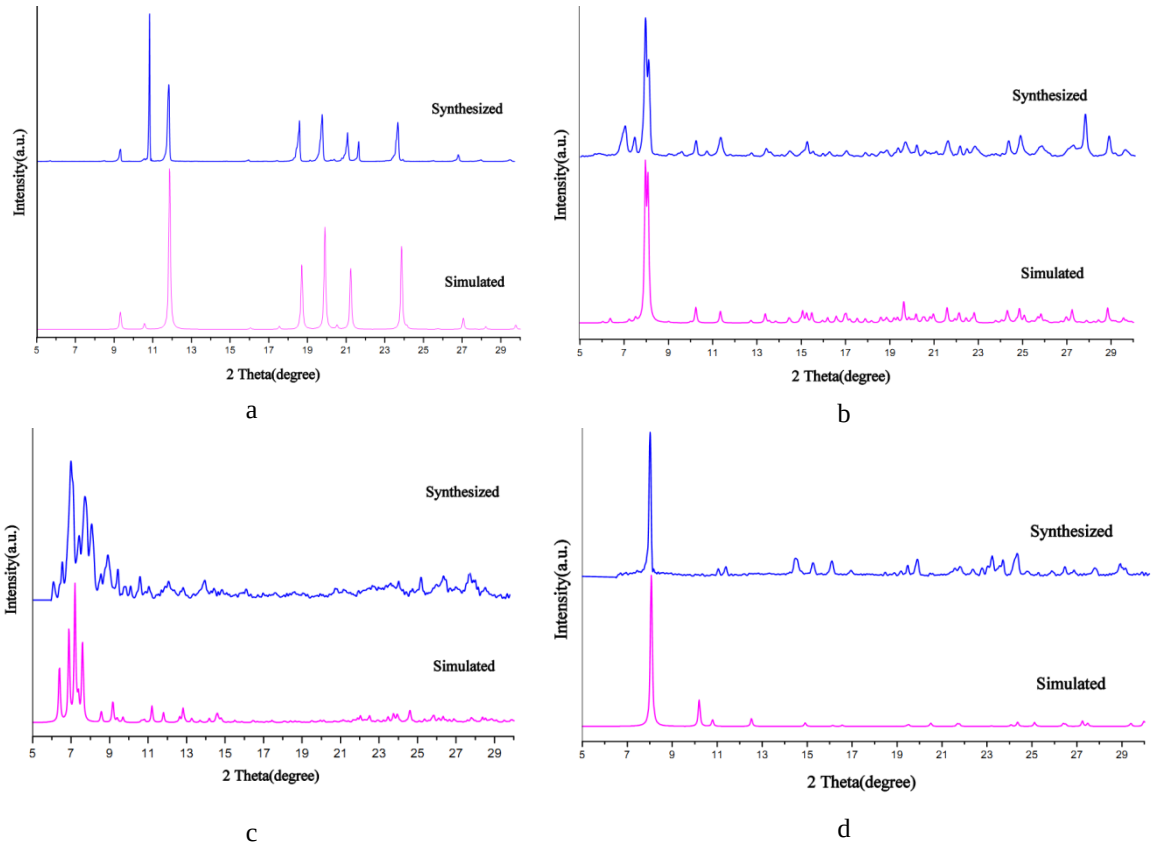

Figure A2.29: PXRD patterns for **3.2**.C_7H_8 (a), **3.15** (b), **3.16** (c) and **3.17** (d). A slight mismatch of the synthesized and simulated patterns for **3.2**, **3.15** and **3.16** is due to the presence of solvated molecules in their single crystal X-ray data

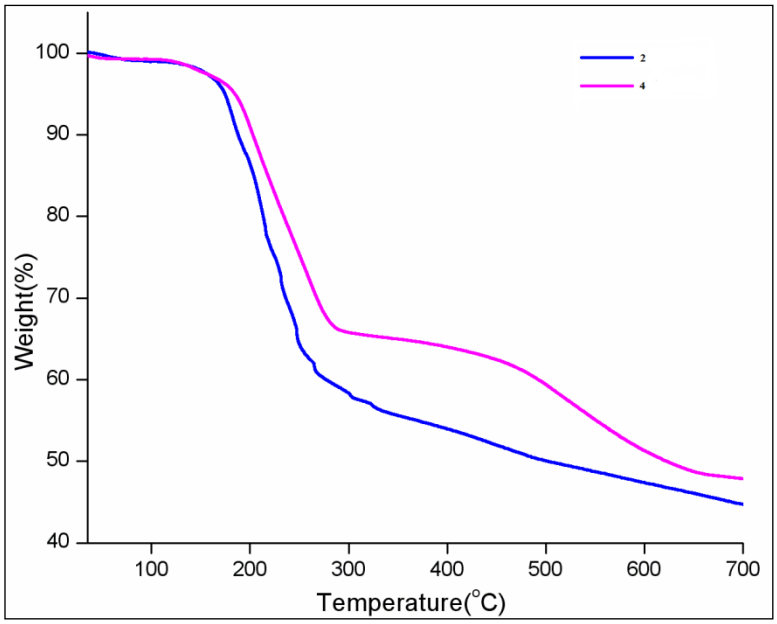

Figure A2.30: TGA traces of the compounds **3.15** and **3.17**

Appendix 3

Table A3.1: Crystallographic Data

Compound	**4.1**	**4.2**·$CH_3OH·H_2O$	**4.3**
Chemical formula	$C_{20}H_{20}N_8PCl$	$C_{16}H_{21}N_6O_3P$	$C_{14}H_{20}N_5O_6PZn$
Formula weight	438.86	376.36	450.69
Temperature (K)	150(2)	296(2)	100(2)K
Crystal system	Cubic	Monoclinic	Orthorhombic
Space group	I-43d	Pc	Pbca
a (Å); α (°)	18.926(5); 90	10.922(6); 90	14.073(2); 90
b (Å); β(°)	18.926(5); 90	9.348(5); 110.05(3)	15.623(3); 90
c (Å); γ (°)	18.926(5); 90	9.763(5); 90	18.459(3); 90
V ($Å^3$); Z	6779(3); 12	936.42(9); 2	4058.3(12); 8
ρ (calc.) mg m^{-3}	1.290	1.335	1.475
μ(Mo K_α) mm^{-1}	0.263	0.176	1.328
$2\theta_{max}$ (°)	56	56	50
R(int)	0.0417	0.0742	0.186
Completeness to θ	99.5 %	98.1 %	99.8%
Data / param.	1398 / 75	4038 / 243	3576 / 253
GOF	1.190	1.070	1.001
R1 [F>4σ(F)]	0.0707	0.0474	0.0499
wR2 (all data)	0.2389	0.2389	0.1302
max. peak/hole (e.$Å^{-3}$)	1.064 / -0.329	1.064 / -0.447	0.973 / -0.445

Compound	**4.3a**	**4.4**	**4.5**
Chemical formula	$C_{12}H_{17}N_4O_6PZn$	$C_{14}H_{20}N_5O_6PZn$	$C_{20}H_{24}N_8O_6P_2Cu$
Formula weight	409.64	450.69	597.95
Temperature (K)	100(2)K	100(2)K	100(2)
Crystal system	Orthorhombic	Monoclinic	Orthorhombic
Space group	Pbca	P2(1)/n	Cccm
a (Å); α (°)	14.135(2); 90	11.522(15); 90	13.16(8); 90
b (Å); β(°)	15.420(3); 90	13.900(19); 103.70(3)	14.94(9); 90
c (Å); γ (°)	18.524(3); 90	11.714(16); 90	16.67(10); 90
V ($Å^3$); Z	4037.5(12); 8	1822.7(4); 4	3277(3); 4
ρ (calc.) mg m^{-3}	1.348	1.642	1.212
μ(Mo K_α) mm^{-1}	1.326	1.478	0.805
$2\theta_{max}$ (°)	56	56	50
R(int)	0.0831	0.0544	0.0541
Completeness to θ	99.5%	99.2%	99.7%
Data / param.	4988 / 215	4492 / 244	2168 / 92
GOF	1.102	1.031	1.129
R1 [F>4σ(F)]	0.0598	0.0470	0.0396
wR2 (all data)	0.1700	0.1194	0.1096
max. peak/hole (e.$Å^{-3}$)	1.335 / -0.511	1.471 / -1.089	0.307 / -0.527

Compound	**4.5a**	**4.6**	**4.7**
Chemical formula	$C_{20}H_{22}N_8O_6P_2Cu$	$C_{10}H_{12}ClN_4O_2P$	$C_{53}H_{65}N_{21}O_{11}P_4Cu_2$
Formula weight	595.93	286.66	1423.22
Temperature (K)	100(2)	296(2)	100(2)
Crystal system	Orthorhombic	Orthorhombic	Monoclinic
Space group	Cccm	Pca2(1)	P2(1)/c
a (Å); α (°)	13.450(14); 90	17.593(9), 90	11.6307(15); 90
b (Å); β(°)	14.052(16); 90	8.610(4), 90	19.702(2); 110.414(3)
c (Å); γ (°)	16.673(17); 90	8.481(4), 90	15.347(19); 90
V ($Å^3$); Z	3375.3(6); 4	1284.7(10), 4	3295.8(7); 2
ρ (calc.) mg m^{-3}	1.173	1.482	1.434
μ(Mo K_α) mm^{-1}	0.782	0.422	0.814
$2\theta_{max}$ (°)	50	50	50
R(int)	0.0353	0.1014	0.0713
Completeness to θ	97.1%	95.5	100%
Data / param.	1541 / 91	2132 / 157	8296 / 438
GOF	1.201	1.004	1.035
R1 [F>4σ(F)]	0.0862	0.0714	0.0469
wR2 (all data)	0.1832	0.1840	0.1239
max. peak/hole (e.$Å^{-3}$)	0.614 / -0.656	0.589 / -0.315	1.097 /-0.490

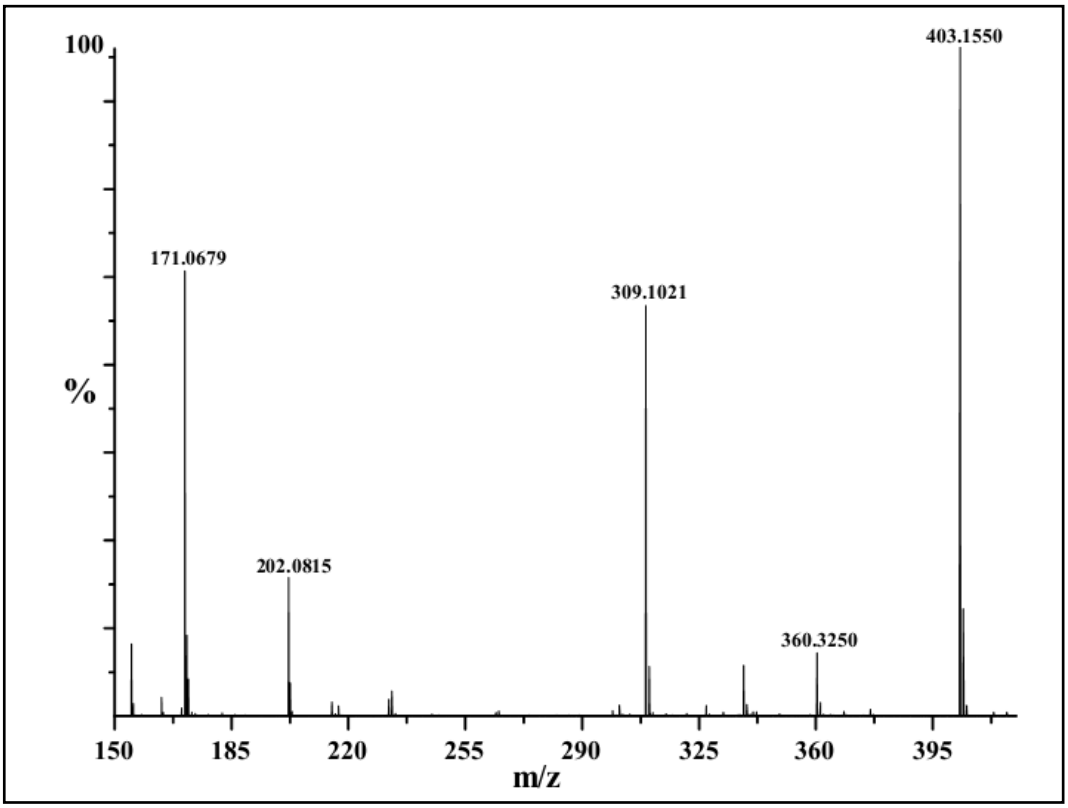

Figure A3.1: MALDI-TOF Mass spectrum of **4.1**.

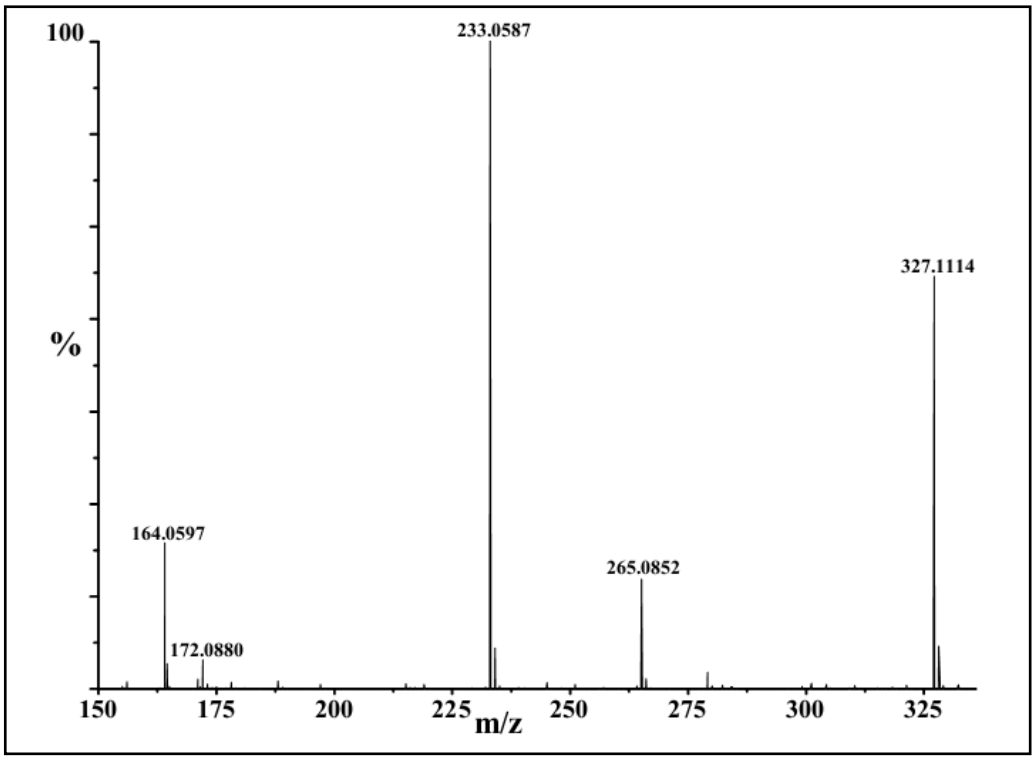

Figure A3.2: ESI (+) Mass spectrum of **4.2**.

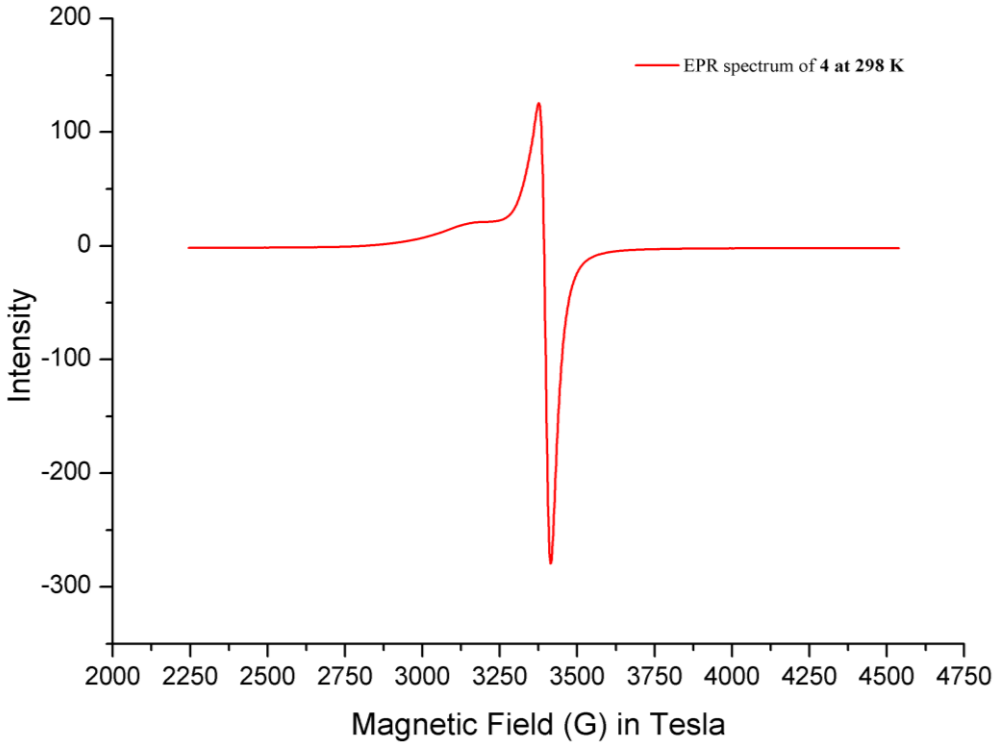

Figure **A3.3**: EPR spectrum of **4** at 298 K

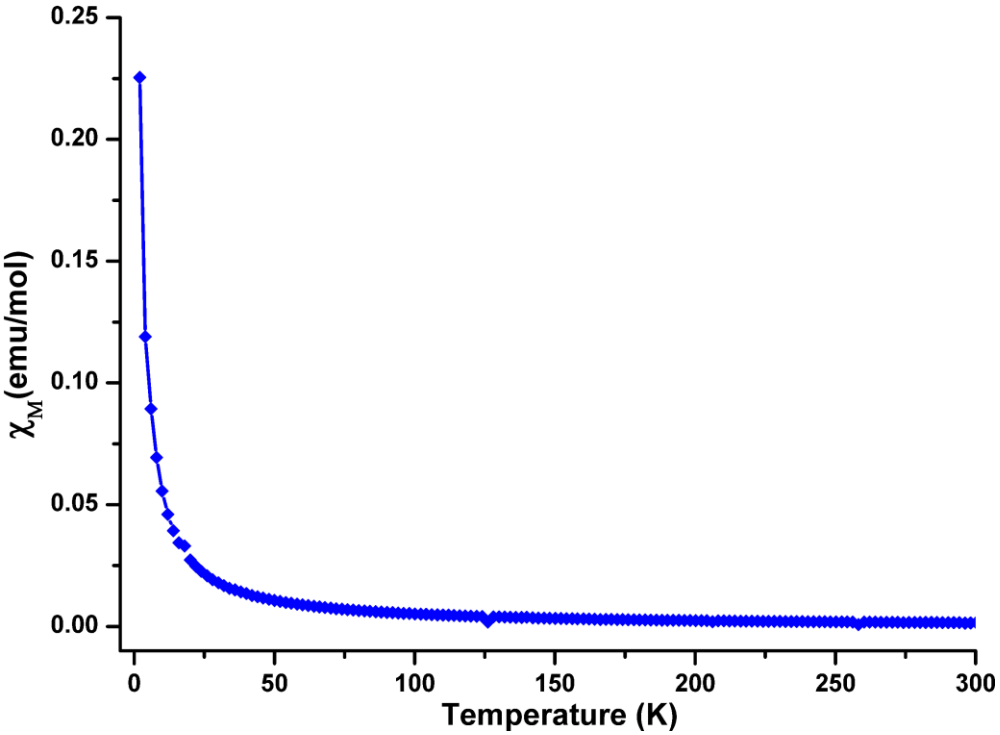

Figure A3.4: Temperature dependence of magnetic susceptibility of **4** measured at 500 Oe field strength

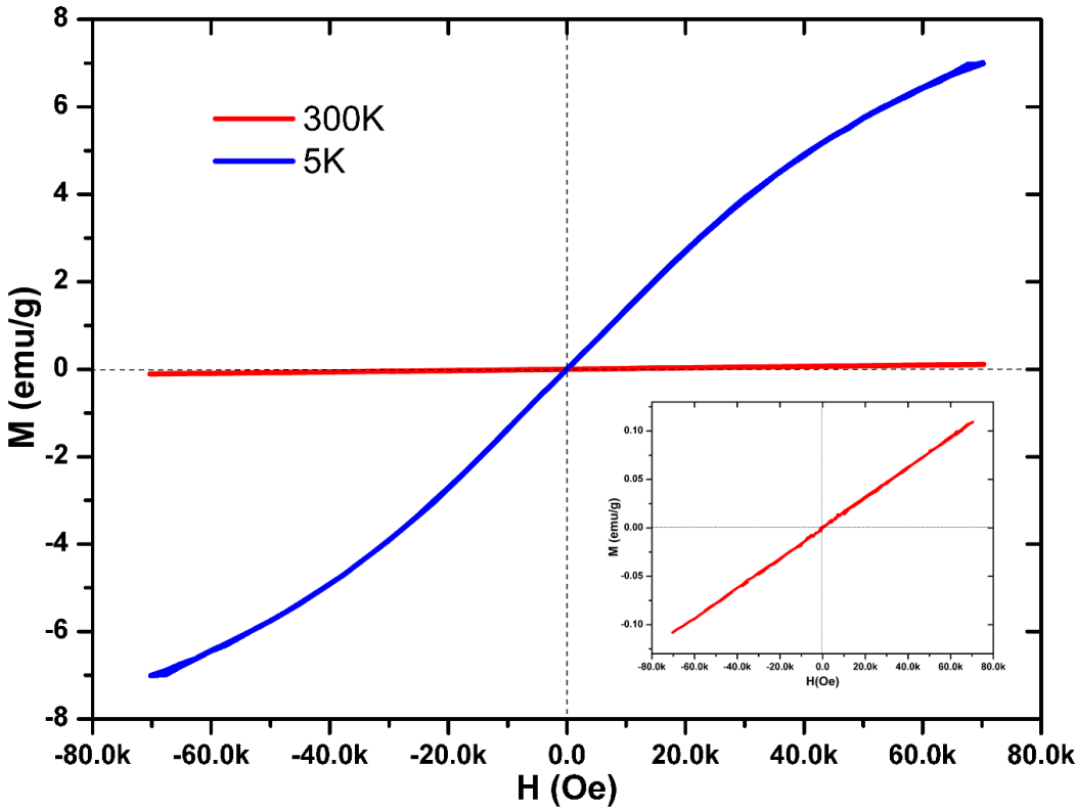

Figure A3.5: M vs H graph of **4** at 300 K and 5 K (Inset shows the expanded view of the 300 K graph).

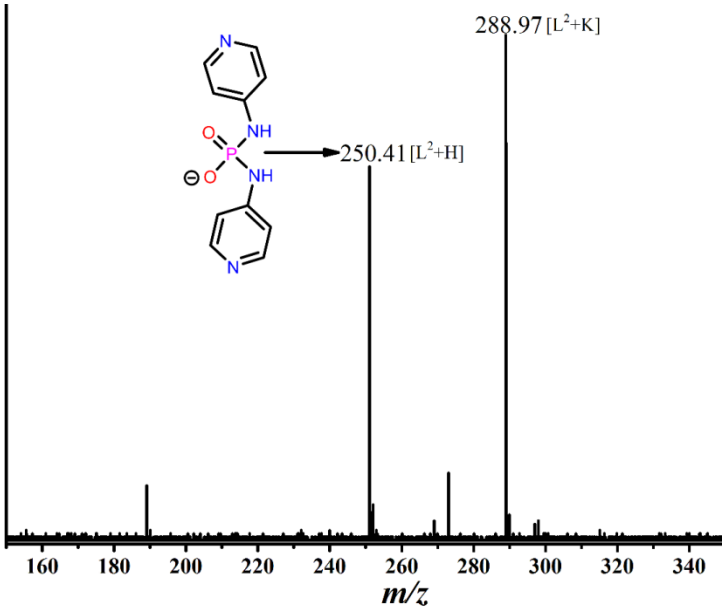

Figure A3.6: MALDI-TOF Mass spectrum of **4.6**.

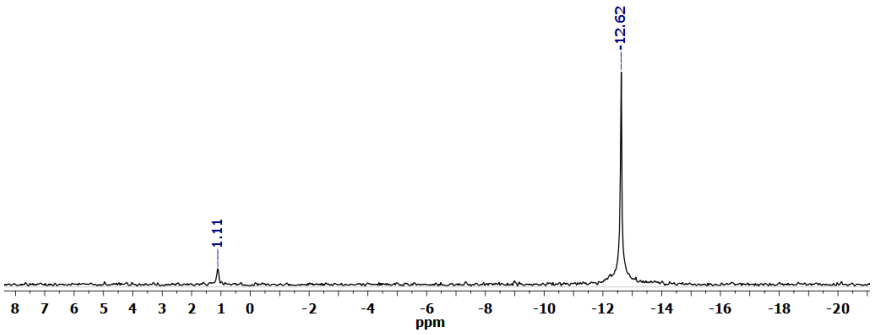

Figure A3.7: ^{31}P-NMR spectrum of **4.6**

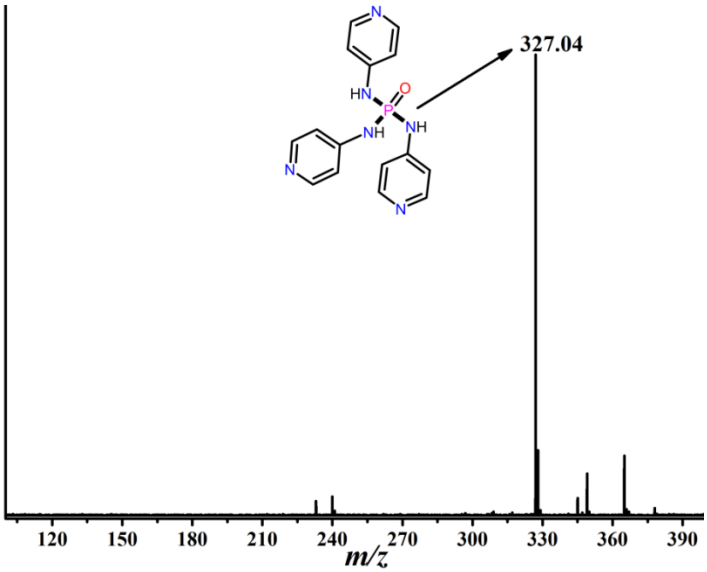

Figure A3.8: MALDI-TOF Mass spectrum of **4.2**treated with 1M HCl at room temperature.

Table A3.2: Selected bond-lengths and angles for **4.1**

Compound	**Bond lengths**	**Bond Angles**
1	P(1)-N(1)#1: 1.631(3) P(1)-N(1)#2: 1.631(3) P(1)-N(1)#3: 1.631(3) P(1)-N(1): 1.631(3)	N(1)#1-P(1)-N(1)#2: 107.02(8) N(1)#1-P(1)-N(1)#3: 107.02(8) N(1)#2-P(1)-N(1)#3: 114.49(16) N(1)#1-P(1)-N(1): 114.49(16) N(1)#2-P(1)-N(1): 107.02(8) N(1)#3-P(1)-N(1): 107.02(8)

Table A3.3. Table of hydrogen bonding parameters for **4.6**

4.6	N(2)-H(2)...Cl(1)#1	2.47	3.232(9)	148.1
	N(24)-H(24)...Cl(1)#2	2.18	3.024(6)	165.9
	N(1)-H(1)...O(1)#3	2.06	2.900(11)	167.1
	N(14)-H(14)...O(2)#4	1.78	2.632(12)	172.6
	Symmetry transformations used to generate equivalent atoms:			
	#1 -x+1/2,y+1,z+1/2 #2 -x+1/2,y+1,z-1/2 #3 -x+1,-y+1,z-1/2			
	#4 x-1/2,-y+1,z			

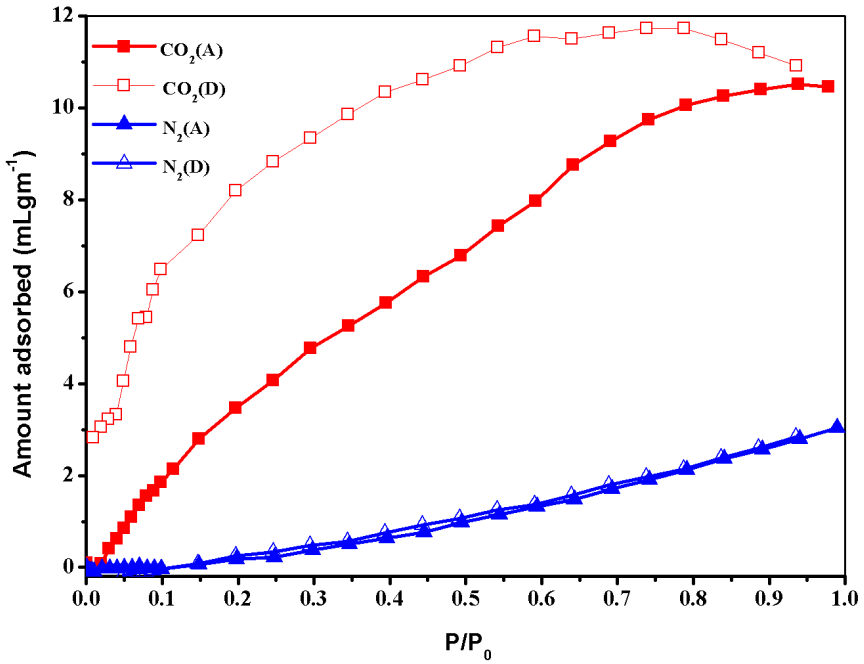

Figure A3.9: CO_2 and N_2 adsorption and desorption isotherms of **4.3b** at room temperature.

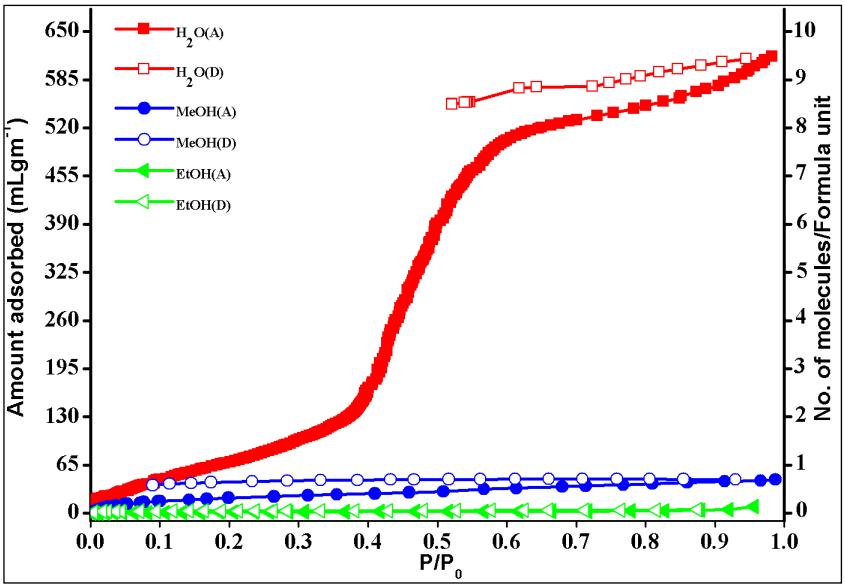

Figure A3.10: Sovent adsorption and desorption isotherms for **4.3b** at 298K

Number of solvent molecules per formula (N) unit has been calculated by

$$N = \frac{\text{Volume adsorbed (V)} \ \mathbf{X} \ \text{Formula weight of the de-solvated sample (F)}}{\text{Molar volume of 1 mol. of a gas at STP (M)}}$$

M = 22.4 litre or 22400 mL for the gases at STP
F = 360.59 g/mol
From the graph, V = 615.91 ml/g for water, V = 45.63 for methanol and V= 8.79 for ethanol
For water adsorption N(w) = 9.91
For methanol adsorption N(m) = 0.734
For ethanol adsorption N(e) = 0.141

The ratio of N(w) / N(m) = 13.5
The ratio of N(w) / N(e) = 70.3

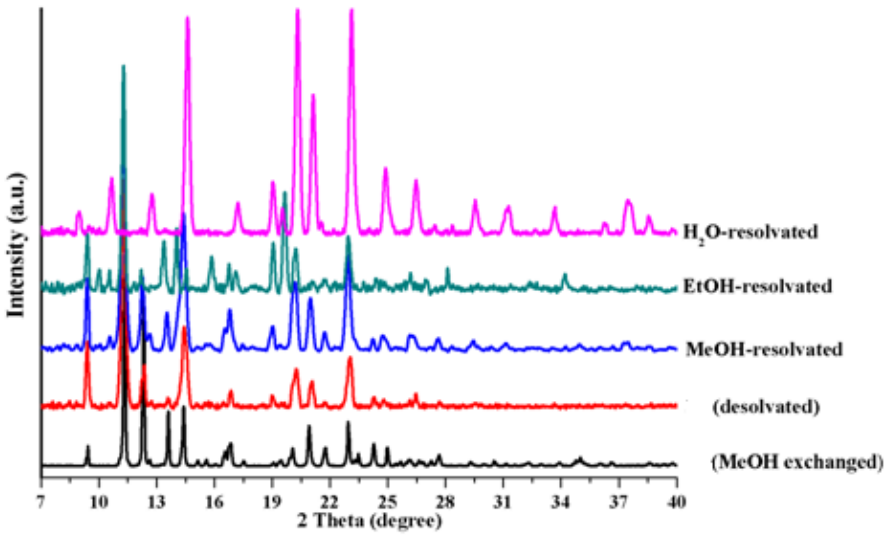

Figure A3.11: Comparitive PXRD patterns for methanol exchanged **(4.3a)**(black), de-solvated **(4.3b)(**red), and various re-solvated samples

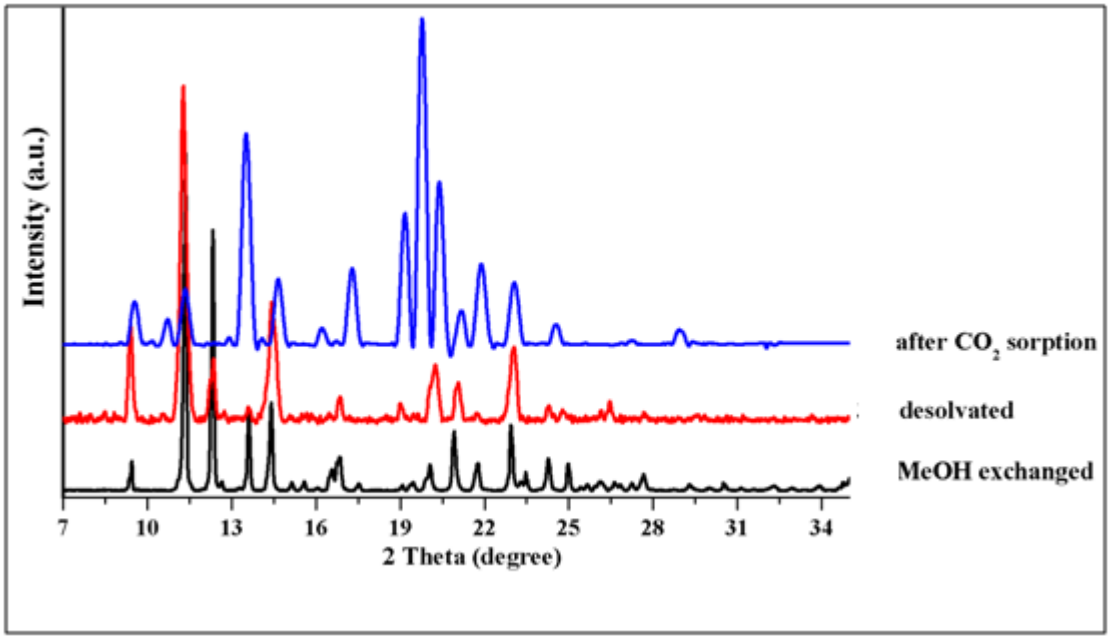

Figure A3.12: Comparitive PXRD patterns for methanol exchanged (4.3a), de-solvated (4.3b), and after CO_2 sorption (4.3e)

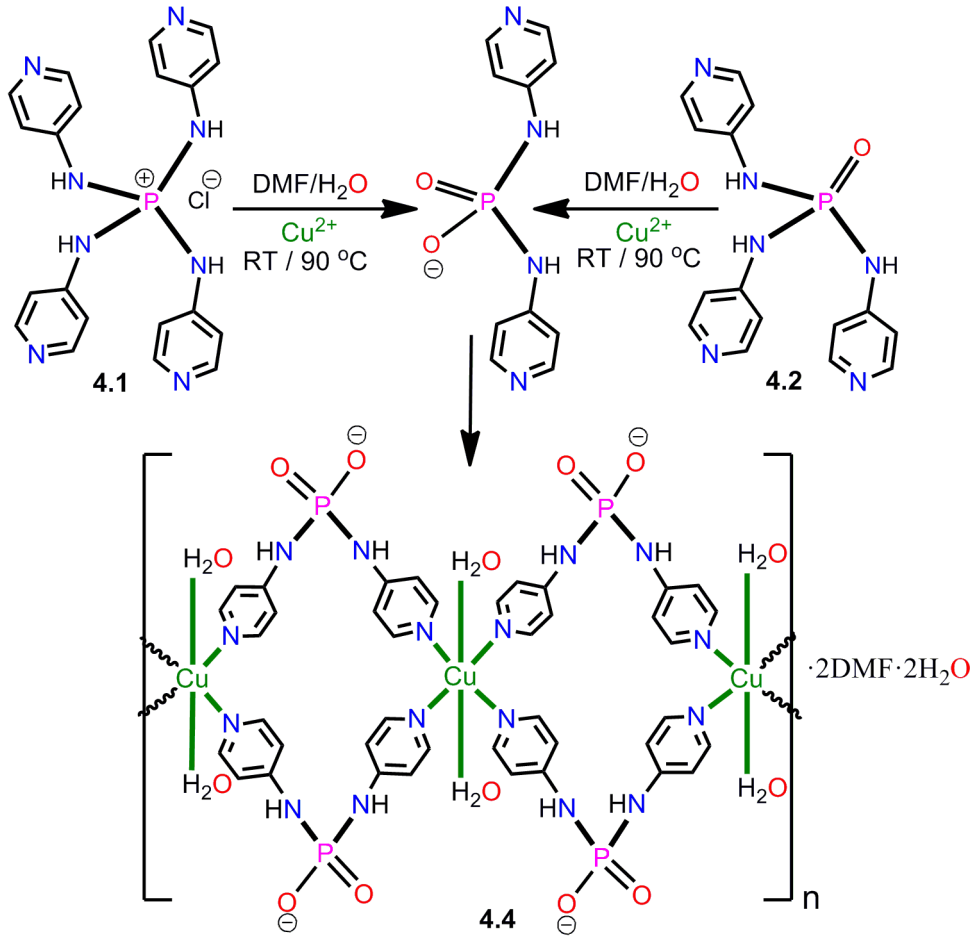

Scheme A3.13: Reaction conditions for the formation of the in-situ ligands and the complexes **4.4**

Details of the TOPOS 4.0 Analysis

```
##################
1: Compound 4 in Cccm
##################
Topology for P1
--------------------
Atom P1 links by bridge ligands and has
Common vertex with                    R(A-A)          f
Cu 1    1.0000    0.0000    0.5000   ( 1 0 0)    5.794A       1
Cu 1    0.5000    0.5000    0.5000   ( 0 0 0)    5.794A       1
Cu 1    1.0000    0.0000    0.0000   ( 1 0 0)    7.320A       1
Cu 1    0.5000    0.5000    0.0000   ( 0 0 0)    7.320A       1
Topology for Cu1
--------------------
Atom Cu1 links by bridge ligands and has
Common vertex with                    R(A-A)          f
P  1    0.2500    0.2500   -0.1779   ( 1 0-1)    5.794A       1
P  1    0.2500    0.2500    0.1779   ( 1 0 0)    5.794A       1
P  1   -0.2500   -0.2500   -0.1779   (-1 0-1)    5.794A       1
P  1   -0.2500   -0.2500    0.1779   (-1 0 0)    5.794A       1
P  1   -0.2500    0.2500    0.3221   (-1 0 0)    7.320A       1
P  1    0.2500   -0.2500    0.3221   ( 1 0 0)    7.320A       1
P  1   -0.2500    0.2500   -0.3221   (-1 0 0)    7.320A       1
P  1    0.2500   -0.2500   -0.3221   ( 1 0 0)    7.320A       1
-------------------------
Structural group analysis
-------------------------
-------------------------
Structural group No 1
-------------------------
Structure consists of 3D framework with CuP2O4N4
Coordination sequences
----------------------
P1:  1  2  3   4   5   6   7   8    9   10
Num  4 20 28  94  76 214 148 382  244  598
Cum  5 25 53 147 223 437 585 967 1211 1809
Rad 6.6(0.9) 10.3(2.3) 15.1(2.8) 18.9(3.7) 24.4(3.9) 28.6(4.5) 33.9(5.0) 38.2(5.5) 43.4(6.2) 47.8(6.7)
Cmp Cu4 P20 Cu28 P94 Cu76 P214 Cu148 P382 Cu244 P598
----------------------
Cu1:  1  2  3   4   5   6   7   8    9   10
Num   8 14 56  50 152 110 296 194  488  302
Cum   9 23 79 129 281 391 687 881 1369 1671
Rad 6.6(0.8) 11.5(1.9) 15.1(2.8) 20.2(3.5) 24.4(3.9) 29.5(4.7) 33.9(5.0) 38.9(5.8) 43.4(6.2) 48.4(7.0)
Cmp P8 Cu14 P56 Cu50 P152 Cu110 P296 Cu194 P488 Cu302
----------------------
```

TD10=1763
Vertex symbols for selected sublattice

P1 Point symbol:{4^4.6^2}
Extended point symbol:[4.4.4(3).4(3).6(6).6(6)]

Cu1 Point symbol:{4^16.6^12}
Extended point symbol:[4.4.4.4.4.4.4.4.4.4.4.4.4.4.4.4.4.4.6(2).6(2).6(2).6(2).6(2).6(2).6(2).6(2).6(2).6(2).6(2).6(2).6(2)]

Point symbol for net: {4^16.6^12}{4^4.6^2}2
4,8-c net with stoichiometry (4-c)2(8-c); 2-nodal net

Topological type:
scu; sqc170 (topos&RCSR.ttd)
{4^16.6^12}{4^4.6^2}2 - VS [4.4.4.4.4.4.4.4.4.4.4.4.4.4.4.4.4.4.8(15).8(15).8(15).8(15).8(15).8(15).8(15).8(15).*.*.*.*]
[4.4.4(3).4(3).8(30).8(30)] (76188 types in 11 databases)
Elapsed time: 19.26 sec.

###################
2: Compound **5** in P2(1)/c
###################

Topology for P1

Atom P1 links by bridge ligands and has
Common vertex with R(A-A) f
Cu 1 1.2550 0.0634 0.0515 (1 0 0) 7.329A 1
Cu 1 0.7450 0.5634 0.4485 (1 0 0) 7.397A 1
Cu 1 0.2550 0.0634 0.0515 (0 0 0) 7.413A 1
Topology for Cu1

Atom Cu1 links by bridge ligands and has
Common vertex with R(A-A) f
P 1 -0.1964 0.2824 0.1470 (-1 0 0) 7.329A 1
P 1 0.1964 -0.2176 0.3530 (1-1 0) 7.397A 1
P 1 0.8036 0.2824 0.1470 (0 0 0) 7.413A 1

Structural group analysis

Structural group No 1

Structure consists of layers (0 0 1) with CuP2O3N12C35H31
Coordination sequences

P1: 1 2 3 4 5 6 7 8 9 10

Num 3 6 9 12 15 18 21 24 27 30
Cum 4 10 19 31 46 64 85 109 136 166
Rad 7.4(0.0) 11.9(1.0) 16.6(2.4) 21.5(2.0) 26.7(2.7) 31.9(2.3) 37.1(2.9) 42.2(2.6) 47.5(3.2) 52.7(3.0)
Cmp Cu3 P6 Cu9 P12 Cu15 P18 Cu21 P24 Cu27 P30

Cu1: 1 2 3 4 5 6 7 8 9 10
Num3 6 9 12 15 18 21 24 27 30
Cum 4 10 19 31 46 64 85 109 136 166
Rad 7.4(0.0) 12.5(1.1) 16.6(2.4) 21.7(1.8) 26.7(2.7) 32.2(2.3) 37.1(2.9) 42.3(2.6) 47.5(3.2) 52.9(3.0)
Cmp P3 Cu6 P9 Cu12 P15 Cu18 P21 Cu24 P27 Cu30

TD10=166
Vertex symbols for selected sublattice

P1 Point symbol :{6^3}
Extended point symbol:[6.6.6]

Cu1 Point symbol :{6^3}
Extended point symbol:[6.6.6]

Point symbol for net: {6^3}
3-c net; uninodal net

Topological type: hcb; Shubnikov hexagonal plane net/ (6,3) (topos&RCSR.ttd)
{6^3} - VS [6.6.6] (76188 types in 11 databases)
Elapsed time: 16.18 sec.

Appendix 4

Table A4.1: Crystallographic Data

Compound	**5.3-H_3**	**5.4-H_3**	**5.6**
Chemical formula	$C_9H_{24}NOP$	$C_{12}H_{30}N_3OP$	$C_{18}H_{36}N_3O_7PPd_3$
Formula weight	221.28	263.37	756.67
Temperature (K)	296(2)	100(2)	100(2)
Crystal system	Monoclinic	Monoclinic	Orthorhombic
Space group	Pnma	P2(1)/c	Cmc2(1)
a (Å); α (°)	9.2210(4); 90	34.883(7); 90	15.899(2); 90
b (Å); β(°)	18.3933(9); 90	13.293(2); 90.318(4)	17.194(3); 90
c (Å); γ (°)	8.1667(4); 90	14.469(3); 90	9.5281(14); 90
V ($Å^3$); Z	1385.11(11); 4	6709(2); 16	2604.8(7); 4
ρ (calc.) mg m^{-3}	1.071	1.040	1.929
μ(Mo K_α) mm^{-1}	0.179	0.157	2.151
$2\theta_{max}$ (°)	50	50	56
R(int)	0.00859	0.0784	0.0262
Completeness to θ	99.6 %	98.8 %	99.8 %
Data / param.	1257 / 74	1167 / 636	3303 / 164
GOF	1.021	1.078	1.292
R1 [F>4σ(F)]	0.0411	0.0745	0.0181
wR2 (all data)	0.1230	0.2232	0.0560
max. peak/hole (e.$Å^{-3}$)	0.237 / -0.199	1.114 / -0.741	0.482 / -0.524

Compound	**5.7·H_2O**	**5.8·$2H_2O$**	**5.9**
Chemical formula	$C_{48}H_{86}N_6O_{15}P_2Pd_6$	$C_{31}H_{64}N_6O_{16}P_2Pd3$	$C_{28}H_{60}N_6O_{12}P_2Pd_6$
Formula weight	1687.57	147.22	1373.16
Temperature (K)	100(2)	100(2)	100(2)
Crystal system	Orthorhombic	Monoclinic	Monoclinic
Space group	C222(1)	C2/c	P2(1)/c
a (Å); α (°)	15.31(2); 90	14.8019(16); 90	24.812(6); 90
b (Å); β(°)	21.694(2); 90	8.678(2); 90.015(4)	32.9964(14); 115.837
c (Å); γ (°)	19.245(3); 90	38.140(4); 90	12.2459(5); 90
V ($Å^3$); Z	6391(14); 4	10545(2); 8	4332.6(3); 4
ρ (calc.) mg m^{-3}	1.754	1.861	2.105
μ(Mo K_α) mm^{-1}	1.764	2.125	2.571
$2\theta_{max}$ (°)	56	50	50
R(int)	0.1249	0.0792	0.0463
Completeness to θ	99.4 %	99.5 %	99.6 %
Data / param.	7897 / 342	9288 / 567	4197 / 272
GOF	1.001	1.108	1.037
R1 [F>4σ(F)]	0.0603	0.0474	0.0373
wR2 (all data)	0.1355	0.0988	0.0887
max. peak/hole (e.$Å^{-3}$)	1.407 / -1.131	1.073 / -1.017	1.262 / -0.834

Compound	**5.10·2DMSO**	**5.11·2H_2O**	**5.12·DMF**
Chemical formula	$C_{30}H_{68}N_6O_{14}P_2Pd_6S_2$	$C_{24}H_{54}N_6O_2P_2Cl_6Pd_6$	$C_{36}H_{66}N_6O_2Cl_6P_2Pd_6$
Formula weight	1501.36	1371.90	1528.13
Temperature (K)	100(2)	100(2)	100(2)
Crystal system	Monoclinic	Hexagonal	Monoclinic
Space group	C2/c	P6(3)/m	P2(1)/c
a (Å); α (°)	24.812(3); 90	9.5919(10); 90	9.2484(16); 90
b (Å); β(°)	9.7381(14); 120.349	9.5919(10); 90	12.526(2); 109.154(4)
c (Å); γ (°)	23.628(3); 90	23.988(3); 120	25.198(4); 90
V ($Å^3$); Z	4926.7(11); 4	1911.3(4); 2	2757.4(8); 2
ρ (calc.) mg m^{-3}	2.024	2.524	1.906
μ(Mo K_α) mm^{-1}	2.355	3.316	2.258
$2\theta_{max}$ (°)	50	55	50
R(int)	0.0463	0.0598	0.0762
Completeness to θ	96.6%	99.5 %	97.3 %
Data / param.	4197 / 272	1535 / 90	4844 / 265
GOF	1.037	1.148	1.017
R1 [F>4σ(F)]	0.0373	0.0495	0.0402
wR2 (all data)	0.0887	0.1277	0.1183
max. peak/hole (e.$Å^{-3}$)	1.262 / -0.834	1.302 / -3.841	1.487 / -0.775

Compound	**5.13**	**5.14**	**5.16.2H_2O**
Chemical formula	$C_{18}H_{42}N_6O_2P_2Cl_6Pd_6$	$C_{24}H_{54}N_6O_2P_2Cl_6Pd_6$	$C_{42}H_{81}N_6O_7PPd_3$
Formula weight	1287.74	1371.77	1132.30
Temperature (K)	100(2)	296(2)	100(2)
Crystal system	Monoclinic	Monoclinic	Trigonal
Space group	P2(1)/n	P2(1)/c	P-3c1
a (Å); α (°)	9.185(4); 90	8.733(3); 90	17.0471(16); 90
b (Å); β(°)	22.919(9); 116.718(9)	17.755(6); 108.067(7)	17.0471(16); 90
c (Å); γ (°)	9.225(4); 90	13.504(5); 90	22.921(3); 120
V ($Å^3$); Z	1734.6(12); 2	1990.6(12); 2	5768(10); 4
ρ (calc.) mg m^{-3}	2.461	2.289	1.304
μ(Mo K_α) mm^{-1}	3.628	3.169	0.996
$2\theta_{max}$ (°)	50	50	56
R(int)	0.1778	0.0316	0.1711
Completeness to θ	99.9%	99.5 %	99.7 %
Data / param.	3055 / 186	4678 / 214	4800 / 181
GOF	1.154	1.052	0.921
R1 [F>4σ(F)]	0.1429	0.0235	0.0652
wR2 (all data)	0.3967	0.0573	0.2330
max. peak/hole (e.$Å^{-3}$)	3.280 / -3.372	1.297 / -0.710	1.099 / -1.060

Compound	**5.17**
Chemical formula	$C_{33}H_{69}N_6O_7PPd_3$
Formula weight	1012.11
Temperature (K)	100(2)
Crystal system	Monoclinic
Space group	P2(1)/n
a (Å); α (°)	11.6709(10); 90
b (Å); β(°)	16.7648(14); 98.2(2)
c (Å); γ (°)	21.993(2); 90
V ($Å^3$); Z	4258.7(6); 4
ρ (calc.) mg m^{-3}	1.579
μ(Mo K_α) mm^{-1}	1.339
$2\theta_{max}$ (°)	56
R(int)	0.0671
Completeness to θ	99.7 %
Data / param.	10546 / 461
GOF	1.021
R1 [F>4σ(F)]	0.0387
wR2 (all data)	0.0847
Flack parameter	-
max. peak/hole (e.$Å^{-3}$)	0.898 / -0.904

Spectral Data for the phenylated trans-alkene products 5.19a – 5.19d.

Butyl cinnamate (5.19a)

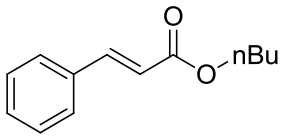

Pale yellow semi-solid; eluent (3% ethyl acetate in hexanes)
^{1}H NMR ($CDCl_3$, 400 MHz):δ7.69 (d, *J*= 16.0Hz, 1 H), 7.54 – 7.52 (m, 2 H), 7.40 – 7.37 (m, 3 H), 6.45 (d, *J*= 16.0Hz, 1 H), 4.22 (t, *J* = 4.0Hz, 2 H), 1.74 – 1.66 (m, 2 H), 1.50 – 1.40 (m, 2 H), 0.97 (t, *J*= 8.0 Hz, 3 H).
^{13}C NMR ($CDCl_3$, 100 MHz):δ167.2, 144.64, 134.5, 130.2, 128.9, 128.1, 118.3, 64.5, 30.8, 19.2, 13.84.
HRMS (ESI): calc. for $[(C_{13}H_{16}O_2)Na]$ $(M+Na)^+$ 227.1048, measured 227.1047.

Methyl cinnamate (5.19b)

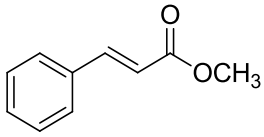

Pale yellow liquid; eluent (3% ethyl acetate in hexanes)
^{1}H NMR ($CDCl_3$, 400 MHz):δ7.71 (d, *J*= 16.0Hz, 1 H), 7.55 – 7.53 (m, 2 H), 7.41 – 7.39 (m, 3 H), 6.46 (d, *J*= 16.0Hz, 1 H), 3.82 (s, 3 H).
^{13}C NMR ($CDCl_3$, 100 MHz):δ167.5, 144.9, 134.4, 130.3, 128.9, 128.1, 117.8, 51.9.
HRMS (ESI): calc. for $[(C_{10}H_{10}O_2)Na]$ $(M+Na)^+$ 185.0578, measured 185.0579.

Cyclohexylcinnamate (5.19c)

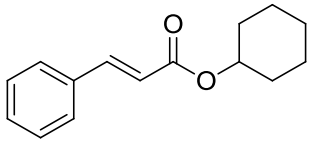

Pale yellow liquid;eluent (3% ethyl acetate in hexanes)
^{1}H NMR ($CDCl_3$, 400 MHz):δ7.68 (d, *J*= 16.0Hz, 1 H), 7.55 – 7.52 (m, 2 H), 7.49 – 7.38 (m, 3 H), 6.44 (d, *J*= 16.0Hz, 1 H), 4.93 – 4.87 (s, 1 H),1.95 – 1.91 (m, 2 H), 1.80 – 1.76 (m, 2 H), 1.60 – 1.54 (m, 1 H), 1.52 – 1.46 (m, 2 H), 1.44 – 1.40 (m, 1 H), 1.34 – 1.26 (m, 2 H).
^{13}C NMR ($CDCl_3$, 100 MHz):δ166.5, 144.3, 134.8, 130.2, 128.9, 128.1, 118.3, 72.8, 31.8, 25.5, 23.9.
HRMS (ESI): calc. for $[(C_{15}H_{18}O_2)Na]$ $(M+Na)^+$ 253.1204, measured 253.1203.

(*E*)-1,2-Diphenylethene (5.19d)

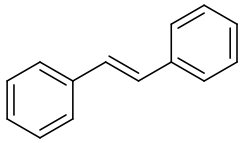

Pale yellow solid; eluent (3% ethyl acetate in hexanes)
^{1}H NMR ($CDCl_3$, 400 MHz):δ7.59 (d, *J*= 8.0Hz, 4 H), 7.43 (t, *J*= 8.0Hz, 4 H), 7.33 (t, *J*= 8.0Hz, 2 H) 7.19 (s, 2 H).
^{13}C NMR ($CDCl_3$, 100 MHz):δ137.4, 128.2, 127.7, 126.8.
HRMS (ESI): calc. for $[(C_{14}H_{12})]^+$ $(M)^+$ 181.1017, measured 181.1018.

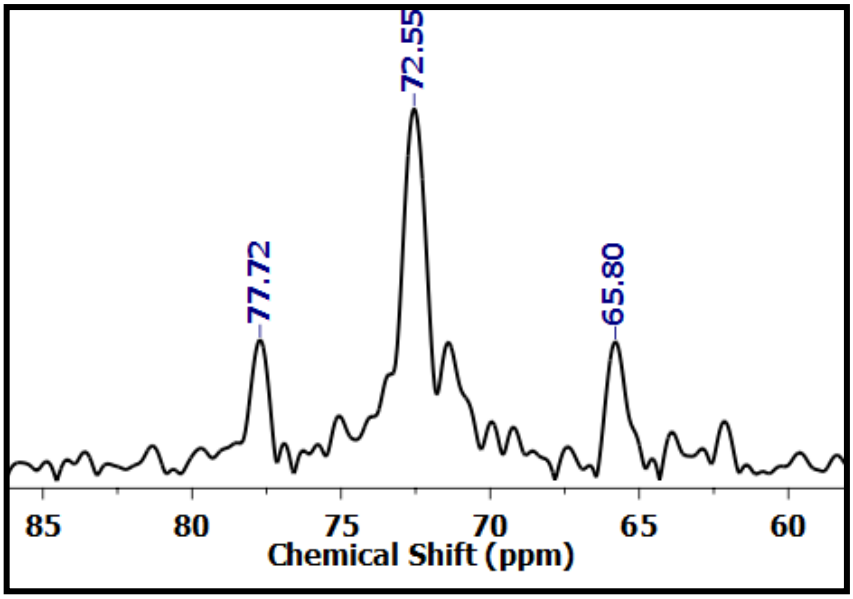

Figure A4.1: ^{31}P-NMR spectra of a reaction mixture of **3-H$_3$**, Pd(OAc)$_2$ in methanol after 12 hours of stirring

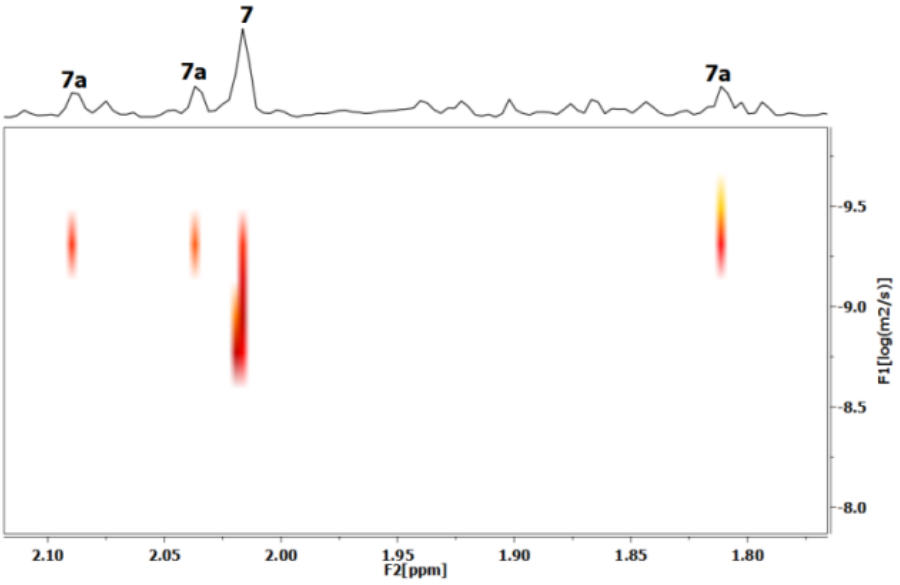

Figure A4.2: ^{1}H-2D- DOSY NMR spectra of a reaction mixture of **3-H$_3$**, Pd(OAc)$_2$ in methanol after 15 hours of stirring

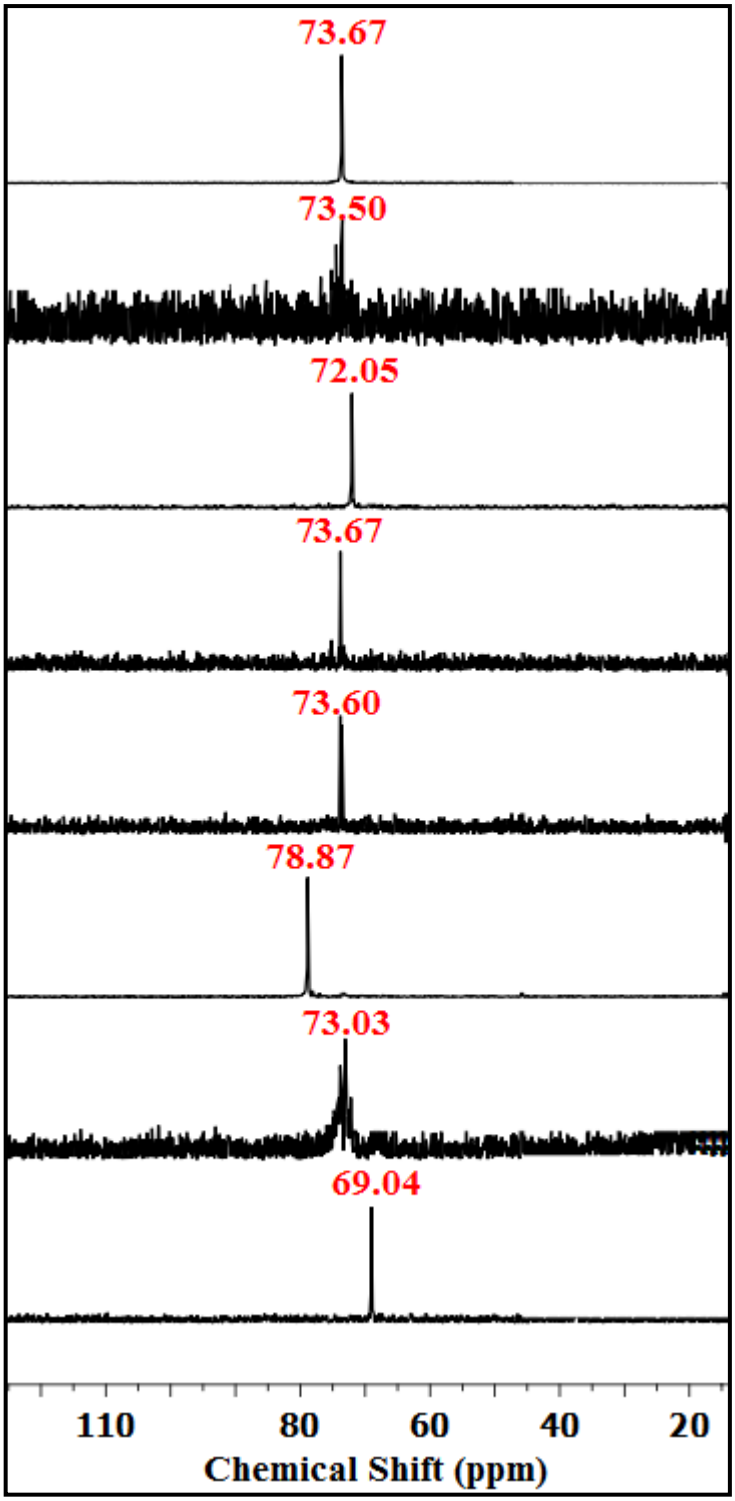

Figure A4.3: ^{31}P NMR spectra of **5.6, 5.7, 5.8, 5.9, 5.10, 5.15, 5.16 and 5.17(order from bottom to top)**

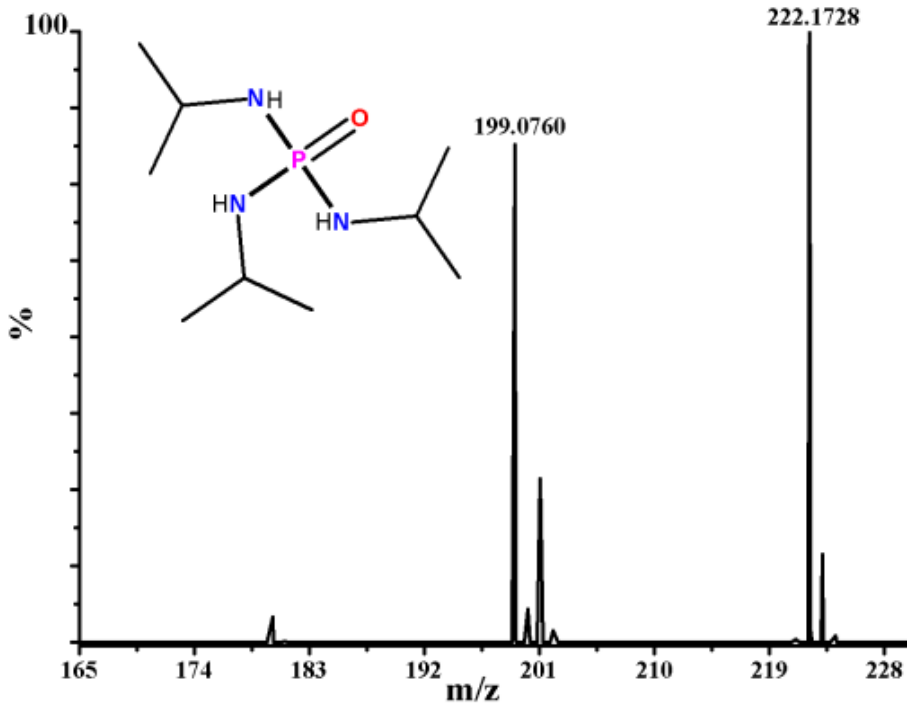

Figure A4.4: ESI (+) HRMS Mass spectra of **5.3**-H_3: m/z = 222.

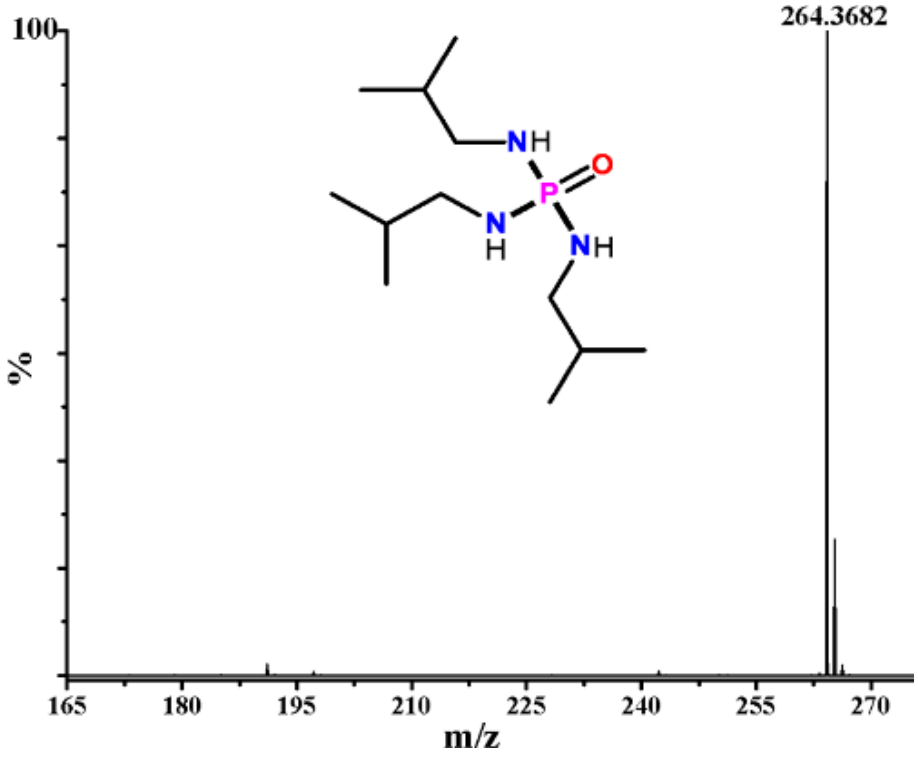

Figure 4.5: ESI (+) HRMS Mass spectra of **5.4**-H_3: m/z = 264.

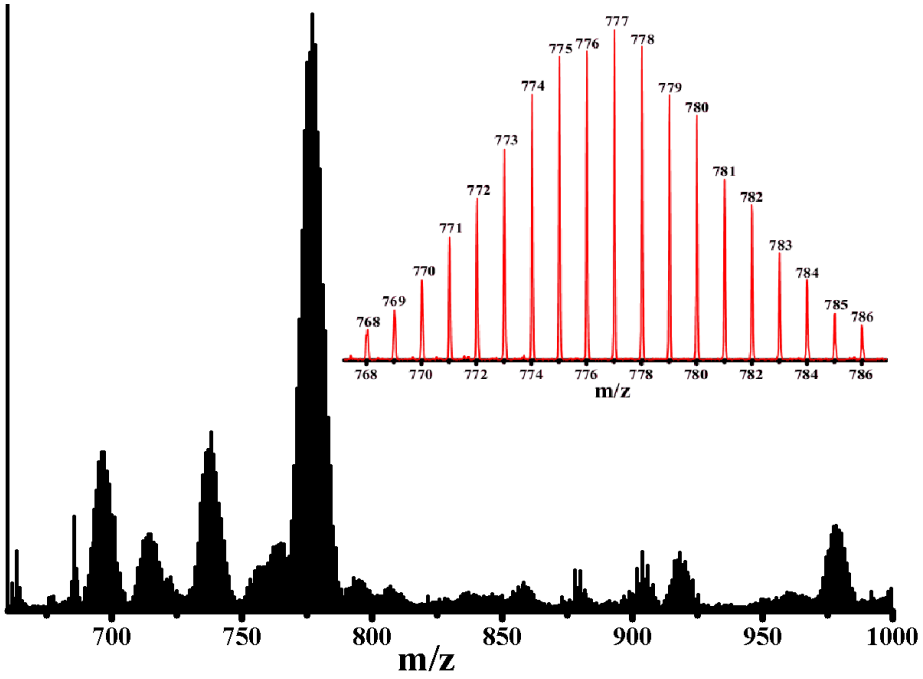

Figure A4.6: ESI (+) HRMS Mass spectra of **5.6**: m/z = 755; $[M+Na]^+$ = 778

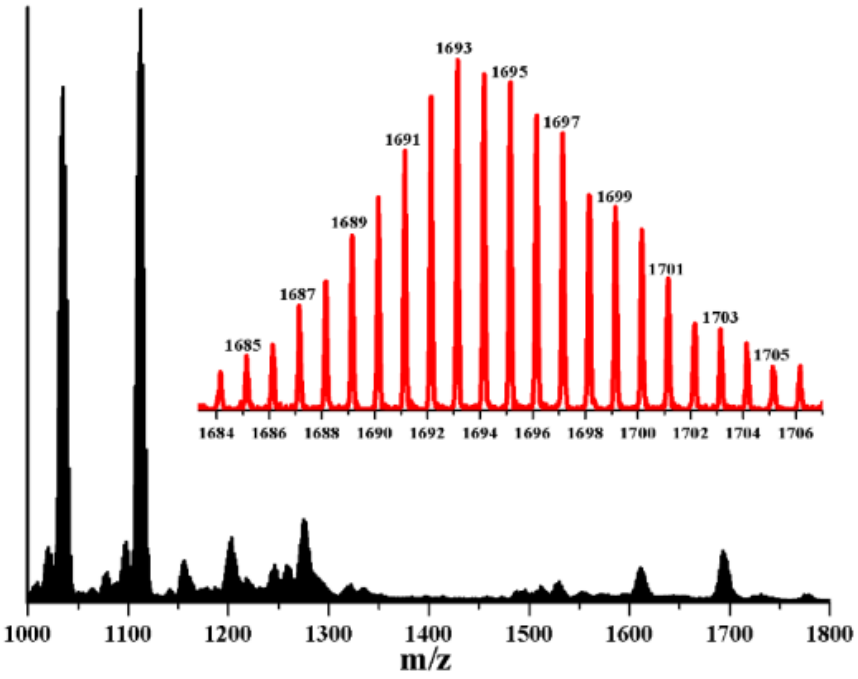

Figure A4.7: ESI (+) HRMS Mass spectra of **5.7**.H_2O:m/z = 1671; $[M+Na]^+$ = 1694.

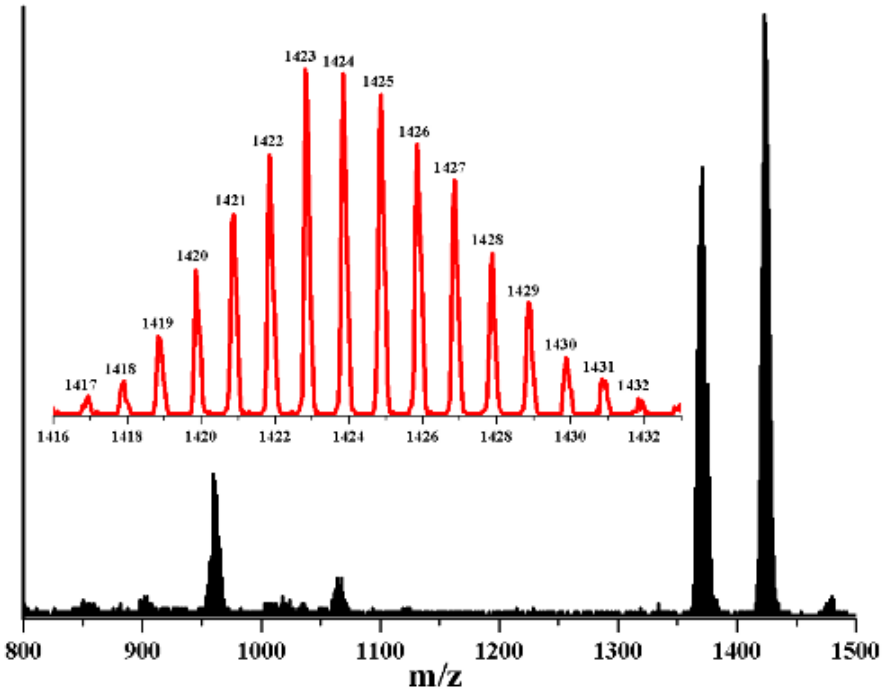

Figure A4.8: MALDI-TOF Mass spectra of **5.8**.2H_2O: m/z 1423.

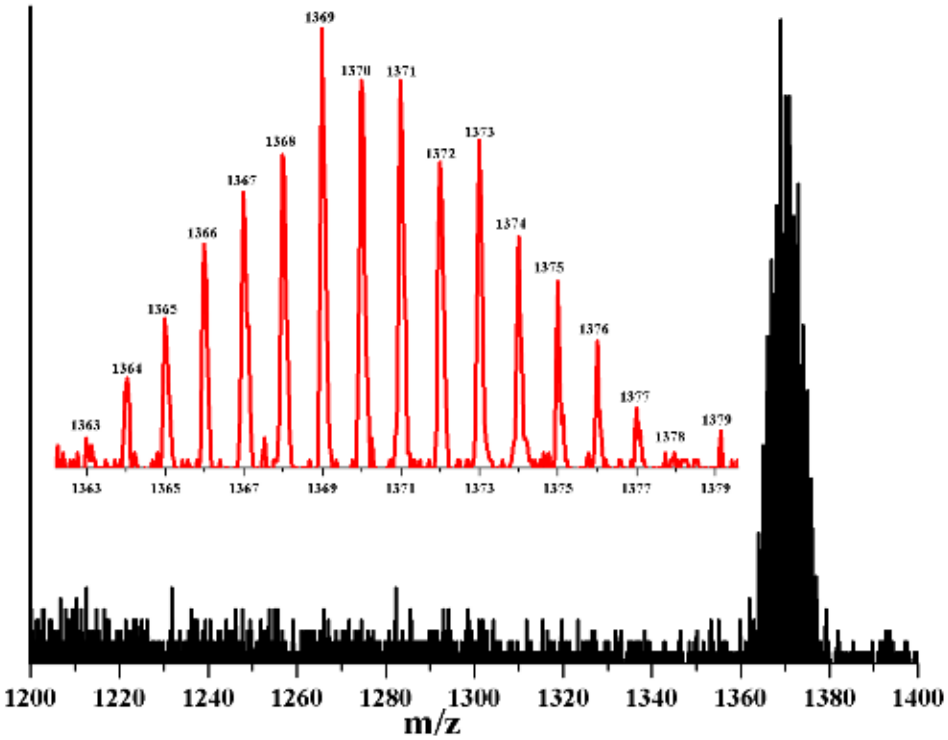

Figure A4.9: MALDI-TOF Mass spectra of **5.9**:m/z = 1369.

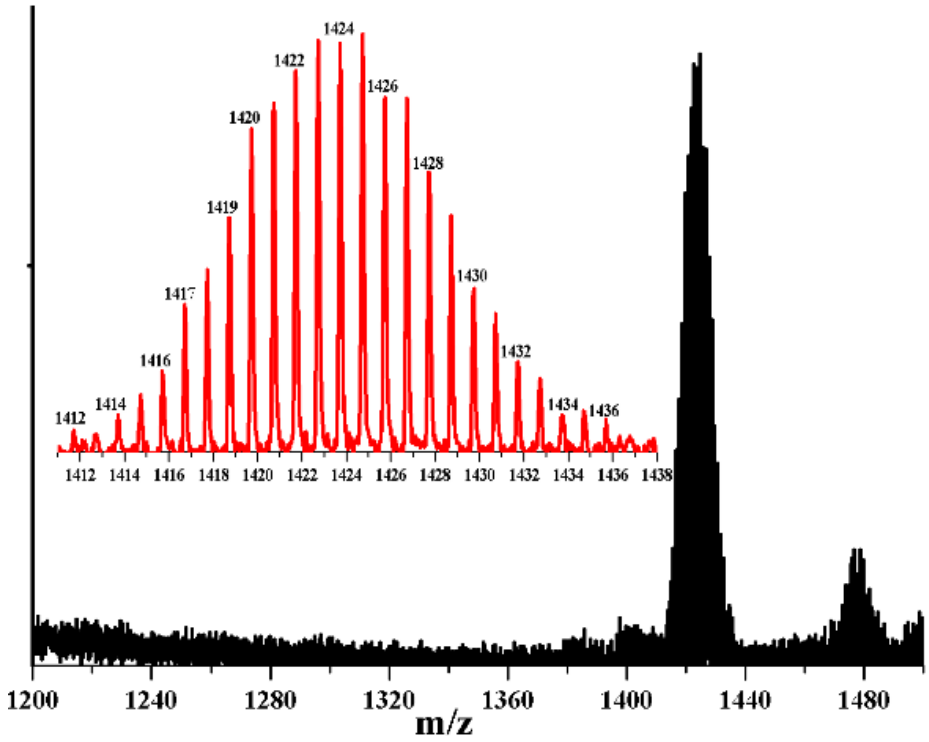

Figure A4.10: MALDI-TOF Mass spectra of **5.10**: $[M+DMSO]^+$ = 1423.

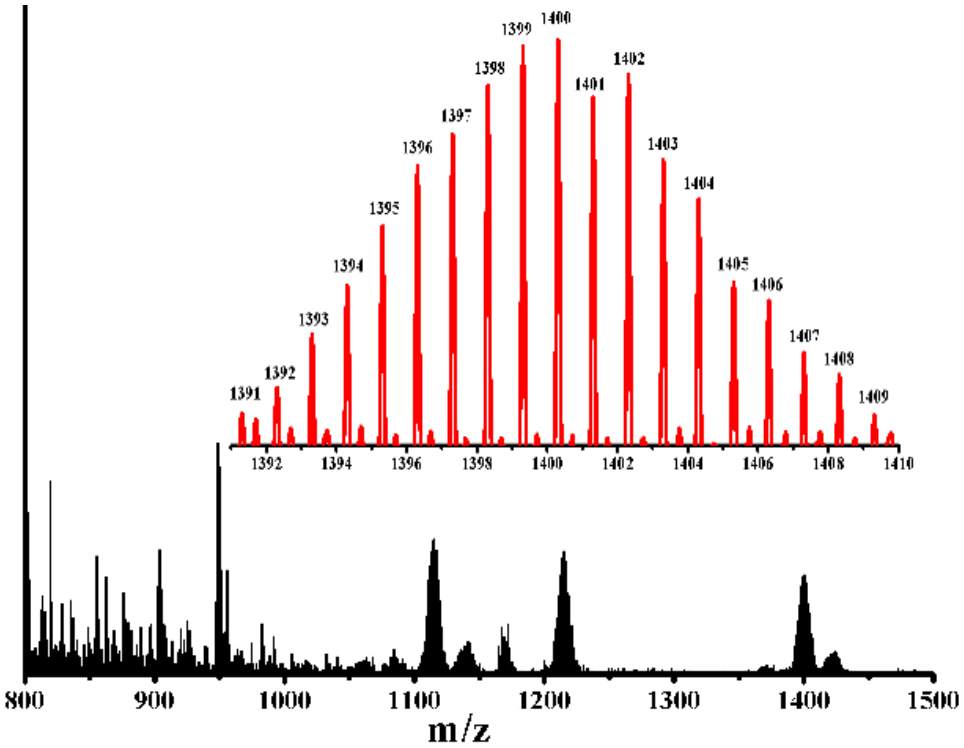

Figure 4.11: ESI (+) HRMS Mass spectra of **5.11**m/z = 1365; $[M+K]^+$ = 1404.

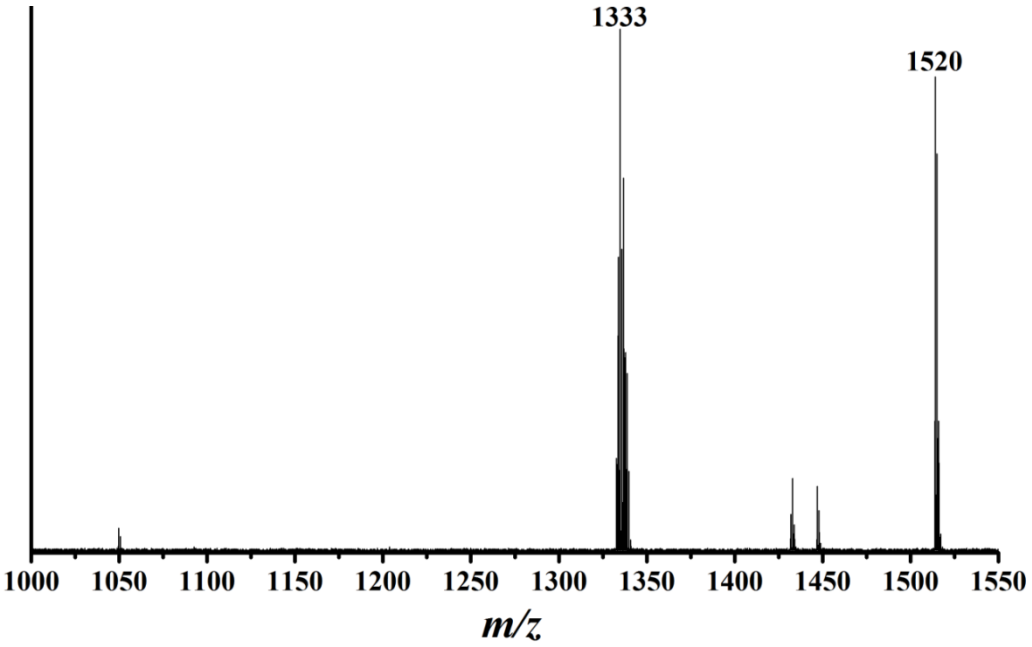

Figure A4.12: MALDI-TOF Mass spectra of **5.12**:m/z = 1520

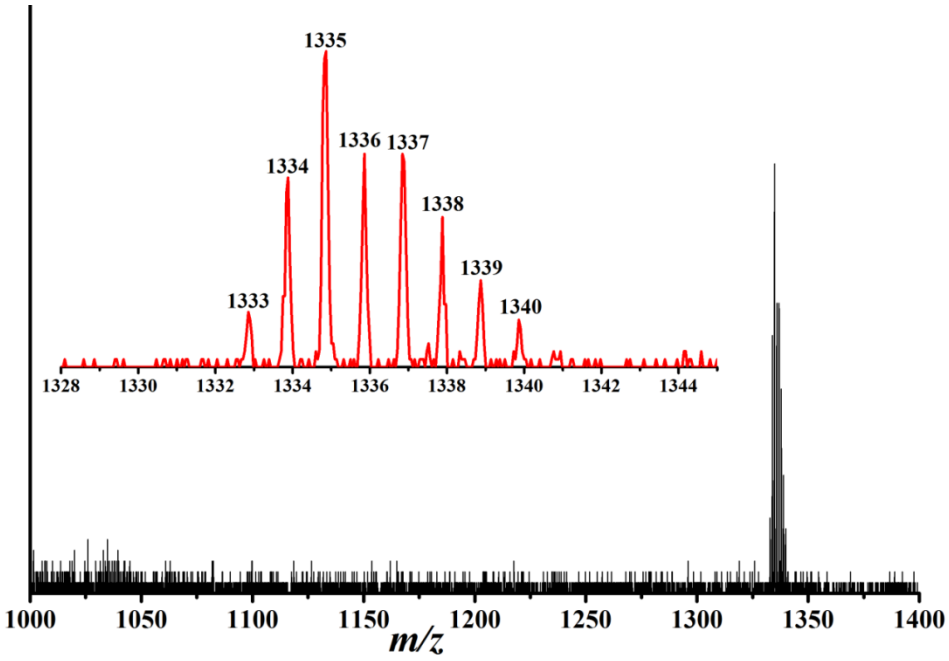

Figure A4.13: MALDI-TOF Mass spectra of **5.13**: m/z = 1287; $[M+K]^+$ = 1326.

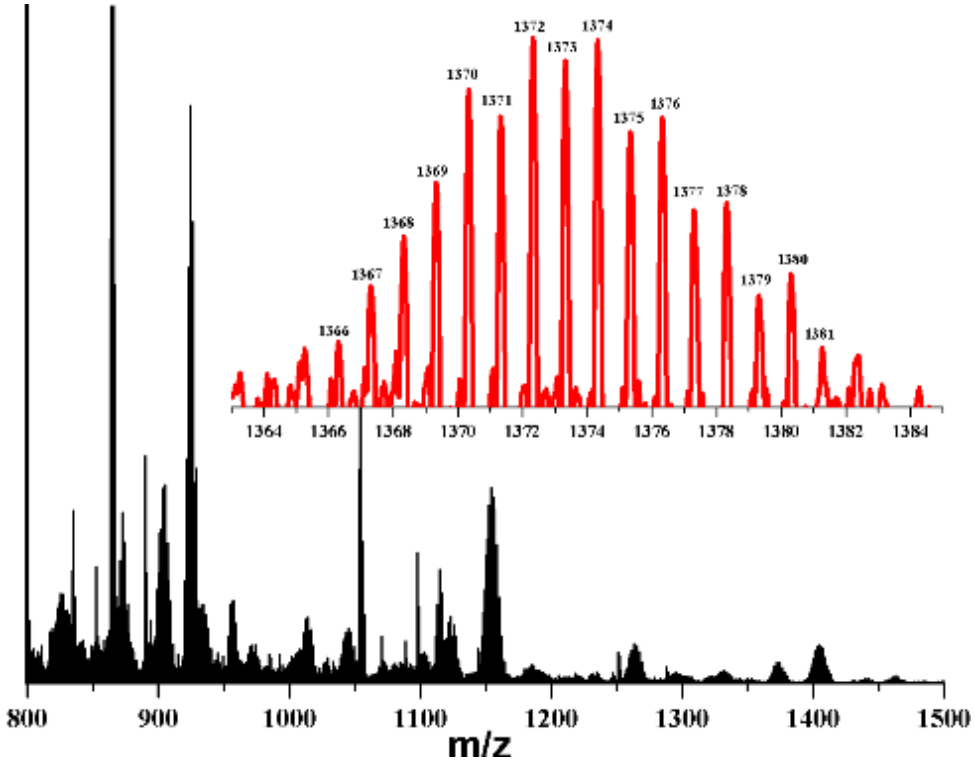

Figure 4.14: ESI (+) HRMS Mass spectra of **5.14:** m/z = 1371

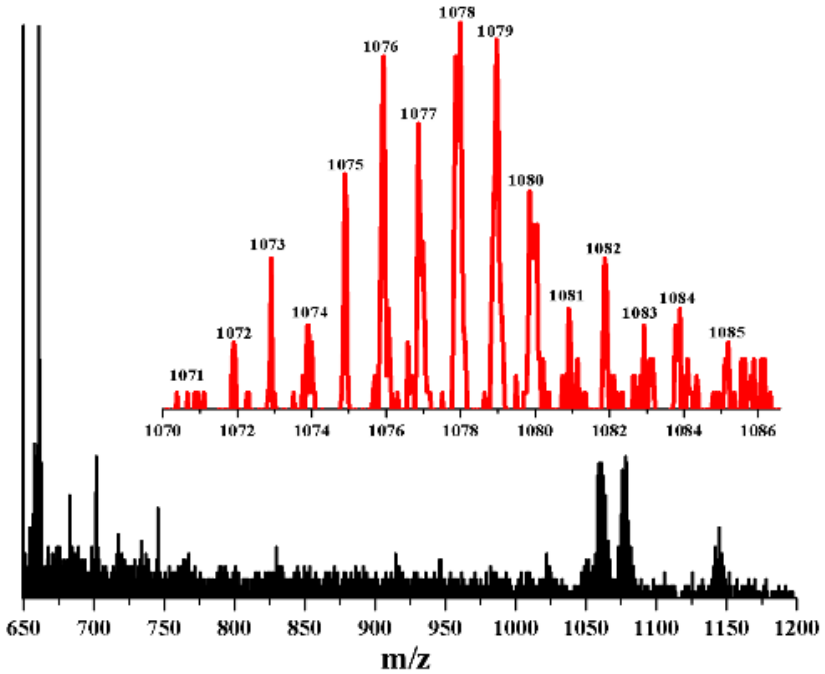

Figure A4.15: MALDI-TOF Mass spectra of 5.15: m/z = 1054; $[M+Na]^+$ = 1077.

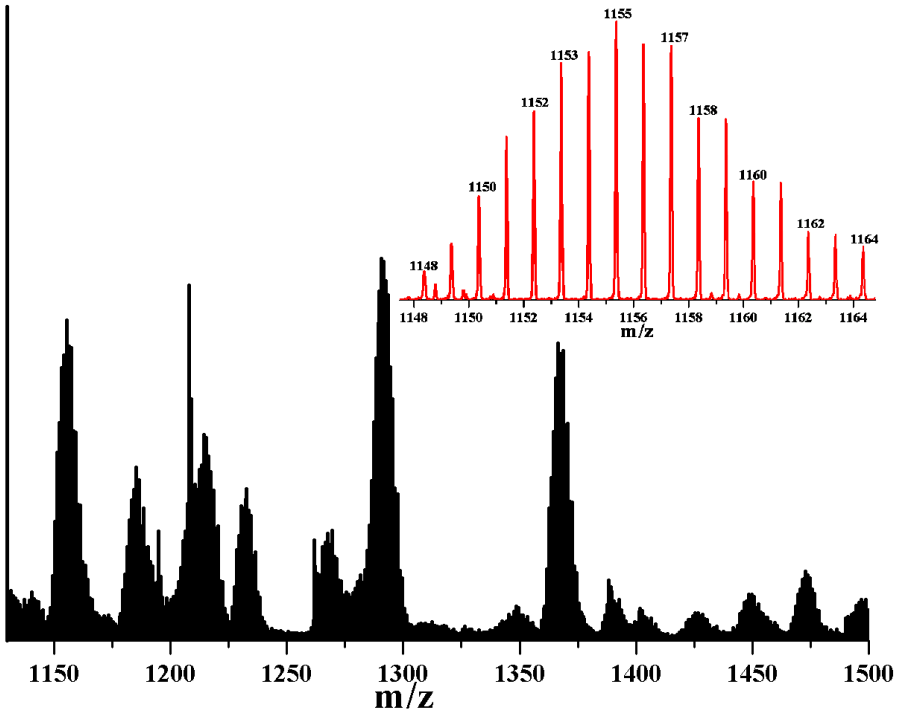

Figure A4.16: ESI (+) HRMS Mass spectra of **5.16**.2H_2O:m/z = 1133; $[M+Na]^+$ = 1154.

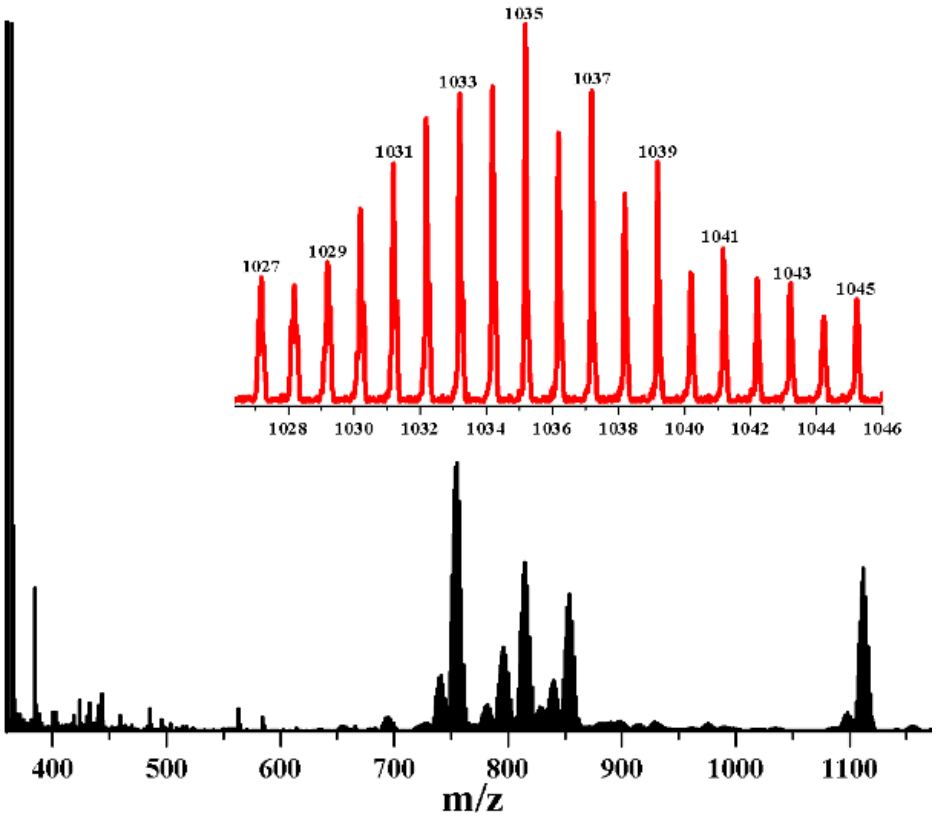

Figure A4.17: ESI (+) HRMS Mass spectra of 5.17: m/z = 1009; $[M+Na]^+$ = 1035.

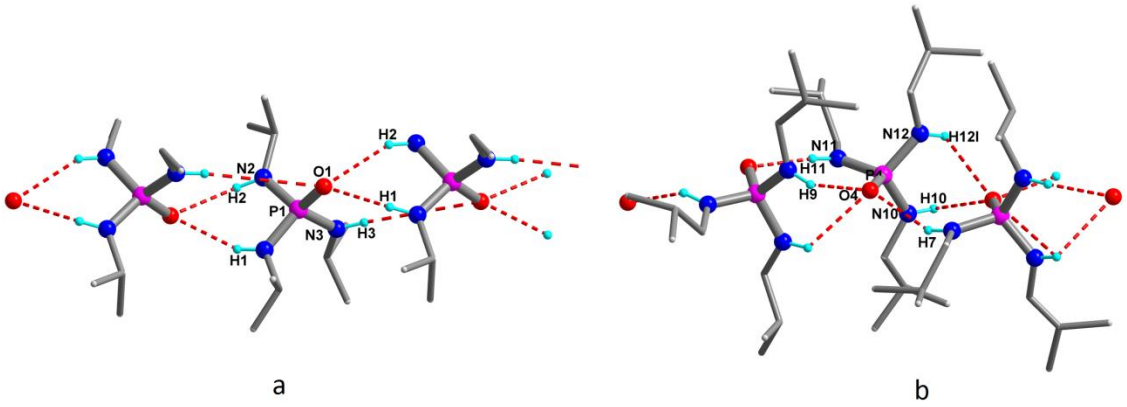

Figure A4.18: Hydrogen bonded network of ligand **3-H3** and **6-H3**

^{1}H and ^{13}C NMR Spectra of Compound **5.19a**

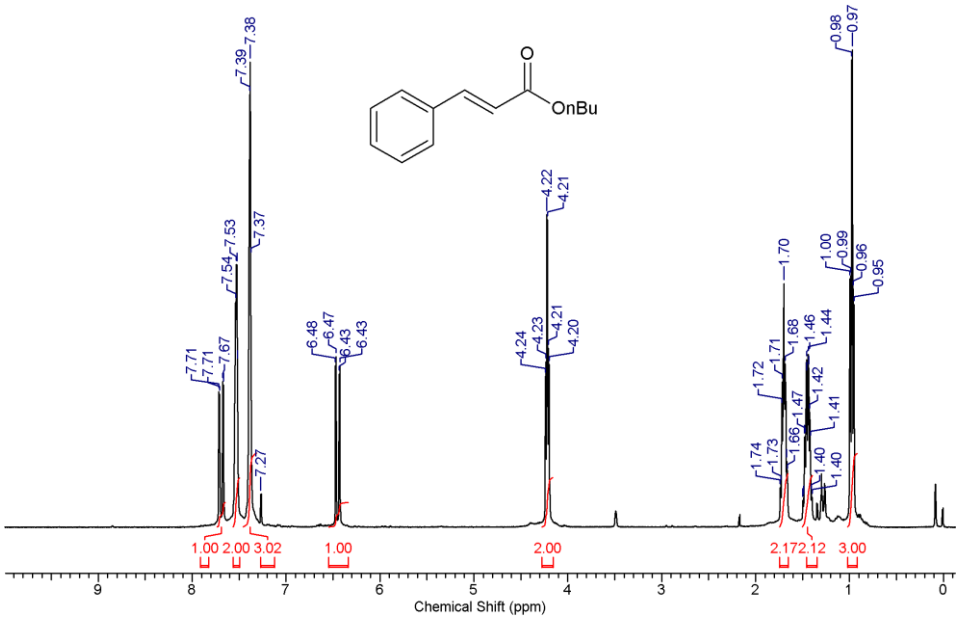

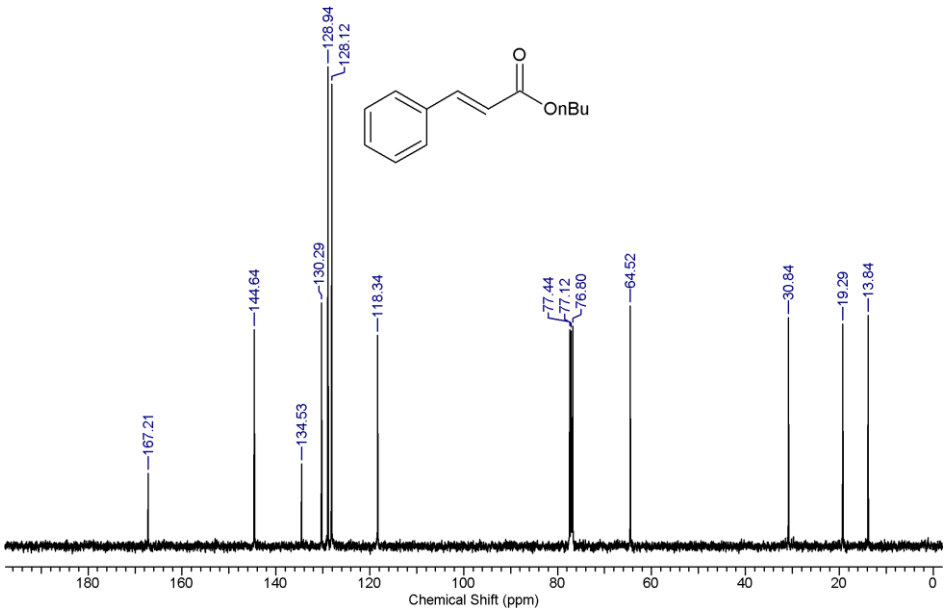

^{1}H and ^{13}C NMR Spectra of Compound 5.19

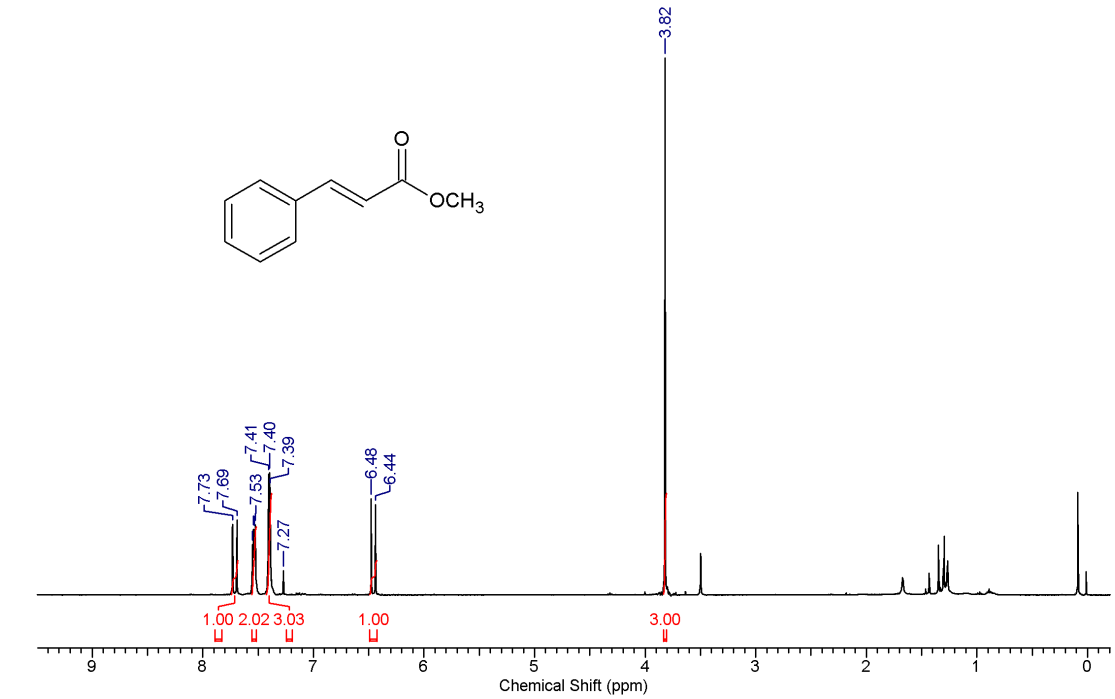

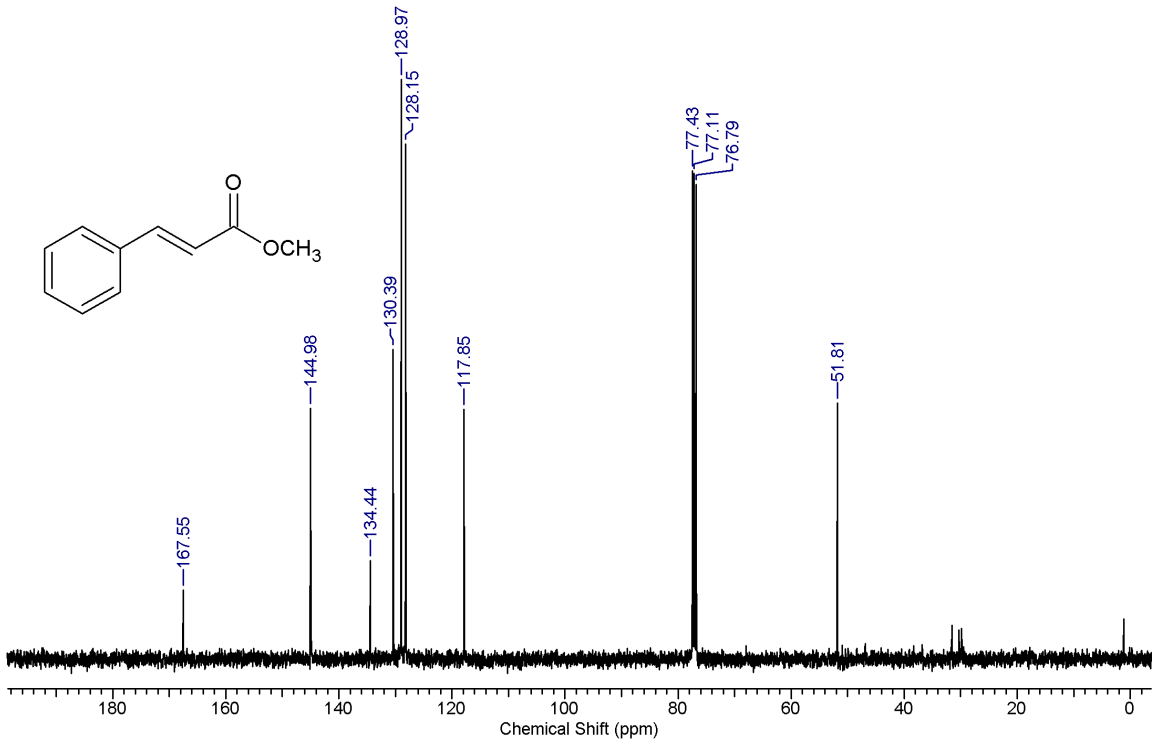

^{1}H and ^{13}C NMR Spectra of Compound 5.19

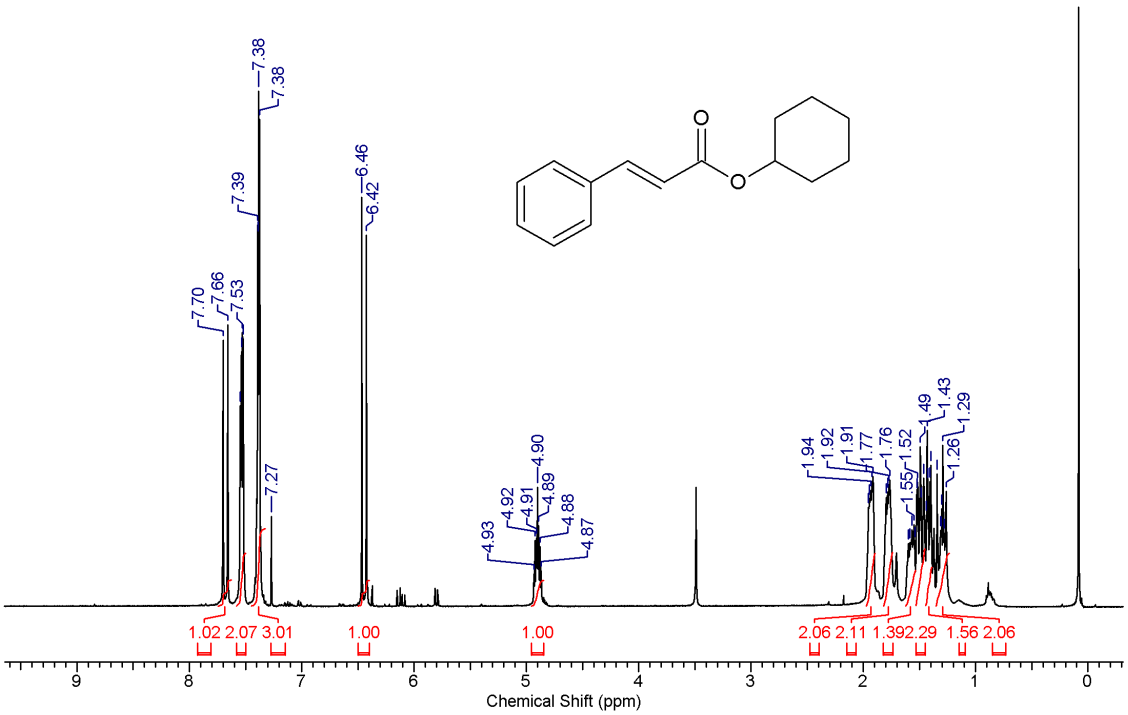

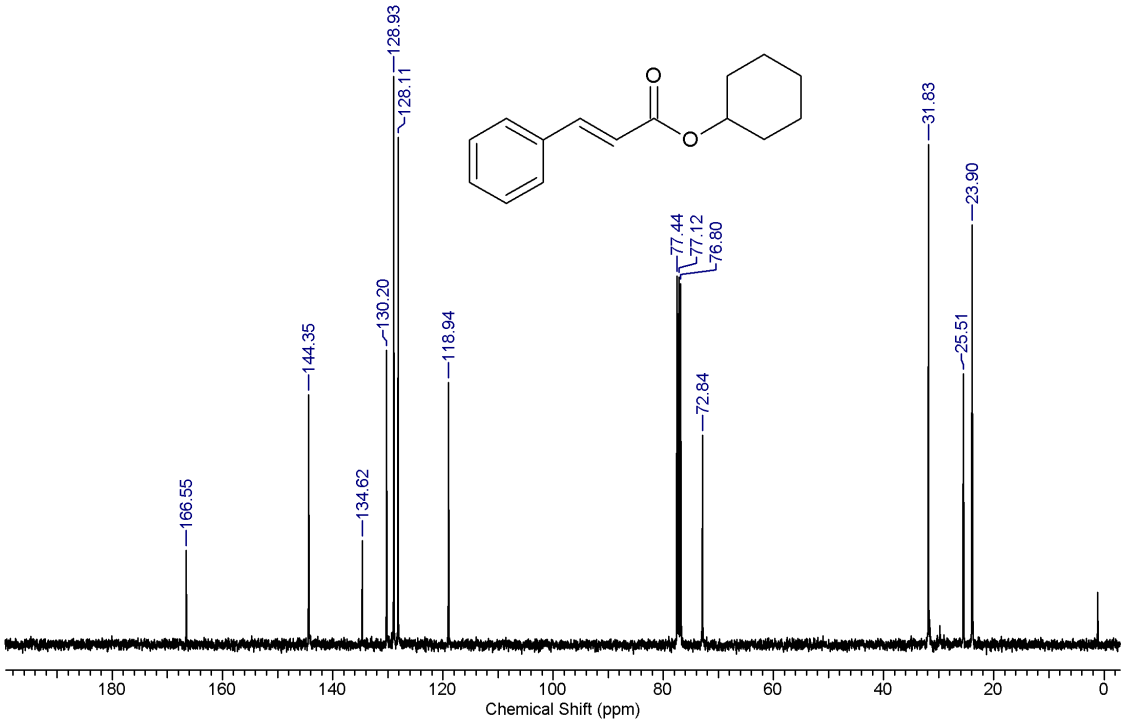

^{1}H and ^{13}C NMR Spectra of Compound 5.19

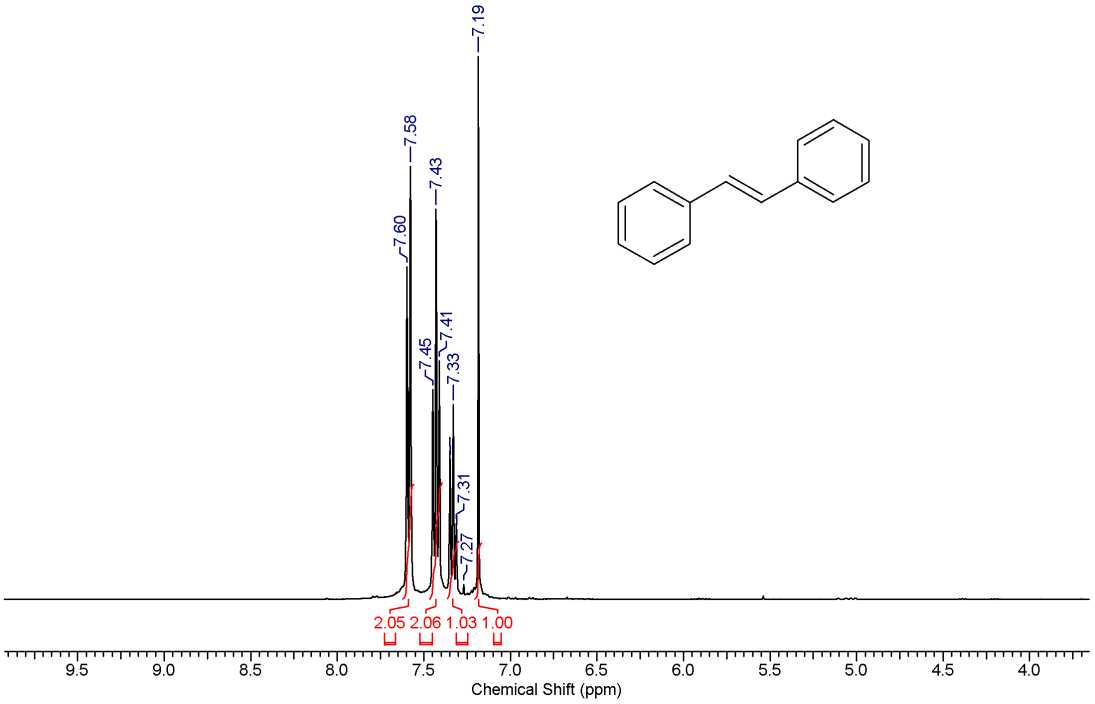

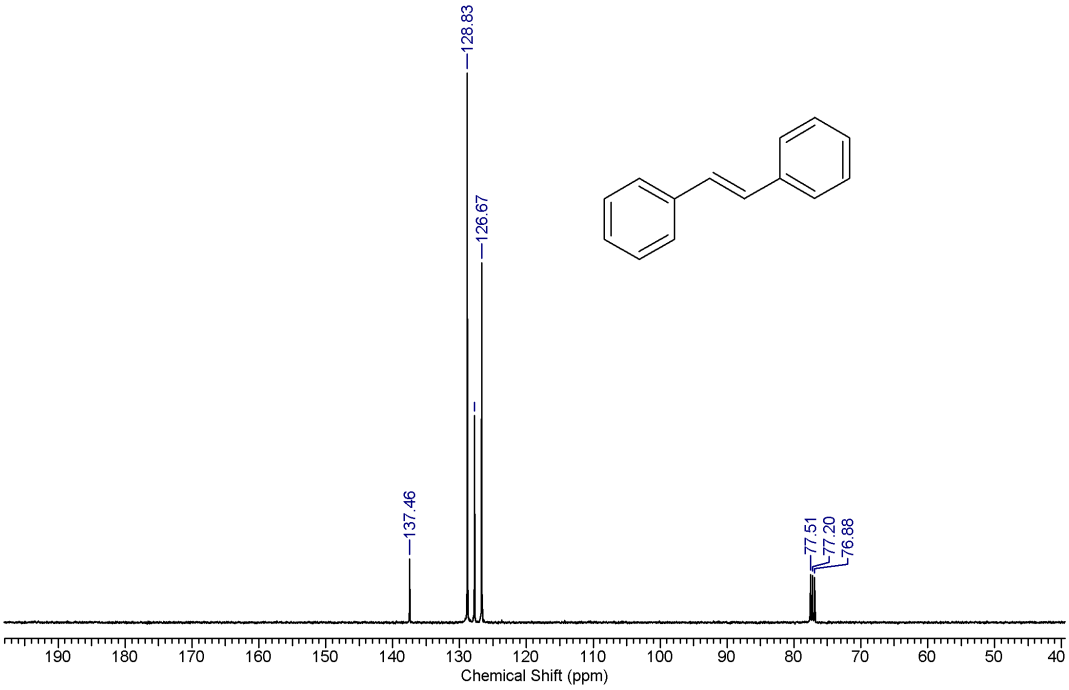

Appendix 5

Table A5.1: Crystallographic Data

Compound	**6.1**·H_2O·CH_3OH	**6.2**	**DMSO⊂6.3**
Chemical formula	$C_{60}H_{72}N_6O_{14}P_2Pd_6$	$C_{42}H_{58}N_6O_{12}Fe_2Pd_6$	$C_{50}H_{90}N_{12}O_{29}P_4Pd_{12}S$
Formula weight	1801.73	1651.11	2756.54
Temperature (K)	100(2)	100(2)	100(2)
Crystal system	Monoclinic	Monoclinic	Orthorhombic
Space group	P2(1)/c	Ia	Cmcm
a (Å); α (°)	14.687(11); 90	19.20(12); 90	18.885(3); 90
b (Å); β(°)	21.730(17); 91.768(17)	16.347(8); 114.768(8)	28.732(9); 90
c (Å); γ (°)	22.327(17); 90	19.392(8); 90	24.969(4); 90
V ($Å^3$); Z	7122(10); 4	5526(5); 4	13548(4); 4
ρ (calc.) mg m^{-3}	2.264	1.959	1.349
μ(Mo K_α) mm^{-1}	3.084	2.526	1.662 (Mo K_α)
$2\theta_{max}$ (°)	57	57	56
R(int)	0.2769	0.2328	0.1953
Completeness to θ	97.4%	99.2	99.7 %
Data / param.	17646 / 842	10852 / 644	8919 / 268
GOF	0.928	0.967	0.931
R1 [F>4σ(F)]	0.0816	0.0967	0.0467
wR2 (all data)	0.2303	0.2506	0.1168
max. peak/hole (e.$Å^{-3}$)	1.506 / -1.822	2.400 / -1.359	0.745/ -1.310

Compound	**C_6H_6⊂6.3**	**CCl_4⊂6.3**	**$CHCl_3$⊂6.3**
Chemical formula	$C_{54}H_{90}N_{12}O_{28}P_4Pd_{12}$	$C_{49}H_{84}N_{12}O_{28}P_4Cl_4P_4d_{12}$	$C_{49}H_{85}N_{12}O_{28}P_4Cl_3Pd_{12}$
Formula weight	2756.05	2831.76	2797.32
Temperature (K)	100(2)	100(2)	100(2)
Wavelength Å	0.71073	1.54178	0.71073
Crystal system	Monoclinic	Monoclinic	Monoclinic
Space group	P2(1)/c	P2(1)/c	P2(1)/n
a (Å); α (°)	17.75(9); 90	18.051(4); 90	17.835(2); 90
b (Å); β(°)	24.00(11); 106.78	23.832(6); 107.46(11)	23.996(3); 107.088(3)
c (Å); γ (°)	29.99(16); 90	29.920(2); 90	29.742(4); 90
V (Å3); Z	12239.3(11); 4	12278.7(5); 4	12167(2); 4
ρ (calc.) mg m-3	1.496	1.532	1.527
μ(Mo Kα) mm-1	1.823 (Mo K_α)	15.569 (Cu K_α)	1.899 (Mo K_α)
2θmax (°)	54	136	50
R(int)	0.0534	0.0396	0.1335
Completeness to θ	99%	98.7%	99.1%
Data / param.	26582 / 986	22240 / 1006	21266 / 994
GOF	0.950	1.079	0.990
R1 [F>4σ(F)]	0.0377	0.0415	0.0566
wR2 (all data)	0.0956	0.1255	0.155
max. peak/hole (e.Å-3)	1.443 / -1.194	1.385 /-0.650	1.880 / -1.998

Compound	**CH_2Cl_2⊂6.3**	**C_7H_8⊄6.3**	**C_6H_5Cl⊄6.3**
Chemical formula	$C_{49}H_{86}N_{12}O_{28}P_4Cl_2Pd_{12}$	$C_{57}H_{98}N_{12}O_{29}P_4SPd_{12}$	$C_{56}H_{95}N_{12}O_{29}P_4SPd_{12}$
Formula weight	2762.88	2848.21	2868.63
Temperature (K)	100(2)	100(2)	100(2)
Wavelength Å	0.71073	0.71073	0.71073
Crystal system	Monoclinic	Monoclinic	Monoclinic
Space group	P2(1)/n	P2(1)/c	P2(1)/c
a (Å); α (°)	17.78(2); 90	21.477(11); 90	21.447(4); 90
b (Å); β(°)	23.96(3); 107.22(2)	28.389(14); 108.41(2)	28.408(4); 108.562(4)
c (Å); γ (°)	29.74(3); 90	17.663(8); 90	17.659(3); 90
V ($Å^3$); Z	12101(2); 4	10218.0(9); 4	10199(3); 4
ρ (calc.) mg m^{-3}	1.517	1.851	1.868
μ(Mo K_α) mm^{-1}	1.887 (Mo K_α)	2.207 (Mo K_α)	2.237 (Mo K_α)
$2\theta_{max}$ (°)	56	50	56
R(int)	0.1611	0.0930	0.1763
Completeness to θ	99.5%	97.4	99.5%
Data / param.	29982 / 982	17570 / 1003	25461 / 1050
GOF	0.823	0.974	0.903
R1 [F>4σ(F)]	0.0684	0.0452	0.0698
wR2 (all data)	0.1807	0.1057	0.1755
max. peak/hole (e.$Å^{-3}$)	1.896 / -1.584	1.929 / -1.064	1.461 /-1.566

Compound	**C_6H_5F⊄6.3**	**6.4**	**6.5·4DMSO**
Chemical formula	$C_{50}H_{90}N_{12}O_{29}P_4SPd_{12}$	$C_{64}H_{100}N_{16}O_{16}P_4Pd_{10}$	$C_{34}H_{51}N_6O_{15}PPd_3S_4$
Formula weight	2756.07	2483.68	1262.22
Temperature (K)	100(2)	100(2)	100(2)
Wavelength Å	0.71073	Triclinic	Monoclinic
Crystal system	Monoclinic	P-1	P2(1)/n
Space group	P2(1)/c	11.74(2); 93.75	16.468(2); 90
a (Å); α (°)	17.780(17); 90	14.95(3); 100.91(3)	13.3297(19); 91.872(3)
b (Å); β(°)	23.911(2); 107.27(2)	15.64(3); 100.70(3)	21.451(3); 90
c (Å); γ (°)	29.859(3); 90	2634(8); 1	4706.2(11); 4
V ($Å^3$); Z	12137(2); 4	1.703	1.781
ρ (calc.) mg m^{-3}	1.504	1.915	1.415
μ(Mo K_α) mm^{-1}	1.855 (Mo K_α)	57	56
$2\theta_{max}$ (°)	56	0.4915	0.0398
R(int)	0.1182	99.3%	99.8%
Completeness to θ	99.7%	13373 / 489	11718 / 640
Data / param.	30249 / 970	0.994	0.70
GOF	0.921	0.1501	0.0266
R1 [F>4σ(F)]	0.0546	0.4870	0.0845
wR2 (all data)	0.1291	-	-
max. peak/hole (e.$Å^{-3}$)	1.274 /-1.523	6.150 /-1.578	0.941 / -0.782

Compound	**6.6·8H_2O**	**6.7**
Chemical formula	$C_{144}H_{192}N_{48}O_{58}P_8Pd_{24}$	$C_{27}H_{49}N_9O_{22}PPd_3$
Formula weight	6324.82	1201.92
Temperature (K)	100(2)	100(2)
Crystal system	Orthorhombic	Monoclinic
Space group	Fddd	P2(1)
a (Å); α (°)	23.423(7); 90	19.307(3); 90
b (Å); β(°)	40.770(12); 90	7.733(14); 119.99
c (Å); γ (°)	72.05(2); 90	19.315(3); 90
V ($Å^3$); Z	68808(36); 8	2497.5(7); 2
ρ (calc.) mg m^{-3}	1.221	1.598
μ(Mo K_α) mm^{-1}	1.308	1.179
$2\theta_{max}$ (°)	44.5	50
R(int)	0.22	0.1256
Completeness to θ	99%	97.9%
Data / param.	10795 / 342	10313 / 544
GOF	0.995	0.986
R1 [F>4σ(F)]	0.1301	0.0781
wR2 (all data)	0.363	0.2126
max. peak/hole ($e.Å^{-3}$)	1.89 / -1.01	1.443 / -1.194

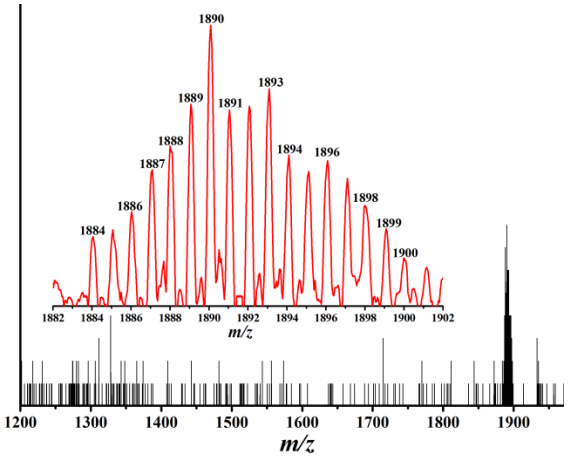

Figure A5.1: MALDI-TOF Mass spectrum of 6.1

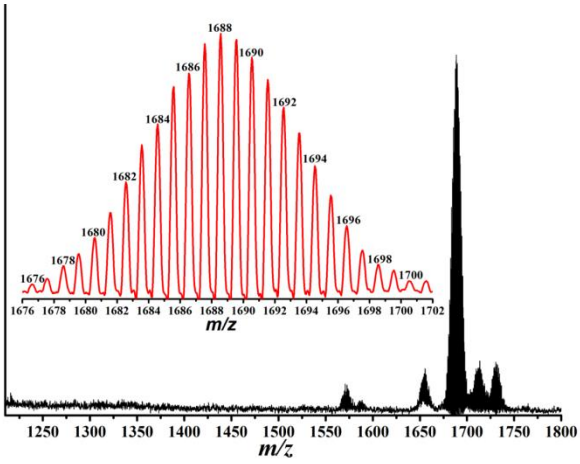

Figure A5.2: MALDI-TOF Mass spectrum of 6.2

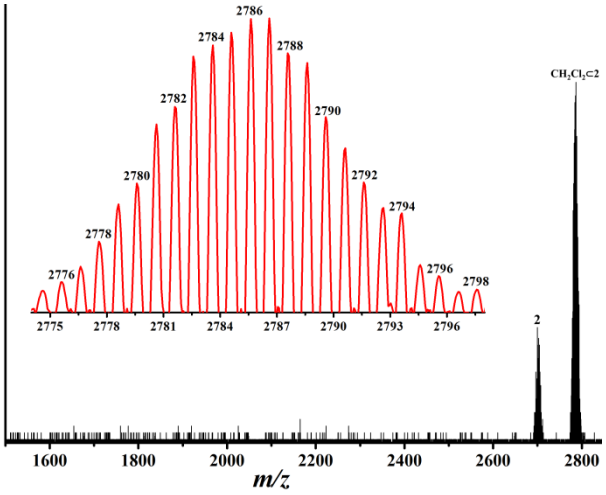

Figure A5.3: MALDI-TOF Mass spectrum of CH_2Cl_2⊂**6.3.**

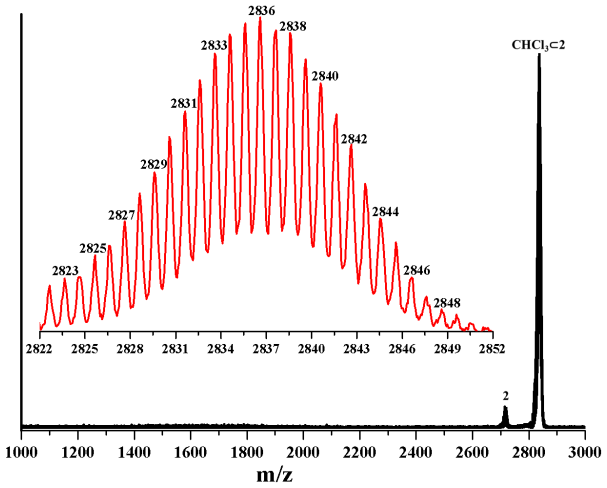

Figure A5.4: MALDI-TOF Mass spectrum of $CHCl_3$⊂**6.3.**

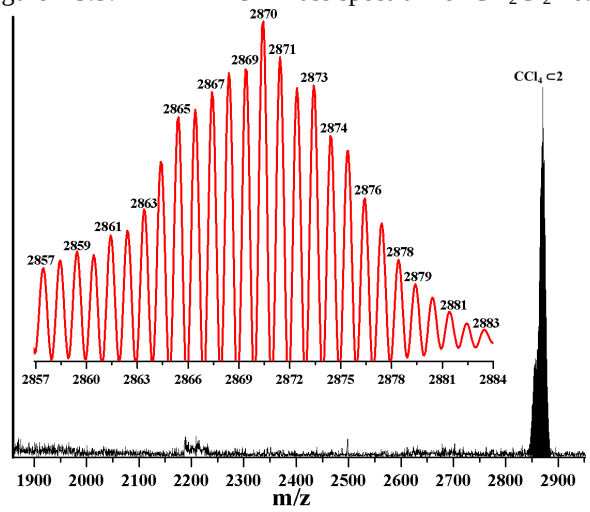

Figure A5.5: MALDI-TOF Mass spectrum of CCl_4⊂**6.3.**

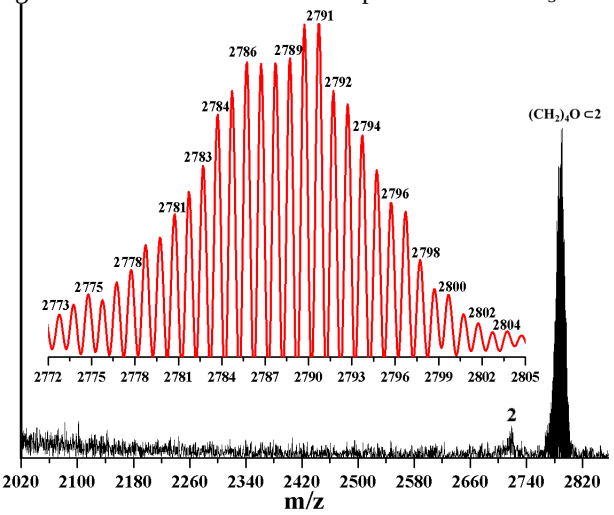

Figure A5.6: MALDI-TOF Mass spectrum of THF⊂**6.3**.

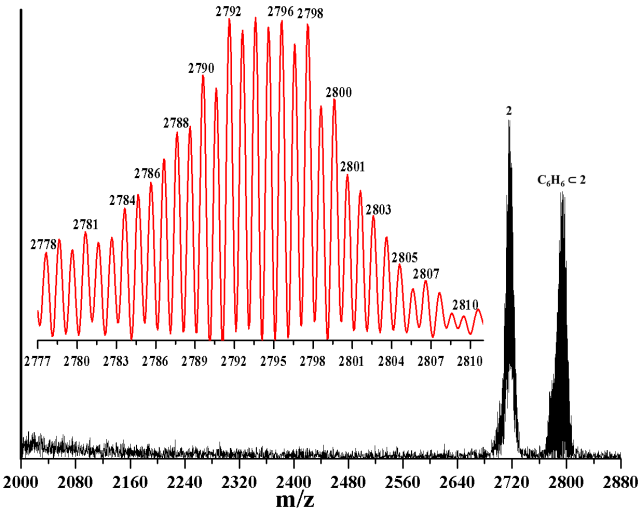

Figure 5.7: MALDI-TOF Mass spectrum of C_6H_6⊂**6.3**.

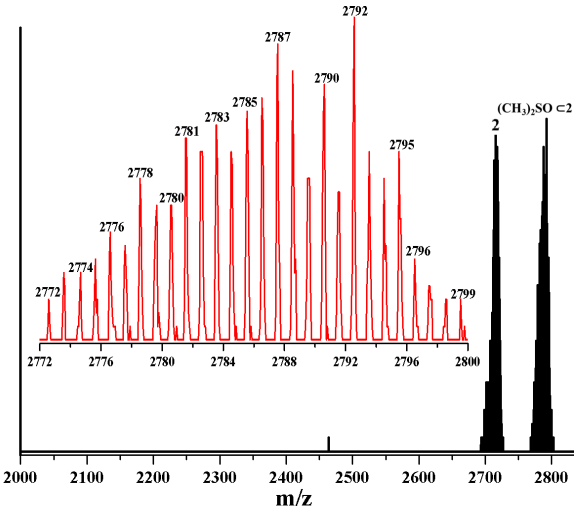

Figure A5.8: Figure A5.6:: MALDI-TOF Mass spectrum of C_6H_5F⊄**6.3.**

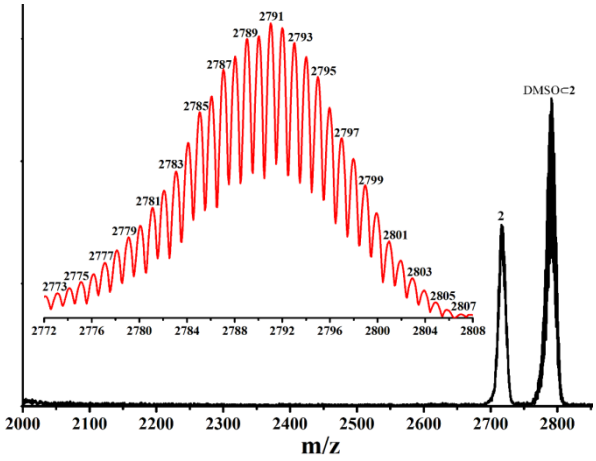

Figure A5.9: MALDI-TOF Mass spectra of C_6H_5Cl⊄**6.3**.

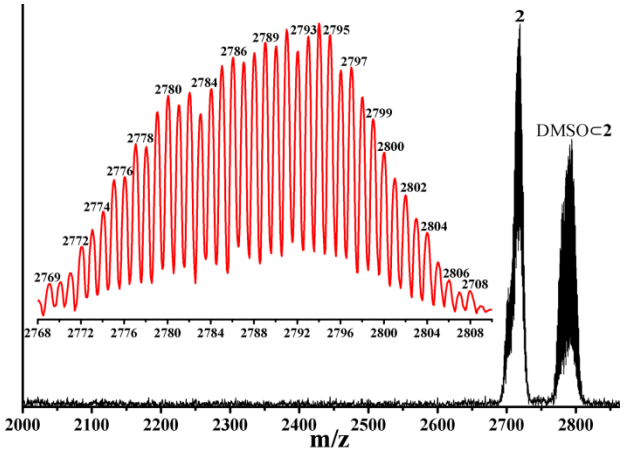

Figure A5.10: MALDI-TOF Mass spectrum of C_6H_{12}⊄**6.3**.

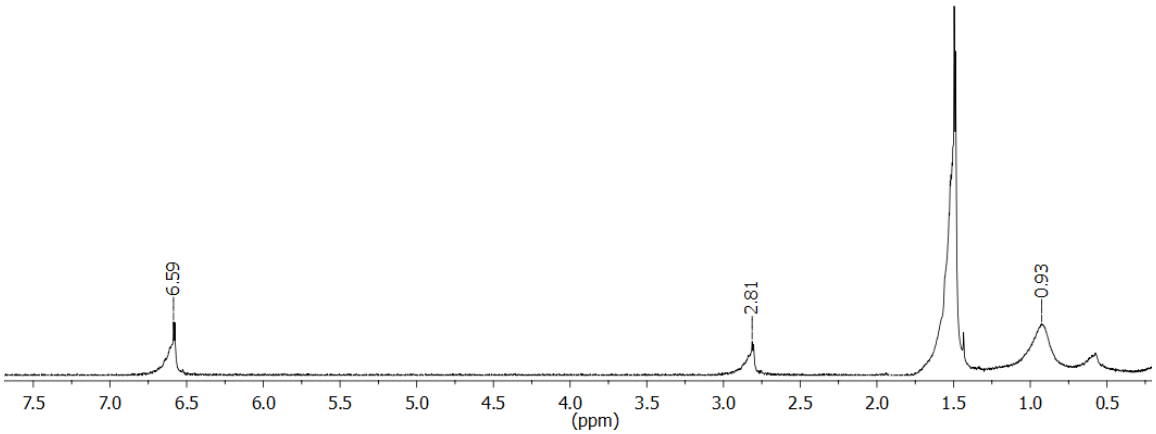

Figure A2.11: ^{1}H-NMR spectra **of 6.6.**

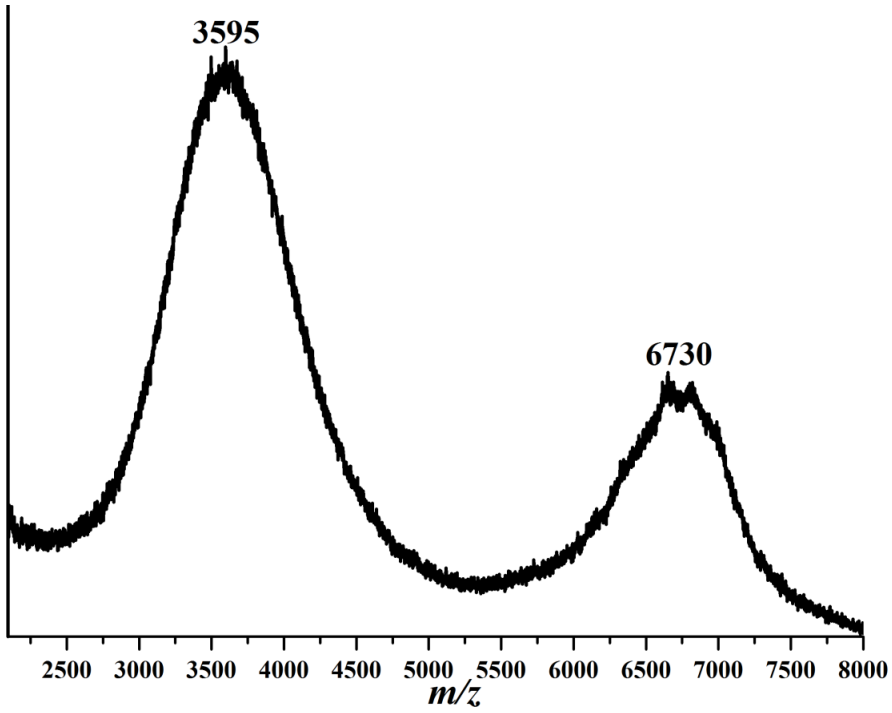

Figure A2.12: MALDI-TOF Mass spectrum of **6.6**showing the existence of approx. *m/z* value